THE UNIVERSITY of ADELAIDE

What do epsilon hafnium isotopic arrays tell us about Wilson cycle tectonics? Implications for the type area in the Appalachian-Variscan Orogen

BONNIE HENDERSON

Geology and Geophysics
School of Physical Sciences
University of Adelaide

This thesis is submitted in fulfillment of the requirements for the degree of Doctor of Philosophy

April 2016

Table of contents

Abstract

The Appalachian Orogen in Atlantic Canada, and its extension into the Variscan Orogen of Europe, are crucial locations for the development of some of the earliest ideas associated with plate tectonic theory. The recognition of a boundary that separated rocks of Gondwanan faunal affinity from those of Laurentian faunal affinity in the northern Appalachians was fundamental in defining a Wilson cycle; the process of opening and closing an oceanic basin that pre-dated the Atlantic Ocean. Tectonic models for the Appalachian Orogen have become increasingly complex as more geological data have become available resulting in the subdivision of distinct exotic terranes (Avalonia, Ganderia and Meguma) and putative multiple subduction/accretion events. These terranes, collectively referred to as "peri-Gondwanan", are generally interpreted to have been rifted from the northern Gondwanan margin in the early Paleozoic and sequentially accreted to the Laurentian margin via the closure various oceans, thereby suggesting successive Wilson cycles during the mid-late Paleozoic. A viable method for testing the model of multiple Wilson cycles is to investigate the hafnium isotopic arrays from zircon grains, which are capable of recording the evolution of complex accretionary orogenic systems. This thesis presents a comprehensive hafnium data set from igneous and sedimentary rocks in the Appalachian and Variscan orogens to assess the isotopic signature of sequential Wilson cycle tectonics.

Hafnium isotopic (εHf) arrays allow the provenance of exotic terranes in the Appalachian-Variscan orogenic system to be established. Ganderia and Avalonia, and probably Meguma, were built on a Mesoproterozoic basement that must have formed along the former Grenvillian suture-zone. In Variscan Europe, εHf arrays show that Iberia was derived from the Saharan metacraton and Armorica from the West African Craton. The Upper Allochthon of Iberia is often linked to the West African Craton, but it is more similar to the εHf array of Avalonia. Hafnium isotopes of magmatic and detrital zircons from Ganderia indicate the terrane hosted a long-lived magmatic arc that began between 800-750 Ma and continued until 450 Ma. The arc initially formed on juvenile Grenvillian crust, but a transition toward more evolved Hf isotopic compositions between 650-600 Ma coincides with accretion of Ganderia to the Gondwanan margin. Increasing amounts of juvenile crustal inputs between ~550-500 Ma are interpreted to reflect subduction roll-back and eventual rifting of Ganderia from the margin, associated with opening of the Rheic Ocean. Juvenile zircons from the leading-edge arc system of Ganderia, the Penobscot-Popelogan-Victoria arcs, indicate that they were exclusively oceanic by ~500 Ma. By contrast, evolved Hf values confirm that the coeval Notre Dame arc developed on the Laurentian margin between ~515-430 Ma. The preservation of very evolved (εHf =-15 to -25) Notre Dame arc zircons in Ganderian overstep sequences confirm the arrival of the leading edge of Ganderia to Laurentia by ~450 Ma.

The Dover Fault separates Ganderia from Avalonia. Monazite geochronology and mineral phase equilibria modelling of amphibolite facies rocks from within the fault system help constrain the younger tectonic evolution of Ganderia. The metamorphic rocks record two major stages of Ganderia evolution: (1) a low pressure (P), high temperature (T) (3-4 kbar, 600°C) event recorded by 460 ± 7 Ma monazites, associated with formation of the adjacent Tetagouche-Exploits back-arc basin, and (2) a higher P, lower T event (5-6 kbar, ~600-650°C) characterised by migmatisation and formation of garnet-sillimanite bearing metamorphic assemblages at 409 ± 6 Ma, interpreted to reflect a short interval of compression associated with the widespread Acadian orogeny.

The Hf isotopic arrays show that Avalonia records a history of arc magmatism dating back to 800-750 Ma, when it formed on Grenvillian-aged crust. A shift to more juvenile (+εHf) values by 700 Ma indicates it had evolved to an oceanic terrane at that stage, but like Ganderia, it also records the transition toward more evolved Hf isotopic compositions between 650-600 Ma, coinciding with accretion onto the Gondwanan margin.

Thereafter, it also records the shift back toward juvenile values as the terrane rifted from Gondwana to open the Rheic Ocean. The isotopic array of Meguma overlaps with those of Ganderia and Avalonia, indicating that it travelled the same journey. Accordingly, the three terranes are combined and referred to as "composite Avalonia".

The characteristic Hf array of composite Avalonia, and comparison with Hf data compilations from cratonic Amazonia, Baltica and Laurentia, allow Neoproterozoic to Paleozoic paleogeographic models to be reassessed. Avalonian continental arc magmatism began at ~800 Ma near the former Grenville suture-zone, most likely along the Laurentian margin. It is proposed that arc magmatism is the southern extension of the Valhalla arc in east Greenland. Propagation of an ocean spreading ridge behind the developing Valhalla Orogen opened the Asgard Sea, separating Baltica and Amazonia from Laurentia, possibly as early as 900 Ma. Subduction was initiated along the Laurentian margin between ~800-750 Ma, and the uniform shift toward juvenile ε(Hf) values between 750-650 Ma suggests the arc retreated from Laurentia to form the microcontinental ribbon of composite Avalonia by 700 Ma, opening proto-Iapetus as a back-arc basin between the ribbon and Laurentia. Migration of the composite Avalonian ribbon and its accretion to Gondwana by 650 Ma closed the Asgard Sea, as shown by the reversal of εHf data to progressively negative values between 650-600 Ma.

Reversal of the isotopic trend to +εHf values between 600-450 Ma for composite Avalonia, along with the Iberian and Amorican terranes of Europe, shows that all developed as a retreating oceanic arc off the north Gondwanan margin. As the ribbon separated the Rheic Ocean formed, with Meguma as the trailing passive margin. Composite Avalonia migrated northward, initially closing the Tornquist Sea as it collided with Baltica, then closing Iapetus at ~450 Ma during protracted collision with Laurentia. Following the final accretion of composite Avalonia by ~440 Ma, subduction stepped outboard into the trailing Rheic Ocean, placing composite Avalonia in an upper plate, suprasubduction zone setting. The εHf array for the northern Appalachian Orogen shows a progressive homogenisation toward CHUR. This "arrow-head" εHf array is interpreted to indicate crustal reworking during tectonic switching, between retreating (e.g. Salinic and Neoacadian orogenies) and advancing (e.g. Acadian orogeny) subduction episodes, which exclusively reworked the juvenile (Late Neoproterozoic) and Grenvillian-type basement.

The Variscan European hafnium array is remarkably similar to the Appalachian array between ~600-450 Ma in that both transition towards increasingly radiogenic values, indicating all the terranes along the northern Gondwanan margin developed into retreating magmatic arcs during subduction rollback. After ~450 Ma, the European arrays also record continual recycling of the former Neoproterozoic arc basement along a typical crustal evolutionary path, with limited input from the depleted mantle and no recycling of ancient Gondwanan crust. Intermittent back-arc opening and closing events, including the Variscan orogeny at ~360 Ma, occurred throughout the Paleozoic and early Mesozoic of Europe. The Mesozoic-Cenozoic εHf array of Variscan Europe simply reflects ongoing subduction-related magmatic activity in Europe associated with opening and closing of basins in the Tethyan oceanic realm, following Pangean amalgamation. A strong negative εHf excursion at 30 Ma indicates subduction and melting of Gondwanan cratonic lithosphere for the first time since 600 Ma, suggesting the arrival of former Gondwana into the subduction zone.

Hf isotopic arrays indicates that the completion of the type-Wilson cycle in the northern Appalachians is marked only by termination of magmatism as the εHf array converged on CHUR at ~300 Ma. Similarly in Europe the collision of Gondwana with Laurentia to form Pangea is not reflected in the εHf array and also reflects only the reworking of composite Avalonia. Therefore, the assembly of Pangea could form only part of a larger, longer-term supercontinental cycle. Accordingly, Hf isotopic arrays provide an opportunity to reassess Precambrian supercontinent reconstructions at a cratonic scale, but are less likely to recognise individual Wilson cycles unless they involve reworking of cratonic crust at the beginning and end of each cycle.

Declaration

I certify that this work contains no material which has been accepted for the award of any other degree or diploma in my name, in any university or other tertiary institution and, to the best of my knowledge and belief, contains no material previously published or written by another person, except where due reference has been made in the text. In addition, I certify that no part of this work will, in the future, be used in a submission in my name, for any other degree or diploma in any university or other tertiary institution without the prior approval of the University of Adelaide and where applicable, any partner institution responsible for the joint-award of this degree.

I give consent to this copy of my thesis when deposited in the University Library, being made available for loan and photocopying, subject to the provisions of the Copyright Act 1968.

The author acknowledges that copyright of published works contained within this thesis resides with the copyright holder(s) of those works.

I also give permission for the digital version of my thesis to be made available on the web, via the University's digital research repository, the Library Search and also through web search engines, unless permission has been granted by the University to restrict access for a period of time.

BONNIE HENDERSON DATE

Publications arising from this thesis

Journal articles

Bonnie Henderson, W. J. Collins, J. Brendan Murphy, Gabriel Gutierrez-Alonso, Martin Hand, (in press), *Gondwanan basement terranes of the Variscan-Appalachian orogen: Baltican, Saharan and West African hafnium isotopic fingerprints in Avalonia, Iberia and the Armorican Terranes,* Tectonophysics, DOI:10.1016/j.tecto.2015.11.020

Bonnie Henderson, W.J. Collins, J. Brendan Murphy, Martin Hand, *A hafnium isotopic record of magmatic arcs and continental growth in the Iapetus Ocean: the contrasting evolution of Ganderia and the peri-Laurentian margin,* (in review), Gondwana Research

Conference abstracts

Bonnie Henderson, W.J. Collins, J. Brendan Murphy, Martin Hand, *What can hafnium isotope ratio arrays tell us about orogenic processes? An insight into geodynamic processes operating in the Alpine/Mediterranean region*, AGU Fall meeting 2013

Bonnie Henderson, W.J Collins, J. Brendan Murphy, Martin Hand, Gabriel Gutierrez-Alonso, Tracking the Neoproterozoic-Permian tectonic evolution of Avalonia in the Canadian Appalachians: a combined U-Pb-Hf detrital zircon study, Gondwana15, Madrid, 2014

W.J Collins, **Bonnie Henderson**, J. Brendan Murphy, Martin Hand, Gabriel Gutierrez-Alonso, *Evolution of Phanerozoic Europe from an Hf isotope perspective: implications for supercontinental and Wilson cycles*, Gondwana15, Madrid, 2014

G. Gutierrez-Alonso, J. Fernandez-Suarez, **Bonnie Henderson,** Daniel Pastor-Galan, Alicia Lopez Carmona, J. Brendan Murphy, Arlo B Weil, M Francisco Pereira, Javier Fernandez-Lozano, *Another model for Western Europe Paleozoic Variscan evolution: questioning redundant subduction and oceans*, Variscan 2015

Erin Martin, W. J. Collins, **Bonnie Henderson**, *Neoproterozoic global geodynamic rearrangement recorded by Hf isotopes in zircon: Birth of the circum-Pacific and dawn of the Phanerozoic,* Australian Earth Science Convention 2014

Acknowledgements

I am incredibly grateful for the life changing opportunities and events that I have been offered and involved in since starting this unpredictable PhD journey. Although the path has not always been clear, and my self-confidence has been tested at times, I know that the past four years have shaped me and allowed me to become a better critical thinker, scientist and hopefully, person.

To my university friends (especially Farid, Nader, Daniel, Louise) who have been around from the start of my geological journey- I wouldn't be writing this without you. Emma, Ryan and Georgy: our adventures in India are what gave me the drive and passion to continue with my post-graduate studies, thank you for your ongoing support and friendship. To those who have travelled on the PhD path with me I am so grateful that you have put up with me for so long! Big thanks go to Morgan, Diana, Laura, Cesco, Rob, Lachy, Kieran, Dan, Funny and Vicki. I am especially grateful to Katherine, Kat, Jade, and Alec. You all have kept me sane and have shown time and time again how patient, empathetic, kind and wickedly funny each of you are, in your own special ways. Seriously, you will always have a friend in me no matter the distance.

Outside of the bubble that is post-graduate life I am supported by the most incredible people who represent different, and equally important, facets of my life. To the girls and guys at the Pole Boutique and Polarise Adelaide you all made me feel so loved and happy when I there were times when I really struggled to be positive. To my school girls Amy, Krystal, Koral, Celeste and Kylie thank you for understanding that sometimes I was just too busy to catch up properly for months! To Jess and Kate, what would I do without you? I wasn't blessed with sisters by blood- but I have you guys and that is just as important to me.

On the technical side I am thankful for the professional and hardworking team at Adelaide Microscopy and to Justin Payne for being a multi-collector guru. Huge thanks go to Donnelly Archibald for providing me with safe transport across Nova Scotia and Newfoundland, invaluable insights into Antigonish geology and for sending samples home to Adelaide when I really needed them!

Perhaps the highlight of my PhD was the time I was lucky to spend in Salamanca and Galicia with Gabriel Gutierrez-Alonso. Gracias for taking the time and having the patience to teach me the intricate details of Iberian geology. Equally enjoyable was the time I spent in Antigonish with my co-supervisor, Brendan Murphy. Your passion and knowledge of Appalachian geology and tectonics is invaluable to not only me, but to the wider geological community.

To Martin Hand, thank you for your faith in my abilities, especially during times when I had many doubts! The breadth of your geological knowledge is astounding and I was lucky to tap into even a little of that. Finally, to my 'primary' supervisor Bill Collins. I absolutely would not have completed this without your support. You encouraged me to think outside the box and to challenge myself constantly. Thank you for everything.

To Debs and Greg, Grandma and Grandad, Sam, Joel and Alex, you are the best family I could ask for, and luckily I just got you by chance. Mum and Dad, thank you for the emotional and at times, financial, support throughout my seemingly never ending university career. I love you very much.

Lastly, to my thanks go to Josh, who has provided me with constant support and love for the last three and half years. I couldn't have done this without you by my side, feeding me and propping me up when I felt particularly blue. Thank you for all that you are.

Chapter 1

INTRODUCTION AND THESIS OUTLINE

1. PLATE TECTONICS AND THE WILSON CYCLE CONCEPT

Plate tectonics is perhaps the most important and fundamental theory in geology, of which the Wilson cycle forms an integral part. The Wilson cycle is coined after Tuzo Wilson (Wilson, 1966), based on his understanding of the Appalachian Orogen. The first stage of a Wilson cycle involves splitting a tectonic plate apart, culminating in the opening of an ocean basin and the generation of oceanic crust as the two plates diverge (Fig. 1a-d). This is the classic "Atlantic-style ocean-opening process. The second phase involves the reversal of plate motion, subduction initiation, consumption of the oceanic plate, and eventual collision of continental margins and subsequent orogenesis (Fig. 1e-g). A complete Wilson cycle, simply put, is the opening and closing of an oceanic basin (Fig. 1).

The northern Appalachian Orogen in Atlantic Canada (Nova Scotia, Newfoundland and New Brunswick) formed an important location for the early stages of defining plate tectonics and the key stages of a Wilson cycle. Crucial for recognising the process of oceanic basin opening and closing was the identification of a suture zone that ran through Atlantic Canada and into Western Europe, separating rocks of Laurentian affinity from those of Gondwanan affinity (Fig. 2, Wilson, 1966; Williams, 1979; Williams et al., 1988). Over the last four decades, technological advancements have further refined the fundamental principles of the Wilson cycle, with much of the work taking place in the type section of Atlantic Canada (Fig. 1). Building on Wilson's (1966) concept, Williams (1979; 1988) recognised important contrasts in the lithology, fauna, metamorphic and igneous record of the Neoproterozoic-Paleozoic rocks of Newfoundland and Nova Scotia (Atlantic Canada), and subdivided them into distinct tectonostratigraphic zones. These are: Ganderia, Avalonia and Meguma, which preserve continental affinity with Gondwana; and two distinct "oceanic" domains that have affinities to Laurentia (Notre Dame Subzone) and Ganderia (Exploits Subzone) and represent vestiges of the closure of the ancient Iapetus Ocean (Fig. 2). The complex geology preserved in the Appalachian Orogen is commonly is now interpreted to be the result of a culmination of multiple Wilson cycles (see van Staal et al., 1998; van Staal et al., 2007; van Staal et al., 2009; Barr et al., 2014 and references therein), and thus represents an ideal natural laboratory to investigate the isotopic record of Wilson cycles and the implications for plate tectonics.

2. GEOLOGICAL FRAMEWORK OF THE APPALACHIAN OROGEN

The three distinct continental blocks in the northern Appalachian Orogen, Ganderia, Avalonia and Meguma (Fig. 2), have been called "peri-Gondwanan" (O'Brien et al., 1983; Nance and Murphy, 1994; Barr and White, 1996; O'Brien et al., 1996), based on their apparent Gondwanan affinity. Avalonia and Ganderia are commonly interpreted to have occupied a location along the Amazonian margin of Gondwana in the latest Neoproterozoic (Nance et al., 2008), whereas the paleogeography of Meguma is more enigmatic. Sparse detrital zircon data suggests an affinity with Avalonia and the West African Craton throughout the late Neoproterozoic-early Cambrian (Waldron et al., 2009). Subtle differences in the geological records of the peri-Gondwanan terranes have resulted in contrasting interpretations for the evolution of the terranes during the late Neoproterozoic-early Paleozoic, as discussed below.

These so-called peri-Gondwanan terranes, and their counterparts in Variscan Europe (Iberia, Armorica, Cadomia and the Pontides of Turkey), are frequently interpreted to have formed by one of two tectonic evolutionary models. The first requires the closure of up to five

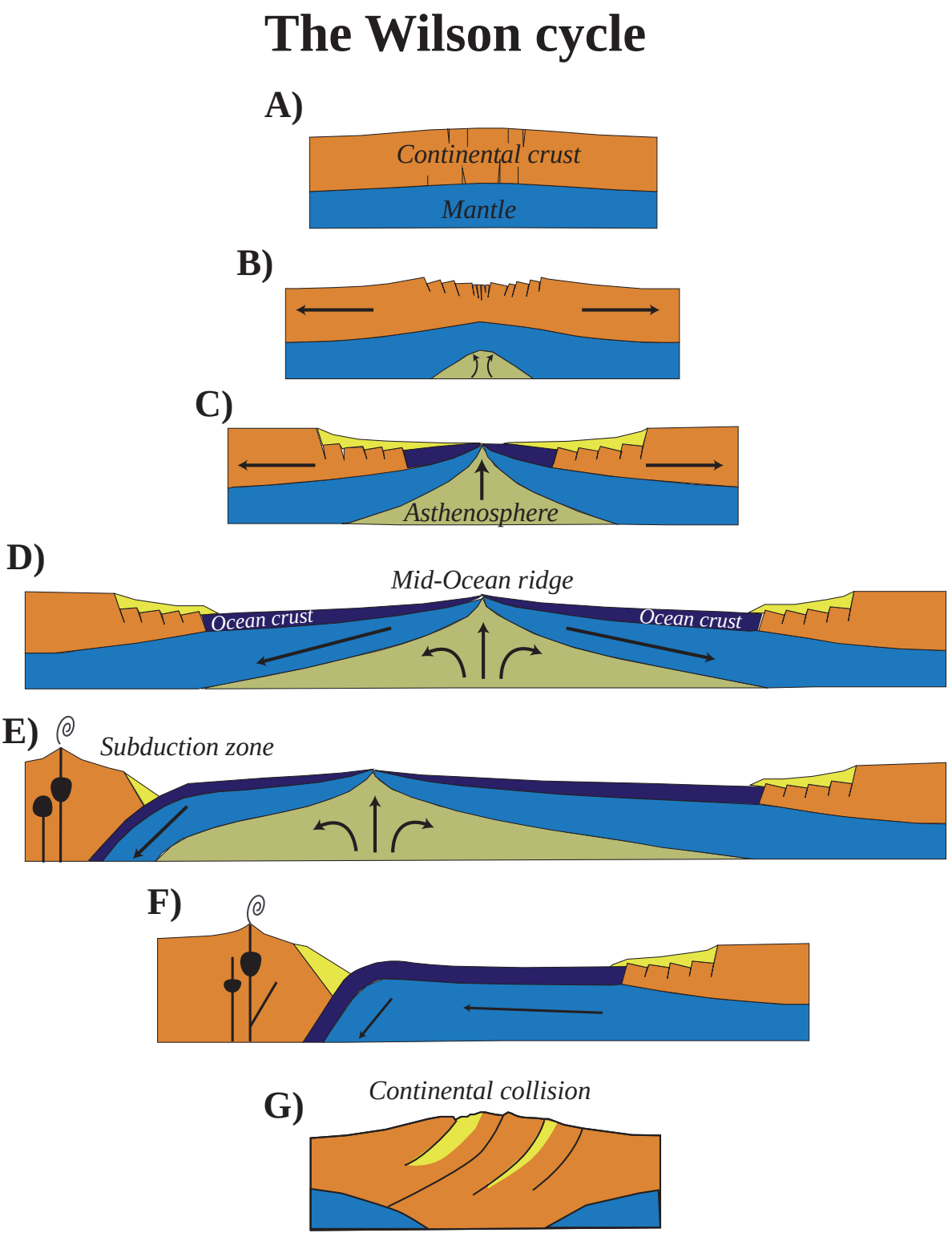

Figure 1
Simplified schematic showing the major stages in an idealised Wilson cycle. a) A single stable craton. b) early-stages of rifting and extension including normal faulting and half-graben development. c) The initiation of plate divergence during the development of a proto-oceanic basin. d) An oceanic basin at its fullest width. e) Subduction of oceanic crust commences along one margin of the ocean-continent boundary, reversing the plate motions. f) Spreading has ceased in the oceanic basin as the mid-ocean ridge is eventually subducted. g) The two continents are drawn together as the ocean closes, completing the Wilson cycle.

ocean basins (see van Staal et al., 1998; van Staal et al., 2007; van Staal et al., 2009; Barr et al., 2014 and references therein) during the protracted accretionary assembly of the peri-Laurentian margin, thus involving five potential Wilson cycles. In this model, Ganderia, Avalonia and Meguma were separate terranes that were diachronously rifted from the Gondwanan margin during the late Cambrian to Silurian (Landing, 2004; Pollock, 2007; Pollock et al., 2009; van Staal et al., 2012; White and Barr, 2012). The leading edge of Ganderia is interpreted to have arrived at the Laurentian margin by ~452 Ma (Pollock et al., 2007; van Staal et al., 2012), and the trailing passive margin at ~435-422 Ma (Pollock et al., 2011), after the closure of the Tetagouche-Exploits back-arc basin (van Staal, 1994; Zagorevski et al., 2007). Avalonia is considered to have arrived almost immediately after following the closure of the Acadian seaway (Zagorevski et al., 2007; van Staal et al., 2014). The arrival of Meguma is contentious, but in the separate terranes model, it arrived during the later stages of the Acadian orogeny or during the Neoacadian orogeny at ~390-370 Ma (Robinson et al., 1998; Moran et al., 2007; Stampfli et al., 2011).

The second model proposes that a contiguous continental terrane (composite Avalonia) closed a single oceanic basin (Iapetus) as it assembled with Laurentia, and opened a second ocean (Rheic) during its departure of Gondwana (Murphy et al., 1999; Stampfli and Borel, 2002; Murphy et al., 2004; Murphy and Keppie, 2005). The latter model requires the completion of a Wilson cycle during the closure of the Iapetus Ocean and the completion of a second cycle during the closure of the Rheic Ocean.

3. THE ZIRCON HAFNIUM METHOD AND ISOTOPIC ARRAYS

Zircon can host up to 1% hafnium in its crystal structure and, because of its very low Lu/Hf ratio, it essentially preserves the initial 176Hf/177Hf ratio (expressed as εHf) of its source magma at the time of crystallisation (Kinny and Maas, 2003). The Hf isotopic composition of a zircon grain can be used as a geochemical tracer of a host rock's origin in the same way that whole-rock Nd isotopes are used. However, the greatest advantage of the Lu/Hf method over the Sm/Nd method is that it allows for greater resolution and detail regarding the source of magmas, with the εHf array generating at least two end-member source components from the population of analysed zircons, whereas the Nd data only provides a single isotopic value, based on a weighted average for the whole rock. The differences between hafnium data from zircons and whole rock Nd data is particularly evident in sedimentary rocks where the sources can be highly varied and Nd data alone are not able to identify the individual components (e.g. Howard et al., 2009). Even in granites, which are commonly considered to have a single source, zircon hosted hafnium isotopes are able to identify mixed sources and inheritance within a single sample (Griffin et al., 2002; Villaros et al., 2011; Zhou et al., 2012), detail that may be lost using whole rock Nd data alone (Hawkesworth and Kemp, 2006).

Hafnium isotope analysis of the zircon grains provides an important second dimension to U-Pb zircon geochronology, allowing the age-data to be presented in statistically robust, composite epsilon hafnium (εHf) arrays. Hafnium isotopes in zircons can be used for a single crystallisation event to describe the crustal and/or mantle contribution to magmatism in individual granitic suites (Griffin et al., 2002; Jiang et al., 2012), in regional studies to describe the tectonomagmatic evolution of cratons (Belousova et al., 2009) or at global scale to describe the nature of supercontinent cycles (Kemp et al., 2006; Condie and Aster, 2010) or crustal growth during the Earth's history (Kemp et al., 2007). Comprehensive hafnium isotopic arrays permit rigorous comparisons to putative source cratons in provenance studies (Howard et al., 2009; Wang et al., 2010; Linnemann et al., 2014), as well as allowing the geodynamic links between dispersed continental blocks to be tested, which would otherwise show only weak

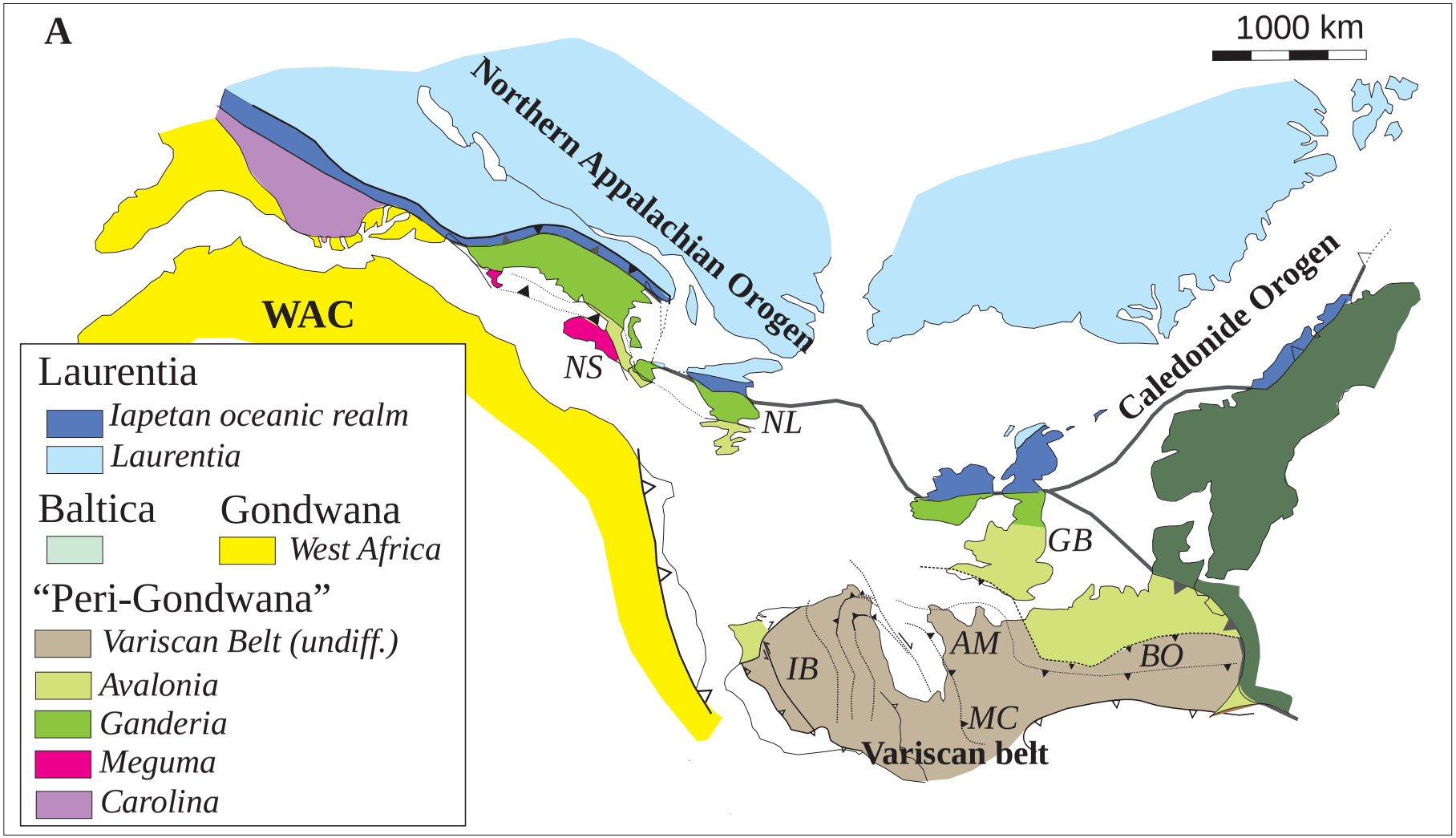

Figure 2

Tectonic map showing the distribution of the Appalachian orogen and the extension into the United Kingdom and Variscan Europe during the late Carboniferous. Shown are the tectonic-stratigraphic subdivisions within the Appalachian orogen including Laurentia, the Iapetan "Dunnage Zone", Ganderian arcs, Ganderia, Avalonia and Meguma. NL: Newfoundland, NS: Nova Scotia, IB: Iberia, AM: Amorica, MC: Massif Centrale, BO: Bohemia, WAC: West African Craton. The figure is modified from Hibbard et al., (2007b), Barreiro et al., (2007), Keppie et al., (2008) and Pollock et al., (2011).

geological connections (Henderson et al., 2016).

More recently, Hf arrays from detrital and magmatic zircons have been used to identify the isotopic signature of the closure phase of Wilson cycles (Collins et al., 2011; Smits et al., 2014). Shifts in hafnium isotopic arrays are indicators of a fundamental change in tectonic conditions. Using Hf arrays from Phanerozoic orogens Collins et al., (2011) identified two distinct orogenic systems that yield contrasting isotopic signatures; the "exterior" circum-pacific orogens and the "interior" Alpine-Himalayan-Indonesian collisional orogens. Circum-pacific orogens are characterised by extensional, accretionary processes and record a long-term shift towards increasingly juvenile hafnium values, which reflect the progressive removal of ancient lower crust and subcontinental lithospheric mantle (SCLM) during continuous subduction processes. In contrast, interior orogens, like the Himalayas, are characterised by the progressive accretion of continental fragments during successive Wilson cycles. Subduction-related magmatism is restricted to periods of ocean closure (Collins et al., 2011) and records an initial excursion towards the depleted mantle reflecting juvenile arc magmas derived from the mantle wedge, followed by mixing with evolved magmas that mirror the composition of the upper plate lithosphere. The result of a long-lived accretionary system is a 'saw-tooth' type pattern in the Hf isotopic array (e.g. Fig. 4a).

A third Hf isotopic array has been recognised by Smits et al. (2014) in central Australia during the Paleoproterozoic-Mesoproterozoic (Fig. 3). The oldest zircons of the orogen are ~1700 Ma and the large vertical array of εHf values, between +12 and -30, suggest a continental arc was built on Archean crust, which can be identified as the West Australian Craton. The isotopic contraction of negative epsilon hafnium values towards positive values during a ~100 myr interval between 1700-1600 Ma has been interpreted to reflect the initiation of subduction retreat and the removal of vast continental ribbon from the West Australian Craton (Fig. 3). The process is marked by the development of an inverted "U-shaped" array, reflecting the transition from a continental arc to an extensional, accretionary orogen analogous to the circum-Pacific array (Collins et al., 2011). The inflection in the Hf array from positive to negative values at ~1500 Ma suggests the continental ribbon then underwent crustal reworking. The next ~300 myr shows the array follows a typical crustal evolutionary path (Lu/Hf= 0.015), indicating that working continued between 1500-1200 Ma, whereby little ancient or juvenile crust contributed to the magmatism (Fig. 3). At ~1200 Ma, a major negative excursion to εHf values of -30 indicates re-introduction of Archean crust into the magmatic system. Given the geological constraints that this interval coincided with major compressive deformation of the Albany-Fraser orogen against the adjacent West Australian Craton, the -εHf excursion was taken to represent amalgamation of the Western and South Australian cratons (Smits et al., 2014). In effect, this was the termination of a long Wilson cycle.

As Hf isotopic arrays are capable of recording complex orogenic systems involving the closure of multiple oceanic basins, the method can be used to test the evolutionary models proposed for the Appalachian-Variscan Orogen. By analysing the hafnium isotopic record of the detrital and magmatic zircons associated with the opening and closure of the Iapetus and Rheic oceans in the Appalachians, it is possible to investigate the presence and duration of Wilson cycles during the assembly of the Apalachian Orogen. If the peri-Gondwanan terranes are separated by a number of individual ocean basins (e.g. Zagorevski et al., 2007; van Staal et al., 2009), then the hafnium isotopic array should record the cyclical nature of consecutive ocean closure events (Fig. 4a), as the arrival of each crustal block should record the culmination of an individual Wilson cycle (Fig. 3). The hafnium array should show a vertical spike that records the development of a continental arc on the upper plate, where magmatism involves mixing between the basement crust and juvenile arc magmas derived from the mantle wedge (e.g. Mueller et al., 2008; Roberts et al., 2013; Linnemann et al., 2014) (Fig. 4a). Following the

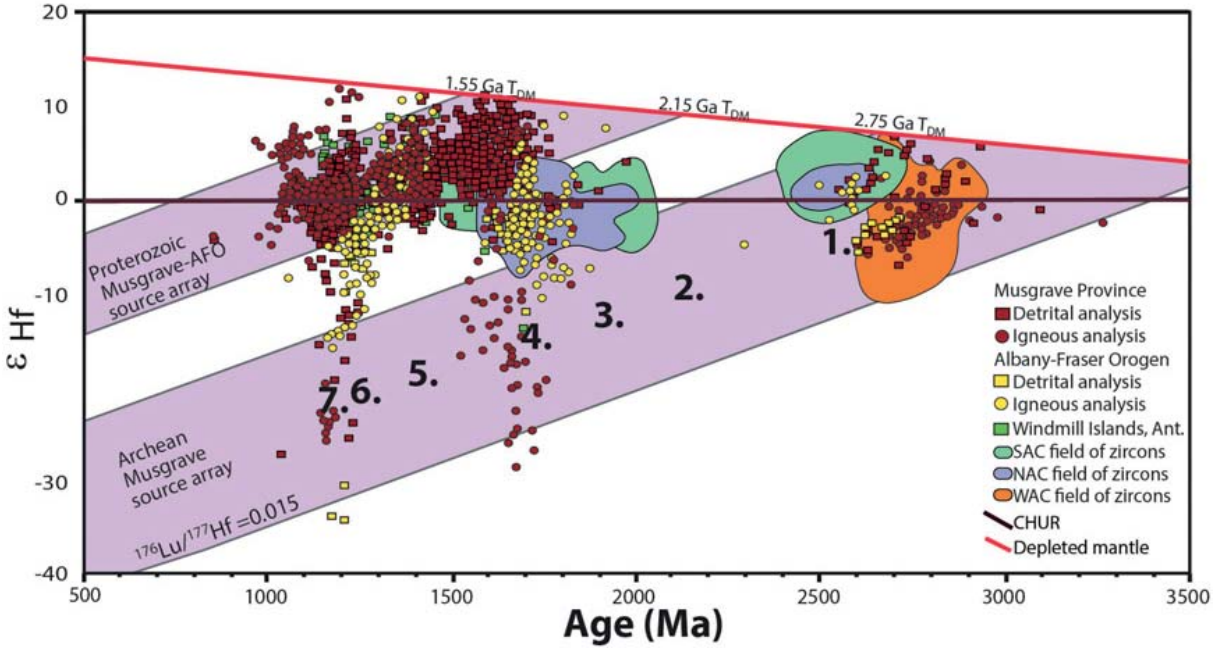

Figure 3

The hafnium isotopic array for the central Australian Musgraves Province, which is from Smits et al. (2014). The numbers correspond to: 1) craton formation, 2) initial continental extension and passive margin development, 3) ocean opening, 4) subduction initiation and back-arc formation, 5) oceanic closure during slow accretion of arc-backarc system and recycling, 6) terminal continental collision and, 7) post-collisional magmatism.

arrival of each terrane, subduction would step outboard into the next ocean basin and the same process should start again with an arc developing on the newly accreted terrane. The overall effect of this evolutionary model is a saw-tooth type pattern in the hafnium array (Fig. 4a). However, if the peri-Gondwanan terranes formed a contiguous "composite Avalonia" terrane (e.g. Murphy et al., 1999), then only a single Wilson cycle should be recorded in the hafnium isotopic array (Fig. 4b) during the early Paleozoic, with a second Wilson cycle associated with the closure of the Rheic Ocean prior to the Alleghenian Orogeny in the late Carboniferous (Williams et al. 1979, Hatcher et al. 1988; Veevers, 2004; Stampfli et al., 2013).

To ensure consistency throughout this thesis, epsilon hafnium (εHf) and T_{DM} (DM=depleted mantle) were calculated using the 176Lu decay constant after Scherer et al., (2001), where T is the time of crystallization of the zircon. T_{DM} and T_{DMc} were calculated using the methods of Griffin et al. (2002), with an average crustal composition of 176Lu/177Hf = 0.015. All data are presented using the epsilon hafnium (εHf) notation, which refers to the deviation of the isotopic composition from CHUR, which at any time yields a value of 0 (Patchett and Tatsumoto, 1980; Blichert-Toft and Albarède, 1997).

Figure 4a *(on the next page)*

The expected hafnium isotopic record of the two main competing theories for the evolution of the northern Appalachian orogen during the Paleozoic. A) The first model considers the peri-Gondwanan terranes to be separate entities that arrived at the Laurentian margin via the closure of multiple oceanic basins (e.g. during consecutive Wilson cycles, see van Staal et al. 2009). The overall effect of this evolutionary model is a "saw-tooth" type pattern in the hafnium array. B) The second model considers the peri-Gondwanan terranes represented a single composite terrane that was accreted to Laurentia in during the Silurian (e.g. Murphy and Keppie 2005). An Andean style continental arc was then built upon the Laurentian margin during the closure of the Rheic Ocean, resulting in a fanning isotopic array that represents the ongoing recycling of juvenile arc magmas with the basement of the continental terrane. As subduction continues it strips the SCLM and replaces it with increasingly juvenile arc magmas, leading to an overall increasingly juvenile arc (see Collins et al., 2011).

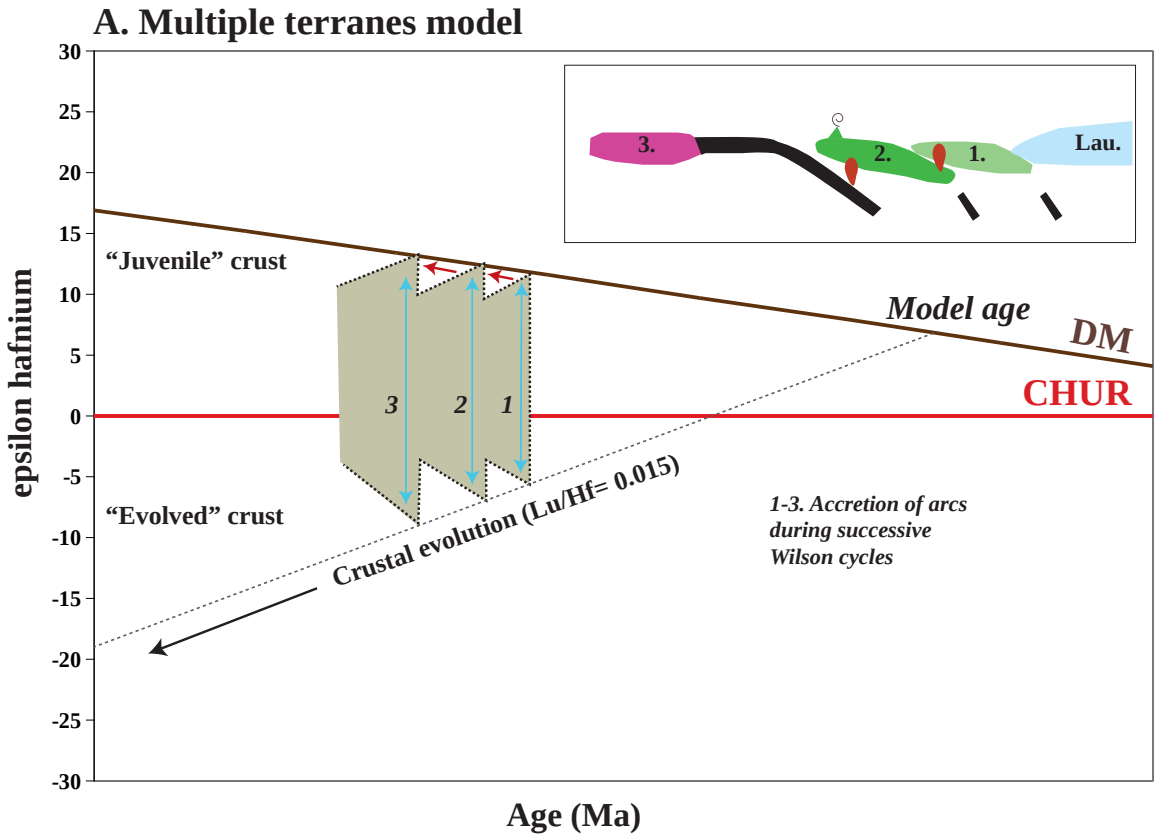
A. Multiple terranes model
epsilon hafnium
30
25
20
15
10
5
0
-5
-10
-15
-20
-25
-30
3.
2.
1.
Lau.
"Juvenile" crust
Model age
DM
CHUR
3
2
1
"Evolved" crust
Crustal evolution (Lu/Hf= 0.015)
1-3. Accretion of arcs during successive Wilson cycles
Age (Ma)

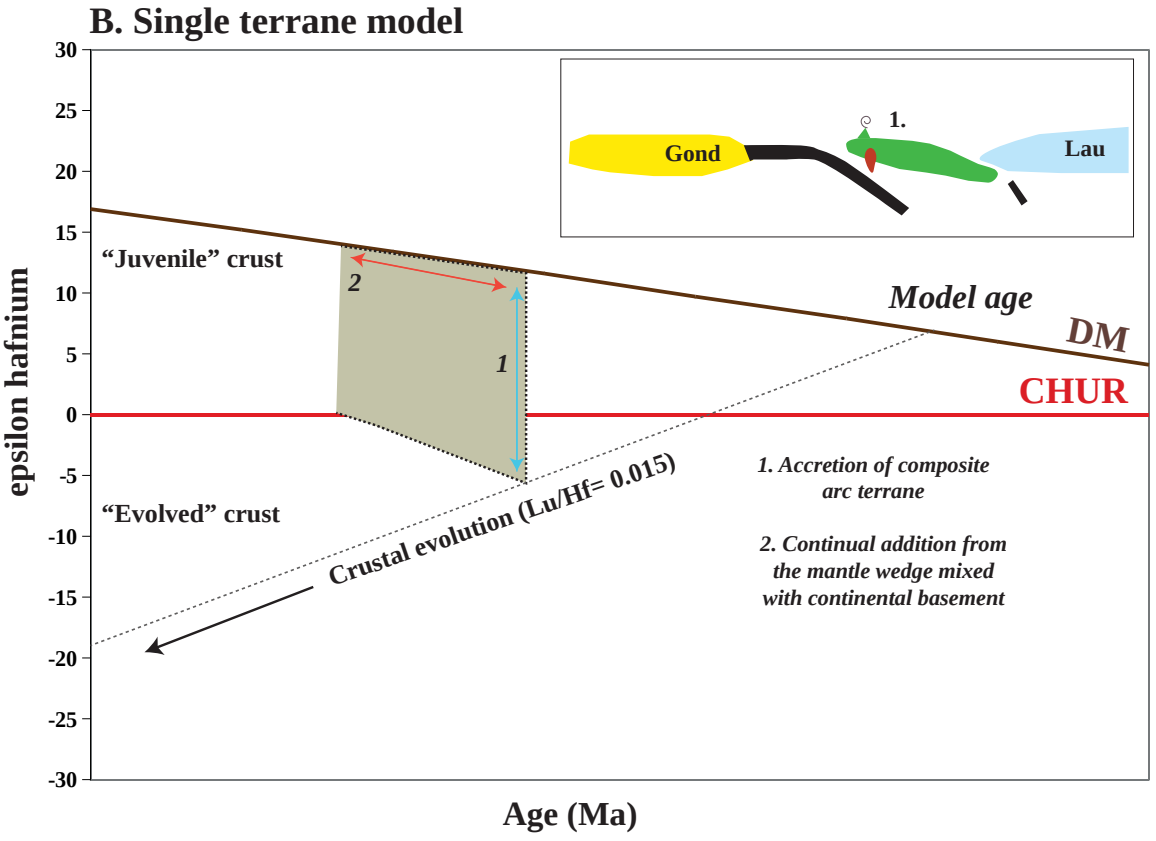
B. Single terrane model
epsilon hafnium
30
25
20
15
10
5
0
-5
-10
-15
-20
-25
-30
Gond
1.
Lau
"Juvenile" crust
2
1
Model age
DM
CHUR
"Evolved" crust
Crustal evolution (Lu/Hf= 0.015)
1. Accretion of composite arc terrane
2. Continual addition from the mantle wedge mixed with continental basement
Age (Ma)

Juvenile components are recognised as (+) εHf(T) values (Fig. 4), falling between the estimated value of the new continental crust from modern island arcs (Dhuime et al., 2011) and the estimated depleted mantle array of Griffin et al. (2004). Evolved components are recognised as negative εHf(T) values (0 to -40), interpreted to have been sourced from magmas that include an ancient crustal component (Fig. 4).

4. PROJECT AIMS

The major aims of this project are:

1. To obtain a comprehensive hafnium isotopic record of the northern Appalachian Orogen, which is the type area of the Wilson cycle (Wilson, 1966) and thus represents an appropriate natural laboratory.
2. To test the test the sensitivity of the hafnium isotopic arrays in documenting complex accretionary processes during continental ribbon transfer from one continental margin to another.
3. To test the metamorphic record of continental ribbon transfer against the associated hafnium isotopic record of magmatism.
4. To propose a geodynamic framework for the Neoproterozoic to late Paleozoic evolution of the Appalachian Orogen (and to a lesser extent, the Variscan Orogen) that accommodates both the hafnium isotopic and geological records.

5. THESIS OUTLINE

Chapter Two presents detrital zircon U-Pb-Hf isotopic data from Neoproterozoic-Silurian sedimentary rocks of Avalonia in the northern Appalachians and Iberia, Spain, to demonstrate that the provenance of the peri-Gondwanan terranes is relatively simple and can be traced back to major cratons in Gondwana and Baltica. Comprehensive hafnium isotopic arrays from Armorica, Baltica, Amazonia and the African cratons each have their own unique signature. Avalonia is commonly considered to have been derived from the Amazonian margin of Gondwana, but the hafnium isotopic characteristics of the detrital zircon grains in early Neoproterozoic rocks bear much stronger similarities to Baltica. The hafnium isotopic array also suggests the early Avalonian oceanic arc was built on a sliver of "Grenvillian-type crust" (~2.0–1.0 Ga) possibly of Baltican affinity at ~800 Ma, prior to accretion with a continental margin at ~640 Ma. Chapter two presents the framework for how hafnium isotopic data is presented and interpreted throughout the remainder of the thesis.

This chapter is published as "Gondwanan basement terranes of the Variscan–Appalachian orogen: Baltican, Saharan and West African hafnium isotopic fingerprints in Avalonia, Iberia and the Armorican Terranes" Henderson, B.J., Collins, W.J., Murphy J.B., Gutierrez-Alonso, G., Hand, M., 2016, Tectonophysics.

Chapter Three presents detrital and magmatic zircon U-Pb-Hf isotopic data from Ganderia and peri-Laurentia in order to test the sensitivity of the hafnium isotopic arrays in documenting complex accretionary orogenic processes. Ganderia hosted a long-lived magmatic arc that began at least by 650 Ma and continued until 450 Ma, but the Hf isotopic record suggests it began earlier, possibly at ~750 Ma. Ganderia appears to have formed on a sliver of "Grenvillian-type" basement, and records a transition toward more evolved Hf isotopic compositions between 650-600 Ma, coinciding with its accretion to the Gondwanan margin. This was followed by increasing amounts of juvenile crustal inputs between ~550-500 Ma, which is interpreted to reflect subduction roll-back from the Gondwana and the opening of the Rheic Ocean. The

Notre Dame arc evolved along the Laurentian margin between ~515-425 Ma, and was built on Archean crust. Suprasubduction zone magmatism occurred at ~490-460 Ma during the closure of the Taconic Seaway and was dominated by the recycling of Laurentian crust, with progressive mixing of evolved and juvenile arc magmas over time. The preservation of very evolved Notre Dame arc zircons in Ganderian overstep sequences confirm the arrival of the leading edge of Ganderia to Laurentia by ~450 Ma.

Chapter three is under review as "A hafnium isotopic record of magmatic arcs and continental growth in the Iapetus Ocean: the contrasting evolution of Ganderia and the peri-Laurentian margin", Henderson, B.J., Collins, W.J., Murphy J.B., Hand, M., 2016, Gondwana Research.

Chapter Four presents monazite geochronology and mineral phase equilibria, calculated for a series of amphibolite facies rocks within the Dover Fault Shear Zone; a brittle-ductile structure that separates the Ganderia terrane from Avalonia in Newfoundland. The purpose of the chapter is to investigate the timing and nature of metamorphism in the Gander Zone during continental ribbon transfer across the Iapetus Ocean. The metamorphic rocks along the Dover Fault Zone record two major stages of the Ganderian evolution. The first is a low pressure, high temperature (3-4 kbar, 600°C) event recorded by 460 ± 7 Ma monazite within andalusite bearing metamorphic assemblages. The second is both a higher pressure event (5-6 kbar, ~600-650°C) and a lower pressure event (3-4 kbar) characterised by migmatisation and the formation of garnet-sillimanite bearing metamorphic assemblages at 409 ± 6 Ma; interpreted to reflect a short interval of compression along the Dover Fault Shear Zone followed by the emplacement of the Hare Bay Gneiss and other granite suites. Ganderia is interpreted to form the locus of intermittent extension and contraction events between the early Ordovician-middle Devonian, most likely relating to the opening and closing of back-arc basins, during the consumption of the Iapetus and the Rheic Oceans.

Chapter Five is a compilation of all the hafnium isotopic data collected throughout chapters two, three and four and also presents new detrital and magmatic U-Pb and Hf isotopic data for late Neoproterozoic-Cambrian and Silurian rocks from Meguma, Silurian-Carboniferous rocks of Avalonia and Neoproterozoic-Devonian igneous rocks from Avalonia/Meguma. Similarity of the εHf arrays for Avalonia, Ganderia and Meguma suggest that were all geodynamically connected, so the term "composite Avalonia" is used.

A revised geodynamic framework for the northern Appalachian Orogen is proposed for the following intervals: (1) the early-late Neoproterozoic evolution of the composite Avalonia and the Iapetus Ocean, and 2) the early-Paleozoic assembly of the Appalachian Orogen and Pangea. The hafnium isotopic array associated with the 800-750 Ma zircons from composite Avalonia suggests it initiated as a continental-type arc between ~800-750 in the former Grenville Orogen, along the Laurentian margin. The orogen is linked to the early Neoproterozoic Valhalla Orogen of East Greenland, and it is suggested that the orogen propagated southward during this interval. A uniform shift in the Hf isotope array toward juvenile values between 800-700 Ma suggests the composite Avalonia retreated from Laurentia to form a microcontinental ribbon at least by 700 Ma. The intervening backarc basin became the proto-Iapetus Ocean. Between ~750-650 Ma, the ribbon transferred by subduction retreat across the Asgard Sea, closing it and colliding with the Gondwanan margin at ~650 Ma. Accretion of the ribbon is reflected in the reversal of εHf data to progressively negative values between 650-600 Ma.

Composite Avalonia separated from Gondwana between 550-500 Ma, forming the Rheic Ocean. All terranes within composite Avalonia show a εHf isotopic trend toward juvenile values, consistent with the transition from continental to a retreating oceanic-arc. The ribbon migrated northward, initially closing the Tornquist Sea as it collided with Baltica, then closing Iapetus

northward, initially closing the Tornquist Sea as it collided with Baltica, then closing Iapetus at ~450 Ma as it finally re-amalgamated with Laurentia. Following the final accretion of to Laurentia by ~430 Ma, subduction stepped outboard into the trailing Rheic Ocean. There is little evidence for the existence of a Late Silurian magmatic arc on the continental ribbon, with most of the magmatism recording rifting in a back-arc setting. This suggests that subduction was initiated outboard, placing the Meguma and the other terranes in an upper plate, back-arc setting. Subsequent Devonian-Carboniferous magmatism migrated inboard, then outboard across the orogen, reflecting switching between a retreating and advancing orogen, resulting in a predominantly extensional tectonic setting interspersed with shorter term compressional and transtensional events. The hafnium isotopic record of magmatism during the Silurian-Carboniferous reflects progressive homogenisation of the Neoproterozoic arc basement of composite Avalonia, with no apparent input from the depleted mantle or ancient Laurentian crust.

Chapter Six presents a comprehensive compilation of new and existing zircon hafnium isotopic data from Phanerozoic Europe. The purpose of the compilation is to test the sensitivity of the hafnium isotopic method against the successive Wilson cycles that have shaped the geology of the European continent. Rather than successive 'U-shaped' hafnium isotopic arrays associated with multiple ocean closures, the European array records a single reworking array extending from ~600 Ma until the Oligocene. Surprisingly, the Pangea defining Variscan orogeny at ~360 Ma also does not change the hafnium isotopic array, but rather reflects reworking of composite Avalonia and the other peri-Gondwanan terranes in Europe. A strong negative εHf excursion at 30 Ma indicates subduction and melting of Gondwanan cratonic lithosphere for the first time since 600 Ma. The inverted U-shaped European εHf isotopic array records the 600 million year closure phase of a supercontinental cycle. Lower and upper εHf model age limits on the post-450 Ma Phanerozoic array corresponds to Nuna and Rodinia breakup events, suggesting that Hf isotopic arrays provide temporal and spatial constraints on supercontinental cycles, which can be reconstructed at a cratonic scale.

Chapter Seven concludes the thesis and summarises the major findings from the previous chapters. The chapter also includes a brief discussion on the implication of the work, and future research and knowledge gaps regarding hafnium isotopic arrays.

REFERENCES

Barr, S.M., White, C.E., 1996. Contrasts in Late Precambrian-Early Paleozoic tectonothermal history between Avalon composite terrane sensu stricto and other possible peri-Gondwanan terranes in southern New Brunswick and Cape Breton Island, Canada. SPECIAL PAPERS-GEOLOGICAL SOCIETY OF AMERICA, 95-108.

Barr, S.M., White, C.E., Davis, D.W., McClelland, W.C., van Staal, C.R., 2014. Infrastructure and provenance of Ganderia: Evidence from detrital zircon ages in the Brookville terrane, southern New Brunswick, Canada. Precambrian Research 246, 358-370.

Belousova, E.A., Reid, A.J., Griffin, W.L., O'Reilly, S.Y., 2009. Rejuvenation vs. recycling of Archean crust in the Gawler Craton, South Australia: Evidence from U–Pb and Hf isotopes in detrital zircon. Lithos 113, 570-582.

Blichert-Toft, J., Albarède, F., 1997. The Lu-Hf isotope geochemistry of chondrites and the evolution of the mantle-crust system. Earth and Planetary Science Letters 148, 243-258.

Collins, W.J., Belousova, E.A., Kemp, A.I.S., Murphy, J.B., 2011. Two contrasting Phanerozoic orogenic systems revealed by hafnium isotope data. Nature Geoscience 4, 333-337.

Condie, K.C., Aster, R.C., 2010. Episodic zircon age spectra of orogenic granitoids: The supercontinent connection and continental growth. Precambrian Research 180, 227-236.

Dhuime, B., Hawkesworth, C., Cawood, P., 2011. When continents formed. Science 331, 154-155.

Griffin, W.L., Wang, X., Jackson, S.E., Pearson, N.J., O'Reilly, S.Y., Xu, X., Zhou, X., 2002. Zircon chemistry and magma mixing, SE China: In-situ analysis of Hf isotopes, Tonglu and Pingtan igneous complexes. Lithos 61, 237-269.

Hatcher, R.D., 1988. Basement -cover relationships in the Appalachian-Caledonian-Variscan orogen: mid-Devonian (end of Acadian orogeny) to end of Permian. Geological society of London 38.

Hawkesworth, C.J., Kemp, A.I.S., 2006. Using hafnium and oxygen isotopes in zircons to unravel the record of crustal evolution. Chemical Geology 226, 144-162.

Henderson, B., Collins, W.J., Murphy, B.J., Gutiérrez-Alonso, G., Hand, M., 2016. Gondwanan basement terranes of the Variscan-Appalachian orogen: Baltican, Saharan and West African hafnium isotopic fingerprints in Avalonia, Iberia and the Armorican Terranes. Tectonophysics.

Howard, K.E., Hand, M., Barovich, K.M., Reid, A., Wade, B.P., Belousova, E.A., 2009. Detrital zircon ages: Improving interpretation via Nd and Hf isotopic data. Chemical Geology 262, 277-292.

Jiang, N., Chen, J., Guo, J., Chang, G., 2012. In situ zircon U–Pb, oxygen and hafnium isotopic compositions of Jurassic granites from the North China craton: evidence for Triassic subduction of continental crust and subsequent metamorphism-related 18 O depletion. Lithos 142, 84-94.

Kemp, A., Hawkesworth, C., Foster, G., Paterson, B., Woodhead, J., Hergt, J., Gray, C., Whitehouse, M., 2007. Magmatic and crustal differentiation history of granitic rocks from Hf-O isotopes in zircon. Science 315, 980-983.

Kemp, A.I.S., Hawkesworth, C.J., Paterson, B.A., Kinny, P.D., 2006. Episodic growth of the Gondwana supercontinent from hafnium and oxygen isotopes in zircon. Nature 439, 580-583.

Kinny, P.D., Maas, R., 2003. Lu-Hf and Sm-Nd isotope systems in zircon, In: Hanchar, J.M., Hoskin, P.W.O. (Eds.), Zircon, pp. 327-341.

Landing, E., 2004. Precambrian–Cambrian boundary interval deposition and the marginal platform of the Avalon microcontinent. Journal of Geodynamics 37, 411-435.

Linnemann, U., Gerdes, A., Hofmann, M., Marko, L., 2014. The Cadomian Orogen: Neoproterozoic to Early Cambrian crustal growth and orogenic zoning along the periphery of the West African Craton—Constraints from U–Pb zircon ages and Hf isotopes (Schwarzburg Antiform, Germany). Precambrian Research 244, 236-278.

Moran, P.C., Barr, S.M., White, C.E., Hamilton, M.A., 2007. Petrology, age, and tectonic setting of the Seal Island Pluton, offshore southwestern Nova Scotia. Canadian Journal of Earth Sciences 44, 1467-1478.

Mueller, P.A., Kamenov, G.D., Heatherington, A.L., Richards, J., 2008. Crustal Evolution in the Southern Appalachian Orogen: Evidence from Hf Isotopes in Detrital Zircons. Journal of Geology 116, 414-422.

Murphy, B.J., van Staal, C.R., Duncan Keppie, J., 1999. Middle to late Paleozoic Acadian orogeny in the northern Appalachians: A Laramide-style plume-modified orogeny? Geology 27, 653-656.

Murphy, J.B., Fernández-Suárez, J., Keppie, J.D., Jeffries, T.E., 2004. Contiguous rather than discrete Paleozoic histories for the Avalon and Meguma terranes based on detrital zircon data. Geology 32, 585-588.

Murphy, J.B., Keppie, J.D., 2005. The Acadian orogeny in the northern Appalachians. International Geology Review 47, 663-687.

Nance, R.D., Murphy, J.B., 1994. Contrasting basement isotopic signatures and the palinspastic restoration of peripheral orogens: example from the Neoproterozoic Avalonian-Cadomian belt. Geology 22, 617-620.

Nance, R.D., Murphy, J.B., Strachan, R.A., Keppie, J.D., Gutiérrez-Alonso, G., Fernández-Suárez, J., Quesada, C., Linnemann, U., D'lemos, R., Pisarevsky, S.A., 2008. Neoproterozoic-early Palaeozoic tectonostratigraphy and palaeogeography of the peri-Gondwanan terranes: Amazonian v. West African connections. Geological Society, London, Special Publications 297, 345-383.

O'Brien, S., O'Brien, B., Dunning, G., Tucker, R., 1996. Late Neoproterozoic Avalonian and related peri-Gondwanan rocks of the Newfoundland Appalachians. SPECIAL PAPERS-GEOLOGICAL SOCIETY OF AMERICA, 9-28.

O'Brien, S., O'Brien, B., Dunning, G.R., TUCKER, R.D., 1983. The Avalon Zone: a Pan African terrane in the Appalachian orogen of Canada. Geology Journal 18.

Patchett, P., Tatsumoto, M., 1980. Hafnium isotope variations in oceanic basalts. Geophysical Research Letters 7, 1077-1080.

Pollock, J.C., 2007. The Neoproterozoic-early Paleozoic tectonic evolution of the peri-Gondwanan margin of the Appalachian Orogen: An integrated geochronological, geochemical and isotopic study from North Carolina and Newfoundland. ProQuest.

Pollock, J.C., Hibbard, J.P., Sylvester, P.J., 2009. Early Ordovician rifting of Avalonia and birth of the Rheic Ocean: U–Pb detrital zircon constraints from Newfoundland. Journal of the Geological Society 166, 501-515.

Pollock, J.C., Hibbard, J.P., van Staal, C.R., 2011. A paleogeographical review of the peri-Gondwanan realm of the Appalachian orogen1 This article is one of a series of papers published in this CJES Special Issue: In honour of Ward Neale on the theme of Appalachian and Grenvillian geology. Canadian Journal of Earth Sciences 49, 259-288.

Roberts, N.W., Slagstad, T., Parrish, R., Norry, M., Marker, M., Horstwood, M.A., 2013. Sedimentary recycling in arc magmas: geochemical and U–Pb–Hf–O constraints on the Mesoproterozoic Suldal Arc, SW Norway. Contributions to Mineralogy and Petrology 165, 507-523.

Robinson, P., Tucker, R.D., Bradley, D., Berry IV, H.N., Osberg, P.H., 1998. Paleozoic orogens in New England, USA. GFF 120, 119-148.

Scherer, E., Münker, C., Mezger, K., 2001. Calibration of the Lutetium-Hafnium Clock. Science 293, 683-687.

Smits, R.G., Collins, W.J., Hand, M., Dutch, R., Payne, J., 2014. A Proterozoic Wilson cycle identified by Hf isotopes in central Australia: Implications for the assembly of Proterozoic Australia and Rodinia. Geology.

Stampfli, G., Borel, G., 2002. A plate tectonic model for the Paleozoic and Mesozoic constrained by dynamic plate boundaries and restored synthetic oceanic isochrons. Earth and Planetary Science Letters 196, 17-33.

Stampfli, G., Hochard, C., Vérard, C., Wilhem, C., vonRaumer, J., 2013. The formation of Pangea. Tectonophysics.

Stampfli, G., Von Raumer, J., Wilhem, C., 2011. The distribution of Gondwana-derived terranes in the Early Paleozoic. Ordovician of the World 14, 567-574.

van Staal, C., Whalen, J., McNicoll, V., Pehrsson, S., Lissenberg, C.J., Zagorevski, A., van Breemen, O., Jenner, G., 2007. The Notre Dame arc and the Taconic orogeny in Newfoundland. Geological Society of America Memoirs 200, 511-552.

van Staal, C.R., 1994. Brunswick subduction complex in the Canadian Appalachians: record of the Late Ordovician to Late Silurian collision between Laurentia and the Gander margin of Avalon.

Tectonics 13, 946-962.

van Staal, C.R., Barr, S.M., Murphy, J.B., 2012. Provenance and tectonic evolution of Ganderia: Constraints on the evolution of the Iapetus and Rheic oceans. Geology 40, 987-990.

van Staal, C.R., Dewey, J., Mac Niocaill, C., McKerrow, W., 1998. The Cambrian-Silurian tectonic evolution of the northern Appalachians and British Caledonides: history of a complex, west and southwest Pacific-type segment of Iapetus. Geological Society, London, Special Publications 143, 197-242.

van Staal, C.R., Whalen, J.B., Valverde-Vaquero, P., Zagorevski, A., Rogers, N., 2009. Pre-Carboniferous, episodic accretion-related, orogenesis along the Laurentian margin of the northern Appalachians. Geological Society, London, Special Publications 327, 271-316.

van Staal, C.R., Zagorevski, A., McNicoll, V.J., Rogers, N., 2014. Time-transgressive Salinic and Acadian orogenesis, magmatism and Old Red Sandstone sedimentation in Newfoundland. Geoscience Canada 41, 138-164.

Veevers, J.J., 2004. Gondwanaland from 650–500 Ma assembly through 320 Ma merger in Pangea to 185–100 Ma breakup: supercontinental tectonics via stratigraphy and radiometric dating. Earth-Science Reviews 68, 1-132.

Villaros, A., Buick, I.S., Stevens, G., 2011. Isotopic variations in S-type granites: an inheritance from a heterogeneous source? Contributions to Mineralogy and Petrology 163, 243-257.

Waldron, J.W., White, C.E., Barr, S.M., Simonetti, A., Heaman, L.M., 2009. Provenance of the Meguma terrane, Nova Scotia: rifted margin of early Paleozoic Gondwana. Canadian Journal of Earth Sciences 46, 1-8.

Wang, L.J., Griffin, W.L., Yu, J.H., O'Reilly, S.Y., 2010. Precambrian crustal evolution of the Yangtze Block tracked by detrital zircons from Neoproterozoic sedimentary rocks. Precambrian Research 177, 131-144.

White, C.E., Barr, S.M., 2012. Meguma terrane revisited: Stratigraphy, metamorphism, paleontology, and provenance. Geoscience Canada 39.

Williams, H., 1979. Appalachian orogen in Canada. Canadian Journal of Earth Sciences 16, 792-807.

Williams, H., Colman-Sadd, S., Swinden, H., 1988. Tectonic-stratigraphic subdivisions of central Newfoundland. Current Research, Part B. Geological Survey of Canada, Paper 88, 91-98.

Wilson, J.T., 1966. Did the Atlantic close and then re-open? Nature.

Zagorevski, A., van Staal, C.R., McNicoll, V.J., 2007. Distinct Taconic, Salinic, and Acadian deformation along the Iapetus suture zone, Newfoundland Appalachians. Canadian Journal of Earth Sciences 44, 1567-1585.

Zhou, Z.-H., Mao, J.-W., Lyckberg, P., 2012. Geochronology and isotopic geochemistry of the A-type granites from the Huanggang Sn–Fe deposit, southern Great Hinggan Range, NE China: Implication for their origin and tectonic setting. Journal of Asian Earth Sciences 49, 272-286.

Chapter 2

This chapter is in press as:

Bonnie Henderson, W. J. Collins, J. Brendan Murphy, Gabriel Gutierrez-Alonso, Martin Hand, (in press), Gondwanan basement terranes of the Variscan-Appalachian orogen: Baltican, Saharan and West African hafnium isotopic fingerprints in Avalonia, Iberia and the Armorican Terranes, Tectonophysics, DOI:10.1016/j.tecto.2015.11.020

Statement of Authorship

Title of Paper	Gondwanan basement terranes of the Variscan-Appalachian orogen: Baltican, Saharan and West African hafnium isotopic fingerprints in Avalonia, Iberia and the Armorican Terranes
Publication Status	☒ Published ☐ Accepted for Publication ☐ Submitted for Publication ☐ Unpublished and Unsubmitted work written in manuscript style
Publication Details	Henderson, B., Collins, W.J., Murphy, B.J., Gutiérrez-Alonso, G., Hand, M., *in press*. Gondwanan basement terranes of the Variscan-Appalachian orogen: Baltican, Saharan and West African hafnium isotopic fingerprints in Avalonia, Iberia and the Armorican Terranes. Tectonophysics.

Principal Author

Name of Principal Author (Candidate)	Bonnie Henderson
Contribution to the Paper	Sample collection, U-Pb and Hafnium zircon analysis, data interpretation, manuscript and figure composition
Overall percentage (%)	85%
Certification:	This paper reports on original research I conducted during the period of my Higher Degree by Research candidature and is not subject to any obligations or contractual agreements with a third party that would constrain its inclusion in this thesis. I am the primary author of this paper.
Signature	Date: 05/04/2016

Co-Author Contributions

By signing the Statement of Authorship, each author certifies that:

i. the candidate's stated contribution to the publication is accurate (as detailed above);
ii. permission is granted for the candidate in include the publication in the thesis; and
iii. the sum of all co-author contributions is equal to 100% less the candidate's stated contribution.

Name of Co-Author	W.J. Collins
Contribution to the Paper	Project design, data interpretation and manuscript revisions
Signature	Date: 5/4/2016

Name of Co-Author	J. Brendan Murphy
Contribution to the Paper	Assistance with sample collection and manuscript revisions
Signature	Date: April 5 2016

Name of Co-Author	Gabriel Gutierrez-Alonso
Contribution to the Paper	Assistance with sample collection and manuscript revisions
Signature	Date: 05/04/2016

Name of Co-Author	Martin Hand
Contribution to the Paper	Manuscript revisions
Signature	Date: 6-4-2016

Gondwanan basement terranes of the Variscan-Appalachian orogen: Baltican, Saharan and West African hafnium isotopic fingerprints in Avalonia, Iberia and the Armorican Terranes

ABSTRACT

Iberia, Avalonia and the "Armorican" terranes form key constituents of the Variscan-Appalachian orogen, but their Neoproterozoic origins along the northern Gondwanan margin continue to be strongly debated. Here, we present a new detrital zircon U-Pb-Hf dataset from Neoproterozoic-Silurian sedimentary sequences in NW Iberia and Avalonia, in conjunction with the comprehensive existing datasets from potential source cratons, to demonstrate that the provenance of each terrane is relatively simple and can be traced back to three major cratons. The enigmatic Tonian-Stenian detrital zircons in autochthonous Iberian rocks were derived from the Saharan metacraton in the latest Neoproterozoic-early Cambrian. Avalonia is commonly considered to have been derived from the Amazonian margin of Gondwana, but the hafnium isotopic characteristics of the detrital zircon grains in early Neoproterozoic rocks bear much stronger similarities to Baltica. The hafnium isotopic array also suggests the early Avalonian oceanic arc was built on a sliver of "Grenvillian-type crust" (~2.0-1.0 Ga) possibly of Baltican affinity at ~800 Ma, prior to accretion with a continental margin at ~640 Ma. The Upper Allochthon of Iberia is frequently linked to the West African Craton in the late Neoproterozoic-early Cambrian, however the hafnium isotopic array presented here does not support this connection; rather it is more similar to the hafnium array from Avalonia. The Armorican terranes have strong detrital zircon isotopic links to the West African Craton during the late Neoproterozoic-Cambrian.

1. INTRODUCTION

Modern provenance studies have routinely focussed on obtaining the U-Pb crystallisation age of individual detrital zircon grains to build statistically significant populations that can be "matched" to the age of tectonomagmatic events recognised in potential source terranes (Ireland et al., 1998; Košler et al., 2002; Anderson, 2005; Dickinson and Gehrels, 2009). The method becomes problematic if the potential source terranes preserve coeval tectonothermal events, because they yield overlapping zircon age spectra. Hafnium isotope analysis of the same zircons allows the data to be presented in composite hafnium (εHf) arrays, thereby allowing for more rigorous comparisons with the evolution of putative source areas (Howard et al., 2009; Wang et al., 2010). Moreover, Hf arrays have the potential to evaluate geodynamic links between dispersed blocks that otherwise show only weak geological connection. Comprehensive hafnium isotope arrays define the nature of the zircon-forming tectonomagmatic events at the cratonic scale (Smits et al., 2014), and as such generate an isotopic "fingerprint" for that craton that can be directly compared to exotic continental terranes.

The interval between the late Neoproterozoic supercontinent Gondwana and the Carboniferous assembly of Pangea is shaped largely by the events surrounding the development and subsequent destruction of the Rheic Ocean and the evolution of the 'peri-Gondwanan' microcontinental terranes that occupied the oceanic realm between Gondwana and Laurussia (Pollock et al., 2011; Nance et al., 2012; van Staal et al., 2012). Closure of the Rheic Ocean was accompanied by collision between Gondwana and Laurussia forming the Appalachian-Variscan Orogen of North America and western Europe (Scotese, 2004; Hibbard et al., 2010; Stampfli et al., 2013). The events prior to the amalgamation of Pangea are controversial essentially because there are insufficient constraints on the late Neoproterozoic-early Paleozoic provenance and paleogeography of the microcontinental terranes that form the basement of the Appalachian-Variscan orogen. Robust paleogeographic constraints for the Late Neoproterozoic microcontinental terranes that

are commonly thought to have formed along the northern Gondwanan margin are required to provide the framework for unravelling the Paleozoic crustal evolution of the Pangean amalgamation.

The late Neoproterozoic provenance and paleogeography of the peri-Gondwanan terranes has been previously constrained by matching the U-Pb zircon age spectra in clastic sedimentary and igneous rocks with coeval tectonothermal events in the potential source cratons of northern Gondwana (see compilation in Eckelmann et al., 2014 and references therein). The addition of hafnium isotope analyses to these U-Pb zircon studies provides a powerful tool in further defining the isotopic "signature" of these terranes, the nature of the tectonomagmatic events and can distinguish between tectonic processes dominated by the input of juvenile crust and those that involve the reworking of older crustal material (Hawkesworth and Kemp, 2006).

The basement terranes of the Variscan-Appalachian orogen include (but are not limited too) Avalonia, Iberia, "Armorican" terranes and the Pontides of Turkey. Avalonia is commonly subdivided into east and west Avalonia, with eastern Avalonia located in Europe and the United Kingdom and western Avalonia underlying much of the eastern seaboard of Atlantic Canada (Cocks et al., 1997). Here, we present a new comprehensive U-Pb-Hf detrital and magmatic zircon data set from Neoproterozoic-Ordovician rocks from NW Iberia and western Avalonia, which we use in conjunction with published data from Iberia and eastern Avalonia, to test the provenance of Iberia and Avalonia during the Neoproterozoic-Ordovician interval. We compare these data against a wealth of hafnium isotopic data published in the last decade from cratonic domains within the Gondwanan supercontinent including: the West African Craton (WAC), Arabian-Nubian Shield (ANS, Morag et al., 2012; Ali et al., 2013; Robinson et al., 2014), Saharan Metacraton (SMC, Iizuka et al., 2013; Be'eri-Shlevin et al., 2014; Meinhold et al., 2014), Amazonia (Hurai et al., 2010; Matteini et al., 2010; Reimann et al., 2010; McGee et al., 2015), the central African region (Congo Craton and Mesoproterozoic orogenic belts) (Iizuka et al., 2013; Foster et al., 2014), and Baltica (Kuznetsov et al., 2010; Kristoffersen, 2011; Beranek et al., 2013; Kuznetsov et al., 2014; Romanyuk et al., 2014).

We use these comprehensive hafnium isotopic arrays from Avalonia, Iberia and Armorica, in addition to major cratonic domains of Gondwana and Baltica, to demonstrate that distinct hafnium isotopic fingerprints are identifiable in the basement terranes of the Variscan-Appalachian orogen. The data have direct implications for late Neoproterozoic paleogeography, the geodynamic evolution of the Rheic Ocean and subsequent amalgamation of Pangea.

2. GEOLOGICAL BACKGROUND

2.1 The evolution of the Variscan-Appalachian Orogen

The evolution of the Paleozoic Variscan-Appalachian orogen is dominated by the late Cambrian-early Ordovician opening and Devonian closure of the Rheic Ocean (Fig. 1). The Rheic Ocean opened when Neoproterozoic arc-related terranes, collectively termed the "peri-Gondwanan" terranes, separated from the northern margin (present coordinates) of West Gondwana in the early Paleozoic (van Staal et al., 1998; Stampfli and Borel, 2002; Pollock et al., 2011; van Staal et al., 2012). These terranes are presently distributed throughout the Paleozoic Variscan and Appalachian orogens of Europe and North America (Von Raumer et al., 2002; Nance et al., 2008) (Fig. 1), and include Avalonia, Iberia, the Pontides of Turkey, and "Armorica".

Vestiges of oceanic arc magmatism

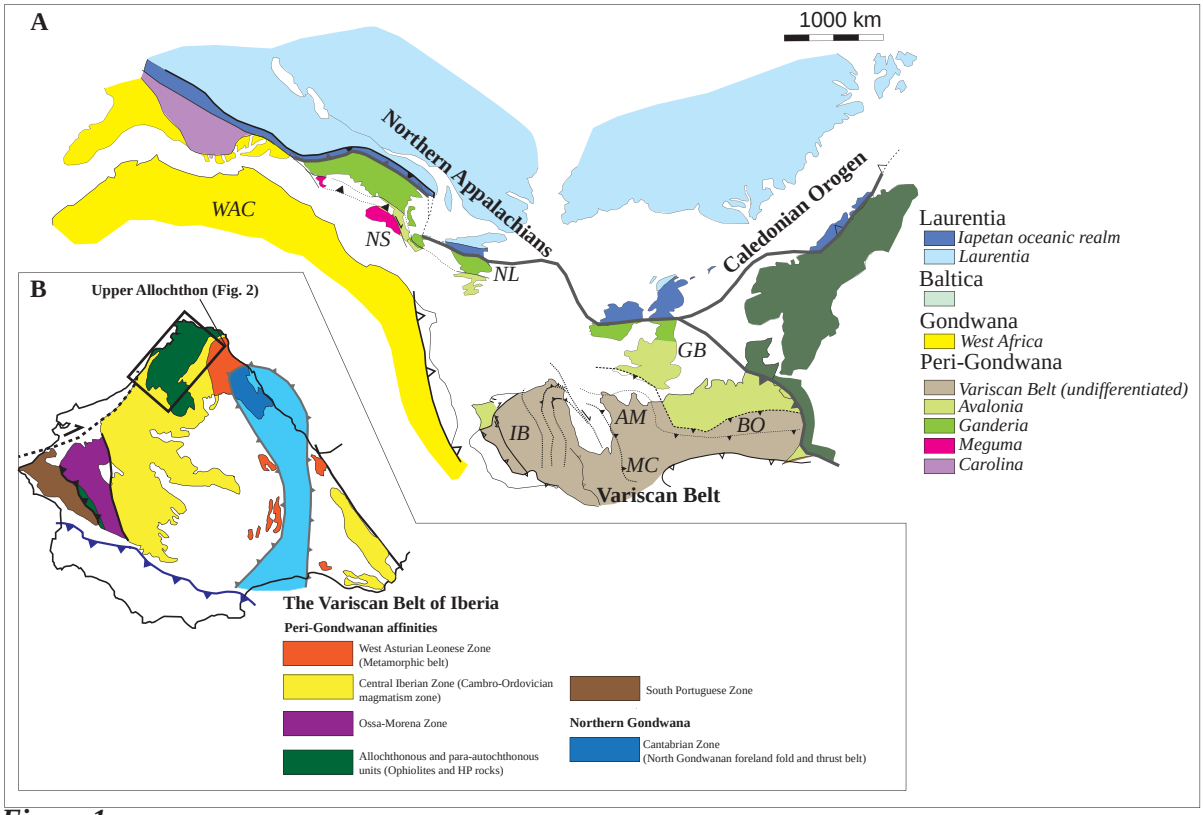

Figure 1

A) Map showing the distribution of the Appalachian, Variscan and Caledonian belts at the end of the Paleozoic. Shown are the major cratonic and microcontinental components within the orogenic belts including Iberia (IB), Amorican Massif (AM), Massif Centrale (MC), Bohemian Massif (BO) and the West African Craton (WAC). This represents the approximate configuration of Pangea following late Paleozoic convergence between Laurentia and Gondwana. The figure is modified from Barreiro et al. (2007) and Keppie et al., (2008).

B) Geology map illustrating the major tectonic subdivisions of Iberia. Upper Allochthon is highlighted in the box and is detailed further in Figure 2.

with ~760-650 Ma ages are recognised across the majority of the peri-Gondwanan terranes (Murphy and Nance, 1989; Murphy et al., 2000; Murphy et al., 2008b), followed by major ensialic continental arc magmatism at ~650-540 Ma, with subduction directed southward beneath the periphery of West Gondwana (Nance et al., 2002; Keppie et al., 2003).

In the late Cambrian-early Ordovician a protracted rifting episode opened the Rheic Ocean with the disputed separation of several peri-Gondwana terranes (Avalonia-Cadomia) from the northern margin of Gondwana (Murphy, 2006; Nance et al., 2010; van Staal et al., 2012).

Widespread rift-related igneous activity is recorded between 495-470 Ma across all of the Iberian Variscides (see Nance et al., 2010 and references therein), and the coeval deposition of a thick passive margin sedimentary sequence are interpreted to be related to the initial rifting and early drift interval associated with the Rheic Ocean (Quesada, 1991; Sánchez-García et al., 2003).

The Iapetus Ocean was closed during a series of accretion events in the late Ordovician to Silurian, whereby the peri-Gondwanan terranes (Ganderia, Carolinia and Avalonia ± Meguma) were accreted to the Laurussian margin (Murphy and Nance, 1991; van Staal et al., 1998; Stampfli and Borel, 2002; Keppie et al., 2003; van Staal et al., 2009; Hibbard et al., 2010). The closure of the Rheic Ocean

culminated in collision between Laurussia, the peri-Gondwanan terranes, and Gondwana in the middle-upper Devonian (Sacks and Secor, 1990; Scotese and McKerrow, 1990; Nance et al., 2012; Arenas et al., 2014).

Some authors use paleomagnetic data to suggest that NW Iberia and the Armorican terranes formed part of a drifting continental ribbon (referred to as the Galatian super terrane, or Armorica) in the Late Silurian (Tait, 1999; von Raumer et al., 2003; Stampfli et al., 2013) that separated from Gondwana to open a second Paleozoic ocean (Paleotethys). In this hypothesis, the collision of the drifting ribbon with Laurussia closes the Rheic Ocean, defining the onset of the Variscan orogeny, and involves either dual subduction of the Rheic oceanic lithosphere beneath southern Laurussia and northern Gondwana, or subduction of the Rheic and Paleotethyan Ocean beneath the Galatian ribbon continent (Stampfli et al., 2013). According to this model, the amalgamation of Pangea followed in the late Carboniferous with the closure of the western end on the Paleotethys and the collision of the Gondwanan margin with Laurussia. In contrast, on the basis of lithostratigraphic and faunal data, many authors place autochthonous and parautochthonous NW Iberia along the northern Gondwanan passive margin throughout the Paleozoic (Quesada, 1991; Robardet, 2003; Linnemann et al., 2004; Simancas et al., 2005; Gutiérrez-Alonso et al., 2008; Linnemann et al., 2008; Martínez Catalán et al., 2009; Arenas et al., 2013; Pastor-Galán et al., 2013; Ballèvre et al., 2014), with Rheic Ocean closure predominantly driven by northward subduction in the Early Devonian (Arenas et al., 2007; Arenas et al., 2014).

2.2 Geological background of Avalonia

Avalonia is one of the largest peri-Gondwanan terranes in the Appalachian-Variscan orogen with Avalonian rocks recognised on both sides of the Atlantic Ocean (Fig. 1). Avalonian rocks located in southern England, Ireland, Wales and parts of western Europe (Belgium, France, northern Germany, the Czech Sudetes) are deemed to represent East Avalonia (Katzung et al., 1995; Verniers et al., 2002), whereas Avalonian rocks are recognised from Boston (USA) through Maritime Canada to the Avalon peninsula of eastern Newfoundland comprise West Avalonia (Murphy and Nance, 2002; Hibbard, 2006; Thompson et al., 2007; Satkoski et al., 2010).

Unequivocal basement is not exposed in Avalonia. However, neodymium isotopic data from late Neoproterozoic - Paleozoic igneous suites suggest derivation from a 0.8 - 1.1 Ga juvenile source in West Avalonia, and a 1.0 to 1.8 Ga continental source in East Avalonia (Nance and Murphy, 1994; Kerr et al., 1995; Hegner and Kröner, 2000; Murphy et al., 2000). Neoproterozoic-early Cambrian rocks of Avalonia preserve a record of early arc and rift development (~760-635 Ma), main stage, voluminous magmatic arc activity (~635 Ma), and late stage rift related volcanism and sedimentation (~590-550 Ma) (Keppie et al., 2003).

Paleomagnetic data indicate that West Avalonia in the Avalon peninsula of Newfoundland had a paleolatitude of 34°±8° at 575 Ma (McNamara et al., 2001), compared to an equatorial position for Laurentia at that time (Nance et al., 2008). The paleogeographic location of Avalonia during the latest Neoproterozoic-early Paleozoic is uncertain. The increasing faunal endemism of Avalonia in the Ordovician has been interpreted to reflect the progressive isolation of Avalonia from West Gondwana (Lees et al., 2002; Fortey and Cocks, 2003), and the subsequent gradual introduction of Baltic and Laurentian fauna to indicate a decreasing distance between Avalonia and Laurussia during the latest Ordovician. However, Landing (1996b) considered there to be no geological or faunal evidence to suggest that Avalonia was contiguous with the West Gondwanan margin in the latest Neoproterozoic-early Cambrian, favouring Avalonia as a separate microcontinent during this interval.

The protracted assembly of Laurussia is

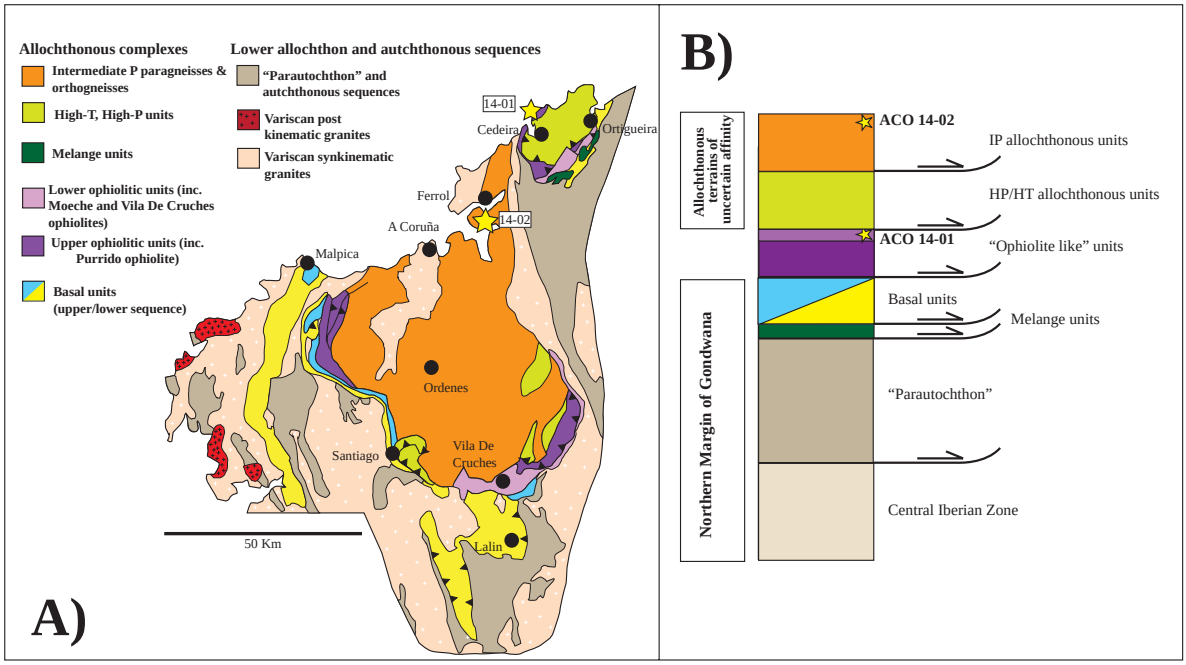

Figure 2

A)Simplified geology map of the Upper Allochthon modified from Arenas et al., (2009, 2013). B) Basic stratigraphic column for the Upper Allochthon and parautochthon/autochthon showing the typical relationships between the subdivided units.

interpreted to have occurred via collision between Baltica and East Avalonia at ~450 Ma, at the expense of the Tornquist Ocean (Torsvik and Rehnström, 2003; Murphy et al., 2004a), prior to collision of composite Avalonia/Baltica with Laurentia (to form Laurussia) diachronously during the final consumption of the Iapetus Ocean in the early-mid Silurian (van Staal et al., 1998; van Staal et al., 2009; Hibbard et al., 2010; van Staal et al., 2012). West Avalonian clastic sedimentary rocks record a Laurussian neodymium isotopic signature in the Late Silurian (Murphy et al., 1996), in broad agreement with the age of Iapetan suture rocks in East Avalonia that indicate closure of Iapetus at ~420 Ma (Soper et al., 1992).

2.3 Geological background of the Iberian terranes

NW Iberia preserves a near complete section of ancient Gondwanan margin in the Variscan orogen. It is divided into several zones that are defined by differences in Lower Paleozoic stratigraphy, Variscan structural characteristics and magmatic and metamorphic activity, all of which broadly reflect the increasing distance from the northern Gondwanan margin. The autochthonous Cantabrian Zone (CZ), West-Asturian-Leonese (WALZ), Central Iberian Zone (CIZ), and Galicia-Tras-os-Montes schistose Zone (GTOMZ) represent the proximal (platformal) coastal to increasingly distal offshore facies, respectively (Fig. 1). The most distal units considered to have been deposited on northern Gondwanan margin are those of the Basal Units of the allochthonous complexes (Fig. 1, Arenas et al., 2014).

2.3.1 NW Iberian allochthonous complexes

The allochthonous complexes consist of, from bottom to top, the "Basal Units" (Gondwanan basement, Martínez Catalán et al., 1996; Arenas et al., 2009; Díez Fernández et al., 2011; Arenas et al., 2013; López-Carmona et al., 2014), structurally overlain by two "ophiolitic" units (Lower and Upper Ophiolites) which yield Early Ordovician (~495 Ma, Arenas et al., 2007; Martínez et al., 2012), and Devonian ages, (~395 Ma, Martínez et al., 2011; Arenas et al., 2013), respectively.

Depositional age	Sample No.	Stratigraphic name	Sample description
	ACO-13-22	Ferrona Formation	Ironstone
	ACO-12-40	Redmans Formation	Sandstone
Ordovician	ACO-12-48	MacKinnons Brook Formation	Conglomerate
	ACO-12-49	Black John Formation	Coarse grained sandstone
Cambrian	ACO-12-38	Malignant Cove Formation	Gritty red conglomerate
	ACO-12-29B	Livingston Cove Formation	Coarse, pebbly conglomerate
	ACO-12-50	James River Formation	Fine grained sandstone
	ACO-12-54	Keppoch Formation	Sandstone
	ACO-12-52A	Gamble Brook Formation	Quartzite
Neoproterozoic	ACO-12-52B	Gamble Brook Formation	Quartzite

Table 1

A list of the samples obtained from the Avalonia terrane in Nova Scotia and Newfoundland, eastern Canada.

Early Ordovician ophiolites reflect Rheic Ocean opening, and are not discussed further, whereas Devonian ophiolites are interpreted to have formed during Rheic Ocean consumption (Fig. 2, Murphy et al., 2009; Martínez et al., 2011; Arenas et al., 2014). These ophiolite complexes are structurally overlain by the upper units (or Upper allochthon) of continental affinity, which comprise high-pressure, high-temperature (HT-HP) rocks structurally overlain intermediate pressure (IP) units (Barreiro et al., 2007; Albert et al., 2014 and references therein).

The "Basal Units" have a continental affinity and contain Ediacaran-Early Ordovician metasedimentary rocks, which are intruded by voluminous calc-alkaline (~493 Ma, Abati et al., 2010) to alkaline-peralkaline (~475-470 Ma, Díez Fernández et al., 2010) granitic bodies. The Basal Units underwent subduction beneath Laurussia during the onset of the Variscan orogeny (Martínez Catalán et al., 1996; Díez Fernández et al., 2011; López-Carmona et al., 2014), and were affected by high pressure and low-intermediate temperature metamorphism (Lopez-Carmona et al., 2013). The "Basal Units" were subsequently exhumed via crustal scale thrusting associated with recumbent folding and subsequent extensional tectonics (Martínez Catalán et al., 1996; Díez Fernández et al., 2011; López-Carmona et al., 2014).

The Lower and Upper Ophiolites (Fig. 2a) are collectively interpreted to preserve a rootless suture zone between the Laurussian and Gondwanan components (Arenas et al., 2007; Martínez Catalán et al., 2009; Arenas et al., 2013; Ballèvre et al., 2014). The most continuous ophiolite units in NW Iberia are the ~395 Ma mafic series, which are also traceable throughout Variscan Europe and are interpreted to have been formed during the final stages of closure of the Rheic Ocean (Martínez et al., 2007). However, the

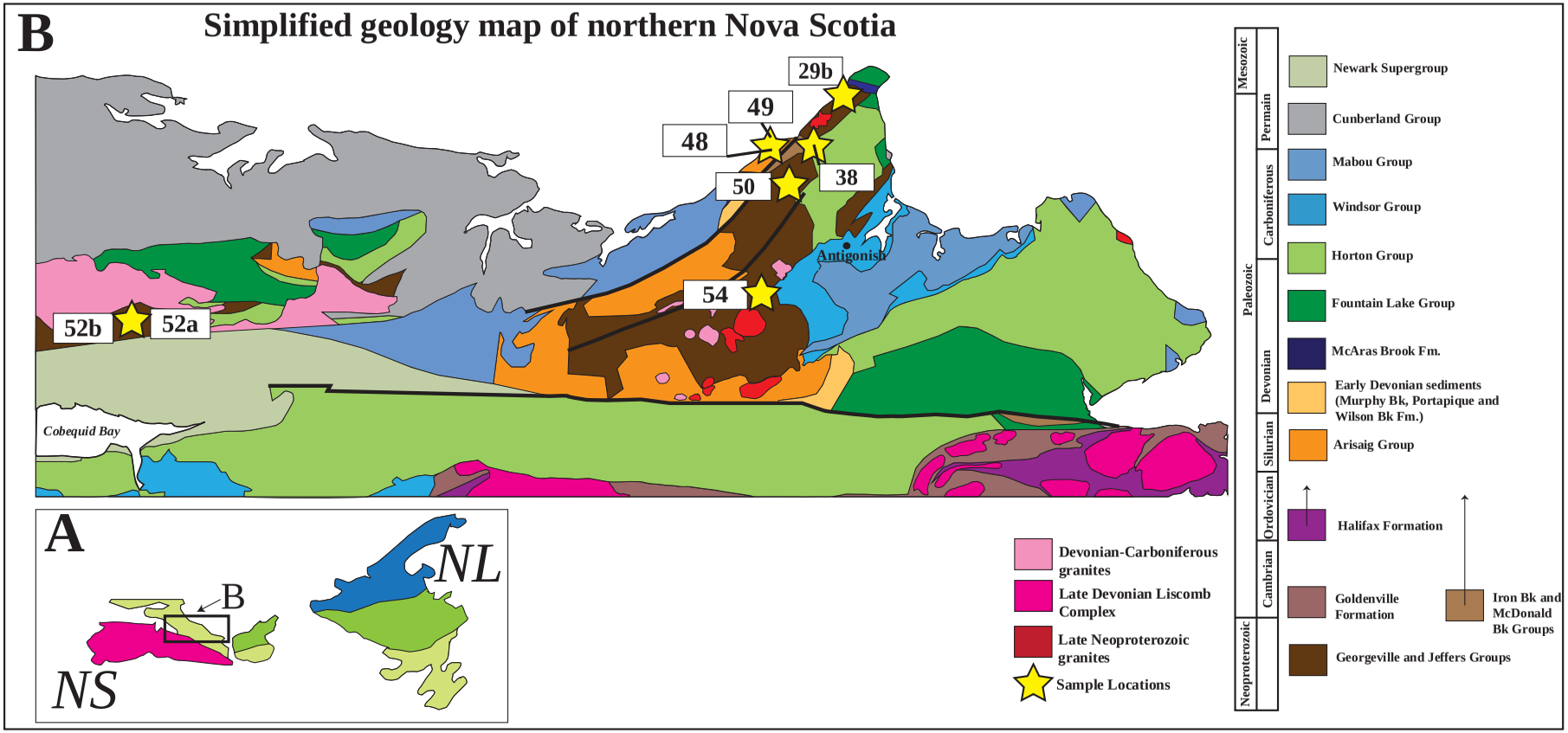

Figure 3

A) Simplified geological subdivision of Nova Scotia and Newfoundland (represented by colours shown in Figure 1). B) Detailed geology of northern Nova Scotia (Avalonia) with the sample locations represented by yellow stars. Map modified from Murphy et al., (1991), Keppie (2000) and White et al. (2012).

Depositional age	Sample No.	Stratigraphic name	Sample description	Reference for U-Pb data
Devonian	G7	Aljibe Quartzite	Quartzite	Gutierrez-Alonso et al., 2015
	Laz32	Base Quartzite Formation	Quartzite	Gutierrez-Alonso et al., 2015
	ACO-14-01	Carreiro Shear Zone	Aluminous metasediment	*New data*
Silurian	PG14	Formigoso Formation	Sandstone	Pastor-Galan et al., 2013
Ordovician	CZ02	Armorican Quartzite	Quartzite	Shaw et al., 2014
Cambrian	ACO-14-02	Ordenes Complex	Sandstone	*New data*
	ACO-12-57	Oville Formation	Quarzite	*New data*
Neoproterozoic	ACO-12-60	Candana Formation	Quartzite	*New data*
	OD4	Monterrubio Formation	Sandstone	Fernandez-Suarez et al., 2014
	OD5	Allande Gp.	Sandstone	Fernandez-Suarez et al., 2014

Table 2

A list of the sedimentary rock samples taken from NW Iberia and the Upper Allochthon of Iberia. Where existing detrital zircon mounts could be obtained (referenced samples), these were used to analyse hafnium isotopic data from the dated zircon grains.

interpretation has been updated in light of Sm-Nd whole rock (Murphy and Gutiérrez-Alonso, 2008) and new U-Pb-Hf zircon isotopic data that suggest that ophiolites were generated by the mixing of juvenile material with an older Mesoproterozoic continental basement (Martínez et al., 2011; Arenas et al., 2013).

The HP-HT units of the Upper Allochthon are composed of ultramafic rocks, mafic-felsic granulites, eclogites, orthogneisses and paragneisses (Albert et al., 2014 and references therein). The Upper Allochthon is commonly considered to have been generated in a volcanic-arc environment, which was part of the early Paleozoic peri-Gondwanan arc system (Abati et al., 1999; Abati et al., 2007; Albert et al., 2014). The protolith ages for the igneous rocks are upper Cambrian (~490 Ma), and the age of metamorphism is ~400-390 Ma (Abati et al., 2007; Fernández-Suárez et al., 2007). The IP units are comprised of a thick series of greywacke, pelitic and conglomeritic sequences, which record maximum depositional ages in the range of 530-500 Ma (Fernández-Suárez et al., 2003). In the Órdenes Complex, the sedimentary rocks were intruded by gabbros and calc-alkaline granitoids, which yield protolith ages of ~490-500 Ma (Abati et al., 1999; Andonaegui et al., 2012).

3. SAMPLE SELECTION

3.1 Avalonia: sample selection

Although some U-Pb-Hf detrital zircon data are available for East Avalonia (Willner et al., 2013; Zlatkin et al., 2014), and West Avalonia (Willner et al., 2013; Pollock et al., 2015), the data do not span the pivotal Late Neoproterozoic-early Paleozoic stratigraphic interval. Moreover, Sm-Nd data (Nance and Murphy, 1994, 1996; Murphy et al., 2000) suggest that East and West Avalonia are underlain by different basements, and the hafnium data that are available for West Avalonia does not presently resolve this. Accordingly, nine siliciclastic samples were collected for U-Pb-Hf detrital zircon analysis from unequivocal West Avalonian rocks in Nova Scotia and Newfoundland, Canada (Table 1, Fig. 3). The samples were

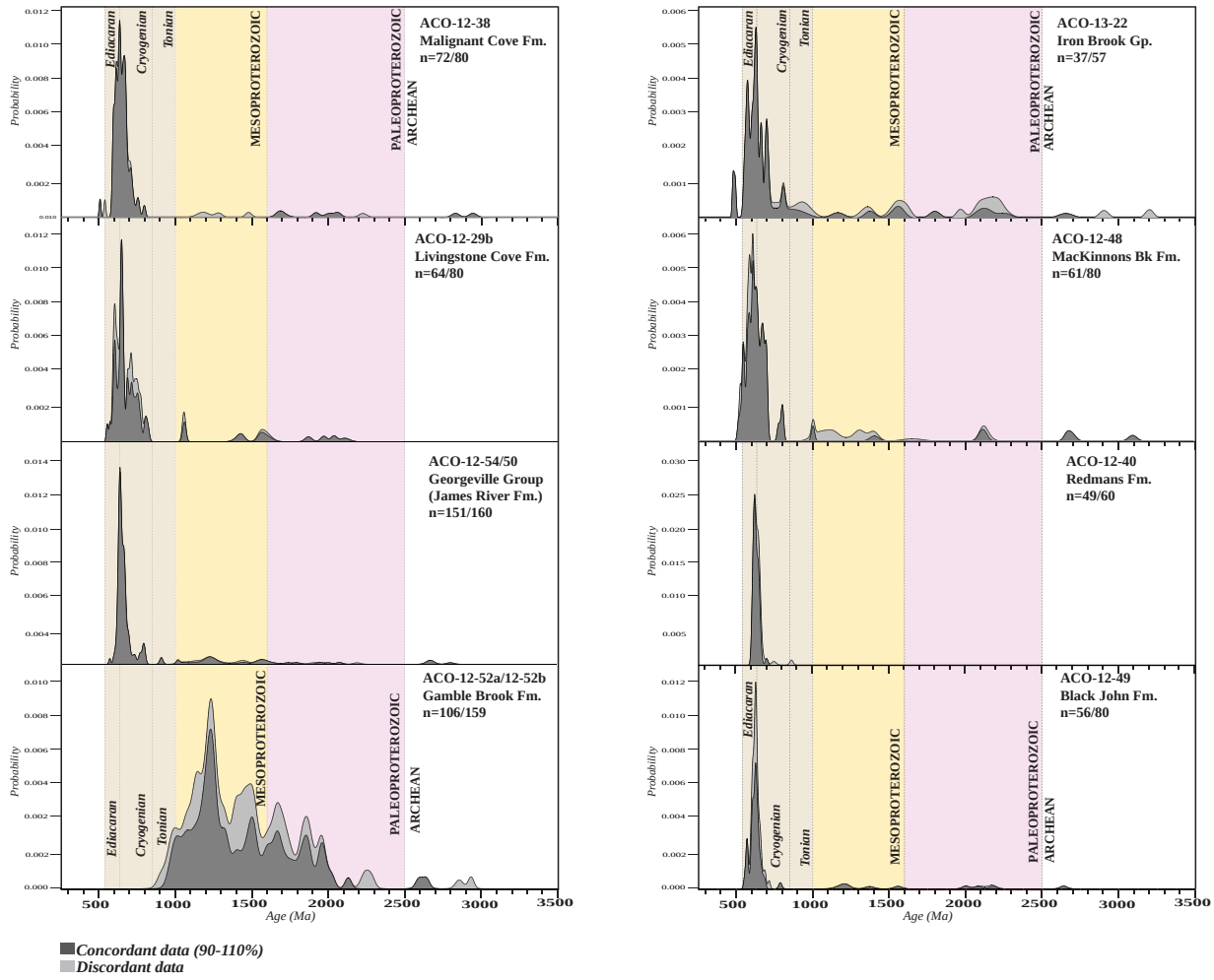

Figure 4

Detrital zircon age probability density distribution plots for sedimentary rocks from Avalonia. Lighter grey fields represent zircon grains that are > 10% discordant. n = xxx/xxx equals number of > 90–110% concordant analyses/number of < 90% or > 110% concordant analyses.

selected to complement the existing data (Willner et al., 2013; Pollock et al., 2015) and to sufficiently cover the Neoproterozoic-Ordovician stratigraphic record in West Avalonia. Two samples were taken from the early Neoproterozoic Gamble Brook Formation (ACO-12-52A, ACO-12-52B), and three samples from the late Neoproterozoic Georgeville Group (Livingstone Cove Formation (ACO-12-29B), James River Formation (ACO-12-50, ACO-12-54).

U-Pb detrital zircon data was previously obtained for the Gamble Brook (Barr et al., 2003), Livingstone Cove (Keppie et al., 1998) and Malignant Cove (Murphy et al., 2004b) formations, but in each study, the number of zircons analysed was insufficient for a statistical analysis of populations and Hf isotopic data are unavailable. The Gamble Brook data yield a maximum depositional age of ca. 1.0 Ga (Murphy, 2002). The deposition of the Livingstone Cove Formation is tightly constrained between the ages of the youngest detrital zircon (613 + 5 Ma, Keppie et al., 1998) and the 607 + 2 Ma age of an igneous complex that intrudes the Georgeville Group (Murphy et al., 1997).

Three samples were selected from Cambrian redbeds in Nova Scotia (Malignant Cove Formation, ACO-12-38, MacKinnon Brook Formation, ACO-12-48, Black John Formation, ACO-12-49), as well as from correlative early Ordovician ironstone layers in both Nova Scotia (Ferrona Formation, ACO-

13-22) and southern Newfoundland (Redmans Formation, ACO-12-40). The Malignant Cove sample is from the same location as that of Murphy et al., (2004b) and is mapped as the Bears Brook Formation by White et al., (2012), enabling direct comparison between these studies. The depositional ages of these formations are constrained by paleontological evidence (Ranger et al., 1984; Landing and Murphy, 1991). Recent U-Pb detrital zircon and Lu-Hf isotopic data from the Redmans Formation (Pollock et al., 2015) are included in our synthesis.

In order to build a comprehensive U-Pb-Hf zircon record for composite (west and east) Avalonia, we have also included the published εHf datasets from other parts of West Avalonia, including Ediacaran-Ordovician cover sequences in Nova Scotia and Newfoundland (Pollock et al., 2015) and the Mira terrane (Cape Breton, Willner et al., 2013). Equivalent data from East Avalonia include the Stavelot-Venn Massif (Belgium) (Willner et al., 2013), and the Pelagonian zone of the Hellenides (Greece, Zlatkin et al., 2014).

3.2 NW Iberia: sample selection

Four samples were collected for U-Pb-Hf detrital zircon analysis (Fig. 2); an upper Cambrian metasandstone from the Betanzos Unit of the Órdenes Complex of the Upper Allochthon and a Devonian amphibolite facies schist from the Carreiro Shear Zone (Upper Allochthon). A Lower Cambrian quartzite from the Cándana Formation (WALZ) and an Upper Cambrian quartzite from the Oville Formation (CZ) were sampled from the autochthonous sequences. In addition, six zircon mounts were obtained from published geochronological studies in order for the zircon grains to be analysed for hafnium isotopes (Table 2). The hafnium isotope analyses were conducted on the zircon mounts as close to, or over the top of, the existing U-Pb isotope analyses. These include: an Ordovician Armorican Quartzite sample from the Cantabrian Zone (CZ02, Shaw et al., 2014), two Neoproterozoic-Cambrian samples from the Cantabrian and Central Iberian Zones, (OD5 and OD4, Fernández-Suárez et al., 2014) and two Devonian samples from the Central Iberian Zone (G7 and LAZ32, Gutiérrez Alonso et al., 2015). The samples selected span the Neoproterozoic-Devonian stratigraphic record in NW Iberia, allowing for a reappraisal of the provenance and paleogeography of the terrane during this period.

U-Pb detrital zircon data have been previously obtained from a greywacke in the Betanzos Unit of the Órdenes Complex (Fernández-Suárez et al., 2003), where a maximum depositional age of ~490 Ma was interpreted. The maximum deposition of the Cándana Formation is constrained by U-Pb detrital zircon data to 532 ± 10 Ma (Fernández-Suárez et al., 2014). The deposition of the Oville Formation is constrained to the mid-Cambrian-Tremadocian by diverse trace fossil occurrences including trilobites (Sdzuy, 1968; Gámez Vintaned et al., 2000), echinoderms (Wotte and Mergl, 2007 and references therein), graptolites (Sdzuy, 1974) and acritarchs (Fombella, 1979). Detrital zircon data have not previously been obtained for the Oville Formation. Similarly, the Carreiro Shear Zone, which is located structurally above the Purrido Ophiolite complex, has no constraints on the age of the protolith.

Also included in the compilation of autochthonous Iberian data are the εHf zircon data from Ediacaran-Cambrian sedimentary rocks of the CIZ (Orejana et al., 2015). Presented in conjunction with the allochthonous Iberian data are the published εHf zircon data from mylonitic greenschists of the Moeche ophiolite (Arenas et al., 2013) and Devonian gabbros of the Purrido ophiolite complex (Martínez et al., 2011). εHf data from the Cariño gneisses of the Cabo Ortegal Complex are also included in the data set for the Upper Allochthon (Albert et al., 2014).

4. ANALYTICAL METHODS

4.1 U-Pb zircon methods

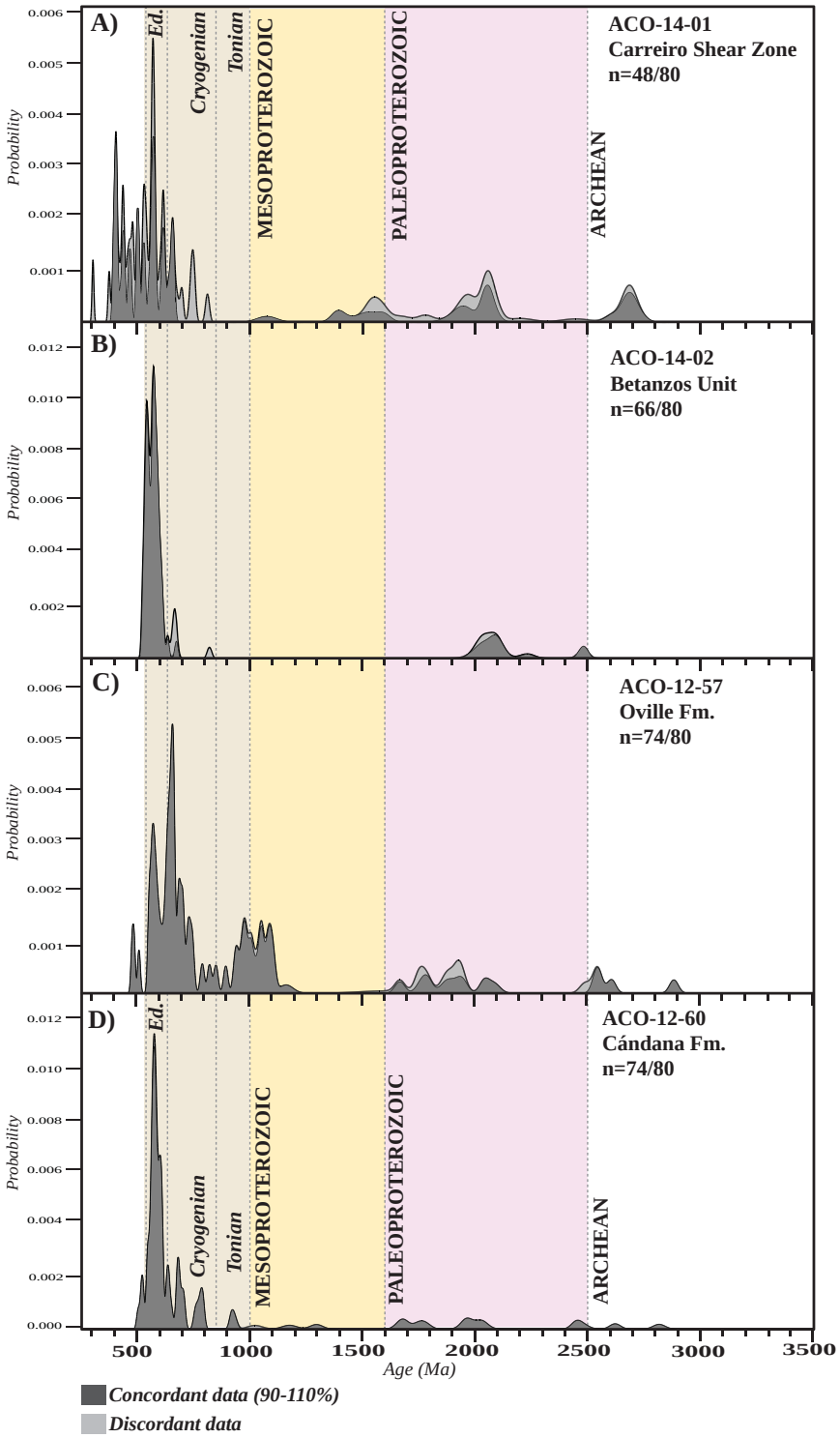

Figure 5
Detrital zircon age probability density distribution plots for sedimentary rocks from Iberia. Lighter grey fields represent zircon grains that are > 10% discordant. n = xxx/xxx equals number of > 90–110% concordant analyses/number of < 90% or > 110% concordant analyses.

Analytical techniques for U–Pb isotopic dating of zircon follow those of Payne et al., (2008) and Payne et al. (2010). U–Th–Pb analysis of zircons was conducted at Adelaide Microscopy, University of Adelaide, South Australia; using an Agilent 7500cs ICPMS,

coupled to a New Wave 213 nm Nd-YAG laser.

U–Pb fractionation was corrected using the GEMOC GJ-1 zircon (TIMS normalisation data 207Pb/206Pb = 608.3 Ma, 206Pb/238U = 600.7 Ma and 207Pb/235U = 602.2 Ma; (Jackson et al., 2004). A second zircon standard (Plesovice, TIMS-ID U–Pb age: 337.1 ± 0.4 Ma, Sláma et al., 2008) was used to monitor the ongoing accuracy of the instrument. GJ-1 produced a weighted average 206Pb/238U age of 600.48 ± 0.92 Ma (n = 270, MSWD = 0.83), and Plesovice a 206Pb/238U age weighted average of 337.9 ± 1.6 Ma (n = 73, MSWD = 1.1).

Data reduction was completed using the program "GLITTER" (Griffin et al., 2008). Weighted average calculations use 207Pb/206Pb ages for zircon populations older than 1000 Ma and 206Pb/238U ages for those populations younger than 1000 Ma. A ± 10% discordancy threshold was applied to zircon analysis during age interpretation (Payne et al., 2006; Howard et al., 2009; Howard et al., 2011).

In order to define the youngest zircon population for each individual samples we utilise the conservative method described by Dickinson and Gehrels (2009) whereby the youngest grain cluster (2σ) (n= >3) grains overlap in age at 2σ error. Where possible at least eighty individual zircon grains were analysed per detrital sample in order to satisfy the minimum recommendation of Anderson (2005). The zircon populations are qualitatively classified by the population size (%) per sample from accessory populations (<5%) through minor (6-19%), major (20-49%), large (50-79%) to dominant populations (80>%) of the total (Anderson, 2005). A population is considered to be greater than 3 grains (2σ) (Dickinson and Gehrels, 2009).

4.2 Lu-Hf isotope method

Zircon can host up to 1% hafnium in its crystal structure and because of its very low Lu/Hf ratio it essentially preserves the initial 176Hf/177Hf ratio of its source magma at the time of crystallisation (Kinny and Maas, 2003). The Hf isotopic composition of a zircon grain can be used as a geochemical tracer of a host rock's origin in the same way that whole-rock Nd isotopes are used. However, Hf is a more sensitive tracer than Nd, as Lu/Hf in the depleted mantle has increased at approximately twice the rate of Sm/Nd relative to CHUR (chrondritic uniform reservoir, Patchett and Tatsumoto, 1980; Patchett, 1983). The biggest advantage of the Lu/Hf method over the Sm/Nd method is that it allows for greater resolution and detail regarding the source of magmas that produced the dated zircons, rather than providing a weighted average for the whole rock.

The zircon mounts prepared for U–Pb LA-ICPMS analysis were also used for Lu–Hf isotopic studies undertaken with Laser Ablation Multi-Collector Inductively Coupled Plasma Mass Spectrometry (LA-MC-ICPMS) at the University of Adelaide – CSIRO joint facility, Waite Campus, South Australia. To ensure the accuracy of the εHf estimates, only grains with U–Pb LA-ICPMS analysis between 95%-105% concordance were analysed for Lu–Hf isotope composition (e.g. Teale et al., 2011; Glorie et al., 2014; Henderson et al., 2014). Analysis spots were placed as close as possible to concordant U–Pb LA-ICP-MS spots, and within the same CL zone, including those zircon mounts analysed by previous studies. Zircons were ablated with a New Wave UP-193 Excimer laser (193 nm) using a spot size of 50 μm, frequency of 5 Hz, 4 ns pulse length and an intensity of ~ 10 J/cm2. Confirmation of accuracy of the technique was monitored using a combination of the Plesovice, Mudtank and QGNG zircon standards. The average 176Hf/177Hf value for Plesovice for the analytical session was 0.282479 ± 0.000022 (2SD, n = 37), which is comparable to the published value of 0.282482 ± 0.000013 (2SD) by Sláma et al., (2008).
εHf(T), TDM (DM=depleted mantle) and

TDMc (TDMc= depleted mantle crustal) were calculated using 176Lu decay constant after Scherer et al., (2001), where T is the time of crystallization of the zircon. TDM and TDMc were calculated using the methods of Griffin et al., (2002) with an average crustal composition of 176Lu/177Hf = 0.015. All data are presented using the epsilon hafnium (εHf) notation, which refers to a comparison of the data from CHUR; which at any time is set at a value of 0 (Patchett and Tatsumoto, 1980; Blichert-Toft and Albarède, 1997). Juvenile components are recognized as εHf(T) values that fall between the estimated value of the new continental crust from modern island arcs (Dhuime et al., 2011) and the estimated depleted mantle array of Griffin et al. (2004).

5. RESULTS U-PB ZIRCON GEOCHRONOLOGY

5.1 Avalonia

The results of the U-Pb zircon geochronology from Neoproterozoic-Ordovician Avalonian rocks are presented in Figure 4 and the full data tables are included in the supplementary data.

5.1.1 ACO-12-52A and ACO-12-52B (Gamble Brook Formation)

Sample ACO-12-52a and ACO-12-52b are fine grained, white quartzite taken from outcrops approximately 25 metres apart. ACO-12-52a had 80 analyses conducted on 80 detrital grains, of which 63 are 90-110% concordant (Fig. 4). ACO-12-52b had 60 analyses conducted on 60 detrital zircon grains, of which 40 grains are concordant. The two samples contain zircon populations restricted to the earliest Neoproterozoic-Mesoproterozoic and the early Paleoproterozoic (~970-2100 Ma). The zircon spectra are dominated by Mesoproterozoic zircons which form 73% of the total population, with Paleoproterozoic, Neoproterozoic and Archean zircons forming the remaining 18%, 3% and 2%, respectively. Within these populations the zircon distribution patterns define major peaks at 1100-1200 Ma (20%), 1220-1290 (20%) and minor peaks at 970-1070 Ma (12%), 1300-1360 Ma (6%), 1400-1500 Ma (9%), 1510-1600 Ma (6%), 1610-1690 Ma (6%), 1720-1790 Ma (7%), 1830-1880 Ma (6%), 1930-2030 Ma (6%) as well as single grains at 2130 ± 21 Ma, 2592 ± 22 Ma and 2640 ± 22 Ma. The youngest detrital zircon population is 975 ± 33 Ma (n=3, MSWD=0.34).

5.1.2 ACO-12-50/ACO-12-54 (James River Formation)

Sample ACO-12-50 is a grey, coarse-grained sandstone and ACO-12-54 is a medium-grained sandstone. In sample ACO-12-50 eighty analyses were conducted on eighty detrital zircon grains, with 76 grains being concordant (Fig. 4). The zircon distribution patterns define a major peak at 635-780 Ma (58%), minor peaks at 610-635 Ma (17%), 1000-1260 Ma (9%) and 1550-1600 Ma (5%), and accessory peaks at 900 Ma (3%), 1630-1730 Ma (3%) and 2670-2690 Ma (3%). Single zircons at 2000 ± 24 Ma and 2801 ± 22 Ma were also analysed. The youngest detrital zircon population is 613 ± 13 Ma (n=4, MSWD= 0.51).

Sample ACO-12-54 also had eighty analyses conducted on eighty detrital zircon grains. Of these, seventy five are concordant, and range from Neoarchean to late Neoproterozoic in age (Fig. 4). The zircon distribution patterns define major peaks at ~610-635 Ma (44%) and 635-790 Ma (41%), an accessory peak at 1100-1250 Ma (8%) and minor peak at 1400-1570 Ma (3%). Single zircon grains at 1793 ± 24 Ma, 1941 ± 22 Ma, 2073 ± 20 Ma and 2652 ± 21 Ma were also analysed. The youngest detrital zircon population is 612 ± 6 Ma (n=4, MSWD= 0.8).

5.1.3 ACO-12-29B (Livingstone Cove Formation)

Sample ACO-12-29B is a coarse grained, pebbly conglomerate. It had eighty

one analyses conducted on eighty one detrital zircon grains. Of these, sixty three analyses are concordant, and range from Neoarchean to late Neoproterozoic in age (Fig. 4). The zircon distribution patterns define a large peak at ~635-800 Ma (55%), a major peak at ~590-635 Ma (27%) and minor 1400-1600 Ma (11%) and accessory ~1850-1950 Ma (5%) peaks. Single zircons were analysed at 1184 ± 23 Ma, 2104 ± 30 Ma and 2677 ± 20 Ma. The youngest detrital zircon population is 590 ± 5 Ma (n=6, MSWD=0.78).

The youngest detrital zircon population (590 Ma) contradicts the tightly constrained depositional ages for the Georgeville Group. The maximum depositional age is constrained by lavas in the basal units of the Georgeville Group whereby U-Pb zircon and monazite ages of 628 and 617 ± 1.6 Ma are recorded, respectively (Murphy et al., 1997). The minimum depositional age of the Georgeville Group is tightly constrained by syn-tectonic and late tectonic plutons at 606 ± 1.16 Ma (TIMS, U-Pb zircon) and 607 ± 3 Ma (TIMS, titanite). From these constraints it is possible to interpret that the Georgeville Group was deposited and deformed between ~617 Ma and 607 Ma. The zircon grains analysed for TIMS in Murphy et al., (1997) were abraded to remove lead loss, we consider the small group (n=9) of concordant zircon grains younger than 607 Ma to likely be the product of minor lead loss resulting from younger magmatic or metamorphic events in Avalonia (i.e. at 570, 540, 360 Ma, Nance et al., 2002; Murphy and Keppie, 2005) leading to slightly younger apparently concordant ages that still sit along the concordia. These data are not considered in the interpretation that follows.

5.1.4 ACO-12-38 (Malignant Cove Formation)

Sample ACO-12-38 is a gritty, coarse grained red conglomerate. It had eighty analyses conducted on eighty detrital zircon grains, of which seventy two grains are concordant (Fig. 4). The zircon distribution patterns define a large peak at 635-750 Ma (52%), a major peak at 590-635 Ma (38%), a minor peak at 1700 Ma (7%) and single zircons at 1918 ± 22 Ma, 2002 ± 27 Ma, 2224 ± 26 Ma and 2637 ± 22 Ma. The youngest detrital zircon population is 593 ± 5 Ma (n=7, MSWD=0.12).

5.1.5 ACO-12-49 (Black John Formation)

Sample ACO-12-49 is a coarse grained conglomerate that had 80 analyses conducted on eighty detrital zircon grains. Of these, seventy eight grains are concordant (Fig. 4). The zircon distribution patterns define a large peak at 560-635 Ma (65%), a major peak at 635-780 Ma (23%) and accessory peaks at ~1200 Ma (6%) and 2000-2200 Ma (4%), and single grains at 1369 ± 27 Ma, 1554 ± 25 Ma and 2637 ± 22 Ma The youngest detrital zircon population is 562 ± 6 Ma (n=5, MSWD=0.95).

5.1.6 ACO-12-48 (MacKinnons Brook Formation)

Sample ACO-12-48 is a coarse-grained, red conglomerate. Eighty analyses were conducted on eighty detrital zircon grains; of these 62 grains were concordant (Fig. 4). The zircon distribution patterns define a large peak at 545-635 Ma (51%), a major peak at 635-800 Ma (32%) and single zircon populations at 512 ± 8 Ma, 526 ± 6 Ma, 1002 ± 10 Ma, 1406 ± 30 Ma, 2126 ± 24 Ma, 2674 ± 22, 2709 ± 25 and 3104 ± 27 Ma. The youngest detrital zircon population is 543 ± 6 Ma (n=4, MSWD=0.49).

5.1.7 ACO-13-22 (Ferrona Formation)

Sample ACO-13-22 is from an ironstone layer of the Ordovician Ferrona Formation. Fifty seven detrital zircon grains were analysed, of which thirty seven grains are concordant (Fig. 4). The zircon distribution patterns define a large 560-635 Ma (54%) peak, a minor 680-720 Ma peak and single zircon grains at 1367 ± 34, 1537 ± 45 Ma, 2085 ± 39 and 2249 ± 48 Ma and 480 ± 7 Ma. The youngest detrital zircon population is 560

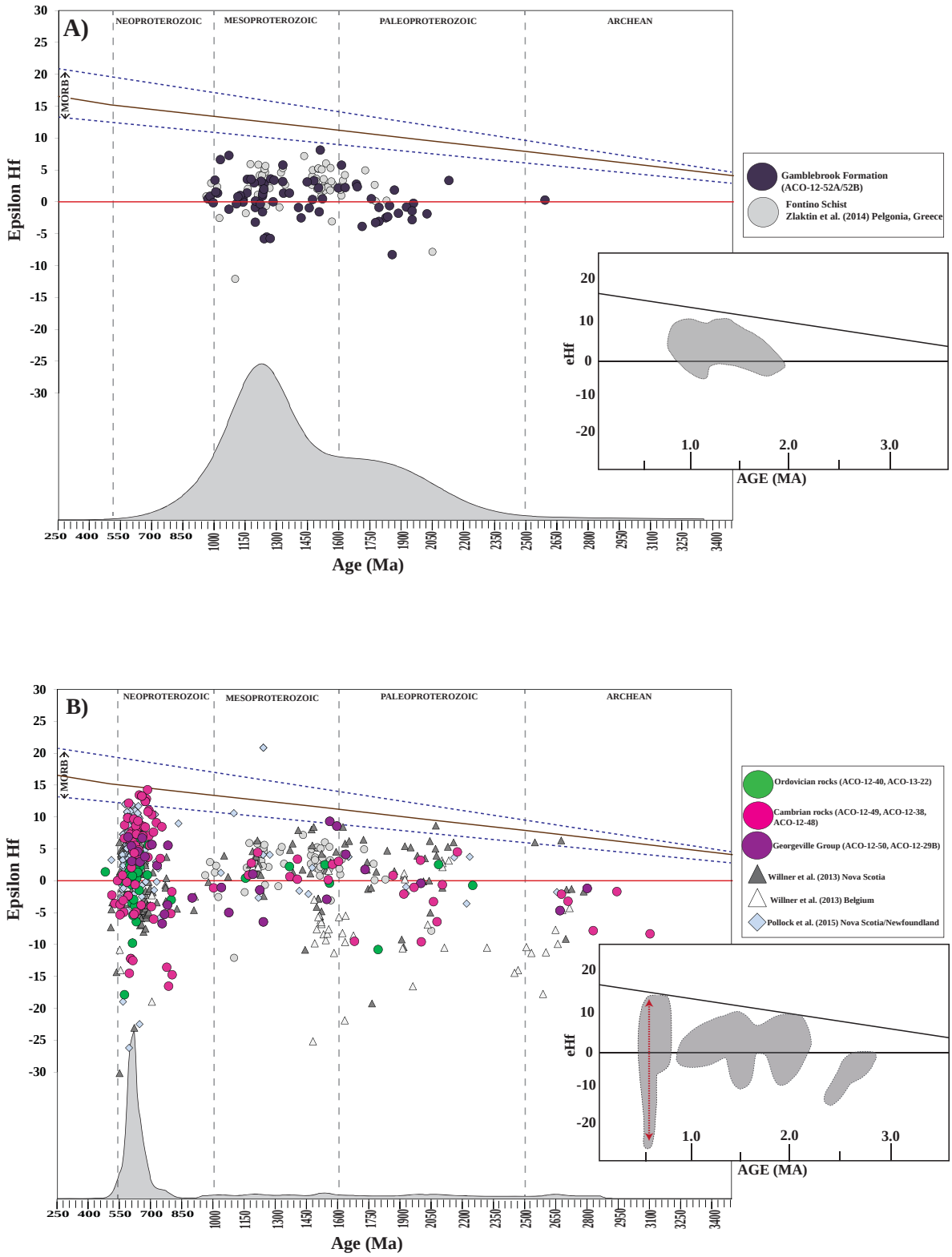

Figure 6

A)εHf values plotted against the U-Pb ages for individual zircon grains from the Gamble Brook Formation (ACO-12-52A/52B) and the Fontino schist (Zlatkin et al., 2014). The inset illustrates a field defining the hafnium isotopic array of the Gamble Brook Formation. B) εHf values plotted against the U-Pb ages for individual zircon grains from the late Neoproterozoic Georgeville Group, Cambrian and Ordovician sedimentary rocks from Avalonia. Also shown are the Avalonian detrital zircon data from Wilner et al., (2013) and Pollock et al., (2015). The inset shows the vertical array associated with late Neoproterozoic magmatism in Avalonia.

± 7 Ma (n=5, MSWD=0.14).

5.1.8 ACO-12-40 (Redmans Formation)

Sample ACO-12-40 is a medium grained, white to grey quartz arenite. Sixty analyses were conducted on sixty detrital zircon grains; of these, forty nine are concordant (Fig. 4). The detrital zircon spectra are limited to a large peak at 600-635 Ma (68%) and a major 635-690 Ma peak (32%). The youngest detrital zircon population is 598 ± 6 Ma (n=6, MSWD= 0.059).

5.2 NW Iberia

The results of U-Pb zircon geochronology from the autochthonous and upper allochthonous Iberian rocks are presented in Figure 5 and the tables with the analytical data are included in the supplementary files.

5.2.1 Upper allochthon: ACO-14-01 (Carreiro Shear Zone) and ACO-14-02 (Órdenes Complex)

Sample ACO-14-01 is from a highly deformed, amphibolite facies schist within the Carreiro Shear Zone (Vogel, 1967; Azcárraga et al., 2002). Eighty analyses were performed on detrital zircon grains extracted from ACO-14-01 of which 48 are concordant (Fig. 5). The interpretation of detrital zircon data in metamorphic rocks can be complex (see Mezger and Krogstad, 1997), however it is unlikely the zircons in sample ACO-14-01 reflect metamorphic ages as zircon disturbance requires granulite facies conditions (Rubatto et al., 2001). However, it is possible that new zircon growth occurred during metamorphism and partial melting at ~400 Ma (Martínez et al., 2011); therefore, it is not plausible to assign a maximum depositional age to the protolith rock. This age is within error of the age of the Purrido ophiolite (395 ± 3 Ma, Martínez et al., 2011). The zircon distribution patterns (Fig. 5) define a major peak at 551-635 Ma (23%), minor peaks at 1910-2060 Ma (15%), 2620-2730 Ma (13%), 1400-1600 Ma (11%), 500-530 Ma (11%), 391-404 Ma (11%) and accessory peaks at 655 Ma (5%), 460 Ma (5%) and 420-440 Ma (6%) .

Sample ACO-14-02 is an upper Cambrian sandstone from a turbiditic sequence (Matte and Capdevila, 1978) in the upper part of the Betanzos Unit of the Órdenes Complex. Sample ACO-14-01 is stratigraphically equivalent to OS-1 in Fernandez-Suarez et al., (2003). Eighty analyses were obtained from detrital zircons of which 66 are concordant (Fig. 5). The youngest detrital zircon population for ACO-14-02 is 528 ± 5 Ma (n=8, MSWD= 0.89). The detrital zircon spectra yield a large peak at 540-610 Ma (61%), a major peak at 521-540 Ma (23%) and a minor peak at 2000-2086 Ma (15%). A single zircon at 671 ± 8 Ma was also analysed (Fig. 6).

5.2.2 West-Asturian-Leonese Zone: ACO-12-60 (Cándana Formation)

Sample ACO-12-60 comes from a thickly bedded (~1 m) clean, white, lower-middle Cambrian quartzite. Of the 80 detrital zircon analyses obtained, 74 grains are concordant (Fig. 5). The maximum sedimentation age is indicated by the youngest population of zircon grains at 527 ± 7 Ma (n=3, MSWD=0.54).

The zircon distribution patterns define a large peak at 550-615 Ma (55%), a major peak at 635-800 Ma (21%) and accessory peaks at 510-530 Ma (5%), 930 Ma (3%), 1670-1780 Ma (6%), 1950-2020 Ma (3%) and 2450 Ma (3%). There is a single Archean grain (2624 ± 24 Ma) (Fig. 5).

5.2.3 Cantabrian Zone: ACO-12-57

Sample ACO-12-57 comes from the upper Cambrian Oville formation in the Cantabrian Zone. It is a glauconite-bearing quartzite, paleontologically constrained to be late Cambrian in age (Lotze and Sdzuy, 1961). Of the 80 detrital zircon analyses obtained, 74 are concordant (Fig. 5). The maximum deposition age, as indicated by the youngest population, is Ediacaran (559 ± 7 Ma; n=3, MSWD=0.57). The zircon distribution patterns define major peaks at 635-825 Ma (34%) and

550-635 Ma (20%), minor peaks at 850-1000 Ma (19%), 1000-1150 Ma (9%), 1670-1800 Ma (9%) and accessory peaks of 2550-2600 Ma (5%) and 490-511 Ma (4%). A single grain at 2885 ± 20 Ma was also analysed.

6. HAFNIUM ISOTOPE RESULTS

6.1 Avalonia

A total of 239 Lu-Hf isotopic analyses were obtained from the Neoproterozoic-Ordovician rocks of West Avalonia. The zircon grains analysed have measured 176Hf/177Hf ratios of 0.280592-0.282793 and initial 176Hf/177Hf ratios of 0.280549-0.282758. Approximately 60% of the zircon grains have εHf values ranging between CHUR and DM (εHf= 0 to +14). The hafnium data are presented in Figure 6 and Figure 7, and will be discussed according to the depositional ages of the clastic rocks; Early Neoproterozoic, Late Neoproterozoic-Cambrian and Ordovician. Full analytical data are included in the supplementary files.

6.1.1 Early Neoproterozoic Gamble Brook Formation

The analyses from the Gamble Brook Formation fall into a restricted detrital zircon spectra that span the interval ~2000-1000 Ma, with the largest population of grains at ~1200 Ma. In general, the zircon grains predominantly cluster around εHf = 0. However, between ~1050-950 and 1650-1550 Ma, a wider range of εHf values extend to more juvenile compositions (Fig. 6a, εHf=0 to +8). A period of crustal recycling is also evident at ~2000-1750 Ma where the grains are predominantly evolved (εHf= +1 to -8), indicating reworking of Archean crust (~2.5-2.6 Ga).

6.1.2 Late Neoproterozoic- Cambrian rocks

The Late Neoproterozoic-Cambrian samples are coeval with the interpreted continental arc magmatic interval that defines the main phase of magmatism in Avalonia (Doig et al., 1991; Kerr et al., 1995; White et al., 2001; Barr et al., 2012; Murphy et al., 2013; Pollock et al., 2015). All the samples contain abundant Cryogenian-Ediacaran populations (Fig. 4). The mid-late Cryogenian (~800-650 Ma) zircon grains span the interval interpreted to represent the early oceanic arc phase in Avalonia (Murphy et al., 2000; Murphy et al., 2008a and references therein; Pollock et al., 2015). The percentage contribution of individual populations may change between samples, but generally all the Neoproterozoic-Cambrian rocks record evidence of a dominant ~540-800 Ma source, and subordinate Mesoproterozoic (~1.0, 1.2 and 1.6 Ga), Paleoproterozoic (1.9-2.2 Ga) and Archean (2.6-2.8 Ga) sources. As their hafnium isotopic arrays are also similar, these rocks will be discussed collectively.

The mid-Neoproterozoic (~800-650 Ma) zircons record two periods of crustal recycling and one of predominantly juvenile magmatism (Fig. 7). Crustal mixing is recorded between ~800-750 Ma where negative (evolved) zircon grains indicate the recycling of a Paleoproterozoic crustal component (εHf= +10 to -20). Between ~750-650 Ma, increasingly juvenile processes dominate and the majority of grains are positive (εHf= -7 to +15). After ~650 Ma crustal mixing processes are indicated by a vertical excursion to evolved values (εHf=+15 to -15) until at least ~590 Ma (Fig. 7). Detrital zircon hafnium data from late Neoproterozoic-Cambrian classic sedimentary rocks in west Avalonia (Cape Breton Island, Nova Scotia and the Avalon terrane, Newfoundland) and east Avalonia (Belgium) consistently overlap with the data presented here from northern Nova Scotia (Willner et al., 2013; Pollock et al., 2015; Fig. 6, Fig. 7); suggesting similar source rocks across Avalonia during the Neoproterozoic-Cambrian interval.

The Mesoproterozoic-Paleoproterozoic detrital zircons from the

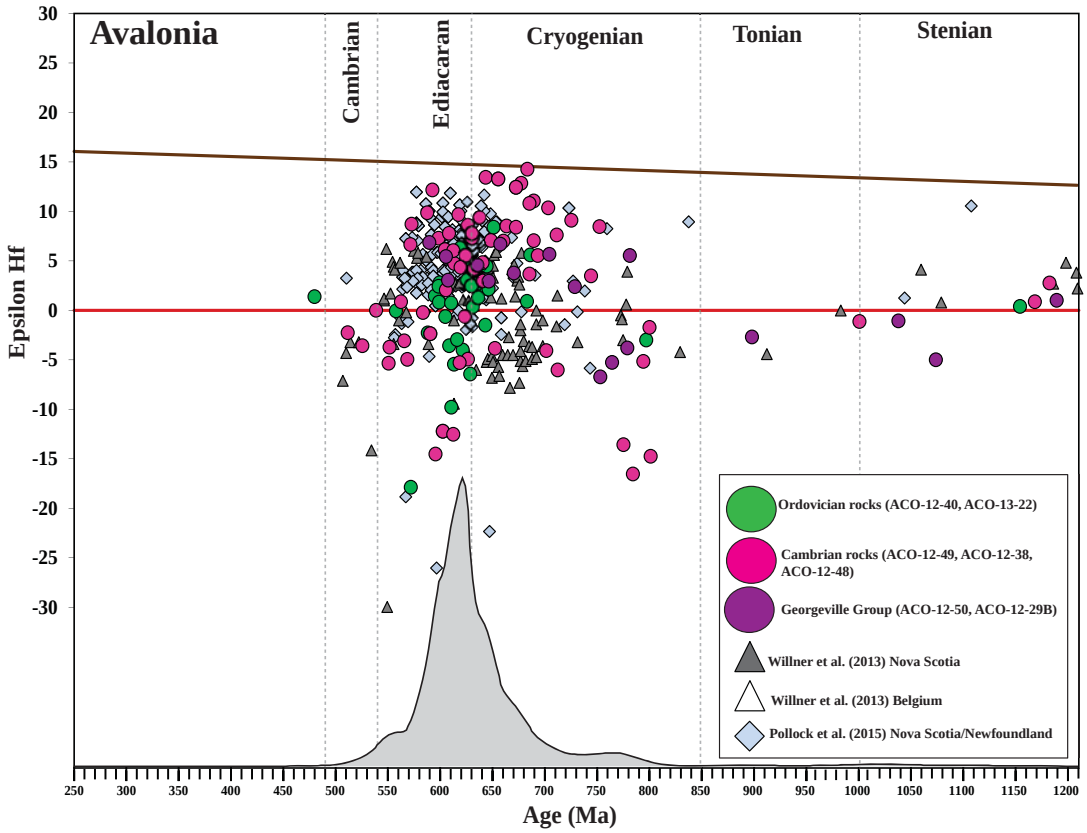

Figure 7

εHf values plotted against the U-Pb ages for individual zircon grains from the late Neoproterozoic Georgeville Group, Cambrian and Ordovician sedimentary rocks from Avalonia. The data is restricted to only the Paleozoic –early Mesoproterozoic interval (250-1200 Ma) to highlight the character of the Avalonian arc system between ~800-550 Ma.

late Neoproterozoic-Cambrian rocks record a similar U-Pb and hafnium isotopic array to that of the early Neoproterozoic Gamble Brook Formation (Fig. 6b). A juvenile input is evident at ~1650-1550 Ma (εHf= +11 to -3). Subsequently, zircons crystallised between ~1.5-1.0 Ga appear to have been predominantly recycled from the juvenile ~1650-1550 Ma magmatism (εHf= +5 to -5). A vertical array at ~1.95-2.1 Ga yields a wide range of hafnium values (εHf= +5 to -10), which include depleted mantle values in the Mira Terrane (Willner et al., 2013). The εHf array indicates that crustal recycling at ~1.9-2.1 Ga involved mixing of depleted mantle material with an Archean source (~2.8-2.6 Ga). All Archean grains (~3.1-2.6 Ga) analysed are evolved (εHf= -1 to -10) and reflect recycled Paleoarchean to Eoarchean crust (TDMC =~3.0-3.9 Ga).

6.1.3 Ordovician rocks

The Early Ordovician samples (ACO-12-40 and ACO-13-22) were deposited during the initial stages of separation of Avalonia from Gondwana (Scotese and McKerrow, 1990; Prigmore et al., 1997; Pollock et al., 2009). In contrast to the Neoproterozoic-Cambrian rocks, the Ordovician samples record a single period of record crustal recycling during the Neoproterozoic), with a weak vertical mixing array at ~650-600 Ma (Fig. 7) indicating the recycling of a Mesoproterozoic-early Paleoproterozoic source (TDMC = ~1.2-1.7 Ga). The few Cryogenian grains (~700-650 Ma) analysed are all juvenile (εHf= +1 to +7), similar to those analysed in the Late Neoproterozoic-Cambrian samples. Sample ACO-12-40 did not have any grains older than

the Mesoproterozoic. Mesoproterozoic grains (~1.2-1.5 Ga) in ACO-13-22 straddle CHUR (± 3 εHf units), and a single ~1795 Ma grain is highly evolved (εHf=-11). Two grains at ~2.0-2.2 Ga also straddle CHUR (± 3 εHf units). The older zircon grains are not statistically robust, but do overlap with the populations of the same age identified in the Neoproterozoic-Cambrian rocks (Fig. 6).

6.2 Iberian Terranes

A total of 260 Lu-Hf isotopic analyses were obtained from detrital zircon grains of Neoproterozoic- Devonian rocks of NW Iberia. The zircon grains analysed have measured 176Hf/177Hf ratios of 0.280569-0.282863 and initial 176Hf/177Hf ratios of 0.280540-0.282833. Approximately 65% of all grains are evolved, recording negative epsilon hafnium values (0 to -37 εHf).The results are divided into the autochthonous and upper allochthonous samples and are shown in Figure 8.

6.2.1 Autochthonous zones: CZ, WALZ and CIZ

Neoproterozoic grains form the largest population in all of the autochthonous Iberian Neoproterozoic-Devonian rocks. Of these, Ediacaran (635-542 Ma) zircons are the most abundant. The Ediacaran zircon grains are highly variable yielding εHf values between -30 and +9; however the majority of the population is between εHf +8 and -16 (Fig. 8a).

A vertical spread of hafnium data is a type of array that is traditionally interpreted as a result of 'mixing' and is commonly attributed to continental arc magmatism (e.g. Mueller et al., 2008; Roberts et al., 2013; Linnemann et al., 2014). Projecting the lower limit of the Ediacaran population (εHf = -37) back to the depleted mantle along a typical crustal evolution line (Lu/Hf= 0.015; Griffin et al., 2000) indicates the zircons were crystallised from a recycled ancient crustal component, yielding a depleted mantle model age (TDMC) of 3.7 Ga.

Cryogenian grains (850-635 Ma) yield 60% positive and 40% negative εHf values, with the majority of the population falling between εHf -15 and +10 (Fig. 8a). The Cryogenian-Ediacaran zircons are bracketed by two negative εHf excursions at ~650-600 Ma and ~1000-900 Ma. In the interval between these events there is a pronounced inverted U-shaped transition between ~900 Ma and ~700 Ma during which the zircon grains are increasingly juvenile, and the previous significant ancient crustal input is subordinate (Fig. 8a). Zircons between ~900-1100 Ma are highly variable (εHf -25 to +17) and define a broad mixing array, between juvenile and ancient sources. A single grain at 1100 Ma is extremely evolved yielding an εHf value of -35. Six zircons aged between ~1200-1400 Ma were analysed for hafnium, recording variable εHf values between -10 and +5. A single zircon at 1300 Ma is extremely evolved with an εHf value of -35. Overall, there are very few Mesoproterozoic grains are recorded in the CZ-CIZ-WALZ rocks.

The broad population of zircons between ~2.1-1.75 Ga in the Ordovician-Devonian rocks are predominantly evolved with εHf values between +3 and -18 (Fig. 8a). The lower limit on the array suggests reworking from a Paleoarchean crustal source. A population at ~2.7-2.5 Ga is also evolved (εHf 0 to -13) and yields a Paleoarchean TDMc (~3.5 Ga) at the lowest limit of the array.

6.2.2 Upper Allochthon: ACO-14-01 and ACO-14-02

Late Neoproterozoic-early Paleozoic grains (~700-500 Ma) predominantly fall in a restricted group between εHf +10 and -10 (Fig. 8b). However, two grains are significantly more evolved (εHf -22 and -37). The lower limit of the main 700-500 Ma population (εHf -10) indicates that the zircons were crystallised via the mixing of crustal sources with juvenile

crust, yielding a lower TDMC limit of ~2.0 Ga. The interval between ~750-1950 Ma marks a lull in the detrital zircon record. However, 1050-1600 Ma zircons are recorded in sample ACO-14-01, the Moeche and Purrido complexes and the Cariño Gneisses and all but one grain record positive εHf values. Zircons with crystallisation ages of ~2.1-1.95 Ga are all positive (εHf +1 to +10). Minor populations at 2.5 and 2.7 Ga are evolved (εHf -10 and -1 to -7, respectively), and yield the same TDMC of ~ 3.5 Ga, indicating recycling of a similar Paleoarchean source.

7. DEFINING HAFNIUM ISOTOPE ARRAYS

7.1 Cryogenian-Ediacaran arc magmatism

Neoproterozoic (Cryogenian-Ediacaran) zircon grains form the largest detrital populations in all late Neoproterozoic-Cambrian samples from NW Iberia, Avalonia and the Armorican terranes (Linnemann et al., 2007; Drost et al., 2011; Linnemann et al., 2014). These grains are commonly attributed to a period of arc-magmatism along the northern Gondwanan margin, referred to as the peri-Gondwanan Avalonian-Cadomian arc system (Murphy and Nance, 1989; Nance and Murphy, 1994), which was active between ~750-550 Ma (Nance et al., 2008; Murphy et al., 2013; Linnemann et al., 2014). Despite similar ages of arc magmatism, Sm-Nd isotopic data (Nance and Murphy, 1994, 1996) indicate that Avalonia and Cadomia were developed on isotopically distinct basements, and so their origin is discussed separately. In addition, as more hafnium isotopic data are produced, it is apparent that the isotopic nature and timing of magmatic activity within the arc system as a whole is highly variable.

Neoproterozoic magmatism is also an important process in the development of the Arabian-Nubian Shield and in the Timanides orogen of Baltica; therefore it is also necessary to discuss the hafnium isotopic character of these arc systems. Collectively, these arrays make it possible to recognise hafnium isotope signatures for different components of the Neoproterozoic magmatic arc systems, and thus trace the source of the zircons. The hafnium isotopic character of components of the Neoproterozoic magmatism is discussed below (Fig. 9); however the crustal evolution of the Avalonian arc-system will be discussed separately.

7.1.1 Cadomian arc

Cadomian (~750-570 Ma) arc magmatism preserved in the Schwarzburg Antiform, Germany have εHf values ranging from near depleted mantle values (+11) to very evolved (-40), including a distinct negative spike of Hf isotopes (Fig. 9), suggesting that Cadomian magmatism involved juvenile magmas that were contaminated with varying amounts of Eburnian and Archean crust (Linnemann et al., 2014). Consequently, the Cadomian arc is interpreted to have been built on the NW margin of the Reguibat shield of the West African Craton, where ancient Archean rocks (3.5-3.4 Ga, 3.0-2.7 Ga) were available for recycling and melting during the Neoproterozoic events (Stern, 1994; Kroner et al., 2001; Linnemann et al., 2014).

7.1.2 Arabian-Nubian Shield

The north-eastern Gondwanan margin is dominated by the Neoproterozoic Arabian-Nubian shield (ANS); located along the eastern boundary of the Saharan Metacraton in the northern East African Orogen. The ANS is comprised of a collage of ~900-760 Ma (Morag et al., 2012; Robinson et al., 2014) juvenile island arcs and back-arc basins which accreted to the Saharan metacraton in the Ediacaran. Cryogenian metasedimentary and arc-metavolcanic rocks in eastern Egypt reveal that arc magmatism was not entirely juvenile and did involve reworking of some pre-Neoproterozoic crust (Ali et al., 2013). Post-collisional magmatism between ~660-580 Ma, appears to have reworked only the juvenile Tonian crust (Morag et al., 2012), as the majority of zircon grains yield positive

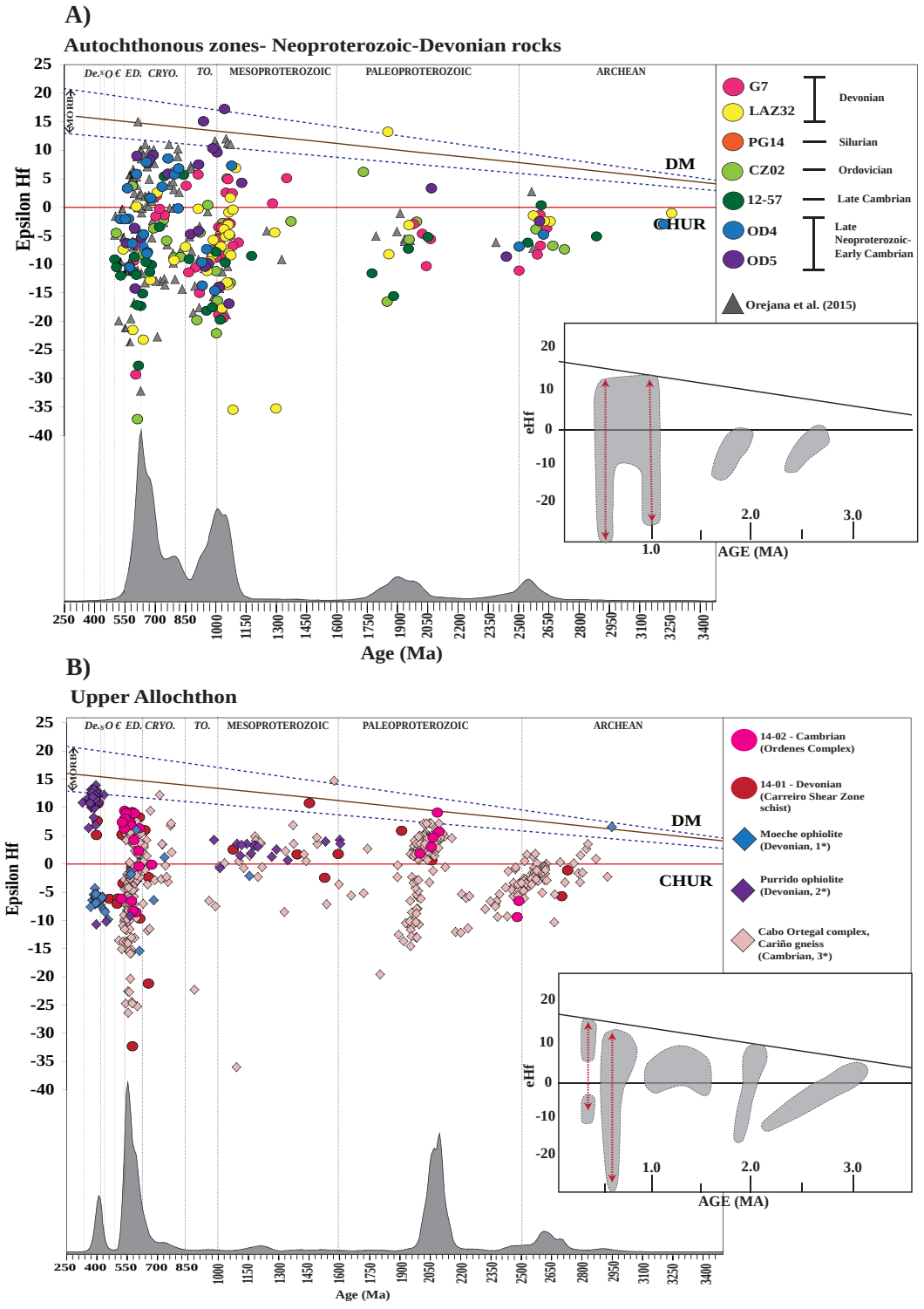

Figure 8

A) εHf values plotted against the U-Pb ages for individual zircon grains from late Neoproterozoic-Devonian sedimentary rocks of the autochthonous zones Iberia. Also shown are the εHf data from detrital zircons in the Central Iberian Zone (Orejana et al., 2015). The inset illustrates the 'U' shaped array with two strong vertical hafnium excursions that characterise the Neoproterozoic zircon data at ~650-600 Ma and ~1000-900 Ma. B) εHf values plotted against the U-Pb ages for individual zircon grains from the late Neoproterozoic- Cambrian sedimentary rocks from the Upper Allochthon, as well as the metasedimentary sample from the Carreiro Shear Zone (ACO-14-01). Also shown are the detrital zircon data from the Moeche ophiolite (1, Arenas et al., 2013) and the Purrido ophiolite (2*, Sanchez-Martinez et al., 2011) and the Carino Gneiss (3*, Albert et al., 2014). The inset highlights two vertical mixing arrays in the allochthonous complex zircon data at ~600 Ma and ~400 Ma.*

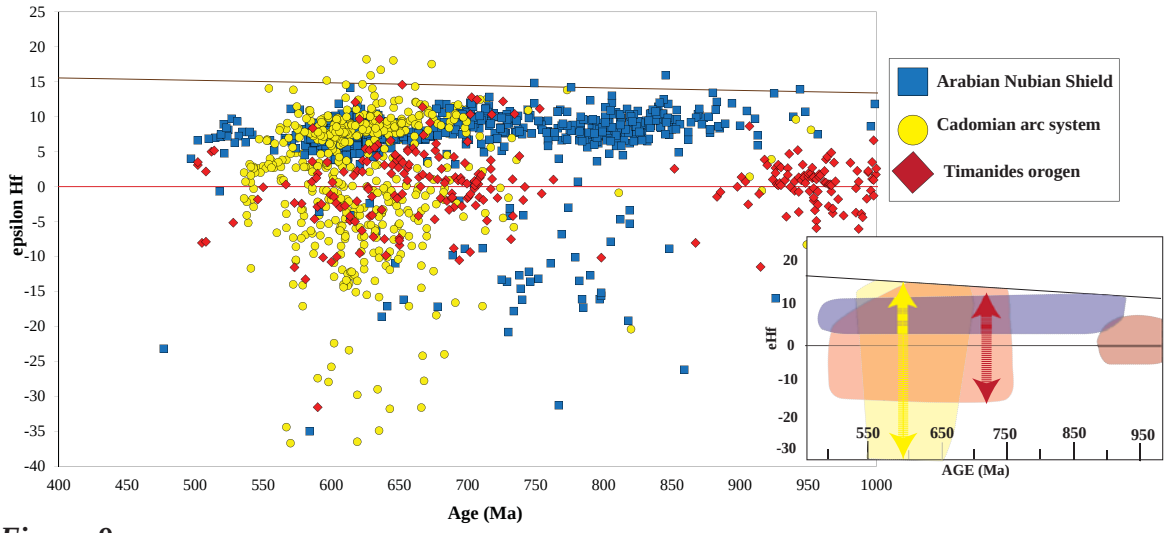

Figure 9

A compilation of the published εHf values for occurrence of Neoproterozoic arc-magmatism in the Timanides, Arabian-Nubian Shield and the Cadomian arc. Data for the Arabian Nubian Shield are from Robinson et al., (2014), Ali et al., (2013), Morag et al., (2011, 2012). Data for Baltica are from Beranek et al., (2013), Romanyuk et al., (2014), Kusnetskov et al., (2010), Kristofferson et al., (2011), Kusnetskov et al., (2014) and Roberts et al., (2013). Data for the Cadomian arc-system are from Linneman et al., (2014).

εHf values (Fig. 9) (Morag et al., 2011; Morag et al., 2012; Ali et al., 2013; Robinson et al., 2014).

7.1.3 Timanides

The Timanide orogen of Baltica is an Ediacaran-Cambrian orogenic belt developed in a continental arc environment on either the margin of Arctida prior to accretion with the passive Timan-Ural margin of Baltica at ~550 Ma (Gee and Pease, 2004; Kuznetsov et al., 2010), or on the margin of Baltica as part of the peri-Gondwanan "Avalonian-Cadomian" arc system (Scarrow et al., 2001; Linnemann et al., 2004) . Magmatism during the development of the Timanide orogen have both depleted mantle and crustal sources, yielding a strong vertical array (Fig. 9), with εHf values extending to -15, likely to reflect development of a continental arc on Paleoproterozoic crust. Minor mixing with an Archean crustal component is suggested by two extremely evolved (εHf=-25 to -30) zircons (Kristoffersen, 2011; Beranek et al., 2013), but was not the dominant magmatic process.

7.2 Cratonic Gondwana and Baltica

A wealth of U-Pb zircon and hafnium isotopic data has been published in the last decade that defines the isotopic composition of the basement rocks of northern African, Arabian, Amazonian and the Baltican cratons (Fig. 10 and Fig. 11). We summarise the available data below in order to emphasise the unique hafnium isotopic signatures recognised in the cratonic domains of northern Gondwana, as well as the cratonic nuclei of Baltica.

7.2.1 West African Craton

The West African Craton forms a significant component of the northern Gondwanan margin. The WAC is comprised of two major Archean and Paleoproterozoic metamorphic and magmatic shields, separated by two sedimentary basins (Taoudeni and Tindouf basins). Its cratonic components are presently exposed in the two main areas of uplift; the Man shield in the south and the Reguibat shield in the north (Mauritania, Morocco and Algeria). The WAC was amalgamated through three orogenic cycles: 1) Leonian cycle (3.5-3.0 Ga) and Liberian cycle (2.95-2.75 Ga), 2)

the Eburnian cycle (2.2-1.75 Ga), and 3) the Pan-African orogenesis (760-660 Ma) (see Abati et al., 2012 and references therein). Crucially, there is a distinct magmatic gap between 1.7-1.0 Ga. During the ~1.7-1.0 Ga interval of quiescence, the WAC underwent cratonisation and was able to develop a thick lithosphere (Black and Liegeois, 1993), prior to remobilisation in the late Neoproterozoic.

The Leonian-Liberian cycles (3.5-2.75 Ga) do not form a distinct hafnium array, but rather form two variable populations at ~3.4 Ga (εHf =0 to -3) and ~3.1-2.6 Ga (εHf =+3 to -17), followed by a period of juvenile magmatism at ~2.5-2.35 Ga. The "Eburnian" cycle (Fig. 10a) extends over 400 myr (~2250-1800 Ma) and is characterised by a period of predominantly juvenile magmatism between ~2250 and 2100 Ma (εHf =+9 to -3), with minor crustal mixing indicated by a small number of evolved grains (εHf= -6 to -9). A vertical array (εHf= +10 to -35) evident in the hafnium data indicate an extended period of crustal recycling between ~2100 and 1800 Ma. During this interval, juvenile material generated during the early stages of the Eburnian and Leonian-Liberian events was reworked.

The Neoproterozoic arc-derived detrital zircon grains of the Anti-Atlas Belt of Morocco (Abati et al., 2012) contrasts with that of the Cadomian arc (Linnemann et al., 2014). The Anti-Atlas records juvenile magmatism at ~700-675 Ma (εHf= +13), prior to a period of mixing with a Paleoproterozoic (Eburnian) source (TDMC =~1.8-2.0 Ga) between ~650-590 Ma (Fig. 9). Consequently, the oceanic magmatic arc is interpreted to have been accreted to the eastern part of the Reguibat Shield at ~650 Ma, which is dominated by Eburnian (~2.1-1.8 Ga) crust (see Walsh et al., 2012).

Mafic-ultra mafic rocks in the Arar Souttouf Massif of the Moroccan Sahara are dated at ~700-550 Ma (Gärtner et al., 2014), and yield predominantly very juvenile εHf values (εHf =+15 to +2), and minor crustal mixing with a Paleoproterozoic source (εHf= +12 to -9) at ~650-600 Ma (Fig. 10a). The dominantly juvenile magmatism has been interpreted to represent an occurrence of oceanic arc magmatism coeval with the main stages of magmatism in the Avalonian-Cadomian arc system (Gärtner et al., 2014).

7.2.2 Saharan Metacraton

The 500,000 km2 area of continental lithosphere occupying the Africa between the Arabian-Nubian shield in the east, the Tuareg shield in the west, and the Congo Craton in the south (Fig. 10b) has been classified as the Saharan 'metacraton' (SMC), which is defined as a 'metacraton' is a "craton that has been variably mobilized during an orogenic event but is still recognisable through its rheological, geochronological and isotopic characteristics" (Abdelsalam et al., 2002; Abdelsalam et al., 2011). The region is dominated by medium to high grade gneisses, metasedimentary rocks, migmatites and smaller outcrops of granulites and low grade volcano-sedimentary rocks (Abdelsalam et al., 2011). Geochronological (Rb-Sr, whole rock) and Sm-Nd isotopic data, indicate the heterogeneous nature of the metacraton, with ages ranges between ~3100-500 Ma (see Abdelsalam et al., 2002 and references therein; Abdelsalam et al., 2011).
Ilzuka et al. (2013) and Be'eri et al. (2014) analysed detrital zircons from the Nile river system, producing a U-Pb-Hf dataset that illustrates the isotopic nature of the Saharan Metacraton and the ANS. The data set (Fig. 10b) yields a double vertical array; one at ~850-550 Ma and a second, distinct Tonian-Stenian (0.85-1.20 Ga) population; an age range not seen in the WAC. The juvenile ~850-550 Ma (εHf= +13) zircons overlap with the mid-late Neoproterozoic juvenile magmatism recorded in the ANS and are conceivably sourced from the ANS. However, the remainder of the hafnium array does not match with the geologic record of the ANS. Notably, the ~1150-850 Ma zircons in the Nile data set are markedly different to those found in the ANS (Fig. 10c) in that they form

an extended vertical array (εHf= +7 to -25). The recognition of similar ~1.2-0.9 Ga zircons from Devonian sandstones in southern Libya (Meinhold et al., 2014) suggest derivation of the Tonian-Stenian (0.85-1.20 Ga) grains from within the SMC. Therefore the Nile River and southern Libya datasets are the most representative of the hafnium isotopic record of the SMC. The SMC is also characterised by a gap in detrital zircon ages between ~1.15-1.9 Ga (Fig. 11b). A period of crustal recycling (vertical mixing array) of an Archean source is evident at ~1.9-2.1 Ga and at ~2.5-2.7 Ga.

7.2.3 Central Africa (Congo Craton and Mesoproterozoic belts)

The Congo Craton records a vertical mixing array between ~900-1150 Ma (Batumike et al., 2009; Iizuka et al., 2013; Foster et al., 2014), generated by mixing Paleoarchean crust with juvenile material (εHf= +15 to -27); comparable to the array seen in the SMC (Fig. 10d). Detrital zircons from the Neoproterozoic Damara Orogen (Foster et al., 2014), which forms the boundary between the Kalahari Craton and southern Congo Craton, also feature a prominent Tonian-Stenian (0.85-1.20 Ga) peak that overlaps with that found in the Congo and Zambezi River sediments (Iizuka et al., 2013).

An important difference between the SMC and Congo Craton is the presence of zircons from the central African Mesoproterozoic Kibaran, Irumide and Namaqua-Natel Belts in the Congo Craton hafnium array (Foster et al., 2014). These orogens contain magmatic and metamorphic provinces that yield varying ages between ~1.6-1.0 Ga, with peaks at ~1.4-1.3 Ga (Linol et al.; De Waele et al., 2003; Foster et al., 2014 and references therein). The hafnium record from the ~1.2-1.4 Ga interval in the Congo Craton is characterised by zircons that straddle CHUR (± 3 εHf units) with reworking of an older crustal source at ~1.3 Ga indicated by a negative spike down to εHf -15 (Fig. 10d). These populations are not abundant in the SMC record and are limited to the central African region.

7.2.4 Baltica

Baltica is not commonly considered as a detritus contributor to the late Neoproterozoic peri-Gondwanan terranes as it is usually interpreted to have been separated from the supercontinent Rodinia during the final stages of break-up at ~650 Ma (Torsvik et al., 1996; Buchan et al., 2000; Johansson, 2014). The model of protracted amalgamation of Gondwana during the ~650-550 Ma interval also did not include Baltica or Laurentia (Johansson, 2014). However, as there are still many unanswered questions regarding its paleogeography (Cawood and Pisarevsky, 2006; Levashova et al., 2013; Meert, 2014) as well as the ultimate provenance of Avalonia, it is necessary to include it while reassessing provenance of the peri-Gondwanan terranes. Whole rock Sm-Nd data from late Neoproterozoic (610-600 Ma) granites of West Avalonia (New England, USA; Thompson et al., 2012) yield early Mesoproterozoic-mid-Paleoproterozoic (~1.0 to 2.2 Ga) model ages and are interpreted to reflect mixing of Svecofennian Baltican crust with juvenile material. A Baltican-Avalonian connection during the Ediacaran is permissible with the available paleomagnetic data, which place both Baltica and Avalonia at moderate south paleolatitude between ~615 and 575 Ma (Thompson et al., 2012). Keppie and Keppie (2014) also consider an Ediacaran connection between Baltica and Avalonia on the basis of 550 Ma paleomagnetic data for Avalonia.

Baltica records an extensive tectonic history that ranges from the Archean to the Paleozoic. Archean rocks (~3.7-2.6 Ga) are well exposed in all the Fennoscandian, Volgo-Uralian and Sarmatian shields (for a detailed review see Bogdanova et al., 2008), which were amalgamated into a coherent craton (East European Craton) during a series of collisions between ~2.0-1.7 Ga. The hafnium record of these events indicates that magmatism

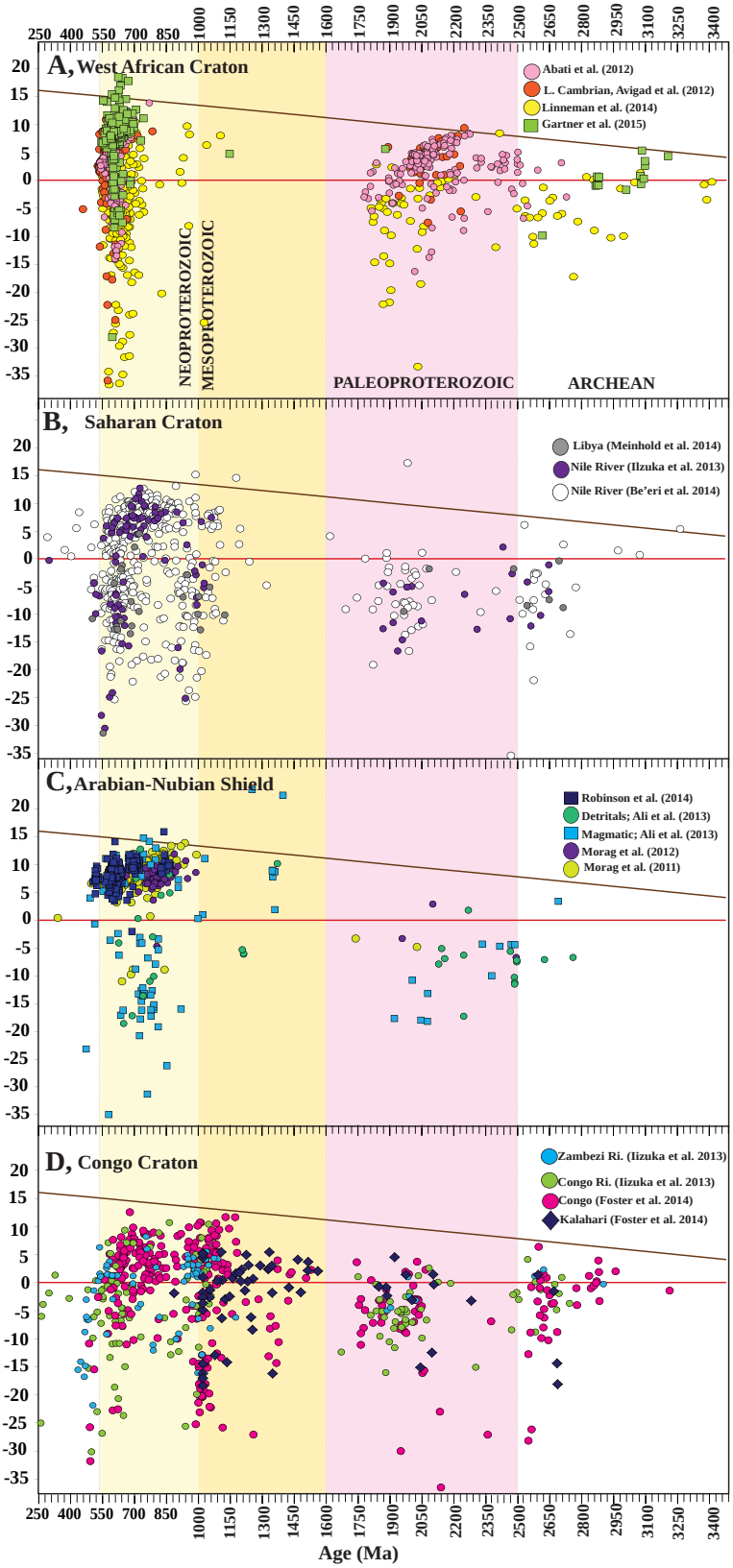

Figure 10

A compilation of the published εHf zircon values for the major African cratons. A) The Saharan Metacraton; data are from Meinhold et al., (2014), Ilzuka et al., (2013) and Be'eri et al., (2014). B) Arabian-Nubian Shield; data are from Robinson et al., (2014), Ali et al., (2013), Morag et al., (2011, 2012). C) Congo craton; data are from Ilzuka et al., (2013) and Foster et al., (2014). D) the West African Craton; data are from Abati et al., (2012), Avigad et al., (2012), Linneman et al., (2014) and Gartner et al., (2015).

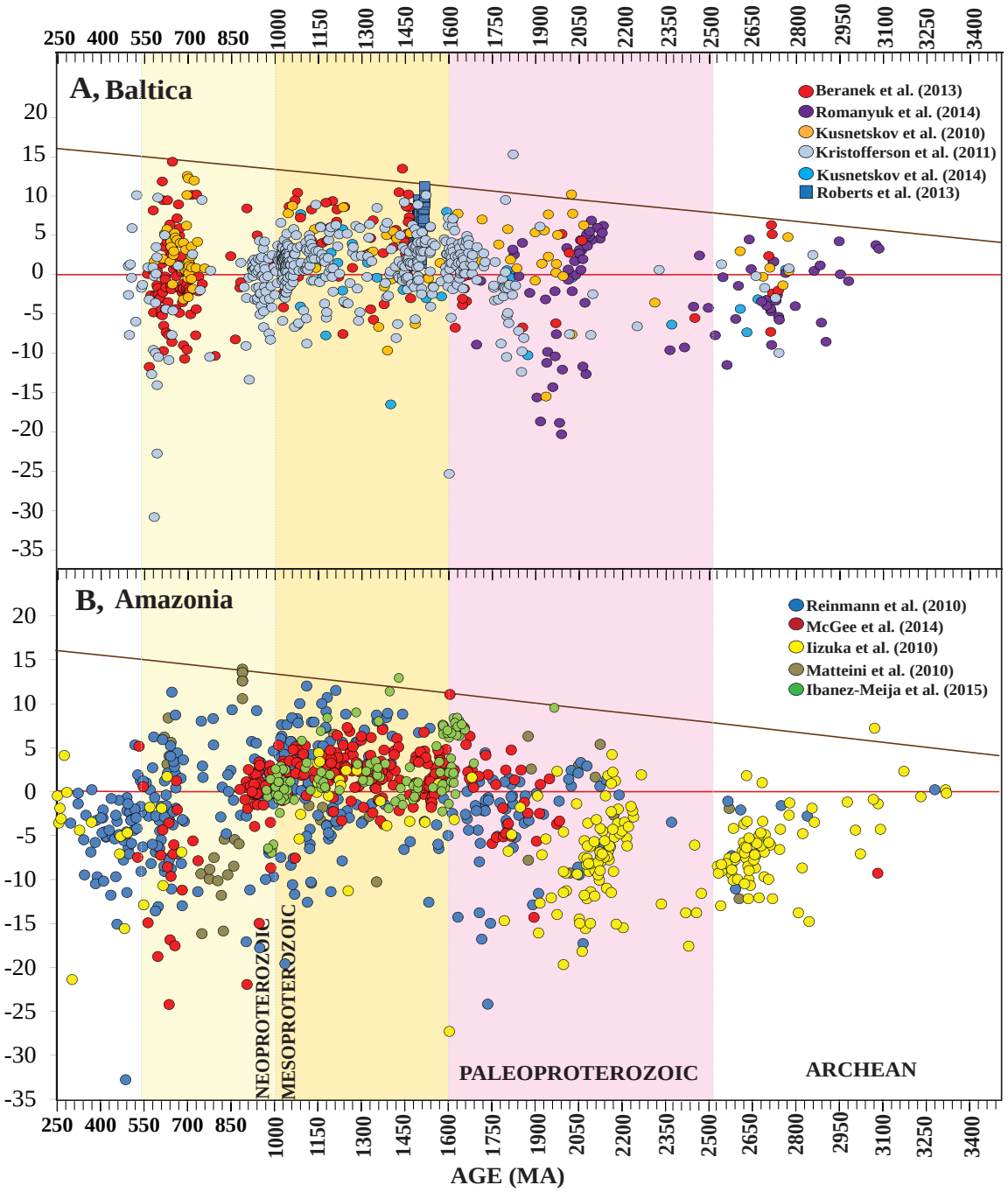

Figure 11

A compilation of the published εHf zircon values for Baltica and Amazonia. A) Baltica; data are from Beranek et al., (2013), Romanyuk et al., (2014), Kusnetskov et al., (2010), Kristofferson et al., (2011), Kusnetskov et al., (2014) and Roberts et al., (2013). B) Amazonia; data are from Reimann et al., (2010) McGee et al., (2014), Iizuka et al., (2010), Ibanez-Mejia et al., (2015) and Matteini et al., (2010).

was initially juvenile at ~2.1-2.2 Ga, prior to crustal mixing processes with a Paleoarchean source until ~1.85 Ga (Andersson et al., 2011) (Fig. 11a). The hafnium array for the late Paleoproterozoic-Mesoproterozoic of Baltica is distinct in that it records no evidence of further recycling of Archean crust until the late Neoproterozoic. Instead, juvenile magmatism is recorded predominantly between ~1.6-1.4 Ga. Subsequently, most of the zircons appear to have been produced from reworked ~1.6-1.4 Ga juvenile crust, with minor input from depleted mantle material (Fig. 11a). The Sveconorwegian orogeny at ~1.2-0.90 Ga

also recycled the 1.6-1.4 Ga Mesoproterozoic crust, with minor additions of juvenile material (Andersen et al., 2002; Andersen et al., 2009).

7.2.5 Amazonia

Amazonia occupies a position adjacent to the West African Craton in most reconstructions of Gondwana (Cordani et al., 2003; Collins and Pisarevsky, 2005). Amazonia has been subdivided into six provinces that range from Archean to early Neoproterozoic in age (Cordani et al., 2009), which were amalgamated during a series of accretionary and collision events during the Paleoproterozoic (Transamazonian Orogeny, ~2.25-2.05 Ga) and Mesoproterozoic (Rio Negro-Juruena Belt, ~1.78-1.55 Ga; Rondonian-San Ignacio orogeny, ~1.55-1.30 Ga; and the Sunsas orogeny, ~1.28-0.92 Ga). The hafnium isotopic record features several isotopic anomalies that distinguish it from the other Gondwanan terranes (Fig. 11b).

The Archean record is dominated by reworking of an initially juvenile Paleoarchean crust (~3.2-3.5 Ga) along a typical crustal evolution path (average Lu/Hf of 0.015; Griffin et al., 2000) (Fig. 11b). A strong vertical array at ~2.25-2.00 Ga corresponding to the Transamazonian event indicates significant recycling of a Paleoarchean crustal source and limited juvenile material. Juvenile magmatism was an important component of the Sunsas Orogeny (1.3-1.0 Ga) and the Goias magmatic arc (0.9-0.6 Ga; Matteini et al., 2010), but both also involved the minor recycling of Paleoproterozoic crust.

8. DISCUSSION

8.1 Provenance of the Gondwanan basement terranes

The U-Pb-Hf isotopic data we present highlight the power of hafnium isotope arrays for defining the crustal evolution of ancient cratonic regions. The comprehensive hafnium arrays can be used to isotopically 'fingerprint' a craton, and we demonstrate that the arrays are traceable through many stages in the evolution of mobile microcontinental terranes.

Using the U-Pb detrital zircon spectra of predominantly Cambrian sedimentary rocks, Dörr et al., (2015) recently proposed that four unique peri-Gondwanan components comprise the majority of the European basement; Amazonian-derived Avalonian terranes, Baltican components, Minoan components (Sicily, Sardinia, Northern Spain and the Mediterranean) and Armorican terranes derived from West Africa. Utilising the addition of hafnium data we propose that the provenance of the European basement terranes is simpler, and can be linked back to three basement components (Fig. 12); Baltica, SMC and the WAC.

8.2 Avalonia

Avalonian components present on the western and eastern margins of the Atlantic Ocean, in the northern Appalachians and Variscan orogens respectively, preserve relatively consistent detrital zircon populations in the late Neoproterozoic-early Palaeozoic sedimentary rocks. These populations are dominated by mid-late Neoproterozoic (~800-550 Ma) detrital zircons, with varying minor percentages of Mesoproterozoic (~1.2-1.6 Ga), Paleoproterozoic (~1.7-2.2 Ga) and Archean populations (~2.6-2.8 Ga).This grouping has led to a consensus that Avalonia resided along the NW margin of Gondwana in the late Neoproterozoic (Pollock et al., 2011; Linnemann et al., 2012).

The West African Craton is commonly dismissed as a source of provenance for Neoproterozoic-Ordovician Avalonian rocks due to the complete absence of Mesoproterozoic source rocks (Murphy et al., 2002; Murphy et al., 2004b). Similarly, the SMC and Congo Craton are also unlikely candidates as they record a distinct Tonian-Stenian vertical mixing array (0.85-1.2 Ga, Fig. 10) that is not preserved in any of the

Neoproterozoic-Ordovician Avalonian rocks. The SMC also lacks ~1.4-1.6 Ga source rocks, which form significant detrital populations in Neoproterozoic-Ordovician Avalonian rocks.
The detrital zircon spectra of late Neoproterozoic Avalonian rocks are most frequently matched to the Amazonian craton (Nance and Murphy, 1994; Keppie et al., 1998; Satkoski et al., 2010; Barr et al., 2012; Willner et al., 2013). However, the tectonic provinces of Baltica also yield significant overlaps with the detrital zircon spectra of Avalonian rocks. The comprehensive hafnium isotope arrays presented here (Fig. 6, Fig. 10, Fig. 11) for Avalonia, Amazonia and Baltica allow the provenance of Avalonian rocks to be tested beyond one dimensional U-Pb zircon age spectra comparisons.

8.2.1 Amazonia versus Baltica: key differences in the hafnium arrays

There are two key differences between the geological evolution of Baltica and Amazonia that differentiate the hafnium isotopic arrays. The first is the Goiás magmatic arc in the Tocantins Province in Amazonia, a Brasiliano/Pan-African orogen that formed during the complex accretion of island and continental magmatic arcs on the western margin of the Sao Francisco craton during the Tonian-Ediacaran (~1.0-0.63 Ga) (Cordani et al., 2009; Pimentel et al., 2011). The arc underwent multiple magmatic events and is recorded by a broad vertical- array that indicates mixing between juvenile and Archean crust εHf= +15 to -17) during the ~0.9-0.6 Ga interval (Matteini et al., 2010). The hafnium array from the same interval (~0.9-0.6 Ga) in Baltica is distinct in that it is characterised by a magmatic "gap" between ~0.9-0.8 Ga, prior to continental arc-type mixing array at ~0.8-0.6 Ga. The vertical-array at ~0.8-06 Ga is defined by εHf values of +15 to -12 and is related to the development of the Timanides orogen (Kuznetsov et al., 2010).

The second distinction between the Amazonian and Baltican hafnium arrays is the timing and nature of Paleoproterozoic magmatism. Paleoproterozoic magmatism in the Amazonian Craton commences at ~2.25 Ga and is characterised by a broad vertical array (εHf= +5 to -22) until ~1.9 Ga (Iizuka et al., 2010). The vertical array (Fig. 11b) indicates the mixing of Archean (~3.2 Ga) crust with varying amounts of younger crustal material. There are no purely juvenile (depleted mantle-type) zircons generated during the ~2.25-1.9 Ga event. The nature of the array indicates that crustal recycling was the dominant process and was likely to be associated with the cratonisation of Amazonia during the ~2.1-2.0 Ga Trans-Amazonian orogeny (see Cordani and Teixeira, 2007 and references therein). By contrast, the Paleoproterozoic hafnium array in Baltica is characterised by the commencement of juvenile magmatism at ~2.1 Ga prior to the evolution of a vertical-mixing array at ~2.05-1.9 Ga (Fig. 11a), whereby depleted mantle material was mixed with Archean crust (~2.9-3.0 Ga).

8.2.2 Provenance of early Neoproterozoic Avalonia (Gamble Brook Formation)

The hafnium isotope array for the Gamble Brook Formation allows a more precise resolution for the earliest history of Avalonia. The maximum depositional age of the early Neoproterozoic Gamble Brook Formation is constrained by the youngest detrital zircon population at 975 ± 33 Ma (present study, Murphy, 2002; Barr et al., 2003). As the Gamble Brook Formation does not contain any early Avalonian magmatic arc populations (~760-730 Ma), it is interpreted to have been deposited between ~970 Ma and ~750 Ma. Given the ~300 million year interval in which the Gamble Brook Formation could have been deposited it seems unlikely to have taken place in an active arc environment, where the youngest zircons commonly overlap with the maximum age of deposition (i.e. Cawood et al., 2012; Zlatkin et al., 2014).

Similar early Neoproterozoic successions to the Gamble Brook are

documented in New England (Westboro Formation, Thompson et al., 2012) and Pelagonia, Greece (Fontino schist, Zlatkin et al., 2014). U-Pb-Hf analyses of detrital zircons from the Fontino schist in Pelagonia overlap with those of the Gamble Brook Fm and indicate a similar source terrane (Zlatkin et al., 2014). The compiled Gamble Brook Fm and Fontino schist hafnium array is restricted to Mesoproterozoic (~1.0-1.6 Ga) to mid-Paleoproterozoic (1.6-2.2 Ga) zircons. The ~2.1-1.75 Ga zircons form a cluster around CHUR (±3 εHf units); whereas ~1.5-1.2 Ga zircons form a predominantly juvenile grouping between εHf +10 and -3. The ~1.2-1.0 zircons are variably mixed between CHUR and +8. The Gamble Brook Formation also preserves very few Archean grains (<2%).

During the ~975-750 Ma window of potential deposition of the Gamble Brook Fm, Baltica and Amazonia are commonly considered to have been contiguous (Nance et al., 2002; Li et al., 2008 and references therein), therefore rocks deposited adjacent to Baltica/Amazonia could potentially yield a mixed detrital signal. However, given the restricted range of detrital zircons (~1.0-2.2 Ga) in the Gamble Brook Formation (and its equivalents in other regions of Avalonia), it seems more feasible that deposition occurred adjacent to Paleoproterozoic-Mesoproterozoic provinces, and not the Archean nuclei of either Baltica or Amazonia.

Crucially, the Gamble Brook Formation does not record ~0.9-0.8 Ga detritus that may be expected if Avalonia was located near the active Goiás arc region of the Amazonian margin (Thompson et al., 2012). Paleoproterozoic zircons in the Gamble Brook Formation and the Fontino schist record magmatism commencing at ~2.1 Ga, which is later than that of the Amazonian hafnium array (~2.25 Ga) and closer to the Baltican record (~2.1 Ga). The increased juvenile composition of the zircons at ~1.5-1.45 Ga in the Avalonia array is also more comparable to the Baltican, rather than the Amazonian, hafnium array (Fig. 11).

Given the isotopic evidence presented here that highlights a number of similarities to Baltica and important differences to Amazonia, we favour the interpretation that Avalonia was located near Baltica in the early Neoproterozoic (~975-750 Ma). The interval coincides with the deposition of the Gamble Brook Formation (and its equivalents New England, Fig. 12), and requires a paleogeographic position closest to the Telemarkia province, Transcandinavian Igneous Belt and the Osnitsk-Mikashevichi Belt, which are dominated by Paleoproterozoic-Mesoproterozoic rocks. This is similar to the location proposed by Thompson et al. (2012) whereby Avalonia occupied a location adjacent to western-end of the Timanides of Baltica and along strike from the Cadomian orogen outboard of West Africa (see Fig. 8, Thompson et al., 2012).

8.2.3 Crustal evolution of the Avalonian arc system in the Cryogenian-Ediacaran

Previous interpretations of the earliest evolution of the Avalonia microcontinent are largely derived from whole rock Sm-Nd isotopic data from vestiges of the early arc magmatism (~760-730 Ma). These include the Economy River Gneiss (734 Ma, Doig et al., 1993) in Nova Scotia, the Burin Group volcanic rocks (~763 Ma, Krogh et al., 1988; Murphy et al., 2008b) in Newfoundland and the Malverns Plutonic Complex (~675 Ma, Tucker and Pharoah, 1991; Strachan et al., 1996) in the English Midlands. Early Mesoproterozoic Sm-Nd model ages (~1.2-1.0 Ga) for the 734 Ma Economy River Gneiss and 675 Ma Malverns Plutonic Complex have led to the interpretation that "proto-Avalonia" developed as juvenile oceanic arcs in the peri-Rodinian ocean in the late Mesoproterozoic (1.2-1.0 Ga) (Murphy et al., 2000; Nance et al., 2002). Consequently, the ~760 Ma arc magmatism represents renewed subduction in an oceanic arc environment, prior to accretion to the Gondwanan margin and subsequent

continental arc magmatism between ~630-570 Ma (Murphy et al., 2013). Hafnium data from zircons crystallised in the Avalonia arc-system provide a more detailed isotopic picture of the arc system, compared to the average given by whole rock Sm-Nd data.

The late Neoproterozoic Georgeville Group and Cambrian samples are dominated by Cryogenian-Ediacaran (~750-550 Ma) zircons. A small number of ~800-760 Ma zircons are also present, but form only accessory populations (<5%) in the rocks. However, the ~800-760 Ma zircons overlap with the hafnium isotopic array of the dominant ~760-650 Ma arc related zircons indicating arc magmatism in Avalonia may have commenced as early as ~800 Ma. The hafnium isotopic array of the ~800-550 Ma zircons describes the crustal nature of the Avalonian arc system. Of these zircons 90% fall into a cluster of εHf values between -7 and +14, which corresponds to a TDMc range of ~0.68 to 1.9 Ga. An interval of increased ancient crustal reworking is apparent at ~640-570 Ma, whereby a small number of zircons record comparatively evolved crustal values (εHf= -12 to -18); which corresponds to TDMc range of ~2.2 to 2.6 Ga.

Previous Sm-Nd whole rock analyses of early arc rocks in West and East Avalonia infer magmatism was a mix of juvenile depleted mantle material with Mesoproterozoic-Paleoproterozoic (~1.0-1.30 Ga, ~1.3-1.8 Ga) crustal contamination (Pharaoh et al., 1987; Thorogood, 1990; Barr and Hegner, 1992; Nance and Murphy, 1994; Whalen and Jenner, 1994; Murphy and Nance, 2002). However, the ~800-550 Ma hafnium array identifies an older Paleoproterozoic crustal component than that of the Sm-Nd whole rock data (e.g. Murphy et al., 2000); and indicates that the early Avalonian arc-system was built on a basement of "Grenvillian-type" crust that records mid-Paleoproterozoic-Mesoproterozoic crustal model ages (~1.0-2.0 Ga) (Daly and McLelland, 1991; Rainbird et al., 1997; Rivers, 1997).

Given that the deposition of the early Neoproterozoic Gamble Brook Fm is interpreted to have occurred adjacent to Baltica, we propose that the early-Avalonian basement originated along the Baltican margin and was subsequently rifted away in the mid-Neoproterozoic. The tectonic setting of "Proto-Avalonia" could have been similar to that of the late Cretaceous margin of eastern Australia, whereby fragmentation and rifting of the continental crust resulted in the separation of a microcontinental ribbon ("Zealandia", Mortimer, 2004; Tulloch et al., 2009); which subsequently formed the upper plate during oceanic and continental arc subduction in the mid-Palaeogene (Kamp, 1999; Stern et al., 2006). Oceanic-arc magmatism in Avalonia at ~800-760 Ma preferentially nucleated on the thinned continental crust. A modern analogue to this could be the Cenozoic oceanic arc Vanuatu (Buys et al., 2014), whereby hafnium isotopes from zircons in arc-related magmas have identified significant crustal contamination in the oceanic arcs of Vanuatu and have allowed the basement to be traced back to its origin along the Australian margin (Buys et al., 2014).

The Avalonian hafnium array shifts at ~640 Ma towards more evolved crustal values and is interpreted to represent the accretion of the Avalonian arc to a cratonic margin (Nance et al., 2002 and references therein). The shift towards crustally derived magmatism also coincides with the onset of continental arc magmatism (Murphy et al., 2013) along the northern Gondwanan margin. Instances of high-intermediate grade metamorphism at ~650 Ma in east Avalonia (Malverns Plutonic Complex, Strachan et al., 1996) and west Avalonia (southern Maine, Cape Breton Island, southern Newfoundland) provide further evidence for the accretion of the oceanic arcs to a continental margin prior to ~640 Ma. Mesoproterozoic (~1.0-1.6 Ga), Paleoproterozoic (~1.8-2.2 Ga) and Archean (~2.5, 3.0 Ga) zircon inheritance during the main stage of continental arc magmatism are

reported in the ~615 Ma Keppoch rhyolite in Nova Scotia (Murphy et al., 1997), Horse Cove Complex, Newfoundland (Skipton et al., 2013) and ~570-560 Ma granites in SW Poland (Mazur et al., 2010). Neodymium isotopic signatures of coeval, crustally derived volcanic and plutonic rocks in Avalonia are also testament to the transition to a continental arc environment between ~650-600 Ma (Nance and Murphy, 1994, 1996).

8.2.4 Provenance and paleogeography of Avalonia during the late Ediacaran-Ordovician

Continental reconstructions for the late Neoproterozoic-early Paleozoic frequently place Avalonia along the Amazonian margin of Gondwana (Stampfli and Borel, 2002; Scotese, 2004; Nance et al., 2008), with some authors suggesting a Baltican or insular location (Landing, 1996a; Thompson et al., 2012; Keppie and Keppie, 2014). The detrital zircon hafnium array from the Ediacaran (Georgeville Group), Cambrian and Ordovician sedimentary rocks allow the paleogeographic scenarios to be tested.

The spread of detrital zircon ages (0.8-0.6 Ga, 1.0-2.1 Ga, 2.5-2.8 Ga) preserved in the Ediacaran Georgeville Group indicate that the sequences are not likely to be recycled solely from the underlying Avalonian rocks (i.e. Gamble Brook Fm., Westboro Fm., Fotino Schist). If this were the case, it is expected that a similar U-Pb-Hf zircon spectra to that of the Gamble Brook Fm would be evident in the ~610-480 Ma sedimentary rocks. Although an isotopically similar spread of Mesoproterozoic-mid Paleoproterozoic (~1.0-2.1 Ga) zircons are indeed found in the younger (~610-480 Ma) Avalonian sequences, they are accompanied by Archean zircons (~2.5-3.0 Ga) and the dominant Neoproterozoic (0.8-0.6 Ga) arc-related populations. The appearance of the Archean zircons suggests the introduction of an ancient cratonic source by the Ediacaran deposition of the Georgeville Group (~620-607 Ma). Therefore, the Georgeville Group is interpreted to have been sourced from a mixture of components, including recycling of the underlying basement (i.e. the Gamble Brook Fm), the adjacent active-arc system and an Archean cratonic source.

An early Neoproterozoic "gap" (~900-800 Ma) in the late Neoproterozoic-Ordovician Avalonian isotopic array is important, because it is an interval of zircon generation associated with the Amazonian Goiás magmatic arc. A period of mixing between juvenile and Paleoproterozoic (~2.4-2.2 Ga) crust at ~1050-900 Ma typical of Amazonia is also not evident in the Avalonian array (Fig. 6). If the Avalonia continent docked along the Amazonian margin during the late Neoproterozoic it is necessary to explain the absence of the ~1.1-0.8 Ga zircons that characterise the Amazonian hafnium array during this interval. A possibility is that the Goiás magmatic arc rocks were physically obstructed from the arc-related basins. As the northern Gondwanan margin is considered to have hosted an Andean-style magmatic-system during the ~640-550 Ma interval (Gutiérrez-Alonso et al., 2003; Murphy et al., 2004b) it is entirely possible that the topography of the Neoproterozoic arc system restricted the drainage into the basins. This is analogous to the redirection of the ancestral Amazon River system following the development of the Andes (Mora et al., 2010; Sacek, 2014).

The hafnium isotopic array for the Mesoproterozoic-Paleoproterozoic (~1.1-2.2 Ga) detrital zircons found in the late Neoproterozoic-Ordovician Avalonian rocks is broadly comparable to both Amazonia and Baltica. The Avalonian array contains Paleoproterozoic detritus as old as ~2.25 Ga, which can be linked to the Trans-Amazonian array in Amazonia and not to the slightly younger Svecofennian array at ~2.1 Ga. However, the two intervals of increased juvenile magmatism at ~1.50-1.45 Ga and ~2.0 Ga in the Avalonian array match closely with events in Baltica; including anorogenic Fennoscandian rapakivi-granitic intrusions

(~1.6-1.45 Ga, references) and early Svecofennian (Sarmatian) juvenile granites (~2.0 Ga, Lahtinen et al., 2002; Shchipansky et al., 2007). Lastly, the hafnium isotopic character of the Archean (~2.5-3.0 Ga) zircons is such that derivation from either Baltica or Amazonia is feasible (Fig. 11) and cannot be used to distinguish a source craton.

Therefore, although the hafnium isotopic record of arc-related zircons support the collision of the Avalonia to a continental margin at ~640 Ma (Fig. 6 and Fig. 7), the hafnium isotopic arrays for the Mesoproterozoic, Paleoproterozoic and Archean detrital zircons in the Georgeville Group, Cambrian and Ordovician rocks cannot be used to confidently distinguish which cratonic margin this was. The hafnium isotopic evidence for provenance from either Amazonia or Baltica is somewhat equivocal due to the similarities between the Baltican and Amazonian arrays. A further complication is the recycling of the Baltican basement inherited during the early Neoproterozoic (~975-800 Ma Gamble Brook Formation, present study), in the Ediacaran-Ordovician rocks.

8.3 Iberia

8.3.1 Saharan metacraton provenance for autochthonous NW Iberia

Autochthonous NW Iberia (CZ, CIZ, WALZ) rocks record a relatively consistent detrital zircon spectrum between the Ediacaran and Silurian, dominated by Ediacaran (635-550 Ma), Cryogenian (850-635 Ma), Tonian-Stenian (0.85-1.20 Ga), mid Paleoproterozoic (~1.9-2.2 Ga) and early Archean (2.5-2.8 Ga) sources (present study, Pastor-Galán et al., 2013; Fernández-Suárez et al., 2014; Shaw et al., 2014; Gutiérrez Alonso et al., 2015). However, an exception to this trend occurs during the interval between the Ediacaran and Cambrian and has been recognised in many geodynamic and paleogeographic studies in Iberia (Fernández-Suárez et al., 2000; Fernández-Suárez et al., 2002; Gutiérrez-Alonso et al., 2003; Díez Fernández et al., 2010; Díez Fernández et al., 2012; Pereira et al., 2012; Talavera et al., 2012; Fernández-Suárez et al., 2014; Orejana et al., 2015; Zimmermann et al., 2015). Lower-middle Cambrian rocks in the Cantabrian and Central Iberian Zones (sample OD1 and OD3, Fernández-Suárez et al., 2014; upper Herrería Formation, Zimmermann et al., 2015) record comparatively minor to absent abundances of Tonian-Stenian (0.85-1.20 Ga) zircons; which is in contrast to the upper Ediacaran rocks where these grains form a significant population (10-20%). Coeval Lower Cambrian sedimentary rocks deposited in the Upper Allochthon (Fig. 6, sample ACO-12-60; Cariño gneisses, Albert et al., 2014) also yield similar detrital zircon records dominated by mid-late Neoproterozoic (850-550 Ma) and mid Paleoproterozoic zircons (1.8-2.2 Ga).

The anomalous upper Ediacaran-Lower Cambrian change in provenance recorded in some Iberian rocks coincides with major adjustments in the geodynamics of the northern Gondwanan margin. It follows the opening of the Iapetus Ocean (~570 Ma, Cawood et al., 2001), precedes the opening of the Rheic Ocean, coincides with the termination of magmatism in the Avalonian-Cadomian arc and with the transition towards a stable platform along northern Gondwana (see Nance et al., 2008; Nance et al., 2012 and references therein). The apparent shift in provenance has been tentatively linked to extension-related exhumation on the Gondwanan side of the active margin exposing an older ~2.0 Ga basement terrane (Fernández-Suárez et al., 2014). As the present study does not include any hafnium data from the Lower Cambrian rocks (e.g. OD1, OD3, Fernández-Suárez et al., 2014) that display the anomalous shift in provenance, we cannot contribute a new perspective to the ongoing debate regarding this. We instead focus on the hafnium isotopic array for the dominant detrital zircon populations seen in the majority of the Ediacaran to Silurian autochthonous

Iberian rocks.

The hafnium isotope array for NW Iberia (Fig. 8a) records evidence for two periods of continental arc-type magmatism during the Neoproterozoic. A vertical array at ~1100-900 Ma is indicative of mixing between a juvenile depleted mantle source and Archean crust (TDMC = ~3.1 Ga). The shift towards a comparatively juvenile population between ~850-700 Ma suggests the transition from a continental arc to an oceanic arc (c.f. Smits et al., 2014), although the trend is subtle. Between ~700-550 Ma continental-arc type magmatism was re-established and involved reworking of significant portions of Archean (εHf= +15 to -40, TDMC= 3.8-3.3 Ga) as well as juvenile depleted mantle material.

The NW Iberia hafnium array favourably compares with the SMC or Congo Craton (Fig. 10), as both record two vertical mixing arrays during the Neoproterozoic. However, the presence of additional Mesoproterozoic zircon populations in the Congo Craton distinguishes the two regions (Fig. 10d). Cryogenian passive margin sequences on the SW Congo contain predominantly ~1.1-1.0 Ga grains, and a minor 1.4-1.2 Ga population. As the Iberian Ediacaran rocks are devoid of ~1.4-1.2 Ga zircon grains, the Congo Craton is a less feasible option than the SMC for provenance in the Ediacaran.

Our data support the interpretation that autochthonous NW Iberia occupied a paleoposition adjacent to the SMC in the Late Neoproterozoic, reinforcing the models proposed by Diez-Fernandez et al., (2010) and Fernandez Suarez et al., (2014). Other basement regions of Europe also record the Tonian-Stenian (0.85-1.20 Ga) population, so we propose that these terranes were also derived from the SMC and may have also occupied a position along the northeastern Gondwanan margin (Fig. 12). Included are, the Peloritani Mountains, Sicily (Williams et al., 2012), the external Hellenides, Greece (Kydonakis et al., 2014; Dörr et al., 2015), the Serbo-Macedonian Massif (Meinhold et al., 2010), the Alpine basement in Switzerland and Austria (von Raumer et al., 2013), the Eastern Carpathians (Balintoni and Balica, 2013) and the Western Carpathians, Slovakia (Vozárová et al., 2012).

8.3.2 Provenance of the Upper Allochthon, Iberia

The relationship of the so called 'exotic' allochthonous complexes with the autochthonous and parautochthonous zones of NW Iberia is contentious (Barreiro et al., 2007; Murphy and Gutiérrez-Alonso, 2008; Catalán et al., 2009; Díez Fernández et al., 2010). The Basal Units of the allochthonous complexes have been interpreted to represent the most outboard region of the Gondwanan margin, and the detrital zircon record of the Basal Units (Díez Fernández et al., 2010) is comparable to the autochthonous Gondwanan sequences (Fernández-Suárez et al., 2002; Gutiérrez-Alonso et al., 2003; Catalán et al., 2004; Catalán et al., 2008) in that they record similar Tonian-Stenian (0.85-1.20 Ga), Paleoproterozoic (~2.2-1.8 Ga) and Archean (~2.8-2.5 Ga) zircon populations. Accordingly, they are likely to also have been derived from the SMC as discussed above. However, the zircon record from the Cambrian rocks in the Upper Allochthon, and the Devonian ophiolite complexes, provide a strong contrast with those in the autochthonous zones.

The Upper Allochthon of Iberia is generally interpreted to have developed as part of the Cadomian-Avalonian arc/back arc system in the late Neoproterozoic adjacent to the West African Craton (WAC) (see Quesada, 1991; Abati et al., 2007 and references therein; Albert et al., 2014). The varying but small percentages of Mesoproterozoic detritus in the Neoproterozoic-Cambrian rocks are interpreted to have been derived from distant cratons to the east, such as the SMC or ANS (Albert et al., 2014).

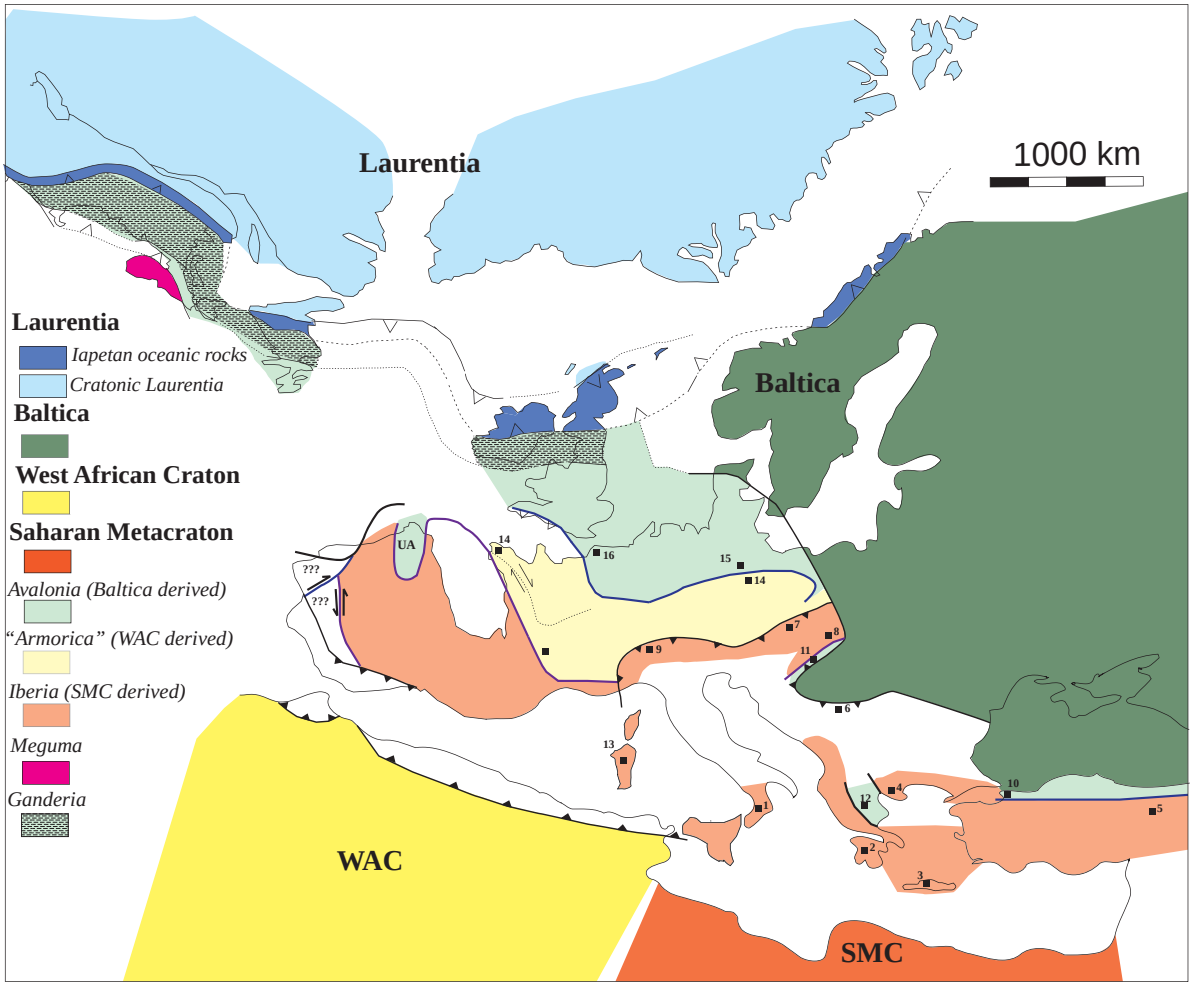

Figure 12

A schematic diagram of the Variscan-Appalachian orogen that indicates the hafnium isotopic affinity of the basement rocks to the West African Craton, Saharan Metacraton or Baltica. "Avalonian" components record an early Neoproterozoic (~975-800 Ma) Baltican history, which then formed the basement to the main stage of the Avalonian arc in the later Neoproterozoic (~750-550 Ma). Autochthonous Iberia records an affinity with the SMC from the late Ediacaran (~550 Ma) and the SMC isotopic signature is recognisable in sequences as young as the Silurian. On the basis of the available detrital zircon hafnium isotopic data for the Armorican terranes and parts of Mediterranean Europe, the late Neoproterozoic-early Cambrian affinity to the West African Craton or the Saharan Metacraton have been interpreted. Where existing hafnium data is not available, detrital zircon geochronology has been used to tentatively link the Neoproterozoic-Cambrian rocks to either the SMC or WAC on the basis of distinct zircon populations. Sequences derived from the SMC are associated with Tonian-Stenian zircon populations (0.85-1.2 Ga) and those derived from the WAC record a magmatic gap between ~1.8-0.75 Ga. The numbers refer to the following geochronological/isotopic studies: 1) Williams et al., (2012), 2) Dorr et al., (2015), 3) Kydonakis et al., (2014), 4) Meinhold et al., (2010), 5) Ustaomer et al., (2012), 6) Carrigan et al., (2006), 7) Vozarova et al., (2012), 8) Balintoni et al., (2014), 9) Von Raumer et al., (2013), 10) Ustaomer et al., (2012), 11) Balintoni & Balica (2013), 12) Zlatkin et al., (2014), 13) Avigad et al., (2012), 14) Linneman et al., 2004, Drost et al., (2011), 15), Eckelmann et al., (2014) 16) Linneman et al., 2012.

The compilation of hafnium data for the Upper Allochthon (Fig. 8b) cannot be easily reconciled with derivation from the WAC (Fig. 11a). The data from the Devonian Moeche and Purrido ophiolites (Martínez et al., 2011; Arenas et al., 2013) are similar to the εHf arrays for the Mesoproterozoic detrital data from both the Cabo Ortegal complex (Albert et al., 2014) and the Carreiro shear zone (Fig. 8b). They are likely to have all

shared the same continental source, which is distinct from the WAC and other northern Gondwanan terranes.

Notable differences between the WAC and the array from the Upper Allochthon include: (1), the Mesoarchean hafnium isotopic array (~3.0-2.4 Ga) that indicates juvenile magmatism at ~3.0 Ga, followed by reworking along a typical crustal evolution array between ~3.0-2.4 Ga (Fig. 8b). The equivalent interval (~3.0-2.4 Ga) in the WAC is not comparable (Fig. 11a), and suggests that juvenile magmatism occurred sporadically between ~3.15 and 2.6 Ga, and was the dominant process at ~2.5 Ga. (2), The "Eburnian" zircon peak at ~2.0 Ga is short-lived in the hafnium array from the Upper Allochthon compared to the Eburnian event recorded in the WAC. The total duration recorded by the detrital zircon grains in the Upper Allochthon occupies the interval ~2.18-1.97 Ga, and is characterised by early juvenile, oceanic-arc magmatism (~2.18-2.1 Ga), followed by an episode of continental-arc type magmatism at ~2.1-1.97 Ga, recorded by a distinct vertical mixing array (εHf= +12 to -17). In contrast, the Eburnian event in the WAC extends from ~2.25 to ~1.8 Ga and indicates a period of juvenile magmatism with minor crustal mixing at ~2.25 Ga, followed by recycling of the ~2.25 Ga juvenile material with an increased crustal input between ~2.2-1.8 Ga.

Perhaps the most distinguishing feature of the hafnium array in the Upper Allochthon is the presence of Mesoproterozoic zircons in the sedimentary rocks and the Devonian 'ophiolite' complexes. The Mesoproterozoic grains (~1.0-1.6 Ga) form ~4% of the total detrital spectra of the Cariño Gneisses and 11% of the Carreiro Schist. They are present in both the Purrido and Moeche 'ophiolites' and overlap in hafnium isotopic space with equivalent zircons from the Cariño Gneisses and Carreiro schist (Fig. 8b). The Cariño Gneisses are also characterised by ~1.6-1.8 Ga Sm-Nd model ages (Albert et al., 2014), suggesting the bulk components of the protolith rocks could be sourced from a Mesoproterozoic-Paleoproterozoic terrane.
Given the occurrence of both juvenile and evolved zircons in the ca. 400 Ma ophiolites (Fig. 8b), the juvenile zircons, with ages close to the crystallization age of the Purrido ophiolite are likely to represent the mantle-derived component of the magmatic system. The Mesoproterozoic zircons are interpreted as xenocrysts (Martinez et al., 2009, Arenas et al., 2013), implying the magma traversed through continental crust.

Arenas et al., (2013) consider the evolved ~400 Ma zircon grains in the Moeche Ophiolite to be inherited into the mafic magmas from a separate continental source, and cite the xenocrystic morphology and oscillatory zoning of the grains as justification. Additionally, the authors also consider the normal mid-ocean-ridge basalt (N-MORB) to transitional island arc tholeitic geochemistry of the Moeche greenschists to be incompatible with a continental source, and therefore must have a mantle provenance. However, Pearce (1996) maintains that MORB-island arc transitional basalts can also be emplaced in evolved marginal (backarc) basins or attenuated continental settings. The εHf arrays for the Moeche and the Purrido ophiolites Devonian 'ophiolites' strongly suggests an environment in which mafic magma intruded a late Mesoproterozoic-early Paleoproterozoic crust. Mafic rocks of the Devonian ophiolites have suprasubduction zone geochemical signatures (Pin et al., 2002; Martínez et al., 2011; Arenas et al., 2013), indicating emplacement in a back-arc setting.

The hafnium isotopic data presented herein cast doubt on the widely assumed WAC derivation of the Upper Allochthon. The terrane with the most similar εHf isotopic record is Avalonia (Fig. 12). The Paleoproterozoic (~2.1-1.9 Ga) tectonomagmatic event recorded in Avalonian zircons overlaps in hafnium space with that in the Upper Allochthon, and the Mesoproterozoic (~1.6-1.4 Ga) zircon grains from the Upper Allochthon are also

consistent with an Avalonian source. Although no true basement is exposed in Avalonia, hafnium data presented here for Avalonia (see Fig. 6 and Fig. 7) and Sm-Nd whole rock data from Neoproterozoic igneous rocks in East Avalonia indicate a Mesoproterozoic-Paleoproterozoic basement (~1.2-1.8 Ga, see Nance and Murphy, 1994 and references therein).

The range of inherited zircons in the Devonian ophiolite requires the interaction with a Mesoproterozoic-Paleoproterozoic (~1.4-1.9 Ga) basement. A similar situation exists in the Cenozoic island arcs of Vanuatu, where basaltic arc rocks contain abundant inherited zircons of crustal affinity (Buys et al., 2014). The proto-Vanuatu arc is interpreted to have formed in response to Cretaceous back arc extension and rifting along the eastern margin of Australia, and is now located ~2000 km east of mainland Australia (Schellart et al., 2006). Basaltic island arc magmas were emplaced in an extended ribbon of continental crust leading to an accumulation of inherited zircons that match the igneous rock record of northern Australia (Buys et al., 2014). This evolved back arc setting could represent a potential modern analogue for the Upper Allochthon. Therefore, the Upper-Allochthon could have hosted island-arc type magmatism built on extended continental lithosphere during the Devonian (~400 Ma); a tectonic scenario that is able to explain the mixed juvenile-crustal isotopic signature and the Mesoproterozoic-Archean inherited zircons of the Devonian ophiolites.

8.4 Provenance for the Armorican terranes

The Armorican terranes include most of the Bohemian Massif, the Massif Centrale of France and the Armorican Massif (Fig. 1). The boundary between WAC-derived terranes and Baltica-derived terranes (Avalonia) is located between the Mid German Crystalline Rise (MGCR) and the Rheno-Hercynian Zone in central Germany. The Rheno-Hercynian Zone of the Bohemian Massif is generally considered to be part of the 'Avalonian' ribbon (Tait et al., 2000; Stampfli and Borel, 2002; Linnemann et al., 2008), whereas the remainder of the Bohemian Massif to the south is considered here to be part of the "Armorican" terranes. We compile and interpret the available U-Pb-Hf zircon data for the first time to assess its likely provenance in the late Neoproterozoic-early Cambrian. The detrital zircon hafnium signature is consistent throughout the Armorican terranes and reinforces the common interpretation that the late Neoproterozoic-early Cambrian rocks in the Armorican terranes are derived from the WAC (Linnemann et al., 2008, Fig. 12).
Gerdes and Zeh (2006) analysed 42 detrital zircon grains from a Cambrian metasedimentary rock in the MGCR in the Bohemian Massif for U-Pb-Hf isotopes. The MGCR separates the Saxo-Thuringian Zone and Moldanubian Zone from the Rheno-Hercynian Zone in central Germany, and marks the collision zone between 'Avalonian' components to the north and 'Armorican' components to the south (Linnemann et al., 2004; Zeh and Gerdes, 2010). The detrital zircon spectrum in the MGCR is dominated by Cryogenian-Cambrian (~720-500 Ma) and Paleoproterozoic (~1.8, 2.1-2.0 Ga) grains, with minor Archean populations (~2.5-2.8 Ga). The limited hafnium array suggests a linkage with the WAC.

The Saxo-Thuringian Zone, located south of the MGCR in central Germany, contains Late Neoproterozoic-early Cambrian sequences that yield Paleoproterozoic (~1.8-2.2 Ga) and Archean (~2.5-3.0 Ga) detritus. The zircons overlap with the age and hafnium isotopic array of the West African Craton (Linnemann et al., 2014). Similar Paleoproterozoic and Archean grains have been found in previous U-Pb detrital zircon studies from the Saxo-Thuringian Zone, however no hafnium analyses were conducted (Linnemann et al., 2004; Linnemann et al., 2007; Linnemann et al., 2008). Similarly, Ediacaran siliciclastic rocks of the Tepla-Barrandian complex farther south in the Bohemian Massif also preserve dominant Neoproterozoic (~700-550 Ma),

Paleoproterozoic (~2.1-1.8 Ga) and Archean (2.8-2.5, 3.2 Ga) populations (Drost et al., 2011), a detrital zircon signature interpreted to be consistent with the WAC.

The Armorican Massif (France) is composed of Neoproterozoic-early Cambrian "Cadomian" magmatic and volcaniclastic rocks which overlie a composite Paleoproterozoic (Icartian gneiss, ~2.0 Ga) basement (Chantraine et al., 2001). εHf data from the ~2.0 Ga zircons in the Icartian gneiss overlap with ~2.0 Ga zircons in the WAC compilation (Fig. 11a). The link between pre-Cadomian arc "Armorican" basement and the WAC are also reinforced by similar whole rock Nd isotopic compositions for the ~2.0 Ga rocks (Samson and D'Lemos, 1998). Detrital zircons from late Neoproterozoic sedimentary rocks in the north Armorican domain of Brittany are devoid of Mesoproterozoic zircons and have also been interpreted to indicate a WAC provenance (Fernández-Suárez et al., 2002).

9. CONCLUDING REMARKS

We present new hafnium isotopic detrital zircon data from Neoproterozoic-Silurian sequences in Avalonia, autochthonous Iberia and the Upper Allochthon of Iberia. We compile this data with existing hafnium isotopic data from Avalonia, Iberia and the Armorican terranes to reassess the provenance of these regions from Gondwana and Baltica during the late Neoproterozoic.

We have compiled comprehensive detrital and magmatic zircon hafnium isotope arrays from the West African Craton, Saharan Metacraton, Arabian-Nubian Shield, Amazonia and Baltica to demonstrate that they are distinctive in character and provide insight into the crustal evolution of the basement rocks in the Appalachian-Variscan orogen. We demonstrate that the hafnium arrays can be used to trace detrital zircons in exotic continental terranes now located within the Appalachian-Variscan orogenic belt to their cratonic sources and provide a more detailed resolution than Sm-Nd whole rock isotopic studies.

The hafnium isotopic data suggest that Avalonia inherited a hitherto unrecognized Baltican hafnium isotopic signature in the early Neoproterozoic (~975-750 Ma) during the deposition of the Gamble Brook Formation. The hafnium array indicates that the oceanic arc was initially built on a sliver of Paleoproterozoic crust (~1.9 Ga) that had previously separated from Baltica. Early oceanic arc magmatism commenced at ~800-760 Ma and involved a mixture of juvenile material with "Grenvillian-type ~2.0-1.0 Ga crust. Together, these rocks form the basement to the Late Neoproterozoic Avalonian arc. At ~640 Ma the hafnium isotope array becomes more evolved and indicates the introduction of an older crustal component (Archean), consistent with the accretion of Avalonia to a continental margin by that time. During the late Neoproterozoic-early Ordovician, Avalonian rocks inherited detritus recycled from the underlying Baltica-derived basement, the proximal ~760-550 Ma arc rocks and an Archean craton (~2.5-2.8 Ga). The hafnium array from Edicaran-Ordovician rocks has isotopic similarities to both Baltica and/or Amazonia, and provenance from either source cannot be confidently interpreted on the basis of the present hafnium isotope arrays.

The autochthonous zones of Iberia have a clear affinity with the Saharan Metacraton in the late Neoproterozoic-Ordovician. The late Neoproterozoic-Cambrian rocks of the Upper Allochthon (NW Iberia) do not display an affinity to cratonic Gondwana; instead the hafnium isotopic array is closest is that of Avalonia. A compilation of published U-Pb-Hf zircon data from the Armorican terranes (Armorican Massif, Massif Centrale of France and the Bohemian Massif) reinforces a strong link to the West African Craton in the late Neoproterozoic.

The data presented here highlight the power of hafnium isotope arrays for defining

the crustal evolution of ancient cratonic regions. These arrays can be used to isotopically 'fingerprint' a craton, and we demonstrate the arrays are traceable through many stages in the evolution of mobile microcontinental terranes. The data have direct implications for late Neoproterozoic paleogeography, the geodynamic evolution of the Rheic Ocean and subsequent amalgamation of Pangea.

ACKNOWLEDGEMENTS

We are delighted to contribute to this special volume in celebration of the career of Cecilio Quesada. We thank Daniel Pastor-Galan for assistance in the field and for providing some Iberian samples. Javier Fernandez-Suarez and Jessica Shaw also provided Iberian samples. We also thank Justin Payne for help with isotope analysis. We thank Donnelly Archibald for invaluable local knowledge and assistance during field work in Nova Scotia. We are grateful to Dr. Antonio Azor for the very helpful revisions of the manuscript. Financial support to G.G.-A was supplied by Research Project ODRE III ('Oroclines and Delamination: Relations and Effects') CGL2013-46061. This work was funded by Australian Research Council DP 120104004 and JBM acknowledges the ongoing support of the N.S.E.R.C Canada. Bonnie Henderson is a recipient of an Australian Post Graduate award.

REFERENCES

Abati, J., Aghzer, A.M., Gerdes, A., Ennih, N., 2012. Insights on the crustal evolution of the West African Craton from Hf isotopes in detrital zircons from the Anti-Atlas belt. Precambrian Research 212–213, 263-274.

Abati, J., Castiñeiras, P., Arenas, R., Fernández-Suárez, J., Gómez Barreiro, J., Wooden, J.L., 2007. Using SHRIMP zircon dating to unravel tectonothermal events in arc environments. The early Palaeozoic arc of NW Iberia revisited. Terra Nova 19, 432-439.

Abati, J., Dunning, G.R., Arenas, R., Díaz García, F., González Cuadra, P., Martínez Catalán, J.R., Andonaegui, P., 1999. Early Ordovician orogenic event in Galicia (NW Spain): Evidence from U-Pb ages in the uppermost unit of the Ordenes Complex. Earth and Planetary Science Letters 165, 213-228.

Abati, J., Gerdes, A., Suárez, J.F., Arenas, R., Whitehouse, M.J., Fernández, R.D., 2010. Magmatism and early-Variscan continental subduction in the northern Gondwana margin recorded in zircons from the basal units of Galicia, NW Spain. Geological Society of America Bulletin 122, 219-235.

Abdelsalam, M.G., Gao, S.S., Liégeois, J.-P., 2011. Upper mantle structure of the Saharan Metacraton. Journal of African Earth Sciences 60, 328-336.

Abdelsalam, M.G., Liégeois, J.-P., Stern, R.J., 2002. The saharan metacraton. Journal of African Earth Sciences 34, 119-136.

Albert, R., Arenas, R., Gerdes, A., Martínez, S.S., Fernández-Suárez, J., Fuenlabrada, J., 2014. Provenance of the Variscan Upper Allochthon (Cabo Ortegal Complex, NW Iberian Massif). Gondwana Research.

Ali, K.A., Wilde, S.A., Stern, R.J., Moghazi, A.-K.M., Ameen, S.M.M., 2013. Hf isotopic composition of single zircons from Neoproterozoic arc volcanics and post-collision granites, Eastern Desert of Egypt: Implications for crustal growth and recycling in the Arabian-Nubian Shield. Precambrian Research 239, 42-55.

Andersen, T., Graham, S., Sylvester, A.G., 2009. The geochemistry, Lu–Hf isotope systematics, and petrogenesis of Late Mesoproterozoic A-type granites in southwestern Fennoscandia. The Canadian Mineralogist 47, 1399-1422.

Andersen, T., Griffin, W., Pearson, N., 2002. Crustal evolution in the SW part of the Baltic Shield: the Hf isotope evidence. Journal of Petrology 43, 1725-1747.

Anderson, T., 2005. Detrital zircons as tracers of sedimentary provenance: limiting conditions from statistics and numerical simulation. Chemical Geology 216, 249-270.

Andersson, U., Begg, G., Griffin, W.L., Högdahl, K., 2011. Ancient and juvenile components in the continental crust and mantle: Hf isotopes in zircon from Svecofennian magmatic rocks and rapakivi granites in Sweden. Lithosphere 3, 409-419.

Andonaegui, P., Castiñeiras, P., Cuadra, P.G., Arenas, R., Martínez, S.S., Abati, J., García, F.D., Catalán, J.R.M., 2012. The Corredoiras orthogneiss (NW Iberian Massif): Geochemistry and geochronology of the Paleozoic magmatic suite developed in a peri-Gondwanan arc. Lithos 128–131, 84-99.

Arenas, R., Catalán, J.R.M., Martínez, S.S., Fernández-Suárez, J., Andonaegui, P., Pearce, J.A., Corfu, F., 2007. The Vila de Cruces ophiolite: a remnant of the early Rheic Ocean in the Variscan suture of Galicia (northwest Iberian Massif). The Journal of geology 115, 129-148.

Arenas, R., Díez Fernández, R., Sánchez Martínez, S., Gerdes, A., Fernández-Suárez, J., Albert, R., 2014. Two-stage collision: Exploring the birth of Pangea in the Variscan terranes. Gondwana Research 25, 756-763.

Arenas, R., Martínez, S.S., Gerdes, A., Albert, R., Fernández, R.D., Andonaegui, P., 2013. Re-interpreting the Devonian ophiolites involved in the Variscan suture: U–Pb and Lu–Hf zircon data of the Moeche Ophiolite (Cabo Ortegal Complex, NW Iberia). Int J Earth Sci (Geol Rundsch), 1-18.

Arenas, R., Sánchez Martínez, S., Castiñeiras, P., Jeffries, T.E., Díez Fernández, R., Andonaegui, P., 2009. The basal tectonic mélange of the Cabo Ortegal Complex (NW Iberian Massif): a key unit in the suture of Pangea.

Azcárraga, J., Ábalos, B., Gil Ibarguchi, J.I., 2002. On the relationship between kilometer-scale sheath folds, ductile thrusts and minor structures in the basal high-pressure units of the Cabo Ortegal complex (NW Spain). Journal of structural geology 24, 1971-1989.

Balintoni, I., Balica, C., 2013. Carpathian peri-Gondwanan terranes in the East Carpathians (Romania): A testimony of an Ordovician, North-African orogeny. Gondwana Research 23, 1053-1070.

Ballèvre, M., Catalán, J.R.M., López-Carmona, A., Pitra, P., Abati, J., Fernández, R.D., Ducassou, C., Arenas, R., Bosse, V., Castiñeiras, P., 2014. Correlation of the nappe stack in the Ibero-Armorican arc across the Bay of Biscay: a joint French–Spanish project. Geological Society, London, Special Publications 405, SP405. 413.

Barr, S.M., Davis, D.W., Kamo, S., White, C.E., 2003. Significance of U–Pb detrital zircon ages in quartzite from peri-Gondwanan terranes, New Brunswick and Nova Scotia, Canada. Precambrian Research 126, 123-145.

Barr, S.M., Hamilton, M.A., Samson, S.D., Satkoski, A.M., White, C.E., Murphy, J.B., 2012. Provenance variations in northern Appalachian Avalonia based on detrital zircon age patterns in Ediacaran and Cambrian sedimentary rocks, New Brunswick and Nova Scotia, Canada. Canadian Journal of Earth Sciences 49, 533-546.

Barr, S.M., Hegner, E., 1992. Nd isotopic compositions of felsic igneous rocks in Cape Breton Island, Nova Scotia. Canadian Journal of Earth Sciences 29, 650-657.

Barreiro, J.G., Catalán, J.R.M., Arenas, R., Castiñeiras, P., Abati, J., García, F.D., Wijbrans, J.R., 2007. Tectonic evolution of the upper allochthon of the Órdenes Complex (northwestern Iberian Massif): structural constraints to a polyorogenic peri-Gondwanan terrane. Geological Society of America Special Papers 423, 315-332.

Batumike, J., Griffin, W., O'Reilly, S., Belousova, E., Pawlitschek, M., 2009. Crustal evolution in the central Congo-Kasai Craton, Luebo, DR Congo: Insights from zircon U–Pb ages, Hf-isotope and

trace-element data. Precambrian Research 170, 107-115.

Be'eri-Shlevin, Y., Avigad, D., Gerdes, A., Zlatkin, O., 2014. Detrital zircon U–Pb–Hf systematics of Israeli coastal sands: new perspectives on the provenance of Nile sediments. Journal of the Geological Society 171, 107-116.

Beranek, L.P., van Staal, C.R., McClelland, W.C., Israel, S., Mihalynuk, M.G., 2013. Detrital zircon Hf isotopic compositions indicate a northern Caledonian connection for the Alexander terrane. Lithosphere 5, 163-168.

Black, R., Liegeois, J.-P., 1993. Cratons, mobile belts, alkaline rocks and continental lithospheric mantle: the Pan-African testimony. Journal of the Geological Society 150, 89-98.

Blichert-Toft, J., Albarède, F., 1997. The Lu-Hf isotope geochemistry of chondrites and the evolution of the mantle-crust system. Earth and Planetary Science Letters 148, 243-258.

Bogdanova, S.V., Bingen, B., Gorbatschev, R., Kheraskova, T.N., Kozlov, V.I., Puchkov, V.N., Volozh, Y.A., 2008. The East European Craton (Baltica) before and during the assembly of Rodinia. Precambrian Research 160, 23-45.

Buchan, K., Mertanen, S., Park, R., Pesonen, L., Elming, S.-Å., Abrahamsen, N., Bylund, G., 2000. Comparing the drift of Laurentia and Baltica in the Proterozoic: the importance of key palaeomagnetic poles. Tectonophysics 319, 167-198.

Buys, J., Spandler, C., Holm, R.J., Richards, S.W., 2014. Remnants of ancient Australia in Vanuatu: Implications for crustal evolution in island arcs and tectonic development of the southwest Pacific. Geology 42, 939-942.

Catalán, J.R.M., Arenas, R., Abati, J., Martínez, S.S., García, F.D., Suárez, J.F., Cuadra, P.G., Castiñeiras, P., Barreiro, J.G., Montes, A.D., 2009. A rootless suture and the loss of the roots of a mountain chain: the Variscan belt of NW Iberia. Comptes Rendus Geoscience 341, 114-126.

Catalán, J.R.M., FernÁndez-SuÁrez, J., Jenner, G.A., Belousova, E., Montes, A., 2004. Provenance constraints from detrital zircon U–Pb ages in the NW Iberian Massif: implications for Palaeozoic plate configuration and Variscan evolution. Journal of the Geological Society 161, 463-476.

Catalán, J.R.M., FERNáNDEZ-SUáREZ, J., Meireles, C., Clavijo, E.G., Belousova, E., Saeed, A., 2008. U–Pb detrital zircon ages in synorogenic deposits of the NW Iberian Massif (Variscan belt): interplay of Devonian–Carboniferous sedimentation and thrust tectonics. Journal of the Geological Society 165, 687-698.

Cawood, P.A., Hawkesworth, C.J., Dhuime, B., 2012. Detrital zircon record and tectonic setting. Geology 40, 875-878.

Cawood, P.A., McCausland, P.J.A., Dunning, G.R., 2001. Opening Iapetus: Constraints from the Laurentian margin in Newfoundland. Geological Society of America Bulletin 113, 443-453.

Cawood, P.A., Pisarevsky, S.A., 2006. Was Baltica right-way-up or upside-down in the Neoproterozoic? Journal of the Geological Society 163, 753-759.

Chantraine, J., Egal, E., Thiéblemont, D., Le Goff, E., Guerrot, C., Ballèvre, M., Guennoc, P., 2001. The Cadomian active margin (North Armorican Massif, France): a segment of the North Atlantic Panafrican belt. Tectonophysics 331, 1-18.

Cocks, L., McKerrow, W., Van Staal, C., 1997. The margins of Avalonia. Geological Magazine 134, 627-636.

Collins, A.S., Pisarevsky, S.A., 2005. Amalgamating eastern Gondwana: The evolution of the Circum-Indian Orogens. Earth-Science Reviews 71, 229-270.

Cordani, U.G., Brito-Neves, B.B., D'Agrella-Filho, M.S., 2003. From Rodinia to Gondwana: A Review of the Available Evidence from South America. Gondwana Research 6, 275-283.

Cordani, U.G., Teixeira, W., 2007. Proterozoic accretionary belts in the Amazonian Craton. Geological Society of America Memoirs 200, 297-320.

Cordani, U.G., Teixeira, W., D'Agrella-Filho, M.S., Trindade, R.I., 2009. The position of the Amazonian Craton in supercontinents. Gondwana Research 15, 396-407.

Daly, J., McLelland, J., 1991. Juvenile middle Proterozoic crust in the Adirondack highlands, Grenville province, northeastern North America. Geology 19, 119-122.

De Waele, B., Wingate, M.T., Fitzsimons, I.C., Mapani, B.S., 2003. Untying the Kibaran knot: A reassessment of Mesoproterozoic correlations in southern Africa based on SHRIMP U-Pb data from the Irumide belt. Geology 31, 509-512.

Dhuime, B., Hawkesworth, C., Cawood, P., 2011. When continents formed. Science 331, 154-155.

Dickinson, W.R., Gehrels, G.E., 2009. U-Pb ages of detrital zircons in Jurassic eolian and associated sandstones of the Colorado Plateau: Evidence for transcontinental dispersal and intraregional recycling of sediment. Geological Society of America Bulletin 121, 408-433.

Díez Fernández, R., Castiñeiras, P., Gómez Barreiro, J., 2012. Age constraints on Lower Paleozoic convection system: Magmatic events in the NW Iberian Gondwana margin. Gondwana Research 21, 1066-1079.

Díez Fernández, R., Catalán, J.R.M., Gerdes, A., Abati, J., Arenas, R., Fernández-Suárez, J., 2010. U–Pb ages of detrital zircons from the Basal allochthonous units of NW Iberia: Provenance and paleoposition on the northern margin of Gondwana during the Neoproterozoic and Paleozoic. Gondwana Research 18, 385-399.

Díez Fernández, R., Martínez Catalán, J.R., Arenas Martín, R., Abati Gómez, J., 2011. Tectonic evolution of a continental subduction-exhumation channel: Variscan structure of the basal allochthonous units in NW Spain. Tectonics 30, TC3009.

Doig, R., Murphy, J.B., Nance, R.D., 1991. U-Pb geochronology of Late Proterozoic rocks of the eastern Cobequid Highlands, Avalon Composite Terrane, Nova Scotia. Canadian Journal of Earth Sciences 28, 504-511.

Doig, R., Murphy, J.B., Nance, R.D., 1993. Tectonic significance of the late Proterozoic Economy River gneiss, Cobequid Highlands, Avalon composite terrane, Nova Scotia. Canadian Journal of Earth Sciences 30, 474-479.

Dörr, W., Zulauf, G., Gerdes, A., Lahaye, Y., Kowalczyk, G., 2015. A hidden Tonian basement in the eastern Mediterranean: Age constraints from U–Pb data of magmatic and detrital zircons of the External Hellenides (Crete and Peloponnesus). Precambrian Research 258, 83-108.

Drost, K., Gerdes, A., Jeffries, T., Linnemann, U., Storey, C., 2011. Provenance of Neoproterozoic and early Paleozoic siliciclastic rocks of the Teplá-Barrandian unit (Bohemian Massif): Evidence from U–Pb detrital zircon ages. Gondwana Research 19, 213-231.

Eckelmann, K., Nesbor, H.-D., Königshof, P., Linnemann, U., Hofmann, M., Lange, J.-M., Sagawe, A., 2014. Plate interactions of Laurussia and Gondwana during the formation of Pangaea — Constraints from U–Pb LA–SF–ICP–MS detrital zircon ages of Devonian and Early Carboniferous siliciclastics of the Rhenohercynian zone, Central European Variscides. Gondwana Research 25, 1484-1500.

Fernández-Suárez, J., Arenas, R., Abati, J., Catalán, J.M., Whitehouse, M., Jeffries, T., 2007. U-Pb chronometry of polymetamorphic high-pressure granulites: An example from the allochthonous terranes of the NW Iberian Variscan belt. Geological Society of America Memoirs 200, 469-488.

Fernández-Suárez, J., Díaz García, F., Jeffries,

T.E., Arenas, R., Abati, J., 2003. Constraints on the provenance of the uppermost allochthonous terrane of the NW Iberian Massif: Inferences from detrital zircon U-Pb ages. Terra Nova 15, 138-144.

Fernández-Suárez, J., Gutiérrez-Alonso, G., Jenner, G., Tubrett, M., 2000. New ideas on the Proterozoic-Early Palaeozoic evolution of NW Iberia: insights from U–Pb detrital zircon ages. Precambrian Research 102, 185-206.

Fernández-Suárez, J., Gutiérrez-Alonso, G., Pastor-Galán, D., Hofmann, M., Murphy, J.B., Linnemann, U., 2014. The Ediacaran–Early Cambrian detrital zircon record of NW Iberia: possible sources and paleogeographic constraints. Int J Earth Sci (Geol Rundsch) 103, 1335-1357.

Fernández-Suárez, J., Gutiérrez Alonso, G., Jeffries, T.E., 2002. The importance of along-margin terrane transport in northern Gondwana: Insights from detrital zircon parentage in Neoproterozoic rocks from Iberia and Brittany. Earth and Planetary Science Letters 204, 75-88.

Fernández-Suárez, J., Alonso, G.G., Cox, R., Jenner, G.A., 2002. Assembly of the Armorica Microplate: A Strike-Slip Terrane Delivery? Evidence from U-Pb Ages of Detrital Zircons. The Journal of geology 110, 619-626.

Fombella, M., 1979. Palinologia de la Formacion Oville al norte y sur de la Cordillera Cantabrica, España. Palinología 1, 1-15.

Fortey, R.A., Cocks, L.R.M., 2003. Palaeontological evidence bearing on global Ordovician–Silurian continental reconstructions. Earth-Science Reviews 61, 245-307.

Foster, D.A., Goscombe, B.D., Newstead, B., Mapani, B., Mueller, P.A., Gregory, L.C., Muvangua, E., 2014. U–Pb age and Lu–Hf isotopic data of detrital zircons from the Neoproterozoic Damara Sequence: Implications for Congo and Kalahari before Gondwana. Gondwana Research.

Gámez Vintaned, J., Mayoral, E., Gozalo, R., 2000. Lower and Middle Cambrian trace fossils from the Láncara and Oville formations in the area of Presa del Porma (Cantabrian Zone, northern Spain). Cambrian from the southern edge. INSUGEO, Miscelánea 6, 91-94.

Gärtner, A., Villeneuve, M., Linnemann, U., Gerdes, A., Youbi, N., Guillou, O., Rjimati, E.-C., 2014. History of the West African Neoproterozoic Ocean: Key to the geotectonic history of circum-Atlantic Peri-Gondwana (Adrar Souttouf Massif, Moroccan Sahara). Gondwana Research.

Gee, D.G., Pease, V., 2004. The Neoproterozoic Timanide Orogen of Eastern Baltica. Geological Society of London.

Gerdes, A., Zeh, A., 2006. Combined U–Pb and Hf isotope LA-(MC-) ICP-MS analyses of detrital zircons: comparison with SHRIMP and new constraints for the provenance and age of an Armorican metasediment in Central Germany. Earth and Planetary Science Letters 249, 47-61.

Glorie, S., De Grave, J., Singh, T., Payne, J.L., Collins, A.S., 2014. Crustal root of the Eastern Dharwar Craton: Zircon U–Pb age and Lu–Hf isotopic evolution of the East Salem Block, southeast India. Precambrian Research 249, 229-246.

Griffin, W., Powell, W., Pearson, N., O'Reilly, S., 2008. GLITTER: data reduction software for laser ablation ICP-MS. Laser Ablation-ICP-MS in the Earth Sciences. Mineralogical Association of Canada Short Course Series 40, 204-207.

Griffin, W.L., Belousova, E.A., Shee, S.R., Pearson, N.J., O'Reilly, S.Y., 2004. Archean crustal evolution in the northern Yilgarn Craton: U–Pb and Hf-isotope evidence from detrital zircons. Precambrian Research 131, 231-282.

Griffin, W.L., Pearson, N.J., Belousova, E., Jackson, S.E., van Achterbergh, E., O'Reilly, S.Y., Shee, S.R., 2000. The Hf isotope composition of cratonic mantle: LAM-MC-ICPMS analysis of zircon megacrysts in kimberlites. Geochimica et Cosmochimica Acta 64, 133-147.

Griffin, W.L., Wang, X., Jackson, S.E., Pearson, N.J., O'Reilly, S.Y., Xu, X., Zhou, X., 2002. Zircon chemistry and magma mixing, SE China: In-situ analysis of Hf isotopes, Tonglu and Pingtan igneous complexes. Lithos 61, 237-269.

Gutiérrez-Alonso, G., Fernández-Suárez, J., Jeffries, T.E., Jenner, G.A., Tubrett, M.N., Cox, R., Jackson, S.E., 2003. Terrane accretion and dispersal in the northern Gondwana margin. An Early Paleozoic analogue of a long-lived active margin. Tectonophysics 365, 221-232.

Gutiérrez-Alonso, G., Fernández-Suárez, J., Weil, A.B., Murphy, J.B., Nance, R.D., Corfú, F., Johnston, S.T., 2008. Self-subduction of the Pangaean global plate. Nature Geoscience 1, 549-553.

Gutiérrez Alonso, G., Fernández-Suárez, J., Pastor-Galán, D., Johnston, S.T., Linnemann, U., Hoffman, M., Shaw, J., Colmenero, J.R., Hernandez, P., 2015. Whence come detrital zircons in Siluro-Devonian rocks from Iberia? Geological Society of America Bulletin.

Hawkesworth, C.J., Kemp, A.I.S., 2006. Using hafnium and oxygen isotopes in zircons to unravel the record of crustal evolution. Chemical Geology 226, 144-162.

Hegner, E., Kröner, A., 2000. Review of Nd isotopic data and xenocrystic and detrital zircon ages from the pre-Variscan basement in the eastern Bohemian Massif: Speculations on palinspastic reconstructions, pp. 113-129.

Henderson, B., Collins, A.S., Payne, J., Forbes, C., Saha, D., 2014. Geologically constraining India in Columbia: The age, isotopic provenance and geochemistry of the protoliths of the Ongole Domain, Southern Eastern Ghats, India. Gondwana Research 26, 888-906.

Hibbard, J., 2006. Lithotectonic Map of the Appalachian Orogen: Canada-United States of America. Commission géologique du Canada.

Hibbard, J.P., van Staal, C.R., Rankin, D.W., 2010. Comparative analysis of the geological evolution of the northern and southern Appalachian orogen: Late Ordovician-Permian. Geological Society of America Memoirs 206, 51-69.

Howard, K.E., Hand, M., Barovich, K.M., Payne, J.L., Belousova, E.A., 2011. U–Pb, Lu–Hf and Sm–Nd isotopic constraints on provenance and depositional timing of metasedimentary rocks in the western Gawler Craton: Implications for Proterozoic reconstruction models. Precambrian Research 184, 43-62.

Howard, K.E., Hand, M., Barovich, K.M., Reid, A., Wade, B.P., Belousova, E.A., 2009. Detrital zircon ages: Improving interpretation via Nd and Hf isotopic data. Chemical Geology 262, 277-292.

Hurai, V., Paquette, J.L., Huraiová, M., Konečný, P., 2010. U–Th–Pb geochronology of zircon and monazite from syenite and pincinite xenoliths in Pliocene alkali basalts of the intra-Carpathian back-arc basin. Journal of Volcanology and Geothermal Research 198, 275-287.

Iizuka, T., Campbell, I.H., Allen, C.M., Gill, J.B., Maruyama, S., Makoka, F., 2013. Evolution of the African continental crust as recorded by U–Pb, Lu–Hf and O isotopes in detrital zircons from modern rivers. Geochimica et Cosmochimica Acta 107, 96-120.

Iizuka, T., Komiya, T., Rino, S., Maruyama, S., Hirata, T., 2010. Detrital zircon evidence for Hf isotopic evolution of granitoid crust and continental growth. Geochimica et Cosmochimica Acta 74, 2450-2472.

Ireland, T.R., Flottmann, T., Fanning, C.M., Gibson, G.M., Preiss, W.V., 1998. Development of the early Paleozoic Pacific margin of Gondwana from detrital-zircon ages across the Delamerian orogen. Geology 26, 243-246.

Jackson, S.E., Pearson, N.J., Griffin, W.L., Belousova, E.A., 2004. The application of laser ablation-inductively coupled plasma-mass spectrometry to in situ U–Pb zircon geochronology. Chemical Geology 211, 47-69.

Johansson, Å., 2014. From Rodinia to Gondwana with the 'SAMBA' model—A distant view from Baltica towards Amazonia and beyond. Precambrian Research 244, 226-235.

Kamp, P.J., 1999. Tracking crustal processes by FT thermochronology in a forearc high (Hikurangi margin, New Zealand) involving Cretaceous subduction termination and mid-Cenozoic subduction initiation. Tectonophysics 307, 313-343.

Katzung, G., Giese, U., Maletz, J., Servais, T., Van Grootel, G., 1995. The eastern end of Avalonia: continuation into northern central Europe.

Keppie, J.D., Davis, D., Krogh, T., 1998. U-Pb geochronological constraints on Precambrian stratified units in the Avalon Composite Terrane of Nova Scotia, Canada: tectonic implications. Canadian Journal of Earth Sciences 35, 222-236.

Keppie, J.D., Keppie, D.F., 2014. Ediacaran–Middle Paleozoic Oceanic Voyage of Avalonia from Baltica via Gondwana to Laurentia: Paleomagnetic, Faunal and Geological Constraints. Geoscience Canada 41, 5-18.

Keppie, J.D., Nance, R.D., Murphy, J.B., Dostal, J., 2003. Tethyan, Mediterranean, and Pacific analogues for the Neoproterozoic-Paleozoic birth and development of peri-Gondwanan terranes and their transfer to Laurentia and Laurussia. Tectonophysics 365, 195-219.

Kerr, A., Jenner, G.A., Fryer, B.J., 1995. Sm–Nd isotopic geochemistry of Precambrian to Paleozoic granitoid suites and the deep-crustal structure of the southeast margin of the Newfoundland Appalachians. Canadian Journal of Earth Sciences 32, 224-245.

Kinny, P.D., Maas, R., 2003. Lu-Hf and Sm-Nd isotope systems in zircon, in: Hanchar, J.M., Hoskin, P.W.O. (Eds.), Zircon, pp. 327-341.

Košler, J., Fonneland, H., Sylvester, P., Tubrett, M., Pedersen, R.B., 2002. U-Pb dating of detrital zircons for sediment provenance studies - A comparison of laser ablation ICPMS and SIMS techniques. Chemical Geology 182, 605-618.

Kristoffersen, M., 2011. Provenance of the Asker Group, Oslo Rift: A detrital zircon U-Pb and Lu-Hf study.

Krogh, T., Strong, D., O'brien, S., Papezik, V., 1988. Precise U-Pb zircon dates from the Avalon Terrane in Newfoundland. Canadian Journal of Earth Sciences 25, 442-453.

Kroner, A., Ekwueme, B.N., Pidgeon, R.T., 2001. The Oldest Rocks in West Africa: SHRIMP Zircon Age for Early Archean Migmatitic Orthogneiss at. Journal of Geology 109, 399.

Kuznetsov, N., Belousova, E., Alekseev, A., Romanyuk, T., 2014. New data on detrital zircons from the sandstones of the lower Cambrian Brusov Formation (White Sea region, East-European Craton): unravelling the timing of the onset of the Arctida–Baltica collision. International Geology Review 56, 1945-1963.

Kuznetsov, N., Natapov, L., Belousova, E., OReilly, S.Y., Griffin, W.L., 2010. Geochronological, geochemical and isotopic study of detrital zircon suites from late Neoproterozoic clastic strata along the NE margin of the East European Craton: implications for plate tectonic models. Gondwana Research 17, 583-601.

Kydonakis, K., Kostopoulos, D., Poujol, M., Brun, J.-P., Papanikolaou, D., Paquette, J.-L., 2014. The dispersal of the Gondwana Super-fan System in the eastern Mediterranean: New insights from detrital zircon geochronology. Gondwana Research 25, 1230-1241.

Lahtinen, R., Huhma, H., Kousa, J., 2002. Contrasting source components of the Paleoproterozoic Svecofennian metasediments: Detrital zircon U–Pb, Sm–Nd and geochemical data. Precambrian Research 116, 81-109.

Landing, E., 1996a. Avalon: Insular continent by the latest Precambrian, pp. 29-63.

Landing, E., 1996b. Avalon: Insular continent by the latest Precambrian. SPECIAL PAPERS-GEOLOGICAL SOCIETY OF AMERICA, 29-64.

Landing, E., Murphy, J.B., 1991. Uppermost Precambrian(?)-lower Cambrian of mainland Nova Scotia: faunas, depositional environments, and stratigraphic revision. Journal of Paleontology 65, 382-396.

Lees, D.C., Fortey, R.A., Cocks, L.R.M., 2002. Quantifying paleogeography using biogeography: a test case for the Ordovician and Silurian of Avalonia based on brachiopods and trilobites. Paleobiology 28, 343-363.

Levashova, N.M., Bazhenov, M.L., Meert, J.G., Kuznetsov, N.B., Golovanova, I.V., Danukalov, K.N., Fedorova, N.M., 2013. Paleogeography of Baltica in the Ediacaran: Paleomagnetic and geochronological data from the clastic Zigan Formation, South Urals. Precambrian Research 236, 16-30.

Li, Z.X., Bogdanova, S.V., Collins, A.S., Davidson, A., De Waele, B., Ernst, R.E., Fitzsimons, I.C.W., Fuck, R.A., Gladkochub, D.P., Jacobs, J., Karlstrom, K.E., Lu, S., Natapov, L.M., Pease, V., Pisarevsky, S.A., Thrane, K., Vernikovsky, V., 2008. Assembly, configuration, and break-up history of Rodinia: A synthesis. Precambrian Research 160, 179-210.

Linnemann, U., Gerdes, A., Drost, K., Buschmann, B., 2007. The continuum between Cadomian orogenesis and opening of the Rheic Ocean: Constraints from LA-ICP-MS U-Pb zircon dating and analysis of plate-tectonic setting (Saxo-Thuringian zone, northeastern Bohemian Massif, Germany). Geological Society of America Special Papers 423, 61-96.

Linnemann, U., Gerdes, A., Hofmann, M., Marko, L., 2014. The Cadomian Orogen: Neoproterozoic to Early Cambrian crustal growth and orogenic zoning along the periphery of the West African Craton—Constraints from U–Pb zircon ages and Hf isotopes (Schwarzburg Antiform, Germany). Precambrian Research.

Linnemann, U., Herbosch, A., Liégeois, J.-P., Pin, C., Gärtner, A., Hofmann, M., 2012. The Cambrian to Devonian odyssey of the Brabant Massif within Avalonia: A review with new zircon ages, geochemistry, Sm–Nd isotopes, stratigraphy and palaeogeography. Earth-Science Reviews 112, 126-154.

Linnemann, U., McNaughton, N.J., Romer, R.L., Gehmlich, M., Drost, K., Tonk, C., 2004. West African provenance for Saxo-Thuringia (Bohemian Massif): Did Armorica ever leave pre-Pangean Gondwana? - U/Pb-SHRIMP zircon evidence and the Nd-isotopic record. Int J Earth Sci (Geol Rundsch) 93, 683-705.

Linnemann, U., Pereira, F., Jeffries, T.E., Drost, K., Gerdes, A., 2008. The Cadomian Orogeny and the opening of the Rheic Ocean: the diacrony of geotectonic processes constrained by LA-ICP-MS U–Pb zircon dating (Ossa-Morena and Saxo-Thuringian Zones, Iberian and Bohemian Massifs). Tectonophysics 461, 21-43.

Linol, B., de Wit, M.J., Barton, E., de Wit, M.J.C., Guillocheau, F., U–Pb detrital zircon dates and source provenance analysis of Phanerozoic sequences of the Congo Basin, central Gondwana. Gondwana Research.

López-Carmona, A., Abati, J., Pitra, P., Lee, J.K., 2014. Retrogressed lawsonite blueschists from the NW Iberian Massif: P–T–t constraints from thermodynamic modelling and 40Ar/39Ar geochronology. Contrib Mineral Petrol 167, 1-20.

Lopez-Carmona, A., Pitra, P., Abati, J., 2013. Blueschist-facies metapelites from the Malpica–Tui Unit (NW Iberian Massif): phase equilibria modelling and H2O and Fe2O3 influence in high-pressure assemblages. Journal of Metamorphic Geology 31, 263-280.

Lotze, F., Sdzuy, K., 1961. Das Kambrium Spaniens. Akademie der Wissenschaften und der Literatur; in Kommision bei F. Steiner, Wiesbaden.

Martínez Catalán, J.R., Arenas, R., Abati, J.,

Martínez, S.S., García, F.D., Suárez, J.F., Cuadra, P.G., Castiñeiras, P., Barreiro, J.G., Montes, A.D., Clavijo, E.G., Pascual, F.J.R., Andonaegui, P., Jeffries, T.E., Alcock, J.E., Fernández, R.D., Carmona, A.L., 2009. A rootless suture and the loss of the roots of a mountain chain: The Variscan belt of NW Iberia. Comptes Rendus - Geoscience 341, 114-126.

Martínez Catalán, J.R., Arenas, R., Díaz García, F., Rubio Pascual, F.J., Abati, J., Marquínez, J., 1996. Variscan exhumation of a subducted Paleozoic continental margin: The basal units of the Ordenes Complex, Galicia, NW Spain. Tectonics 15, 106-121.

Martínez, S.S., Arenas, R., García, F.D., Catalán, J.R.M., Gómez-Barreiro, J., Pearce, J.A., 2007. Careón ophiolite, NW Spain: suprasubduction zone setting for the youngest Rheic Ocean floor. Geology 35, 53-56.

Martínez, S.S., Arenas, R., Gerdes, A., Castiñeiras, P., Potrel, A., Fernández-Suárez, J., 2011. Isotope geochemistry and revised geochronology of the Purrido Ophiolite (Cabo Ortegal Complex, NW Iberian Massif): Devonian magmatism with mixed sources and involved Mesoproterozoic basement. Journal of the Geological Society 168, 733-750.

Martínez, S.S., Gerdes, A., Arenas, R., Abati, J., 2012. The Bazar Ophiolite of NW Iberia: a relic of the Iapetus–Tornquist Ocean in the Variscan suture. Terra Nova 24, 283-294.

Matte, P., Capdevila, R., 1978. Tectonique en grands plis couchés et plissements superposés d'âge hercynien dans la série de Ordenes–Betanzos (Galice Occidentale). Cuadernos del seminario de estudios cerámicos de Sargadelos 27, 193-201.

Matteini, M., Junges, S.L., Dantas, E.L., Pimentel, M.M., Bühn, B., 2010. In situ zircon U–Pb and Lu–Hf isotope systematic on magmatic rocks: Insights on the crustal evolution of the Neoproterozoic Goiás Magmatic Arc, Brasília belt, Central Brazil. Gondwana Research 17, 1-12.

Mazur, S., Kröner, A., Szczepański, J., Turniak, K., Hanžl, P., Melichar, R., Rodionov, N.V., Paderin, I., Sergeev, S.A., 2010. Single zircon U–Pb ages and geochemistry of granitoid gneisses from SW Poland: evidence for an Avalonian affinity of the Brunian microcontinent. Geological Magazine 147, 508-526.

McGee, B., Collins, A.S., Trindade, R.I., Payne, J., 2015. Age and provenance of the Cryogenian to Cambrian passive margin to foreland basin sequence of the northern Paraguay Belt, Brazil. Geological Society of America Bulletin 127, 76-86.

McNamara, A.K., Niocaill, C.M., van der Pluijm, B.A., Van der Voo, R., 2001. West African proximity of the Avalon terrane in the latest Precambrian. Bulletin of the Geological Society of America 113, 1161-1170.

Meert, J.G., 2014. Ediacaran–Early Ordovician paleomagnetism of Baltica: A review. Gondwana Research 25, 159-169.

Meinhold, G., Kostopoulos, D., Frei, D., Himmerkus, F., Reischmann, T., 2010. U–Pb LA-SF-ICP-MS zircon geochronology of the Serbo-Macedonian Massif, Greece: palaeotectonic constraints for Gondwana-derived terranes in the Eastern Mediterranean. Int J Earth Sci (Geol Rundsch) 99, 813-832.

Meinhold, G., Morton, A.C., Fanning, C.M., Howard, J.P., Phillips, R.J., Strogen, D., Whitham, A.G., 2014. Insights into crust formation and recycling in North Africa from combined U–Pb, Lu–Hf and O isotope data of detrital zircons from Devonian sandstone of southern Libya. Geological Society, London, Special Publications 386, 281-292.

Mezger, K., Krogstad, E., 1997. Interpretation of discordant U□Pb zircon ages: An evaluation. Journal of metamorphic Geology 15, 127-140.

Mora, A., Baby, P., Roddaz, M., Parra, M., Brusset, S., Hermoza, W., Espurt, N., 2010. Tectonic history of the Andes and sub-Andean zones: implications for the development of the Amazon drainage basin. Amazonia: Landscape and species

evolution, 38-60.

Morag, N., Avigad, D., Gerdes, A., Belousova, E., Harlavan, Y., 2011. Crustal evolution and recycling in the northern Arabian-Nubian Shield: New perspectives from zircon Lu-Hf and U-Pb systematics. Precambrian Research 186, 101-116.

Morag, N., Avigad, D., Gerdes, A., Harlavan, Y., 2012. 1000–580Ma crustal evolution in the northern Arabian-Nubian Shield revealed by U–Pb–Hf of detrital zircons from late Neoproterozoic sediments (Elat area, Israel). Precambrian Research 208, 197-212.

Mortimer, N., 2004. New Zealand's Geological Foundations. Gondwana Research 7, 261-272.

Mueller, P.A., Kamenov, G.D., Heatherington, A.L., Richards, J., 2008. Crustal Evolution in the Southern Appalachian Orogen: Evidence from Hf Isotopes in Detrital Zircons. Journal of Geology 116, 414-422.

Murphy, J.B., 2002. Geochemistry of the Neoproterozoic metasedimentary Gamble Brook Formation, Avalon Terrane, Nova Scotia: Evidence for a rifted-arc environment along the West Gondwanan margin of Rodinia. Journal of Geology 110, 407-419.

Murphy, J.B., 2006. Fault-controlled emplacement of arc-related magmas along the Neoproterozoic northern Gondwanan margin: An example from the Antigonish Highlands, Nova Scotia. Precambrian Research 147, 305-319.

Murphy, J.B., Dostal, J., Keppie, J.D., 2008a. Neoproterozoic-Early Devonian magmatism in the Antigonish Highlands, Avalon terrane, Nova Scotia: Tracking the evolution of the mantle and crustal sources during the evolution of the Rheic Ocean. Tectonophysics 461, 181-201.

Murphy, J.B., Fernández-Suárez, J., Jeffries, T.E., 2004a. Lithogeochemical and Sm-Nd and U-Pb isotope data from the Silurian-Lower Devonian Arisaig Group clastic rocks, Avalon terrane, Nova Scotia: A record of terrane accretion in the Appalachian-Caledonide orogen. Bulletin of the Geological Society of America 116, 1183-1201.

Murphy, J.B., Fernández-Suárez, J., Jeffries, T.E., Strachan, R.A., 2004b. U-Pb (LA-ICP-MS) dating of detrital zircons from Cambrian elastic rocks in Avalonia: Erosion of a Neoproterozoic arc along the northern Gondwanan margin. Journal of the Geological Society 161, 243-254.

Murphy, J.B., Gutiérrez-Alonso, G., 2008. The origin of the Variscan upper allochthons in the Ortegal Complex, northwestern Iberia: Sm-Nd isotopic constraints on the closure of the Rheic Ocean. Canadian Journal of Earth Sciences 45, 651-668.

Murphy, J.B., Gutiérrez-Alonso, G., Nance, R.D., Fernández-Suárez, J., Keppie, J.D., Quesada, C., Dostal, J., Braid, J.A., 2009. Rheic Ocean mafic complexes: Overview and synthesis, pp. 343-369.

Murphy, J.B., Keppie, J.D., 2005. The Acadian orogeny in the northern Appalachians. International Geology Review 47, 663-687.

Murphy, J.B., Keppie, J.D., Davis, D., Krogh, T.E., 1997. Regional significance of new U-Pb age data for Neoproterozoic igneous units in Avalonian rocks of northern mainland Nova Scotia, Canada. Geological Magazine 134, 113-120.

Murphy, J.B., Keppie, J.D., Dostal, J., Waldron, J.W.F., Cude, M.P., 1996. Geochemical and isotopic characteristics of early Silurian clastic sequences in Antigonish Highlands, Nova Scotia, Canada: Constraints on the accretion of Avalonia in the Appalachian - Caledonide Orogen. Canadian Journal of Earth Sciences 33, 379-388.

Murphy, J.B., McCausland, P.J.A., O'Brien, S.J., Pisarevsky, S., Hamilton, M.A., 2008b. Age, geochemistry and Sm-Nd isotopic signature of the 0.76 Ga Burin Group: Compositional equivalent of Avalonian basement? Precambrian Research 165, 37-48.

Murphy, J.B., Nance, R.D., 1989. Model for the evolution of the Avalonian-Cadomian belt.

Geology 17, 735-738.

Murphy, J.B., Nance, R.D., 1991. Supercontinent model for the contrasting character of late Proterozoic orogenic belts. Geology 19, 469-472.

Murphy, J.B., Nance, R.D., 2002. Sm-Nd isotopic systematics as tectonic tracers: An example from West Avalonia in the Canadian Appalachians. Earth-Science Reviews 59, 77-100.

Murphy, J.B., Nance, R.D., Keppie, J.D., 2002. Discussion and reply: West African proximity of the Avalon terrane in the latest Precambrian Discussion. Geological Society of America Bulletin 114, 1049-1050.

Murphy, J.B., Pisarevsky, S., Nance, R.D., 2013. Potential geodynamic relationships between the development of peripheral orogens along the northern margin of Gondwana and the amalgamation of West Gondwana. Mineralogy and Petrology 107, 635-650.

Murphy, J.B., Strachan, R.A., Nance, R.D., Parker, K.D., Fowler, M.B., 2000. Proto-Avalonia: A 1.2-1.0 Ga tectonothermal event and constraints for the evolution of Rodinia. Geology 28, 1071-1074.

Nance, R.D., Gutiérrez-Alonso, G., Keppie, J.D., Linnemann, U., Murphy, J.B., Quesada, C., Strachan, R.A., Woodcock, N.H., 2010. Evolution of the Rheic Ocean. Gondwana Research 17, 194-222.

Nance, R.D., Gutiérrez-Alonso, G., Keppie, J.D., Linnemann, U., Murphy, J.B., Quesada, C., Strachan, R.A., Woodcock, N.H., 2012. A brief history of the Rheic Ocean. Geoscience Frontiers 3, 125-135.

Nance, R.D., Murphy, J.B., 1994. Contrasting basement isotopic signatures and the palinspastic restoration of peripheral orogens: example from the Neoproterozoic Avalonian-Cadomian belt. Geology 22, 617-620.

Nance, R.D., Murphy, J.B., 1996. Basement isotopic signatures and Neoproterozoic paleogeography of Avalonian-Cadomian and related terranes in the circum-North Atlantic, Special Paper of the Geological Society of America, pp. 333-346.

Nance, R.D., Murphy, J.B., Keppie, J.D., 2002. A Cordilleran model for the evolution of Avalonia. Tectonophysics 352, 11-31.

Nance, R.D., Murphy, J.B., Strachan, R.A., Keppie, J.D., Gutiérrez-Alonso, G., Fernández-Suárez, J., Quesada, C., Linnemann, U., D'lemos, R., Pisarevsky, S.A., 2008. Neoproterozoic-early Palaeozoic tectonostratigraphy and palaeogeography of the peri-Gondwanan terranes: Amazonian v. West African connections. Geological Society, London, Special Publications 297, 345-383.

Orejana, D., Martínez, E.M., Villaseca, C., Andersen, T., 2015. Ediacaran–Cambrian paleogeography and geodynamic setting of the Central Iberian Zone: Constraints from coupled U–Pb–Hf isotopes of detrital zircons. Precambrian Research 261, 234-251.

Pastor-Galán, D., Gutiérrez-Alonso, G., Murphy, J.B., Fernández-Suárez, J., Hofmann, M., Linnemann, U., 2013. Provenance analysis of the Paleozoic sequences of the northern Gondwana margin in NW Iberia: passive margin to Variscan collision and orocline development. Gondwana Research 23, 1089-1103.

Patchett, P., Tatsumoto, M., 1980. Hafnium isotope variations in oceanic basalts. Geophysical Research Letters 7, 1077-1080.

Patchett, P.J., 1983. Importance of the Lu-Hf isotopic system in studies of planetary chronology and chemical evolution. Geochimica et Cosmochimica Acta 47, 81-91.

Payne, J.L., Barovich, K.A., Hand, M., 2006. Provenance of metasedimentary rocks in the northern Gawler Craton, Australia: Implications for palaeoproterozoic reconstructions. Precambrian Research 148, 275-291.

Payne, J.L., Ferris, G., Barovich, K.M., Hand,

M., 2010. Pitfalls of classifying ancient magmatic suites with tectonic discrimination diagrams: An example from the Paleoproterozoic Tunkillia Suite, southern Australia. Precambrian Research 177, 227-240.

Payne, J.L., Hand, M., Barovich, K.M., Wade, B.P., 2008. Temporal constraints on the timing of high-grade metamorphism in the northern Gawler Craton: implications for assembly of the Australian Proterozoic. Australian Journal of Earth Sciences 55, 623-640.

Pearce, J., 1996. A user's guide to basalt discrimination diagrams.

Pereira, M.F., Linnemann, U., Hofmann, M., Chichorro, M., Solá, A.R., Medina, J., Silva, J.B., 2012. The provenance of Late Ediacaran and Early Ordovician siliciclastic rocks in the Southwest Central Iberian Zone: Constraints from detrital zircon data on northern Gondwana margin evolution during the late Neoproterozoic. Precambrian Research 192-195, 166-189.

Pharaoh, T., Webb, P., Thorpe, R., Beckinsale, R., 1987. Geochemical evidence for the tectonic setting of late Proterozoic volcanic suites in central England. Geological Society, London, Special Publications 33, 541-552.

Pimentel, M.M., Rodrigues, J.B., DellaGiustina, M.E.S., Junges, S., Matteini, M., Armstrong, R., 2011. The tectonic evolution of the Neoproterozoic Brasília Belt, central Brazil, based on SHRIMP and LA-ICPMS U–Pb sedimentary provenance data: A review. Journal of South American Earth Sciences 31, 345-357.

Pin, C., Paquette, J., Zalduegui, J.S., Ibarguchi, J.G., 2002. Early Devonian suprasubduction-zone ophiolite related to incipient collisional processes in the Western Variscan Belt: The Sierra de Careón unit, Ordenes Complex, Galicia. SPECIAL PAPERS-GEOLOGICAL SOCIETY OF AMERICA, 57-72.

Pollock, J.C., Hibbard, J.P., Sylvester, P.J., 2009. Early Ordovician rifting of Avalonia and birth of the Rheic Ocean: U–Pb detrital zircon constraints from Newfoundland. Journal of the Geological Society 166, 501-515.

Pollock, J.C., Hibbard, J.P., van Staal, C.R., 2011. A paleogeographical review of the peri-Gondwanan realm of the Appalachian orogen1 This article is one of a series of papers published in this CJES Special Issue: In honour of Ward Neale on the theme of Appalachian and Grenvillian geology. Canadian Journal of Earth Sciences 49, 259-288.

Pollock, J.C., Sylvester, P.J., Barr, S.M., Murphy, B., 2015. Lu–Hf zircon and Sm–Nd whole-rock isotope constraints on the extent of juvenile arc crust in Avalonia: examples from Newfoundland and Nova Scotia, Canada. Canadian Journal of Earth Sciences 52, 1-21.

Prigmore, J.K., Butler, A.J., Woodcock, N.H., 1997. Rifting during separation of Eastern Avalonia from Gondwana: Evidence from subsidence analysis. Geology 25, 203-206.

Quesada, C., 1991. Geological constraints on the Paleozoic tectonic evolution of tectonostratigraphic terranes in the Iberian Massif. Tectonophysics 185, 225-245.

Rainbird, R.H., McNicoll, V., Theriault, R., Heaman, L., Abbott, J., Long, D., Thorkelson, D., 1997. Pan-continental river system draining Grenville Orogen recorded by U-Pb and Sm-Nd geochronology of Neoproterozoic quartzarenites and mudrocks, northwestern Canada. The Journal of Geology, 1-17.

Ranger, M., Pickerill, R., Flllion, D., 1984. Lithostratigraphy of the Cambrian?-Lower Ordovician Bell Island and Wabana groups of Bell, Little Bell, and Kellys islands, Conception Bay, eastern Newfoundland. Canadian Journal of Earth Sciences 21, 1245-1261.

Reimann, C., Bahlburg, H., Kooijman, E., Berndt, J., Gerdes, A., Carlotto, V., Lopez, S., 2010. Geodynamic evolution of the early Paleozoic Western Gondwana margin 14–17 S reflected by the detritus of the Devonian and Ordovician basins of southern Peru and northern Bolivia. Gondwana

Research 18, 370-384.

Rivers, T., 1997. Lithotectonic elements of the Grenville Province: review and tectonic implications. Precambrian Research 86, 117-154.

Robardet, M., 2003. The Armorica 'microplate': fact or fiction? Critical review of the concept and contradictory palaeobiogeographical data. Palaeogeography, Palaeoclimatology, Palaeoecology 195, 125-148.

Roberts, N.W., Slagstad, T., Parrish, R., Norry, M., Marker, M., Horstwood, M.A., 2013. Sedimentary recycling in arc magmas: geochemical and U–Pb–Hf–O constraints on the Mesoproterozoic Suldal Arc, SW Norway. Contrib Mineral Petrol 165, 507-523.

Robinson, F.A., Foden, J.D., Collins, A.S., Payne, J.L., 2014. Arabian Shield magmatic cycles and their relationship with Gondwana assembly: Insights from zircon U–Pb and Hf isotopes. Earth and Planetary Science Letters 408, 207-225.

Romanyuk, T., Kuznetsov, N., Maslov, A., Belousova, E., Krupenin, M., Ronkin, Y.L., Gorozhanin, V., Gorozhanina, E., 2014. Geochemical and Lu/Hf isotopic (LA-ICP-MS) signature of detrital zircons from sandstones of the basal levels of the Riphean stratotype, Dokl. Earth Sc. Springer, pp. 1356-1360.

Rubatto, D., Williams, I.S., Buick, I.S., 2001. Zircon and monazite response to prograde metamorphism in the Reynolds Range, central Australia. Contrib Mineral Petrol 140, 458-468.

Sacek, V., 2014. Drainage reversal of the Amazon River due to the coupling of surface and lithospheric processes. Earth and Planetary Science Letters 401, 301-312.

Sacks, P.E., Secor, D.T., 1990. Kinematics of Late Paleozoic continental collision between Laurentia and Gondwana. Science 250, 1702-1705.

Samson, S., D., D'Lemos, R., S, 1998. U–Pb geochronology and Sm–Nd isotopic composition of Proterozoic gneisses, Channel Islands, UK. Journal of the Geological Society 155, 609-618.

Sánchez-García, T., Bellido, F., Quesada, C., 2003. Geodynamic setting and geochemical signatures of Cambrian–Ordovician rift-related igneous rocks (Ossa-Morena Zone, SW Iberia). Tectonophysics 365, 233-255.

Satkoski, A.M., Barr, S.M., Samson, S.D., 2010. Provenance of Late Neoproterozoic and Cambrian Sediments in Avalonia: Constraints from Detrital Zircon Ages and Sm-Nd Isotopic Compositions in Southern New Brunswick, Canada. Journal of Geology 118, 187-200.

Scarrow, J.H., Pease, V., Fleutelot, C., Dushin, V., 2001. The late neoproterozoic enganepe ophiolite, Polar Urals, Russia: An extension of the Cadomian arc? Precambrian Research 110, 255-275.

Schellart, W.P., Lister, G.S., Toy, V.G., 2006. A Late Cretaceous and Cenozoic reconstruction of the Southwest Pacific region: Tectonics controlled by subduction and slab rollback processes. Earth-Science Reviews 76, 191-233.

Scherer, E., Münker, C., Mezger, K., 2001. Calibration of the Lutetium-Hafnium Clock. Science 293, 683-687.

Scotese, C.R., 2004. A Continental Drift Flipbook. Journal of Geology 112, 729-741.

Scotese, C.R., McKerrow, W.S., 1990. Revised world maps and introduction. Geological Society, London, Memoirs 12, 1-21.

Sdzuy, K., 1968. Biostratigrafia de la griotte Cambrica de Los Barrios de Luna (Leon) y de otras sucesiones comparables. Trabajos de Geología 2, 45-59.

Sdzuy, K., 1974. Mittelkambrische Graptolithen aus NW-Spanien. Paläontologische Zeitschrift 48, 110-139.

Shaw, J., Gutiérrez-Alonso, G., Johnston, S., Galán, D.P., 2014. Provenance variability along the Early Ordovician north Gondwana margin: Paleogeographic and tectonic implications of U-Pb detrital zircon ages from the Armorican Quartzite of the Iberian Variscan belt. Geological Society of

America Bulletin 126, 702-719.

Shchipansky, A.A., Samsonov, A.V., Petrova, A.Y., Larionova, Y.O., 2007. Geodynamics of the eastern margin of Sarmatia in the Paleoproterozoic. Geotecton. 41, 38-62.

Simancas, J.F., Tahiri, A., Azor, A., Lodeiro, F.G., Martínez Poyatos, D.J., El Hadi, H., 2005. The tectonic frame of the Variscan–Alleghanian orogen in Southern Europe and Northern Africa. Tectonophysics 398, 181-198.

Skipton, D.R., Dunning, G.R., Sparkes, G.W., Murphy, B., 2013. Late Neoproterozoic arc-related magmatism in the Horse Cove complex, eastern Avalon zone, Newfoundland. Canadian Journal of Earth Sciences 50, 462-482.

Sláma, J., Košler, J., Condon, D.J., Crowley, J.L., Gerdes, A., Hanchar, J.M., Horstwood, M.S.A., Morris, G.A., Nasdala, L., Norberg, N., Schaltegger, U., Schoene, B., Tubrett, M.N., Whitehouse, M.J., 2008. Plešovice zircon - A new natural reference material for U-Pb and Hf isotopic microanalysis. Chemical Geology 249, 1-35.

Smits, R.G., Collins, W.J., Hand, M., Dutch, R., Payne, J., 2014. A Proterozoic Wilson cycle identified by Hf isotopes in central Australia: Implications for the assembly of Proterozoic Australia and Rodinia. Geology.

Soper, N., Strachan, R., Holdsworth, R., Gayer, R., Greiling, R., 1992. Sinistral transpression and the Silurian closure of Iapetus. Journal of the Geological Society 149, 871-880.

Stampfli, G., Borel, G., 2002. A plate tectonic model for the Paleozoic and Mesozoic constrained by dynamic plate boundaries and restored synthetic oceanic isochrons. Earth and Planetary Science Letters 196, 17-33.

Stampfli, G., Hochard, C., Vérard, C., Wilhem, C., vonRaumer, J., 2013. The formation of Pangea. Tectonophysics.

Stern, R.J., 1994. ARC Assembly and Continental Collision in the Neoproterozoic East African Orogen: Implications for the Consolidation of Gondwanaland. Annual Review of Earth and Planetary Sciences 22, 319-351.

Stern, T., Stratford, W., Salmon, M., 2006. Subduction evolution and mantle dynamics at a continental margin: Central North Island, New Zealand. Reviews of Geophysics 44.

Strachan, R.A., Nance, R.D., Dallmeyer, R.D., D'Lemos, R.S., Murphy, J.B., Watt, G.R., 1996. Late Precambrian tectonothermal evolution of the Malverns Complex. Journal of the Geological Society 153, 589-600.

Tait, J., 1999. New Early Devonian paleomagnetic data from NW France: Paleogeography and implications for the Armorican microplate hypothesis. Journal of Geophysical Research: Solid Earth (1978–2012) 104, 2831-2839.

Tait, J., Schätz, M., Bachtadse, V., Soffel, H., 2000. Palaeomagnetism and Palaeozoic palaeogeography of Gondwana and European terranes. Geological Society, London, Special Publications 179, 21-34.

Talavera, C., Montero, P., Martínez Poyatos, D., Williams, I.S., 2012. Ediacaran to Lower Ordovician age for rocks ascribed to the Schist–Graywacke Complex (Iberian Massif, Spain): Evidence from detrital zircon SHRIMP U–Pb geochronology. Gondwana Research 22, 928-942.

Teale, W., Collins, A.S., Foden, J., Payne, J.L., Plavsa, D., Chetty, T.R.K., Santosh, M., Fanning, M., 2011. Cryogenian (□830 Ma) mafic magmatism and metamorphism in the northern Madurai Block, southern India: A magmatic link between Sri Lanka and Madagascar? Journal of Asian Earth Sciences 42, 223-233.

Thompson, M., Grunow, A., Ramezani, J., 2007. Late Neoproterozoic paleogeography of the Southeastern New England Avalon Zone: insights from U-Pb geochronology and paleomagnetism. Geological Society of America Bulletin 119, 681-696.

Thompson, M.D., Barr, S.M., Grunow, A.M.,

2012. Avalonian perspectives on Neoproterozoic paleogeography: Evidence from Sm-Nd isotope geochemistry and detrital zircon geochronology in SE New England, USA. Bulletin of the Geological Society of America 124, 517-531.

Thorogood, E.J., 1990. Provenance of the pre-Devonian sediments of England and Wales: Sm-Nd isotopic evidence. Journal of the Geological Society 147, 591-594.

Torsvik, T., Smethurst, M., Meert, J.G., Van der Voo, R., McKerrow, W., Brasier, M., Sturt, B., Walderhaug, H., 1996. Continental break-up and collision in the Neoproterozoic and Palaeozoic—a tale of Baltica and Laurentia. Earth-Science Reviews 40, 229-258.

Torsvik, T.H., Rehnström, E.F., 2003. The Tornquist Sea and Baltica–Avalonia docking. Tectonophysics 362, 67-82.

Tucker, R.D., Pharoah, T.C., 1991. U-Pb zircon ages for Late Precambrian igneous rocks in southern Britain. Journal of the Geological Society 148, 435-443.

Tulloch, A., Ramezani, J., Mortimer, N., Mortensen, J., van den Bogaard, P., Maas, R., 2009. Cretaceous felsic volcanism in New Zealand and Lord Howe Rise (Zealandia) as a precursor to final Gondwana break-up. Geological Society, London, Special Publications 321, 89-118.

van Staal, C.R., Barr, S.M., Murphy, J.B., 2012. Provenance and tectonic evolution of Ganderia: Constraints on the evolution of the Iapetus and Rheic oceans. Geology 40, 987-990.

van Staal, C.R., Dewey, J., Mac Niocaill, C., McKerrow, W., 1998. The Cambrian-Silurian tectonic evolution of the northern Appalachians and British Caledonides: history of a complex, west and southwest Pacific-type segment of Iapetus. Geological Society, London, Special Publications 143, 197-242.

van Staal, C.R., Whalen, J.B., Valverde-Vaquero, P., Zagorevski, A., Rogers, N., 2009. Pre-Carboniferous, episodic accretion-related, orogenesis along the Laurentian margin of the northern Appalachians. Geological Society, London, Special Publications 327, 271-316.

Verniers, J., Pharaoh, T., André, L., Debacker, T., De Vos, W., Everaerts, M., Herbosch, A., Samuellson, J., Sintubin, M., Vecoli, M., 2002. The Cambrian to mid Devonian basin development and deformation history of Eastern Avalonia, east of the Midlands Microcraton: new data and a review. Geological Society, London, Special Publications 201, 47-93.

Vogel, D.E., 1967. Petrology of an eclogite- and pyrigarnite-bearing polymetamorphic rock complex at Cabo Ortegal, NW Spain. [s.n.], [S.l.].

Von Raumer, J., Stampfli, G., Borel, G., Bussy, F., 2002. Organization of pre-Variscan basement areas at the north-Gondwanan margin. Int J Earth Sci (Geol Rundsch) 91, 35-52.

von Raumer, J.F., Bussy, F., Schaltegger, U., Schulz, B., Stampfli, G.M., 2013. Pre-Mesozoic Alpine basements—Their place in the European Paleozoic framework. Geological Society of America Bulletin 125, 89-108.

von Raumer, J.F., Stampfli, G.M., Bussy, F., 2003. Gondwana-derived microcontinents — the constituents of the Variscan and Alpine collisional orogens. Tectonophysics 365, 7-22.

Vozárová, A., Šarinová, K., Rodionov, N., Laurinc, D., Paderin, I., Sergeev, S., Lepekhina, E., 2012. U–Pb ages of detrital zircons from Paleozoic metasandstones of the Gelnica Terrane (Southern Gemeric Unit, Western Carpathians, Slovakia): evidence for Avalonian–Amazonian provenance. Int J Earth Sci (Geol Rundsch) 101, 919-936.

Walsh, G.J., Benziane, F., Aleinikoff, J.N., Harrison, R.W., Yazidi, A., Burton, W.C., Quick, J.E., Saadane, A., 2012. Neoproterozoic tectonic evolution of the Jebel Saghro and Bou Azzer—El Graara inliers, eastern and central Anti-Atlas, Morocco. Precambrian Research 216–219, 23-62.

Wang, L.J., Griffin, W.L., Yu, J.H., O'Reilly, S.Y., 2010. Precambrian crustal evolution of the Yangtze Block tracked by detrital zircons from

SUPPLEMENTARY MATERIAL

Sample	Analysis_#	Pb207/Pb206		Pb206/U238		Pb207/U235		Pb208/Th232		Concordancy	Pb207/Pb206		Pb206/U238		Pb207/U235		Pb208/Th232	
ACO-12-52a	1	0.0858	0.0011	0.2278	0.0027	2.6939	0.0359	0.0686	0.0012	99	1332.9	24.2	1323.2	13.99	1326.8	9.87	1341.3	22.28
ACO-12-52a	2	0.1033	0.0013	0.2999	0.0035	4.2698	0.0568	0.0841	0.0015	100	1684.1	23.18	1690.6	17.34	1687.6	10.95	1632.4	28.38
ACO-12-52a	3	0.0939	0.0011	0.2713	0.0032	3.5102	0.0451	0.079	0.0014	103	1505.4	22.28	1547.3	16.05	1529.5	10.15	1536	26.73
ACO-12-52a	4	0.1736	0.0023	0.4748	0.0056	11.363	0.1569	0.15	0.0032	97	2592.7	22.35	2504.5	24.53	2553.4	12.89	2825	56.77
ACO-12-52a	5	0.0818	0.0011	0.2056	0.0025	2.3179	0.033	0.0579	0.0011	97	1240	26.41	1205.5	13.09	1217.8	10.09	1137.9	21.78
ACO-12-52a	6	0.0816	0.001	0.2058	0.0024	2.3148	0.0294	0.0607	0.001	98	1235.9	23.22	1206.2	12.63	1216.8	9.01	1190.9	19.31
ACO-12-52a	7	0.0915	0.0011	0.2497	0.0029	3.1497	0.0399	0.0722	0.0013	99	1456.9	22.59	1436.9	14.68	1444.9	9.77	1409.7	23.56
ACO-12-52a	8	0.2136	0.0025	0.2293	0.0026	6.7515	0.0846	0.3181	0.0056	45	2933.2	19.11	1330.5	13.78	2079.4	11.08	5581.9	86.16
ACO-12-52a	9	0.0777	0.001	0.1905	0.0022	2.0404	0.0271	0.0549	0.001	99	1139.2	24.95	1124	11.91	1129.1	9.04	1080	19.97
ACO-12-52a	10	0.0814	0.0011	0.2093	0.0025	2.3497	0.0332	0.0599	0.0012	99	1232.1	26.63	1225	13.09	1227.5	10.07	1175.3	23.15
ACO-12-52a	11	0.0986	0.0013	0.2786	0.0032	3.7871	0.0503	0.0788	0.0015	99	1597.6	23.68	1584.5	16.09	1590	10.66	1532.8	28.78
ACO-12-52a	12	0.0823	0.0011	0.2035	0.0024	2.3087	0.0312	0.0572	0.0011	95	1252.5	25.12	1194	12.56	1215	9.59	1124.7	20.96
ACO-12-52a	13	0.0946	0.0012	0.2635	0.003	3.4381	0.044	0.0762	0.0014	99	1520.8	22.82	1507.8	15.3	1513.2	10.07	1484.7	26.82
ACO-12-52a	14	0.1096	0.0029	0.3247	0.0051	4.9026	0.1241	0.0728	0.0033	101	1793	47.02	1812.6	24.92	1802.7	21.34	1421	62.18
ACO-12-52a	15	0.1003	0.0015	0.2877	0.0035	3.9793	0.062	0.0723	0.0021	100	1630.3	28.02	1630.2	17.61	1630	12.64	1411.5	39.31
ACO-12-52a	16	0.1403	0.0022	0.247	0.0029	4.7755	0.073	0.1143	0.0034	64	2230.7	26.76	1422.7	14.74	1780.6	12.84	2186.8	61.83
ACO-12-52a	17	0.0871	0.0013	0.2302	0.0028	2.7628	0.0429	0.0591	0.0015	98	1361.5	29.17	1335.8	14.64	1345.6	11.59	1160.4	28.93
ACO-12-52a	18	0.0941	0.0014	0.2234	0.0027	2.8964	0.0451	0.0175	0.0005	86	1509.2	28.68	1299.7	14.16	1381	11.75	350.3	10.09
ACO-12-52a	19	0.099	0.0017	0.2703	0.0034	3.6896	0.0627	0.0683	0.0023	96	1605.9	31.19	1542.5	17.07	1569.1	13.57	1335.8	42.92
ACO-12-52a	20	0.1127	0.0016	0.3254	0.0038	5.0573	0.0716	0.0856	0.0021	99	1843.7	24.85	1816.2	18.45	1829	12	1660.1	39.77
ACO-12-52a	21	0.0778	0.0017	0.1874	0.0025	2.0076	0.0426	0.0453	0.0018	97	1140.5	42.57	1107	13.8	1118.1	14.39	894.5	33.95
ACO-12-52a	22	0.115	0.0016	0.2362	0.0027	3.7431	0.0522	0.0966	0.0023	73	1879.2	24.74	1366.7	14.11	1580.6	11.18	1863.1	42.77
ACO-12-52a	23	0.0994	0.0018	0.2533	0.003	3.4695	0.0609	0.0839	0.0031	90	1612	33.62	1455.7	15.53	1520.3	13.83	1628.1	57.75
ACO-12-52a	24	0.0856	0.0011	0.2244	0.0027	2.6477	0.0375	0.0726	0.0017	98	1329.1	25.6	1304.8	14.15	1314	10.43	1416.4	32.45
ACO-12-52a	25	0.0714	0.001	0.1645	0.002	1.6192	0.0236	0.0519	0.0011	100	969.2	28.14	981.6	10.82	977.7	9.13	1022.6	21.56
ACO-12-52a	26	0.1202	0.0015	0.3495	0.0041	5.7901	0.0768	0.1042	0.0022	99	1958.8	21.96	1932.1	19.57	1944.9	11.48	2003.7	40.66
ACO-12-52a	27	0.0937	0.0012	0.2604	0.0031	3.3635	0.0463	0.0818	0.0018	99	1501.8	24.41	1491.9	15.74	1495.9	10.78	1589.3	32.83
ACO-12-52a	28	0.0777	0.001	0.1901	0.0022	2.0352	0.0272	0.059	0.0013	99	1138.1	24.97	1121.8	11.87	1127.3	9.09	1157.7	24.77
ACO-12-52a	29	0.0759	0.001	0.1711	0.002	1.7896	0.0252	0.0576	0.0013	93	1091.7	26.68	1018.1	11.04	1041.7	9.17	1131.9	25.5
ACO-12-52a	30	0.0731	0.001	0.1684	0.002	1.6963	0.024	0.0561	0.0013	99	1016	27.27	1003.1	10.85	1007.1	9.04	1103.3	25.18
ACO-12-52a	31	0.1142	0.0015	0.3345	0.0039	5.2662	0.0705	0.0994	0.0023	100	1867.1	22.81	1860.3	18.66	1863.4	11.42	1915.7	42.03
ACO-12-52a	32	0.0718	0.0012	0.1535	0.0019	1.5186	0.0252	0.0503	0.0013	98	979.8	32.74	920.3	10.6	937.9	10.17	991.8	25.07
ACO-12-52a	33	0.1116	0.0015	0.3181	0.0038	4.8953	0.068	0.0945	0.0022	97	1826.3	23.48	1780.2	18.55	1801.4	11.72	1825.5	41.31
ACO-12-52a	34	0.08	0.0012	0.2033	0.0025	2.243	0.0343	0.0635	0.0017	100	1197.4	28.76	1193.1	13.19	1194.6	10.74	1243.4	32.16
ACO-12-52a	35	0.1419	0.0021	0.1782	0.0022	3.4849	0.0522	0.1033	0.0028	47	2250.3	25.05	1056.9	11.77	1523.8	11.82	1987.3	50.9
ACO-12-52a	36	0.1135	0.0016	0.3272	0.0039	5.1208	0.074	0.0969	0.0025	98	1856.6	24.6	1824.7	19.04	1839.6	12.28	1870.1	46.79
ACO-12-52a	37	0.1035	0.0016	0.2932	0.0036	4.186	0.0649	0.0866	0.0024	98	1688.6	27.35	1657.7	17.94	1671.3	12.7	1679.2	44.23
ACO-12-52a	38	0.0812	0.0012	0.2071	0.0025	2.317	0.0346	0.0639	0.0018	99	1225.3	28.09	1213.2	13.1	1217.5	10.59	1252	34.92
ACO-12-52a	39	0.0831	0.0013	0.2074	0.0025	2.3751	0.0385	0.0662	0.002	96	1271	30.63	1214.8	13.44	1235.1	11.57	1295.8	38.17
ACO-12-52a	40	0.1122	0.0017	0.3237	0.0039	5.0062	0.0767	0.0924	0.0027	99	1834.8	26.44	1807.9	19.2	1820.4	12.96	1786.5	50.43

ACO-12-52a	41	0.0926	0.0018	0.2592	0.0035	3.3073	0.0644	0.0814	0.0033	100	1479	35.75	1485.5	17.83	1482.8	15.18	1582	62.06				
ACO-12-52a	42	0.0784	0.0012	0.192	0.0024	2.0758	0.0336	0.0602	0.0019	98	1157.4	30.88	1132.3	12.71	1140.8	11.09	1182	35.54				
ACO-12-52a	43	0.0994	0.0018	0.2727	0.0036	3.7357	0.0707	0.0856	0.0036	96	1612.5	33.8	1554.2	18.27	1579.1	15.17	1660.7	67.19				
ACO-12-52a	44	0.0825	0.0012	0.1628	0.002	1.8503	0.0271	0.0654	0.0015	77	1256.4	26.94	972.1	10.88	1063.5	9.65	1280.9	28.51				
ACO-12-52a	45	0.118	0.0019	0.3316	0.0044	5.3935	0.0911	0.0962	0.0031	96	1925.7	28.62	1846.1	21.11	1883.8	14.47	1856.1	57.78				
ACO-12-52a	46	0.1016	0.0015	0.2531	0.0032	3.546	0.054	0.0877	0.0024	88	1654.4	26.19	1454.2	16.29	1537.5	12.05	1699	44.23				
ACO-12-52a	47	0.08	0.001	0.2047	0.0024	2.258	0.0304	0.0649	0.0015	100	1197.8	24.96	1200.2	12.72	1199.3	9.48	1271.1	27.87				
ACO-12-52a	48	0.1447	0.0019	0.3039	0.0036	6.0647	0.0842	0.138	0.0031	75	2284.6	22.61	1710.8	18	1985.2	12.1	2613.3	54.4				
ACO-12-52a	49	0.091	0.0013	0.1884	0.0023	2.3619	0.0342	0.0682	0.0016	77	1445.4	26.11	1112.5	12.3	1231.1	10.34	1332.7	29.45				
ACO-12-52a	50	0.1184	0.0027	0.2515	0.0034	4.1039	0.0888	0.0979	0.0046	75	1931.7	39.6	1446	17.47	1655.1	17.67	1888.4	84.99				
ACO-12-52a	51	0.0897	0.0014	0.2379	0.003	2.941	0.046	0.0722	0.0019	97	1418	28.56	1376	15.35	1392.5	11.86	1408.9	35.16				
ACO-12-52a	52	0.0723	0.001	0.1682	0.002	1.6767	0.0245	0.0511	0.0013	100	994.8	28.31	1002.1	10.97	999.7	9.29	1007.3	24.87				
ACO-12-52a	53	0.1786	0.0023	0.4889	0.0059	12.04	0.1673	0.135	0.0032	97	2640.1	21.61	2566	25.49	2607.5	13.03	2560.1	57.3				
ACO-12-52a	54	0.0827	0.0014	0.2047	0.0026	2.3335	0.0408	0.0669	0.0023	95	1262.2	32.58	1200.3	14.13	1222.5	12.41	1309.3	44.06				
ACO-12-52a	55	0.0985	0.0026	0.2429	0.0038	3.2968	0.0834	0.0753	0.0028	88	1595.2	47.6	1401.5	19.67	1480.3	19.7	1467	52.67				
ACO-12-52a	56	0.0746	0.0011	0.1656	0.002	1.7035	0.0258	0.0539	0.0015	93	1057.5	29.11	988	11.11	1009.9	9.68	1060.8	29.07				
ACO-12-52a	57	0.0785	0.0014	0.1861	0.0024	2.0134	0.0356	0.0559	0.002	95	1158.9	33.72	1100.2	13	1120	12	1099.3	37.6				
ACO-12-52a	58	0.0963	0.0014	0.2456	0.003	3.2592	0.0491	0.0898	0.0026	91	1552.8	26.66	1415.7	15.47	1471.4	11.7	1737.4	48.73				
ACO-12-52a	59	0.1135	0.0021	0.2656	0.0035	4.1569	0.0772	0.1014	0.0041	82	1856.7	32.58	1518.2	17.87	1665.6	15.2	1951.7	74.7				
ACO-12-52a	60	0.0963	0.0016	0.2143	0.0027	2.843	0.0473	0.0742	0.0022	81	1552.6	30.3	1251.4	14.22	1367	12.49	1447	41.22				
ACO-12-52a	61	0.08	0.0018	0.1992	0.0028	2.1976	0.0482	0.0608	0.0027	98	1197.1	42.73	1171.1	15	1180.3	15.3	1192.4	52.09				
ACO-12-52a	62	0.1096	0.0021	0.3136	0.0042	4.7385	0.0929	0.09	0.0039	98	1792.5	34.99	1758.4	20.73	1774.1	16.44	1741	71.31				
ACO-12-52a	63	0.1016	0.0027	0.2526	0.0035	3.5384	0.0902	0.0837	0.0056	88	1653.4	47.84	1452.1	17.96	1535.8	20.17	1624	103.8				
ACO-12-52a	64	0.0771	0.0012	0.192	0.0024	2.0411	0.0323	0.0572	0.0014	101	1124.3	30.11	1132	12.78	1129.3	10.77	1123.4	26.19				
ACO-12-52a	65	0.0814	0.0011	0.204	0.0025	2.29	0.0336	0.0609	0.0013	97	1231.8	27.11	1196.7	13.18	1209.2	10.36	1194.8	24.72				
ACO-12-52a	66	0.1117	0.0014	0.2213	0.0026	3.4086	0.0469	0.0938	0.002	71	1827.6	23.21	1288.8	13.94	1506.4	10.81	1811.2	37.23				
ACO-12-52a	67	0.0923	0.0012	0.2504	0.003	3.1853	0.0435	0.0744	0.0016	98	1472.7	24.07	1440.6	15.32	1453.6	10.54	1449.5	30.49				
ACO-12-52a	68	0.0727	0.001	0.1699	0.002	1.7035	0.0237	0.0516	0.0012	100	1006.8	26.18	1011.4	11.11	1009.9	8.89	1017.4	22.22				
ACO-12-52a	69	0.0798	0.0011	0.2001	0.0024	2.201	0.0314	0.0608	0.0014	99	1191.6	26.37	1175.9	12.86	1181.4	9.96	1192.5	27.38				
ACO-12-52a	70	0.0815	0.0013	0.2073	0.0026	2.3286	0.0378	0.061	0.0018	99	1232.5	30.15	1214.6	13.96	1221	11.52	1196.1	34.09				
ACO-12-52a	71	0.0838	0.0014	0.2115	0.0027	2.4438	0.0413	0.0647	0.0017	96	1287.9	31.89	1236.9	14.25	1255.6	12.17	1267.4	32.64				
ACO-12-52a	72	0.1074	0.0016	0.316	0.0039	4.6794	0.0717	0.0868	0.0024	101	1755.9	26.41	1770.2	19.24	1763.6	12.83	1683	44.19				
ACO-12-52a	73	0.089	0.0013	0.2357	0.0029	2.8912	0.0436	0.071	0.0018	97	1403.3	27.28	1364.5	15.04	1379.6	11.38	1386.4	34.5				
ACO-12-52a	74	0.2037	0.0033	0.2692	0.0034	7.5581	0.1214	0.184	0.0055	54	2856	25.81	1536.5	17.39	2179.9	14.4	3413.2	93.58				
ACO-12-52a	75	0.0947	0.002	0.2738	0.0038	3.573	0.0749	0.0768	0.0035	103	1521.6	38.61	1559.8	19.34	1543.6	16.62	1494.6	65.12				
ACO-12-52a	76	0.0814	0.0013	0.2031	0.0024	2.2797	0.0365	0.065	0.0022	97	1231.3	30.71	1192.1	13.07	1206	11.31	1272.8	41.66				
ACO-12-52a	77	0.0955	0.0016	0.2072	0.0026	2.7279	0.0453	0.081	0.0025	79	1537.7	30.3	1214	13.81	1336.1	12.33	1573.8	47.42				
ACO-12-52a	78	0.082	0.0013	0.2059	0.0025	2.3265	0.0367	0.0624	0.002	97	1244.5	29.74	1206.9	13.21	1220.4	11.2	1223.7	38.85				
ACO-12-52a	79	0.1056	0.0016	0.3027	0.0037	4.4065	0.0683	0.0874	0.0028	99	1724.8	27.21	1704.5	18.19	1713.6	12.82	1693.3	51.44				
ACO-12-52a	80	0.1222	0.0019	0.3647	0.0044	6.1444	0.0977	0.1043	0.0036	101	1988.6	27.52	2004.5	20.73	1996.6	13.89	2006	65.14				

ACO-12-52B	1	0.0852	0.0011	0.2299	0.0027	2.698	0.0375	0.0419	0.001	99	1318.8	25.59	1333.8	14.38	1327.9	10.29	829.2	19.64	
ACO-12-52B	2	0.2067	0.4294	9.717	34.762	278.04	*********	*********	**********	#VALUE!	2880	1712.8	*******	********	5718	4071.4	-NaN	*******	
ACO-12-52B	3	0.0856	0.0012	0.231	0.0028	2.7269	0.0397	0.048	0.0013	99	1330.1	26.9	1339.7	14.61	1335.8	10.82	948.4	24.96	
ACO-12-52B	4	0.0934	0.0012	0.2796	0.0029	3.5985	0.0444	0.0764	0.0018	94	1495.2	23.77	1589.3	14.72	1549.2	9.81	1487.3	34.11	
ACO-12-52B	5	0.0792	0.001	0.2079	0.0023	2.2699	0.029	0.0525	0.0011	97	1177.3	25.07	1217.6	11.99	1203	8.99	1033.7	21.24	
ACO-12-52B	6	0.1324	0.0016	0.4006	0.0043	7.3144	0.0872	0.0934	0.0019	98	2130.5	20.59	2172	19.84	2150.6	10.65	1804.8	35.85	
ACO-12-52B	7	0.0804	0.0011	0.1688	0.0019	1.8703	0.0264	0.0521	0.0014	120	1206.2	27.23	1005.5	10.66	1070.6	9.35	1027.4	27.21	
ACO-12-52B	8	0.1198	0.0014	0.3697	0.004	6.1053	0.0729	0.0719	0.0015	96	1953.2	20.97	2027.9	18.79	1991	10.41	1403.3	27.28	
ACO-12-52B	9	0.0896	0.0012	0.1902	0.0021	2.3506	0.031	0.0504	0.0012	126	1417.8	25.08	1122.5	11.27	1227.7	9.38	994.5	22.17	
ACO-12-52B	10	0.0802	0.0013	0.2176	0.0027	2.4048	0.0405	0.0513	0.0021	95	1201.7	32.33	1269	14.22	1244	12.06	1010.6	39.97	
ACO-12-52B	11	0.0814	0.001	0.213	0.0022	2.3895	0.0292	0.0533	0.0014	99	1230.4	24.12	1244.8	11.78	1239.5	8.75	1049.1	27	
ACO-12-52B	12	0.0851	0.0011	0.2435	0.0027	2.8567	0.0369	0.0525	0.0012	94	1317.5	24.78	1405	13.79	1370.6	9.7	1034.6	22.86	
ACO-12-52B	13	0.1086	0.0018	0.3173	0.004	4.751	0.0793	0.0625	0.0022	100	1776.4	29.87	1776.5	19.52	1776.3	14	1226.2	42.63	
ACO-12-52B	14	0.0873	0.0015	0.2779	0.0036	3.345	0.0581	0.0258	0.0008	87	1367.6	33.26	1580.8	18.15	1491.6	13.57	515	15.26	
ACO-12-52B	15	0.078	0.001	0.2296	0.0025	2.4701	0.0305	0.0443	0.001	86	1147.5	24.02	1332.6	12.99	1263.3	8.93	876.7	19.94	
ACO-12-52B	16	0.0712	0.0009	0.1892	0.0021	1.8566	0.0232	0.0357	0.0008	86	962.1	25.16	1117.3	11.16	1065.8	8.23	708.7	16.3	
ACO-12-52B	17	0.0804	0.0013	0.2205	0.0027	2.4423	0.0406	0.0511	0.0021	94	1206	32.19	1284.3	14.09	1255.2	11.99	1007.6	40.25	
ACO-12-52B	18	0.1021	0.0015	0.3158	0.0037	4.4458	0.0652	0.0626	0.0021	94	1663.1	26.35	1769.1	18.15	1720.9	12.16	1227.6	39.16	
ACO-12-52B	19	0.078	0.0011	0.2213	0.0025	2.3784	0.0322	0.036	0.0008	89	1146	26.57	1288.6	12.99	1236.1	9.67	715	16.35	
ACO-12-52B	20	0.0836	0.002	0.2189	0.0032	2.5222	0.0584	0.0433	0.0017	101	1283.3	45.67	1276.2	16.75	1278.5	16.83	856.6	33.29	
ACO-12-52B	21	0.1247	0.0015	0.3744	0.0043	6.431	0.0824	0.0549	0.0013	99	2024.6	21.4	2050	20.35	2036.5	11.25	1079.3	24.63	
ACO-12-52B	22	0.083	0.0011	0.2105	0.0025	2.4064	0.0324	0.037	0.0009	103	1269.9	25.07	1231.2	13.16	1244.5	9.65	734.9	17.99	
ACO-12-52B	23	0.0908	0.0012	0.2929	0.0031	3.6674	0.0467	0.0673	0.0017	87	1442.7	24.44	1656.1	15.63	1564.3	10.17	1315.9	31.57	
ACO-12-52B	24	0.0818	0.0013	0.2161	0.0026	2.4355	0.038	0.032	0.0008	98	1240.8	30.13	1261.3	13.93	1253.1	11.22	636.8	15.69	
ACO-12-52B	25	0.0717	0.001	0.1817	0.002	1.7952	0.0241	0.0406	0.001	91	976.7	26.69	1076.3	11.13	1043.7	8.75	805.1	18.85	
ACO-12-52B	26	0.0751	0.0012	0.1894	0.0023	1.9595	0.0312	0.049	0.0022	96	1070.8	31.05	1118.1	12.63	1101.7	10.71	966.7	42.35	
ACO-12-52B	27	0.1021	0.0013	0.2697	0.0029	3.796	0.0473	0.0681	0.0016	108	1662.9	22.76	1539.1	14.88	1591.9	10	1332.4	30.4	
ACO-12-52B	28	0.0911	0.0016	0.2495	0.0032	3.1289	0.0532	0.0336	0.001	101	1447.5	32.28	1435.7	16.53	1439.8	13.07	667.9	19.22	
ACO-12-52B	29	0.0696	0.0012	0.1762	0.0022	1.6895	0.029	0.0373	0.0012	88	916.1	35	1046.1	11.84	1004.6	10.97	740.7	22.94	
ACO-12-52B	30	0.1064	0.0013	0.3463	0.0039	5.0811	0.0626	0.055	0.0011	91	1739.3	21.91	1917	18.49	1832.9	10.45	1082.1	21.75	
ACO-12-52B	31	0.1174	0.0017	0.2702	0.0032	4.3731	0.0624	0.0751	0.0025	124	1917.6	25.06	1541.8	16	1707.3	11.8	1464.2	47.74	
ACO-12-52B	32	0.1143	0.0014	0.3596	0.004	5.6628	0.0695	0.0482	0.0009	94	1868	21.62	1980.3	19.02	1925.7	10.59	951.9	17.67	
ACO-12-52B	33	0.0795	0.001	0.223	0.0024	2.4431	0.0302	0.0561	0.0015	91	1184.2	23.72	1297.5	12.81	1255.4	8.9	1102.3	28.15	
ACO-12-52B	34	0.0887	0.0014	0.2765	0.0032	3.3805	0.0508	0.0692	0.0022	89	1397.7	28.8	1573.6	16.08	1499.9	11.78	1352	41.15	
ACO-12-52B	35	0.1051	0.0026	0.2244	0.0031	3.2524	0.076	0.0736	0.0046	132	1716.8	44.72	1305	16.35	1469.7	18.15	1435.3	86.13	
ACO-12-52B	36	0.0818	0.0009	0.2076	0.0023	2.3387	0.0273	0.0466	0.0009	102	1239.5	22.11	1215.7	12.07	1224.1	8.3	921	18.18	
ACO-12-52B	37	0.081	0.001	0.2112	0.0023	2.3584	0.0299	0.055	0.0017	99	1221.9	24.23	1234.9	12.29	1230.1	9.03	1081.7	32.23	
ACO-12-52B	38	0.1198	0.0018	0.3762	0.0044	6.2114	0.095	0.0938	0.0047	95	1953	26.88	2058.5	20.41	2006.1	13.38	1812.2	85.87	
ACO-12-52B	39	0.0891	0.0013	0.2441	0.0028	2.9971	0.0436	0.0686	0.0024	100	1405.6	27.58	1408	14.42	1406.9	11.07	1341.6	44.4	
ACO-12-52B	40	0.0767	0.0011	0.1864	0.0022	1.9705	0.0284	0.0355	0.0012	101	1113	27.6	1102	11.98	1105.5	9.7	704.1	22.67	
ACO-12-52B	41	0.0845	0.001	0.2498	0.0028	2.9094	0.0368	0.0467	0.0008	91	1303.6	23.78	1437.6	14.43	1384.4	9.56	923.1	16.29	

ACO-12-52B	42	0.1049	0.0014	0.298	0.0033	4.3089	0.0577	0.0895	0.0025	102	1712.4	24.76	1681.4	16.22	1695.1	11.03	1731.6	45.54			
ACO-12-52B	43	0.0694	0.0009	0.1804	0.002	1.7253	0.0223	0.0296	0.0006	85	909.8	25.87	1069.3	11.04	1018	8.3	589.6	10.8			
ACO-12-52B	44	0.0814	0.0011	0.2183	0.0024	2.4493	0.0324	0.0551	0.0012	97	1230.7	25.3	1273	12.94	1257.2	9.54	1084.3	23.32			
ACO-12-52B	45	0.0751	0.0009	0.1841	0.0021	1.9063	0.0245	0.0416	0.0008	98	1071.3	24.86	1089.5	11.23	1083.3	8.55	822.9	16.15			
ACO-12-52B	46	0.0882	0.001	0.2883	0.0032	3.5051	0.0411	0.0443	0.0008	85	1387.3	21.49	1632.8	15.89	1528.4	9.26	875.1	14.78			
ACO-12-52B	47	0.0736	0.0011	0.1846	0.0022	1.8728	0.0289	0.0455	0.0018	94	1030.5	30.21	1092.2	11.93	1071.5	10.2	899.8	35.48			
ACO-12-52B	48	0.0726	0.0013	0.1765	0.0022	1.7667	0.0305	0.0313	0.0009	96	1003.8	34.52	1047.8	12.15	1033.3	11.21	621.9	18.16			
ACO-12-52B	49	0.1045	0.0012	0.3491	0.0039	5.0286	0.0599	0.0555	0.0011	88	1705.7	20.99	1930.3	18.46	1824.2	10.09	1091.3	21.02			
ACO-12-52B	50	0.0751	0.001	0.1781	0.002	1.8424	0.0241	0.0344	0.0007	101	1070	25.5	1056.6	10.94	1060.7	8.61	684.1	13.46			
ACO-12-52B	51	0.0941	0.0013	0.2668	0.003	3.4604	0.047	0.0794	0.0022	99	1510.1	25.26	1524.4	15.24	1518.2	10.71	1544.6	41.25			
ACO-12-52B	52	0.0915	0.0015	0.3022	0.0034	3.8096	0.06	0.0739	0.0033	86	1456.1	30.59	1701.9	16.7	1594.8	12.67	1440.8	62			
ACO-12-52B	53	0.1211	0.0016	0.3879	0.0045	6.4705	0.0862	0.0583	0.0014	93	1971.7	22.94	2112.9	20.93	2041.9	11.71	1145.7	26.61			
ACO-12-52B	54	0.083	0.0016	0.2576	0.0031	2.9474	0.0538	0.0622	0.0028	86	1268.9	36.41	1477.7	15.69	1394.2	13.85	1219.6	53.12			
ACO-12-52B	55	0.1154	0.0016	0.3293	0.004	5.2385	0.0745	0.0475	0.0012	103	1886.6	24.82	1835.2	19.16	1858.9	12.13	937.6	23.61			
ACO-12-52B	56	0.0735	0.0014	0.1791	0.0022	1.8154	0.0341	0.0413	0.0015	97	1029	38.09	1061.9	12.17	1051	12.28	817.8	29.1			
ACO-12-52B	57	0.0913	0.0011	0.3031	0.0034	3.8119	0.0481	0.0473	0.0011	85	1451.7	23.22	1706.8	16.77	1595.2	10.16	933.3	20.19			
ACO-12-52B	58	0.082	0.0025	0.2062	0.0033	2.3291	0.067	0.0354	0.0025	103	1245.4	57.42	1208.4	17.36	1221.2	20.44	702.1	48.27			
ACO-12-52B	59	0.0764	0.0012	0.1867	0.0022	1.9669	0.0304	0.0311	0.0008	100	1106.3	30.53	1103.7	12.04	1104.3	10.41	618.2	16.08			
ACO-12-52B	60	0.0924	0.0012	0.3137	0.0035	3.996	0.0516	0.0597	0.0016	84	1475.9	23.74	1759	17.22	1633.4	10.49	1172.4	29.59			
ACO-12-52B	61	0.0812	0.001	0.2326	0.0026	2.6021	0.0331	0.0495	0.0012	91	1225.1	24	1347.9	13.51	1301.2	9.32	976	22.97			
ACO-12-52B	62	0.0901	0.0019	0.1565	0.0022	1.9442	0.0395	0.0241	0.0008	152	1427.1	39.37	937.4	11.97	1096.4	13.64	482.1	14.82			
ACO-12-52B	63	0.078	0.001	0.2184	0.0025	2.3473	0.0299	0.0337	0.0007	90	1146	24.29	1273.2	13.03	1226.7	9.08	669.4	14.21			
ACO-12-52B	64	0.0933	0.0016	0.2963	0.0038	3.8137	0.0657	0.0297	0.0009	89	1494	32.15	1672.9	18.99	1595.6	13.85	591	18.31			
ACO-12-52B	65	0.0769	0.0017	0.2172	0.0028	2.302	0.0479	0.0505	0.0025	88	1117.8	42.4	1267	14.67	1212.9	14.74	995.8	47.78			
ACO-12-52B	66	0.1023	0.0012	0.2916	0.0033	4.1121	0.0498	0.0446	0.0009	101	1665.7	21.45	1649.6	16.25	1656.7	9.89	881.3	17.13			
ACO-12-52B	67	0.0884	0.0012	0.2641	0.003	3.2181	0.0441	0.0503	0.0013	92	1390.2	25.44	1511	15.45	1461.5	10.62	991.2	24.29			
ACO-12-52B	68	0.0973	0.0024	0.2689	0.0037	3.6091	0.0857	0.0718	0.0044	103	1573.8	45.91	1535	18.92	1551.5	18.88	1401.2	82.65			
ACO-12-52B	69	0.0935	0.0016	0.2843	0.0036	3.6661	0.0628	0.0549	0.0019	93	1498.6	31.86	1612.8	18.03	1564	13.66	1080.7	36.36			
ACO-12-52B	70	0.1012	0.0017	0.3488	0.0042	4.867	0.0815	0.0763	0.0031	85	1646.1	31.32	1929	19.96	1796.6	14.1	1486.5	58.43			
ACO-12-52B	71	0.0747	0.0012	0.2038	0.0025	2.1006	0.0342	0.029	0.0007	89	1061.6	32.64	1195.8	13.21	1149	11.2	577.8	14.29			
ACO-12-52B	72	0.0775	0.001	0.2376	0.0027	2.5394	0.0326	0.0386	0.001	83	1134.1	24.46	1374.4	13.98	1283.4	9.35	764.8	18.95			
ACO-12-52B	73	0.1021	0.0031	0.3172	0.0051	4.465	0.1272	0.0755	0.0048	94	1661.9	54.4	1776.1	25.09	1724.5	23.63	1470.2	89.89			
ACO-12-52B	74	0.0879	0.0012	0.2714	0.0032	3.2889	0.0467	0.046	0.0013	89	1380.1	26.51	1547.8	16.03	1478.4	11.06	909	25.33			
ACO-12-52B	75	0.0774	0.0011	0.2263	0.0027	2.4161	0.0357	0.0365	0.001	86	1132	28.81	1315.3	13.98	1247.4	10.62	725.2	20.18			
ACO-12-52B	76	0.0843	0.0015	0.2611	0.0034	3.0352	0.0532	0.0339	0.0014	87	1299.3	33.19	1495.3	17.13	1416.5	13.39	672.9	26.5			
ACO-12-52B	77	0.0891	0.0013	0.2782	0.0033	3.4188	0.0503	0.0487	0.0015	89	1407.1	27.44	1582.1	16.53	1508.7	11.57	961.9	29.29			
ACO-12-52B	78	0.0825	0.0012	0.2604	0.0031	2.9598	0.0441	0.0502	0.0019	84	1256.3	27.97	1491.7	15.71	1397.4	11.32	990.6	36.4			
ACO-12-52B	79	0.0758	0.0011	0.2132	0.0025	2.2273	0.0322	0.0441	0.0016	87	1089.1	28.06	1245.8	13.11	1189.7	10.13	873.1	31.3			
ACO-12-52B	80	0.1042	0.0016	0.3491	0.0041	5.015	0.0757	0.0758	0.0028	88	1700	27.13	1930.4	19.75	1821.9	12.78	1476	53.39			
ACO-12-54	1	0.0603	0.0007	0.1028	0.0011	0.8544	0.0103	0.0288	0.0006	101	615	25.55	630.5	6.41	627	5.66	574.7	12.04			

ACO-12-54	2	0.0601	0.0009	0.1024	0.0011	0.8482	0.0119	0.0307	0.0008	101	607	31.28	628.3	6.2	623.6	6.52	610.6	15.34
ACO-12-54	3	0.0612	0.0008	0.1039	0.0011	0.877	0.0117	0.0307	0.0007	100	647.2	28.69	637.2	6.52	639.3	6.34	610.9	13.28
ACO-12-54	4	0.0615	0.001	0.102	0.0012	0.8655	0.0138	0.0264	0.0006	99	657.6	34.2	626.4	6.82	633.1	7.51	525.9	11.9
ACO-12-54	5	0.0591	0.0009	0.1036	0.0011	0.8448	0.0119	0.0317	0.0008	102	571.6	31.25	635.7	6.37	621.8	6.53	630	15.74
ACO-12-54	6	0.0613	0.0007	0.1021	0.0011	0.8627	0.0105	0.0238	0.0005	99	648.7	25.83	626.9	6.38	631.6	5.74	475	9.58
ACO-12-54	7	0.0711	0.0009	0.1697	0.0018	1.6632	0.0212	0.0424	0.001	102	960.2	25.81	1010.3	10.1	994.6	8.09	840	18.76
ACO-12-54	8	0.0713	0.001	0.1023	0.0011	1.0061	0.0142	0.0288	0.0007	89	966.6	28.96	628	6.63	706.9	7.21	574.2	13.05
ACO-12-54	9	0.0591	0.0008	0.1038	0.0012	0.8455	0.0122	0.0257	0.0007	102	570.4	30.64	636.5	6.87	622.2	6.69	513.1	13
ACO-12-54	10	0.0596	0.0009	0.1043	0.0012	0.8569	0.0128	0.0243	0.0006	102	588	32.06	639.8	6.91	628.4	7	484.7	11.68
ACO-12-54	11	0.0761	0.0013	0.1118	0.0013	1.1734	0.0189	0.0244	0.0006	62	1097.9	32.68	683.4	7.49	788.3	8.83	487.5	11.84
ACO-12-54	12	0.0605	0.0008	0.1018	0.0011	0.849	0.0113	0.0279	0.0007	100	620.7	28.37	625.1	6.45	624.1	6.18	555.3	14.27
ACO-12-54	13	0.0628	0.0009	0.112	0.0012	0.9692	0.0138	0.0322	0.0009	99	700.2	30.16	684.4	7.15	688	7.09	640.9	16.92
ACO-12-54	14	0.0645	0.0009	0.1299	0.0014	1.154	0.0161	0.033	0.0009	101	756.6	29.31	787.1	8.15	779.1	7.59	657	17.19
ACO-12-54	15	0.0616	0.0009	0.1052	0.0012	0.8928	0.0124	0.0314	0.0009	100	658.8	29.77	644.8	6.69	647.9	6.67	625.2	18.3
ACO-12-54	16	0.0604	0.0009	0.1018	0.0011	0.8468	0.0128	0.029	0.0009	100	616.4	32.77	624.7	6.61	622.9	7.04	577.5	17.56
ACO-12-54	17	0.0803	0.0011	0.2183	0.0023	2.4178	0.0319	0.0636	0.0022	106	1205.1	26.18	1273	12.3	1247.9	9.48	1245.9	41.37
ACO-12-54	18	0.1097	0.0015	0.3216	0.0036	4.8624	0.0662	0.0782	0.0026	100	1793.6	24.26	1797.7	17.68	1795.8	11.47	1521.6	48.53
ACO-12-54	19	0.0613	0.0011	0.0981	0.0012	0.8288	0.0152	0.0194	0.0007	98	648.8	38.73	603.4	7.28	612.9	8.46	389	14.02
ACO-12-54	20	0.0606	0.002	0.1015	0.0016	0.8478	0.0276	0.024	0.0013	100	624.3	70.63	623.2	9.59	623.4	15.16	479.7	25.16
ACO-12-54	21	0.0603	0.0008	0.1011	0.0011	0.8397	0.0111	0.0253	0.0005	100	613.4	28.3	620.5	6.44	619	6.15	505.5	10.23
ACO-12-54	22	0.0612	0.0007	0.103	0.0011	0.869	0.0105	0.0294	0.0006	100	646.1	25.4	632	6.44	635	5.72	585.1	12.49
ACO-12-54	23	0.0594	0.0009	0.1032	0.0012	0.8447	0.0126	0.0289	0.0007	102	581.8	32.21	632.8	6.71	621.7	6.91	575.2	12.69
ACO-12-54	24	0.0598	0.0008	0.1029	0.0011	0.848	0.0115	0.0316	0.0008	101	595.3	30.14	631.3	6.45	623.6	6.33	628.3	15.32
ACO-12-54	25	0.0603	0.0009	0.0914	0.001	0.7603	0.0111	0.0225	0.0005	98	615.5	30.98	563.8	6.13	574.2	6.41	449.8	10.6
ACO-12-54	26	0.0638	0.0012	0.1013	0.0011	0.8901	0.0161	0.0322	0.0011	96	733.8	39.77	621.7	6.67	646.4	8.67	641.1	20.66
ACO-12-54	27	0.0614	0.0014	0.1012	0.0013	0.8564	0.0189	0.026	0.0008	99	653	47.5	621.4	7.72	628.2	10.31	518.7	16.01
ACO-12-54	28	0.0603	0.0009	0.1026	0.0011	0.8527	0.0125	0.0287	0.0007	101	613.8	31.5	629.6	6.64	626.1	6.83	571.6	14.17
ACO-12-54	29	0.0614	0.0009	0.1011	0.0011	0.856	0.0119	0.0276	0.0007	99	654.6	29.58	620.6	6.51	627.9	6.51	549.9	13.61
ACO-12-54	30	0.0629	0.0009	0.1025	0.0011	0.8892	0.0129	0.0331	0.0009	97	706.2	30.93	628.9	6.55	645.9	6.91	657.8	18.48
ACO-12-54	31	0.0605	0.0009	0.1012	0.0011	0.8448	0.0118	0.029	0.0008	100	622.4	29.86	621.7	6.49	621.8	6.48	577	15.48
ACO-12-54	32	0.0604	0.0008	0.1024	0.0011	0.8528	0.0115	0.0292	0.0008	100	619.3	28.62	628.2	6.52	626.2	6.27	581.3	15.48
ACO-12-54	33	0.0595	0.0009	0.1028	0.0012	0.8428	0.0129	0.0299	0.0009	102	584.1	33.33	630.9	6.73	620.7	7.13	595.3	17.29
ACO-12-54	34	0.0772	0.0012	0.1905	0.0022	2.0272	0.0304	0.0515	0.0015	100	1126.6	29.91	1123.8	11.71	1124.7	10.2	1015.6	28.95
ACO-12-54	35	0.061	0.0016	0.1072	0.0014	0.9007	0.0228	0.0364	0.0017	101	637.4	56.12	656.4	7.97	652.1	12.17	722.9	33.43
ACO-12-54	36	0.0596	0.0016	0.1032	0.0013	0.8481	0.0213	0.0326	0.0017	102	589.9	56.22	633	7.62	623.6	11.7	647.6	33.88
ACO-12-54	37	0.0606	0.0009	0.104	0.0012	0.8688	0.0124	0.0299	0.0009	100	624.5	30.49	637.9	6.7	634.9	6.72	595.6	17.95
ACO-12-54	38	0.0613	0.0022	0.0972	0.0015	0.821	0.0281	0.0295	0.0012	98	650	74.97	597.7	8.92	608.6	15.64	587.7	24.38
ACO-12-54	39	0.0643	0.0016	0.1025	0.0015	0.9081	0.022	0.0208	0.001	96	752.3	51	628.9	8.53	656.1	11.7	416.4	20.56
ACO-12-54	40	0.0605	0.0009	0.1014	0.0011	0.8452	0.0126	0.0279	0.0009	100	620.5	31.96	622.6	6.6	622	6.91	557	18.53
ACO-12-54	41	0.1282	0.0015	0.377	0.0041	6.662	0.078	0.0991	0.0022	99	2073.2	20.1	2062.2	18.98	2067.6	10.34	1910.4	39.51
ACO-12-54	42	0.0601	0.0008	0.1004	0.0011	0.8325	0.0106	0.0256	0.0005	100	608.2	27.08	616.9	6.38	615	5.89	510.5	10.28

ACO-12-54	43	0.0625	0.0008	0.0996	0.0011	0.8576	0.0109	0.0275	0.0006	97	690.1	26.48	612	6.31	628.8	5.93	548.2	11.92			
ACO-12-54	44	0.0807	0.0015	0.2062	0.0024	2.2943	0.0393	0.0604	0.002	100	1214	35.05	1208.7	12.54	1210.5	12.12	1184.4	37.3			
ACO-12-54	45	0.091	0.0011	0.2485	0.0027	3.1173	0.0395	0.0616	0.0015	99	1446.6	23.68	1430.5	14.09	1437	9.74	1209.1	28.11			
ACO-12-54	46	0.0855	0.002	0.1704	0.0023	2.0092	0.044	0.0491	0.0014	76	1327.4	43.64	1014.3	12.59	1118.6	14.85	969.3	26.51			
ACO-12-54	47	0.0657	0.0008	0.1257	0.0014	1.138	0.0146	0.0346	0.0008	99	795.9	26.4	763.2	7.82	771.5	6.93	688	16.41			
ACO-12-54	48	0.0623	0.0009	0.1003	0.0011	0.8616	0.0119	0.026	0.0006	98	684.3	29.01	616.3	6.48	631	6.46	519	12.32			
ACO-12-54	49	0.1369	0.0019	0.1336	0.0015	2.5203	0.0343	0.0566	0.0014	37	2188.2	23.78	808.1	8.67	1277.9	9.9	1112	26.33			
ACO-12-54	50	0.0801	0.0013	0.2113	0.0025	2.3322	0.0379	0.0584	0.0017	103	1198.5	32.33	1235.8	13.2	1222.2	11.56	1147.9	32.93			
ACO-12-54	51	0.119	0.0015	0.352	0.0039	5.7761	0.0716	0.0817	0.0021	100	1941.8	21.66	1944	18.42	1942.8	10.73	1586.4	38.67			
ACO-12-54	52	0.0914	0.0016	0.1061	0.0013	1.3372	0.0233	0.0329	0.0009	45	1455.6	33.91	649.9	7.5	862	10.11	653.8	18.16			
ACO-12-54	53	0.0599	0.0008	0.1026	0.0011	0.8469	0.0112	0.029	0.0008	101	598.1	28.06	629.9	6.56	622.9	6.14	578.6	15.68			
ACO-12-54	54	0.0606	0.001	0.1025	0.0012	0.8566	0.0138	0.0296	0.0009	100	626.1	34.68	628.9	6.82	628.2	7.52	589	17.56			
ACO-12-54	55	0.0607	0.0014	0.1037	0.0013	0.8671	0.0197	0.0276	0.0009	100	627.3	49.8	636	7.77	634	10.73	550.3	16.79			
ACO-12-54	56	0.0891	0.0019	0.255	0.0035	3.1315	0.0652	0.0633	0.0029	104	1405.9	39.64	1464.2	18.09	1440.5	16.03	1240.6	54.91			
ACO-12-54	57	0.062	0.001	0.1028	0.0012	0.8792	0.0145	0.0287	0.0011	98	675.4	34.68	630.8	7.18	640.6	7.85	571.6	21.83			
ACO-12-54	58	0.06	0.0009	0.1049	0.0012	0.8673	0.0136	0.0282	0.001	101	602.9	33.47	642.9	7.08	634.1	7.39	562.8	19.21			
ACO-12-54	59	0.1799	0.0024	0.5402	0.0062	13.398	0.1815	0.1235	0.004	105	2652	21.95	2784.4	26.11	2708.2	12.8	2352.9	72.7			
ACO-12-54	60	0.0972	0.0015	0.2814	0.0033	3.7712	0.058	0.0783	0.0028	102	1571.6	28.89	1598.2	16.56	1586.6	12.35	1523.1	51.58			
ACO-12-54	61	0.0626	0.0012	0.103	0.0013	0.8884	0.0165	0.0258	0.0008	98	694.3	39.03	631.7	7.56	645.5	8.86	514.7	15.26			
ACO-12-54	62	0.0599	0.0009	0.1078	0.0013	0.8904	0.0134	0.0297	0.0008	102	599.2	31.66	660.2	7.3	646.6	7.18	591.4	16.14			
ACO-12-54	63	0.0603	0.0009	0.1061	0.0012	0.8813	0.0127	0.0293	0.0008	101	612.8	30.91	650	6.9	641.7	6.87	583.2	14.65			
ACO-12-54	64	0.06	0.001	0.1073	0.0013	0.8877	0.0155	0.0289	0.001	102	604.5	36.81	656.8	7.69	645.1	8.31	575.1	19.13			
ACO-12-54	65	0.0614	0.0008	0.1065	0.0012	0.9013	0.0123	0.0279	0.0007	100	653.4	28.77	652.2	6.85	652.4	6.56	556.4	13.93			
ACO-12-54	66	0.0595	0.0009	0.1062	0.0012	0.8713	0.0132	0.0299	0.0009	102	586.5	32.37	650.4	7.03	636.3	7.14	594.6	17.27			
ACO-12-54	67	0.0603	0.001	0.1037	0.0012	0.8621	0.0136	0.0274	0.0008	101	615.2	33.78	635.7	6.99	631.2	7.42	546.2	15.71			
ACO-12-54	68	0.0599	0.0008	0.1069	0.0012	0.8821	0.0124	0.0302	0.0008	102	598.8	30.12	654.5	6.9	642.1	6.7	601.1	16.33			
ACO-12-54	69	0.061	0.0009	0.1069	0.0012	0.8996	0.0126	0.0316	0.0009	101	640.1	30.1	654.8	6.76	651.5	6.72	628	18.38			
ACO-12-54	70	0.0616	0.0009	0.1066	0.0012	0.9058	0.0132	0.0315	0.001	100	660.7	31.35	653.1	6.86	654.8	7.05	626.9	19.52			
ACO-12-54	71	0.0602	0.0009	0.1022	0.0011	0.8481	0.0119	0.0289	0.0009	101	610	30.22	627.4	6.57	623.6	6.55	576.6	16.73			
ACO-12-54	72	0.0816	0.0011	0.2147	0.0024	2.4169	0.034	0.0542	0.0015	101	1236.8	27.26	1253.9	12.88	1247.6	10.11	1065.8	29.5			
ACO-12-54	73	0.0626	0.0011	0.1174	0.0014	1.0131	0.0171	0.0332	0.001	101	693.6	36.02	715.8	7.89	710.4	8.62	659.5	19.8			
ACO-12-54	74	0.0663	0.0011	0.1316	0.0014	1.2019	0.0191	0.0372	0.0014	99	814.9	34.34	796.8	8.12	801.4	8.82	738.9	26.6			
ACO-12-54	75	0.0602	0.0008	0.1077	0.0012	0.8945	0.012	0.0287	0.0008	102	612.2	28.45	659.4	6.91	648.8	6.44	571	16.11			
ACO-12-54	76	0.0603	0.0008	0.1094	0.0012	0.9086	0.0126	0.0303	0.0009	102	612.5	29.54	669.1	7.06	656.3	6.72	603.7	17.49			
ACO-12-54	77	0.0616	0.001	0.1064	0.0012	0.9037	0.0143	0.0286	0.0009	100	659.4	33.64	652	7.13	653.7	7.61	569.2	16.94			
ACO-12-54	78	0.0588	0.001	0.1064	0.0013	0.8628	0.0144	0.0283	0.001	103	560.8	35.81	651.6	7.36	631.7	7.84	564.4	19.4			
ACO-12-54	79	0.0597	0.0008	0.1054	0.0012	0.867	0.012	0.0282	0.0009	102	591.7	29.4	645.9	6.81	633.9	6.5	562.4	16.81			
ACO-12-54	80	0.063	0.0008	0.1299	0.0014	1.1284	0.015	0.0359	0.0011	103	707.5	27.68	787.5	8.15	767	7.15	712.8	21.71			
ACO-12-50	1	0.0985	0.0013	0.2805	0.0032	3.8068	0.0494	0.0738	0.0018	100	1595.4	23.53	1593.7	15.89	1594.2	10.42	1438.7	34.12			
ACO-12-50	2	0.062	0.0011	0.109	0.0013	0.9313	0.0168	0.0345	0.001	100	674.4	39	666.9	7.42	668.3	8.81	685.7	19.07			

ACO-12-50	3	0.0967	0.0013	0.2739	0.0032	3.6514	0.0512	0.0624	0.0016	100	1561.1	25.12	1560.6	16.42	1560.8	11.17	1222.8	31.25
ACO-12-50	4	0.0704	0.0011	0.1498	0.0018	1.4536	0.0231	0.0415	0.0012	99	940	31.74	899.7	10.08	911.4	9.55	822.7	24.15
ACO-12-50	5	0.061	0.0013	0.0987	0.0013	0.8307	0.0174	0.0256	0.0008	99	640.6	44.76	606.8	7.6	614	9.65	511.5	15.76
ACO-12-50	6	0.0625	0.0011	0.1076	0.0013	0.9269	0.0161	0.0272	0.0008	99	690.7	37.07	658.9	7.47	666	8.5	541.4	14.76
ACO-12-50	7	0.0635	0.0015	0.105	0.0013	0.9189	0.0212	0.031	0.0012	97	724.4	50.25	643.8	7.73	661.8	11.19	616.4	23.52
ACO-12-50	8	0.0612	0.0009	0.1038	0.0012	0.8755	0.0128	0.0277	0.0008	100	646.5	30.71	636.5	6.9	638.6	6.91	551.6	14.79
ACO-12-50	9	0.106	0.0015	0.3204	0.0038	4.6803	0.0664	0.0654	0.0017	103	1731.2	25.57	1791.7	18.34	1763.7	11.87	1279.4	31.55
ACO-12-50	10	0.0622	0.0011	0.0959	0.0011	0.8219	0.0143	0.028	0.001	97	680.6	37.66	590.3	6.54	609.1	7.98	558.5	18.63
ACO-12-50	11	0.0611	0.001	0.1066	0.0012	0.8973	0.0139	0.029	0.0009	100	641.9	32.94	652.9	7.17	650.3	7.45	576.9	16.91
ACO-12-50	12	0.0667	0.0009	0.1014	0.0012	0.9315	0.0134	0.0223	0.0006	93	827.3	29.26	622.4	6.78	668.4	7.02	446.4	12.15
ACO-12-50	13	0.0645	0.0018	0.1084	0.0015	0.9632	0.026	0.0338	0.0016	97	757.6	58.62	663.2	8.59	684.9	13.44	671.6	31.19
ACO-12-50	14	0.0648	0.0013	0.129	0.0015	1.1525	0.0222	0.0395	0.0017	100	768.7	41.65	782.1	8.66	778.4	10.47	783.9	33.87
ACO-12-50	15	0.1838	0.0025	0.5609	0.0063	14.204	0.195	0.1581	0.0061	107	2687.1	22.66	2870.1	25.93	2763.4	13.02	2967	106.55
ACO-12-50	16	0.0633	0.0012	0.1078	0.0013	0.9401	0.0181	0.0311	0.0012	98	717.9	41.14	659.9	7.63	672.9	9.45	619.4	23.46
ACO-12-50	17	0.0626	0.001	0.1198	0.0014	1.0329	0.0157	0.0325	0.0011	101	693.1	31.92	729.4	7.95	720.4	7.86	646.6	21.79
ACO-12-50	18	0.0685	0.0013	0.1007	0.0012	0.9508	0.0177	0.0296	0.0011	91	883.6	38.72	618.5	7.26	678.5	9.23	588.7	20.88
ACO-12-50	19	0.0577	0.0012	0.1099	0.0014	0.8737	0.0174	0.0329	0.0013	105	517	44.34	672.3	7.83	637.6	9.45	654.7	25.6
ACO-12-50	20	0.0624	0.001	0.099	0.0012	0.8524	0.014	0.0241	0.0011	97	688.9	33.56	608.7	7.1	625.9	7.65	481.8	20.76
ACO-12-50	21	0.0782	0.0013	0.1044	0.0013	1.1258	0.0181	0.0281	0.0007	84	1152.8	31.63	639.9	7.32	765.7	8.64	559.6	12.79
ACO-12-50	22	0.0624	0.0013	0.1035	0.0013	0.8897	0.0177	0.0291	0.0008	98	686.7	42.49	634.7	7.6	646.2	9.49	578.9	15.77
ACO-12-50	23	0.0618	0.001	0.1119	0.0013	0.953	0.0156	0.0352	0.0011	101	667.1	35.46	683.6	7.34	679.7	8.12	698.9	21.31
ACO-12-50	24	0.0659	0.0018	0.101	0.0015	0.9178	0.0242	0.0262	0.001	94	803.5	55.35	620.2	8.78	661.2	12.8	522.1	18.99
ACO-12-50	25	0.0594	0.0013	0.1061	0.0013	0.868	0.0183	0.0332	0.0011	102	579.8	46.29	650	7.67	634.5	9.92	660.8	20.61
ACO-12-50	26	0.062	0.0008	0.1038	0.0012	0.8876	0.0115	0.0264	0.0007	99	673.9	26.45	636.9	6.85	645.1	6.2	526.1	12.78
ACO-12-50	27	0.0619	0.0012	0.1055	0.0013	0.8998	0.0168	0.0283	0.0008	99	670.1	39.81	646.3	7.57	651.6	8.97	563.3	15.7
ACO-12-50	28	0.0649	0.0013	0.1084	0.0014	0.9689	0.0191	0.0313	0.0009	96	769.6	41.59	663.2	7.92	687.9	9.84	622.8	18.39
ACO-12-50	29	0.0667	0.001	0.1303	0.0014	1.1981	0.0182	0.0392	0.0015	99	829.3	32.09	789.3	8.19	799.7	8.41	776.4	28.53
ACO-12-50	30	0.0627	0.0013	0.104	0.0013	0.8991	0.0182	0.0325	0.0012	98	698.6	42.91	637.6	7.73	651.2	9.71	645.8	22.89
ACO-12-50	31	0.1159	0.0018	0.1452	0.0018	2.3212	0.0362	0.041	0.0012	72	1894.6	27.75	874	10.02	1218.8	11.06	812.5	23.95
ACO-12-50	32	0.123	0.0017	0.357	0.0042	6.0562	0.085	0.0739	0.0022	98	2000.6	24.19	1968	20.03	1984	12.24	1440.2	40.95
ACO-12-50	33	0.0811	0.0012	0.2204	0.0026	2.4653	0.0359	0.0583	0.0019	105	1224.3	27.84	1284.1	13.57	1261.9	10.52	1144.7	35.86
ACO-12-50	34	0.0614	0.0013	0.1057	0.0013	0.8949	0.0185	0.0321	0.0016	100	654.2	45.61	647.6	7.38	649	9.94	637.8	30.66
ACO-12-50	35	0.0739	0.0009	0.1756	0.002	1.7901	0.0235	0.0475	0.0015	100	1039.4	25.2	1043	10.91	1041.9	8.54	937.5	29.32
ACO-12-50	36	0.096	0.0015	0.2757	0.0032	3.6474	0.0553	0.0777	0.0031	101	1546.9	28.32	1569.7	16.12	1559.9	12.07	1512.1	57.54
ACO-12-50	37	0.0601	0.0013	0.1081	0.0013	0.8962	0.0189	0.032	0.0016	102	607.6	46.65	661.9	7.65	649.7	10.13	636.1	30.96
ACO-12-50	38	0.0624	0.0016	0.113	0.0015	0.9715	0.0244	0.0387	0.0019	100	686.9	54.81	690	8.73	689.2	12.58	766.9	36.51
ACO-12-50	39	0.0631	0.0013	0.1157	0.0014	1.0059	0.0208	0.0386	0.0018	100	710.1	44.66	705.8	8.22	706.8	10.52	765.5	35.36
ACO-12-50	40	0.0649	0.0014	0.1032	0.0013	0.9235	0.0199	0.0305	0.0012	95	771.7	45.72	633	7.86	664.2	10.52	607.4	23.28
ACO-12-50	41	0.0829	0.0014	0.2091	0.0026	2.3905	0.0397	0.053	0.0013	97	1267.7	32.03	1223.8	13.72	1239.8	11.88	1043.4	25.73
ACO-12-50	42	0.0652	0.0013	0.108	0.0013	0.9697	0.0186	0.0321	0.001	96	779.7	41	660.8	7.55	688.3	9.58	638.9	19.21
ACO-12-50	43	0.062	0.0012	0.1097	0.0013	0.9377	0.0177	0.034	0.0011	100	674.5	41.13	671	7.52	671.7	9.27	676.6	21.46

ACO-12-50	44	0.0602	0.0012	0.1024	0.0012	0.8494	0.0167	0.0307	0.0011	101	609.9	43.6	628.5	7.06	624.3	9.18	611.9	22.08			
ACO-12-50	45	0.0606	0.0017	0.101	0.0014	0.8439	0.0227	0.0338	0.0012	100	624.5	59.09	620.5	8.21	621.3	12.5	671.3	23.65			
ACO-12-50	46	0.0623	0.0012	0.1072	0.0013	0.9209	0.0176	0.0332	0.0011	99	685	41.2	656.5	7.53	662.8	9.29	660	20.6			
ACO-12-50	47	0.0631	0.0011	0.1031	0.0012	0.8966	0.0152	0.0339	0.0011	97	712.4	36.29	632.2	6.94	649.9	8.11	672.9	21.74			
ACO-12-50	48	0.0624	0.001	0.1082	0.0013	0.9305	0.0149	0.0308	0.0009	99	687	33.8	662.3	7.38	667.9	7.85	612.8	17.01			
ACO-12-50	49	0.0617	0.0012	0.1008	0.0012	0.8581	0.0162	0.028	0.0008	98	665.2	40.46	619.1	7.24	629.1	8.85	558	15.96			
ACO-12-50	50	0.0897	0.0014	0.2826	0.0033	3.4938	0.0538	0.0818	0.0028	113	1418.5	29.08	1604.5	16.79	1525.8	12.16	1588.6	52.73			
ACO-12-50	51	0.0672	0.0014	0.1241	0.0017	1.1489	0.0237	0.0226	0.0009	97	842.7	41.97	753.9	9.84	776.7	11.2	451.6	16.94			
ACO-12-50	52	0.0629	0.0012	0.1136	0.0014	0.9846	0.0184	0.0355	0.0012	100	703.9	39.98	693.6	7.94	696	9.39	705.2	23.57			
ACO-12-50	53	0.066	0.0013	0.1109	0.0014	1.0086	0.0192	0.0358	0.0013	96	806.2	40.37	677.7	7.85	708.2	9.73	710.7	24.85			
ACO-12-50	54	0.0948	0.0015	0.2785	0.0034	3.6406	0.0588	0.0834	0.0037	104	1524.3	29.79	1584	17.07	1558.5	12.86	1619.1	69.75			
ACO-12-50	55	0.1008	0.0016	0.2904	0.0035	4.0348	0.0623	0.0769	0.0028	100	1638.5	28.2	1643.4	17.44	1641.2	12.56	1498	52.61			
ACO-12-50	56	0.197	0.0027	0.5644	0.0069	15.328	0.2193	0.112	0.0037	103	2801.2	22.56	2884.7	28.21	2835.9	13.64	2144.9	66.88			
ACO-12-50	57	0.0665	0.001	0.1286	0.0015	1.1795	0.0182	0.0373	0.0013	99	823.3	31.87	779.7	8.49	791.1	8.47	739.5	25.78			
ACO-12-50	58	0.0613	0.0012	0.1047	0.0012	0.8852	0.0171	0.0337	0.0017	100	651	42.67	641.9	7.13	643.8	9.18	670.6	33.44			
ACO-12-50	59	0.0609	0.001	0.1091	0.0013	0.9158	0.0153	0.0291	0.0012	101	634.2	35.03	667.7	7.7	660.1	8.09	579.3	23.2			
ACO-12-50	60	0.0619	0.0011	0.1121	0.0013	0.9564	0.0165	0.0331	0.0013	100	670.8	36.93	684.7	7.68	681.4	8.55	658.9	25.07			
ACO-12-50	61	0.0753	0.0017	0.1748	0.0022	1.8137	0.0384	0.0548	0.002	97	1075.1	43.79	1038.5	12.1	1050.4	13.85	1077.9	37.35			
ACO-12-50	62	0.0612	0.001	0.1017	0.0011	0.8586	0.014	0.0302	0.001	99	647.2	35.83	624.3	6.59	629.4	7.65	600.7	20.05			
ACO-12-50	63	0.0614	0.0011	0.1137	0.0013	0.9623	0.0168	0.0355	0.0012	101	652	38.31	694.4	7.49	684.5	8.71	705.8	24.06			
ACO-12-50	64	0.0641	0.0013	0.1079	0.0013	0.9528	0.0192	0.0331	0.0012	97	743.4	43.2	660.4	7.73	679.6	9.99	658.8	23.74			
ACO-12-50	65	0.0608	0.0009	0.1045	0.0012	0.8756	0.0129	0.0243	0.0006	100	631.5	30.93	640.9	7.01	638.6	6.97	485.3	11.7			
ACO-12-50	66	0.0627	0.0012	0.1081	0.0013	0.9343	0.018	0.0284	0.0008	99	697.8	41.16	661.9	7.77	669.9	9.45	566.7	15.97			
ACO-12-50	67	0.0637	0.0013	0.1083	0.0014	0.9509	0.0192	0.0292	0.0009	98	731.8	42.86	662.9	7.96	678.6	9.98	581.3	17.61			
ACO-12-50	68	0.0628	0.0012	0.104	0.0013	0.9001	0.0171	0.0275	0.0009	98	702.5	40.34	637.5	7.58	651.8	9.16	547.3	17.04			
ACO-12-50	69	0.1819	0.0022	0.4953	0.0057	12.416	0.1586	0.1002	0.0027	97	2670.4	20.21	2593.6	24.43	2636.4	12	1930.3	48.85			
ACO-12-50	70	0.0657	0.0013	0.126	0.0016	1.1417	0.0214	0.0305	0.001	99	798.3	39.22	765.1	8.93	773.3	10.13	607.8	18.66			
ACO-12-50	71	0.0646	0.0013	0.1197	0.0016	1.0635	0.022	0.0276	0.0011	99	759.6	42.85	728.9	9.24	735.6	10.82	549.6	20.78			
ACO-12-50	72	0.0726	0.001	0.1096	0.0013	1.0969	0.0159	0.0326	0.001	89	1003.4	28.67	670.5	7.34	751.8	7.7	647.5	20.35			
ACO-12-50	73	0.0618	0.001	0.112	0.0013	0.9545	0.0155	0.0341	0.0014	101	666.7	35.24	684.5	7.31	680.4	8.07	677.5	27.7			
ACO-12-50	74	0.0644	0.0015	0.1036	0.0014	0.9195	0.0211	0.0288	0.0011	96	755.7	48.86	635.3	8.1	662.1	11.16	573	20.92			
ACO-12-50	75	0.0798	0.0018	0.1973	0.0025	2.1699	0.0472	0.055	0.0027	97	1190.9	44.19	1160.7	13.69	1171.5	15.12	1082	52.14			
ACO-12-50	76	0.0693	0.0011	0.1507	0.0018	1.4378	0.0236	0.0411	0.0016	100	906.2	33.33	904.8	10.04	904.8	9.82	814.6	30.14			
ACO-12-50	77	0.0585	0.0012	0.1036	0.0013	0.8351	0.0171	0.0294	0.0012	103	547.4	45.49	635.6	7.5	616.4	9.44	585.4	24.17			
ACO-12-50	78	0.0818	0.0018	0.2093	0.0026	2.3634	0.0508	0.0558	0.0036	99	1241.2	43.38	1224.9	14	1231.6	15.33	1098.3	68.46			
ACO-12-50	79	0.0617	0.0012	0.1047	0.0013	0.8897	0.0173	0.0285	0.0011	99	663.1	41.63	641.9	7.64	646.2	9.3	567.2	22.32			
ACO-12-50	80	0.0829	0.0021	0.2128	0.003	2.4326	0.0593	0.0617	0.0037	98	1266.5	48.65	1243.9	15.8	1252.3	17.53	1210.4	71.04			
ACO-12-29B	1	0.0605	0.0008	0.1041	0.0011	0.8686	0.0111	0.0294	0.0005	101	622.8	26.87	638.3	6.59	634.8	6.01	585.7	10.38			
ACO-12-29B	2	0.0696	0.0014	0.1166	0.0015	1.1191	0.0225	0.0377	0.0011	93	917.7	40.92	710.9	8.86	762.5	10.78	748.4	21.22			
ACO-12-29B	3	0.0961	0.0011	0.2507	0.0028	3.3213	0.0394	0.0644	0.0011	93	1550.2	21.25	1441.8	14.16	1486.1	9.25	1261.9	21.34			

ACO-12-29B	4	0.0795	0.001	0.1776	0.0019	1.9461	0.0236	0.0568	0.0012	89	1184	23.82	1054	10.31	1097.1	8.15	1117.1	22.64				
ACO-12-29B	5	0.0744	0.0011	0.0951	0.0011	0.9745	0.0137	0.0291	0.0005	85	1050.9	28.13	585.6	6.26	690.8	7.05	579.4	10.63				
ACO-12-29B	6	0.0649	0.0009	0.1263	0.0014	1.1303	0.0148	0.0379	0.0007	100	771.5	27.23	766.8	7.85	767.9	7.06	752	14.15				
ACO-12-29B	7	0.0602	0.0009	0.1011	0.0011	0.8394	0.0119	0.0308	0.0006	100	612.1	30.94	620.8	6.34	618.8	6.56	612.1	12.05				
ACO-12-29B	8	0.0766	0.0014	0.0996	0.0012	1.0514	0.0188	0.0341	0.0008	84	1109.8	35.68	612.2	7.23	729.6	9.31	678.5	16.02				
ACO-12-29B	9	0.0603	0.0008	0.1043	0.0011	0.8667	0.0111	0.0317	0.0006	101	614.3	27.68	639.4	6.39	633.8	6.01	629.8	11.77				
ACO-12-29B	10	0.1103	0.0019	0.1189	0.0015	1.8079	0.0307	0.0428	0.0009	69	1803.7	31.66	724.5	8.51	1048.3	11.12	847.5	16.77				
ACO-12-29B	11	0.0621	0.0009	0.103	0.0011	0.8819	0.012	0.0308	0.0006	98	678.1	29.23	632	6.44	642	6.46	612.2	12.05				
ACO-12-29B	12	0.0668	0.0012	0.1137	0.0013	1.0473	0.0183	0.0357	0.0008	95	832.1	37.11	694.2	7.62	727.6	9.08	708.7	16.09				
ACO-12-29B	13	0.0983	0.0012	0.176	0.0018	2.385	0.028	0.0381	0.0009	66	1591.9	22.75	1045.3	9.74	1238.1	8.4	755.4	16.59				
ACO-12-29B	14	0.2262	0.0049	0.1135	0.0017	3.5394	0.0686	0.0508	0.0012	45	3025.4	34.38	693.1	9.96	1536.1	15.35	1001.2	23.62				
ACO-12-29B	15	0.1207	0.0014	0.3678	0.004	6.1204	0.0722	0.0859	0.0015	103	1967	20.29	2018.8	18.97	1993.2	10.29	1665.6	27.64				
ACO-12-29B	16	0.065	0.0011	0.1231	0.0015	1.1032	0.0189	0.0351	0.0009	99	775.6	34.82	748.1	8.83	754.9	9.11	696.9	17.61				
ACO-12-29B	17	0.0901	0.0011	0.2427	0.0028	3.0127	0.0382	0.0606	0.0013	98	1426.8	22.29	1400.7	14.66	1410.8	9.67	1189	24.39				
ACO-12-29B	18	0.0617	0.001	0.1047	0.0012	0.8906	0.0143	0.0332	0.0008	99	664.4	34.94	641.7	6.82	646.7	7.69	660.1	14.93				
ACO-12-29B	19	0.0791	0.0018	0.0948	0.0012	1.0333	0.0227	0.0297	0.0008	81	1173.4	45.25	584	7.06	720.6	11.31	591.1	16				
ACO-12-29B	20	0.0664	0.001	0.1225	0.0014	1.1209	0.0161	0.0375	0.0007	98	817.5	29.91	745.2	7.83	763.4	7.72	744.2	14.21				
ACO-12-29B	21	0.0615	0.0008	0.1049	0.0011	0.8891	0.0119	0.0327	0.0006	100	655.3	28.56	643.3	6.64	645.9	6.41	651.2	12.44				
ACO-12-29B	22	0.0723	0.0022	0.0976	0.0015	0.9735	0.0287	0.0317	0.001	87	995.6	61.32	600.4	8.66	690.3	14.77	630.9	19.66				
ACO-12-29B	23	0.068	0.0027	0.1103	0.0019	1.0337	0.0387	0.0358	0.0021	94	867.8	79.14	674.5	11.23	720.8	19.32	711.6	41.08				
ACO-12-29B	24	0.0624	0.0008	0.1244	0.0014	1.0701	0.014	0.0322	0.0006	102	687.5	27.3	755.9	7.81	738.8	6.85	641.3	11.1				
ACO-12-29B	25	0.0992	0.0017	0.115	0.0014	1.5714	0.0253	0.0394	0.0009	73	1608.3	30.69	701.5	7.86	959	9.99	780.7	17.23				
ACO-12-29B	26	0.0606	0.0007	0.1061	0.0011	0.8862	0.0103	0.0312	0.0006	101	624.6	24.28	650	6.58	644.3	5.55	620.1	10.8				
ACO-12-29B	27	0.0624	0.001	0.1209	0.0014	1.0402	0.0166	0.0364	0.0007	102	688	34.28	735.8	7.89	724	8.28	722.9	13.73				
ACO-12-29B	28	0.062	0.0008	0.104	0.0011	0.8884	0.0122	0.0302	0.0006	99	672.5	28.89	637.9	6.68	645.5	6.53	601.4	10.77				
ACO-12-29B	29	0.066	0.0016	0.0883	0.0011	0.8037	0.018	0.0291	0.0009	91	807.5	48.85	545.4	6.37	598.9	10.15	579.9	17.25				
ACO-12-29B	30	0.0681	0.0012	0.1103	0.0012	1.0353	0.017	0.0345	0.0009	93	871.2	35.25	674.5	7.01	721.6	8.47	686.2	16.82				
ACO-12-29B	31	0.0613	0.0009	0.1109	0.0012	0.9369	0.0131	0.0323	0.0006	101	649.4	29.8	677.9	7.06	671.3	6.86	643.4	12.33				
ACO-12-29B	32	0.0659	0.0014	0.1112	0.0013	1.0095	0.0198	0.0347	0.0011	96	801.7	42.76	679.7	7.47	708.6	10.02	689.9	20.83				
ACO-12-29B	33	0.0651	0.0009	0.119	0.0013	1.0678	0.0151	0.0347	0.0007	98	776.7	29.59	725	7.53	737.7	7.39	688.4	13.3				
ACO-12-29B	34	0.0694	0.0011	0.1185	0.0014	1.1336	0.0183	0.033	0.0007	94	909.6	33.46	722.2	7.92	769.5	8.73	656.9	13.06				
ACO-12-29B	35	0.061	0.0009	0.1032	0.0011	0.8673	0.013	0.0313	0.0007	100	638.2	32.29	633	6.67	634.1	7.05	622.1	12.64				
ACO-12-29B	36	0.0619	0.0008	0.1027	0.0011	0.8768	0.0109	0.029	0.0005	99	671.8	25.89	630.2	6.49	639.3	5.89	578.6	10.33				
ACO-12-29B	37	0.0615	0.0008	0.101	0.0011	0.8558	0.0117	0.0294	0.0006	99	655.3	28.92	620.3	6.49	627.8	6.39	584.9	11.24				
ACO-12-29B	38	0.0617	0.0008	0.096	0.0011	0.8167	0.0111	0.0277	0.0006	97	664.7	28.71	590.8	6.16	606.2	6.18	552.8	10.98				
ACO-12-29B	39	0.0782	0.0015	0.0993	0.0012	1.07	0.0194	0.0365	0.0009	83	1151.1	36.51	610.3	7.08	738.8	9.5	723.8	17.13				
ACO-12-29B	40	0.0974	0.0015	0.2613	0.0033	3.509	0.0553	0.0613	0.0014	95	1574.9	28.65	1496.7	16.65	1529.2	12.45	1202.8	26.76				
ACO-12-29B	41	0.1827	0.0022	0.5012	0.0058	12.624	0.1608	0.1263	0.003	98	2677.5	19.84	2618.9	25.08	2652	11.98	2404.4	54.62				
ACO-12-29B	42	0.0891	0.0014	0.2433	0.0032	2.9877	0.0499	0.0516	0.0021	100	1405.6	30.23	1403.9	16.61	1404.5	12.69	1016.4	40.41				
ACO-12-29B	43	0.0611	0.0008	0.1124	0.0013	0.9468	0.0132	0.0309	0.0009	101	643.7	29.03	686.4	7.36	676.4	6.87	614.6	16.58				
ACO-12-29B	44	0.0669	0.0008	0.1324	0.0015	1.2206	0.0155	0.0341	0.0008	99	834.3	25.4	801.4	8.35	810	7.08	677.3	15.75				

ACO-12-29B	45	0.0647	0.001	0.1161	0.0014	1.0344	0.0157	0.0318	0.0009	98	762.8	30.98	707.8	7.86	721.1	7.81	631.8	17.22		
ACO-12-29B	46	0.0677	0.0012	0.1064	0.0013	0.9932	0.0167	0.03	0.0008	93	859.6	34.9	651.8	7.34	700.3	8.51	597.4	15.59		
ACO-12-29B	47	0.0641	0.001	0.1307	0.0014	1.1545	0.0174	0.0389	0.0011	102	744.3	32.32	791.8	8.17	779.4	8.21	770.5	21.04		
ACO-12-29B	48	0.0959	0.0014	0.1259	0.0015	1.6636	0.0241	0.0428	0.0013	77	1545.2	26.81	764.3	8.36	994.8	9.2	847.9	24.97		
ACO-12-29B	49	0.0722	0.0012	0.1346	0.0016	1.34	0.0216	0.0387	0.0012	94	992.3	32.2	813.9	9.13	863.2	9.35	767	22.99		
ACO-12-29B	50	0.0626	0.001	0.1061	0.0011	0.9156	0.0138	0.0318	0.0011	99	694.4	32.94	650.2	6.61	660	7.3	633	21.14		
ACO-12-29B	51	0.0614	0.001	0.1042	0.0012	0.8814	0.0135	0.03	0.0009	100	652.1	32.78	638.9	6.89	641.8	7.3	596.4	16.61		
ACO-12-29B	52	0.0592	0.0009	0.1052	0.0012	0.8583	0.0135	0.0306	0.0009	102	574.3	34.18	644.7	6.89	629.2	7.35	610.1	18.41		
ACO-12-29B	53	0.0685	0.0011	0.1157	0.0014	1.0926	0.0172	0.0277	0.0009	94	883.1	31.75	705.9	7.97	749.8	8.35	552.8	17.82		
ACO-12-29B	54	0.0636	0.001	0.1151	0.0013	1.0085	0.0153	0.0329	0.001	99	726.6	32	702.4	7.49	708.1	7.72	654.1	19.87		
ACO-12-29B	55	0.0612	0.0008	0.0975	0.0011	0.8223	0.0115	0.0239	0.0008	98	644.7	29.33	599.9	6.44	609.3	6.41	476.3	14.89		
ACO-12-29B	56	0.0637	0.0013	0.0984	0.0013	0.8638	0.0174	0.0243	0.0011	96	730.6	41.86	605.1	7.72	632.2	9.49	485.2	21.66		
ACO-12-29B	57	0.0639	0.0012	0.1052	0.0013	0.9265	0.0167	0.0318	0.0011	97	737.6	38.19	644.8	7.35	665.8	8.78	633.3	21.43		
ACO-12-29B	58	0.1141	0.0015	0.3291	0.0036	5.178	0.0669	0.0849	0.0027	98	1866.2	22.81	1834	17.62	1849	11	1647.7	50.71		
ACO-12-29B	59	0.0798	0.0016	0.1214	0.0016	1.3357	0.0261	0.0346	0.0015	86	1192.2	38.2	738.7	9.19	861.4	11.34	686.6	29.07		
ACO-12-29B	60	0.1305	0.0024	0.3862	0.0053	6.9469	0.1315	0.0753	0.0042	100	2104.6	32.05	2104.9	24.45	2104.7	16.8	1467.3	79.03		
ACO-12-29B	61	0.1253	0.0014	0.3329	0.0036	5.7497	0.0662	0.0775	0.0015	91	2032.7	19.55	1852.4	17.44	1938.9	9.96	1509.3	28.6		
ACO-12-29B	62	0.0641	0.0009	0.1039	0.0011	0.9175	0.0129	0.031	0.0008	96	743.9	30.03	637	6.56	661	6.84	617.4	14.95		
ACO-12-29B	63	0.0638	0.0014	0.0962	0.0012	0.8454	0.0173	0.0313	0.001	95	733.4	44.55	592	6.85	622.1	9.54	622.3	18.93		
ACO-12-29B	64	0.0628	0.0009	0.0997	0.0011	0.8629	0.0122	0.0286	0.0007	97	701.7	29.99	612.4	6.43	631.7	6.64	569	13.14		
ACO-12-29B	65	0.0636	0.0009	0.103	0.0011	0.9041	0.0122	0.0281	0.0007	97	729.8	28.01	632.2	6.65	653.9	6.48	560	12.73		
ACO-12-29B	66	0.1053	0.0032	0.0969	0.0015	1.4064	0.0396	0.0384	0.0014	67	1718.8	54.44	596.3	9	891.7	16.73	762.3	27.34		
ACO-12-29B	67	0.064	0.001	0.0969	0.001	0.8557	0.013	0.0288	0.0009	95	742.4	33.14	596.4	6.12	627.7	7.13	574.2	17.04		
ACO-12-29B	68	0.0615	0.0011	0.1044	0.0012	0.8855	0.015	0.0294	0.0009	99	656.7	37.32	640.3	6.74	643.9	8.06	585.4	18.17		
ACO-12-29B	69	0.0617	0.0012	0.0913	0.001	0.7768	0.0143	0.027	0.0011	97	663.3	40.93	563.5	5.97	583.7	8.15	537.6	22.39		
ACO-12-29B	70	0.0604	0.0008	0.1072	0.0011	0.8935	0.0112	0.0309	0.0009	101	619.4	27.4	656.6	6.46	648.3	6	614.9	17.73		
ACO-12-29B	71	0.1341	0.0029	0.1139	0.0017	2.1058	0.0431	0.0576	0.0021	60	2152.7	36.64	695.4	9.61	1150.7	14.09	1131.8	40.15		
ACO-12-29B	72	0.0659	0.0008	0.0942	0.0011	0.8564	0.0114	0.0234	0.0007	92	803.5	26.3	580.5	6.42	628.1	6.22	466.9	12.84		
ACO-12-29B	73	0.0615	0.0012	0.0979	0.0013	0.829	0.0165	0.0192	0.0008	98	656.1	41.64	602	7.79	613.1	9.15	384.5	15.22		
ACO-12-29B	74	0.0734	0.0016	0.1006	0.0014	1.0175	0.0214	0.0235	0.0009	87	1025.3	42.38	617.8	8.07	712.7	10.76	469.9	17.68		
ACO-12-29B	75	0.0644	0.002	0.0952	0.0014	0.8451	0.0254	0.0285	0.0016	94	755.8	64.57	585.9	8.5	622	13.97	567	31.61		
ACO-12-29B	76	0.0704	0.0011	0.1766	0.0022	1.713	0.0267	0.0299	0.001	112	939.3	30.84	1048.4	11.78	1013.4	9.98	595.6	19.98		
ACO-12-29B	77	0.0667	0.0018	0.1214	0.0018	1.1163	0.0293	0.0318	0.0014	97	828.8	55.13	738.7	10.47	761.2	14.06	632.9	26.73		
ACO-12-29B	78	0.0767	0.0014	0.1273	0.0016	1.3459	0.0245	0.0351	0.0012	89	1112.5	36.28	772.5	9.14	865.8	10.58	697.5	24.3		
ACO-12-29B	79	0.0604	0.0009	0.0965	0.0011	0.8034	0.0115	0.02	0.0006	99	618.1	30	593.7	6.6	598.7	6.49	399.3	12.66		
ACO-12-29B	80	0.099	0.0019	0.2745	0.0036	3.745	0.0692	0.0561	0.0023	97	1604.9	34.5	1563.3	18.34	1581.1	14.81	1102.4	43.72		
ACO-12-38	1	0.059	0.0008	0.108	0.0013	0.8793	0.0128	0.0309	0.0007	103.15	568.1	30.67	660.8	7.28	640.6	6.92	615.1	12.77		
ACO-12-38	2	0.0632	0.0011	0.0817	0.001	0.7115	0.0121	0.0265	0.0006	92.74	713.7	36.45	506	5.7	545.6	7.19	528.9	11.06		
ACO-12-38	3	0.0617	0.0017	0.124	0.0018	1.0555	0.0285	0.0349	0.0009	102.98	663.7	58.75	753.4	10.09	731.6	14.07	693	18.31		
ACO-12-38	4	0.0634	0.001	0.1104	0.0013	0.9656	0.0158	0.0295	0.0005	98.37	721.2	34.37	675	7.58	686.2	8.13	588.1	10.36		

ACO-12-38	5	0.0597	0.001	0.102	0.0012	0.8395	0.0143	0.031	0.0007	101.16	590.8	36.9	626.1	7.07	618.9	7.91	616.5	14.04		
ACO-12-38	6	0.0621	0.0015	0.1016	0.0013	0.8704	0.0198	0.0298	0.0007	98.11	677	49.99	623.8	7.55	635.8	10.77	593	13.96		
ACO-12-38	7	0.0592	0.0012	0.0992	0.0012	0.8103	0.0157	0.0312	0.0008	101.18	575	42.45	609.7	7.05	602.6	8.78	620.5	16.23		
ACO-12-38	8	0.0587	0.0007	0.0966	0.0011	0.7819	0.0098	0.0288	0.0005	101.36	554.1	26.48	594.6	6.23	586.6	5.58	573.4	10.36		
ACO-12-38	9	0.0925	0.001	0.2237	0.0027	2.8553	0.035	0.0277	0.0005	88.11	1477.2	20.62	1301.5	14.11	1370.2	9.21	551.7	9.86		
ACO-12-38	10	0.0588	0.001	0.0969	0.0011	0.7865	0.013	0.0289	0.0006	101.17	561.3	36.6	596.1	6.45	589.2	7.41	576.2	11.64		
ACO-12-38	11	0.0603	0.0011	0.1009	0.0012	0.8398	0.015	0.0303	0.0006	100.15	614.4	38.99	619.9	6.98	619	8.29	603.3	12.35		
ACO-12-38	12	0.0592	0.001	0.1008	0.0011	0.8237	0.0136	0.0304	0.0007	101.51	574.7	36.64	619.3	6.59	610.1	7.57	604.5	14.1		
ACO-12-38	13	0.0605	0.0008	0.103	0.0012	0.86	0.0114	0.0233	0.0004	100.27	621.8	27.07	631.8	6.91	630.1	6.2	466.4	7.84		
ACO-12-38	14	0.0604	0.0008	0.1035	0.0012	0.8624	0.0118	0.0279	0.0005	100.51	617.9	28.27	634.6	6.92	631.4	6.41	556.2	10.17		
ACO-12-38	15	0.0641	0.0011	0.1193	0.0014	1.0543	0.0184	0.0424	0.0009	99.37	743.8	36.99	726.4	8.25	731	9.1	839.9	17.87		
ACO-12-38	16	0.0662	0.0012	0.1039	0.0013	0.9484	0.0166	0.0252	0.0005	94.05	811.6	36.07	636.9	7.57	677.2	8.65	503	9.84		
ACO-12-38	17	0.0626	0.001	0.1042	0.0012	0.9006	0.0138	0.0306	0.0006	98.01	695.6	32.09	639	7.07	652	7.35	609.2	11.91		
ACO-12-38	18	0.0616	0.0015	0.1071	0.0014	0.9099	0.0209	0.0321	0.0009	99.82	659.9	50.2	655.8	8.14	657	11.13	637.6	17.46		
ACO-12-38	19	0.0608	0.0013	0.101	0.0013	0.8474	0.0182	0.0297	0.0008	99.50	632.7	46.49	620.1	7.64	623.2	9.98	591.4	15.86		
ACO-12-38	20	0.0615	0.001	0.1101	0.0013	0.934	0.0157	0.0344	0.0008	100.49	657.2	36.01	673.1	7.54	669.8	8.25	683.4	15.45		
ACO-12-38	21	0.0789	0.0016	0.1707	0.0021	1.8561	0.037	0.067	0.0025	86.92	1168.5	40.71	1015.7	11.62	1065.6	13.15	1309.8	46.42		
ACO-12-38	22	0.063	0.0011	0.1031	0.0012	0.8956	0.0153	0.0275	0.0008	97.43	708.2	36.24	632.7	7.18	649.4	8.22	548.9	14.9		
ACO-12-38	23	0.0651	0.0018	0.1133	0.0015	1.017	0.0263	0.0342	0.0013	97.14	776.5	55.7	692	8.93	712.4	13.22	680.4	24.58		
ACO-12-38	24	0.0618	0.0013	0.1107	0.0014	0.9425	0.0191	0.0326	0.0011	100.36	666.5	43.7	676.6	8.06	674.2	10	647.5	20.54		
ACO-12-38	25	0.0637	0.0012	0.1171	0.0014	1.0284	0.0185	0.0359	0.0012	99.39	731.2	38.8	713.7	7.88	718.1	9.26	712.2	23.68		
ACO-12-38	26	0.0611	0.0013	0.1059	0.0014	0.892	0.0192	0.0316	0.001	100.26	641.7	46.58	649.1	7.88	647.4	10.28	628.1	19.02		
ACO-12-38	27	0.0637	0.0021	0.1165	0.0018	1.0238	0.0321	0.0423	0.0022	99.25	732	67.87	710.4	10.18	715.8	16.08	836.5	43.53		
ACO-12-38	28	0.0602	0.0017	0.1081	0.0015	0.8973	0.0247	0.0352	0.0015	101.77	610.7	60.36	661.8	8.96	650.3	13.21	699.9	29.1		
ACO-12-38	29	0.0614	0.0021	0.1108	0.0017	0.9378	0.0299	0.0312	0.0019	100.88	651.8	70.15	677.6	9.57	671.7	15.68	620.1	37		
ACO-12-38	30	0.0619	0.0009	0.1029	0.0012	0.8782	0.0125	0.0266	0.0008	98.63	671.6	29.43	631.2	6.91	640	6.74	530.8	15.54		
ACO-12-38	31	0.0617	0.001	0.1042	0.0012	0.8863	0.0149	0.0298	0.001	99.12	664.8	35.59	638.7	7.24	644.4	8	593.6	19.77		
ACO-12-38	32	0.0623	0.0014	0.1069	0.0015	0.9189	0.0205	0.0277	0.0011	98.96	685.8	47.45	654.9	8.42	661.8	10.83	551.7	21.54		
ACO-12-38	33	0.0598	0.001	0.1081	0.0013	0.8911	0.0151	0.0294	0.001	102.27	596.6	36.37	661.6	7.5	646.9	8.11	585.3	20.05		
ACO-12-38	34	0.0589	0.001	0.1085	0.0013	0.8811	0.015	0.034	0.0013	103.48	563.8	36.92	663.9	7.48	641.6	8.11	676.4	25.3		
ACO-12-38	35	0.0608	0.001	0.1156	0.0014	0.9679	0.0156	0.0293	0.001	102.55	630.6	34.1	704.9	7.89	687.4	8.03	584.1	19.26		
ACO-12-38	36	0.2006	0.0032	0.528	0.0059	14.603	0.227	0.1756	0.0102	96.55	2830.8	25.75	2733.2	24.78	2789.7	14.77	3269.9	174.85		
ACO-12-38	37	0.0589	0.001	0.1068	0.0013	0.8667	0.0144	0.0329	0.0013	103.22	561.5	35.74	654.2	7.35	633.8	7.82	653.3	24.95		
ACO-12-38	38	0.0599	0.0021	0.0961	0.0015	0.7935	0.0267	0.0282	0.0013	99.66	600.6	74.02	591.2	8.86	593.2	15.1	561.4	26.14		
ACO-12-38	39	0.0635	0.0016	0.1089	0.0014	0.9536	0.0229	0.0439	0.0025	97.99	725	52.01	666.3	8.29	680	11.88	868.8	48.18		
ACO-12-38	40	0.0609	0.0015	0.1052	0.0014	0.8829	0.0208	0.0365	0.002	100.33	635	51.71	644.6	7.9	642.5	11.21	725.1	38.7		
ACO-12-38	41	0.0597	0.001	0.1095	0.0013	0.9016	0.0144	0.0312	0.001	102.67	592.9	33.64	670	7.45	652.6	7.68	620.1	18.53		
ACO-12-38	42	0.0627	0.0011	0.1095	0.0013	0.9461	0.0158	0.0285	0.0008	99.08	696.3	35.28	669.9	7.56	676.1	8.22	567.5	16.26		
ACO-12-38	43	0.1274	0.0017	0.3964	0.0046	6.9616	0.0926	0.0842	0.0022	104.40	2061.7	22.83	2152.5	21.2	2106.5	11.81	1633	40.21		
ACO-12-38	44	0.1031	0.0015	0.3046	0.0038	4.3298	0.0648	0.0633	0.0022	102.03	1680.2	26.21	1714.3	18.62	1699.1	12.35	1241.4	41.54		
ACO-12-38	45	0.2152	0.0034	0.5653	0.0064	16.778	0.252	0.1663	0.0082	98.09	2944.9	25.29	2888.6	26.38	2922.2	14.39	3109.6	141.19		

ACO-12-38	46	0.0641	0.0014	0.1313	0.0015	1.1602	0.0232	0.0484	0.0024	101.69	743.6	43.92	795.3	8.78	782.1	10.92	956.1	46.26				
ACO-12-38	47	0.0606	0.0011	0.1067	0.0012	0.8918	0.0152	0.0368	0.0015	100.96	624.9	37.73	653.5	6.95	647.3	8.14	730.5	29.73				
ACO-12-38	48	0.06	0.0011	0.1058	0.0012	0.8756	0.0156	0.0345	0.0015	101.53	603.3	39.62	648.4	6.97	638.6	8.42	685.3	29.5				
ACO-12-38	49	0.1043	0.0021	0.2941	0.0036	4.2273	0.0804	0.0991	0.0057	97.69	1701.1	36.71	1661.8	17.68	1679.3	15.61	1909.9	104.01				
ACO-12-38	50	0.0627	0.0015	0.1111	0.0014	0.9599	0.0224	0.0366	0.0018	99.37	696.6	51.5	678.9	8.09	683.2	11.62	726.6	34.25				
ACO-12-38	51	0.0647	0.0023	0.124	0.002	1.106	0.0378	0.0399	0.002	99.67	762.9	73.84	753.8	11.25	756.3	18.21	790.3	38.76				
ACO-12-38	52	0.1398	0.0021	0.3583	0.0041	6.909	0.1026	0.1051	0.0047	88.72	2224.9	26.19	1974	19.29	2099.8	13.17	2020.3	85.97				
ACO-12-38	53	0.0593	0.0009	0.0989	0.0011	0.8092	0.0128	0.0283	0.0011	101.03	578.8	34.21	608.2	6.69	602	7.18	563.7	20.6				
ACO-12-38	54	0.0605	0.001	0.1035	0.0012	0.8625	0.0134	0.0318	0.0013	100.51	619.8	33.9	634.7	6.77	631.5	7.3	631.9	25.65				
ACO-12-38	55	0.062	0.0009	0.1131	0.0013	0.9665	0.0141	0.0331	0.0013	100.58	673.7	30.96	690.6	7.37	686.6	7.27	657.6	24.39				
ACO-12-38	56	0.0619	0.0011	0.1065	0.0013	0.9082	0.0163	0.03	0.0012	99.39	669.7	38.81	652.1	7.38	656.1	8.69	598.2	22.57				
ACO-12-38	57	0.0637	0.001	0.096	0.0011	0.8422	0.0127	0.0259	0.001	95.24	729.9	31.98	590.8	6.42	620.3	7.02	517.3	19.3				
ACO-12-38	58	0.0596	0.0014	0.1029	0.0014	0.8454	0.019	0.0242	0.0012	101.45	589.8	48.79	631.1	8.07	622.1	10.45	483.1	23.42				
ACO-12-38	59	0.0612	0.0011	0.1039	0.0012	0.8771	0.0146	0.0315	0.0014	99.66	647.3	36.54	637.2	6.9	639.4	7.92	626.8	27.61				
ACO-12-38	60	0.0613	0.0011	0.1154	0.0013	0.9754	0.0171	0.0349	0.0016	101.84	650.6	38.16	703.9	7.74	691.2	8.76	693.6	30.79				
ACO-12-38	61	0.1175	0.0015	0.354	0.0039	5.7313	0.072	0.0944	0.0022	101.83	1918.4	22.05	1953.5	18.63	1936.1	10.86	1823.5	40.67				
ACO-12-38	62	0.0621	0.0015	0.0995	0.0012	0.8511	0.0196	0.0302	0.0012	97.78	677	50.83	611.3	7.18	625.2	10.73	601.7	22.52				
ACO-12-38	63	0.0835	0.001	0.0641	0.0007	0.7377	0.0092	0.017	0.0004	71.38	1281.4	23.87	400.5	4.26	561.1	5.39	340.4	7.75				
ACO-12-38	64	0.0628	0.0018	0.1038	0.0014	0.899	0.024	0.0328	0.0013	97.77	702.4	58.21	636.7	8.33	651.2	12.85	651.9	26.3				
ACO-12-38	65	0.0611	0.0012	0.1086	0.0013	0.9143	0.0177	0.0317	0.0009	100.83	641.2	42.14	664.8	7.63	659.3	9.4	630.1	18.14				
ACO-12-38	66	0.0619	0.001	0.1098	0.0013	0.9372	0.0154	0.035	0.0011	100.01	671.8	35.46	671.5	7.24	671.4	8.06	694.6	21.16				
ACO-12-38	67	0.0681	0.0011	0.1034	0.0012	0.9697	0.0155	0.0337	0.0011	92.11	870.8	33.33	634	6.86	688.3	7.97	670.5	22.31				
ACO-12-38	68	0.0602	0.0012	0.0996	0.0012	0.8258	0.0159	0.0317	0.0013	100.11	609.6	42.82	612	6.72	611.3	8.84	629.9	24.45				
ACO-12-38	69	0.0618	0.0009	0.0988	0.0011	0.8412	0.0125	0.0292	0.001	97.97	666.7	31.73	607.2	6.45	619.8	6.88	582.6	18.67				
ACO-12-38	70	0.0688	0.0011	0.0869	0.001	0.8239	0.0127	0.0285	0.0009	88.05	891.7	31.76	537.3	5.92	610.2	7.08	567.7	16.9				
ACO-12-38	71	0.0703	0.0013	0.1012	0.0012	0.9804	0.0181	0.0328	0.0011	89.58	935.9	38.35	621.5	7.21	693.8	9.3	651.5	22.26				
ACO-12-38	72	0.0797	0.0015	0.0873	0.0011	0.9589	0.0176	0.0319	0.0011	79.05	1188.5	36.76	539.7	6.34	682.7	9.11	634.6	21.3				
ACO-12-38	73	0.0757	0.0019	0.1136	0.0017	1.1851	0.0296	0.0293	0.0016	87.38	1087.9	50.39	693.5	9.66	793.7	13.75	583.7	30.57				
ACO-12-38	74	0.0627	0.0011	0.097	0.0011	0.8378	0.0144	0.0296	0.0012	96.54	697.4	37.24	596.5	6.49	617.9	7.95	590.4	23.64				
ACO-12-38	75	0.1232	0.0019	0.3537	0.0046	6.0028	0.0977	0.054	0.002	97.48	2002.6	27.77	1952.2	21.91	1976.2	14.17	1063.7	37.82				
ACO-12-38	76	0.063	0.0019	0.0963	0.0013	0.8361	0.0239	0.0301	0.0018	96.01	709.3	62.63	592.4	7.8	617	13.21	599.7	34.57				
ACO-12-38	77	0.0624	0.0012	0.0962	0.0012	0.8276	0.0155	0.0292	0.0012	96.68	688	40.21	592	6.81	612.3	8.6	581.9	22.64				
ACO-12-38	78	0.0603	0.0012	0.0996	0.0012	0.828	0.0164	0.0297	0.0014	99.92	614.2	43.67	612	6.87	612.5	9.08	591.6	28.23				
ACO-12-38	79	0.0605	0.0015	0.0993	0.0013	0.828	0.0202	0.0326	0.0018	99.66	620.6	53.75	610.4	7.55	612.5	11.2	647.5	34.57				
ACO-12-38	80	0.0622	0.001	0.0991	0.0011	0.8506	0.0136	0.0299	0.0013	97.50	682	33.88	609.4	6.71	625	7.45	595.4	25.01				
ACO-13-22	1	0.1292	0.0027	0.267	0.0034	4.7578	0.0944	0.1239	0.0093	73	2087.2	35.82	1525.6	17.24	1777.5	16.64	2361.5	166.47				
ACO-13-22	2	0.0601	0.0023	0.1025	0.0018	0.8492	0.031	0.0277	0.0054	101	605.5	78.9	629.3	10.22	624.2	17.01	552.3	106.76				
ACO-13-22	3	0.0584	0.0021	0.099	0.0017	0.7974	0.0282	0.1021	0.0403	102	546.3	77.34	608.6	10.08	595.4	15.94	1965	739.09				
ACO-13-22	4	0.0873	0.0016	0.2353	0.003	2.8336	0.0509	0.0767	0.0041	100	1367.4	34.3	1362.2	15.38	1364.5	13.48	1493	76.98				
ACO-13-22	5	0.0664	0.0035	0.1128	0.0024	1.0326	0.0519	0.0409	0.0035	96	819.8	105.81	688.9	14.05	720.2	25.94	809.5	68.36				

ACO-13-22	6	0.0624	0.0014	0.1119	0.0014	0.9628	0.0205	0.0395	0.003	100	688.7	46.71	683.5	7.99	684.8	10.62	783.1	58.09				
ACO-13-22	7	0.0621	0.0011	0.1012	0.0013	0.867	0.0159	0.0378	0.0022	98	677.9	38.39	621.6	7.43	633.9	8.65	749.5	43.12				
ACO-13-22	8	0.0609	0.0012	0.0991	0.0012	0.8327	0.016	0.0344	0.0022	99	636.8	41.79	609.1	7.04	615.1	8.86	683.7	42.96				
ACO-13-22	9	0.0582	0.0012	0.0915	0.0011	0.7336	0.0145	0.0293	0.0017	101	535.8	43.52	564.1	6.73	558.7	8.47	583.5	33.93				
ACO-13-22	10	0.0571	0.0017	0.0773	0.0011	0.6094	0.0175	0.0259	0.0017	99	496.6	64.44	480.2	6.58	483.2	11.06	516.8	33.07				
ACO-13-22	11	0.0616	0.0013	0.0994	0.0013	0.8441	0.0169	0.0342	0.0022	98	658.9	42.88	611.1	7.32	621.4	9.32	678.6	42.26				
ACO-13-22	12	0.0614	0.0012	0.1011	0.0013	0.8555	0.0166	0.0338	0.0023	99	653	41.59	620.6	7.38	627.6	9.1	671.1	44.42				
ACO-13-22	13	0.0955	0.0023	0.2611	0.0033	3.4373	0.0789	0.1017	0.0106	97	1537.8	45.25	1495.5	16.89	1513	18.06	1958.2	193.98				
ACO-13-22	14	0.1291	0.0029	0.3786	0.0049	6.7347	0.1458	0.1133	0.0101	99	2085.2	39.02	2069.8	22.88	2077.2	19.14	2168.4	184.15				
ACO-13-22	15	0.0563	0.0014	0.0613	0.0008	0.4762	0.0112	0.0209	0.0016	97	464.6	52.72	383.6	4.91	395.5	7.67	418.2	31.02				
ACO-13-22	16	0.0619	0.0014	0.0956	0.0012	0.8161	0.0175	0.0318	0.0013	97	671.5	45.92	588.6	7.13	605.9	9.79	632.4	25.76				
ACO-13-22	17	0.0564	0.0028	0.0907	0.0016	0.7047	0.0332	0.0318	0.0019	103	469	105.47	559.4	9.52	541.6	19.77	633.6	37.61				
ACO-13-22	18	0.2533	0.0046	0.3329	0.0044	11.625	0.2177	0.3215	0.0201	58	3205.4	28.65	1852.5	21.04	2574.7	17.51	5634.1	306.63				
ACO-13-22	19	0.0654	0.003	0.0904	0.0017	0.8139	0.036	0.0313	0.0023	92	785.9	93.44	557.6	10.26	604.6	20.15	623.2	45.56				
ACO-13-22	20	0.0619	0.0021	0.0945	0.0014	0.806	0.0266	0.031	0.0019	97	670.5	71.03	582	8.44	600.2	14.98	617	37.66				
ACO-13-22	21	0.059	0.0018	0.0904	0.0014	0.736	0.0222	0.0279	0.0017	100	568.3	65.65	558.1	8.09	560.1	13.01	556.4	33.32				
ACO-13-22	22	0.1204	0.0019	0.2591	0.003	4.2983	0.0669	0.0859	0.0043	76	1961.9	27.4	1485.1	15.14	1693	12.81	1666.1	80.86				
ACO-13-22	23	0.0672	0.002	0.1011	0.0015	0.936	0.0269	0.0319	0.0019	93	842.7	60.13	620.8	8.82	670.8	14.11	634.4	37.19				
ACO-13-22	24	0.0854	0.0018	0.1135	0.0014	1.3361	0.0271	0.0475	0.0027	80	1325.6	39.94	692.9	8.15	861.5	11.79	938.7	52.41				
ACO-13-22	25	0.0994	0.0016	0.1033	0.0012	1.4142	0.0237	0.0406	0.0021	71	1612.2	30.4	633.4	7.24	894.9	9.95	804.2	40.36				
ACO-13-22	26	0.0697	0.0021	0.1183	0.0018	1.1371	0.0339	0.0358	0.0033	93	919.8	61.19	720.8	10.62	771.1	16.08	710.2	63.41				
ACO-13-22	27	0.1418	0.0041	0.4074	0.0064	7.9656	0.2246	0.1096	0.0105	98	2249.6	48.71	2202.9	29.46	2227.1	25.43	2102.1	190.79				
ACO-13-22	28	0.0711	0.0018	0.1047	0.0015	1.0267	0.0256	0.04	0.0034	90	960.7	50.4	642	8.73	717.3	12.82	791.9	65.16				
ACO-13-22	29	0.0618	0.0023	0.0903	0.0015	0.7696	0.0273	0.0276	0.002	96	667.7	76.23	557.4	8.7	579.5	15.64	550.1	39.11				
ACO-13-22	30	0.21	0.0042	0.1188	0.0016	3.4403	0.0664	0.116	0.0069	48	2905.8	31.74	723.8	9	1513.7	15.19	2218.6	124.58				
ACO-12-48	1	0.0652	0.0009	0.1326	0.0015	1.1913	0.0167	0.0371	0.0009	101	781.1	28.63	802.4	8.65	796.6	7.74	736	17.8				
ACO-12-48	2	0.062	0.001	0.0946	0.0011	0.8081	0.0125	0.0236	0.0007	97	673.5	33.21	582.7	6.32	601.4	7.03	470.5	13.25				
ACO-12-48	3	0.0755	0.0019	0.1022	0.0015	1.0636	0.0265	0.0246	0.0009	85	1081.1	50.46	627.4	8.97	735.6	13.04	490.2	17.96				
ACO-12-48	4	0.0599	0.001	0.1111	0.0013	0.9168	0.0147	0.0265	0.0007	103	598.9	34.38	679.2	7.61	660.7	7.81	529	12.97				
ACO-12-48	5	0.0676	0.0012	0.1093	0.0013	1.0178	0.018	0.0272	0.0007	94	856.3	36.71	668.4	7.77	712.8	9.04	543.3	13.53				
ACO-12-48	6	0.06	0.001	0.0923	0.0011	0.7637	0.0128	0.0243	0.0007	99	605	35.89	569.1	6.46	576.1	7.34	485.6	13.57				
ACO-12-48	7	0.0606	0.0009	0.0984	0.0012	0.8217	0.0122	0.0225	0.0006	99	624.3	31.23	605.3	6.75	609	6.81	449.6	11.65				
ACO-12-48	8	0.059	0.0012	0.0983	0.0012	0.7994	0.0159	0.0223	0.0007	101	567.1	43.64	604.6	7.21	596.5	8.99	445.8	12.83				
ACO-12-48	9	0.0687	0.0018	0.0965	0.0015	0.9134	0.0232	0.0173	0.0008	90	888.7	52.45	593.6	8.57	658.8	12.31	346	15.6				
ACO-12-48	10	0.0618	0.0011	0.128	0.0016	1.0902	0.0189	0.0245	0.0008	104	666.5	36	776.6	9.35	748.6	9.19	489.1	16.63				
ACO-12-48	11	0.0629	0.0011	0.0957	0.0012	0.8292	0.014	0.0173	0.0006	96	703	35.04	589.4	7.03	613.2	7.79	347.4	11.38				
ACO-12-48	12	0.0611	0.0012	0.1018	0.0013	0.8567	0.0171	0.0233	0.0008	99	642.6	42.77	624.7	7.66	628.3	9.35	465.3	15.69				
ACO-12-48	13	0.0653	0.0013	0.1068	0.0014	0.9602	0.0188	0.0241	0.0009	96	782.8	41.07	653.9	7.97	683.4	9.74	481.7	17.25				
ACO-12-48	14	0.0717	0.001	0.1682	0.0019	1.6625	0.0235	0.0444	0.0015	102	978.2	28.29	1002.4	10.54	994.3	8.94	878.8	28.94				
ACO-12-48	15	0.0624	0.0011	0.0982	0.0012	0.8438	0.0151	0.0243	0.0008	97	687.7	38.41	603.6	6.94	621.3	8.32	486	16.04				

ACO-12-48	16	0.0661	0.0012	0.1064	0.0013	0.9681	0.0176	0.0346	0.0014	95	808.9	38.78	651.6	7.37	687.5	9.09	688.1	26.93
ACO-12-48	17	0.1823	0.0025	0.5548	0.0065	13.934	0.1886	0.1148	0.0037	106	2674.1	22.03	2844.9	26.81	2745.3	12.82	2196.1	66.18
ACO-12-48	18	0.0849	0.0016	0.0815	0.001	0.9526	0.0172	0.0196	0.0007	74	1311.9	35.16	505	6.14	679.4	8.92	392.8	14.31
ACO-12-48	19	0.134	0.0025	0.097	0.0013	1.7911	0.0317	0.0348	0.0012	57	2150.7	32.01	597.1	7.37	1042.2	11.52	690.5	23.91
ACO-12-48	20	0.1862	0.0029	0.527	0.0059	13.511	0.2004	0.134	0.0066	101	2709	25.09	2728.7	24.91	2716	14.02	2542.4	117.6
ACO-12-48	21	0.0657	0.001	0.0962	0.0012	0.8705	0.0135	0.0188	0.0005	93	795.4	31.47	592.2	6.76	635.8	7.3	376	10.19
ACO-12-48	22	0.0707	0.0013	0.0982	0.0012	0.9563	0.0169	0.0236	0.0006	89	947.6	36.24	603.8	7.03	681.4	8.75	470.6	11.08
ACO-12-48	23	0.063	0.0011	0.1138	0.0014	0.988	0.0168	0.0246	0.0007	100	707.4	35.34	694.9	8.09	697.7	8.56	490.7	12.97
ACO-12-48	24	0.0606	0.0009	0.0873	0.001	0.7298	0.0107	0.0272	0.0008	97	626.2	31.52	539.6	5.8	556.4	6.29	543.2	15.92
ACO-12-48	25	0.0676	0.001	0.0946	0.0011	0.8811	0.0134	0.022	0.0006	91	854.7	30.89	582.9	6.58	641.6	7.23	439.4	11.76
ACO-12-48	26	0.0884	0.0016	0.0877	0.0011	1.0691	0.019	0.0178	0.0005	73	1391.9	34.49	541.9	6.51	738.3	9.34	356.2	9.77
ACO-12-48	27	0.063	0.0011	0.088	0.001	0.7647	0.0127	0.0266	0.0009	94	708.1	35.7	544	6.04	576.7	7.33	530.7	17.6
ACO-12-48	28	0.4687	0.0094	0.1738	0.0027	11.222	0.2151	0.239	0.0129	25	4145.7	29.51	1032.9	15.03	2541.7	17.87	4332	209.8
ACO-12-48	29	0.0609	0.0015	0.0931	0.0012	0.7815	0.018	0.0281	0.0012	98	636.4	50.55	573.5	7.05	586.3	10.25	559.4	23
ACO-12-48	30	0.0588	0.0012	0.1108	0.0014	0.8989	0.0181	0.0287	0.0012	104	561.1	44.61	677.3	7.84	651.1	9.68	571.2	22.54
ACO-12-48	31	0.064	0.0013	0.0937	0.0012	0.8269	0.0161	0.0292	0.0012	94	742.6	41.6	577.2	6.79	611.9	8.94	580.7	23.56
ACO-12-48	32	0.0611	0.001	0.1111	0.0013	0.9358	0.0148	0.0281	0.0009	101	642.8	33.47	678.9	7.61	670.7	7.78	560.8	17.55
ACO-12-48	33	0.0778	0.0014	0.0854	0.0011	0.9164	0.0164	0.0277	0.001	80	1142.1	35.26	528.3	6.37	660.5	8.67	552.3	20.35
ACO-12-48	34	0.0637	0.0011	0.1048	0.0013	0.9201	0.0159	0.0275	0.001	97	730.8	36.06	642.4	7.51	662.4	8.41	548.6	19.59
ACO-12-48	35	0.0581	0.0012	0.114	0.0014	0.9141	0.0182	0.0347	0.0015	106	534	44.4	696	8.08	659.2	9.63	690	29.94
ACO-12-48	36	0.1322	0.0019	0.4049	0.0046	7.3799	0.1053	0.1203	0.0055	103	2126.8	24.79	2191.4	21.18	2158.5	12.76	2296.3	99.99
ACO-12-48	37	0.0605	0.0009	0.1001	0.0012	0.8355	0.0129	0.0273	0.001	100	622.2	32.37	614.9	6.91	616.6	7.12	543.3	19.55
ACO-12-48	38	0.0614	0.0009	0.1023	0.0012	0.866	0.0131	0.03	0.0012	99	652.4	31.43	627.9	6.99	633.4	7.1	597.1	23.51
ACO-12-48	39	0.0614	0.001	0.0997	0.0012	0.8447	0.0138	0.0401	0.002	99	654.3	34.42	612.5	6.92	621.7	7.59	795.1	38.5
ACO-12-48	40	0.0579	0.0009	0.1137	0.0014	0.9077	0.0147	0.029	0.0012	106	525	34.91	694.1	7.87	655.8	7.82	576.7	22.61
ACO-12-48	41	0.061	0.0017	0.095	0.0013	0.7985	0.0215	0.0283	0.0011	98	639.9	59.39	584.9	7.66	596	12.15	563.8	21
ACO-12-48	42	0.0632	0.001	0.0985	0.0012	0.8579	0.0139	0.0247	0.0006	96	715.5	33.36	605.9	7.02	629	7.57	493.9	12.43
ACO-12-48	43	0.1018	0.0038	0.1153	0.0022	1.6155	0.0567	0.0325	0.0014	72	1656.6	67.65	703.5	12.97	976.2	22	646.9	26.51
ACO-12-48	44	0.0653	0.0011	0.0874	0.0011	0.7863	0.0136	0.0211	0.0006	92	785.3	35.22	540.3	6.57	589.1	7.72	421.1	11.73
ACO-12-48	45	0.0673	0.0014	0.0905	0.0012	0.8397	0.0174	0.0265	0.0009	90	847.4	43.48	558.7	6.87	619	9.6	528.9	17.75
ACO-12-48	46	0.0619	0.001	0.0955	0.0012	0.8144	0.0137	0.0177	0.0007	97	671.9	34.49	588.2	7.22	604.9	7.68	353.6	14.38
ACO-12-48	47	0.0629	0.0012	0.1039	0.0013	0.9002	0.0169	0.0338	0.0011	98	704.1	40.19	637.1	7.41	651.8	9.04	670.9	21.49
ACO-12-48	48	0.0591	0.001	0.0987	0.0012	0.8033	0.0133	0.026	0.0008	101	571	35.46	606.6	6.89	598.7	7.48	517.9	15.58
ACO-12-48	49	0.0595	0.0014	0.0852	0.0011	0.6973	0.0158	0.0235	0.0008	98	583.9	49.2	526.8	6.7	537.2	9.42	469.1	16.56
ACO-12-48	50	0.0761	0.002	0.109	0.0017	1.1408	0.0291	0.0196	0.0008	86	1097	51.57	666.9	9.61	772.9	13.81	392.8	14.82
ACO-12-48	51	0.0731	0.0015	0.1022	0.0014	1.0277	0.0207	0.0205	0.0007	87	1015.7	40.62	627.2	7.88	717.8	10.37	411	13.36
ACO-12-48	52	0.0663	0.0013	0.098	0.0013	0.8937	0.0172	0.0225	0.0007	93	814.4	39.8	602.8	7.48	648.3	9.23	448.8	14.44
ACO-12-48	53	0.0623	0.0011	0.0894	0.0011	0.7666	0.0133	0.0163	0.0005	96	684.5	36.06	552.2	6.71	577.8	7.65	325.8	10.32
ACO-12-48	54	0.0696	0.0012	0.0926	0.0011	0.8883	0.0152	0.0283	0.001	88	917.7	34.97	571	6.59	645.5	8.16	564.3	19.38
ACO-12-48	55	0.0648	0.0015	0.1016	0.0013	0.9069	0.0205	0.0322	0.0017	95	766.7	49.06	623.5	7.44	655.4	10.92	639.8	33.22
ACO-12-48	56	0.0618	0.0027	0.1079	0.0019	0.9192	0.0387	0.0344	0.0031	100	665.9	92.11	660.5	11.15	662	20.46	682.6	60.89

ACO-12-48	57	0.0597	0.0016	0.1086	0.0016	0.8918	0.0232	0.0243	0.0011	103	593.6	56.19	664.4	9.25	647.3	12.44	486	22.4
ACO-12-48	58	0.062	0.0011	0.1046	0.0013	0.8925	0.0161	0.027	0.001	99	672.7	38.46	641.4	7.47	647.7	8.64	538.1	18.63
ACO-12-48	59	0.0593	0.0024	0.0828	0.0014	0.6771	0.0255	0.0261	0.0019	98	577.1	83.78	512.9	8.02	525	15.43	521	37.96
ACO-12-48	60	0.0753	0.0024	0.0894	0.0014	0.9279	0.0278	0.0231	0.0013	83	1075.8	62.29	552.2	7.97	666.5	14.65	461.5	25.97
ACO-12-48	61	0.131	0.002	0.3616	0.0048	6.5228	0.1041	0.0374	0.001	94	2111	26.93	1989.7	22.63	2049	14.05	742.2	19.51
ACO-12-48	62	0.0818	0.0024	0.119	0.0018	1.3415	0.0372	0.0253	0.0009	84	1241.5	55.71	724.5	10.55	863.9	16.11	505	17.16
ACO-12-48	63	0.0614	0.0011	0.1001	0.0012	0.8466	0.0152	0.0295	0.0008	99	652.6	38.23	614.8	7.12	622.8	8.34	587.4	15.98
ACO-12-48	64	0.0646	0.0013	0.0932	0.0012	0.8302	0.0171	0.0195	0.0007	94	762.6	42.83	574.6	7.31	613.7	9.47	390.1	13.04
ACO-12-48	65	0.0658	0.0013	0.1083	0.0015	0.9816	0.0197	0.0238	0.0008	95	798.8	41.4	663.1	8.41	694.4	10.08	475.6	15.1
ACO-12-48	66	0.0626	0.0009	0.1034	0.0012	0.8919	0.0132	0.0255	0.0007	98	694.5	30.84	634.2	6.98	647.4	7.09	508.8	13.35
ACO-12-48	67	0.0659	0.0015	0.1148	0.0015	1.043	0.0229	0.037	0.0014	97	802.7	46.95	700.3	8.36	725.4	11.36	735.2	27.67
ACO-12-48	68	0.0591	0.0008	0.1012	0.0012	0.8242	0.012	0.0259	0.0007	102	569.5	30.75	621.6	6.78	610.4	6.65	517.3	14.36
ACO-12-48	69	0.065	0.0011	0.132	0.0016	1.1832	0.0199	0.0336	0.001	101	775.1	35.05	799.3	8.92	792.8	9.23	668.8	20.15
ACO-12-48	70	0.063	0.0015	0.1037	0.0013	0.9014	0.02	0.0322	0.0012	97	709.6	48.25	635.8	7.64	652.5	10.7	640.3	24.3
ACO-12-48	71	0.0643	0.001	0.1024	0.0012	0.9084	0.014	0.0257	0.0008	96	752.8	31.87	628.7	7	656.2	7.45	512.1	16.57
ACO-12-48	72	0.0847	0.0014	0.1514	0.0018	1.7678	0.0295	0.0303	0.0011	88	1308.5	32.49	908.8	10.14	1033.7	10.81	602.6	21.57
ACO-12-48	73	0.0628	0.0015	0.0916	0.0011	0.7939	0.0181	0.0298	0.0013	95	701.6	49.84	565	6.76	593.4	10.24	592.7	26.17
ACO-12-48	74	0.0684	0.0014	0.0955	0.0012	0.9003	0.0175	0.0235	0.0008	90	880.7	40.56	587.9	6.97	651.9	9.34	469.2	16.19
ACO-12-48	75	0.0648	0.0014	0.089	0.0012	0.7949	0.0171	0.0224	0.001	93	768.2	45.24	549.7	6.97	593.9	9.66	447	18.96
ACO-12-48	76	0.0618	0.0011	0.1131	0.0014	0.9623	0.0176	0.0294	0.0012	101	665.5	38.65	690.7	8.08	684.5	9.08	585.9	23.87
ACO-12-48	77	0.0612	0.001	0.1092	0.0013	0.9209	0.015	0.0291	0.0011	101	645.7	34.95	668	7.35	662.8	7.94	579.2	21.32
ACO-12-48	78	0.0891	0.0015	0.2309	0.0027	2.8365	0.0455	0.0659	0.0027	95	1406.4	30.74	1339.3	14.12	1365.2	12.03	1289.7	51.39
ACO-12-48	79	0.2377	0.0042	0.6044	0.008	19.799	0.3579	0.0977	0.0052	98	3104.9	27.87	3047.6	32.09	3081.6	17.47	1884	95.42
ACO-12-48	80	0.0723	0.0013	0.0846	0.001	0.8432	0.0151	0.0203	0.0009	84	994.2	36.43	523.7	6.15	620.9	8.33	406.8	16.8
ACO-12-49	1	0.0789	0.0014	0.2028	0.0024	2.2066	0.0372	0.0572	0.0015	98.286	1170.1	33.8	1190.5	12.69	1183.1	11.77	1123.5	28.38
ACO-12-49	2	0.0624	0.0008	0.0927	0.001	0.7981	0.0106	0.0228	0.0005	104.23	689.3	28.06	571.5	5.94	595.7	6	455.1	9.69
ACO-12-49	3	0.0618	0.0011	0.1012	0.0012	0.8623	0.0152	0.0251	0.0006	101.63	667.7	37.98	621.3	6.88	631.4	8.27	501.8	12.68
ACO-12-49	4	0.0631	0.0013	0.1018	0.0011	0.8846	0.0168	0.0319	0.0014	103.01	710.3	42.05	624.7	6.63	643.5	9.05	634.4	26.54
ACO-12-49	5	0.0612	0.0009	0.1019	0.0011	0.8595	0.0127	0.0323	0.001	100.67	645.4	32.4	625.6	6.38	629.8	6.95	642.2	18.69
ACO-12-49	6	0.061	0.0012	0.0956	0.0011	0.8039	0.0152	0.0232	0.0006	101.78	639.5	41.13	588.5	6.68	599	8.55	464.1	12.35
ACO-12-49	7	0.0622	0.0009	0.102	0.0011	0.8737	0.013	0.0307	0.001	101.85	679.3	31.91	626	6.52	637.6	7.03	610.5	18.92
ACO-12-49	8	0.0627	0.0012	0.1013	0.0011	0.8763	0.0158	0.032	0.0012	102.7	699.5	39.71	622.2	6.62	639	8.56	635.9	24.02
ACO-12-49	9	0.066	0.0014	0.0956	0.0012	0.87	0.0176	0.025	0.0008	108.02	807.5	42.91	588.4	6.88	635.6	9.53	499.7	15.75
ACO-12-49	10	0.1331	0.0028	0.1132	0.0014	2.076	0.0405	0.0602	0.0026	165.08	2139.4	36.54	691.1	8.3	1140.9	13.38	1181.5	48.53
ACO-12-49	11	0.1229	0.0015	0.3683	0.004	6.238	0.0787	0.0953	0.0028	98.857	1998.3	22.04	2021.4	18.65	2009.8	11.03	1840.7	52.41
ACO-12-49	12	0.0596	0.0009	0.0997	0.0011	0.8192	0.0121	0.0231	0.0007	99.151	588.6	31.74	612.8	6.47	607.6	6.73	461.4	13.26
ACO-12-49	13	0.0651	0.0012	0.103	0.0012	0.924	0.0166	0.022	0.0006	105.13	776.2	37.91	632.1	7.2	664.5	8.77	439.7	12.42
ACO-12-49	14	0.0593	0.0008	0.1065	0.0012	0.8704	0.0122	0.0244	0.0007	97.456	577.7	30.18	652.4	6.8	635.8	6.63	487.7	14.1
ACO-12-49	15	0.0598	0.0012	0.1006	0.0012	0.8288	0.016	0.0241	0.0008	99.191	594.5	42.49	618	7.04	613	8.88	482.1	15.01
ACO-12-49	16	0.0576	0.001	0.0988	0.0012	0.7847	0.0137	0.023	0.0008	96.823	514.5	38.27	607.5	6.86	588.2	7.79	459.4	15.42

ACO-12-49	17	0.0605	0.0009	0.0984	0.0011	0.8209	0.0128	0.0227	0.0008	100.58	621.9	33.12	605.1	6.61	608.6	7.13	454.5	15.15
ACO-12-49	18	0.0602	0.0012	0.1081	0.0012	0.8965	0.0163	0.0324	0.0017	98.202	610.5	40.9	661.7	6.88	649.8	8.74	645	33.25
ACO-12-49	19	0.066	0.0013	0.092	0.0011	0.8367	0.0164	0.0267	0.0011	108.76	804.6	41.4	567.6	6.65	617.3	9.09	533.4	21.17
ACO-12-49	20	0.0629	0.0011	0.1023	0.0012	0.8872	0.0146	0.0258	0.0009	102.67	704.6	35.1	628.1	6.84	644.9	7.86	515.1	18.13
ACO-12-49	21	0.0623	0.0008	0.1006	0.0011	0.865	0.0115	0.0241	0.0005	102.39	685.8	28	618.1	6.4	632.9	6.25	481.3	10.42
ACO-12-49	22	0.061	0.0008	0.103	0.0011	0.8663	0.0118	0.027	0.0006	100.3	640.1	29.06	631.7	6.56	633.6	6.44	538.5	12.43
ACO-12-49	23	0.0571	0.0009	0.1005	0.0011	0.7917	0.012	0.0244	0.0006	95.903	495.6	33.3	617.5	6.56	592.2	6.77	487.6	11.68
ACO-12-49	24	0.0609	0.0012	0.1032	0.0012	0.8662	0.0171	0.0314	0.001	100.03	634.7	43.13	633.3	7.19	633.5	9.29	624.3	19.28
ACO-12-49	25	0.0586	0.0011	0.098	0.0012	0.7917	0.0145	0.0261	0.0007	98.209	551.1	40.36	602.9	6.76	592.1	8.23	521.1	14.54
ACO-12-49	26	0.0597	0.0008	0.1038	0.0011	0.854	0.0113	0.0263	0.0007	98.43	591	28.09	636.9	6.58	626.9	6.17	525.4	13.11
ACO-12-49	27	0.0622	0.001	0.1008	0.0012	0.8646	0.0139	0.0284	0.0008	102.21	682.1	34.33	618.9	6.71	632.6	7.56	565.8	15.49
ACO-12-49	28	0.0595	0.0009	0.1018	0.0012	0.8354	0.0131	0.0264	0.0007	98.624	585.3	33.84	625.2	6.72	616.6	7.23	526.1	14.65
ACO-12-49	29	0.0589	0.001	0.0919	0.0011	0.7457	0.0123	0.0207	0.0006	99.859	562.5	34.86	566.5	6.51	565.7	7.13	414	12.56
ACO-12-49	30	0.0599	0.0009	0.0975	0.0011	0.8058	0.0117	0.0275	0.0008	100.03	600.7	31.24	599.9	6.37	600.1	6.6	548	15.44
ACO-12-49	31	0.059	0.0008	0.1023	0.0011	0.8318	0.0116	0.0243	0.0007	97.913	566.8	29.91	627.7	6.61	614.6	6.44	485.8	13.11
ACO-12-49	32	0.0683	0.0012	0.101	0.0013	0.9503	0.0168	0.021	0.0007	109.39	876.3	35.3	620.1	7.54	678.3	8.73	420.6	14.06
ACO-12-49	33	0.1286	0.0019	0.3748	0.0045	6.6444	0.0994	0.085	0.0026	101.28	2078.4	26.19	2052.1	20.88	2065.3	13.21	1649.4	48.23
ACO-12-49	34	0.0623	0.001	0.1024	0.0011	0.8796	0.0134	0.0317	0.0013	102.01	685.8	33.18	628.2	6.4	640.8	7.22	631.6	25.67
ACO-12-49	35	0.057	0.0012	0.0894	0.0011	0.7027	0.0146	0.0231	0.0009	97.952	492.4	45.91	551.7	6.65	540.4	8.73	461.4	17.32
ACO-12-49	36	0.0602	0.0013	0.0983	0.0012	0.8162	0.0172	0.0254	0.0009	100.23	611.3	45.89	604.5	7.19	605.9	9.6	506.9	16.85
ACO-12-49	37	0.1359	0.0019	0.3931	0.0045	7.3675	0.1041	0.0953	0.003	101.82	2176.1	24.26	2137.2	20.95	2157	12.63	1840.5	55.07
ACO-12-49	38	0.0619	0.0009	0.1123	0.0013	0.9588	0.0138	0.0514	0.0024	99.475	670.8	30.13	686.3	7.28	682.7	7.13	1012.8	46.07
ACO-12-49	39	0.0589	0.0009	0.0989	0.0011	0.8037	0.0126	0.0247	0.0009	98.503	564.8	33.84	608	6.63	598.9	7.11	492.4	16.8
ACO-12-49	40	0.0605	0.0012	0.0998	0.0011	0.8325	0.0152	0.0335	0.0018	100.31	622.2	40.61	613.1	6.53	615	8.43	665.6	35.54
ACO-12-49	41	0.0624	0.0009	0.1073	0.0012	0.9227	0.0132	0.0276	0.0007	101.04	687.3	30.07	657	7.02	663.8	6.99	550.9	13.14
ACO-12-49	42	0.0805	0.0015	0.2009	0.0025	2.2286	0.0408	0.0627	0.0024	102.36	1208.1	35.82	1180.2	13.56	1190.1	12.82	1228.5	45.7
ACO-12-49	43	0.0598	0.0009	0.1012	0.0012	0.8341	0.0131	0.0277	0.0008	99.099	595	34.28	621.5	6.79	615.9	7.27	552.6	14.94
ACO-12-49	44	0.0582	0.0009	0.0973	0.0011	0.7809	0.012	0.0264	0.0007	97.895	537.3	33.87	598.6	6.5	586	6.85	527	13.64
ACO-12-49	45	0.0807	0.0011	0.208	0.0023	2.3145	0.0319	0.0569	0.0015	99.68	1214.3	26.57	1218.2	12.49	1216.7	9.77	1118.4	28.42
ACO-12-49	46	0.0632	0.0015	0.1	0.0013	0.8715	0.0198	0.0316	0.0014	103.58	715.4	48.59	614.4	7.74	636.4	10.73	628.2	26.97
ACO-12-49	47	0.076	0.0012	0.0961	0.0011	1.006	0.0156	0.0353	0.0011	119.55	1094.2	31.25	591.3	6.43	706.9	7.9	701.1	20.51
ACO-12-49	48	0.0607	0.0009	0.1033	0.0012	0.8643	0.0129	0.0279	0.0008	99.811	628.6	31.58	633.6	6.85	632.4	7.01	555.4	15.31
ACO-12-49	49	0.0614	0.0012	0.097	0.0011	0.821	0.0157	0.0301	0.0011	102.01	653.7	41.96	596.6	6.71	608.6	8.77	599.6	20.63
ACO-12-49	50	0.0601	0.0012	0.0911	0.0012	0.754	0.0151	0.0165	0.0006	101.51	605.5	42.31	562	7.18	570.5	8.75	330.3	11.56
ACO-12-49	51	0.0603	0.0009	0.1022	0.0012	0.8495	0.0124	0.0276	0.0008	99.522	613.8	31.02	627.4	6.75	624.4	6.81	550.1	15.91
ACO-12-49	52	0.0599	0.0008	0.0985	0.0011	0.8134	0.0114	0.0263	0.0008	99.769	599.3	29.73	605.8	6.48	604.4	6.39	523.9	15.29
ACO-12-49	53	0.062	0.0009	0.098	0.0011	0.837	0.0122	0.0278	0.0009	102.51	673.6	30.55	602.4	6.49	617.5	6.72	554.6	16.92
ACO-12-49	54	0.0624	0.0013	0.112	0.0014	0.9631	0.0201	0.0334	0.0013	100.06	686.5	45.23	684.5	8	684.9	10.37	663.2	24.56
ACO-12-49	55	0.0648	0.0018	0.1073	0.0016	0.9594	0.0258	0.0279	0.0015	103.91	768.8	56.86	657.3	9.16	683	13.36	556.7	28.79
ACO-12-49	56	0.0585	0.0009	0.1015	0.0012	0.8177	0.0132	0.0258	0.0008	97.415	546.8	34.86	622.9	6.88	606.8	7.35	514	16.07
ACO-12-49	57	0.0616	0.0009	0.1059	0.0012	0.8985	0.0138	0.0274	0.0009	100.34	658.8	32.54	648.7	7.07	650.9	7.38	547.2	18.38

ACO-12-49	58	0.0591	0.0013	0.0929	0.0011	0.7572	0.0158	0.0268	0.001	99.965	571.9	45.84	572.6	6.75	572.4	9.1	535.4	20.48
ACO-12-49	59	0.1783	0.0024	0.508	0.0059	12.49	0.1754	0.0669	0.0025	99.596	2637.2	22.34	2647.9	25.37	2642	13.2	1309.4	47.98
ACO-12-49	60	0.0702	0.0015	0.1296	0.0018	1.2538	0.0265	0.0304	0.0017	105.07	933.5	42.43	785.3	10.1	825.1	11.92	604.3	33.65
ACO-12-49	61	0.0594	0.0008	0.1042	0.0012	0.8533	0.0116	0.0257	0.0006	98.059	582.5	28.48	638.8	6.89	626.4	6.37	512.1	11.24
ACO-12-49	62	0.0619	0.0009	0.1018	0.0012	0.8683	0.0123	0.0278	0.0007	101.52	669.1	29.41	625.2	6.78	634.7	6.67	554.4	13.61
ACO-12-49	63	0.0595	0.0009	0.1051	0.0012	0.8615	0.0127	0.0336	0.001	97.921	583.6	31.73	644.4	6.88	631	6.94	667.8	18.71
ACO-12-49	64	0.063	0.0011	0.0986	0.0012	0.8552	0.0154	0.0262	0.0008	103.53	706.7	37.61	606.1	7.18	627.5	8.4	523.4	15.55
ACO-12-49	65	0.0964	0.0013	0.2774	0.0033	3.6833	0.0517	0.0723	0.0021	98.536	1554.9	25.26	1578	16.41	1567.8	11.21	1410.3	39.79
ACO-12-49	66	0.0605	0.0018	0.0979	0.0014	0.8165	0.0231	0.0301	0.0012	100.65	621.7	62.58	602.2	7.95	606.1	12.89	598.6	24.19
ACO-12-49	67	0.0622	0.001	0.1168	0.0013	1.0011	0.0162	0.0351	0.0014	98.919	681.3	35.17	712.1	7.52	704.4	8.23	696.9	27.24
ACO-12-49	68	0.059	0.0017	0.105	0.0016	0.8529	0.0243	0.0189	0.0007	97.251	565.8	62.11	643.9	9.41	626.2	13.32	379.2	14.46
ACO-12-49	69	0.0596	0.0008	0.1059	0.0012	0.8697	0.0121	0.0281	0.0008	97.92	588.7	29.25	648.9	6.97	635.4	6.56	560.5	15.35
ACO-12-49	70	0.0612	0.0011	0.11	0.0013	0.928	0.0164	0.0288	0.0008	99.049	646	37.94	673	7.69	666.6	8.66	573.8	16.03
ACO-12-49	71	0.0874	0.0013	0.2456	0.003	2.9554	0.0446	0.0495	0.0015	96.729	1369.2	27.74	1415.5	15.54	1396.2	11.45	975.7	28.75
ACO-12-49	72	0.0605	0.001	0.098	0.0011	0.8163	0.013	0.0309	0.0013	100.55	619.9	34.89	602.7	6.34	606	7.24	615.2	24.61
ACO-12-49	73	0.0601	0.001	0.102	0.0011	0.8443	0.0133	0.0334	0.0015	99.297	607.5	34.91	625.9	6.52	621.5	7.34	663.5	29.02
ACO-12-49	74	0.0569	0.001	0.1027	0.0011	0.8049	0.0135	0.0317	0.0014	95.114	485.9	38.41	630.4	6.65	599.6	7.61	629.9	27.66
ACO-12-49	75	0.061	0.001	0.1072	0.0012	0.9009	0.0145	0.0316	0.0013	99.33	638.7	35.1	656.6	6.99	652.2	7.75	628.6	25.52
ACO-12-49	76	0.0611	0.001	0.101	0.0011	0.85	0.0131	0.0296	0.0011	100.71	641.4	33.1	620.3	6.65	624.7	7.18	589.7	22.33
ACO-12-49	77	0.0609	0.0013	0.0917	0.0011	0.7695	0.0156	0.0289	0.0012	102.51	636.2	44.11	565.3	6.62	579.5	8.93	575.3	24.1
ACO-12-49	78	0.0602	0.0013	0.1042	0.0013	0.8633	0.0179	0.0321	0.0015	98.935	609.5	45.92	638.7	7.34	631.9	9.76	639.3	29.86
ACO-12-49	79	0.0621	0.0009	0.1008	0.0012	0.8617	0.0131	0.0272	0.001	101.97	677.5	31.58	618.9	6.91	631.1	7.14	542.2	20.51
ACO-12-49	80	0.0586	0.0009	0.1045	0.0012	0.8444	0.0123	0.0284	0.001	96.958	552.8	31.33	641	6.93	621.5	6.79	565.7	20.37
ACO-12-40	1	0.1018	0.0013	0.1068	0.0014	1.4978	0.0221	0.0379	0.0009	70.339	1656.9	24.21	653.8	8.22	929.5	8.96	751.5	17.17
ACO-12-40	2	0.0595	0.0012	0.1026	0.0014	0.8415	0.0169	0.0286	0.0007	101.53	585.6	41.4	629.5	8.24	620	9.31	569.3	14.6
ACO-12-40	3	0.0611	0.0009	0.0975	0.0013	0.8202	0.0134	0.0274	0.0007	98.569	641.1	32.06	599.4	7.55	608.1	7.45	545.8	13.79
ACO-12-40	4	0.0616	0.001	0.0999	0.0013	0.8476	0.0148	0.0285	0.0008	98.444	659	34.61	613.7	7.86	623.4	8.13	568.2	15.04
ACO-12-40	5	0.0612	0.001	0.1004	0.0014	0.8467	0.0149	0.0284	0.0008	99.004	646.1	34.98	616.6	7.96	622.8	8.19	566.1	15.66
ACO-12-40	6	0.0603	0.001	0.0985	0.0013	0.8188	0.0144	0.0281	0.0008	99.671	615.1	35.11	605.4	7.75	607.4	8.02	559.5	15.73
ACO-12-40	7	0.0732	0.0011	0.1025	0.0014	1.0347	0.0167	0.0294	0.0009	87.204	1020.2	29.84	629	7.98	721.3	8.34	584.9	16.87
ACO-12-40	8	0.0611	0.0008	0.105	0.0014	0.8841	0.0135	0.03	0.0009	100.06	642.4	29.1	643.6	8.03	643.2	7.27	596.7	17.78
ACO-12-40	9	0.0622	0.001	0.1048	0.0014	0.899	0.0149	0.0285	0.0009	98.695	681.1	32.18	642.7	8.13	651.2	7.94	568.2	17.51
ACO-12-40	10	0.061	0.0014	0.1021	0.0015	0.8589	0.0203	0.0285	0.0011	99.523	640.8	49.11	626.5	8.78	629.5	11.09	567	20.95
ACO-12-40	11	0.0639	0.0015	0.1002	0.0015	0.8828	0.0206	0.0289	0.0011	95.813	738.5	47.8	615.6	8.52	642.5	11.12	575.7	20.82
ACO-12-40	12	0.0596	0.0009	0.1032	0.0014	0.8477	0.0144	0.0299	0.0011	101.54	588.8	33.88	633	8.05	623.4	7.92	596.2	20.85
ACO-12-40	13	0.0602	0.0009	0.1009	0.0013	0.8376	0.0134	0.0294	0.0011	100.32	610.3	31.2	619.8	7.8	617.8	7.41	585.3	20.71
ACO-12-40	14	0.063	0.002	0.1052	0.0018	0.9132	0.0287	0.0323	0.0017	97.905	706.5	66.43	645	10.24	658.8	15.23	642	32.87
ACO-12-40	15	0.0615	0.0012	0.1051	0.0015	0.8915	0.0175	0.0324	0.0016	99.567	657.2	39.48	644.4	8.76	647.2	9.38	644.5	30.93
ACO-12-40	16	0.0713	0.0011	0.1041	0.0014	1.0232	0.017	0.0282	0.0012	89.196	966.1	31.1	638.2	8.1	715.5	8.54	561.4	22.55
ACO-12-40	17	0.0612	0.0011	0.103	0.0015	0.8682	0.0169	0.0312	0.0017	99.543	644.8	39.02	631.7	8.63	634.6	9.17	620.2	32.5

ACO-12-40	18	0.0611	0.0012	0.1036	0.0015	0.873	0.0183	0.0315	0.0018	99.765	641.9	42.83	635.7	8.89	637.2	9.93	627.7	35.36
ACO-12-40	19	0.0615	0.0011	0.1031	0.0015	0.8742	0.0162	0.0323	0.0019	99.153	656.6	36.43	632.4	8.52	637.8	8.75	642.1	37.66
ACO-12-40	20	0.0624	0.0017	0.1006	0.0016	0.8656	0.024	0.0307	0.0019	97.599	686.9	58.13	618	9.43	633.2	13.05	611.4	37.53
ACO-12-40	21	0.0617	0.0016	0.0992	0.0016	0.8439	0.0218	0.0274	0.0016	98.117	663.3	54.38	609.6	9.32	621.3	12.01	545.4	32.27
ACO-12-40	22	0.0619	0.0011	0.1056	0.0015	0.9005	0.0171	0.0302	0.0013	99.218	669.2	38.2	646.9	8.61	652	9.13	601.5	25.82
ACO-12-40	23	0.0613	0.0021	0.1027	0.0017	0.8683	0.0292	0.0288	0.0014	99.323	649.6	71.77	630.4	9.95	634.7	15.88	574	27.22
ACO-12-40	24	0.0615	0.0009	0.1038	0.0014	0.8801	0.014	0.0295	0.0011	99.329	656.5	31.11	636.7	7.96	641	7.57	587.3	22.38
ACO-12-40	25	0.0595	0.0012	0.1132	0.0016	0.9276	0.0188	0.0316	0.0013	103.69	584.3	42.18	691	8.96	666.4	9.88	629.7	24.52
ACO-12-40	26	0.1527	0.0027	0.1416	0.002	2.9807	0.053	0.0819	0.0038	60.854	2376.5	29.25	853.6	11.39	1402.7	13.51	1590.4	71.35
ACO-12-40	27	0.0801	0.0011	0.1066	0.0014	1.1773	0.0176	0.0361	0.0015	82.646	1200.2	26.59	652.9	7.96	790	8.2	716	29.19
												45.12	598.9	8.14	597.8	9.72	565.8	26.62
ACO-12-40	28	0.0597	0.0013	0.0974	0.0014	0.8017	0.0173	0.0284	0.0014	100.18	594.1							
ACO-12-40	29	0.0613	0.001	0.097	0.0013	0.8195	0.0142	0.0309	0.0014	98.174	650.2	35.2	596.7	7.42	607.8	7.92	615.4	26.81
ACO-12-40	30	0.0677	0.0014	0.1018	0.0015	0.9509	0.0195	0.0332	0.002	92.101	860.6	40.84	625	8.61	678.6	10.14	660.6	38.8
ACO-12-40	31	0.0896	0.0015	0.1013	0.0014	1.2506	0.0221	0.0394	0.0022	75.513	1416.3	32.05	622	8.02	823.7	9.97	780.9	42.25
ACO-12-40	32	0.0948	0.0024	0.1063	0.0017	1.3898	0.0345	0.0346	0.0024	73.638	1524.5	46.83	651.4	10.07	884.6	14.64	687	47.62
ACO-12-40	33	0.0611	0.0012	0.0998	0.0013	0.8394	0.0163	0.0311	0.0016	99.063	641.9	40.26	613	7.77	618.8	8.97	619.6	30.67
ACO-12-40	34	0.0663	0.0014	0.1043	0.0015	0.9524	0.0207	0.0324	0.002	94.112	814.9	44.47	639.3	8.84	679.3	10.78	644.7	38.42
ACO-12-40	35	0.0593	0.0011	0.0996	0.0013	0.8134	0.0145	0.0311	0.0018	101.24	578.2	37.85	611.9	7.47	604.4	8.1	618.9	34.54
ACO-12-40	36	0.062	0.0023	0.1022	0.0017	0.8732	0.0302	0.0355	0.0035	98.431	672.3	75.99	627.3	10.19	637.3	16.35	704.9	67.52
ACO-12-40	37	0.0614	0.0016	0.101	0.0014	0.8545	0.0215	0.03	0.0017	98.884	654.7	53.42	620.1	8.2	627.1	11.75	597.6	33.57
ACO-12-40	38	0.0827	0.0014	0.105	0.0014	1.1961	0.0201	0.0392	0.0023	80.583	1262.3	31.45	643.7	7.91	798.8	9.3	778	44.77
ACO-12-40	39	0.0624	0.0012	0.0989	0.0013	0.8492	0.0166	0.0314	0.0021	97.389	686.7	41.67	607.9	7.63	624.2	9.1	625.1	41.23
ACO-12-40	40	0.0622	0.0013	0.0984	0.0013	0.8427	0.0175	0.0315	0.0022	97.487	680.9	44.7	605.1	7.74	620.7	9.65	627.5	43.23
ACO-12-40	41	0.0595	0.0009	0.104	0.0013	0.8533	0.0129	0.0303	0.0011	101.84	585.8	30.66	638	7.49	626.5	7.09	603.2	20.68
ACO-12-40	42	0.0954	0.0015	0.1092	0.0015	1.4361	0.0239	0.0339	0.0014	73.919	1535.9	29.76	668.3	8.42	904.1	9.98	674.6	27.24
ACO-12-40	43	0.0649	0.0014	0.1009	0.0013	0.903	0.019	0.0321	0.0012	94.858	771.7	43.48	619.8	7.78	653.4	10.13	639.2	24.14
ACO-12-40	44	0.0632	0.0014	0.0999	0.0013	0.8702	0.0187	0.0313	0.0013	96.586	714.3	44.96	614	7.75	635.7	10.16	623.1	24.61

ACO-12-40	45	0.0967	0.0043	0.1213	0.0027	1.6177	0.066	0.0504	0.0062	75.55	1561.6	81.11	738.2	15.33	977.1	25.59	994.5	118.51
ACO-12-40	46	0.0583	0.0011	0.0987	0.0013	0.7928	0.0147	0.0288	0.0011	102.36	540.3	39.82	606.7	7.56	592.7	8.34	573.7	21.77
ACO-12-40	47	0.0593	0.001	0.1	0.0013	0.817	0.014	0.0282	0.0011	101.35	576.8	35.22	614.6	7.56	606.4	7.8	561.7	21.33
ACO-12-40	48	0.0583	0.0016	0.0988	0.0014	0.7938	0.021	0.0304	0.0014	102.38	540.7	58.45	607.4	8.23	593.3	11.89	605.8	26.7
ACO-12-40	49	0.0603	0.0014	0.1065	0.0015	0.8841	0.0199	0.029	0.0015	101.4	612.9	47.81	652.2	8.9	643.2	10.71	578.1	28.83
ACO-12-40	50	0.06	0.0014	0.0995	0.0014	0.8224	0.0194	0.0283	0.0014	100.3	603.8	50.47	611.2	8.33	609.4	10.82	564.1	27.67
ACO-12-40	51	0.0594	0.0017	0.0995	0.0015	0.8134	0.0222	0.0312	0.0022	101.14	580.1	60.66	611.3	8.72	604.4	12.43	621.4	43.74
ACO-12-40	52	0.059	0.0013	0.0979	0.0013	0.7957	0.0172	0.0268	0.0013	101.3	566.4	46.29	602.1	7.87	594.4	9.72	534.3	25.65
ACO-12-40	53	0.0606	0.0011	0.0992	0.0013	0.828	0.0157	0.0284	0.0014	99.51	624.8	39.67	609.5	7.66	612.5	8.7	566.9	26.77
ACO-12-40	54	0.0631	0.0016	0.0998	0.0014	0.8678	0.0217	0.028	0.0014	96.69	710.8	52.91	613.4	8.36	634.4	11.78	557.6	27.52
ACO-12-40	55	0.062	0.0012	0.0986	0.0013	0.8417	0.0158	0.0277	0.0014	97.758	672.5	39.23	606.2	7.6	620.1	8.73	552.6	27.18
ACO-12-40	56	0.0602	0.0012	0.0973	0.0013	0.8068	0.0165	0.0267	0.0014	99.684	609.1	43.63	598.8	7.72	600.7	9.29	532.4	28.1
ACO-12-40	57	0.0601	0.0015	0.0971	0.0014	0.8034	0.0202	0.0264	0.0015	99.766	605.9	54.26	597.3	8.16	598.7	11.37	526.5	29.83
ACO-12-40	58	0.0619	0.0013	0.1035	0.0014	0.8821	0.018	0.0285	0.0017	98.894	669	43.18	635	8.26	642.1	9.7	568.2	33.68
ACO-12-40	59	0.0686	0.0017	0.0999	0.0015	0.9442	0.0225	0.0296	0.002	90.92	886.2	49.53	613.8	8.73	675.1	11.76	589.6	38.36
ACO-12-40	60	0.11	0.0018	0.103	0.0013	1.5603	0.0256	0.0418	0.0023	66.174	1799.4	29.44	631.7	7.49	954.6	10.16	827.2	44.94

Iberia U-Pb data tables

Sample	Analysis #	Pb207/Pb206		Pb206/U238		Pb207/U235		Pb208/Th232		Concordancy	Pb207/Pb206		Pb206/U238		Pb207/U235		Pb208/Th232	
14-01-01	1	0.05856	0.0012 8	0.0893 4	0.0011 6	0.72138	0.0155 8	0.02552	0.0006 1	100.036	550.8	47.06	551.7	6.88	551.5	9.19	509.4	11.95
14-01-02	2	0.12724	0.0021 4	0.3477	0.0044 3	6.09918	0.1044 8	0.10165	0.0029	93.3696	2060.2	29.44	1923.6	21.2	1990.1	14.9 4	1956.8	53.25
14-01-03	3	0.06069	0.0010 3	0.0920 7	0.0011 3	0.77043	0.0132 6	0.03017	0.0006 9	97.8793	628.4	36.13	567.7	6.67	580	7.61	600.7	13.62
14-01-04	4	0.06298	0.0009 3	0.0695 2	0.0008 4	0.60362	0.0092 8	0.02478	0.0006	90.3441	707.5	31.07	433.2	5.06	479.5	5.87	494.7	11.77
14-01-05	5	0.07019	0.0011 2	0.0769 9	0.0009 4	0.74498	0.0121 8	0.03732	0.0009	84.5746	933.8	32.45	478.1	5.62	565.3	7.08	740.6	17.57
14-01-06	6	0.06195	0.0010 2	0.0705 5	0.0008 5	0.60259	0.0100 5	0.02768	0.0006 4	91.7519	672.3	34.86	439.4	5.12	478.9	6.37	551.9	12.51
14-01-07	7	0.08354	0.0010 6	0.1140 8	0.0013 2	1.314	0.0176	0.03933	0.0007 4	81.7467	1281.7	24.63	696.4	7.61	851.9	7.72	779.8	14.36
14-01-08	8	0.06119	0.0013 8	0.0749 7	0.001	0.6325	0.0141	0.02851	0.0010 4	93.6307	645.9	47.66	466	6.02	497.7	8.77	568.2	20.34
14-01-09	9	0.064	0.0009 4	0.0799 8	0.0009 2	0.70578	0.0105 5	0.03034	0.0006 4	91.4792	741.7	30.77	496	5.52	542.2	6.28	604.1	12.55
14-01-10	10	0.09654	0.0019 7	0.1211 9	0.0016 5	1.61308	0.0331 1	0.09343	0.0034 1	75.6075	1558.4	37.89	737.4	9.51	975.3	12.8 7	1805.3	63.11
14-01-11	11	0.10861	0.0015 6	0.0969 3	0.0011 6	1.45146	0.0216 9	0.10359	0.0024 4	65.5025	1776.2	25.96	596.4	6.83	910.5	8.98	1992.2	44.73
14-01-12	12	0.34528	0.0220 5	0.1809 7	0.0076 2	8.61076	0.4650 2	0.45048	0.0394 7	29.0861	3686.3	94.15	1072.2	41.6 2	2297.7	49.1 3	7516.8	550.05
14-01-13	13	0.06182	0.0013 4	0.0922	0.0012 5	0.78603	0.0171 1	0.02882	0.0010 5	96.5529	667.8	45.68	568.6	7.38	588.9	9.73	574.3	20.61
14-01-14	14	0.11093	0.0021 5	0.0847 6	0.0011 3	1.2963	0.0252 2	0.03191	0.0010 1	62.1372	1814.7	34.79	524.5	6.69	844.1	11.1 5	635	19.69
14-01-15	15	0.1298	0.003 9	0.1100 8	0.0015 8	1.97005	0.0453 7	0.15714	0.0067 2	60.9156	2095.2	40	673.3	9.18	1105.3	15.5 1	2950.1	117.46
14-01-16	16	0.09371	0.0021 4	0.0476 4	0.0006 7	0.61567	0.014	0.0364	0.0014 3	61.589	1502.4	42.6	300	4.13	487.1	8.8	722.6	27.87
14-01-17	17	0.08678	0.0012 7	0.1340 6	0.0015 9	1.60396	0.0242 1	0.05853	0.0014 2	83.4534	1355.5	27.88	811	9.01	971.8	9.44	1149.6	27.06
14-01-18	18	0.09738	0.0032 6	0.0925 3	0.0015 4	1.24165	0.0405 8	0.03529	0.0022 2	69.6071	1574.6	61.45	570.5	9.11	819.6	18.3 8	701.1	43.26
14-01-19	19	0.06086	0.0014 8	0.0646 8	0.0009 5	0.54271	0.0131 5	0.02943	0.0013 4	91.7765	634.5	51.63	404	5.48	440.2	8.66	586.3	26.4
14-01-20	20	0.12152	0.0023 1	0.2245 7	0.0029 5	3.76247	0.0729 8	0.09896	0.0035 2	66.0063	1978.6	33.53	1306	15.5 5	1584.8	15.5 6	1907.3	64.82
14-01-21	21	0.0775	0.0014 1	0.0693 4	0.0008 7	0.74101	0.0134 8	0.02582	0.0006 8	76.7673	1134.2	35.88	432.2	5.27	563	7.86	515.2	13.39
14-01-22	22	0.05991	0.0010 5	0.1001 9	0.0012 2	0.82752	0.0145 2	0.02165	0.0005	100.539	600.2	37.48	615.5	7.15	612.2	8.07	432.9	9.84
14-01-23	23	0.13843	0.0051 3	0.3559 1	0.0070 7	6.79832	0.2411 5	0.08133	0.0056	88.911	2207.6	62.97	1962.8	33.6 2	2085.5	31.4	1580.4	104.62
14-01-24	24	0.08874	0.0019 1	0.0917 9	0.0012 4	1.12298	0.0236 2	0.03577	0.0010 6	74.0581	1398.4	40.58	566.1	7.32	764.4	11.3	710.3	20.71
14-01-25	25	0.12262	0.0026 6	0.2816 1	0.0038 7	4.75975	0.1025 2	0.03958	0.0019 5	80.1875	1994.7	38.12	1599.5	19.4 8	1777.8	18.0 7	784.5	38.01
14-01-26	26	0.04957	0.0022 1	0.0162 9	0.0002 8	0.11134	0.0047 9	0.00372	0.0001 6	97.2015	174.8	101.0 2	104.2	1.8	107.2	4.37	75.1	3.12
14-01-27	27	0.05995	0.0011	0.0996	0.0012	0.82383	0.0156	0.02762	0.0007	100.377	601.9	41.38	612.5	7.01	610.2	8.71	550.6	14.36

ACO-12-60	6	0.06226	0.00104	0.11577	0.00142	0.99436	0.0171	0.03286	0.00154	100.756	683	35.27	706.2	8.21	700.9	8.71	653.6	30.17
ACO-12-60	7	0.05943	0.0013	0.08452	0.0011	0.69281	0.01515	0.02478	0.00136	97.8672	582.7	46.83	523.1	6.51	534.5	9.09	494.8	26.89
ACO-12-60	8	0.06638	0.00134	0.10522	0.00121	0.9638	0.01894	0.03866	0.00262	94.1048	818.3	41.75	644.9	7.05	685.3	9.79	766.6	51.05
ACO-12-60	9	0.05985	0.00089	0.08873	0.00101	0.73295	0.01111	0.02792	0.00137	98.1551	598	31.89	548	5.98	558.3	6.51	556.6	26.97
ACO-12-60	10	0.06205	0.00185	0.09012	0.00117	0.77165	0.0223	0.02733	0.00215	95.7982	675.8	62.65	556.3	6.9	580.7	12.78	544.9	42.25
ACO-12-60	11	0.06135	0.00146	0.08606	0.00103	0.7289	0.01695	0.02526	0.00159	95.7366	651.5	50.29	532.2	6.1	555.9	9.96	504.2	31.37
ACO-12-60	12	0.06199	0.00101	0.08931	0.00103	0.76415	0.01251	0.02802	0.0016	95.6801	673.7	34.49	551.5	6.08	576.4	7.2	558.5	31.39
ACO-12-60	13	0.06068	0.00132	0.09674	0.00117	0.81003	0.01727	0.02862	0.00178	98.805	627.8	46.08	595.3	6.85	602.5	9.69	570.3	35.03
ACO-12-60	14	0.06377	0.00119	0.09165	0.00101	0.80568	0.01461	0.03078	0.00138	94.2167	734	38.93	565.3	5.97	600	8.22	612.7	27.01
ACO-12-60	15	0.10899	0.00154	0.29542	0.00356	4.44026	0.06618	0.08826	0.00424	93.6048	1782.6	25.65	1668.6	17.71	1719.9	12.35	1709.6	78.79
ACO-12-60	16	0.06476	0.00114	0.11256	0.00139	1.00518	0.01809	0.03655	0.00185	97.3386	766.7	36.8	687.6	8.06	706.4	9.16	725.7	36.03
ACO-12-60	17	0.12123	0.00238	0.31519	0.00427	5.26806	0.10578	0.09304	0.00675	89.455	1974.4	34.55	1766.2	20.93	1863.7	17.14	1798.2	124.85
ACO-12-60	18	0.06003	0.00096	0.09117	0.00111	0.75464	0.01256	0.02877	0.00145	98.5111	604.6	34.34	562.4	6.59	570.9	7.27	573.4	28.54
ACO-12-60	19	0.08433	0.00122	0.12598	0.00143	1.4646	0.02157	0.06652	0.00308	83.5135	1300	27.91	764.9	8.18	915.9	8.89	1301.6	58.37
ACO-12-60	20	0.1205	0.00153	0.33903	0.00378	5.63217	0.07443	0.09792	0.0046	95.8444	1963.6	22.43	1882	18.2	1921	11.39	1888.2	84.7
ACO-12-60	21	0.06052	0.00099	0.09346	0.00108	0.77984	0.01297	0.02913	0.00142	98.3772	622.3	34.94	575.9	6.37	585.4	7.4	580.5	27.87
ACO-12-60	22	0.06154	0.00101	0.09506	0.00111	0.80652	0.01349	0.02903	0.00148	97.4854	658.1	34.73	585.4	6.55	600.5	7.58	578.5	29
ACO-12-60	23	0.06307	0.00119	0.10455	0.00125	0.90904	0.01727	0.03093	0.00164	97.639	710.5	39.53	641	7.28	656.5	9.19	615.6	32.12
ACO-12-60	24	0.06	0.00121	0.09381	0.00122	0.77622	0.01583	0.02782	0.00193	99.0914	603.7	42.92	578	7.17	583.3	9.05	554.6	38.04
ACO-12-60	25	0.07932	0.00136	0.17333	0.00205	1.89557	0.03294	0.05376	0.00329	87.3072	1180.2	33.53	1030.4	11.25	1079.5	11.55	1058.3	63.09
ACO-12-60	26	0.06864	0.00117	0.12758	0.00157	1.20721	0.02124	0.03926	0.00249	96.2931	887.8	34.78	774.1	8.98	803.9	9.77	778.4	48.33
ACO-12-60	27	0.05906	0.00076	0.09551	0.00106	0.77712	0.01022	0.02355	0.00061	100.737	569.5	27.59	588.1	6.22	583.8	5.84	470.5	12.09
ACO-12-60	28	0.06187	0.00079	0.11221	0.00123	0.95629	0.01248	0.0268	0.00074	100.616	669.6	27.22	685.6	7.14	681.4	6.48	534.5	14.6
ACO-12-60	29	0.05992	0.00096	0.09462	0.00112	0.7814	0.01272	0.03404	0.00178	99.403	600.5	34.16	582.8	6.58	586.3	7.25	676.5	34.7
ACO-12-60	30	0.06336	0.00081	0.11691	0.00131	1.02059	0.01341	0.03799	0.00109	99.804	720.2	26.96	712.8	7.54	714.2	6.74	753.6	21.26
ACO-12-60	31	0.05872	0.00104	0.09352	0.00107	0.75659	0.01327	0.02075	0.0006	100.752	556.9	37.77	576.3	6.29	572	7.67	415.2	11.9
ACO-12-60	32	0.06448	0.00324	0.09385	0.00141	0.83349	0.041	0.01944	0.00074	93.9561	757.4	102.47	578.3	8.32	615.5	22.7	389.1	14.67
ACO-12-	33	0.10362	0.0013	0.3169	0.0035	4.52528	0.0578	0.05792	0.0016	105.018	1689.9	23.14	1774.7	17.2	1735.6	10.6	1138	32.15

60			1	2	3		7		8					6		4		
ACO-12-60	34	0.05595	0.0008	0.1001	0.0010	0.77232	0.0106	0.01699	0.0006	105.834	450.2	30.99	615	6.2	581.1	6.11	340.5	11.88
ACO-12-60	35	0.15961	0.0021	0.4448	0.0051	9.78746	0.1355	0.12489	0.0058	96.7734	2451.5	22.56	2372.4	22.7	2415	12.7	2378.8	104.69
ACO-12-60	36	0.054	0.0013	0.0981	0.0011	0.73378	0.0173	0.0192	0.0009	107.981	370.7	54.41	603.4	6.91	558.8	10.1	384.3	17.95
ACO-12-60	37	0.05816	0.0011	0.0851	0.0009	0.68247	0.0136	0.01619	0.0005	99.6593	535.1	44.7	526.5	5.84	528.3	8.26	324.6	11.14
ACO-12-60	38	0.05883	0.0010	0.1310	0.0014	1.07355	0.0182	0.02603	0.0012	107.225	560.8	38.53	794	8.16	740.5	8.94	519.3	25.34
ACO-12-60	39	0.06453	0.0013	0.0953	0.0011	0.84874	0.0169	0.01792	0.0005	94.0705	759.1	42.63	587	6.55	624	9.33	359	11.7
ACO-12-60	40	0.05077	0.0023	0.0949	0.0014	0.67237	0.0296	0.01666	0.0008	112.048	230.2	101.2	585	8.25	522.1	17.9	334	16.63
ACO-12-60	41	0.05974	0.0025	0.0991	0.0016	0.81645	0.0336	0.02916	0.0018	100.544	594	89.73	609.4	9.73	606.1	18.7	581	36.61
ACO-12-60	42	0.06219	0.0024	0.0822	0.0011	0.70831	0.0271	0.02281	0.0013	93.673	680.6	82.51	509.3	6.84	543.7	16.1	455.8	25.61
ACO-12-60	43	0.10711	0.0015	0.3010	0.0033	4.44282	0.0631	0.08053	0.0034	96.8986	1750.8	25.89	1696.5	16.6	1720.4	11.7	1565.5	65.16
ACO-12-60	44	0.06482	0.0012	0.0968	0.0012	0.86445	0.0168	0.0309	0.0016	94.166	768.4	40.31	595.6	7.17	632.5	9.17	615	32.23
ACO-12-60	45	0.06239	0.0008	0.0895	0.0010	0.7704	0.0111	0.02743	0.0011	95.3621	687.3	29.98	553.1	6	580	6.39	547	21.59
ACO-12-60	46	0.06069	0.0011	0.0918	0.0011	0.76828	0.0148	0.02924	0.0017	97.8576	628.3	41.32	566.4	6.63	578.8	8.5	582.5	34.82
ACO-12-60	47	0.06736	0.0011	0.1073	0.0012	0.99718	0.0167	0.05058	0.0025	93.6076	849	34.46	657.5	7.3	702.4	8.5	997.2	48.49
ACO-12-60	48	0.12546	0.0017	0.2403	0.0023	4.16254	0.0554	0.04018	0.0019	68.2341	2035.2	24.91	1388.7	12.3	1666.7	10.9	796.2	38.06
ACO-12-60	49	0.19922	0.0033	0.4728	0.0057	12.9815	0.2200	0.08716	0.0054	88.5134	2819.8	26.94	2495.9	25.1	2678.3	15.9	1689.2	100.44
ACO-12-60	50	0.07078	0.0017	0.1565	0.0021	1.52743	0.0367	0.0532	0.0047	99.5858	950.9	49.78	937.6	11.7	941.5	14.7	1047.7	90.74
ACO-12-60	51	0.05886	0.0014	0.0942	0.0012	0.76468	0.0178	0.03065	0.0024	100.659	561.9	51.06	580.5	7.21	576.7	10.2	610.2	48.18
ACO-12-60	52	0.16225	0.0028	0.4521	0.0056	10.114	0.1769	0.12539	0.0081	96.999	2479.2	29.12	2404.8	24.8	2445.2	16.1	2387.6	146.74
ACO-12-60	53	0.06012	0.0017	0.0990	0.0013	0.82116	0.0237	0.0312	0.0023	100.049	608	62.94	609	8.12	608.7	13.2	621	46.89
ACO-12-60	54	0.06535	0.0011	0.0941	0.0011	0.84842	0.0148	0.04225	0.0028	92.9945	785.6	36.37	580.1	6.66	623.8	8.18	836.4	54.74
ACO-12-60	55	0.0627	0.0010	0.1120	0.0012	0.97012	0.0156	0.02451	0.0007	99.4336	698.2	34.17	684.6	7.19	688.5	8.05	489.4	14.93
ACO-12-60	56	0.05818	0.0010	0.0945	0.0010	0.75917	0.0139	0.02162	0.0007	101.517	536.1	40.73	582.2	6.26	573.5	8.04	432.3	14.28
ACO-12-60	57	0.05985	0.0010	0.0927	0.0010	0.76658	0.0137	0.01767	0.0005	98.9616	598.3	38.89	571.8	6.15	577.8	7.91	354	10.31
ACO-12-60	58	0.10257	0.0014	0.2895	0.0030	4.11602	0.0548	0.03131	0.0009	98.0911	1671.1	25.12	1639.2	15.1	1657.5	10.8	623.1	18.57
ACO-12-60	59	0.05854	0.0010	0.0995	0.0011	0.80471	0.0142	0.01583	0.0004	102.085	549.9	38.81	612	6.55	599.5	8.04	317.4	9.39
ACO-12-60	60	0.05882	0.0010	0.0938	0.0010	0.76221	0.0137	0.01511	0.0004	100.539	560.6	39.39	578.4	6.25	575.3	7.94	303.1	8.45

ACO-12-60	61	0.05939	0.0009 5	0.0986 9	0.0011 5	0.80879	0.0128 9	0.01943	0.0006 8	100.814	581.5	34.4	606.7	6.47	601.8	7.24	388.9	13.48
ACO-12-60	62	0.0592	0.0008 3	0.0930 1	0.0010 2	0.75991	0.0107	0.01575	0.0004 7	99.878	574.5	30.28	573.3	6	574	6.18	315.8	9.35
ACO-12-60	63	0.07051	0.0012 2	0.1539 5	0.0017 5	1.49808	0.0255 8	0.0232	0.0007	99.29	943.2	35.02	923	9.79	929.6	10.4	463.5	13.74
ACO-12-60	64	0.05863	0.0008 5	0.0956 6	0.0010 5	0.77392	0.0112 3	0.01695	0.0005 8	101.186	553.5	31.31	588.9	6.2	582	6.43	339.7	11.51
ACO-12-60	65	0.05419	0.0016 6	0.1037	0.0013	0.776	0.0232 6	0.00978	0.0004 1	109.053	378.7	67.39	636	7.6	583.2	13.3	196.8	8.13
ACO-12-60	66	0.05984	0.0013 1	0.0923 9	0.0010 8	0.76286	0.0164 4	0.0125	0.0003 9	98.9404	597.9	46.7	569.6	6.4	575.7	9.47	251.1	7.76
ACO-12-60	67	0.06454	0.0014 8	0.1313 4	0.0015 5	1.16981	0.0265 2	0.02564	0.0008 6	101.131	759.5	47.77	795.5	8.8	786.6	12.4 1	511.7	17
ACO-12-60	68	0.05916	0.0007 9	0.1	0.0011	0.8159	0.0111 1	0.024	0.0007 3	101.42	573	28.94	614.4	6.42	605.8	6.21	479.5	14.42
ACO-12-60	69	0.05962	0.0008 5	0.0979	0.0010 9	0.80493	0.0116 1	0.02306	0.0007 5	100.417	589.8	30.49	602.1	6.42	599.6	6.53	460.8	14.88
ACO-12-60	70	0.06109	0.0016 3	0.0937 9	0.0011 2	0.79046	0.0206 3	0.0179	0.0006	97.7173	642.4	56.42	577.9	6.61	591.4	11.7	358.7	11.88
ACO-12-60	71	0.06611	0.0012 1	0.1254 9	0.0014 8	1.14386	0.0209 3	0.03539	0.0015	98.4244	809.7	37.91	762.1	8.5	774.3	9.91	702.9	29.19
ACO-12-60	72	0.06292	0.0010 9	0.0968 5	0.0011 3	0.84032	0.0146 1	0.02498	0.0010 1	96.2215	705.6	36.43	595.9	6.64	619.3	8.06	498.7	19.9
ACO-12-60	73	0.06024	0.0008 2	0.0979 2	0.0010 7	0.81358	0.0111 9	0.02282	0.0008 5	99.6195	612	29.16	602.2	6.27	604.5	6.26	456.1	16.87
ACO-12-60	74	0.17698	0.0025 8	0.4919 5	0.0058 9	12.0048	0.1825 3	0.1297	0.0067 3	98.2589	2624.8	24.01	2579.1	25.4 5	2604.8	14.2 5	2464.8	120.37
ACO-12-60	75	0.12411	0.0029 7	0.3244 7	0.0039 3	5.56878	0.1282 2	0.12333	0.0140 8	89.8517	2016.1	41.84	1811.5	19.1 1	1911.3	19.8 2	2350.7	253.37
ACO-12-60	76	0.05979	0.0010 1	0.0925 7	0.0010 7	0.76326	0.0128 9	0.02705	0.0014	99.0971	596.1	36.03	570.7	6.33	575.9	7.42	539.5	27.53
ACO-12-60	77	0.06003	0.0010 6	0.0955 3	0.0010 8	0.79093	0.0139 2	0.02691	0.0013 5	99.4085	604.7	37.89	588.2	6.35	591.7	7.89	536.7	26.52
ACO-12-60	78	0.07347	0.0012 4	0.1659 9	0.0019	1.68146	0.0284 3	0.04715	0.0025	98.8517	1027	33.89	990	10.5 3	1001.5	10.7 7	931.3	48.28
ACO-12-60	79	0.06295	0.0020 8	0.1147	0.0015 9	0.99601	0.0317 7	0.03738	0.0063 4	99.7435	706.7	68.64	700	9.18	701.8	16.1 6	741.8	123.48
ACO-12-60	80	0.06016	0.0011 7	0.0998 3	0.0011 6	0.82803	0.0159 4	0.03017	0.0019 4	100.147	609.4	41.48	613.4	6.79	612.5	8.85	600.8	38.05

			6	7			4		3								
14-01-28	28	0.08845	0.0013 1	0.2327 2	0.0026 3	2.83786	0.0419 9	0.05747	0.0013 6	96.8754	1392.2	28.09	1348.7	13.7 6	1365.6	11.1 1	1129.4	26.04
14-01-29	29	0.05784	0.0018 1	0.0640 4	0.0009 4	0.51067	0.0154 2	0.01522	0.0005 5	95.5359	523.3	67.41	400.2	5.71	418.9	10.3 6	305.4	11.03
14-01-30	30	0.18251	0.0028 2	0.4774 4	0.0056 7	12.0138	0.1880 5	0.11121	0.0030 8	94.0317	2675.8	25.36	2516.1	24.7 6	2605.5	14.6 7	2131.4	56.05
14-01-31	31	0.07461	0.0015 1	0.0769 6	0.0009 6	0.79165	0.0156 1	0.02738	0.0008 4	80.7296	1057.7	40.49	478	5.76	592.1	8.85	546	16.53
14-01-32	32	0.05938	0.0023 1	0.0924 7	0.0015	0.75699	0.0283 6	0.02653	0.0009 6	99.6156	580.9	82.44	570.1	8.83	572.3	16.3 9	529.2	19
14-01-33	33	0.0975	0.0015 9	0.1946 5	0.0023	2.61663	0.0426 3	0.07792	0.0024 3	72.7106	1576.8	30.23	1146.5	12.4	1305.3	11.9 7	1516.5	45.51
14-01-34	34	0.18447	0.0037 6	0.4713 8	0.0061 5	11.9878	0.2421 5	0.11283	0.0063 5	92.4299	2693.5	33.25	2489.6	26.9 6	2603.5	18.9 3	2160.9	115.37
14-01-35	35	0.10277	0.0023 5	0.2453 9	0.0033 6	3.47647	0.0781 9	0.0666	0.0033 1	84.4689	1674.7	41.63	1414.6	17.4 1	1521.9	17.7 4	1303.2	62.65
14-01-36	36	0.11925	0.0024	0.3372 1	0.0043 9	5.54422	0.1106 3	0.0925	0.0039 8	96.3136	1945	35.58	1873.3	21.1 8	1907.5	17.1 6	1788.2	73.6
14-01-37	37	0.06126	0.0019 3	0.0928 5	0.0014 2	0.78428	0.0239	0.02847	0.0013 5	97.3635	648.5	66.31	572.4	8.37	587.9	13.6	567.3	26.56
14-01-38	38	0.09501	0.0017 7	0.2635 1	0.0032 3	3.45182	0.0630 3	0.07743	0.0027 3	98.6586	1528.3	34.6	1507.8	16.4 7	1516.3	14.3 8	1507.4	51.14
14-01-39	39	0.08831	0.0019 6	0.0868	0.0011 3	1.05679	0.0226 6	0.03785	0.0014 2	73.286	1389.2	41.94	536.6	6.73	732.2	11.1 9	750.9	27.68
14-01-40	40	0.05755	0.0029 6	0.0675 7	0.0013 9	0.53611	0.0262 5	0.02093	0.0021 5	96.6965	512.5	109.3 8	421.5	8.42	435.9	17.3 5	418.7	41.65
14-01-41	41	0.18453	0.0037 9	0.4551	0.0065 9	11.5779	0.2339 8	0.13238	0.0043 9	89.7513	2694	33.52	2417.9	29.1 8	2570.9	18.8 9	2512.8	78.28
14-01-42	42	0.06379	0.0012 4	0.0933 8	0.0011 5	0.82131	0.0157	0.02839	0.0006	94.5302	734.8	40.67	575.5	6.76	608.8	8.75	565.9	11.87
14-01-43	43	0.12153	0.0025 9	0.3435 8	0.0048 6	5.75683	0.1207 7	0.09501	0.0034 3	96.2149	1978.8	37.48	1903.9	23.3 3	1939.9	18.1 5	1834.5	63.32
14-01-44	44	0.12681	0.0018 7	0.3662 5	0.0041 8	6.40266	0.0938 7	0.10374	0.0023 9	97.9311	2054.2	25.86	2011.7	19.7	2032.6	12.8 8	1995	43.85
14-01-45	45	0.18901	0.0038 7	0.5044 2	0.0068 7	13.1436	0.2672 9	0.13329	0.0052 2	96.3161	2733.5	33.31	2632.8	29.4 4	2690	19.1 9	2529.1	93.05
14-01-46	46	0.06224	0.0013 1	0.1068 2	0.0013 8	0.91662	0.0190 3	0.03314	0.0008 9	99.0463	682.3	44.29	654.3	8.05	660.6	10.0 8	659	17.43
14-01-47	47	0.12717	0.0016 7	0.3715 2	0.0041 7	6.51383	0.0874 8	0.12882	0.0027 9	98.9025	2059.2	22.99	2036.6	19.5 8	2047.8	11.8 2	2449.1	49.98
14-01-48	48	0.1087	0.0015 4	0.1237 2	0.0014 3	1.85413	0.0267 5	0.05733	0.0013 2	70.6076	1777.7	25.72	751.9	8.2	1064.9	9.51	1126.7	25.28
14-01-49	49	0.05535	0.0009 2	0.0646 9	0.0007 5	0.49361	0.0081 2	0.0194	0.0004 7	99.19	426	36.02	404.1	4.51	407.4	5.52	388.4	9.27
14-01-50	50	0.12775	0.0024 4	0.2890 6	0.0038 5	5.09113	0.0963 8	0.1027	0.0030 4	79.1757	2067.3	33.32	1636.8	19.2 5	1834.6	16.0 7	1976	55.8
14-01-51	51	0.18562	0.0028 7	0.5002 9	0.0059 5	12.8028	0.2011 7	0.11404	0.0032 2	96.7193	2703.7	25.28	2615	25.5 7	2665.2	14.8	2182.7	58.34
14-01-52	52	0.07526	0.0017	0.1717 2	0.0022 5	1.78143	0.0392 2	0.0498	0.0019 5	94.9972	1075.4	44.65	1021.6	12.3 5	1038.7	14.3 2	982.3	37.55
14-01-53	53	0.06457	0.0011 4	0.1070 7	0.0012 9	0.95322	0.0168	0.03596	0.0013 5	96.4548	760.4	36.9	655.7	7.52	679.8	8.74	714	26.27
14-01-54	54	0.06118	0.0012	0.1038	0.0012 7	0.87548	0.0168 8	0.03222	0.0010 1	99.7181	645.5	41.56	636.7	7.41	638.5	9.14	641	19.68

14-01-55	55		0.09133	0.0027	0.2551	0.0040	9	3.21311	0.0929	5	0.06901	0.0034	3	100.798	1453.4	55.71	1465	21.0	3	1460.3	22.4	1348.8	64.95
				2	5	9			5			3											
14-01-56	56		0.09304	0.0021	0.0726		0.93181	0.0209	4	0.05125	0.0019	4	67.6189	1488.8	42.91	452.1	6.01		668.6	11.0	1010.2	37.33
				4	4	0.001														1		
14-01-57	57		0.06042	0.0011	0.0914	0.0011	0.76166	0.0144	3	0.03	0.0009	3	98.087	618.6	40.77	564	6.62		575	8.32	597.5	17.63
				6	4	2																
14-01-58	58		0.06407	0.0012	0.1069	0.0013	0.94497	0.0182	6	0.04159	0.0019	2	96.9948	744	40.56	655.2	7.79		675.5	9.54	823.5	37.33
				5	8	4																
14-01-59	59		0.05947	0.0022	0.0741	0.0012	0.60785	0.0219	2	0.02984	0.0017	6	95.6242	584.3	79.47	461.1	7.32		482.2	13.8	594.3	34.56
				3	5	2														4		
14-01-60	60		0.0839	0.0033	0.0662	0.0012	0.76626	0.0290	8	0.03247	0.0017	6	71.572	1290.1	75.76	413.4	7.47		577.6	16.7	646	34.52
				4	3	4														2		
14-01-61	61		0.0693	0.0012	0.0917	0.0011	0.87637	0.0152	8	0.02968	0.0006	4	88.5446	907.7	36.03	565.8	6.47		639	8.27	591.3	12.66
				3	3	1																
14-01-62	62		0.05622	0.0012	0.0636	0.0008	0.49306	0.0108	6	0.01809	0.0007	1	97.6904	460.4	48.38	397.6	5.29		407	7.39	362.4	14.01
				4	1	7																
14-01-63	63		0.05858	0.0014	0.0813	0.0010	0.65707	0.0154	5	0.0274	0.0006	8	98.3229	551.6	51.73	504.2	6.42		512.8	9.47	546.3	13.32
				1	6	8																
14-01-64	64		0.06957	0.0011	0.0870	0.001	0.83494	0.0134	3	0.04047	0.0010	3	87.2972	915.6	33.2	538.1	5.92		616.4	7.41	801.8	20.1
				3	6																	
14-01-65	65		0.09581	0.0013		0.0020	2.40402	0.0348	4	0.06315	0.0015	5	69.8077	1544.1	26.86	1077.9	11.3		1243.8	10.3	1237.8	29.42
				8	0.182	9											9			9		
14-01-66	66		0.12957	0.0021	0.2993	0.0037	5.34641	0.0905	5	0.05197	0.0015		80.6845	2092.1	29.05	1688	18.5		1876.3	14.4	1024	28.9
				6	4	4											7			9		
14-01-67	67		0.06072	0.0009	0.0834	0.0010	0.71547	0.0109	5	0.02691	0.0006	6	96.4781	629.4	32.02	528.7	5.98		548	6.48	536.7	12.99
				1	7	1																
14-01-68	68		0.09134	0.0014	0.1223	0.0014	1.54069	0.0246	3	0.04347	0.0013	5	78.5805	1453.6	30.36	744	8.27		946.8	9.84	860.1	26.22
				7	4	4																
14-01-69	69		0.06016	0.0011	0.0806	0.0009	0.66929	0.0124	8	0.025	0.0007	5	96.1561	609.2	41.05	500.3	5.67		520.3	7.59	499.2	14.85
				6	9	5																
14-01-70	70		0.05929	0.0012	0.0846	0.0010	0.69222	0.0138	1	0.02653	0.0007	7	98.109	577.7	44.15	524	6.08		534.1	8.29	529.2	15.22
				2	9	2																
14-01-71	71		0.12883	0.0023	0.3703	0.0046	6.57788	0.1161	9	0.10527	0.0032	6	97.5505	2082.1	31.07	2031.1	21.8		2056.4	15.5	2023.1	59.54
				6	6	4											1			7		
14-01-72	72		0.07086	0.0018	0.0594	0.0008	0.58095	0.0148	7	0.02584	0.0008	1	80.0688	953.4	53.69	372.4	5.04		465.1	9.55	515.6	15.92
				9	7	3																
14-01-73	73		0.11696	0.0031	0.3262	0.0049	5.25876	0.1369	2	0.09473	0.0049	2	95.2835	1910.3	47.65	1820.2	23.8		1862.2	22.2	1829.3	90.79
				5	5	1											8			1		
14-01-74	74		0.06284	0.0025	0.0992	0.0018	0.85907	0.0338	2	0.03028	0.0018	8	96.871	702.8	85.22	609.9	10.5		629.6	18.4	602.9	36.82
				9	3	1											9			7		
14-01-75	75		0.09849	0.0016	0.2733	0.0032	3.71117	0.0608	1	0.07822	0.0022	6	97.6062	1595.8	30.78	1557.6	16.2		1573.8	13.1	1522.2	42.33
				4	1	1											7			1		
14-01-76	76		0.17645	0.0036	0.4507	0.0059	10.9626	0.2211	6	0.12719	0.0049	8	91.549	2619.8	33.95	2398.4	26.4		2520	18.7	2420	89.32
				4	1	5											6			7		
14-01-77	77		0.05883	0.0013	0.0625	0.0008	0.50716	0.0115	5	0.019	0.0007	2	93.8776	560.9	50.29	391	4.99		416.5	7.78	380.3	14.31
				8	3	2																
14-01-78	78		0.0962	0.0017	0.0999	0.0012	1.32562	0.0238	5	0.08626	0.0027	4	71.6569	1551.7	34.45	614.1	7.1		857	10.4	1672.4	51.03
				9	5	1														1		
14-01-79	79		0.10908	0.0021	0.2563	0.0031	3.85496	0.0739	6	0.08546	0.0031	3	82.4505	1784.1	36.02	1471	16.0		1604.3	15.4	1657.4	58.23
				8	2	2											2			7		
14-01-80	80		0.15994	0.0067	0.3972	0.0073	8.75833	0.3503	4	0.09454	0.0087	1	87.8371	2455	69.81	2156.4	33.8		2313.2	36.4	1825.9	160.85
				7	6	3											4			5		
ACO-14-02		1	0.0612	0.0011	0.0850	0.0010		0.0136			0.0004											
				9	7	2	0.71769	7	0.02559		3		95.8129	646.1	41.27	526.3	6.07		549.3	8.08	510.7	8.47

ACO-14-02	2	0.05976	0.0009 1	0.0842 4	0.0009 6	0.69406	0.0105 5	0.02475	0.0003 7	97.4215	594.6	32.94	521.4	5.68	535.2	6.33	494.2	7.3	
ACO-14-02	3	0.1263	0.0023 1	0.3192 3	0.0043	5.55894	0.1010 8	0.09168	0.0024 1	87.2454	2047.1	31.95	1786	21.0 3	1909.8	15.6 5	1772.9	44.56	
ACO-14-02	4	0.06164	0.0008 3	0.1031 3	0.0011 5	0.87632	0.0120 2	0.03263	0.0004 7	99.0141	661.5	28.71	632.7	6.72	639	6.5	648.9	9.14	
ACO-14-02	5	0.06105	0.0011 9	0.0873 3	0.0010 9	0.73492	0.0141 6	0.02523	0.0004 7	96.4784	640.9	41.3	539.7	6.45	559.4	8.29	503.6	9.26	
ACO-14-02	6	0.06816	0.0020 5	0.0979 3	0.0015 2	0.92018	0.0268 4	0.03202	0.0010 4	90.9132	873.3	61.12	602.3	8.95	662.5	14.1 9	637.1	20.28	
ACO-14-02	7	0.06107	0.0011 9	0.0965	0.0011 8	0.8125	0.0155 7	0.02952	0.0005 3	98.3275	641.8	41.32	593.8	6.91	603.9	8.72	587.9	10.44	
ACO-14-02	8	0.06267	0.001	0.1096 9	0.0013	0.94776	0.0152 1	0.03203	0.0005 4	99.1284	697.2	33.52	671	7.54	676.9	7.93	637.3	10.59	
ACO-14-02	9	0.05841	0.0007 7	0.0860 3	0.0009 6	0.69286	0.0093 6	0.02626	0.0003 9	99.5323	545.3	28.54	532	5.72	534.5	5.62	523.8	7.73	
ACO-14-02	10	0.123	0.0025 3	0.3568 5	0.0051 5	6.04735	0.1249 5	0.0873	0.0027 1	98.3502	2000.2	36.04	1967.2	24.4 5	1982.7	18	1691.7	50.37	
ACO-14-02	11	0.06212	0.0010 5	0.0988 7	0.0011 7	0.84616	0.0142 6	0.03102	0.0005 2	97.5743	678.3	35.65	607.4	6.88	622.5	7.84	617.5	10.15	
ACO-14-02	12	0.05965	0.0011 1	0.0868 3	0.0010 4	0.7139	0.0130 8	0.02685	0.0005 5	98.1173	590.8	39.74	536.8	6.17	547.1	7.75	535.5	10.78	
ACO-14-02	13	0.06134	0.0013 8	0.0925 7	0.0012 2	0.78281	0.0173 5	0.02832	0.0006	97.2066	651.3	47.68	570.7	7.17	587.1	9.88	564.5	11.88	
ACO-14-02	14	0.09938	0.0014 4	0.0902 8	0.0010 6	1.23692	0.0181 4	0.04072	0.0006 3	68.159	1612.5	26.84	557.2	6.29	817.5	8.24	806.7	12.3	
ACO-14-02	15	0.05801	0.0010 9	0.0906 6	0.0011	0.72487	0.0135 5	0.02666	0.0005	101.084	529.6	41.12	559.5	6.52	553.5	7.98	531.9	9.76	
ACO-14-02	16	0.23638	0.0031 2	0.1082 1	0.0012 9	3.5264	0.0471 5	0.13112	0.0019 6	43.1972	3095.8	20.91	662.3	7.51	1533.2	10.5 8	2490.3	35.01	
ACO-14-02	17	0.06004	0.0010 5	0.0876	0.0010 8	0.72501	0.0128 6	0.02701	0.0005 3	97.7782	605	37.56	541.3	6.4	553.6	7.57	538.6	10.47	
ACO-14-02	18	0.05983	0.0009 6	0.0992 9	0.0011 8	0.81889	0.0133 2	0.02957	0.0004 9	100.461	597.3	34.41	610.2	6.91	607.4	7.43	589.1	9.55	
ACO-14-02	19	0.06109	0.0008 1	0.0947 9	0.0010 9	0.79755	0.0110 3	0.02746	0.0004 9	97.9678	642.3	28.26	583.3	6.42	595.4	6.23	547.6	7.77	
ACO-14-02	20	0.05935	0.0011 2	0.0870 1	0.0010 9	0.71199	0.0134 9	0.02776	0.0005 2	98.5345	580.1	40.6	537.9	6.45	545.9	8	553.4	10.3	
ACO-14-02	21	0.05982	0.0009 9	0.0888 7	0.0011 7	0.73297	0.0124 5	0.02706	0.0004 6	98.3163	597	35.4	548.9	6.53	558.3	7.3	539.8	9.15	
ACO-14-02	22	0.13041	0.0031 5	0.3475 4	0.0055 1	6.24892	0.1467 5	0.08931	0.0032 4	91.4096	2103.5	41.85	1922.8	26.3 5	2011.3	20.5 6	1729.1	60.03	
ACO-14-02	23	0.059	0.0012 3	0.0934 2	0.0012 1	0.75985	0.0158 3	0.02805	0.0005 6	100.314	567	44.79	575.7	7.15	573.9	9.13	559.2	11.1	
ACO-14-02	24	0.05808	0.0009 1	0.0931 6	0.0011 4	0.74598	0.0121 4	0.02847	0.0005 1	101.467	532.3	34.58	574.2	6.7	565.9	7.06	567.5	10.02	
ACO-14-02	25	0.12697	0.0026 8	0.3748 4	0.0054 6	6.5629	0.1382 5	0.10241	0.0029	99.7909	2056.4	36.79	2052.1	25.5 8	2054.4	18.5 6	1970.7	53.1	
ACO-14-02	26	0.05861	0.0011 3	0.0957 6	0.0012 4	0.77367	0.0151 4	0.02806	0.0006 3	101.306	552.6	41.59	589.5	7.3	581.9	8.67	559.4	12.42	
ACO-14-02	27	0.05799	0.0009 3	0.0890 6	0.0011	0.71207	0.0117 5	0.02579	0.0004 4	100.733	529	34.96	550	6.51	546	6.97	514.7	8.59	
ACO-14-02	28	0.13184	0.0017 1	0.3856 3	0.0045 8	7.00956	0.0970 7	0.08382	0.0014 5	99.053	2122.6	22.52	2102.5	21.3 2	2112.6	12.3 1	1627	27.05	
ACO-14-	29	0.125	0.0021	0.3729	0.0048	6.42766	0.1155	0.10455	0.0033	100.705	2028.8	30.56	2043.1	22.9	2036.1	15.7	2009.9	61.88	

ACO-14-02	57	0.12763	0.00368	0.38958	0.00623	6.85833	0.18955	0.10152	0.00546	102.677	2065.6	49.94	2120.9	28.88	2093.3	24.49	1954.4	100.2
ACO-14-02	58	0.05951	0.00115	0.09513	0.00123	0.78049	0.01515	0.02747	0.00067	100	585.7	41.29	585.8	7.23	585.8	8.64	547.8	13.09
ACO-14-02	59	0.12701	0.00248	0.3887	0.00543	6.80659	0.13253	0.10227	0.00331	102.912	2056.9	34.01	2116.8	25.21	2086.6	17.24	1968	60.69
ACO-14-02	60	0.13065	0.00346	0.41467	0.00674	7.4698	0.1906	0.11363	0.00505	106.147	2106.7	45.78	2236.2	30.69	2169.4	22.85	2175.4	91.58
ACO-14-02	61	0.0584	0.00149	0.09385	0.0013	0.75544	0.01898	0.03015	0.00071	101.19	544.7	54.83	578.2	7.68	571.4	10.98	600.3	13.85
ACO-14-02	62	0.16328	0.00186	0.47611	0.00553	10.7165	0.1338	0.13103	0.00219	100.819	2489.9	19.09	2510.3	24.14	2498.9	11.6	2488.7	39.19
ACO-14-02	63	0.16253	0.00225	0.47434	0.0056	10.628	0.1513	0.12488	0.0027	100.826	2482.1	23.15	2502.6	24.49	2491.2	13.21	2378.5	48.5
ACO-14-02	64	0.07611	0.0023	0.10707	0.00169	1.12329	0.03277	0.03197	0.00104	85.7685	1098	59.31	655.7	9.83	764.5	15.67	636.1	20.31
ACO-14-02	65	0.05918	0.00116	0.08815	0.00115	0.71914	0.01424	0.02714	0.00063	98.9822	573.8	42.17	544.6	6.79	550.2	8.41	541.3	12.31
ACO-14-02	66	0.05811	0.00087	0.08665	0.00105	0.6941	0.01081	0.02734	0.00048	100.075	533.3	32.96	535.7	6.22	535.3	6.48	545.2	9.43
ACO-14-02	67	0.06125	0.00134	0.08872	0.00118	0.74914	0.0163	0.02763	0.00056	96.5299	648.1	46.43	548	6.96	567.7	9.46	550.8	10.92
ACO-14-02	68	0.0587	0.00112	0.08736	0.00114	0.70695	0.01367	0.02746	0.00059	99.4474	556.1	41.1	539.9	6.73	542.9	8.13	547.6	11.66
ACO-14-02	69	0.05904	0.00098	0.08698	0.00107	0.70789	0.012	0.02649	0.00051	98.9144	568.5	35.68	537.6	6.36	543.5	7.13	528.5	10.07
ACO-14-02	70	0.13906	0.00871	0.3244	0.00861	6.22237	0.37059	0.11672	0.01615	81.7513	2215.5	104.78	1811.2	41.89	2007.6	52.1	2231.3	292.32
ACO-14-02	71	0.06131	0.00097	0.09861	0.0012	0.8334	0.0136	0.03012	0.00059	98.489	650	33.78	606.2	7.06	615.5	7.53	599.7	11.62
ACO-14-02	72	0.05826	0.00097	0.08846	0.00109	0.7105	0.01213	0.02623	0.00052	100.257	538.9	36.74	546.4	6.44	545	7.18	523.3	10.3
ACO-14-02	73	0.05837	0.00102	0.08625	0.00107	0.69404	0.01227	0.0257	0.00052	99.645	543.7	37.69	533.3	6.35	535.2	7.36	512.9	10.22
ACO-14-02	74	0.05756	0.00091	0.08648	0.00105	0.68629	0.01106	0.02612	0.00054	100.773	512.7	34.53	534.7	6.21	530.6	6.66	521.1	10.55
ACO-14-02	75	0.05873	0.00111	0.09154	0.00115	0.74114	0.01399	0.02795	0.0007	100.266	557	40.65	564.6	6.79	563.1	8.16	557.2	13.81
ACO-14-02	76	0.12521	0.00238	0.27282	0.0036	4.70958	0.08962	0.08272	0.0029	76.538	2031.8	33.21	1555.1	18.24	1768.9	15.94	1606.3	54.11
ACO-14-02	77	0.06092	0.00101	0.08896	0.00109	0.74709	0.01262	0.02634	0.00059	96.9815	636.3	35.43	549.4	6.45	566.5	7.33	525.5	11.57
ACO-14-02	78	0.06168	0.00146	0.08741	0.00118	0.74332	0.01725	0.0288	0.00076	95.7292	663.1	49.88	540.2	7	564.3	10.05	573.9	14.83
ACO-14-02	79	0.06096	0.00089	0.08445	0.00101	0.70983	0.01066	0.02603	0.00062	95.9603	637.9	30.95	522.6	5.99	544.6	6.33	519.4	12.18
ACO-14-02	80	0.05786	0.00122	0.08481	0.00109	0.67655	0.01407	0.02518	0.00067	100.019	524.1	45.78	524.8	6.49	524.7	8.52	502.6	13.21
ACO-12-57	1	0.09855	0.00604	0.12267	0.0034	1.6667	0.09515	0.11008	0.00855	74.8971	1596.9	110.3	745.9	19.5	995.9	36.23	2110.8	155.75
ACO-12-57	2	0.06035	0.00077	0.10356	0.00113	0.86178	0.01107	0.01956	0.00054	100.65	616.3	27.2	635.2	6.58	631.1	6.04	391.5	10.72
ACO-12-57	3	0.06049	0.00109	0.10122	0.00123	0.84419	0.0151	0.02029	0.00052	100.016	621.2	38.36	621.6	7.22	621.5	8.31	406	10.25

ACO-12-57	4	0.06344	0.0007 4	0.1492 9	0.0016 9	1.30574	0.0160 3	0.02084	0.0003 6	105.741	723	24.7	897	9.45	848.3	7.06	417	7.07
ACO-12-57	5	0.20746	0.0024 9	0.5597 1	0.0064	16.0087	0.2007 3	0.11004	0.0026 8	99.2931	2885.8	19.36	2865.4	26.4 4	2877.3	11.9 8	2110.1	48.87
ACO-12-57	6	0.06104	0.0008 6	0.1125 6	0.0013 5	0.94709	0.0139 6	0.02052	0.0005 8	101.626	640.5	30.14	687.6	7.81	676.6	7.28	410.6	11.52
ACO-12-57	7	0.0602	0.0010 4	0.1308 9	0.0015 3	1.08642	0.0185 2	0.03322	0.0010 6	106.173	610.7	36.9	792.9	8.73	746.8	9.01	660.5	20.67
ACO-12-57	8	0.05695	0.0011 5	0.0904 8	0.0011 1	0.71046	0.0140 7	0.02213	0.0006 7	102.459	489	44.17	558.4	6.54	545	8.35	442.4	13.31
ACO-12-57	9	0.11941	0.0015 8	0.3644 3	0.0043 4	5.99944	0.0828 4	0.06332	0.0017 3	102.855	1947.5	23.44	2003.1	20.5	1975.8	12.0 2	1241	32.92
ACO-12-57	10	0.06385	0.0009 4	0.1365 3	0.0015 9	1.2019	0.0180 1	0.02848	0.0007 3	102.932	736.7	30.95	825	9.04	801.5	8.31	567.6	14.31
ACO-12-57	11	0.1184	0.0013 1	0.4053 2	0.0045 5	6.61668	0.0766 2	0.04273	0.0007 6	113.523	1932.2	19.61	2193.5	20.8 9	2061.6	10.2 1	845.7	14.73
ACO-12-57	12	0.05712	0.0008 8	0.0826 3	0.001	0.65077	0.0102 4	0.0103	0.0002 5	100.55	495.5	33.89	511.8	5.96	509	6.3	207.1	5.01
ACO-12-57	13	0.05636	0.0007 3	0.0775 9	0.0009 2	0.60303	0.0081 2	0.00679	0.0001 5	100.522	465.7	28.82	481.7	5.49	479.2	5.14	136.8	3.06
ACO-12-57	14	0.10735	0.0012 6	0.2544 3	0.0028 8	3.76592	0.0459 9	0.03154	0.0006 7	83.2744	1754.8	21.19	1461.3	14.8	1585.5	9.8	627.6	13.04
ACO-12-57	15	0.05864	0.0012 2	0.094	0.0012 3	0.75999	0.0156 9	0.01561	0.0007 4	100.889	553.8	44.75	579.1	7.27	574	9.05	313	14.76
ACO-12-57	16	0.0622	0.0009 8	0.1085 7	0.0012 9	0.93108	0.0147 2	0.01958	0.0005 2	99.4313	680.9	33.21	664.4	7.48	668.2	7.74	392	10.24
ACO-12-57	17	0.05796	0.0010 1	0.1234 4	0.0014 5	0.98648	0.0169 7	0.03043	0.0013 7	107.677	527.9	38.02	750.4	8.32	696.9	8.67	605.8	26.8
ACO-12-57	18	0.07363	0.0014 4	0.2099 1	0.0026 1	2.13111	0.0406 7	0.06428	0.003	119.1	1031.4	38.92	1228.4	13.8 9	1158.9	13.1 9	1259.3	57.06
ACO-12-57	19	0.06084	0.0009 2	0.1127 5	0.0013 5	0.94577	0.0144 6	0.02699	0.0010 4	101.894	633.6	32.38	688.7	7.55	675.9	7.54	538.2	20.42
ACO-12-57	20	0.05896	0.0009 2	0.1151 4	0.0013 5	0.93588	0.0147 8	0.02627	0.0009 2	104.741	565.4	33.74	702.5	7.81	670.7	7.75	524.2	18.17
ACO-12-57	21	0.06009	0.0010 7	0.1162 5	0.0013 7	0.96301	0.0168 8	0.02774	0.0008 6	103.504	606.9	38.12	708.9	7.88	684.9	8.73	553.1	16.97
ACO-12-57	22	0.06152	0.0007 9	0.1039 6	0.0011 7	0.88164	0.0116 9	0.02093	0.0004 7	99.3301	657.3	27.3	637.6	6.85	641.9	6.31	418.6	9.27
ACO-12-57	23	0.06277	0.0010 8	0.1156 2	0.0013 4	1.00046	0.0168 4	0.02784	0.0009 7	100.185	700.5	36.12	705.3	7.71	704	8.55	555.1	19.02
ACO-12-57	24	0.05863	0.0008 9	0.1059 7	0.0012 3	0.85652	0.0131 6	0.02379	0.0006 2	103.359	553.4	32.78	649.3	7.19	628.2	7.2	475.3	12.24
ACO-12-57	25	0.1261	0.0015 3	0.3770 7	0.0042 8	6.55521	0.0830 7	0.07259	0.0016 7	100.895	2044.3	21.31	2062.6	20.0 2	2053.3	11.1 6	1416.4	31.46
ACO-12-57	26	0.07194	0.0010 3	0.1877 6	0.0021 6	1.86211	0.0265 6	0.03989	0.0012 9	112.712	984.1	28.75	1109.2	11.4 1	1067.7	9.42	790.6	25
ACO-12-57	27	0.06862	0.0011 3	0.1640 5	0.0019 3	1.5521	0.0254 8	0.03712	0.0011 9	102.943	887.5	33.78	979.3	10.7	951.3	10.1 4	736.7	23.23
ACO-12-57	28	0.06034	0.0007 8	0.0790 1	0.0009 1	0.65718	0.0086 9	0.00682	0.0001 3	95.5742	615.8	27.55	490.2	5.46	512.9	5.32	137.3	2.57
ACO-12-57	29	0.0593	0.0008 8	0.1083 7	0.0012 7	0.88609	0.0134 3	0.01936	0.0004 7	102.949	578.2	32.07	663.3	7.38	644.3	7.23	387.5	9.22
ACO-12-57	30	0.06128	0.0009	0.1090 8	0.0012 6	0.92152	0.0137 8	0.02367	0.0006 4	100.633	649	31.34	667.4	7.32	663.2	7.28	472.8	12.67
ACO-12-57	31	0.06588	0.0009	0.1415	0.0016	1.28565	0.0182	0.0274	0.0007	101.68	802.4	28.71	853.5	9.2	839.4	8.1	546.4	15.22

57			1	7	3		3		7									
ACO-12-57		32	0.0007 9	0.1195 6	0.0013 5	1.02548	0.0135 3	0.02383	0.0006 4	101.577	681.5	26.91	728	7.78	716.7	6.78	475.9	12.65
ACO-12-57		33	0.0010 4	0.1856 5	0.0022	1.82314	0.0274 3	0.03422	0.0010 8	113.868	964.1	29.65	1097.8	11.9 8	1053.8	9.87	680.1	21.17
ACO-12-57		34	0.0007 4	0.0994 7	0.0011 3	0.81349	0.0105 1	0.01124	0.0002 5	101.142	578.9	26.95	611.3	6.61	604.4	5.89	225.9	5.04
ACO-12-57		35	0.0010 2	0.1845	0.0021 2	1.87338	0.0266 6	0.03805	0.0011 6	105.776	1031.9	27.87	1091.5	11.5 2	1071.7	9.42	754.7	22.54
ACO-12-57		36	0.0008 2	0.1082 3	0.0012 4	0.8963	0.0125 2	0.01999	0.0005 9	101.955	606.2	29.1	662.4	7.2	649.7	6.7	400	11.65
ACO-12-57		37	0.0009 3	0.1568 5	0.0018 5	1.49323	0.0204	0.01689	0.0004	101.251	900.5	27.43	939.2	10.0 5	927.6	8.31	338.6	7.93
ACO-12-57		38	0.0011 6	0.1888 3	0.0022 2	1.91318	0.0303 8	0.03798	0.0012 9	108.516	1027.5	31.27	1115	12.0 6	1085.7	10.5 9	753.5	25.16
ACO-12-57		39	0.0014 3	0.3082 8	0.0035 5	4.59002	0.0620 6	0.03589	0.0009 1	98.0916	1765.9	24.02	1732.2	17.5 2	1747.5	11.2 7	712.7	17.67
ACO-12-57		40	0.0009 3	0.0936	0.0011 1	0.76173	0.0120 6	0.01213	0.0003 2	100.313	568.2	34.07	576.8	6.52	575	6.95	243.8	6.33
ACO-12-57		41	0.0009 2	0.1828 2	0.0021 3	1.77562	0.0241 4	0.03241	0.0006 9	114.965	941.5	26.44	1082.4	11.6 1	1036.6	8.83	644.7	13.42
ACO-12-57		42	0.4821 9	0.0056 1	11.198	0.1420 4	0.08199	0.0019 5	99.7797	2542.4	19.73	2536.8	24.4 1	2539.7	11.8 2	1592.7	36.39	
ACO-12-57		43	0.16846	0.002	0.0020 2	0.0055 1	11.9489	0.1445 1	0.09256	0.0021	99.2411	2609.1	19.04	2589.3	23.7 9	2600.4	11.3 3	1789.2	38.77
ACO-12-57		44	0.17532	0.05954	0.0013 1	0.0927 4	0.0011 6	0.76139	0.0162 7	0.01617	0.0005 8	99.4607	586.7	47.1	571.7	6.83	574.8	9.38	324.3	11.47
ACO-12-57		45	0.07132	0.001	0.1778 6	0.0020 3	1.74885	0.0247 9	0.03708	0.001	109.188	966.5	28.27	1055.3	11.1 2	1026.7	9.16	736	19.46
ACO-12-57		46	0.16927	0.0019 7	0.5042 9	0.0057 2	11.7695	0.1446 4	0.08677	0.0019 4	103.203	2550.5	19.4	2632.2	24.5 3	2586.2	11.5	1681.9	36	
ACO-12-57		47	0.05826	0.0009 2	0.0976 8	0.0011 6	0.78463	0.0124 4	0.01533	0.0003 4	102.159	538.8	34.74	600.8	6.81	588.1	7.08	307.6	6.73	
ACO-12-57		48	0.10972	0.0013 2	0.3410 2	0.0038 1	5.15875	0.0645 6	0.06134	0.0016 6	105.399	1794.7	21.77	1891.6	18.3 3	1845.8	10.6 4	1203.2	31.57	
ACO-12-57		49	0.0787	0.0012 5	0.1949	0.0023 9	2.1147	0.0337 4	0.02747	0.0006 6	98.5576	1164.7	31.11	1147.9	12.8 9	1153.6	11	547.8	13.07	
ACO-12-57		50	0.0602	0.0010 2	0.1072 2	0.0012 9	0.88992	0.0151 4	0.02253	0.0006	101.594	610.8	36.26	656.6	7.5	646.3	8.11	450.4	11.95	
ACO-12-57		51	0.05768	0.0009 5	0.1059 6	0.0012 6	0.84214	0.0139 1	0.02229	0.0006 4	104.611	517.2	36.05	648.9	7.34	620.3	7.67	445.5	12.65	
ACO-12-57		52	0.10249	0.0012 4	0.2966 3	0.0035 6	4.1884	0.0503 9	0.00906	0.0001 8	100.293	1669.7	22.29	1674.6	17.7	1671.8	9.86	182.3	3.55	
ACO-12-57		53	0.06717	0.0010 5	0.1651 7	0.0019 2	1.5296	0.0238	0.03505	0.0013 3	104.574	843.1	32.05	985.4	10.6 3	942.3	9.55	696.3	26.07	
ACO-12-57		54	0.05892	0.0007 2	0.0900 7	0.0010 3	0.73167	0.0093 7	0.01638	0.0004 3	99.713	564.2	26.47	555.9	6.06	557.5	5.49	328.4	8.56	
ACO-12-57		55	0.06098	0.0009 1	0.1053 1	0.0012	0.88537	0.0132 3	0.02087	0.0008 5	100.248	638.4	31.77	645.5	7.02	643.9	7.12	417.6	16.77	
ACO-12-57		56	0.05855	0.0011	0.1223 5	0.0014 7	0.98778	0.0181 6	0.0268	0.0012 3	106.666	550.6	40.38	744.1	8.45	697.6	9.27	534.5	24.19	
ACO-12-57		57	0.06011	0.0016 1	0.0966 5	0.0013 7	0.801	0.0207 6	0.01206	0.0003 2	99.548	607.6	56.93	594.7	8.05	597.4	11.7	242.3	6.33	
ACO-12-57		58	0.06564	0.001	0.1586	0.0019 3	1.43519	0.0225 5	0.027	0.0010 6	105.013	795	31.78	949	10.7 5	903.7	9.4	538.5	20.9	

ACO-12-57	59	0.11556	0.00195	0.20582	0.00241	3.27877	0.0546	0.04758	0.00256	63.8799	1888.7	30.11	1206.5	12.91	1476	12.96	939.5	49.34
ACO-12-57	60	0.05586	0.00091	0.09497	0.00112	0.73139	0.01195	0.02079	0.00088	104.934	446.6	35.63	584.9	6.59	557.4	7.01	415.9	17.46
ACO-12-57	61	0.05803	0.00103	0.11289	0.00133	0.90327	0.01574	0.02348	0.00067	105.509	530.6	38.66	689.5	7.72	653.5	8.4	469.1	13.23
ACO-12-57	62	0.07169	0.0009	0.16926	0.00186	1.67317	0.02136	0.03553	0.00101	100.962	977.3	25.4	1008	10.24	998.4	8.12	705.7	19.69
ACO-12-57	63	0.06111	0.00081	0.1204	0.00136	1.0144	0.01376	0.02217	0.00054	103.066	643.1	28.21	732.9	7.83	711.1	6.94	443.2	10.59
ACO-12-57	64	0.16357	0.0024	0.26965	0.003	6.08118	0.08755	0.03242	0.0013	61.7353	2492.9	24.47	1539	15.25	1987.6	12.55	644.8	25.39
ACO-12-57	65	0.11725	0.002	0.3192	0.00362	5.15874	0.08552	0.0328	0.00193	93.2679	1914.7	30.28	1785.8	17.68	1845.8	14.1	652.3	37.81
ACO-12-57	66	0.05401	0.00067	0.09277	0.00105	0.69061	0.00875	0.00607	0.00011	107.258	371.1	27.98	571.9	6.17	533.2	5.25	122.2	2.13
ACO-12-57	67	0.05932	0.00097	0.10793	0.00128	0.88268	0.01439	0.01907	0.00046	102.849	578.9	35.02	660.7	7.42	642.4	7.76	381.9	9.05
ACO-12-57	68	0.05915	0.00078	0.10727	0.00122	0.87479	0.01184	0.0182	0.00043	102.93	572.6	28.42	656.9	7.09	638.2	6.41	364.6	8.57
ACO-12-57	69	0.05869	0.00093	0.10879	0.00128	0.88018	0.01398	0.01475	0.00035	103.837	555.6	34.28	665.7	7.44	641.1	7.55	296	6.89
ACO-12-57	70	0.07372	0.00127	0.18412	0.00228	1.87133	0.03244	0.03563	0.00135	105.368	1033.9	34.5	1089.4	12.39	1071	11.47	707.6	26.34
ACO-12-57	71	0.05912	0.00106	0.09572	0.0012	0.78019	0.01376	0.00876	0.00023	100.632	571.7	38.47	589.3	7.04	585.6	7.85	176.2	4.57
ACO-12-57	72	0.0599	0.00099	0.10484	0.00124	0.8658	0.0143	0.01758	0.00048	101.484	600	35.39	642.7	7.25	633.3	7.78	352.3	9.63
ACO-12-57	73	0.11459	0.0017	0.3441	0.00391	5.43551	0.08045	0.06864	0.00267	101.762	1873.4	26.56	1906.4	18.74	1890.5	12.69	1341.9	50.52
ACO-12-57	74	0.07276	0.00112	0.18243	0.00215	1.82988	0.02847	0.03315	0.00122	107.248	1007.2	30.95	1080.2	11.72	1056.2	10.22	659.2	23.79
ACO-12-57	75	0.07026	0.00099	0.16226	0.00187	1.57172	0.02241	0.02489	0.00068	101.063	936	28.57	969.3	10.36	959.1	8.85	496.9	13.34
ACO-12-57	76	0.05543	0.00075	0.09159	0.00104	0.69982	0.00954	0.01043	0.00026	104.864	429.2	29.6	564.9	6.15	538.7	5.7	209.7	5.24
ACO-12-57	77	0.12924	0.00198	0.42662	0.00488	7.60099	0.11618	0.07286	0.00308	109.714	2087.7	26.7	2290.5	22.06	2185	13.72	1421.5	57.94
ACO-12-57	78	0.06026	0.00104	0.10242	0.00122	0.85078	0.01463	0.02023	0.00074	100.56	612.8	36.94	628.6	7.12	625.1	8.03	404.8	14.69
ACO-12-57	79	0.07015	0.00117	0.178	0.00215	1.72158	0.02865	0.02389	0.00077	113.195	932.9	33.88	1056	11.79	1016.6	10.69	477.2	15.15
ACO-12-57	80	0.07205	0.00119	0.18423	0.00219	1.83005	0.03026	0.03485	0.00128	110.379	987.6	33.29	1090.1	11.93	1056.3	10.86	692.4	24.94
ACO-12-60	1	0.06525	0.00185	0.09924	0.00129	0.89296	0.02492	0.02599	0.00097	94.1358	782.3	58.34	610	7.59	648	13.37	518.5	19.01
ACO-12-60	2	0.06326	0.00164	0.09539	0.0013	0.83224	0.02132	0.02245	0.00098	95.5115	717	54.03	587.3	7.64	614.9	11.81	448.6	19.36
ACO-12-60	3	0.0621	0.00114	0.11207	0.00144	0.95989	0.01813	0.03387	0.00152	100.234	677.6	38.72	684.8	8.37	683.2	9.39	673.2	29.71
ACO-12-60	4	0.06613	0.00177	0.10421	0.00138	0.95057	0.02488	0.03633	0.00216	94.1922	810.5	55.04	639	8.08	678.4	12.95	721.2	42.13
ACO-12-60	5	0.06688	0.0013	0.12942	0.00152	1.19452	0.02301	0.03872	0.00184	98.3085	834	39.93	784.6	8.7	798.1	10.65	767.8	35.86

Avalonia hafnium isotopic data tables

Sample N	Analysis N	Hf176/Hf177	1 S.D.	Lu176/Hf177	Yb176/Hf177	U/Pb AGE	Hf_i	epsilon	1se	T(DM) (Ga)	T(DM) (crustal)	Hf Chur (t)	Hf DM (t)
52a	12-52a-01	0.28199848	3.02E-05	0.000840552	0.026171613	1332.9	0.281977	1.3	1.1	1.76	2.00	0.281939	0.282284
52a	12-52a-02	0.28182956	2.3E-05	0.001206626	0.035560086	1684.1	0.281791	2.8	0.8	2.01	2.18	0.281713	0.282026
52a	12-52a-03	0.28181165	1.63E-05	0.000968136	0.02868388	1505.4	0.281784	-1.6	0.6	2.02	2.32	0.281828	0.282158
52a	12-52a-04	0.28115369	1.83E-05	0.00051096	0.015329391	2592.7	0.281128	0.3	0.7	2.89	3.08	0.281120	0.281349
52a	12-52a-05	0.28209107	2.06E-05	0.000478609	0.014463186	1240	0.282080	2.9	0.7	1.61	1.83	0.281999	0.282353
52a	12-52a-06	0.28206568	1.65E-05	0.000665307	0.019916295	1235.9	0.282050	1.7	0.6	1.66	1.90	0.282002	0.282356
52a	12-52a-07	0.28187922	2.4E-05	0.001693497	0.051729099	1456.9	0.281833	-1.0	0.9	1.97	2.25	0.281860	0.282193
52a	12-52a-08	0.28212017	2.85E-05	0.001024615	0.02722178	1300	0.282095	4.8	1.0	1.60	1.77	0.281960	0.282309
52a	12-52a-09	0.282089	2.77E-05	0.000744738	0.021267861	1139.2	0.282073	0.3	1.0	1.63	1.91	0.282063	0.282426
52a	12-52a-10	0.28204221	2.24E-05	0.000525591	0.015302892	1232.1	0.282030	0.9	0.8	1.68	1.95	0.282004	0.282358
52a	12-52a-11	0.2818538	2.07E-05	0.00078774	0.022433255	1597.6	0.281830	2.2	0.7	1.95	2.16	0.281769	0.282090
52a	12-52a-12	0.2818538	2.07E-05	0.00078774	0.022433255	1252.5	0.281835	-5.5	0.7	1.95	2.34	0.281991	0.282343
52a	12-52a-13	0.2818538	2.07E-05	0.00078774	0.022433255	1520.8	0.281831	0.5	0.7	1.95	2.20	0.281818	0.282146
52a	12-52a-14	0.28163566	2.05E-05	0.000526917	0.015127971	1793	0.281618	-0.9	0.7	2.24	2.51	0.281642	0.281945
52a	12-52a-15	0.28183162	2.24E-05	0.00067825	0.019196868	1630.3	0.281811	2.2	0.8	1.98	2.18	0.281748	0.282066
52a	12-52a-17	0.28198533	2.14E-05	0.001015477	0.028228101	1361.5	0.281959	1.4	0.8	1.78	2.03	0.281921	0.282263
52a	12-52a-20	0.28160615	1.63E-05	0.000384662	0.009918664	1843.7	0.281593	-0.6	0.6	2.27	2.54	0.281610	0.281908
52a	12-52a-24	0.28205033	1.84E-05	0.000757539	0.019964587	1329.1	0.282031	3.2	0.7	1.68	1.88	0.281942	0.282287
52a	12-52a-25	0.28219686	2.16E-05	0.000644835	0.019183981	969.2	0.282185	0.5	0.8	1.48	1.76	0.282172	0.282551
52a	12-52a-26	0.28154858	1.89E-05	0.000548819	0.015320906	1958.8	0.281528	-0.2	0.7	2.36	2.61	0.281535	0.281822
52a	12-52a-27	0.28191658	2E-05	0.000850617	0.024200823	1501.8	0.281892	2.2	0.7	1.87	2.09	0.281831	0.282160
52a	12-52a-28	0.28208238	1.96E-05	0.00091798	0.026644421	1138.1	0.282063	-0.1	0.7	1.64	1.92	0.282064	0.282427
52a	12-52a-30	0.2821911	1.47E-05	0.00054512	0.014952172	1016	0.282181	1.4	0.5	1.48	1.76	0.282142	0.282516
52a	12-52a-31	0.28169345	2.45E-05	0.001337269	0.036814757	1867.1	0.281646	1.8	0.9	2.21	2.39	0.281594	0.281890
52a	12-52a-32	0.2822005	1.66E-05	0.000554233	0.016088863	979.8	0.282190	0.9	0.6	1.47	1.75	0.282165	0.282543
52a	12-52a-	0.28159649	1.77E-05	0.001324623	0.038275902	1826.3	0.281551	-2.5	0.6	2.34	2.62	0.281621	0.281921

	33												
52a	12-52a-34	0.28201453	1.63E-05	0.00059309	0.016218782	1197.4	0.282001	-0.9	0.6	1.72	2.02	0.282026	0.282384
52a	12-52a-36	0.28142432	1.96E-05	0.001599822	0.04264495	1856.6	0.281368	-8.3	0.7	2.60	3.01	0.281601	0.281898
52a	12-52a-37	0.28180864	1.99E-05	0.001015357	0.026268515	1688.6	0.281776	2.3	0.7	2.03	2.23	0.281710	0.282022
52a	12-52a-38	0.28210962	1.18E-05	0.00045145	0.012266763	1225.3	0.282099	3.2	0.4	1.59	1.79	0.282008	0.282363
52a	12-52a-39	0.28210985	1.64E-05	0.001228518	0.033890877	1271	0.282080	3.6	0.6	1.62	1.81	0.281979	0.282330
52a	12-52a-40	0.2815905	1.52E-05	0.001178453	0.030997093	1834.8	0.281549	-2.3	0.5	2.34	2.64	0.281615	0.281914
52a	12-52a-41	0.2819581	1.78E-05	0.000700261	0.018436303	1479	0.281939	3.3	0.6	1.81	2.00	0.281845	0.282177
52a	12-52a-42	0.28210927	1.39E-05	0.000829624	0.021892836	1157.4	0.282091	1.4	0.5	1.60	1.85	0.282052	0.282413
52a	12-52a-43	0.28194394	1.57E-05	0.000749655	0.019872156	1612.5	0.281921	5.7	0.6	1.83	1.96	0.281759	0.282079
52a	12-52a-45	0.28156845	2.36E-05	0.000971631	0.025783401	1925.7	0.281533	-0.8	0.8	2.36	2.61	0.281556	0.281847
52a	12-52a-47	0.28204186	1.8E-05	0.000546428	0.01492875	1197.8	0.282030	0.1	0.6	1.68	1.98	0.282026	0.282384
52a	12-52a-51	0.28182775	1.68E-05	0.000527315	0.01507305	1418	0.281814	-2.5	0.6	1.98	2.31	0.281885	0.282222
52a	12-52a-52	0.28216156	4E-05	0.000526885	0.014010909	994.8	0.282152	-0.1	1.4	1.52	1.83	0.282156	0.282532
52a	12-52a-57	0.2821691	1.87E-05	0.000856817	0.024286503	1158.9	0.282150	3.5	0.7	1.52	1.72	0.282051	0.282412
52a	12-52a-61	0.28195229	1.73E-05	0.000713377	0.020638214	1197.1	0.281936	-3.2	0.6	1.82	2.18	0.282026	0.282384
52a	12-52a-62	0.28159454	2.54E-05	0.001131454	0.032205334	1792.5	0.281556	-3.1	0.9	2.33	2.65	0.281643	0.281946
52a	12-52a-64	0.28211213	2.33E-05	0.000530003	0.01640488	1124.3	0.282101	1.0	0.8	1.59	1.86	0.282073	0.282437
52a	12-52a-65	0.28203453	3.99E-05	0.003222103	0.102072907	1231.8	0.281960	-1.6	1.4	1.82	2.11	0.282004	0.282359
52a	12-52a-67	0.28188129	2.29E-05	0.000780787	0.021970742	1472.7	0.281860	0.4	0.8	1.92	2.18	0.281849	0.282182
52a	12-52a-68	0.28220575	2.35E-05	0.000724351	0.022531838	1006.8	0.282192	1.6	0.8	1.47	1.73	0.282148	0.282523
52a	12-52a-69	0.28212545	1.65E-05	0.00050829	0.014998621	1191.6	0.282114	3.0	0.6	1.57	1.79	0.282030	0.282388
52a	12-52a-70	0.28205304	1.92E-05	0.00063747	0.019624654	1232.5	0.282038	1.2	0.7	1.67	1.92	0.282004	0.282358
52a	12-52a-71	0.28208477	2.36E-05	0.000872841	0.025815956	1287.9	0.282064	3.4	0.8	1.64	1.87	0.281968	0.282317
52a	12-52a-72	0.28170664	2.02E-05	0.000804325	0.024041448	1755.9	0.281680	0.5	0.7	2.16	2.42	0.281666	0.281973
52b	52B_48	2.82E-01	1.10E-05	9.67E-04	4.52E-02	1003	0.28224675	3.409	0.39	1.393	1.619	0.28215057	0.28252593
52b	52b_56	2.82E-01	1.20E-05	4.50E-04	2.05E-02	1029	0.28232028	6.604	0.425	1.286	1.429	0.28213396	0.28250696
52b	52B_45	2.82E-01	1.10E-05	7.96E-04	3.73E-02	1070	0.28207496	-1.163	0.39	1.628	1.952	0.28210776	0.28247701
52b	52B_50	2.82E-01	1.40E-05	2.59E-03	1.31E-01	1070	0.28231273	7.266	0.496	1.309	1.424	0.28210776	0.28247701
52b	52b_59	2.82E-01	1.20E-05	5.31E-04	2.30E-02	1106	0.28207592	-0.313	0.425	1.622	1.909	0.28208474	0.2824507
52b	52B_40	2.82E-01	5.40E-06	6.46E-04	2.76E-02	1113	0.28210246	0.787	0.191	1.587	1.869	0.28208026	0.28244558
52b	52B_5	2.82E-01	1.50E-05	9.35E-04	3.82E-02	1177	0.28213924	3.544	0.532	1.538	1.742	0.28203929	0.28239876
52b	52B_37	2.82E-01	7.30E-06	8.39E-04	3.70E-02	1221	0.28200168	-0.334	0.259	1.726	2.016	0.28201109	0.28236654
52b	52B_36	2.82E-01	6.60E-06	1.66E-03	6.88E-02	1239	0.28205528	1.976	0.234	1.661	1.879	0.28199955	0.28235335
52b	52B_24	2.82E-01	7.00E-06	7.39E-04	2.76E-02	1240	0.28183572	-5.787	0.248	1.953	2.366	0.28199891	0.28235261
52b	52B_22	2.82E-01	7.10E-06	9.97E-04	3.70E-02	1269	0.28181811	-5.752	0.252	1.981	2.383	0.28198031	0.28233135
52b	52B_20	2.82E-01	7.10E-06	7.51E-04	2.48E-02	1283	0.28197182	0.017	0.252	1.765	2.048	0.28197133	0.28232109
52b	52B_3	2.82E-01	1.50E-05	6.37E-04	2.10E-02	1330	0.28210401	5.777	0.532	1.581	1.732	0.28194115	0.2822866
52b	52B_39	2.82E-01	1.40E-05	1.09E-03	4.62E-02	1405	0.281868	-0.885	0.497	1.91	2.19	0.28189293	0.2822315
52b	52B_28	2.82E-01	1.00E-05	1.37E-03	5.60E-02	1447	0.28195362	3.112	0.355	1.793	1.989	0.28186591	0.28220061
52b	52B_51	2.82E-01	1.40E-05	9.11E-04	4.15E-02	1510	0.28205397	8.113	0.496	1.648	1.732	0.28182532	0.28215423
52b	52B_42	2.82E-01	1.00E-05	8.94E-04	3.99E-02	1712	0.28158601	-3.865	0.355	2.288	2.636	0.28169488	0.28200515
52b	52B_13	2.82E-01	1.20E-05	1.44E-03	5.61E-02	1776	0.28156158	-3.262	0.426	2.328	2.623	0.28165345	0.2819578
52b	52b_55	2.82E-01	1.20E-05	7.15E-04	3.11E-02	1886	0.28153141	-1.801	0.426	2.356	2.645	0.28158213	0.28187629
52b	52B_38	2.82E-01	1.30E-05	7.76E-04	3.28E-02	1953	0.28149821	-1.435	0.462	2.401	2.675	0.28153861	0.28182656
52b	52B_8	2.81E-01	1.40E-05	5.28E-04	1.90E-02	1953	0.28145943	-2.813	0.497	2.451	2.757	0.28153861	0.28182656
52b	52B_21	2.81E-01	1.50E-05	1.47E-03	5.64E-02	2024	0.28143948	-1.882	0.533	2.488	2.757	0.28149244	0.28177379
52b	52B_6	2.82E-01	1.30E-05	7.22E-04	2.36E-02	2130	0.28151776	3.353	0.462	2.37	2.519	0.28142339	0.28169488
29b	29B_69	2.82E-01	1.20E-05	2.26E-03	1.00E-01	563	0.28245516	0.879	0.425	1.132	1.433	0.28243034	0.28284568
29b	29B_79	2.83E-01	1.20E-05	6.13E-04	2.58E-02	593	0.28275519	12.175	0.424	0.688	0.743	0.28241134	0.28282396
29b	29B_7	2.83E-01	1.00E-05	1.52E-03	5.65E-02	620	0.28251727	4.357	0.354	1.030	1.261	0.28239423	0.2828044
29b	29B_1	2.83E-01	1.40E-05	9.80E-04	4.02E-02	638	0.28264728	9.365	0.495	0.840	0.960	0.28238282	0.28279136
29b	29B_52	2.83E-01	1.00E-05	1.05E-03	4.19E-02	644	0.28275836	13.434	0.354	0.683	0.706	0.28237901	0.28278701
29b	29B_70	2.83E-01	1.60E-05	3.79E-03	1.84E-01	656	0.28274634	13.278	0.566	0.703	0.728	0.2823714	0.28277831
29b	29B_70	2.83E-01	1.60E-05	3.79E-03	1.84E-01	656	0.28274634	13.278	0.566	0.703	0.726	0.2823714	0.28277831
29b	29B_43	2.83E-01	1.30E-05	6.40E-04	2.66E-02	686	0.28265776	10.816	0.460	0.823	0.908	0.28235236	0.28275656
29b	29B_54	2.82E-01	1.10E-05	7.78E-04	3.15E-02	702	0.28222775	-4.054	0.390	1.423	1.803	0.28234221	0.28274495
29b	29B_20	2.82E-01	8.90E-06	1.10E-03	4.67E-02	745	0.28241356	3.495	0.315	1.168	1.397	0.28231489	0.28271374
29b	29B_44	2.82E-01	1.70E-05	1.94E-03	7.93E-02	801	0.28223085	-1.716	0.602	1.436	1.784	0.28227929	0.28267305
29b	29B_4	2.82E-01	1.00E-05	9.54E-04	3.99E-02	1184	0.28211269	2.762	0.354	1.575	1.775	0.28203481	0.28239364
29b	29B_42	2.82E-01	2.30E-05	1.89E-03	5.62E-02	1405	0.28189973	0.241	0.816	1.876	2.142	0.28189293	0.2822315
29b	29B_40	2.82E-01	1.00E-05	1.44E-03	6.21E-02	1574	0.28185603	2.555	0.355	1.925	2.122	0.28178405	0.28210706
29b	29B_80	2.82E-01	2.20E-05	1.14E-03	4.80E-02	1604	0.28185033	3.039	0.780	1.929	2.114	0.28176468	0.28208492
29b	29B_58	2.82E-01	1.00E-05	7.72E-04	3.23E-02	1866	0.28161868	0.837	0.355	2.238	2.476	0.28159511	0.28189112
29b	29B_15	2.82E-01	7.70E-06	1.61E-03	6.74E-02	1967	0.28149998	-1.049	0.273	2.408	2.661	0.28152951	0.28181616
29b	29B_60	2.81E-01	9.90E-06	6.81E-04	2.75E-02	2104	0.28142273	-0.626	0.352	2.500	2.756	0.28144034	0.28171425
29b	29B_41	2.81E-01	1.10E-05	4.22E-04	1.66E-02	2677	0.28100539	-2.117	0.391	3.050	3.301	0.2810649	0.28128518
50	50_10	2.83E-01	1.70E-05	3.97E-03	1.11E-01	590	0.28260712	6.865	0.601	0.925	1.079	0.28241324	0.28282613
50	50_5	2.83E-01	1.20E-05	8.92E-04	3.26E-02	606	0.28255686	5.445	0.425	0.968	1.165	0.2824031	0.28281455
50	50_20	2.83E-01	1.20E-05	1.73E-03	7.45E-02	608	0.28248824	3.060	0.425	1.074	1.304	0.28240183	0.2828131

50	50_8	2.83E-01	1.10E-05	9.08E-04	2.89E-02	636	0.28251316	4.571	0.389	1.028	1.240	0.28238408	0.28279281
50	50_34	2.82E-01	1.10E-05	1.85E-03	6.70E-02	647	0.28246057	2.956	0.389	1.113	1.351	0.28237711	0.28278484
50	50_6	2.83E-01	2.00E-05	1.53E-03	5.77E-02	658	0.28255908	6.692	0.708	0.969	1.116	0.28237013	0.28277686
50	50_43	2.82E-01	1.30E-05	1.88E-03	7.71E-02	671	0.28246832	3.769	0.460	1.102	1.337	0.28236188	0.28276744
50	50_39	2.83E-01	1.80E-05	1.35E-03	5.46E-02	705	0.28250011	5.660	0.637	1.049	1.247	0.2823403	0.28274277
50	50_17	2.82E-01	1.60E-05	1.99E-03	8.40E-02	729.4	0.28239271	2.405	0.567	1.209	1.451	0.28232481	0.28272506
50	50_51	2.82E-01	1.20E-05	1.16E-03	5.00E-02	753.9	0.28211956	-6.719	0.425	1.580	1.978	0.28230924	0.28270727
50	50_70	2.82E-01	8.80E-06	9.09E-04	3.85E-02	765.1	0.28215393	-5.249	0.312	1.527	1.955	0.28230212	0.28269914
50	50_57	2.82E-01	1.30E-05	5.51E-04	1.94E-02	779.7	0.28218594	-3.787	0.461	1.475	1.883	0.28229284	0.28268853
50	50_14	2.82E-01	1.50E-05	1.56E-03	4.58E-02	782.1	0.28244807	5.553	0.531	1.122	1.316	0.28229131	0.28268679
50	50_4	2.82E-01	1.70E-05	1.54E-03	6.03E-02	899	0.28214098	-2.690	0.602	1.553	1.926	0.2822169	0.28260174
50	50_35	2.82E-01	5.10E-06	1.15E-03	4.60E-02	1039.4	0.28209751	-1.056	0.181	1.602	1.933	0.28212732	0.28249936
50	50_61	2.82E-01	1.50E-05	9.61E-04	4.17E-02	1075.1	0.28196354	-4.997	0.532	1.785	2.204	0.2821045	0.28247329
50	50_75	2.82E-01	8.50E-06	7.19E-04	3.38E-02	1190.9	0.28205886	1.009	0.301	1.646	1.927	0.28203039	0.28238858
50	50_33	2.82E-01	4.30E-05	4.70E-03	1.89E-01	1224.3	0.28196836	-1.440	1.524	1.835	2.096	0.28200898	0.28236412
50	50_78	2.82E-01	6.20E-06	1.53E-03	6.54E-02	1241.2	0.28181618	-6.452	0.220	1.995	2.393	0.28199814	0.28235173
50	50_36	2.82E-01	3.00E-05	1.22E-03	3.83E-02	1546.9	0.28171928	-2.919	1.065	2.114	2.448	0.28180153	0.28212704
50	50_3	2.82E-01	1.70E-05	1.43E-03	5.42E-02	1561.1	0.28205464	9.307	0.603	1.647	1.698	0.28179237	0.28211657
50	50_1	2.82E-01	1.30E-05	5.38E-04	2.29E-02	1595.4	0.28201175	8.571	0.461	1.703	1.773	0.28177024	0.28209127
50	50_55	2.82E-01	1.30E-05	1.43E-03	6.38E-02	1638.5	0.28185859	4.124	0.461	1.919	2.086	0.2817424	0.28205946
50	50_9	2.82E-01	1.80E-05	1.53E-03	4.26E-02	1731.2	0.28173173	1.749	0.639	2.094	2.299	0.28168246	0.28199095
50	50_32	2.82E-01	1.20E-05	8.02E-04	3.13E-02	2000	0.2814965	-0.410	0.426	2.403	2.659	0.28150805	0.28179163
50	50_69	2.81E-01	1.20E-05	6.24E-04	2.65E-02	2670	0.28093815	-4.674	0.427	3.142	3.443	0.28106951	0.28129044
50	50_56	2.81E-01	1.30E-05	2.39E-04	9.94E-03	2801	0.28094919	-1.208	0.463	3.122	3.343	0.28098313	0.28119172
38	38_38	2.82E-01	1.40E-05	0.0016926	0.0644292	591	0.28234624	-2.350	0.496	1.277	1.613	0.28241261	0.28282541
38	38_38	2.82E-01	1.40E-05	0.0016926	0.0644292	591	0.28234624	-2.350	0.496	1.277	1.624	0.28241261	0.28282541
38	38_10	2.82E-01	1.10E-05	0.0002058	0.0143139	596	0.2819997	-14.509	0.390	1.724	2.408	0.28240944	0.28282179
38	38_7	2.83E-01	8.20E-06	0.0005158	0.0177833	609	0.28262111	7.787	0.290	0.875	1.035	0.2824012	0.28281237
38	38_11	2.82E-01	1.30E-05	0.0012908	0.0581575	619	0.28224601	-5.271	0.461	1.410	1.860	0.28239486	0.28280513
38	38_30	2.83E-01	1.80E-05	0.0021289	0.0855825	631	0.2826068	7.775	0.637	0.906	1.055	0.28238725	0.28279643
38	38_30	2.83E-01	1.80E-05	0.0021289	0.0855825	631	0.2826068	7.775	0.637	0.906	1.029	0.28238725	0.28279643
38	38_26	2.83E-01	1.30E-05	0.0007030	0.0280079	649	0.28257544	7.069	0.460	0.939	1.114	0.28237584	0.28278339
38	38_18	2.81E-01	2.40E-05	0.0007575	0.0372315	655	0.28147569	-31.743	0.853	2.457	3.500	0.28237203	0.28277904
38	38_65	2.83E-01	1.40E-05	0.0022965	0.0736757	664	0.28260738	8.537	0.495	0.904	1.019	0.28236632	0.28277251
38	38_20	2.83E-01	1.40E-05	0.0012877	0.0359466	673	0.28259774	8.398	0.495	0.911	1.050	0.28236061	0.28276599
38	38_55	2.83E-01	7.70E-06	0.0016034	0.0603068	690	0.28266223	11.065	0.272	0.820	0.895	0.28234982	0.28275366
38	38_35	2.83E-01	1.30E-05	0.0012589	0.0438223	704	0.28263336	10.357	0.460	0.859	0.951	0.28234094	0.2827435
38	38_25	2.82E-01	1.20E-05	0.0016799	0.0736121	713	0.28216551	-6.011	0.425	1.529	1.982	0.28233522	0.28273697
38	38_15	2.83E-01	2.60E-05	0.0025512	0.0665008	726	0.28258422	9.112	0.920	0.936	1.047	0.28232697	0.28272753
38	38_51	2.83E-01	1.00E-05	0.0005206	0.0219517	753	0.28254864	8.460	0.354	0.973	1.096	0.28230981	0.28270793
38	38_46	2.82E-01	1.40E-05	0.0018345	0.0733606	795	0.2821376	-5.155	0.496	1.568	1.990	0.28228311	0.28267741
38	38_44	2.82E-01	3.00E-05	0.0041121	0.1237850	1680	0.28144812	-9.494	1.065	2.551	2.963	0.28171558	0.2820288
38	38_49	2.83E-01	1.30E-05	0.0019690	0.0638425	1701	0.28256453	30.619	0.460	0.908	0.450	0.281702	0.28201328
38	38_61	2.82E-01	9.60E-06	0.0015015	0.0684048	1918	0.28150232	-2.097	0.341	2.405	2.700	0.28156135	0.28185254
38	38_75	2.81E-01	1.10E-05	0.0020125	0.0621272	2002	0.28123744	-9.567	0.391	2.780	3.225	0.28150675	0.28179015
38	38_43	2.81E-01	8.10E-06	0.0011467	0.0407234	2061	0.28137607	-3.279	0.288	2.570	2.832	0.28146835	0.28174626
38	38_36	2.81E-01	1.90E-05	0.0005878	0.0254359	2830	0.28074414	-7.824	0.677	3.398	3.780	0.28096398	0.28116983
38	38_45	2.81E-01	1.10E-05	0.0015054	0.0689901	2944	0.28084103	-1.693	0.392	3.275	3.469	0.28088859	0.28108367
48	48_59	2.82E-01	1.40E-05	2.17E-03	7.61E-02	512	0.28239914	-2.247	0.496	1.215	1.588	0.28246262	0.28288257
48	48_49	2.82E-01	1.90E-05	1.91E-03	8.58E-02	526	0.28235315	-3.562	0.673	1.275	1.680	0.28245377	0.28287245
48	48_24	2.82E-01	2.10E-05	1.61E-03	6.43E-02	539	0.28244574	0.007	0.743	1.136	1.468	0.28244554	0.28286304
48	48_53	2.82E-01	1.90E-05	2.59E-03	8.44E-02	552	0.28233217	-3.723	0.673	1.318	1.716	0.28243731	0.28285364
48	48_6	2.82E-01	1.30E-05	2.38E-03	7.37E-02	569	0.28228662	-4.954	0.460	1.378	1.799	0.28242654	0.28284134
48	48_29	2.83E-01	2.50E-05	4.19E-03	1.85E-01	573	0.28266998	8.709	0.884	0.832	0.934	0.28242401	0.28283844
48	48_41	2.82E-01	1.50E-05	2.38E-03	9.84E-02	584	0.28241092	-0.217	0.531	1.197	1.522	0.28241704	0.28283048
48	48_15	2.82E-01	2.80E-05	2.47E-03	1.04E-01	603	0.28206004	-12.215	0.993	1.707	2.178	0.282405	0.28281672
48	48_15	2.82E-01	2.80E-05	2.47E-03	1.04E-01	603	0.28206004	-12.215	0.993	1.707	2.178	0.282405	0.28281672
48	48_48	2.83E-01	2.60E-05	3.49E-03	1.23E-01	606	0.28246135	2.063	0.920	1.138	1.396	0.2824031	0.28281455
48	48_63	2.83E-01	1.50E-05	1.90E-03	7.57E-02	614	0.28253208	4.747	0.531	1.013	1.218	0.28239803	0.28280875
48	48_12	2.82E-01	3.70E-05	2.27E-03	6.54E-02	624	0.28237446	-0.610	1.310	1.245	1.565	0.28239169	0.28280151
48	48_38	2.82E-01	1.60E-05	1.21E-03	5.16E-02	627	0.28225073	-4.924	0.567	1.402	1.847	0.28238979	0.28279933
48	48_58	2.82E-01	3.40E-05	1.92E-03	6.26E-02	641	0.28246487	2.973	1.204	1.109	1.366	0.28238091	0.28278919
48	48_13	2.82E-01	1.60E-05	1.24E-03	4.69E-02	653	0.28226479	-3.843	0.567	1.382	1.801	0.2823733	0.28278049
48	48_32	2.83E-01	2.00E-05	2.18E-03	9.06E-02	678	0.28272032	12.852	0.707	0.738	0.772	0.28235744	0.28276236
48	48_76	2.83E-01	2.60E-05	2.11E-03	6.88E-02	690	0.28254871	7.044	0.920	0.987	1.116	0.28234982	0.28275366
48	48_23	2.83E-01	2.10E-05	2.49E-03	1.02E-01	694	0.28250359	5.536	0.743	1.056	1.248	0.28234729	0.28275075
48	48_10	2.82E-01	6.90E-04	3.41E-03	1.13E-01	776	0.28191235	-13.562	#####	1.938	2.498	0.28229519	0.28269122
48	48_1	2.82E-01	1.80E-05	2.35E-03	7.22E-02	802	0.28186265	-14.738	0.639	1.974	2.592	0.28227866	0.28267232
48	48_14	2.82E-01	3.10E-05	1.88E-03	7.78E-02	1002	0.28211957	-1.121	1.099	1.584	1.910	0.2821512	0.28252666
48	48_78	2.82E-01	3.30E-05	2.94E-03	9.66E-02	1406	0.28198778	3.387	1.170	1.761	1.941	0.28189229	0.28223076
48	48_36	2.83E-01	1.50E-05	1.07E-03	4.87E-02	2126	0.28247472	37.264	0.531	1.041	0.348	0.281426	0.28169786
48	48_20	2.81E-01	2.30E-05	8.42E-04	2.98E-02	2709	0.28095336	-3.218	0.819	3.124	3.398	0.28104382	0.28126108
48	48_79	2.81E-01	1.30E-05	7.19E-04	2.40E-02	3104	0.28054914	-8.311	0.463	3.655	3.988	0.28078251	0.28096244
49	49_35	2.82E-01	1.00E-05	1.06E-03	4.95E-02	551	0.28228701	-5.344	0.354	1.350	1.809	0.28243794	0.28285436
49	49_29	2.82E-01	9.90E-06	1.81E-03	7.90E-02	566	0.28234184	-3.066	0.351	1.287	1.635	0.28242844	0.28284351
49	49_58	2.83E-01	8.10E-06	9.43E-04	4.14E-02	572	0.28261288	6.665	0.287	0.890	1.079	0.28242464	0.28283916
49	49_6	2.83E-01	1.30E-05	2.45E-03	1.06E-01	588	0.28269297	9.860	0.460	0.785	0.881	0.28241451	0.28282758
49	49_30	2.83E-01	1.00E-05	9.37E-04	4.10E-02	599	0.28261348	7.292	0.354	0.889	1.061	0.28240754	0.28281962
49	49_52	2.83E-01	8.10E-06	1.23E-03	5.21E-02	605	0.28257701	6.136	0.287	0.942	1.137	0.28240374	0.28281527
49	49_52	2.83E-01	8.10E-06	1.23E-03	5.21E-02	605	0.28257701	6.136	0.287	0.942	1.139	0.28240374	0.28281527
49	49_40	2.83E-01	1.40E-05	1.63E-03	7.34E-02	613	0.2825692	6.039	0.495	0.957	1.141	0.28239867	0.28280947
49	49_42	2.82E-01	9.90E-06	5.85E-04	2.78E-02	613	0.28204527	-12.514	0.351	1.672	2.304	0.28239867	0.28280947
49	49_15	2.83E-01	1.10E-05	1.03E-03	4.17E-02	618	0.28266904	9.687	0.389	0.810	0.925	0.2823955	0.28280585
49	49_73	2.83E-01	9.50E-06	6.10E-04	2.52E-02	625	0.28254685	5.517	0.336	0.979	1.182	0.28239106	0.28280078
49	49_51	2.83E-01	1.10E-05	1.21E-03	5.57E-02	627	0.28263282	8.606	0.389	0.862	1.000	0.28238979	0.28279933

49	49_48	2.83E-01	1.00E-05	1.11E-03	5.00E-02	633	0.28250477	4.206	0.354	1.042	1.282	0.28238599	0.28279498
49	49_80	2.83E-01	1.00E-05	1.05E-03	4.50E-02	641	0.28251742	4.834	0.354	1.024	1.234	0.28238091	0.28278919
49	49_18	2.83E-01	9.10E-06	1.38E-03	5.92E-02	661	0.28256586	6.999	0.322	0.958	1.129	0.28236823	0.28277469
49	49_70	2.83E-01	1.40E-05	2.86E-03	1.27E-01	673	0.28271186	12.440	0.495	0.752	0.792	0.28236061	0.28276599
49	49_70	2.83E-01	1.40E-05	2.86E-03	1.27E-01	673	0.28271186	12.440	0.495	0.752	0.795	0.28236061	0.28276599
49	49_54	2.83E-01	9.90E-06	1.04E-03	4.94E-02	684	0.2827567	14.275	0.350	0.684	0.687	0.28235363	0.28275801
49	49_38	2.82E-01	7.00E-06	6.21E-04	2.89E-02	686	0.28245601	3.671	0.248	1.104	1.358	0.28235236	0.28275656
49	49_67	2.83E-01	1.10E-05	8.16E-04	3.36E-02	712	0.2825511	7.624	0.389	0.973	1.129	0.28233586	0.28273769
49	49_60	2.82E-01	2.20E-05	1.59E-03	6.86E-02	785	0.28182261	-16.538	0.781	2.007	2.684	0.28228947	0.28268468
49	49_1	2.82E-01	1.10E-05	9.19E-04	4.38E-02	1170	0.28206872	0.885	0.390	1.636	1.918	0.28204377	0.28240388
49	49_45	2.82E-01	1.30E-05	7.97E-04	3.91E-02	1214	0.28214076	4.439	0.461	1.534	1.731	0.28201558	0.28237166
49	49_71	2.82E-01	1.10E-05	1.16E-03	5.53E-02	1369	0.2819341	0.639	0.390	1.820	2.092	0.28191608	0.28225795
49	49_65	2.82E-01	8.90E-06	4.71E-04	2.29E-02	1554	0.28180114	0.149	0.316	1.991	2.269	0.28179695	0.2821218
49	49_11	2.82E-01	1.10E-05	3.95E-04	1.88E-02	1998	0.28160001	3.220	0.391	2.258	2.430	0.28150935	0.28179312
49	49_33	2.81E-01	1.20E-05	9.33E-04	4.41E-02	2078	0.28127613	-6.436	0.427	2.703	3.051	0.28145728	0.28173361
49	49_37	2.82E-01	9.40E-06	4.93E-04	2.36E-02	2176	0.28152058	4.520	0.334	2.364	2.490	0.28139338	0.28166058
49	49_59	2.83E-01	2.10E-05	1.16E-03	3.85E-02	2637	0.28256138	52.301	0.743	0.900	-0.226	0.28109124	0.28131528
13-22	10	0.28252937	2.86E-05	0.000849503	0.032566123	480.2	0.282522	1.4	1.0	1.02	1.31	0.282483	0.282906
13-22	21	0.28244809	4.18E-05	0.001558433	0.060463379	558.1	0.282432	-0.1	1.5	1.15	1.47	0.282433	0.282849
13-22	38	0.28192585	2.53E-05	0.000579032	0.02063996	572.3	0.281920	-17.9	0.9	1.85	2.60	0.282424	0.282839
13-22	16	0.28236656	2.82E-05	0.001522213	0.051624706	588.6	0.282350	-2.3	1.0	1.27	1.60	0.282414	0.282827
13-22	37	0.28246266	2.87E-05	0.001085975	0.032808367	595.4	0.282451	1.4	1.0	1.12	1.40	0.282410	0.282822
13-22	54	0.28249261	2.5E-05	0.000619097	0.021237576	599.8	0.282486	2.8	0.9	1.06	1.34	0.282407	0.282819
13-22	8	0.28234683	6.86E-05	0.004050426	0.117200854	609.1	0.282301	-3.6	2.4	1.39	1.75	0.282401	0.282812
13-22	11	0.28214628	4.01E-05	0.001969721	0.067142302	611.1	0.282124	-9.8	1.4	1.60	2.07	0.282400	0.282811
13-22	47	0.28229017	2.56E-05	0.000852633	0.029979136	622	0.282280	-4.0	0.9	1.35	1.79	0.282393	0.282803
13-22	2	0.28221028	2.24E-05	0.000277495	0.010603566	629.3	0.282207	-6.4	0.8	1.44	1.91	0.282388	0.282798
13-22	52	0.28262437	2.59E-05	0.001052047	0.031025615	651.7	0.282612	8.4	0.9	0.89	1.03	0.282374	0.282781
13-22	6	0.28240028	4.04E-05	0.001596905	0.064402578	683.5	0.282380	0.9	1.4	1.22	1.50	0.282354	0.282758
13-22	55	0.28252936	4.04E-05	0.001491663	0.053778445	686.7	0.282510	5.6	1.4	1.04	1.25	0.282352	0.282756
13-22	57	0.28221704	5.68E-05	0.001351341	0.058693736	797.7	0.282197	-3.0	2.0	1.47	1.88	0.282281	0.282675
13-22	33	0.28207891	3.13E-05	0.000668665	0.025024265	1155.7	0.282064	0.4	1.1	1.64	1.94	0.282053	0.282414
13-22	4	0.28200298	2.98E-05	0.000890312	0.035404618	1367.4	0.281980	2.2	1.1	1.75	1.99	0.281917	0.282259
13-22	13	0.28192722	2.97E-05	0.001701836	0.0495311	1537.8	0.281878	2.5	1.1	1.90	2.11	0.281807	0.282134
13-22	53	0.28180954	3.35E-05	0.000921075	0.03365146	1560	0.281782	-0.4	1.2	2.02	2.31	0.281793	0.282117
13-22	40	0.28141329	4.23E-05	0.002214712	0.080946782	1794.2	0.281338	-10.8	1.5	2.65	3.14	0.281642	0.281944
13-22	14	0.28155905	3.23E-05	0.000879616	0.027282388	2085.2	0.281524	2.5	1.1	2.36	2.54	0.281453	0.281728
13-22	27	0.28137304	3.06E-05	0.001122873	0.045058079	2249.6	0.281325	-0.7	1.1	2.63	2.88	0.281345	0.281606
12-40	28	0.2824868	1.98E-05	0.000938176	0.031963579	598.9	0.282476	2.4	0.7	1.08	1.38	0.282408	0.282820
12-40	3	0.28244796	5.07E-05	0.001533955	0.045124569	599.4	0.282431	0.8	1.8	1.15	1.47	0.282407	0.282819
12-40	6	0.28239647	2.28E-05	0.000962262	0.030685322	605.4	0.282386	-0.6	0.8	1.21	1.56	0.282403	0.282815
12-40	35	0.28243445	1.9E-05	0.001182927	0.04008577	611	0.282421	0.7	0.7	1.16	1.50	0.282400	0.282811
12-40	4	0.2822521	2.04E-05	0.000637874	0.020923431	613.7	0.282245	-5.4	0.7	1.40	1.87	0.282398	0.282809
12-40	5	0.2823184	2.39E-05	0.000466135	0.016790364	616.6	0.282313	-3.0	0.8	1.30	1.71	0.282396	0.282807
12-40	13	0.28259354	4.49E-05	0.001838406	0.063570139	619.8	0.282572	6.3	1.6	0.95	1.14	0.282394	0.282805
12-40	10	0.28248413	2.25E-05	0.000618617	0.022342226	626.5	0.282477	3.1	0.8	1.08	1.35	0.282390	0.282800
12-40	2	0.28252648	2.07E-05	0.000587706	0.021326432	629.5	0.282520	4.7	0.7	1.02	1.25	0.282388	0.282798
12-40	23	0.28246442	2.23E-05	0.000559905	0.020832503	630.4	0.282458	2.5	0.8	1.10	1.39	0.282388	0.282797
12-40	17	0.28240889	2.9E-05	0.001025683	0.033995989	631.7	0.282397	0.4	1.0	1.19	1.52	0.282387	0.282796
12-40	12	0.28251761	2.41E-05	0.001539926	0.055503419	633	0.282499	4.0	0.9	1.05	1.29	0.282386	0.282795
12-40	18	0.28247614	4.31E-05	0.00134698	0.049856806	635.7	0.282460	2.7	1.5	1.11	1.38	0.282384	0.282793
12-40	24	0.2824301	2E-05	0.000800155	0.027257582	636.7	0.282421	1.3	0.7	1.16	1.47	0.282384	0.282792
12-40	9	0.28245378	1.82E-05	0.000680694	0.024071788	642.7	0.282446	2.3	0.6	1.12	1.41	0.282380	0.282788
12-40	8	0.28234672	2.27E-05	0.000778035	0.025277479	643.6	0.282337	-1.5	0.8	1.27	1.65	0.282379	0.282787
12-40	15	0.28245152	2.35E-05	0.000847851	0.02834731	644.4	0.282441	2.2	0.8	1.13	1.42	0.282379	0.282787
12-40	14	0.28251501	2.02E-05	0.000826715	0.030389163	645	0.282505	4.5	0.7	1.04	1.27	0.282378	0.282786
12-40	22	0.28245748	3.82E-05	0.001591657	0.059404815	646.9	0.282438	2.2	1.4	1.14	1.42	0.282377	0.282785

Iberia Hafnium isotopic data tables

							Scherer et al., 2001 - ^{176}Lu decay constant (1.865x10^{-11})						
							Hf_i	epsilon	1se	T(DM)	T(DM)		
Sample N	No. #	Hf176/Hf177	1 S.D.	Lu176/Hf177	Yb176/Hf177	U/Pb AGE				(Ga)	(crustal)	Hf Chur (t)	Hf DM (t)
14-01	14-01-01	0.2823617	1.777E-05	0.00185699	0.0507655	551.7	0.282342	-3.4	0.6	1.29	1.69	0.282437	0.282854
14-01	14-01-03	0.28225575	1.921E-05	0.00060344	0.01506293	567.7	0.282249	-6.3	0.7	1.39	1.88	0.282427	0.282842
14-01	14-01-27	0.2821332	2.52E-05	0.00066054	0.01502066	612.5	0.282126	-9.7	0.9	1.56	2.09	0.282399	0.282810
14-01	14-01-28	0.28198008	2.424E-05	0.00118157	0.03221624	1392	0.281949	1.7	0.9	1.80	2.05	0.281901	0.282241
14-01	14-01-29	0.28275817	4.376E-05	0.00119548	0.02793649	400.2	0.282749	7.6	1.5	0.70	0.88	0.282533	0.282963
14-01	14-01-32	0.28259366	2.647E-05	0.00145128	0.03873063	570.1	0.282578	5.4	0.9	0.94	1.16	0.282426	0.282841
14-01	14-01-37	0.28242608	5.419E-05	0.00183068	0.04851182	572.4	0.282406	-0.6	1.9	1.19	1.51	0.282424	0.282839
14-01	14-01-38	0.28176906	3.335E-05	0.00085287	0.02117802	1528	0.281744	-2.5	1.2	2.07	2.41	0.281814	0.282141
14-01	14-01-42	0.28151503	2.854E-05	0.00041739	0.01093241	575.5	0.281511	-32.3	1.0	2.39	3.36	0.282422	0.282837
14-01	14-01-44	0.28159363	2.779E-05	0.00076391	0.01965442	2054	0.281564	3.2	1.0	2.31	2.45	0.281473	0.281751
14-01	14-01-45	0.28102053	4.398E-05	0.00047409	0.01243594	2734	0.280996	-1.1	1.6	3.06	3.26	0.281028	0.281243
14-01	14-01-47	0.2815291	3.585E-05	0.0010666	0.03031901	2059	0.281487	0.6	1.3	2.42	2.65	0.281470	0.281748
14-01	14-01-49	0.2828631	4.638E-05	0.00392672	0.10264742	404.1	0.282833	10.7	1.6	0.60	0.67	0.282531	0.282961
14-01	14-01-51	0.28091913	2.788E-05	0.00062004	0.01531041	2704	0.280887	-5.7	1.0	3.21	3.54	0.281047	0.281265
14-01	14-01-52	0.28219146	3.992E-05	0.00076145	0.01908821	1075	0.282176	2.5	1.4	1.49	1.74	0.282104	0.282473
14-01	14-01-53	0.2823092	3.086E-05	0.00032372	0.00830136	655.7	0.282305	-2.4	1.1	1.31	1.71	0.282372	0.282779
14-01	14-01-54	0.28256439	3.604E-05	0.00098944	0.02182758	636.7	0.282553	6.0	1.3	0.97	1.16	0.282384	0.282792
14-01	14-01-55	0.28220081	6.202E-05	0.00128664	0.03144573	1453	0.282165	10.8	2.2	1.49	1.52	0.281862	0.282196
14-01	14-01-58	0.28178093	2.65E-05	0.00060561	0.01311318	655.2	0.281773	-21.2	0.9	2.04	2.88	0.282372	0.282779
14-01	14-01-59	0.28232356	2.701E-05	0.00039449	0.00907792	461.1	0.282320	-6.2	1.0	1.29	1.80	0.282495	0.282919
14-01	14-01-62	0.28268153	5.089E-05	0.00024866	0.00543749	397.6	0.282680	5.1	1.8	0.79	1.04	0.282535	0.282965
14-01	14-01-63	0.28230335	3.303E-05	0.00092515	0.02330903	504.2	0.282295	-6.1	1.2	1.34	1.83	0.282468	0.282888
14-01	14-01-67	0.2823695	3.97E-05	0.00143728	0.03722309	528.7	0.282355	-3.4	1.4	1.26	1.68	0.282452	0.282870
14-01	14-01-69	0.28228223	2.248E-05	0.00120004	0.03040689	500.3	0.282271	-7.0	0.8	1.38	1.88	0.282470	0.282891
14-01	14-01-70	0.28261605	3.601E-05	0.00147499	0.03729912	524	0.282602	5.2	1.3	0.91	1.11	0.282455	0.282874
14-01	14-01-73	0.28176522	3.821E-05	0.00092254	0.0219935	1910	0.281732	5.9	1.4	2.08	2.19	0.281566	0.281858
14-01	14-01-74	0.28264657	3.365E-05	0.00111948	0.02576923	609.9	0.282634	8.3	1.2	0.86	1.00	0.282401	0.282812
14-01	14-01-75	0.28185326	2.655E-05	0.00111308	0.02872478	1596	0.281820	1.8	0.9	1.97	2.21	0.281770	0.282091
14-02	2	0.28229457	2.132E-05	0.00076431	0.01956968	521.4	0.282287	-6.0	0.8	1.34	1.83	0.282457	0.282876
14-02	7	0.28217996	2.191E-05	0.00051326	0.01238594	593.8	0.282174	-8.4	0.8	1.49	1.98	0.282411	0.282823
14-02	8	0.28237066	1.641E-05	0.00090102	0.02189011	671	0.282359	-0.1	0.6	1.24	1.58	0.282362	0.282767
14-02	10	0.28158515	1.747E-05	0.00066536	0.01582746	2000	0.281560	1.8	0.6	2.31	2.52	0.281508	0.281791
14-02	11	0.28239172	1.198E-05	7.4102E-05	0.00248036	607.4	0.282391	-0.4	0.4	1.19	1.55	0.282402	0.282814
14-02	12	0.28271521	1.589E-05	0.00057758	0.01478251	536.8	0.282709	9.3	0.6	0.75	0.88	0.282447	0.282865
14-02	17	0.28264265	2.152E-05	0.00063541	0.01443632	541.3	0.282636	6.8	0.8	0.86	1.05	0.282444	0.282861
14-02	18	0.28258473	1.747E-05	0.00070452	0.01743571	610.2	0.282577	6.2	0.6	0.94	1.14	0.282400	0.282812
14-02	19	0.28255851	3.109E-05	0.00200539	0.05231878	583.3	0.282537	4.2	1.1	1.01	1.21	0.282417	0.282831
14-02	21	0.28263575	2.394E-05	0.00050758	0.0129172	548.9	0.282631	6.8	0.8	0.86	1.05	0.282439	0.282856
14-02	25	0.28158978	1.858E-05	0.00087183	0.02360241	2056	0.281556	3.0	0.7	2.32	2.49	0.281471	0.281750
14-02	27	0.28270611	2.405E-05	0.00134738	0.03568245	550	0.282692	9.0	0.9	0.78	0.92	0.282439	0.282855
14-02	32	0.28267731	1.771E-05	0.00050793	0.0141982	569.5	0.282672	8.7	0.6	0.80	0.95	0.282426	0.282841
14-02	34	0.28268521	1.573E-05	0.00078239	0.02063065	561.1	0.282677	8.7	0.6	0.80	0.93	0.282432	0.282847
14-02	33	0.2826846	1.797E-05	0.00052743	0.01432767	575	0.282679	9.1	0.6	0.79	0.93	0.282423	0.282837
14-02	35	0.28176268	2.696E-05	0.00148312	0.03851294	2087	0.281704	9.0	1.0	2.12	2.14	0.281452	0.281727
14-02	36	0.2826826	1.809E-05	0.00126935	0.03283827	580.3	0.282669	8.8	0.6	0.81	0.93	0.282419	0.282833
14-02	37	0.28263884	1.704E-05	0.00050091	0.01271688	565	0.282634	7.2	0.6	0.86	1.04	0.282429	0.282844
14-02	47	0.28163657	2.23E-05	0.00077253	0.01760233	2095	0.281606	5.7	0.8	2.25	2.35	0.281446	0.281721
14-02	52	0.2822478	1.51E-05	0.00034907	0.00923798	571.2	0.282244	-6.4	0.5	1.39	1.84	0.282425	0.282840
14-02	53	0.2826238	1.906E-05	0.0005919	0.01529443	567.7	0.282618	6.7	0.7	0.88	1.07	0.282427	0.282842
14-02	57	0.28162955	1.292E-05	0.00086282	0.02036717	2066	0.281596	4.6	0.5	2.27	2.40	0.281465	0.281743
14-02	58	0.28267596	2.033E-05	0.00098114	0.02338627	585.8	0.282665	8.8	0.7	0.82	0.93	0.282416	0.282829
14-02	61	0.28219653	1.964E-05	0.00050589	0.01269596	578.2	0.282191	-8.1	0.7	1.47	1.93	0.282421	0.282835
14-02	62	0.28102646	1.163E-05	0.00039393	0.00855545	2490	0.281008	-6.4	0.4	3.05	3.42	0.281188	0.281426
14-02	63	0.28095582	1.55E-05	0.00045741	0.01234942	2482	0.280934	-9.2	0.6	3.15	3.59	0.281193	0.281432
14-02	65	0.28269804	1.84E-05	0.00051398	0.01198336	544.6	0.282693	8.9	0.7	0.78	0.92	0.282442	0.282859
14-02	66	0.2826307	2.174E-05	0.00085448	0.02080647	535.7	0.282622	6.2	0.8	0.88	1.08	0.282448	0.282865
14-02	68	0.28267411	1.356E-05	0.00051901	0.01357974	539.9	0.282669	7.9	0.5	0.81	0.97	0.282445	0.282862
14-02	71	0.28248491	2.199E-05	0.00135341	0.03316158	606.2	0.282470	2.4	0.8	1.10	1.39	0.282403	0.282814
14-02	80	0.28266723	2.214E-05	0.00069957	0.01946058	524.8	0.282660	7.3	0.8	0.82	1.00	0.282455	0.282873
ACO-12-57	3	0.28198197	1.63E-05	0.00010076	0.0028248	621	0.281981	-14.6	0.6	1.75	2.37	0.282394	0.282804
ACO-12-57	5	0.28083745	1.406E-05	0.00065112	0.01653525	2885	0.280801	-4.5	0.5	3.32	3.61	0.280928	0.281128
ACO-12-57	9	0.2813712	1.463E-05	0.00046339	0.01352276	1947	0.281354	-6.7	0.5	2.59	3.01	0.281543	0.281831
ACO-12-57	10	0.28246756	1.885E-05	0.00142711	0.04062428	825	0.282445	6.4	0.7	1.12	1.30	0.282264	0.282656
ACO-12-57	12	0.282152	2.105E-05	0.00124553	0.03752418	511	0.282140	-11.4	0.7	1.56	2.16	0.282463	0.282883
ACO-12-57	13	0.28226188	1.902E-05	0.00237288	0.07396252	481	0.282241	-8.6	0.7	1.45	1.95	0.282482	0.282905
ACO-12-57	15	0.28219862	1.728E-05	0.00070964	0.02248851	579	0.282191	-8.1	0.6	1.48	2.01	0.282420	0.282834
ACO-12-57	16	0.28210672	1.843E-05	0.00074529	0.0194801	664	0.282097	-9.5	0.7	1.60	2.16	0.282366	0.282773
ACO-12-57	22	0.28214391	1.74E-05	0.00122978	0.03660095	637	0.282129	-9.0	0.6	1.57	2.05	0.282383	0.282792
ACO-12-57	23	0.28226992	1.506E-05	0.0006116	0.01733223	705	0.282262	-2.8	0.5	1.37	1.78	0.282340	0.282743
ACO-12-57	25	0.28137246	1.579E-05	0.00056691	0.01595776	2044	0.281350	-4.6	0.6	2.60	2.95	0.281479	0.281759
ACO-12-57	28	0.28220492	1.443E-05	0.00097933	0.02780464	490	0.282196	-9.9	0.5	1.48	2.04	0.282477	0.282898
ACO-12-57	31	0.28202681	1.644E-05	0.00130845	0.03642463	853	0.282006	-8.5	0.6	1.74	2.25	0.282246	0.282635
ACO-12-57	32	0.28252491	1.995E-05	0.00181511	0.04699741	728	0.282500	6.2	0.7	1.05	1.23	0.282326	0.282726

ACO-12-57	34	0.28193939	1.502E-05	0.0012541	0.03698743	611	0.281925	-16.8	0.5	1.86	2.50	0.282400	0.282811
ACO-12-57	37	0.28170361	1.902E-05	0.00064004	0.0163462	939	0.281692	-17.7	0.7	2.15	2.78	0.282191	0.282573
ACO-12-57	39	0.28138403	1.808E-05	0.00100333	0.0276915	1765	0.281350	-11.0	0.6	2.61	3.05	0.281661	0.281966
ACO-12-57	42	0.28103204	1.881E-05	0.00072831	0.01857841	2542	0.280997	-5.6	0.7	3.07	3.41	0.281154	0.281387
ACO-12-57	43	0.28127046	3.776E-05	0.00262945	0.09787004	2609	0.281139	1.1	1.3	2.89	3.05	0.281110	0.281336
ACO-12-57	44	0.28213011	1.442E-05	0.00055122	0.01572146	571	0.282124	-10.7	0.5	1.56	2.13	0.282425	0.282840
ACO-12-57	47	0.28164833	2.436E-05	0.00136962	0.04354527	600	0.281633	-27.4	0.9	2.27	3.20	0.282407	0.282819
ACO-12-57	49	0.28183738	1.477E-05	0.00061874	0.01629228	1164	0.281824	-7.9	0.5	1.97	2.46	0.282048	0.282408
ACO-12-57	50	0.28208246	2.108E-05	0.00128056	0.04126803	656	0.282067	-10.8	0.7	1.66	2.23	0.282371	0.282778
ACO-12-57	54	0.28218671	2.417E-05	0.00261368	0.07699433	555	0.282160	-9.8	0.9	1.57	2.09	0.282435	0.282851
ACO-12-57	55	0.28219266	2.377E-05	0.0015651	0.0432116	645	0.282174	-7.2	0.8	1.52	1.99	0.282378	0.282786
ACO-12-57	57	0.281948	2.031E-05	0.00074601	0.01988982	594	0.281940	-16.7	0.7	1.82	2.52	0.282411	0.282823
ACO-12-57	62	0.28163991	2.361E-05	0.00191993	0.04700939	1008	0.281603	-19.3	0.8	2.32	3.04	0.282147	0.282522
ACO-12-57	70	0.28191058	1.845E-05	0.00186317	0.0507498	1033	0.281874	-9.1	0.7	1.93	2.38	0.282131	0.282504
ACO-12-57	71	0.2820975	1.52E-05	0.00030084	0.00722719	589	0.282094	-11.3	0.5	1.60	2.19	0.282414	0.282827
ACO-12-57	73	0.28119862	1.543E-05	0.00091694	0.02642121	1873	0.281166	-15.1	0.5	2.86	3.45	0.281591	0.281886
ACO-12-57	75	0.28171646	1.729E-05	0.00141518	0.03797429	969	0.281691	-17.1	0.6	2.18	2.90	0.282172	0.282551
ACO-12-57	80	0.28198048	1.735E-05	0.00126646	0.03997558	987	0.281957	-7.2	0.6	1.80	2.28	0.282161	0.282538
G7	a08	0.28214613	1.764E-05	9.4727E-05	0.00316515	595.6	0.282145	-9.4	0.6	1.52	2.08	0.282410	0.282822
G7	a10	0.28107313	1.63E-05	0.00019297	0.00569257	2623	0.281063	-1.3	0.6	2.97	3.20	0.281101	0.281326
G7	a14	0.28183351	3.495E-05	0.00321538	0.09377483	923.7	0.281778	-15.0	1.2	2.12	2.68	0.282201	0.282584
G7	a15	0.28179188	2.548E-05	0.00257835	0.07606389	1033	0.281742	-13.8	0.9	2.14	2.70	0.282132	0.282504
G7	a20	0.281898	1.942E-05	0.0005078	0.01364169	1035	0.281888	-8.6	0.7	1.88	2.37	0.282130	0.282503
G7	a21	0.28167252	2.461E-05	0.00324043	0.08533716	1019	0.281610	-18.8	0.9	2.35	3.02	0.282141	0.282514
G7	a22	0.2820034	1.849E-05	0.0006541	0.01786716	1288	0.281987	0.7	0.7	1.74	2.01	0.281968	0.282317
G7	a26	0.28223104	1.752E-05	0.00063313	0.01814162	599.8	0.282224	-6.5	0.6	1.43	1.90	0.282407	0.282819
G7	a30	0.2820877	2.108E-05	0.00083277	0.02493533	1358	0.282066	5.1	0.7	1.63	1.80	0.281923	0.282266
G7	a31	0.28204499	2.358E-05	0.00055202	0.01569445	1067	0.282034	-2.7	0.8	1.68	2.00	0.282110	0.282479
G7	a33	0.28198479	2.886E-05	0.00070447	0.0193149	1024	0.281971	-5.9	1.0	1.77	2.17	0.282137	0.282511
G7	a35	0.28088513	2.129E-05	0.00058511	0.01689925	2518	0.280857	-11.1	0.8	3.25	3.72	0.281169	0.281404
G7	a36	0.28120958	1.967E-05	0.00070905	0.02223145	2055	0.281182	-10.3	0.7	2.83	3.30	0.281472	0.281751
G7	a37	0.28238671	2.329E-05	0.0011094	0.02803306	916.9	0.282368	5.7	0.8	1.23	1.41	0.282206	0.282589
G7	a39	0.28206219	2.112E-05	0.00103882	0.03282065	1019	0.282042	-3.5	0.7	1.68	2.01	0.282141	0.282515
G7	a40	0.28199641	2.121E-05	0.00073924	0.02044894	1024	0.281982	-5.5	0.8	1.76	2.18	0.282137	0.282510
G7	a50	0.28100092	2.658E-05	0.00047197	0.01242971	2656	0.280977	-3.6	0.9	3.09	3.37	0.281079	0.281301
G7	a51	0.28221535	3.976E-05	0.00128016	0.03542881	1056	0.282190	2.6	1.4	1.47	1.72	0.282117	0.282488
G7	a58	0.28192795	2.548E-05	0.00072818	0.0215935	904.4	0.281916	-10.6	0.9	1.85	2.40	0.282213	0.282598
G7	a62	0.28235726	1.876E-05	0.00041323	0.01153313	856.4	0.282351	3.8	0.7	1.25	1.45	0.282244	0.282633
G7	a65	0.28204302	1.615E-05	0.0006204	0.01732525	1033	0.282031	-3.6	0.6	1.69	2.08	0.282132	0.282504
G7	a66	0.28092837	1.664E-05	0.0010321	0.0296896	2609	0.280877	-8.3	0.6	3.23	3.62	0.281109	0.281336
G7	**a07**	0.28228232	2.192E-05	0.00061131	0.01681061	**748.4**	0.282274	-1.4	0.8	1.36	1.67	0.282313	0.282711
G7	**a18**	0.2819438	2.408E-05	0.00178333	0.05121033	**868.8**	0.281915	-11.4	0.9	1.88	2.42	0.282236	0.282624
G7	**a19**	0.28092886	1.518E-05	0.00037299	0.01004131	**2625**	0.280910	-6.7	0.5	3.18	3.54	0.281099	0.281324
G7	**a24**	0.28203519	1.625E-05	0.00061428	0.01668021	**1077**	0.282023	-2.9	0.6	1.70	2.06	0.282104	0.282472
G7	**a25**	0.28191395	1.79E-05	0.00064822	0.01733451	**1007**	0.281902	-8.7	0.6	1.86	2.38	0.282148	0.282523
G7	**a32**	0.28217504	3.084E-05	0.00043339	0.01204268	**1087**	0.282166	2.5	1.1	1.50	1.75	0.282097	0.282464
G7	**a35**	0.28230024	1.507E-05	0.00032151	0.01011882	**705.7**	0.282296	-1.6	0.5	1.32	1.66	0.282340	0.282742
G7	**a38**	0.2815762	1.664E-05	6.6676E-05	0.00192617	**604.9**	0.281575	-29.3	0.6	2.29	3.29	0.282404	0.282815
G7	**a40**	0.28131697	2.046E-05	0.00038986	0.01024723	**2076**	0.281302	-5.6	0.7	2.66	3.00	0.281459	0.281735
G7	**a43**	0.28226432	1.924E-05	0.00075392	0.02143891	**1066**	0.282249	4.9	0.7	1.39	1.56	0.282111	0.282480
G7	**a47**	0.28144896	1.578E-05	0.00048589	0.01282124	**1992**	0.281431	-2.9	0.6	2.49	2.80	0.281514	0.281798
G7	**a57**	0.28139856	2.342E-05	0.0011261	0.03070892	**2035**	0.281355	-4.6	0.8	2.60	2.95	0.281485	0.281765
G7	**a58**	0.28191717	1.833E-05	0.0006648	0.01748574	**1118**	0.281903	-6.2	0.7	1.86	2.31	0.282077	0.282442
G7	**a59**	0.28240048	1.481E-05	0.00042019	0.01177071	**708.3**	0.282395	2.0	0.5	1.19	1.47	0.282338	0.282740
G7	**a62**	0.28232961	1.592E-05	0.00064802	0.01704066	**724.3**	0.282321	-0.3	0.6	1.29	1.62	0.282328	0.282729
G7	**a64**	0.28191784	1.761E-05	0.0006398	0.01649236	**1090**	0.281905	-6.8	0.6	1.86	2.35	0.282095	0.282463
G7	**a65**	0.28158924	1.72E-05	0.00053256	0.01254553	**1041**	0.281579	-19.4	0.6	2.30	3.05	0.282126	0.282498
laz32	a01	0.28188171	1.744E-05	0.00102739	0.02645312	961	0.281863	-11.1	0.6	1.93	2.50	0.282177	0.282556
laz32	a02	0.28174275	1.673E-05	0.00082927	0.02338406	1067	0.281726	-13.6	0.6	2.11	2.71	0.282110	0.282480
laz32	a04	0.28240977	2.078E-05	0.00033787	0.01076823	608	0.282406	0.2	0.7	1.17	1.51	0.282402	0.282813
laz32	a11	0.28191457	2.113E-05	0.00172201	0.04494725	1072	0.281880	-8.0	0.7	1.92	2.38	0.282107	0.282476
laz32	a14	0.2820406	1.53E-05	0.00135498	0.03792574	797	0.282020	-9.3	0.5	1.72	2.24	0.282282	0.282676
laz32	a16	0.28209237	1.24E-05	0.00049324	0.0127634	1070	0.282082	-0.9	0.4	1.61	1.94	0.282108	0.282477
laz32	a24	0.28194625	1.78E-05	0.00122006	0.03302548	992	0.281923	-8.3	0.6	1.85	2.35	0.282158	0.282534
laz32	a26	0.28205817	1.754E-05	0.00050307	0.01340742	854	0.282050	-6.9	0.6	1.66	2.13	0.282246	0.282635
laz32	a27	0.2817392	1.442E-05	0.0011646	0.03042632	642	0.281725	-23.2	0.5	2.13	2.93	0.282380	0.282788
laz32	a37	0.28097281	1.953E-05	0.00039007	0.0084136	1305	0.280963	-35.2	0.7	3.12	4.02	0.281957	0.282305
laz32	a38	0.28186038	2.383E-05	0.00095788	0.02589908	1299	0.281837	-4.4	0.8	1.95	2.34	0.281961	0.282309
laz32	a39	0.28069999	1.517E-05	0.00100806	0.0267573	3280	0.280636	-1.0	0.5	3.54	3.70	0.280666	0.280829
laz32	a44	0.28175757	1.706E-05	0.00054315	0.0144708	1020	0.281747	-13.9	0.6	2.07	2.70	0.282140	0.282513
laz32	a50	0.28230395	1.816E-05	0.00111573	0.03132672	1104	0.282281	6.9	0.6	1.34	1.47	0.282086	0.282452
laz32	a51	0.28192419	1.742E-05	0.00126728	0.03590649	975	0.281901	-9.5	0.6	1.88	2.39	0.282169	0.282547
laz32	a58	0.28102099	1.575E-05	0.00045305	0.01089034	2673	0.280998	-2.5	0.6	3.06	3.28	0.281068	0.281288
laz32	a59	0.28204086	1.756E-05	0.00081254	0.02336195	1067	0.282025	-3.0	0.6	1.70	2.07	0.282110	0.282479
laz32	B13	0.28110271	2.283E-05	0.00042531	0.00915998	2590	0.281082	-1.4	0.8	2.95	3.18	0.281122	0.281351

laz32	b07	0.28187802	2.113E-05	0.00064785	0.01767591	1080	0.281865	-8.4	0.7	1.91	2.40	0.282102	0.282470
laz32	B12	0.28110271	2.283E-05	0.00042531	0.00915998	1090	0.281094	-35.5	0.8	2.95	3.97	0.282095	0.282462
laz32	b21	0.28209806	2.135E-05	0.00074181	0.02265205	1090	0.282083	-0.4	0.8	1.62	1.91	0.282095	0.282462
laz32	b24	0.281516	2.143E-05	0.00201923	0.05092365	1969	0.281440	-3.1	0.8	2.50	2.79	0.281528	0.281815
laz32	b27	0.28139855	2.707E-05	0.00103325	0.02851486	1868	0.281362	-8.2	1.0	2.59	3.03	0.281594	0.281890
laz32	b31	0.28203848	2.295E-05	0.00119982	0.03119761	1046	0.282015	-3.8	0.8	1.72	2.10	0.282123	0.282495
laz32	b35	0.28196555	2.518E-05	0.00136505	0.03842419	1031	0.281939	-6.9	0.9	1.83	2.29	0.282133	0.282505
laz32	b37	0.28218627	2.429E-05	0.00177106	0.05174544	1077	0.282150	1.7	0.9	1.53	1.79	0.282103	0.282472
laz32	b38	0.28242094	2.507E-05	0.00090338	0.03589385	713	0.282409	2.6	0.9	1.17	1.40	0.282335	0.282737
laz32	b43	0.28200299	2.143E-05	0.00155735	0.04079386	1054	0.281972	-5.2	0.8	1.78	2.21	0.282118	0.282489
laz32	b44	0.2810502	1.533E-05	0.00064617	0.0190622	2645	0.281018	-2.4	0.5	3.04	3.29	0.281086	0.281309
laz32	b47	0.28226157	1.937E-05	0.00263376	0.07617016	542	0.282235	-7.4	0.7	1.46	1.91	0.282443	0.282861
laz32	b49	0.28221605	2.207E-05	0.00105529	0.0267189	917	0.282198	-0.3	0.8	1.46	1.79	0.282206	0.282589
laz32	b57	0.28165332	2.585E-05	0.00119565	0.03253486	1035	0.281630	-17.7	0.9	2.25	2.94	0.282130	0.282502
laz32	b59	0.28181986	2.233E-05	0.00131039	0.04147503	590	0.281805	-21.5	0.8	2.03	2.83	0.282413	0.282826
laz32	c07	0.28176706	1.833E-05	0.00124908	0.0354801	1062	0.281742	-13.2	0.7	2.10	2.68	0.282113	0.282483
laz32	c10	0.28200395	2.155E-05	0.00054802	0.01422147	678	0.281997	-12.8	0.8	1.74	2.31	0.282357	0.282762
laz32	c21	0.28200594	2.22E-05	0.00164298	0.04904586	1072	0.281973	-4.7	0.8	1.78	2.15	0.282107	0.282476
laz32	c24	0.28220255	2.801E-05	0.00127301	0.0402091	1970	0.282155	22.3	1.0	1.49	1.21	0.281528	0.281814
laz32	c27	0.28200115	2.095E-05	0.00088998	0.02477094	1863	0.281970	13.2	0.7	1.76	1.69	0.281597	0.281893
laz32	c28	0.2820096	2.604E-05	0.00075711	0.02119246	992	0.281995	-5.7	0.9	1.74	2.12	0.282157	0.282534
pg14	a09	0.28105529	9.362E-05	0.00077592	0.02869643	2518	0.281018	-5.4	3.3	3.04	3.37	0.281169	0.281405
pg14	a10	0.28219664	3.803E-05	0.00074733	0.02015355	643	0.282188	-6.8	1.3	1.48	1.92	0.282380	0.282788
pg14	a23	0.28215036	8.021E-05	0.00113199	0.03075881	958	0.282130	-1.7	2.8	1.56	1.90	0.282179	0.282559
pg14	b01	0.28146078	3.353E-05	0.00162973	0.04638219	1932	0.281401	-5.4	1.2	2.55	2.90	0.281553	0.281842
pg14	b10	0.2822757	4.708E-05	0.00195839	0.04980131	1066	0.282236	4.5	1.7	1.41	1.61	0.282110	0.282480
pg14	b38	0.28208147	5.16E-05	0.00603066	0.19282066	1056	0.281962	-5.5	1.8	1.90	2.22	0.282117	0.282487
pg14	b41	0.28209287	9.724E-05	0.00095278	0.02399005	911	0.282077	-4.7	3.4	1.63	2.01	0.282209	0.282593
pg14	b42	0.28232147	4.196E-05	0.00036879	0.00886474	711	0.282317	-0.7	1.5	1.29	1.64	0.282336	0.282738
pg14	b49	0.28156221	6.253E-05	0.00137292	0.03682502	2106	0.281507	2.4	2.2	2.39	2.55	0.281439	0.281713
pg14	b56	0.28241959	3.662E-05	0.00151471	0.03614551	986	0.282391	8.1	1.3	1.19	1.32	0.282162	0.282539
pg14	b58	0.28158098	5.057E-05	0.00085279	0.02042589	1962	0.281549	0.6	1.8	2.33	2.53	0.281533	0.281820
CZ02	a07	0.28086757	1.563E-05	0.00103885	0.02949274	2745	0.280813	-7.4	0.6	3.31	3.67	0.281020	0.281234
CZ02	a08	0.28105265	1.917E-05	0.00094647	0.02773424	2602	0.281006	-3.9	0.7	3.06	3.35	0.281114	0.281341
CZ02	a10	0.28197802	1.512E-05	0.00058287	0.016956	1016	0.281967	-6.2	0.5	1.77	2.23	0.282142	0.282516
CZ02	a12	0.2820427	1.464E-05	0.00060429	0.0175054	797	0.282034	-8.8	0.5	1.69	2.22	0.282282	0.282676
CZ02	a13	0.28202876	2.232E-05	0.0008466	0.02436306	829	0.282016	-8.7	0.8	1.72	2.16	0.282262	0.282653
CZ02	a14	0.28226314	1.916E-05	0.00160657	0.05624833	695	0.282242	-3.7	0.7	1.42	1.81	0.282347	0.282750
CZ02	a24	0.28091468	2.765E-05	0.00088241	0.02760757	2687	0.280869	-6.7	1.0	3.24	3.59	0.281058	0.281278
CZ02	a32	0.28208769	1.976E-05	0.0007609	0.02349448	926	0.282074	-4.4	0.7	1.63	2.02	0.282200	0.282582
CZ02	a47	0.28220027	1.769E-05	0.00079496	0.02258672	965	0.282186	0.4	0.6	1.48	1.79	0.282175	0.282554
CZ02	a57	0.2825273	2.461E-05	0.00173433	0.05221423	1818	0.282467	29.9	0.9	1.05	0.59	0.281626	0.281926
CZ02	a60	0.28235075	2.603E-05	0.00131134	0.03957065	508	0.282338	-4.5	0.9	1.28	1.71	0.282465	0.282886
CZ02	b03	0.28252755	2.656E-05	0.00061483	0.01923579	588	0.282521	3.8	0.9	1.02	1.27	0.282415	0.282828
CZ02	b07	0.28207845	1.616E-05	0.00145828	0.03812772	1038	0.282050	-2.8	0.6	1.67	2.04	0.282128	0.282500
CZ02	b08	0.28167115	1.993E-05	0.00097994	0.0267529	1006	0.281653	-17.6	0.7	2.22	2.91	0.282149	0.282524
CZ02	b10	0.28227215	2.764E-05	0.00133032	0.03581937	744	0.282254	-2.2	1.0	1.40	1.77	0.282315	0.282714
CZ02	b11	0.28153208	1.753E-05	0.00037822	0.01001944	1008	0.281525	-22.1	0.6	2.37	3.18	0.282147	0.282522
CZ02	b20	0.2822322	1.899E-05	0.0005127	0.01659508	603	0.282226	-6.3	0.7	1.42	1.91	0.282405	0.282817
CZ02	b24	0.28186672	2.986E-05	0.00170474	0.06328097	1004	0.281834	-11.2	1.1	1.98	2.53	0.282150	0.282525
CZ02	b25	0.2824692	2.532E-05	0.00097226	0.02891627	799	0.282455	6.2	0.9	1.11	1.29	0.282280	0.282674
CZ02	b31	0.28215094	2.252E-05	0.00049638	0.01235596	641	0.282145	-8.4	0.8	1.53	2.07	0.282381	0.282789
CZ02	b35	0.28166268	1.778E-05	0.00063233	0.01707153	910	0.281652	-19.8	0.6	2.21	2.96	0.282210	0.282593
CZ02	b37	0.28241012	9.584E-06	0.00023767	0.00645063	674	0.282407	1.7	0.3	1.17	1.46	0.282360	0.282765
CZ02	b42	0.28202699	2.11E-05	0.00145318	0.04241087	1029	0.281999	-4.8	0.7	1.75	2.12	0.282134	0.282507
CZ02	b49	0.28199616	1.996E-05	0.00048721	0.01361504	1018	0.281987	-5.5	0.7	1.74	2.18	0.282141	0.282515
CZ02	b53	0.28115354	1.882E-05	0.00055266	0.01548917	1859	0.281134	-16.5	0.7	2.89	3.54	0.281599	0.281896
CZ02	b60	0.28173141	2.051E-05	0.00255321	0.06651218	1013	0.281683	-16.4	0.7	2.22	2.80	0.282144	0.282519
CZ02	c04	0.2821547	1.59E-05	0.00099662	0.02876852	760	0.282140	-5.8	0.6	1.55	2.01	0.282306	0.282703
CZ02	c09	0.28187434	1.52E-05	0.00071796	0.02117248	1742	0.281851	6.2	0.5	1.92	2.03	0.281676	0.281983
CZ02	c10	0.28136295	2.034E-05	0.0011016	0.03333727	614	0.281350	-37.1	0.7	2.65	3.76	0.282398	0.282809
CZ02	c12	0.28199414	1.859E-05	0.00139566	0.04166134	1074	0.281966	-4.9	0.7	1.79	2.16	0.282105	0.282474
CZ02	c16	0.28228175	1.993E-05	0.00129207	0.03285421	1061	0.282256	5.0	0.7	1.38	1.55	0.282114	0.282484
CZ02	c17	0.28141461	2.82E-05	0.0012304	0.03328384	1970	0.281369	-5.7	1.0	2.58	2.95	0.281528	0.281814
CZ02	c18	0.28146905	2.112E-05	0.00094822	0.02854465	2067	0.281433	-2.5	0.8	2.49	2.78	0.281504	0.281787
CZ02	c19	0.28175478	2.126E-05	0.00125338	0.03491829	1077	0.281729	-13.3	0.8	2.12	2.75	0.282103	0.282472
CZ02	B50	0.28185712	1.921E-05	0.0006759	0.01787886	1380	0.281840	-2.5	0.7	1.94	2.30	0.281909	0.282250
OD4	a03	0.28237589	1.929E-05	0.00056268	0.01635654	569	0.282370	-2.0	0.7	1.22	1.62	0.282427	0.282841
OD4	a08	0.28239928	1.5E-05	0.00065037	0.01681216	529	0.282393	-2.1	0.5	1.19	1.53	0.282452	0.282870
OD4	a14	0.28213529	1.915E-05	0.00080396	0.02279782	573	0.282127	-10.5	0.7	1.57	2.15	0.282424	0.282838
OD4	a19	0.28100256	2.025E-05	0.00055255	0.01533219	2518	0.280976	-6.9	0.7	3.09	3.47	0.281169	0.281405
OD4	a24	0.28224473	1.707E-05	0.00082189	0.0235578	588	0.282236	-6.3	0.6	1.42	1.91	0.282415	0.282828
OD4	a30	0.28243497	2.825E-05	0.00093604	0.03263449	737	0.282422	3.6	1.0	1.15	1.40	0.282320	0.282720
OD4	b18	0.28238232	1.784E-05	0.00043916	0.01152873	553	0.282378	-2.1	0.6	1.21	1.61	0.282437	0.282853
OD4	b46	0.28241854	2.469E-05	0.00122315	0.03220778	680	0.282403	1.7	0.9	1.19	1.44	0.282356	0.282761
OD4	b49	0.2825782	2.108E-05	0.00108993	0.02659444	609	0.282566	5.8	0.7	0.96	1.16	0.282401	0.282812
OD4	c02	0.2817606	2.03E-05	0.00039221	0.00991749	2507	0.281742	20.1	0.7	2.06	1.77	0.281177	0.281413
OD4	c04	0.28253682	2.263E-05	0.00119732	0.02810143	564	0.282524	3.3	0.8	1.02	1.28	0.282430	0.282845
OD4	c06	0.28245495	2.207E-05	0.00079295	0.02006466	799	0.282443	5.8	0.8	1.12	1.32	0.282281	0.282675
OD4	c07	0.28255648	2.67E-05	0.00094389	0.02375808	766	0.282543	8.5	0.9	0.98	1.11	0.282302	0.282698
OD4	c21	0.2821424	1.794E-05	0.00019759	0.00700322	661	0.282140	-8.1	0.6	1.53	2.07	0.282368	0.282775
OD4	c27	0.28260664	1.751E-05	0.00105927	0.03044204	658	0.282594	7.9	0.6	0.92	1.07	0.282370	0.282777
OD4	c42	0.28225431	2.104E-05	0.00078954	0.0218699	644	0.282245	-4.8	0.7	1.40	1.83	0.282379	0.282787
OD4	c44	0.2822703	2.104E-05	0.00042355	0.01056823	817	0.282264	-0.2	0.7	1.37	1.69	0.282269	0.282661
OD4	c47	0.2823138	2.896E-05	0.00043736	0.00957595	1084	0.282305	7.3	1.0	1.31	1.44	0.282099	0.282467

OD4	c58	0.28176452	2.535E-05	0.00126961	0.03570418	1000	0.281741	-14.6	0.9	2.10	2.73	0.282152	0.282528
OD4	c15	0.28181925	2.793E-05	0.00077785	0.02037747	937	0.281806	-13.7	1.0	2.00	2.62	0.282193	0.282574
OD4	c24	0.28194211	1.981E-05	0.0011581	0.03587724	936	0.281922	-9.6	0.7	1.85	2.38	0.282194	0.282575
OD4	c34	0.2819854	1.857E-05	0.00079055	0.02437752	960	0.281971	-7.3	0.7	1.77	2.17	0.282178	0.282557
OD4	c37	0.28246881	1.88E-05	0.00057136	0.01357915	819.4	0.282460	6.8	0.7	1.10	1.24	0.282268	0.282660
OD4	c38	0.28064905	2.203E-05	0.00061263	0.01400612	3238	0.280611	-2.9	0.8	3.57	3.81	0.280693	0.280860
OD4	c51	0.28097518	2.508E-05	0.00039721	0.0106538	2640	0.280955	-4.8	0.9	3.12	3.43	0.281089	0.281313
0D5	a03	0.28191235	2.108E-05	0.00089718	0.02377069	967	0.281896	-9.8	0.7	1.88	2.41	0.282173	0.282552
0D5	a08	0.28164834	2.414E-05	0.00084464	0.02461994	1071	0.281631	-16.9	0.9	2.24	2.83	0.282107	0.282476
0D5	a14	0.28191383	3.514E-05	0.00134706	0.03464968	952	0.281890	-10.4	1.2	1.90	2.38	0.282183	0.282563
0D5	a19	0.28107467	4.035E-05	0.00080296	0.02104338	2620	0.281034	-2.4	1.4	3.02	3.28	0.281102	0.281328
0D5	a24	0.28156736	3.009E-05	0.00045355	0.01092045	2081	0.281549	3.3	1.1	2.33	2.48	0.281456	0.281732
0D5	a30	0.28266445	1.718E-05	0.00092491	0.02399371	611.7	0.282654	9.0	0.6	0.83	0.96	0.282399	0.282810
0D5	b18	0.28175977	2.463E-05	0.00082733	0.01980667	1023	0.281744	-14.0	0.9	2.09	2.72	0.282138	0.282512
0D5	b26	0.28243155	2.28E-05	0.00092783	0.0206334	919	0.282416	7.5	0.8	1.16	1.30	0.282204	0.282587
0D5	b46	0.28260013	2.034E-05	0.00133139	0.03290888	663.6	0.282584	7.7	0.7	0.93	1.08	0.282367	0.282773
0D5	b49	0.28247562	1.557E-05	0.00057899	0.01532773	766.3	0.282467	5.9	0.6	1.09	1.28	0.282301	0.282698
0D5	c02	0.28262584	2.006E-05	0.00068999	0.01448509	943	0.282614	15.1	0.7	0.88	0.85	0.282189	0.282569
0D5	c04	0.28226368	2.011E-05	0.00070871	0.01890967	558.8	0.282256	-6.3	0.7	1.39	1.86	0.282433	0.282849
0D5	c06	0.28245816	2.169E-05	0.00223933	0.05810718	2817	0.282337	48.6	0.8	1.16	0.16	0.280972	0.281179
0D5	c07	0.28263639	7.316E-05	0.00143129	0.03701881	1048	0.282608	17.2	2.6	0.88	0.80	0.282122	0.282493
0D5	c21	0.28056907	0.0010807	0.00191776	0.0519212	806.6	0.280540	-61.5	38.5	3.80	5.39	0.282276	0.282669
0D5	c27	0.28212564	4.348E-05	0.00108476	0.02614239	1951	0.282085	19.4	1.5	1.59	1.37	0.281540	0.281828
0D5	c42	0.282316	2.279E-05	0.00096827	0.02825626	599	0.282305	-3.6	0.8	1.32	1.73	0.282408	0.282820
0D5	c44	0.28212122	2.095E-05	0.00145776	0.03675836	878.5	0.282097	-4.7	0.7	1.61	2.02	0.282230	0.282617
0D5	c47	0.28245772	2.831E-05	0.002135	0.05864668	1011	0.282417	9.6	1.0	1.16	1.24	0.282146	0.282520
0D5	c58	0.28221192	2.239E-05	0.00112443	0.03382177	1134	0.282188	4.3	0.8	1.47	1.67	0.282067	0.282430
0D5	d07	0.28225195	6.874E-05	0.00142862	0.03893696	634.1	0.282235	-5.3	2.4	1.43	1.88	0.282385	0.282794
0D5	d09	0.28262448	1.919E-05	0.001328	0.03945232	692.1	0.282607	9.2	0.7	0.90	1.01	0.282349	0.282752
0D5	d11	0.28201057	2.415E-05	0.00062061	0.01773342	602	0.282004	-14.2	0.9	1.73	2.31	0.282406	0.282817
0D5	d12	0.2821214	1.929E-05	0.0018988	0.05683318	917	0.282089	-4.1	0.7	1.63	2.02	0.282205	0.282589
0D5	d15	0.28099324	2.928E-05	0.00054371	0.01645056	2455	0.280968	-8.7	1.0	3.10	3.53	0.281211	0.281452
0D5	d50	0.28247527	4.968E-05	0.00132322	0.03271875	990	0.282451	10.3	1.8	1.11	1.18	0.282159	0.282535
0D5	d53	0.28260561	2.708E-05	0.00078873	0.02075681	674.9	0.282596	8.4	1.0	0.91	1.06	0.282359	0.282765

Chapter 3

This chapter is submitted as:

Henderson B.J, Collins, W.J, Murphy, J.B, Hand, M, 2016, A hafnium isotopic record of magmatic arcs and continental growth in the Iapetus Ocean: the contrasting evolution of Ganderia and the peri-Laurentian margin, Gondwana Research

Statement of Authorship

Title of Paper	A hafnium isotopic record of magmatic arcs and continental growth in the Iapetus Ocean: the contrasting evolution of Ganderia and the peri-Laurentian margin
Publication Status	☐ Published ☐ Accepted for Publication ☒ Submitted for Publication ☐ Unpublished and Unsubmitted w ork w ritten in manuscript style
Publication Details	Henderson, B., Collins, W.J., Murphy, B.J., Hand, M., *in review*. A hafnium isotopic record of magmatic arcs and continental growth in the Iapetus Ocean: the contrasting evolution of Ganderia and the peri-Laurentian margin, Gondwana research

Principal Author

Name of Principal Author (Candidate)	Bonnie Henderson
Contribution to the Paper	Sample collection, U-Pb and Hafnium zircon analysis, data interpretation, manuscript and figure composition
Overall percentage (%)	85%
Certification:	This paper reports on original research I conducted during the period of my Higher Degree by Research candidature and is not subject to any obligations or contractual agreements with a third party that would constrain its inclusion in this thesis. I am the primary author of this paper.
Signature	Date: 05/04/2016

Co-Author Contributions

By signing the Statement of Authorship, each author certifies that:

i. the candidate's stated contribution to the publication is accurate (as detailed above);

ii. permission is granted for the candidate in include the publication in the thesis; and

iii. the sum of all co-author contributions is equal to 100% less the candidate's stated contribution.

Name of Co-Author	W.J. Collins
Contribution to the Paper	Project design, data interpretation and manuscript revisions
Signature	Date: 5/4/2016

Name of Co-Author	J. Brendan Murphy
Contribution to the Paper	Assistance with sample collection and manuscript revisions
Signature	Date: April 5 2016

Name of Co-Author	Martin Hand
Contribution to the Paper	Manuscript revisions
Signature	Date: 6-4-2016

Name of Co-Author	
Contribution to the Paper	
Signature	Date:

A hafnium isotopic record of magmatic arcs and continental growth in the Iapetus Ocean: the contrasting evolution of Ganderia and the peri-Laurentian margin

ABSTRACT

We test the sensitivity of combined U-Pb-Hf isotopic analyses of detrital and magmatic zircons to document complex processes in accretionary orogens, using Ganderia from the Canadian Appalachian orogen as an example. Ganderia hosted a long-lived magmatic arc that began at least by 650 Ma and continued until 450 Ma, but its isotopic record reveals distinct links to Avalonia, suggesting it began earlier, possibly at ~750 Ma. The U-Pb-Hf zircon isotopic array suggests that Ganderia formed on a sliver of "Grenvillian-type" basement (TDMc = 2.2-1.1 Ga). A transition toward more evolved Hf isotopic compositions between 650-600 Ma coincides with its accretion to the Gondwanan margin, consistent with other geological evidence. This was followed by increasing amounts of juvenile crustal inputs between ~550-500 Ma, which is interpreted to reflect subduction roll-back from the Gondwanan margin. Trench retreat culminated in the separation of the Ganderia arc and formation of the exclusively oceanic ~510-450 Ma Penobscot-Popelogan-Victoria arcs on Ganderia. Accretion of Ganderia to the active Notre Dame Subzone along the Laurentian margin occurred in the late Ordovician and is marked by the abrupt termination of Ganderian arc magmatism.

The Notre Dame arc evolved along the Laurentian margin between ~515-430 Ma, and was built on Archean (T(DM)c = 2.5-2.9 Ga) crust. Suprasubduction zone magmatism occurred at ~490-460 Ma during the closure of the Taconic Seaway and was dominated by the recycling of Laurentian crust, with progressive mixing of evolved and juvenile arc magmas over time. The preservation of very evolved Notre Dame arc zircons in Ganderian overstep sequences confirm the arrival of the leading edge of Ganderia to Laurentia by ~450 Ma. The hafnium isotopic method is proven here to be a powerful tool when used in conjunction with geological constraints, and is able to identify the changing nature of magmatism during the evolution of complex accretionary systems.

1. INTRODUCTION

In recent years, a plethora of studies have utilised U-Pb-Hf isotopes in zircon to focus on the link between U-Pb crystallisation age and Hf isotopic evolution of zircon in relation to with the timing of magmatic events (e.g. Griffin et al., 2004; Batumike et al., 2009; Belousova et al., 2009; Mišković and Schaltegger, 2009) and growth of the continental crust (e.g. Blichert-Toft and Albarède, 1997; Kemp et al., 2007; Amelin et al., 2010; Belousova et al., 2010).

Hafnium isotopes in detrital zircon are also proving extremely useful for provenance studies as they provide a further dimension to U-Pb zircon age data (e.g. Sevastjanova et al., 2011; Zlatkin et al., 2013; Henderson et al., 2016). However, few studies have tested the sensitivity of the combined U-Pb-Hf isotopic approach in documenting accretionary orogenic processes, e.g. the rifting and migration of a geological terrane from its cratonic home, to its transfer to a foreign craton in an accretionary environment. As accretionary orogenic processes are fundamental to understanding the evolution of the continental crust (Collins, 2002; Cawood and Buchan, 2007; Cawood et al., 2009), the combined U-Pb-Hf isotopic approach has the potential to provide first-order insights into such processes.

Ganderia, a terrane of the Canadian Appalachians (Fig. 1), was transferred from Gondwana to Laurentia during the Paleozoic. All major stages in this transfer have been

documented (e.g. van Staal et al., 1998; van Staal et al., 2009; van Staal et al., 2012) and so Ganderia is an ideal terrane to test the sensitivity of the combined U-Pb-Hf isotopic approach. Ganderia occupied a location along the northern Gondwanan margin in the late Neoproterozoic-early Paleozoic, prior to transfer as an active arc across the Iapetus Ocean to the Notre Dame Subzone on the Laurentian margin in the late Ordovician. Newfoundland exposes vestiges of the peri-Laurentian margin, the Iapetan oceanic realm and the Ganderian terrane. It therefore provides a unique opportunity to investigate the sensitivity of the zircon hafnium isotopic method during continental ribbon transfer across an oceanic basin; from birth along an active margin, through to rifting and accretion to a continental margin.

In this paper, we present U-Pb detrital and magmatic zircon geochronology and hafnium isotopes in zircon from late Neoproterozoic to Silurian sedimentary and magmatic rocks from the Ganderia terrane and peri-Laurentian Notre Dame Subzone in Newfoundland. We find that combined U-Pb-Hf isotopic methods not only distinguish the different phases of arc-related magmatism in Ganderia, they reveal the contrasting nature of magmatism in peri-Laurentia, and provide additional insights into the waxing and waning of juvenile versus ancient crust contributions to magmatism during accretionary processes. The combined U-Pb-Hf isotopic data presented here are used to propose a revised geodynamic model for the early history of Ganderia.

2. GEOLOGICAL FRAMEWORK

The north-eastern section of the Appalachian-Caledonian orogen is composed of deformed Laurentian crust and a collage of exotic terranes, collectively termed the 'peri-Gondwanan' terranes (Pollock et al., 2011). The peri-Gondwanan terranes (Avalonia, Ganderia, Cadomia, Carolina ± Meguma) are continental ribbons interpreted to originate along the northern margin of Amazonia and North Africa in the Neoproterozoic (Nance and Murphy, 1994; O'Brien et al., 1996; Keppie et al., 2003; Murphy et al., 2004). During the opening and closing of the Iapetus and Rheic Oceans, the peri-Gondwana terranes are purported to have been transferred from the Gondwanan margin to the Baltican/Laurussian margin (van Staal et al., 1998; Murphy and Keppie, 2005; Pollock et al., 2011). Closure of the Rheic Ocean was accompanied by continental collision between Gondwana and Laurussia forming the Appalachian-Variscan Orogen of North America and western Europe (Scotese, 2004; Hibbard et al., 2010; Stampfli et al., 2013).

Ganderia consists of several distinct, but tectonically related terranes, which form the most inboard of the peri-Gondwanan terranes along the Laurentian margin. Ganderian fragments are now thought to be located in New Brunswick, Cape Breton and Newfoundland in Maritime Canada, and New England in the USA (Fig. 1). Across the Atlantic Ocean, they are also recognised in southern Ireland and central Britain (Waldron et al., 2014), and are interpreted to form parts of the southern Carpathians (Balintoni et al., 2014). However detailed geochemical, geological and isotopic studies of the Ganderian terrane have provided insight into the evolution of Ganderia prior to, and during, the transfer across the Iapetus Ocean and subsequent accretion to Laurentia (Holdsworth, 1994; van Staal, 1994; van Staal et al., 1996; Schofield and D'Lemos, 2000; Rogers et al., 2006; Pollock et al., 2007; Zagorevski et al., 2007; Zagorevski et al., 2010; van Staal et al., 2012; Barr et al., 2014; Kellett et al., 2014). The evolution of the Ganderia during the late Neoproterozoic-early Silurian interval is complex and involves the generation of two successive magmatic arcs and associated back arc systems (~515-485 Ma, 478-450 Ma), separated by a brief hiatus, and multiple deformation events associated with the docking of Ganderia with Laurentia (van Staal et al., 2009).

The late Neoproterozoic

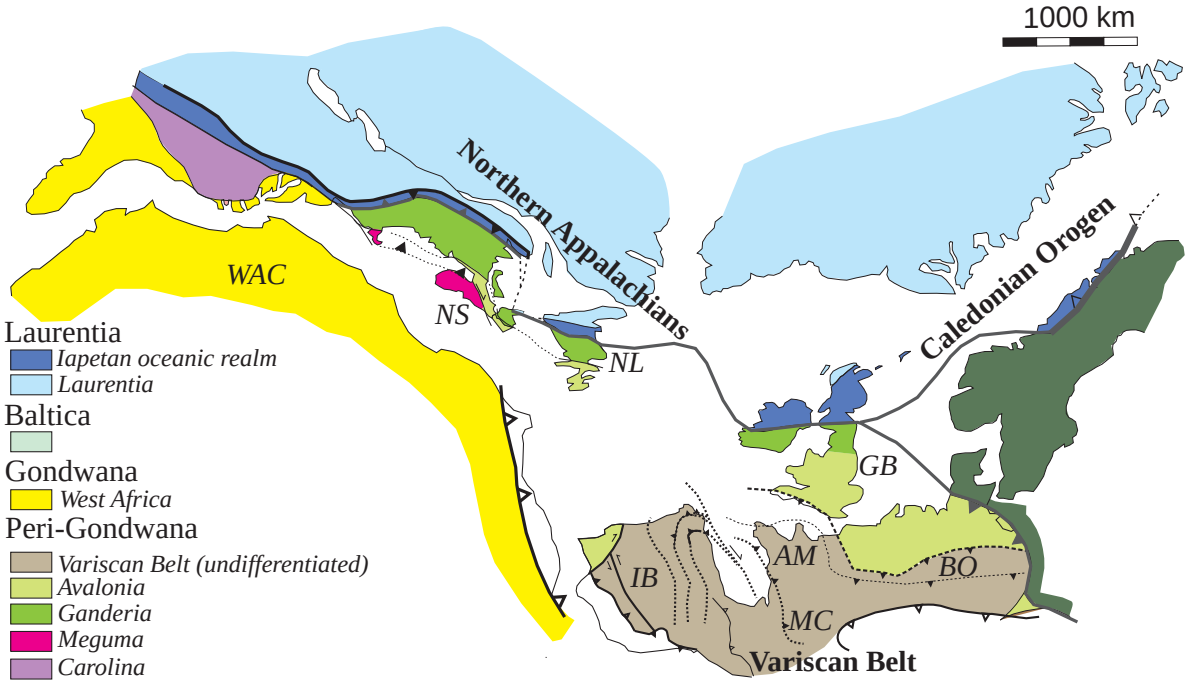

Figure 1

Tectonic map showing the distribution of the Appalachian, Variscan and Caledonian belts at the end of the Paleozoic. Shown are the major cratonic and microcontinental components within the orogenic belts including Iberia (IB), Amorican Massif (AM), Massif Centrale (MC), Bohemian Massif (BO) and the West African Craton (WAC). This represents the approximate configuration of Pangea following late Paleozoic convergence between Laurentia and Gondwana. The figure is modified from Hibbard et al., (2007), Barreiro et al. (2007), Keppie et al., (2008) and Pollock et al., (2011).

paleogeography of Ganderia is poorly constrained, but the terrane is commonly considered to have been located somewhere along the Amazonian margin (Nance et al., 2008; Fyffe et al., 2009; van Staal et al., 2012). Detrital zircon populations in late Neoproterozoic-Cambrian Ganderian rocks (Fyffe et al., 2009; van Staal et al., 2012; Barr et al., 2014; Waldron et al., 2014; Willner et al., 2014) are dominated by Mesoproterozoic (1.0-1.2 Ga, 1.5 Ga), Paleoproterozoic (~1.7-2.2 Ga) and minor Archean (~2.5-3.1 Ga) peaks. Mesoproterozoic rocks are abundant in the Rondonian- San Ignacio (1.5-1.3 Ga) and Sunsas (1.25-1.0 Ga) orogenic belts of Amazonia and provide an plausible source for the dominant detrital populations in Ganderian rocks. Evidence for a major transgression in the Middle Cambrian autochthonous cover of Columbia suggests the departure of a major crustal fragment (Ramos, 2009), which is coeval with the ~509-505 Ma bimodal rift-related volcanism and the deposition of transgressive middle to upper Cambrian black shales in Ganderia (White et al., 1994; Schulz et al., 2008). On the basis of these lines of evidence van Staal et al., (2012) suggest that Ganderia was located along the paleo-Caribbean (Amazonian) margin in the early Paleozoic.

2.1 Ganderian geology in the Canadian Appalachians

The oldest Ganderian rocks are found in New Brunswick and include a 978 ± 7 Ma alkalic anorthosite (Tesfai, 2011), the stromatolite-bearing carbonates and quartzites of the Cryogenian Green Head Group in New Brunswick (Barr et al., 2003a; Barr et al., 2014) and Cryogenian (minimum age) Seven Hundred Acre Island Formation in coastal Maine (Stewart et al., 2001). Detrital zircon populations in the lower unit of the Green Head Group (Ashburn Formation)

cluster between ~1200-2000 Ma with minor Archean grains (2.5-3.0 Ga) and provide a maximum depositional age of ~1230 Ma (Barr et al., 2003a; Barr et al., 2014). The upper unit of the Green Head Group (Martinon Formation) yields similar Mesoproterozoic-Paleoproterozoic populations in addition to younger Neoproterozoic peaks (~1.0 Ga, 0.8-0.6 Ga) (Barr et al., 2014). The Seven Hundred Acre Island Formation is constrained to a minimum deposition age of ~0.7 Ga based on 40Ar/39Ar ages of hornblende in amphibolite facies rocks (Stewart et al., 2001).

The earliest evidence of Ediacaran magmatic arc activity is only found in the Brookville and New River terranes of southern New Brunswick (~652 Ma, Lingley Suite, Currie and McNicoll, 1999; ~622 Ma, Blacks Harbour Granite, Barr et al., 2003b), whereas the younger phase (~580-540 Ma) is more abundant and widespread across Ganderia. In Newfoundland, this younger phase is represented by the Roti Suite (~578-564 Ma, Kerr et al., 1995) and Cripple Back Granite (~565 Ma, Rogers et al., 2006), in Cape Breton the plutonic suites of the Bras d'Or terrane (Barr et al., 1990)(~565-555 Ma), and in New Brunswick the Simpsons Island Formation (539 ± 4 Ma, Barr et al., 2003b) and the Golden Grove Plutonic Suite (553-527 Ma, White et al., 2002; Barr et al., 2014). Coeval volcanic sequences of the Sandy Brook Group (565 Ma, Rogers et al., 2006) in Newfoundland record continental-arc type geochemistry. The younger phase of magmatism is also associated with metamorphism and deformation variably dated between ~570-540 Ma (see Nance et al., 2008 and references therein).

The Middle Cambrian to early Ordovician in Ganderia is also marked by arc magmatism and the concurrent deposition of clastic sedimentary rocks (van Staal et al., 1998; Hibbard et al., 2010; van Staal and Barr, 2011). The juxtaposition of the magmatic activity and clastic sedimentation is explained by the development of an active arc on the outboard edge of Ganderia, with an associated back-arc (Penobscot arc-backarc system), and a trailing passive edge known as the 'Gander margin' (van Staal, 1994). The Cambro-Ordovician arc activity in Ganderia is divided into two virtually consecutive arc systems; the Penobscot arc at ~515-485 Ma, and the Popelogan-Victoria (P-V) arc and associated Tetagouche-Exploits back-arc basin between ~478-450 Ma (van Staal et al., 2009; Zagorevski et al., 2010). In Newfoundland, the Penobscot and P-V arc rocks are restricted to the region between the Red Indian Line in the west and the GRUB line- Day Cove fault system, collectively known as the Exploits Subzone (Fig. 2) (Williams et al., 1988; Williams et al., 1993).

The ~515-485 Ma Penobscot arc is interpreted to have formed in an intra-oceanic setting outboard of the Gander margin above a west-dipping subduction zone (MacLachlan and Dunning, 1998; van Staal et al., 1998; Zagorevski et al., 2007). Inferred ongoing subduction resulted in the collision of the arc system and the obduction of supra-subduction zone ophiolites (Colman-Sadd et al., 1992; Jenner and Swinden, 1993) onto the Gander margin. The apparent collision of the Penobscot arc to the Gander margin is assigned to the Penobscot orogeny at ~485 Ma (van Staal et al., 1998). Subduction reversal heralded the onset of magmatism within the Popelogan-Victoria arc system at ~478 Ma (van Staal et al., 1998; van Staal et al., 2009), which remained active until ~455 Ma, when it was terminated upon arrival to the peri-Laurentian Red Indian Lake arc, thereby closing the main Iapetan Ocean (van Staal and Barr, 2011).

The Gander margin is broadly equivalent to the Gander Zone of Williams (1979), and is coeval with the development of the Penobscot arc. It comprises of a series of Lower Cambrian to Lower Ordovician siliciclastic sequences of arenite, siltstones and shales interpreted to have formed on the outer shelf to slope of a passive margin (Williams et al., 1988; van Staal et al., 1996).

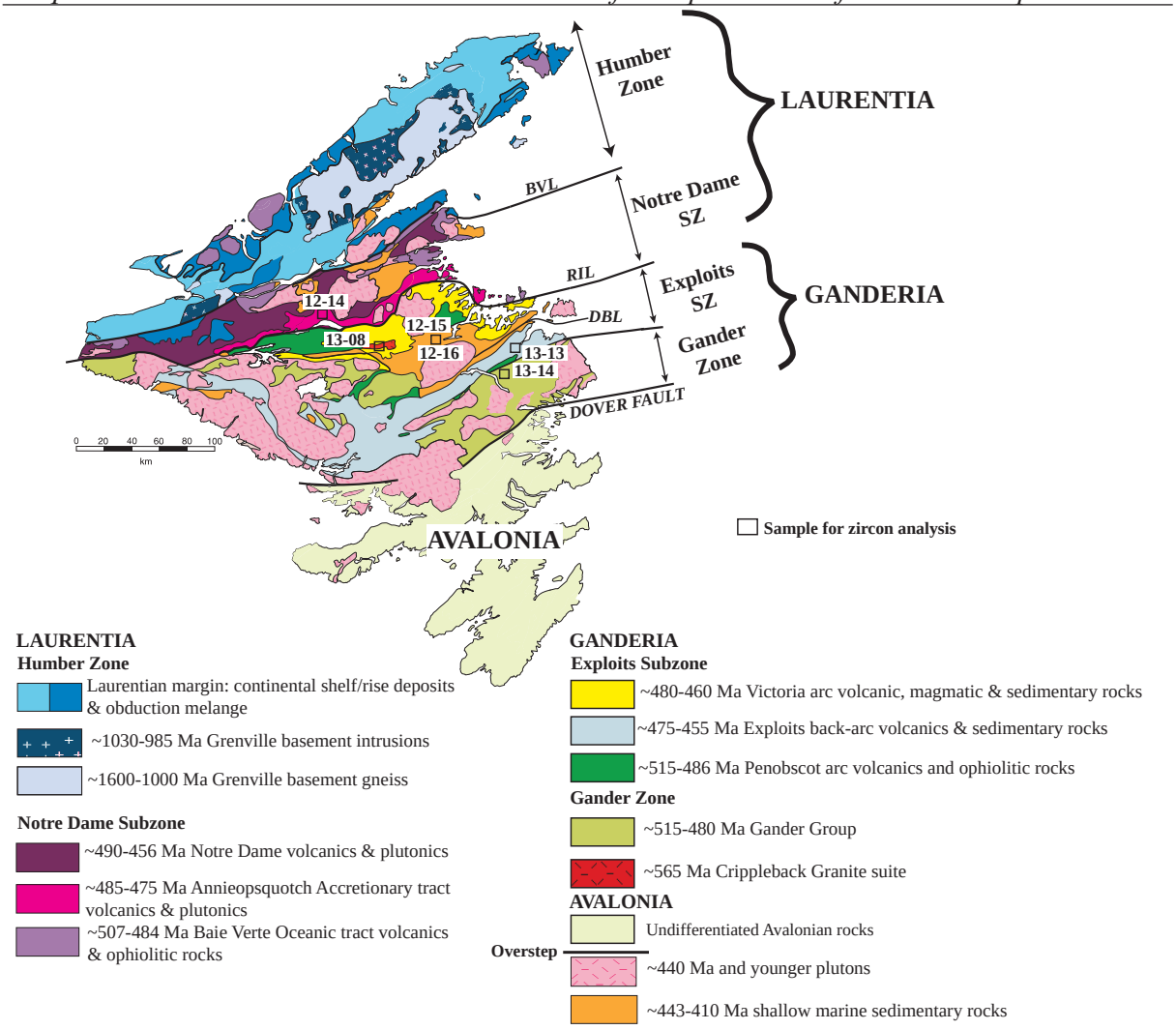

Figure 2

Detailed geology map of Newfoundland, Canada showing the division into the major tectonic terranes of the Appalachian Orogen. Included within "Laurentia" are the Humber Zone and Notre Dame Subzone, and in "Ganderia" the Exploits Subzone and Gander Margin. The Notre Dame Subzone and Exploits Subzones are considered to be the Iapetan Oceanic realms developed on either side of the Iapetus Ocean. Sample locations are shown by the filled white boxes with accompanying sample number. The figure is modified after van Staal et al. (2007), van Staal and Barr (2011) and Piercey et al. (2014). BVL: Baie Verte Line, RIL: Red Indian Line, DBL: Dog Bay Line.

It is uncertain as to whether the Gander margin was deposited on the trailing edge of Ganderia facing Gondwana and/or on the passive margin of the Penobscot back-arc basin (see van Staal, 1994; Zagorevski et al., 2007; Zagorevski et al., 2010; van Staal et al., 2012).

2.2 Ganderia in Newfoundland

A NW-SE transect of the Newfoundland Appalachians includes most of the Laurentian and Gondwanan components involved in the orogen (Fig. 2). From west to east these components are: (i) the Neoproterozoic-early Ordovician Laurentian passive margin (Humber Zone), which includes inliers of the Mesoproterozoic Grenville Province; (ii) the Dunnage Zone (Williams, 1979), which preserves vestiges of the Iapetan oceanic realm including the peri-Laurentian Notre Dame Subzone (NDSz) and the peri-Ganderian Exploits Subzone; and (iii) the Gander margin.

The Gander margin in Newfoundland is composed of predominantly Cambrian-Silurian metasedimentary rocks with metamorphic grade increasing from greenschist to upper amphibolite towards the

Sample Number	Stratigraphic name	Depositional age	Tectonic Affinity	Coordinates (N)	Coordinates (W)
ACO-13-08	Cripple Back Granite	565 Ma (magmatic age)	Ganderia (continental arc)	48°44'29.85"N	56° 8'54.02"W
ACO-13-14	Outflow Formation	~450 Ma	Gander Margin	49°19'43.08"N	54°28'51.55"W
ACO-13-13	Jonathans Pond Formation	~490 Ma	Exploits back-arc basin	49° 1'45.38"N	54°35'56.50"W
ACO-12-15b	Goldson Formation	~440 Ma	Composite Laurentia (Exploits Subzone)	48°57'11.87"N	55°56'46.72"W
ACO-12-16	Wigwam Formation	~420 Ma	Composite Laurentia (Exploits Subzone)	49° 1'38.26"N	55°27'41.81"W
ACO-12-14	Skidder Formation	~455-445 Ma	Notre Dame Subzone	48°46'17.47"N	56°52'51.34"W

Table 1

Sample descriptions for the rocks analysed in the present study.

eastern boundary, marked by the Dover Fault Shear Zone (DFSZ, Fig. 2). The DFSZ is up to 25 km wide and forms a N-NE to NE-SW oriented high strain zone, which marks the surface expression of the tectonic boundary between Ganderia and Avalonia (D'Lemos et al., 1997). The boundary is defined by seismic-reflection studies as a crustal-scale structure that offsets the Moho (Keen et al., 1986; Marillier et al., 1989; Stockmal et al., 1990) . Paragneisses and migmatites of the Square Pond and Hare Bay Gneiss (Schofield and D'Lemos, 2000) exist within the DFSZ. The DFSZ is truncated by the Ackley granite suite, which has a U-Pb zircon crystallisation age of 377 ± 3 Ma (O'Brien et al., 1986; Kerr et al., 1993; Kellett et al., 2014).

2.3 Geology of the peri-Laurentian Notre Dame Subzone

The Notre Dame Subzone (NDSz) preserves remnants of a peri-Laurentian microcontinent (Dashwoods terrane, Waldron and van Staal, 2001) and rocks that record the complex geological evolution of the Taconic Orogeny (~495-450 Ma, van Staal et al., 2007) involving the protracted formation of supra-subduction zone oceanic crust, overprinted by continental arc magmatism and interaction with Laurentian crust (Colman-Sadd et al., 1992; Waldron and van Staal, 2001; Zagorevski et al., 2006). The NDSz is separated from the Humber Zone to the west by the Baie Verte-Brompton Line and to the east from the Exploits Subzone by the Red Indian Line (Fig. 2). The earliest event to affect the Notre Dame Subzone was the protracted opening of the Iapetus Ocean (see Cawood et al., 2001). Rifting and separation from Amazonia at 570 Ma is inferred to herald the opening of Iapetus with a rift-drift phase between ~540-535 Ma (Cawood et al., 2001). A proposed inboard ridge jump from the main oceanic tract of Iapetus led to the opening of the narrow Taconic Seaway (van Staal et al., 2007) at ~540-530 Ma.

The opening of the Taconic Seaway was accompanied by the removal of one or several large microcontinental fragments from the Laurentian margin, the Dashwoods terrane (Waldron and van Staal, 2001; Lissenberg and van Staal, 2002). The Dashwoods terrane formed the basement of the Notre Dame arc (van Staal et al., 2007). Representatives of Taconic oceanic crust include the ~510-495 Ma Lushs Bight Oceanic Tract (LBOT) (Kean et al., 1995) and ~495-489 Ma Baie

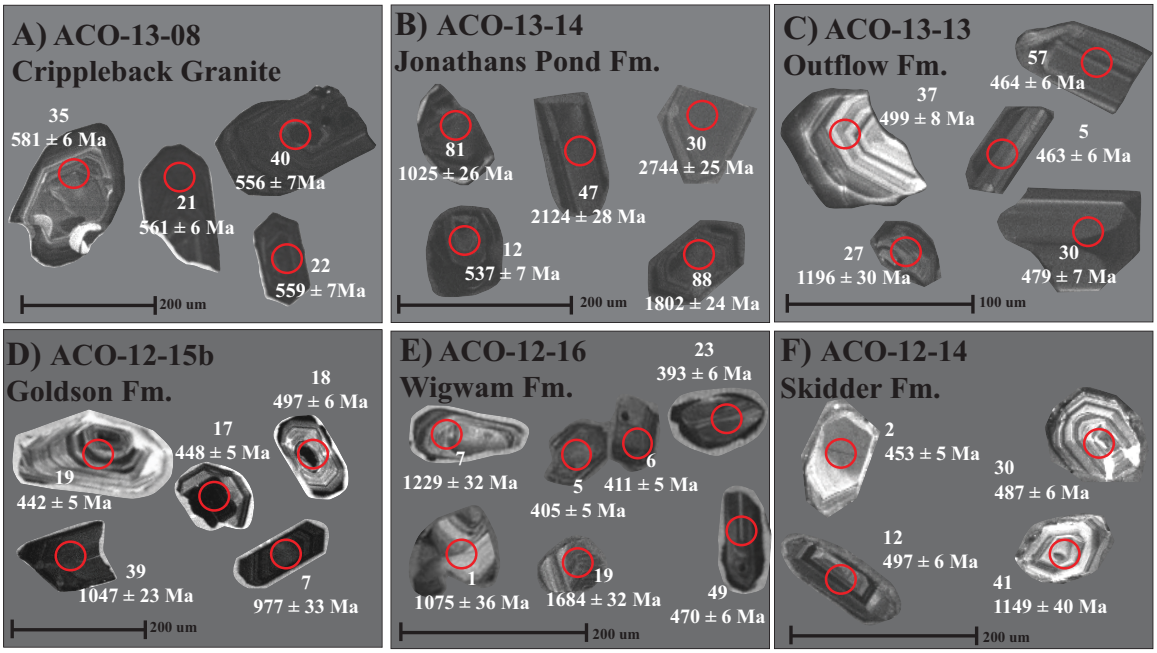

Figure 3

Representative cathodoluminescence images for zircon grains from Ganderia and the Notre Dame Subzone. A) sample ACO-13-08 (Cripple Back Granite) magmatic zircons 35, 21, 40 and 20; B) Sample ACO-13-14 (Jonathans Pond Formation) detrital zircons 81, 12, 47, 30 and 88; C) sample ACO-13-13 (Outflow Formation) detrital zircons 37, 27, 5, 57 & 30; D) sample ACO-12-15b (Goldson Formation) detrital zircons 19, 39, 17, 18 & 7; E) sample ACO-12-16 (Wigwam Formation) detrital zircons 7, 1, 19, 5, 6, 23 & 49; F) sample ACO-12-14 (Skidder Formation) detrital zircons 2, 12, 30 and 41.

Verte Oceanic Tract (BVOT) (Kerr et al., 2008; Skulski et al., 2010). Subduction in the Taconic Seaway led to the formation of the 490-480 supra-subduction BVOT (Dunning and Krogh, 1985; Jenner et al., 1991) in the forearc position of the leading edge of Dashwoods (see van Staal et al., 2007) and initiated the earliest phases of magmatism in the Notre Dame arc (~495-490 Ma) (see Fig. 12.3 in Zagorevski and Van Staal, 2011). Progressive closure of the Taconic seaway between ~488-477 Ma led to the obduction of the BVOT onto the Humber margin, triggering westward dipping subduction in the Iapetus Ocean (see Fig. 12.3 in Zagorevski and Van Staal, 2011) and the development of the supra-subduction zone Annieopsquotch accretionary tract (Zagorevski et al., 2006). Magmatism continued intermittently in the Notre Dame arc until ~435 Ma (van Staal and Barr, 2011).

3. SAMPLE SELECTION

Six samples were collected for U-Pb and hafnium isotope analysis across the Ganderian and Notre Dame Subzones in Newfoundland, Canada. Five samples are from mid-Cambrian-Silurian (Wenlock) sedimentary rocks and one is from an Ediacaran granite. Sample locations are shown on Figure 2 and precise coordinates are given in Table 1.

3.1 Samples for U-Pb-Hf zircon analysis

A sample was taken from the Ediacaran Cripple Back Granite in the Victoria Lake region (Fig. 2), previously dated at 565 ± 4 Ma (Evans et al., 1990), in order to clarify the age and nature of Neoproterozoic magmatism. The oldest sample collected for detrital zircon analysis is from the late Cambrian-early Ordovician Gander Group (ACO-13-14), a thick sequence of variably deformed and metamorphosed clastic metasedimentary rocks that occupy much of the west portion of Ganderia. The Gander Group is subdivided into the lower quartz-rich clastic Jonathans Pond Formation, considered to have been derived from a continental source, and the overlying Indian Bay Big Pond Formation that

contains significantly more volcanic detritus (Holdsworth, 1994). Sample ACO-13-14 is from the Jonathans Pond Formation, which has no existing detrital zircon or fossil-age constraints. Sample ACO-13-13 is from the mid-Ordovician Outflow Formation, which forms the upper sequence of the platform marine Davidsville Group. Pollock et al. (2007) analyzed detrital zircons from the Outflow Formation and report the youngest detrital zircon population at 443 ± 22 Ma.

The Badger Group is a marine turbidite sequence comprised of upward-coarsening sequence of graywackes, siltstones and conglomerates (Williams et al., 1993). Sample ACO-12-15b is from the Goldson Formation in the Silurian Badger Group, which has previously been analyzed for detrital zircon provenance and yields a maximum deposition age of 439 Ma (Pollock et al., 2007). The Botwood Group overlies the Badger Group, and is an extensive thick sequence of volcanic rocks (Lawrenceton Formation) overlain by the fluvial, cross bedded sandstones of the Wigwam Formation (Pollock et al., 2007). Sample ACO-12-16 is from the Wigwam Formation and the minimum age is constrained as Wenlockian by the intrusion of felsic dykes that have a U-Pb zircon age of 422 ± 3 Ma (Elliot et al., 1991). The Badger and the Botwood Groups are interpreted to have been deposited as part of an overstep sequence following the arrival of the Ganderian leading arc to the Laurentian margin in the Ashgill-Llandovery (449-443 Ma, Pollock et al., 2007).

In order to help define the crustal evolution of the Laurentian Notre Dame arc, a sample was taken from the Ordovician Skidder Formation in the peri-Laurentian Notre-Dame Subzone. The Skidder Formation is predominantly a sequence of tholeitic basalts associated with volcanogenic massive sulphide-style mineralisation, pillow breccia and interstitial jasper (Pickett, 1987). Sample ACO-12-14 is from a rare volcanoclastic conglomerate within the Skidder Formation.

4. ANALYTICAL METHODS

4.1 U-Pb zircon geochronology method

Analytical techniques for U–Pb isotopic dating of zircon follow those of Payne et al., (2008) and Payne et al., (2010). U–Th–Pb analysis of zircons was also conducted at Adelaide Microscopy, at the University of Adelaide, South Australia; using an Agilent 7500cs ICPMS, coupled to a New Wave 213 nm Nd-YAG laser. Prior to analysis, zircon grains were imaged at Adelaide Microscopy, The University of Adelaide, using a Phillips XL20 SEM with attached Gatan cathodoluminescence (CL) detector. Representative cathodoluminescence images of the detrital and magmatic zircons are shown in Figure 3.

Pb fractionation was corrected using the GEMOC GJ-1 zircon (TIMS normalisation data 207Pb/206Pb = 608.3 Ma, 206Pb/238U = 600.7 Ma and 207Pb/235U = 602.2 Ma; (Jackson et al., 2004). A second zircon standard (Plesovice, TIMS-ID U–Pb age: 337.1 ± 0.4 Ma, Sláma et al., 2008) was used to monitor the ongoing accuracy of the instrument. GJ-1 produced a weighted average 206Pb/238U age of 600.56 ± 0.86 Ma (n = 289, MSWD = 0.90), and Plesovice a 206Pb/238U age weighted average of 338.1 ± 1.2 Ma (n = 79, MSWD = 0.95). Data reduction was completed using the program "GLITTER" (Griffin et al., 2008). Weighted average calculations use 207Pb/206Pb ages for zircon populations older than 1000 Ma and 206Pb/238U ages for those populations younger than 1000 Ma. A ± 10% discordancy threshold was applied to zircon analysis during age interpretation (Payne et al., 2006; Howard et al., 2009; Howard et al., 2011).

In order to define the youngest zircon population for each individual samples we utilise the conservative method described by Dickinson and Gehrels (2009) whereby the youngest grain cluster (2σ) (n= >3) grains overlap in age at 2σ error. Where possible at least eighty individual zircon grains were analyzed per detrital sample in order to

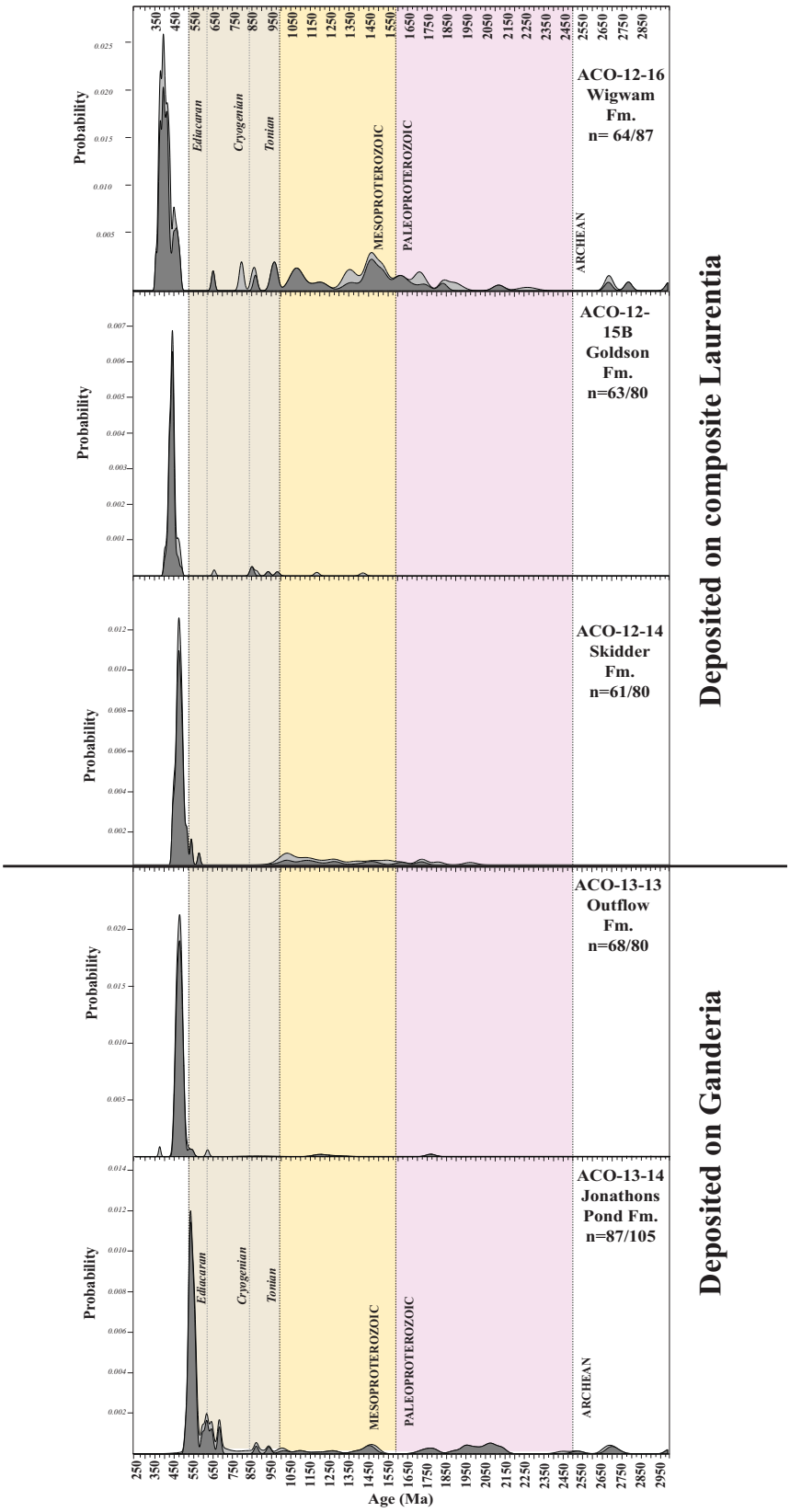

Figure 4

Detrital zircon age probability density distribution plots from Ganderian Mid-Cambrian to Silurian sedimentary rocks and the Ordovician Skidder Formation of the Notre Dame Subzone. Lighter grey fields represent zircon grains that are > 10% discordant. n = xxx/xxx equals number of > 90–110%

satisfy the minimum recommendation of Anderson (2005). The zircon populations are qualitatively classified by the population size (%) per sample from accessory populations (<5%) through minor (6-19%), major (20-49%), large (50-79%) to dominant populations (80>%) of the total (Anderson, 2005). A population is considered to be greater than 3 grains (2σ) (Dickinson and Gehrels, 2009).

4.2 Lu-Hf isotope method

The zircon mounts prepared for U–Pb LA-ICPMS analysis were also used for Lu–Hf isotopic studies undertaken with Laser Ablation Multi-Collector Inductively Coupled Plasma Mass Spectrometry (LA-MC-ICPMS) at the joint CSIRO/University of Adelaide facilities on the Waite campus, South Australia. To ensure the accuracy of the epsilon hafnium estimates, only grains with U–Pb LA-ICPMS analysis between 95%-105% concordance were analyzed for Lu–Hf isotope composition (e.g. Teale et al., 2011; Glorie et al., 2014; Henderson et al., 2014). Analysis spots were placed as close as possible to concordant U–Pb LA-ICP-MS spots, and within the same CL zone, including those zircon mounts analyzed by previous studies. Zircons were ablated with a New Wave UP-193 Excimer laser (193 nm) using a spot size of 50 μm, frequency of 5 Hz, 4 ns pulse length and an intensity of ~ 10 J/cm2. Confirmation of accuracy of the technique was monitored using a combination of the Plesovice, Mudtank and QGNG zircon standards. The average 176Hf/177Hf value for Plesovice for the analytical session was 0.282477 ± 0.000027 (2SD, n = 41), which is comparable to the published value of 0.282482 ± 0.000013 (2SD) by Sláma et al., (2008).

εHf(T), T(DM) (DM=depleted mantle) and TDMc (DMc= depleted mantle crustal model age) were calculated using 176Lu decay constant after Scherer et al., (2001), where T is the time of crystallization of the zircon. T(DM) and TDMc were calculated using the methods of Griffin et al., (2002) with an average crustal composition of 176Lu/177Hf = 0.015. All data are presented using the epsilon hafnium (εHf) notation, referring to a comparison of the data with CHUR; which at any time is set at a value of 0 (Patchett et al., 1981; Blichert-Toft and Albarède, 1997). Juvenile zircons are recognized as those with εHf(T) values that fall between the estimated value of the new continental crust from modern island arcs (Dhuime et al., 2011) and the estimated depleted mantle array of Griffin et al., (2004).

5. RESULTS

5.1 U-PB zircon geochronology

A summary of representative cathodoluminescence images of zircon textures are shown in Figure 3. U–Pb zircon data are presented in supplementary files. Age spectra and concordia diagrams are presented in Figure 4 and Figure 5.

5.1.1 Sample ACO-13-14 (Ganderia)

Sample ACO-13-14 is a moderately sorted grey sandstone from the late Cambrian-early Ordovician Jonathans Pond Formation. Of the one hundred and five analyses obtained, eighty-seven are concordant. The youngest detrital zircon population is 534 ± 6 Ma (n=6, MSWD=0.21). Ediacaran (~635-542 Ma) grains form 51% of the total population. Lower Cambrian (~542-530 Ma) and Paleoproterozoic (~1700-2100 Ma) zircons form 17% and 15% of the concordant population, respectively. Mesoproterozoic zircons (9%, ~1000-1400 Ma), Archean (6%, 2536 ± 30 Ma, ~2700-2750, 3005 ± 18 Ma) and Tonian (2%, 883 ± 10, 948 ± 11 Ma) zircons make up the remainder of the complex detrital zircon spectra (Fig. 4).

5.1.2 Sample ACO-13-13 (Ganderia)

Sample ACO-13-13 is a poorly sorted, pebbly conglomerate from the mid-Ordovician Outflow Formation. Of the eighty detrital zircon analyses conducted, sixty-eight are concordant (Fig. 4). The youngest detrital

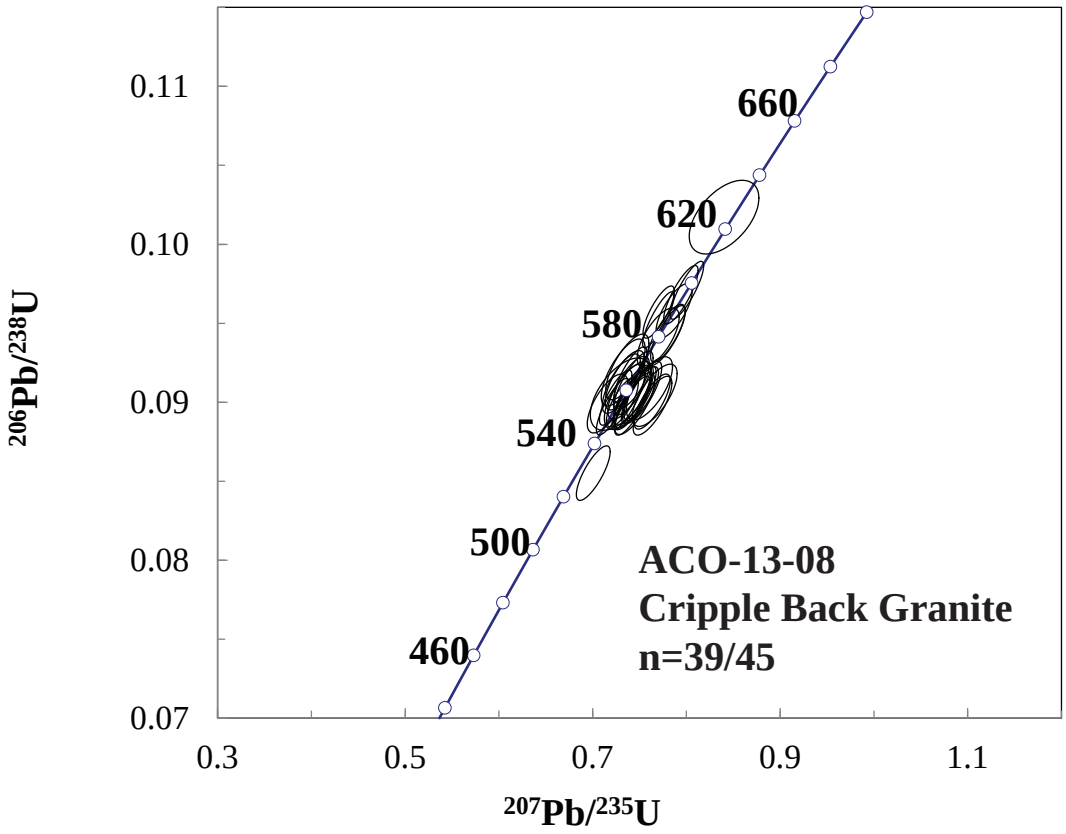

Figure 5

Concordia plots for zircon grains from the Cripple Back Granite. Mean ages displayed are 206Pb/238U ages with mean errors quoted at the one standard deviation level.

population is 450 ± 5 Ma (n=5, MSWD=0.29). Ordovician (~446-488 Ma) zircons form 75% of the total population, followed by Cambrian grains (20%, ~490-500, 525 Ma). Two Mesoproterozoic grains (1136 ± 14, 1233 ± 20 Ma) and a singular Paleoproterozoic (1170 ± 23 Ma) zircon were also analyzed. The young (~375 Ma) grain is discordant and is not considered further.

5.1.5 Sample ACO-12-14 (peri-Laurentian)

Sample ACO-12-14 is from the Ordovician Skidder Formation within the peri-Laurentian Dunnage Zone (Fig. 4). It is a poorly sorted, volcaniclastic conglomerate with pebbles (1-3 cm) of granitic and mafic clasts. Of the eighty analyses obtained, sixty-one are concordant. The youngest detrital zircon population is 455 ± 5 Ma (n=5, MSWD=0.65). The dominant zircon populations are Ordovician (49%, ~450-488 Ma) and middle-upper Cambrian (30%, ~490-520 Ma). Mesoproterozoic (13%, ~1000-1350 Ma) zircon, Ediacaran (5%, ~545 Ma, 587 ± 6 Ma) and Paleoproterozoic (3%, 1627 ± 30, 1728 ± 25 Ma) form comparatively minor detrital populations.

5.1.3 Sample ACO-12-15B (peri-Laurentian)

Sample ACO-12-15b is a gritty, poorly sorted sandstone from the Goldson Formation in the Silurian Badger Group. Of the eighty detrital zircon analyses obtained, sixty-three are concordant (Fig. 4). The youngest detrital zircon population is 430 ± 3 Ma (n=10, MSWD=0.94). The dominant zircon populations are Ordovician (59%, ~440-460 Ma) and Silurian (33%, ~430-440 Ma). A minor Tonian population (6%, ~860 Ma, ~950-990 Ma) and a single Cambrian zircon at 497 ± 5 Ma were also analyzed.

5.1.4 Sample ACO-12-16 (peri-Laurentian)

Sample ACO-12-16 is a moderately sorted sandstone interbedded with fine

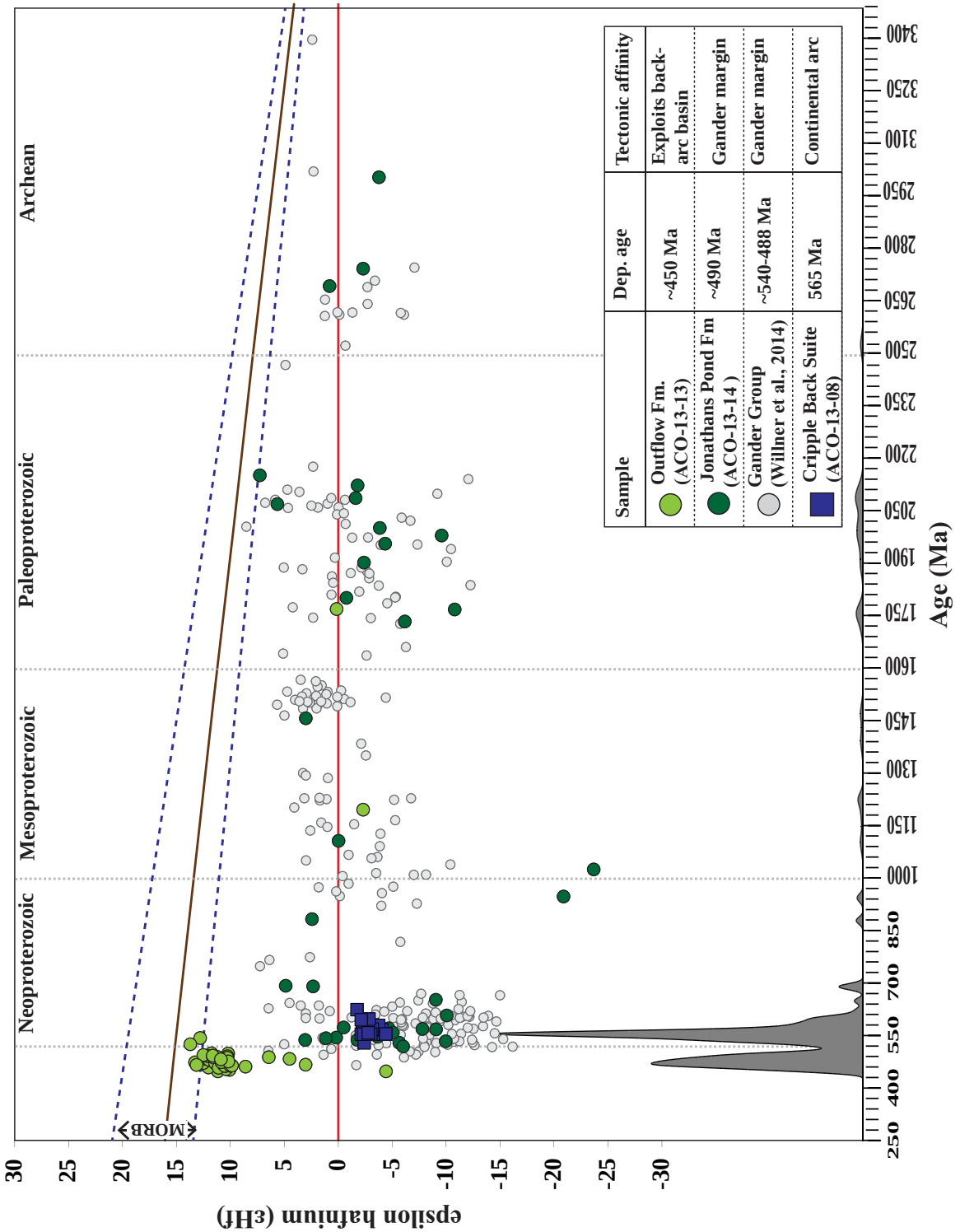

Figure 6
εHf values plotted against the U-Pb ages for individual zircon grains from the Ganderian mid-Cambrian-early Ordovician sedimentary rocks and the Ediacaran Cripple Back Granite. Also plotted are the εHf analyses from the Gander Group (Willner et al., 2014). The crustal evolution limits were projected to the depleted mantle curve using Lu/Hf ratio of average crust (0.015, Griffin et al., 2004), CHUR= chondritic uniform reservoir. The field defined for the depleted mantle array and MORB is from Dhuime et al., (2011) and Griffin et al., (2004), and are also illustrated in Figures 6 and 7.

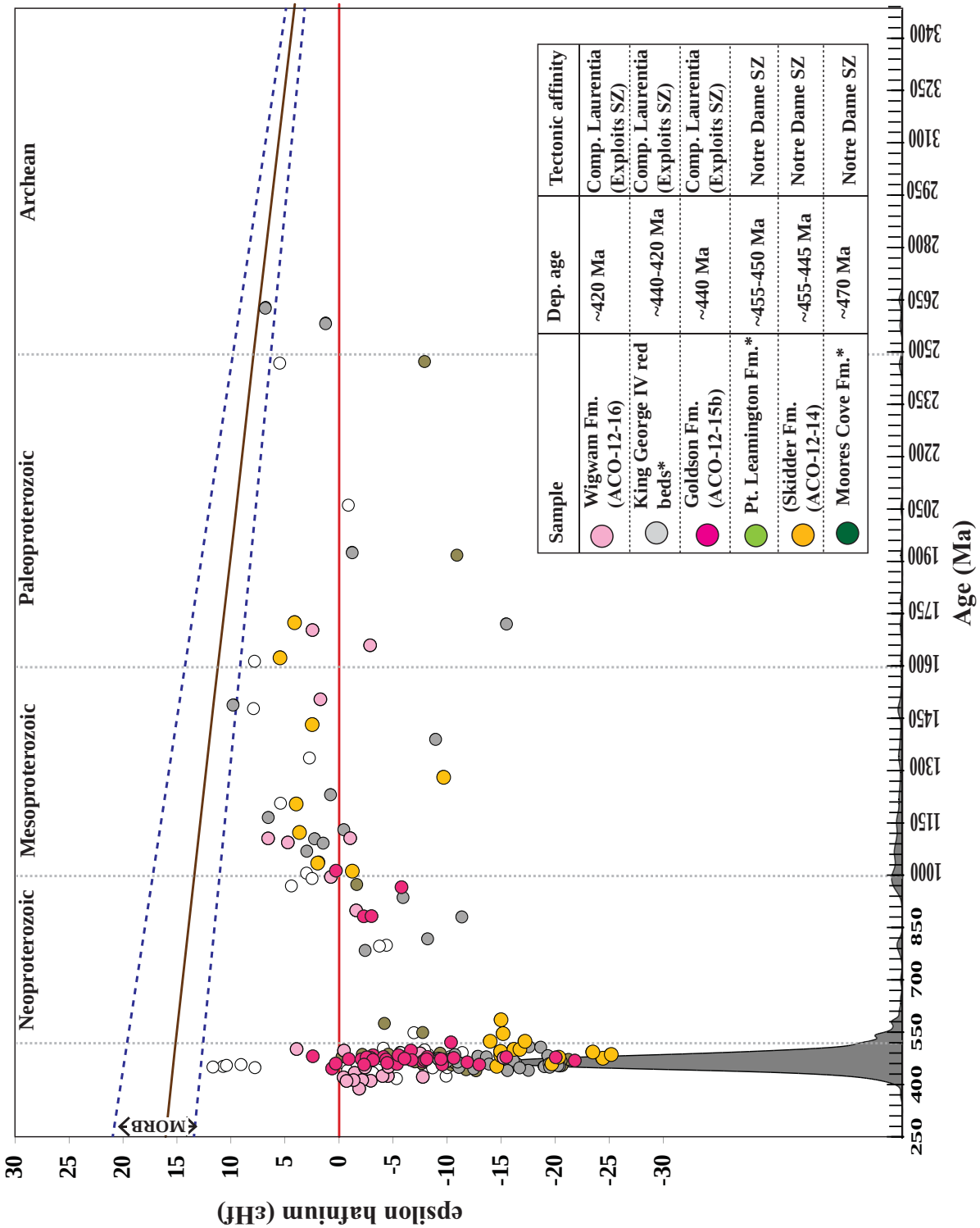

Figure 7
Epsilon hafnium plot for peri-Laurentia εHf values plotted against the U-Pb ages for individual zircon grains from the peri-Laurentian margin (ACO-12-14) and the Silurian Badger and Botwood groups (interpreted to contain peri-Laurentian detritus). Indicated by the "" are the peri-Laurentian εHf zircon analyses from the Moores Cove Formation, Point Leamington Formation and the King George IV red beds from Willner et al. (2014).*

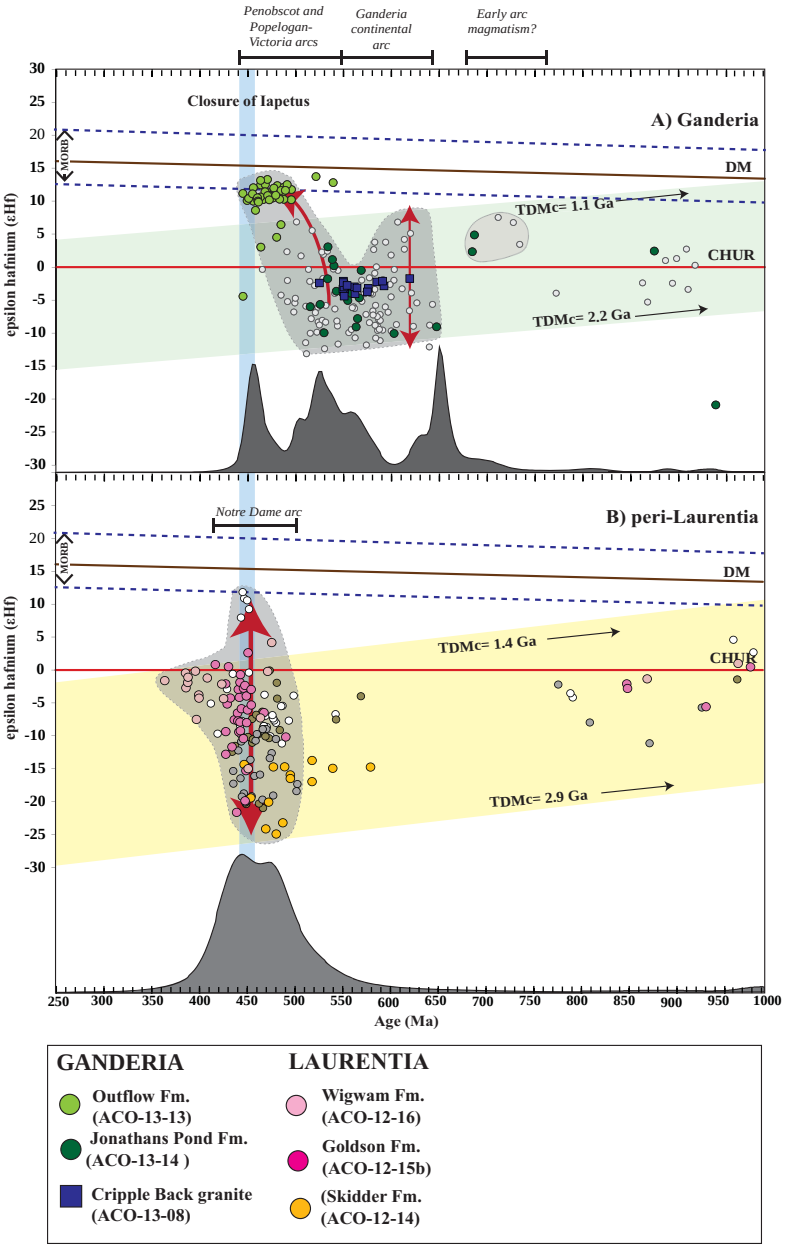

Figure 8

εHf plots showing only U-Pb zircon data between 250-1000 Ma in order to highlight the character of the late Neoproterozoic-early Paleozoic magmatism in the peri-Laurentian Notre Dame Subzone and Ganderian terrane. Included in the diagrams are probability density plots (shown as solid grey fields) for the concordant zircon data associated with the samples displayed. The data set includes the data from Willner et al. (2014). A) εHf isotopic array for Ganderia in the late Neoproterozoic-early Paleozoic. Key tectonic events are highlighted including the lifespan of the Ganderian continental arc, the Penobscot and Popelogan-Victoria arcs and the closure of the Iapetus Ocean. Also shown in the small grey field are the juvenile zircons associated with the possible early arc history of Ganderia. The 770-700 Ma zircons overlap with the record in Avalonia. The crustal evolution field defined by the upper and lower limits of the array in the latest Neoproterozoic suggest the Ganderia is built on a basement of Mesoproterozoic-Paleoproterozoic crust (~2.2-1.1 Ga). A red vertical arrow at ~630 Ma indicates a period of crustal mixing between juvenile and ancient crustal material during continental arc-type magmatism. The second red arrow between ~550-500 Ma illustrates the progressive shift towards juvenile magmatism. B) εHf isotopic array for peri-Laurentia in the late Neoproterozoic-early Paleozoic. The lifespan of the Notre Dame arc magmatism is highlighted between ~520-430 Ma. The crustal evolution field is defined by lower and upper limits that suggest recycling of Mesoproterozoic-Archean crust (1.4 to 2.9 Ga) dominated the magmatic processes in the Notre Dame arc. The red vertical arrow at ~460 Ma highlights an interval of mixing between juvenile and Archean crust during typical continental-arc magmatism.

(1-2 mm) horizons of silt, from the upper Silurian Wigwam Formation. Of the eighty-seven detrital zircon analyses, sixty-four are concordant. The youngest detrital zircon population is 388 ± 4 Ma (n=7, MSWD=0.80), which is younger than the previously assigned upper Silurian maximum deposition age (Pollock et al., 2007). The detrital zircon spectra is complex (Fig. 4) with the largest population coming from Mesoproterozoic (28%, ~1100-1600 Ma) sources. Devonian (24%, ~380-415 Ma) zircons form the second largest population. The remainder of the highly variable detrital zircon spectra is composed of Silurian (15%, ~420-440 Ma), Paleoproterozoic (13%, ~1650-1750 Ma, ~1850 Ma, 2130 ± 30 Ma), Ordovician (8%, ~470-480 Ma), Tonian (6%, ~970-980 Ma) and singular Cambrian (491 ± 6 Ma), Cryogenian (662 ± 9 Ma) and Archean (2695 ± 20 Ma) zircons.

5.1.6 Sample ACO-13-08 (Ganderia)

Sample ACO-13-08 is a K-feldspar, biotite-bearing granite from the Ediacaran Cripple Back Granite, considered to represent the oldest Ganderian rock in Newfoundland. A total of forty-five analyses were obtained from prismatic, euhedral zircons (Fig. 3), with thirty-nine concordant (Fig. 5). The 206Pb/238U weighted average age of the dominant population is 559 ± 3 Ma (MSWD=0.27), with a single younger outlier (529 ± 6 Ma) and a small population of inherited older zircon grains with an age range of ~580-624 Ma. These inherited ages conform to the age range from detrital zircons (Fig. 4) thereby suggesting that this 500-650 Ma age-peak is locally derived and represents the basement.

5.2 Hf isotopes

A total of 197 Lu-Hf isotopic analyses were obtained from four sedimentary rocks and two igneous rocks from Neoproterozoic-Devonian Ganderia. There were also 22 hafnium isotopic analyses obtained from the peri-Laurentian Skidder Formation. The zircon grains analyzed have measured 176Hf/177Hf ratios of 0.280769- 0.2828997 and initial 176Hf/177Hf ratios of 0.280742- 0.282853. Only 30% of the Ganderian and Laurentian zircon grains are juvenile (εHf =0 to +14). The hafnium data are presented in Figures 6 and 7 and are detailed below as: Ganderian detrital zircon analyses, Ganderian magmatic zircon analyses and peri-Laurentian hafnium data, respectively. In order to consider the hafnium isotopic data in a more complete manner, we have also included the Ganderian and Laurentian hafnium dataset from Willner et al. (2014). Full hafnium isotopic data tables are included in the supplementary files.

5.2.1 Ganderian detrital zircons

The late Cambrian-early Ordovician Jonathans Pond Fm (ACO-13-14) is the oldest sedimentary rock analyzed. It is dominated by Ediacaran-Cambrian detrital zircon grains, with the weighted average of the population at ~550 Ma. All but five of the Ediacaran-Cambrian grains are evolved, yielding εHf values between 0 and -12, which correspond to model ages of 1.5 to 2.2 Ga. The positive grains range between εHf +5 and +1, with model ages of 1.3 to 1.5, respectively (Fig. 6). Mesoproterozoic and Paleoproterozoic zircons form comparatively minor populations and yield highly variable hafnium ratios. Two analyses at ~1.0 Ga yield highly evolved εHf values of -21 and -23, corresponding to model ages of 3.1 to 3.3 Ga. A single analysis at 1.2 Ga is chondritic (εHf= 0), and a single grain at 1.5 Ga is comparatively juvenile (εHf= +3). Paleoproterozoic grains (~1.75-2.2 Ga) are relatively juvenile at ~2.2 Ga (εHf= +10 to -1) and become progressively more evolved between ~2.0 and ~1.75 Ga (εHf= 0 to -12). Archean zircons are chondritic-sub chondritic (εHf= +1 to -4).

The Ordovician Outflow Formation (ACO-13-13) has distinct hafnium isotopic spectra dominated by Ordovician and late Cambrian zircons (~500-450 Ma), all of which are juvenile (εHf= +2 to +13).

A single Mesoproterozoic (~1.2 Ga) and Paleoproterozoic (~1.85 Ga) yield chondritic to slightly evolved εHf values (Fig. 6).

5.2.2 Ganderian magmatic zircons

Zircon grains extracted from the (Cripple Back Granite (ACO-13-08) indicate a crystallisation age of 559 ± 3 Ma (Fig. 6). All the zircon grains analyzed yield very consistent measured 176Hf/177Hf ratios of 0.282309-0.282392 and initial 176Hf/177Hf ratios of 0.282302- 0.282375, which correspond to εHf values of -2 to -4. The TDMc for these zircon grains is 1.64-1.78 Ga, indicating that the Cripple Back Granite crystallized from magmas that predominantly recycled Paleoproterozoic crust.

5.3 Peri-Laurentia (ACO-12-14) and Silurian rocks deposited on composite Laurentia

The Ordovician Skidder Formation (ACO-12-14) yields a dominant Ordovician (~488-450 Ma) zircon population which overlaps with the main phase of arc-magmatism in the Notre Dame arc (van Staal et al., 2007). The ~488-450 Ma zircons are evolved and yield εHf values of -15 to -25, which corresponds to T(DM) of ~2.3-2.9 Ga. εHf values of Cambrian zircons (~490-525 Ma) also cluster between -24 to -15 (Fig. 7). Early Mesoproterozoic zircons (~1000-1350 Ma) predominantly straddle CHUR (0 ± 4 εHf) recording εHf values **between** +4 and -1. Upper Mesoproterozoic-early Paleoproterozoic zircons (~1450-1750 Ma) all record positive εHf values between +2.5 to +6.

The hafnium isotopic arrays from the Silurian Goldson and Wigwam Formation samples (ACO-12-16 and ACO-12-15B) are interpreted to reflect deposition in the Tetagouche-Exploits back-arc basin, immediately following the accretion of the Popelogan-Victoria arc to the Laurentian margin (Pollock, 2007). The Goldson Formation is dominated by Ordovician and Silurian zircons that are all chondritic to evolved, forming a well-defined vertical 'spike' (see Fig. 8a) at ~470-440 Ma with εHf values varying between +2 to -21 (Fig. 7), corresponding to model ages of 1.2 to 2.7 Ga. Minor populations of early late Mesoproterozoic zircons (~1.2-1.0 Ga) and early Paleoproterozoic (1.5-1.7 Ga) are chondritic to juvenile (εHf= -1 to +6). The mid-Silurian Wigwam Formation contains an Ordovician population that overlaps with the zircons in the Badger Fm (Fig. 7). The Wigwam Formation also contains a Devonian population that are all evolved and indicate recycling of Paleoproterozoic crustal material (εHf= 0 to -9).

6. DISCUSSION

6.1 The crustal evolution of the Ganderian continental arc

Mid Cryogenian- early Cambrian zircon populations (~650-535 Ma) dominate the detrital zircon age spectra in the late Cambrian Jonathans Pond Formation, the Gander Group (Willner et al., 2014) and the late Neoproterozoic sequences in New Brunswick and Maine (Fyffe et al., 2009). Taking into account the hafnium isotopic data presented here and from elsewhere in the Gander Group (Willner et al., 2014), 84% of all ~650-500 Ma zircons fall in a mixed array between εHf 0 and -15 (Fig. 8a) . The remainder of the ~650-500 Ma zircons (16%) that are comparatively 'juvenile' (εHf=0 to +6) cluster into two intervals; 650-600 Ma and 550-500 Ma. The hafnium array for the ~650-550 Ma zircons yields an upper and lower limit (Lu/Hf=0.015) that intersects the depleted mantle at ~1.1 Ga and 2.2 Ga, respectively (Fig. 8a). The hafnium isotopic array from the Cripple Back Granite (559 ± 3 Ma) completely overlaps with the detrital zircon array, demonstrating that the Hf array is "endemic" to Ganderia.

Volcanic rocks within the ~563 Ma Sandy Brook Group and the Cripple Back Granite have a continental-arc geochemical signature (Evans et al., 1990; Rogers et al., 2006), consistent with the extended vertical

mixing array for the ~650-550 Ma zircons from Ganderia (Fig. 6). The array supports the hypothesis that Ganderia occupied a continental-arc setting during the late Cryogenian-late Neoproterozoic (Rogers et al., 2006 and references therein). Ganderian continental-arc magmatism was dominated by the recycling of Mesoproterozoic-Paleoproterozoic crust with variable input of juvenile mantle material, and confirms that the basement of Ganderia is composed of "Grenvillian-type" Mesoproterozoic-Paleoproterozoic (2.2-1.1 Ga) crust (Fig. 8a).

Late Neoproterozoic-early Cambrian continental-arc magmatism is common throughout the peri-Gondwanan terranes (Keppie et al., 2003; Murphy et al., 2013; Balintoni et al., 2014) with the main phase of continental arc magmatism occurring between ~650-550 Ma. However, Ganderian continental arc zircons (~650-550 Ma) are comparatively evolved (Fig. 8a) relative to Avalonia (Willner et al., 2013; Pollock et al., 2015; Henderson et al., 2016). No Ganderian zircons fall within the depleted mantle array (new crust and traditional depleted mantle of Griffin et al., 2004; Dhuime et al., 2011), contrasting with Avalonia where juvenile zircons are a common feature of the mid-late Neoproterozoic Avalonian continental arc (Henderson et al., 2016, see Fig. 9b).

6.3 Provenance of Ganderia in the early Paleozoic

The hafnium isotopic array (Fig. 8a) indicates that Ganderia was a continental arc between ~650-550 Ma. The continental margin to which Ganderia accreted can be further investigated by investigating the detrital zircon spectra from the mid-Cambrian-early Ordovician Ganderian sequences. Although Neoproterozoic (770-550 Ma) "arc-related" detritus dominates the detrital zircon spectra of Ganderia, minor populations of Mesoproterozoic (1.0-1.2 Ga, 1.5 Ga), Paleoproterozoic (~1.7-2.2 Ga) and Archean (~2.5-3.1 Ga) are also found (present study, Pollock, 2007; Fyffe et al., 2009; Willner et al., 2014).

The older age ranges in Ganderia have been previously matched to known tectonothermal events in Amazonia (Fyffe et al., 2009; van Staal et al., 2012; Barr et al., 2014; Waldron et al., 2014; Willner et al., 2014). A compilation of available Amazonian hafnium isotopic data (Fig. 9a, Henderson et al., 2016) enables a direct comparison to the detrital zircons from Ganderia. Many of the similarities and differences between the Ganderian and Amazonian hafnium isotope arrays are subtle. Although there are Proterozoic populations that overlap between Ganderia and Amazonia, the isotopic nature of the detrital populations are not always comparable. For example, both the Ganderian and Amazonia hafnium arrays record Paleoproterozoic magmatism commencing at ~2.2-2.25 Ga, but the Ganderian zircons are markedly more juvenile (εHf= +11 to -14) than the coeval Amazonian zircons (εHf= +6 to -23). The Mesoproterozoic array from Ganderia also records subtle differences to that of Amazonia. Amazonia records predominantly juvenile magmatism throughout the Mesoproterozoic (Fig. 9a), whereas Ganderia records almost exclusively reworking of Paleoproterozoic crust throughout the Mesoproterozoic (Fig. 6). Apparent mixing between juvenile and Paleoproterozoic (~2.4-2.2 Ga) crust at ~1050-900 Ma, typical of Amazonia, is also not evident in the Ganderian array; with the exception of two extremely evolved zircons at ~1.0 Ga (Fig. 8a). Also, the scarcity of ~900-800 Ma zircons in Ganderia is inconsistent with the Amazonian record, which is marked by abundant zircon crystallisation during this interval (see Cordani et al., 2009; Pimentel et al., 2011).

There are similarities in the detrital zircon age spectra and hafnium isotopic arrays of Avalonia and Ganderia (Willner et al., 2014; Pollock et al., 2015) (Fig. 9b). The detrital zircon age spectra and isotopic array from Mesoproterozoic, Paleoproterozoic

and Archean zircons in Ganderian rocks closely overlap in with those of Avalonia (Fig. 9b), although there are comparatively fewer Mesoproterozoic and older detrital zircons preserved in the sedimentary rocks of Ganderia.

The Paleoproterozoic peak at ~2.2 Ga in Ganderia and Avalonia both record mixing between depleted mantle crust (εHf=+11) and Paleoproterozoic crust (εHf= -15) that continues until the early Mesoproterozoic. The early Mesoproterozoic (~1550-1400 Ma) features a large population of mixed zircons that plot in a mixed array between the depleted mantle and -10 in Avalonia. By comparison, the ~1550-1400 Ma population in Ganderia is more restricted yielding an εHf range between 7+ to -2. Both the Avalonian and Ganderian isotopic arrays record reworking along a typical crustal array in zircons between ~1400-950 Ma (Fig. 6, Fig. 9b). Both Ganderia and Avalonia also record a magmatic gap between 800-900 Ma, which contrasts with the Amazonian record.

Both Ganderia and Avalonia also preserve a small population of predominantly juvenile ~770-700 Ma zircons (Fig. 8a, Fig. 9b). Although the ~770-700 Ma detrital zircon population is relatively minor in Ganderia, it is ubiquitous throughout late Neoproterozoic-early Paleozoic Ganderian sequences, such as the mid-Cambrian Jonathans Pond Formation, the Gander Group (Willner et al., 2014) and from Ediacaran Ganderian sequences in New Brunswick and coastal Maine (USA) (see Fyffe et al. 2009). The ubiquitous presence of ~770-700 Ma zircons indicates a proximal volcanic source was available to Ganderia throughout the late Neoproterozoic-early Paleozoic. The hafnium isotopic character of the ~770-700 Ma zircons is uniform, yielding positive εHf values of +9 to +2, indicating recycling of early Neoproterozoic-Mesoproterozoic crust (TDMc= 0.96-1.2 Ga).

Avalonia preserves Cryogenian granitic and volcanic rocks including the 734 Ma Economy River Gneiss in Nova Scotia (Doig et al. 1993), the 763 Ma Burin Group Volcanics in Newfoundland (Krogh et al. 1988; Murphy et al. 2008) and the 675 Ma Malverns Plutonic Complex in the English Midlands (Strachan et al., 1996), which are testament to the early magmatic-arc history in Avalonia. The nature of the magmatism at ~750-700 Ma in Avalonia is generated from a mix of depleted mantle melts and Paleoproterozoic crust (TDMc = ~0.68 to 1.9 Ga) with εHf values between -7 and +14 (Henderson et al., 2016, Pollock et al. 2015). Early arc magmatism in Avalonia is interpreted to have nucleated on a continental ribbon that originated in Baltica, or the Grenvillian region of Laurentia (Henderson et al. 2016), before accretion to the northern Gondwanan margin by ~650 Ma (Murphy et al., 2013) . The ~760-700 Ma early arc rocks of Avalonia are a potential source for the ~700-700 Ma zircons found in Cambrian Ganderian sequences.

6.4 Crustal evolution of the Penobscot and Popelogan-Victoria arcs

The oldest Paleozoic rocks in the Exploits Subzone of Ganderia are attributed to the Penobscot arc-backarc system (~515-485 Ma, Colman-Sadd et al., 1992), which was initially proposed to have formed via intraoceanic subduction outboard of the Gondwanan margin in the mid-Cambrian (MacLachlan and Dunning, 1998; van Staal et al., 1998), prior to accretion to Gondwana during the Penobscot Orogeny (~490 Ma). However, evolved neodymium isotopic data, late Neoproterozoic inherited zircons and other geochemical data from the ~511 Ma Tally Pond Group Volcanics, suggest that the Penobscot arc was built on Ganderian basement (see Pollock and Wilton, 2001; Evans and Kean, 2002; Rogers et al., 2006 and references therein).

Hafnium data from late Neoproterozoic-early Ordovician zircons in the late Cambrian Jonathans Pond Formation and the Ordovician Outflow Formation allow the tectonic

evolution of the Penobscot and Popelogan-Victoria arcs to be tested. The Penobscot arc was active from ~515-490 Ma but there is no appreciable magmatic gap between the late Neoproterozoic Ganderian continental arc and the commencement of the Penobscot arc (Figs. 4, 8a). Furthermore, the Hf isotopic arrays show a smooth transition within this interval. Rather, the continuous magmatism from~650-450 Ma suggests ongoing arc magmatism associated with consumption of the same oceanic plate throughout the late Neoproterozoic- early Paleozoic.

The shift in isotopic composition of the zircons between ~550-500 Ma (Fig. 8a) suggests a gradual change in the source of the magmatism and/or a shift in the tectonic environment. The transition towards increasingly positive (depleted mantle) εHf values between ~550-500 Ma is indicative of a retreating subduction zone analogous to the Tasmanides of Australia (Kemp et al., 2009). Ongoing subduction-related magmatism (together with roll-back) in the Penobscot arc system would progressively remove the lower crust and SCLM (Collins et al., 2011), leading to increasingly positive εHf values that reflect the increasing but continual input of juvenile material from the underlying mantle wedge.

We suggest that Ganderia underwent extensional processes and crustal thinning during slab roll back and subduction retreat, driving the development of the Penobscot backarc basin at ~490-485 Ma (Jenner and Swinden, 1993; van Staal et al., 2012) in a similar setting to the modern day Tonga-Kermadec arc – back-arc systems (Ewart et al., 1998; Smith and Price, 2006). The existence of multiple back-arc basin systems through the Ordovician (Penobscot back-arc, Tetagouche-Exploits basins), which separated the leading oceanic arcs from the trailing passive margin of Gander (Zagorevski et al., 2007; Zagorevski et al., 2010), is also consistent with a primitive, retreating subduction zone (e.g. Rosenbaum and Lister, 2004).

There is also no demonstrable magmatic gap between the Penobscot Orogeny (~486-478 Ma) and the commencement of the Popelogan-Victoria (P-V) arc magmatism at 475 Ma. The hafnium data from the upper Ordovician Outflow Formation emphasises the juvenile nature of the (P-V) arc; all zircons preserve a restricted εHf range (+14 to +3, average = +10) between 550-540 Ma. Therefore, P-V magmatism did not rework significant portions of the ~1.1-2.2 Ga Ganderian basement. The primitive hafnium isotopic array from the P-V arc implies it was an oceanic arc, and its existence requires that Ganderia retreated from the Gondwanan margin with the leading magmatic arc becoming increasingly juvenile. Juvenile magmatism was abruptly terminated at ~450 Ma, consistent with the existing constraints on the arrival of Ganderia to the peri-Laurentian margin (Pollock et al., 2007; Zagorevski and Van Staal, 2011; van Staal et al., 2012; Willner et al., 2014) .

6.5 Crustal evolution of the Notre Dame Subzone

Extensive rifting along the Humber margin between ~565-550 Ma resulted in the opening of the Taconic Seaway and the separation of the Dashwoods microcontinent from Laurentia by ~540 Ma (Waldron and van Staal, 2001; van Staal and Barr, 2011). A complex supra-subduction zone and continental arc environment ensued in the Taconic Seaway and Dashwoods terrane between ~515-470 Ma (van Staal et al., 2007; van Staal et al., 2009; van Staal and Barr, 2011), evident as arc tholeiites, boninites and ophiolites and subduction-related granites (see Kean et al., 1995; Szybinski, 1995; Swinden, 1996; Kurth et al., 1998; Skulski et al., 2010; Zagorevski et al., 2010; Castonguay et al., 2014). Closure of the Taconic seaway at ~468 Ma culminated in the re-accretion of the Dashwoods microcontinent to the Humber margin (Schroetter et al., 2006; Tremblay et al., 2009).

Hafnium data from the peri-Laurentian domain (Figs. 7, 8b) span the ~515-470 Ma interval of complex Taconic tectonic activity, and despite the apparent oceanic setting, the hafnium isotopic array indicates that crustal recycling processes dominated the magmatic record of the NDSz (Fig. 8b). Evidence of crustal contamination and zircon inheritance has long been recognised within the peri-Laurentian Dashwoods realm (Skulski et al., 2010) and hafnium data confirm that the peri-Laurentian Dashwoods microcontinent (Waldron and van Staal, 2001) comprises in part an Archean basement. Crustal model ages of ~2.5-2.9 Ga for ~450-500 Ma NDSz zircons imply that Dashwoods microcontinent may potentially represent a ribbon of the >2.5 Ga Superior Province (Percival, 2007), albeit overprinted by Mesoproterozoic and Grenvillian events (Whitmeyer and Karlstrom, 2007).

The U-Pb-Hf data from the NDSz zircons indicate that magmatism involved significant recycling of Paleoproterozoic-Archean crust, commencing as early as ~515 Ma and continuing until ~425 Ma, with the majority of zircons yielding εHf values between 0 and -25 (Fig. 8b). However, a cluster of ~460-445 Ma zircons from the Silurian King George red beds (Fig. 8b, Willner et al., 2014), are significantly more juvenile (εHf= +7 to +12), implying that an important juvenile component of magmatism contributed to the Notre Dame arc. When all available data are considered together (Fig. 8b), the NDSz records mixing between ancient Archean and juvenile crustal components yielding a mixed array typical of continental arcs (e.g. Mueller et al., 2008; Roberts et al., 2013; Linnemann et al., 2014).

A marked shift in the hafnium array occurs between ~460-445 Ma, when mixing between depleted mantle and ancient Laurentian crust occurred (εHf= +12 to -20). This shift is preceded by an interval of extensive tonalite emplacement at 467-459 Ma (van Staal et al., 2007), prior to intrusion of 445-435 Ma calc-alkaline gabbros to granodiorites (van Staal and Barr, 2011 and references therein). The influx of juvenile crust evident in the hafnium array may be attributed to slab break off in the Taconic seaway and/or possibly delamination beneath the Notre Dame arc (van Staal et al., 2007; van Staal et al., 2009; van Staal and Barr, 2011). A simple alternative explanation is that it reflects the mixing of juvenile and continental crust in a typical continental arc setting (e.g. Mueller et al., 2008; Roberts et al., 2013; Linnemann et al., 2014).

The mixing array ceased by ~445-450 Ma (Fig. 8b) coinciding with the arrival of the P-V arc to composite Laurentia (present study, Pollock, 2007; Zagorevski et al., 2007; van Staal and Barr, 2011; van Staal et al., 2012), but post-collisional magmatism continued until at least 425 Ma (van Staal and Barr, 2011 and references therein). Epsilon Hf values ranging from 0 to -20 for the ~445-425 Ma magmatism (T(DM) = 1.3-2.0 Ga) imply dominant recycling of Laurentian crust. The final phase of magmatism (>439 Ma) in the Notre Dame Subzone is a bimodal magmatic suite that has been previously attributed to slab-breakoff (Whalen et al., 1996; Whalen et al., 2006) following the closure of the Tetagouche-Exploits backarc basin. The hafnium from zircons crystallised between ~440-370 Ma indicates a shift towards CHUR (εHf= -6 to 0), indicating a decreasing input from ancient Laurentian crust into arc magmas.

6.6 Revised geodynamic model for Ganderia

The late Neoproterozoic to Silurian evolution of Ganderia occurred during complex plate tectonic changes largely associated with development of the Iapetus Ocean. Geochronological, biological and paleomagnetic constraints have led to a broad framework for the evolution of Ganderia, the composite Laurentian margin, and the Iapetus Ocean (Hibbard, 2006; Pollock et al., 2007; Murphy et al., 2010; Zagorevski et al., 2010; van Staal and Barr, 2011; van Staal et al., 2012;

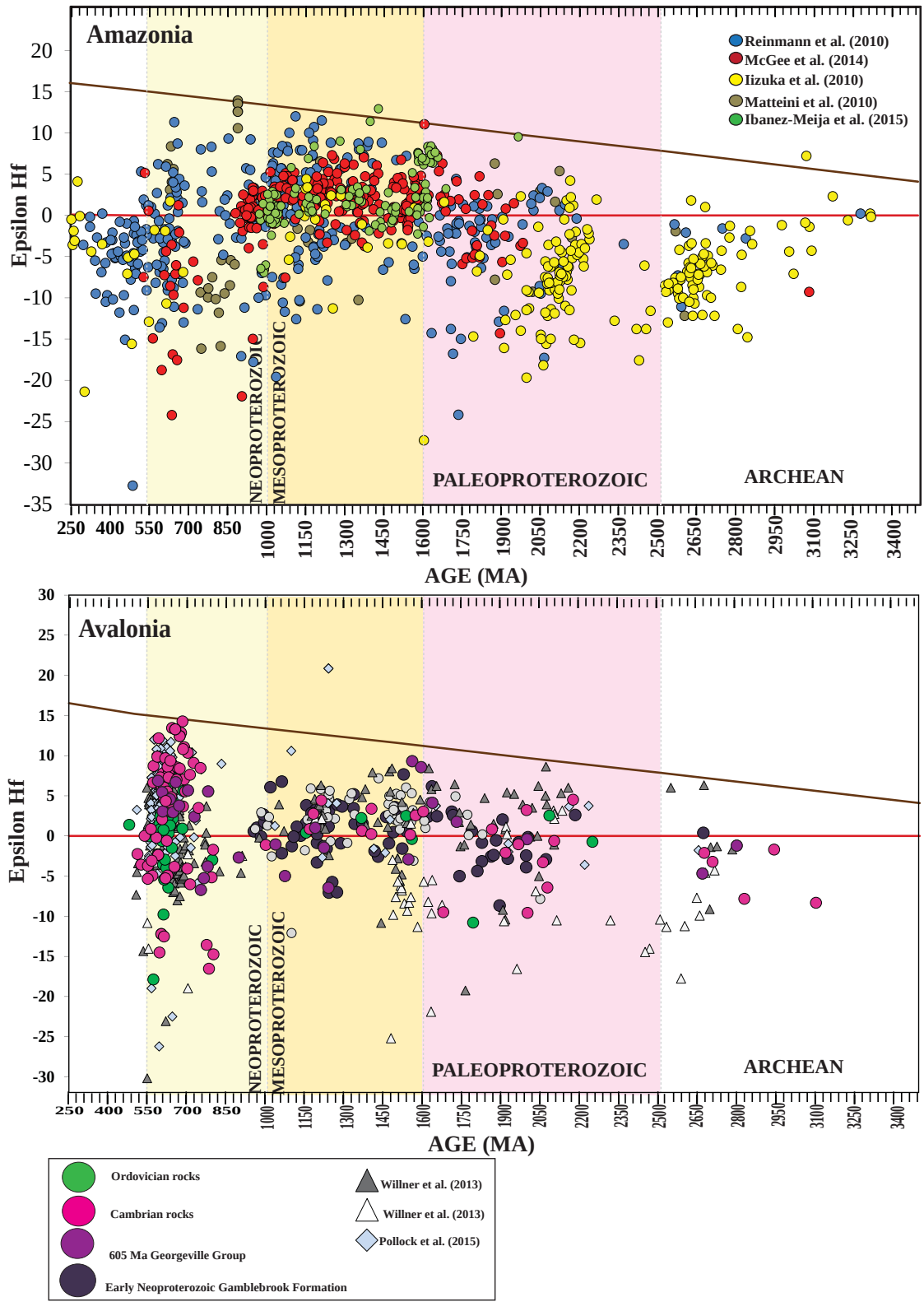

Figure 9

A compilation of the published εHf zircon values for Amazonia and Avalonia. A) Amazonia; data are from Reimann et al., (2010), McGee et al., (2015), Iizuka et al., (2010) and Matteini et al., (2010). B) Avalonian data are from Henderson et al. (2016), Pollock et al. (2015) and Willner et al. (2013). The figure is modified from Henderson et al. (2016).

Willner et al., 2014). The comprehensive hafnium isotopic record presented here from the coeval, but contrasting, arc systems hosted on Ganderia and peri-Laurentia provides additional insights into the late Neoproterozoic-early Paleozoic evolution of the Iapetus Ocean and the process of continental ribbon transfer, details of which cannot be discerned using geochronological methods alone. We present a revised model for the evolution of Ganderia and the nature of the magmatism in the Notre Dame Subzone (Fig. 10).

The earliest record of arc magmatism in Ganderia is evident in the ~770-700 Ma zircons that persistently appear throughout the late Neoproterozoic-Cambrian sedimentary rocks (Pollock et al., 2007; Fyffe et al., 2009; Willner et al., 2014). The positive εHf values of the ~770-700 Ma Ganderia zircons (Fig. 8a) indicates a predominantly juvenile source mixed with Mesoproterozoic crust (1.1-1.4 Ga), similar to the ~750-700 Ma record in Avalonia (Fig. 9b, 10a). Sm-Nd whole rock model ages of 0.9-1.2 Ga from igneous and sedimentary rocks from Ganderia and Avalonia have been previously interpreted to reflect the formation of juvenile lithosphere ("proto-Avalonia") within the peri-Rodinian Mirovoi Ocean during the early Neoproterozoic (Nance and Murphy, 1994, 1996; Murphy et al., 2000). Early arc magmatism (770-650 Ma) in Avalonia was subsequently considered to have formed during renewed subduction and predominantly involved the recycling of the 0.9-1.2 Ga juvenile lithosphere (Murphy et al., 2013 and references therein). However, hafnium isotopes from ~800-650 Ma Avalonian and Ganderian zircons yield zircons with εHf model ages of ~1.0-2.2 Ga, indicating that the basement is actually likely to be Mesoproterozoic-Paleoproterozoic, similar to that of the Grenville Orogen (Dickin et al., 1990; Daly and McLelland, 1991; Dickin, 2000).

We consider that Ganderia records an early arc history built on a sliver of Mesoproterozoic-Paleoproterozoic crust prior to accretion with the Gondwanan margin at ~650 Ma (Fig. 10a), similar to that of Avalonia (Henderson et al., 2016). A modern analogue to this is the Cenozoic oceanic arcs of Vanuatu in the South Pacific. Hafnium isotopes from zircons in arc-related magmas have identified a continental basement to the oceanic arcs, which has allowed the continental ribbon to be traced to its point of origin along the Australian margin (Buys et al., 2014). The hafnium isotopic data indicates that Ganderia (and Avalonia) must have been derived from an appropriate Mesoproterozoic-Paleoproterozoic cratonic source during the early Neoproterozoic; such as the Grenville regions of Laurentia and Sveconorwegian Baltica (Dickin, 2000; Bingen et al., 2008).

The overlapping εHf array between Ganderia and Avalonia at 650-600 Ma (compare Figs. 8a, 9b) suggests Ganderia formed part of the same continental arc system as Avalonia by 650 Ma (Fig. 10b). Like Avalonia, continental-arc type magmatism continued in Ganderia throughout the Neoproterozoic, yielding a mixed isotopic array that recycled predominantly a Mesoproterozoic-Paleoproterozoic basement with varying amounts of juvenile crust until ~550 Ma (Fig. 10b).

The record of ~650 Ma arc accretion onto Gondwana is much clearer in Avalonia than Ganderia, where instances of high-intermediate grade metamorphism at ~650 Ma are preserved in east Avalonia (Malverns Plutonic Complex, Strachan et al., 1996) and west Avalonia (southern Maine, Cape Breton Island, southern Newfoundland, O'Brien et al., 1996). Given that there is no appreciable magmatic gap in Ganderia from ~750 Ma to the Paleozoic, the transition away from positive εHf values between 650-550 Ma in both Ganderia and Avalonia is consistent with growth of a continental arc following accretion to Gondwana (Fig. 10b). The hafnium record of the Ganderian arc contrasts with that of the Cadomian arc built on the West African Craton (Linnemann et al., 2014), where juvenile arc

magmas are mixed with Archean (possibly Hadean) crust yielding a large vertical mixing array (εHf = +11 to -38) between 750-540 Ma (Linnemann et al., 2014), compared to the +11 to -15 εHf array for Avalonia-Ganderia, though some of the εHf values for Ganderia reach -30 (Fig. 9b). It is evident from the hafnium arrays that Ganderia was not part of the Cadomian arc system that formed on the margin of the West African Craton. In light of new isotopic and geochronological data, it is clear that the nature of late Neoproterozoic continental-arc magmatism along the peri-Gondwanan margin is highly variable and if more characterised precisely, can be utilised for provenance studies and paleogeographic reconstructions (e.g. Henderson et al., 2016).

Between ~550 Ma to 500 Ma, the εHf values shifted towards the depleted mantle composition (Fig. 10b). The ancient crustal contribution progressively diminished and was replaced by a very juvenile mantle input. This contraction to positive values is consistent with a reversion to an oceanic arc realm that normally occurs during subduction retreat (Kemp et al., 2009; Collins et al., 2011). The latter stages of this inferred retreat was associated with a period of extension, indicated by the emplacement of bimodal volcanics, including the Ellsworth Schist and unconformably overlying Castine volcanics; dated at 508 Ma and 503 Ma, respectively (Schulz et al., 2008). It also coincides with development of the Penobscot and Popelogan-Victoria arcs outboard of Ganderia (Fig. 10c). We interpret the characteristics of the ~550-500 Ma interval in the Ganderian hafnium isotopic array to indicate the onset of subduction rollback from ~550 Ma leading to retreat of the magmatic arc away from the continental margin. Other existing geological, geochronological and isotopic data (van Staal et al., 2012 and references therein) imply progressive rifting of Ganderia from a continental margin by ~510 Ma, which is the point (510-500 Ma) in the hafnium array where magmatism becomes extremely juvenile (Fig. 8a). The timing of the rifting also overlaps with the existing constraints on the opening of the Rheic Ocean (~500 Ma) in the Ganderian realm (Nance et al., 2012 and references therein).

The metamorphic record in Ganderia is also consistent with extension during the Early Paleozoic. An early flat-lying fabric preserved in the Gander Zone is loosely constrained to pre ~470 Ma (King, 1997) and a subsequent high T, low P metamorphic assemblage overprints the earlier fabric and is dated at 469 ± 5 Ma by insitu monazite analysis (Henderson, in prep). The early horizontal fabric could represent extension associated with either the opening of the Penobscot back-arc at ~497-482 Ma (Johnson et al., 2012) or Rheic Ocean initiation (~500 Ma), with the later metamorphic assemblage coeval with the development of the Tetagouche-Exploits back-arc basin (Fig. 10c) between 470-460 Ma (Zagorevski et al., 2010).

Juvenile magmatism persisted in the Popelogan-Victoria arc until ~450 Ma (Fig. 8a), when termination of the arc is interpreted to reflect its arrival at the peri-Laurentian Red Indian Lake arc, resulting in a Moluccan Sea-style arc-arc convergence (van Staal and Barr, 2011). Evidence for the arrival of Ganderia is the shift in provenance recorded in the late Ordovician- early Silurian Badger and Botwood Groups deposited within the Exploits Subzone (Fig. 10d). The upper-most unit of the 449-443 Ma Badger Group contains zircons that overlap in epsilon Hf space with peri-Laurentian Notre Dame arc detritus (Fig. 7), and contrast significantly with the juvenile zircons produced in the Ganderian P-V arc system (Fig. 10c, d). However, detrital zircons from the late Ordovician Point Leamington Formation in the Gander Zone (Willner et al., 2014) are sourced from the peri-Laurentian Notre Dame arc (Fig. 8b), and thus confirm the earliest isotopic evidence of the arrival of Ganderia to Laurentia by 452 Ma (Fig. 10d).

On the peri-Laurentian margin, the lack of significant mantle input into the Notre Dame arc throughout most of its history (Fig.

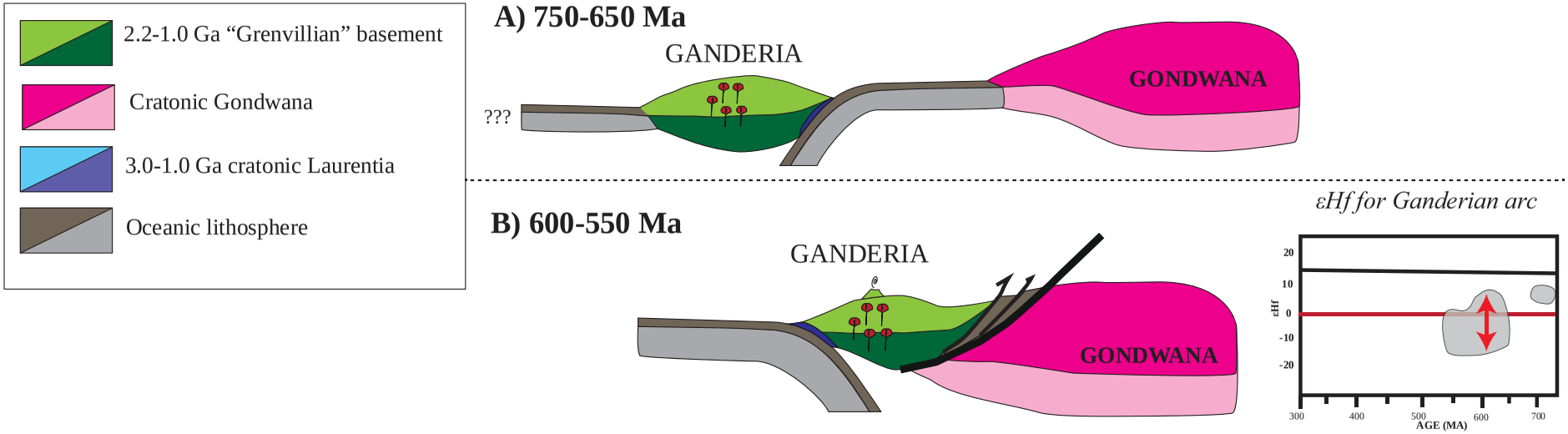

Figure 10

A geodynamic model that illustrates the possible evolution of the Ganderian terrane and the Notre Dame Subzone. The schematic cross sections encompass the hafnium isotopic constraints and existing geological models. The figures are modified after van Staal et al. (1998; 2007; 2009).

a) 750-650 Ma: *early juvenile detrital zircons indicate Ganderia formed on a rifted Mesoproterozoic-Paleoproterozoic continental ribbon prior to accretion with the northern Gondwanan margin.* ***b) 600-550 Ma:*** *Ganderia had accreted to the Gondwanan margin by ~650 Ma and subduction then stepped outboard beneath Ganderia-Gondwana to establish a continental-arc. The hafnium inset illustrates the mixing between Paleoproterozoic-Mesoproterozoic "Grenvillian" type crust and juvenile arc magmas during arc magmatism.*

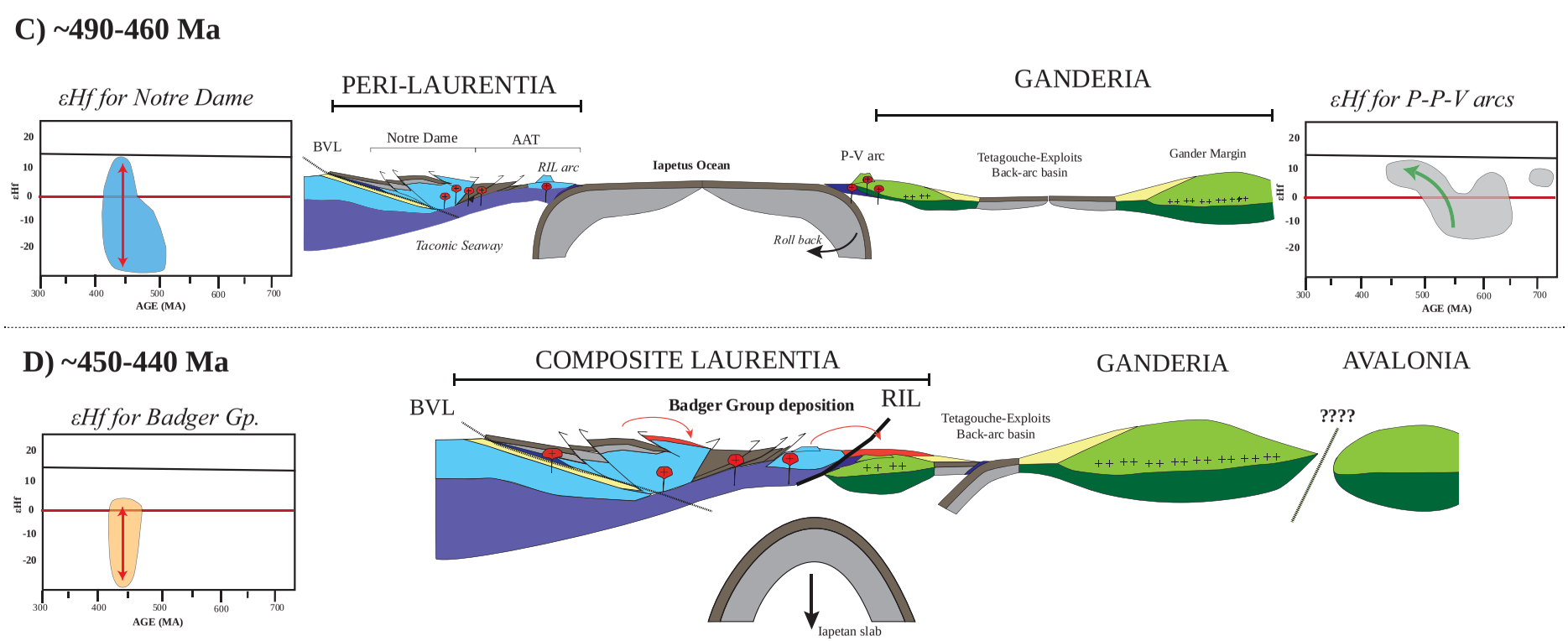

Figure 10 (cont.)

c) 490-460 Ma: *Subduction begins to roll back from the Gondwanan margin at ~550 Ma leading to the eventual rifting and separation of Ganderia by ~510 Ma. The process is recorded in the continuous magmatism in the Gander arc associated with a shift from predominantly recycling continental crust, towards increasingly juvenile magmatism. The development of the exclusively oceanic Penobscot and Popelogan-Victoria arcs generates juvenile magmatism on the leading Ganderia margin between ~500-450 Ma. On the Laurentian margin, a coeval arc system is established leading to the generation of a continental arc (Notre Dame arc). The hafnium inset indicates the basement of the Dashwoods terrane is underlain by Archean crust (~2.9 Ga), which is recycled continuously with younger crustal material throughout the ~515-460 Ma interval. RIL arc: Red Indian Lake arc.* ***d) 450-440 Ma*** *Following the arrival of Ganderia to Laurentia subduction is interpreted to step in the Tetagouche-Exploits back-arc basin. The deposition of the Silurian Badger and Botwood Groups record peri-Laurentian arc detritus on Ganderian crust. The hafnium array from the Badger/Botwood Groups is isotopically comparable to the Laurentian array and in contrast to the juvenile Ganderian arcs. RIL: Red Indian Line. Dual subduction of the Iapetan slab is after van Staal and Barr (2011).*

8b) could be a reflection of the general inability of mafic rocks to yield significant zircon, or it could indicate that very little magmatism was generated from the depleted mantle during this interval. Recently, the Taconic Seaway was proposed to have been magma poor and generated via extremely slow spreading, and was floored by thinned Laurentian lithosphere with partially exhumed mantle and limited oceanic crust (see Castonguay et al., 2014). During closure of the Taconic Seaway at ~475-465 Ma, the thinned Laurentian lithosphere, embryonic oceanic crust and the leading edge of the Humber margin were all thrust beneath the Dashwoods terrane (van Staal and Barr, 2011). The hafnium array records mainly records the reworking of Laurentian crust during this interval, and suggests that minimal oceanic crust was recycled during this event.

Following Taconic Seaway closure by ~465 Ma (~465, Hibbard et al., 2010), subduction likely stepped outboard (see van Staal et al., 2009) coinciding with an influx of juvenile crust evident in the hafnium array at ~465-445 Ma (Fig. 8a, 10c). Although Notre Dame arc magmatism during the ~460-445 Ma interval is commonly considered to be post-collisional (van Staal and Barr, 2011 and references therein), mixing between juvenile and continental crust is typical of continental-arc settings (e.g. Mueller et al., 2008; Roberts et al., 2013; Linnemann et al., 2014) and is a simple explanation for the vertical mixing array at ~465-445 Ma. In the model (Fig. 10c), the subduction stepped outboard (eastward) following the Taconic orogeny and W-dipping subduction continued beneath Laurentia. This scenario would place the Annieopsquotch Accretionary Tract (Zagorevski et al., 2009) in a back-arc setting and the Red Indian Lake arc as the outboard (easternmost) magmatic system following subduction retreat (Fig. 10c, d).

Ultimately, the hafnium isotopic array for the Notre Dame Subzone does not record the detailed evolution of the complex oceanic processes associated with the geological evolution of peri-Laurentia (Zagorevski et al., 2006; van Staal et al., 2009; Zagorevski and Van Staal, 2011) instead broadly recording the development of a continental arc built on Archean crust between ~520-440 Ma. Magmatism predominantly reworked the Archean basement of the Notre Dame Subzone during these events with minor input from the mantle wedge.

7. CONCLUDING REMARKS

We use the hafnium isotopic method on detrital and magmatic zircons from Ganderia and the peri- Laurentian Notre Dame Subzone to test the sensitivity of the method against the tectonic evolution of the Ganderia terrane in the late Neoproterozoic-early Paleozoic. The hafnium isotopic method is proven to be a powerful tool when used in conjunction with sound geological constraints, and is able to identify the changing nature of magmatism during the evolution of complex accretionary orogens. Of particular significance is the recognition that hafnium isotopes are able to characterise the early evolution of Ganderia, which has not been previously identified and is largely lost from the geological record.

The present study finds the hafnium method is broadly consistent with geological framework previously defined for Ganderia, but provides additional insight into the geodynamic driving forces behind continental ribbon transfer; a process that is important for continental growth. The hafnium isotope array identifies an interval of continental arc magmatism at ~650-550 Ma, which coincides with continental arc magmatism in Avalonia. The Hf data also show that Ganderia is built on a basement of Paleoproterozoic-Mesoproterozoic "Grenvillian-type" crust (~2.2-1.1 Ga) crust, which was recycled during the main phase of Neoproterozoic magmatism. A similar hafnium isotopic array for ~750-550 Ma magmatism in Avalonia, on compositionally similar basement, suggests a previously unrecognised shared early Neoproterozoic history. A progressive

shift in the hafnium isotopic array towards increasingly juvenile magmatism between ~550-500 Ma in Ganderia represents the onset of subduction retreat, leading to the rifting and separation of Ganderia from Gondwana. During terrane transfer the ~510-485 Ma Penobscot and immediate successor (475-455 Ma) Popelogan-Victoria arcs were almost exclusively juvenile oceanic arcs. The peri-Laurentian Notre Dame arc recycled Archean Laurentian crust in an arc- back-arc environment, which underwent multiple extensional and contractional events during the closure of Iapetus. Despite the record of oceanic-arc magmatism on peri-Laurentian between ~510-450 Ma, the detail of these processes are not preserved in the hafnium isotopic record. The preservation of very evolved Notre Dame arc zircons in Ganderian overstep sequences confirm the arrival of the leading edge of Ganderia to Laurentia by ~450 Ma.

ACKNOWLEDGEMENTS

We thank Justin Payne and Benjamin Wade for help with isotope analysis. We thank Donnelly Archibald, Cees van Staal and Alexandre Zagorevski for invaluable local knowledge and assistance during field work in Nova Scotia. This work was funded by Australian Research Council DP 120104004 and JBM acknowledges the ongoing support of the N.S.E.R.C Canada. Bonnie Henderson is a recipient of an Australian Post Graduate award.

REFERENCES

Amelin, Y., Kamo, S.L., Lee, D.-C., 2010. Evolution of early crust in chondritic or non-chondritic Earth inferred from U–Pb and Lu–Hf data for chemically abraded zircon from the Itsaq Gneiss Complex, West GreenlandThis article is one of a series of papers published in this Special Issue on the theme of Geochronology in honour of Tom Krogh. Canadian Journal of Earth Sciences 48, 141-160.

Anderson, T., 2005. Detrital zircons as tracers of sedimentary provenance: limiting conditions from statistics and numerical simulation. Chemical Geology 216, 249-270.

Balintoni, I., Balica, C., Ducea, M.N., Hann, H.-P., 2014. Peri-Gondwanan terranes in the Romanian Carpathians: A review of their spatial distribution, origin, provenance, and evolution. Geoscience Frontiers 5, 395-411.

Barr, S.M., Davis, D.W., Kamo, S., White, C.E., 2003a. Significance of U–Pb detrital zircon ages in quartzite from peri-Gondwanan terranes, New Brunswick and Nova Scotia, Canada. Precambrian Research 126, 123-145.

Barr, S.M., Dunning, G.R., Raeside, R.P., Jamieson, R.A., 1990. Contrasting U–Pb ages from plutons in the Bras d'Or and Mira terranes of Cape Breton Island, Nova Scotia. Canadian Journal of Earth Sciences 27, 1200-1208.

Barr, S.M., White, C.E., Davis, D.W., McClelland, W.C., van Staal, C.R., 2014. Infrastructure and provenance of Ganderia: Evidence from detrital zircon ages in the Brookville terrane, southern New Brunswick, Canada. Precambrian Research 246, 358-370.

Barr, S.M., White, C.E., Miller, B.V., 2003b. Age and geochemistry of Late Neoproterozoic and Early Cambrian igneous rocks in southern New Brunswick: similarities and contrasts. Atlantic Geology 39.

Barreiro, J.G., Catalán, J.R.M., Arenas, R., Castiñeiras, P., Abati, J., García, F.D., Wijbrans, J.R., 2007. Tectonic evolution of the upper allochthon of the Órdenes Complex (northwestern Iberian Massif): structural constraints to a polyorogenic peri-Gondwanan terrane. Geological Society of America Special Papers 423, 315-332.

Batumike, J., Griffin, W., O'Reilly, S., Belousova, E., Pawlitschek, M., 2009. Crustal evolution in the central Congo-Kasai Craton, Luebo, DR Congo: Insights from zircon U–Pb ages, Hf-isotope and trace-element data. Precambrian Research 170, 107-115.

Belousova, E.A., Kostitsyn, Y.A., Griffin, W.L., Begg, G.C., O'Reilly, S.Y., Pearson, N.J., 2010. The growth of the continental crust: Constraints from zircon Hf-isotope data. Lithos 119, 457-466.

Belousova, E.A., Reid, A.J., Griffin, W.L., O'Reilly, S.Y., 2009. Rejuvenation vs. recycling of Archean crust in the Gawler Craton, South Australia: Evidence from U–Pb and Hf isotopes in detrital zircon. Lithos 113, 570-582.

Bingen, B., Nordgulen, Ø., Viola, G., 2008. A four-phase model for the sveconorwegian orogeny, SW Scandinavia. Norsk Geologisk Tidsskrift 88, 43-72.

Blichert-Toft, J., Albarède, F., 1997. The Lu-Hf isotope geochemistry of chondrites and the evolution of the mantle-crust system. Earth and Planetary Science Letters 148, 243-258.

Buys, J., Spandler, C., Holm, R.J., Richards, S.W., 2014. Remnants of ancient Australia in Vanuatu: Implications for crustal evolution in island arcs and tectonic development of the southwest Pacific. Geology 42, 939-942.

Castonguay, S., van Staal, C.R., Joyce, N., Skulski, T., Hibbard, J.P., 2014. Taconic Metamorphism Preserved in the Baie Verte Peninsula, Newfoundland Appalachians: Geochronological Evidence for Ophiolite Obduction and Subduction and Exhumation of the Leading Edge of the Laurentian (Humber) Margin During Closure of the Taconic. Geoscience Canada 41, 459-482.

Cawood, P.A., Buchan, C., 2007. Linking accretionary orogenesis with supercontinent assembly. Earth-Science Reviews 82, 217-256.

Cawood, P.A., Kröner, A., Collins, W.J., Kusky, T.M., Mooney, W.D., Windley, B.F., 2009. Accretionary orogens through Earth history, pp. 1-36.

Cawood, P.A., McCausland, P.J.A., Dunning, G.R., 2001. Opening Iapetus: Constraints from the Laurentian margin in Newfoundland. Geological Society of America Bulletin 113, 443-453.

Collins, W., 2002. Hot orogens, tectonic switching, and creation of continental crust. Geology 30, 535-538.

Collins, W.J., Belousova, E.A., Kemp, A.I.S., Murphy, J.B., 2011. Two contrasting Phanerozoic orogenic systems revealed by hafnium isotope data. Nature Geoscience 4, 333-337.

Colman-Sadd, S., Stone, P., Swinden, H., Barnes, R., 1992. Parallel geological development in the Dunnage Zone of Newfoundland and the Lower Palaeozoic terranes of southern Scotland: an assessment. Transactions of the Royal Society of Edinburgh: Earth Sciences 83, 571-594.

Cordani, U.G., Teixeira, W., D'Agrella-Filho, M.S., Trindade, R.I., 2009. The position of the Amazonian Craton in supercontinents. Gondwana Research 15, 396-407.

Currie, K., McNicoll, V., 1999. New data on the age and geographic distribution of Neoproterozoic plutons near Saint John, New Brunswick. Atlantic Geology 35.

D'Lemos, R.S., Schofield, D.I., Holdsworth, R.E., King, T.R., 1997. Deep crustal and local rheological controls on the siting and reactivation of fault and shear zones, northeastern Newfoundland. Journal of the Geological Society 154, 117-121.

Daly, J., McLelland, J., 1991. Juvenile middle Proterozoic crust in the Adirondack highlands, Grenville province, northeastern North America. Geology 19, 119-122.

Dhuime, B., Hawkesworth, C., Cawood, P., 2011. When continents formed. Science 331, 154-155.

Dickin, A., 2000. Crustal formation in the Grenville Province: Nd-isotope evidence. Canadian Journal of Earth Sciences 37, 165-181.

Dickin, A., McNutt, R., Clifford, P., 1990. A neodymium isotope study of plutons near the Grenville Front in Ontario, Canada. Chemical Geology 83, 315-324.

Dickinson, W.R., Gehrels, G.E., 2009. U-Pb ages of detrital zircons in Jurassic eolian and associated sandstones of the Colorado Plateau: Evidence for transcontinental dispersal and intraregional

recycling of sediment. Geological Society of America Bulletin 121, 408-433.

Dunning, G., Krogh, T., 1985. Geochronology of ophiolites of the Newfoundland Appalachians. Canadian Journal of Earth Sciences 22, 1659-1670.

Elliot, C.G., Duninng, G.R., Williams, P.F., 1991. New U/Pb zircon age constraints on the timing of deformation in north-central Newfoundland and implications for early Paleozoic Appalachian orogenesis. Geological Society of America Bulletin 103, 125-135.

Evans, D., Kean, B., 2002. The Victoria Lake Supergroup, central Newfoundland-its definition, setting and volcanogenic massive sulphide mineralization. Newfoundland and Labrador Department of Mines and Energy, Geological Survey.

Evans, D., Kean, B., Dunning, G., 1990. Geological studies, Victoria Lake Group, central Newfoundland. Current Research. Newfoundland Department of Mines and Energy, Geological Survey Branch, Report, 90-91.

Ewart, A., Collerson, K., Regelous, M., Wendt, J., Niu, Y., 1998. Geochemical evolution within the Tonga–Kermadec–Lau arc–back-arc systems: the role of varying mantle wedge composition in space and time. Journal of Petrology 39, 331-368.

Fyffe, L.R., Barr, S.M., Johnson, S.C., McLeod, M.J., McNicoll, V.J., Valverde-Vaquero, P., van Staal, C.R., White, C.E., 2009. Detrital zircon ages from Neoproterozoic and Early Paleozoic conglomerate and sandstone units of New Brunswick and coastal Maine: implications for the tectonic evolution of Ganderia. Atlantic Geology 45, 110-144.

Glorie, S., De Grave, J., Singh, T., Payne, J.L., Collins, A.S., 2014. Crustal root of the Eastern Dharwar Craton: Zircon U–Pb age and Lu–Hf isotopic evolution of the East Salem Block, southeast India. Precambrian Research 249, 229-246.

Griffin, W., Powell, W., Pearson, N., O'Reilly, S., 2008. GLITTER: data reduction software for laser ablation ICP-MS. Laser Ablation-ICP-MS in the Earth Sciences. Mineralogical Association of Canada Short Course Series 40, 204-207.

Griffin, W.L., Belousova, E.A., Shee, S.R., Pearson, N.J., O'Reilly, S.Y., 2004. Archean crustal evolution in the northern Yilgarn Craton: U–Pb and Hf-isotope evidence from detrital zircons. Precambrian Research 131, 231-282.

Griffin, W.L., Wang, X., Jackson, S.E., Pearson, N.J., O'Reilly, S.Y., Xu, X., Zhou, X., 2002. Zircon chemistry and magma mixing, SE China: In-situ analysis of Hf isotopes, Tonglu and Pingtan igneous complexes. Lithos 61, 237-269.

Henderson, B., in prep. The P-T-t evolution of Ganderia in the Paleozoic: the metamorphic record of back-arc basin tectonics and continental ribbon transfer The University of Adelaide.

Henderson, B., Collins, A.S., Payne, J., Forbes, C., Saha, D., 2014. Geologically constraining India in Columbia: The age, isotopic provenance and geochemistry of the protoliths of the Ongole Domain, Southern Eastern Ghats, India. Gondwana Research 26, 888-906.

Henderson, B., Collins, W.J., Murphy, B.J., Gutiérrez-Alonso, G., Hand, M., 2016. Gondwanan basement terranes of the Variscan-Appalachian orogen: Baltican, Saharan and West African hafnium isotopic fingerprints in Avalonia, Iberia and the Armorican Terranes. Tectonophysics.

Hibbard, J., 2006. Lithotectonic Map of the Appalachian Orogen: Canada-United States of America. Commission géologique du Canada.

Hibbard, J.P., Van Staal, C.R., Rankin, D.W., 2007. A comparative analysis of pre-Silurian crustal building blocks of the northern and the southern Appalachian orogen. American Journal of Science 307, 23-45.

Hibbard, J.P., van Staal, C.R., Rankin, D.W., 2010. Comparative analysis of the geological evolution of the northern and southern Appalachian orogen: Late Ordovician-Permian. Geological Society of America Memoirs 206, 51-69.

Holdsworth, R., 1994. Structural evolution of the Gander-Avalon terrane boundary: a reactivated transpression zone in the NE Newfoundland Appalachians. Journal of the Geological Society 151, 629-646.

Howard, K.E., Hand, M., Barovich, K.M., Payne, J.L., Belousova, E.A., 2011. U–Pb, Lu–Hf and Sm–Nd isotopic constraints on provenance and depositional timing of metasedimentary rocks in the western Gawler Craton: Implications for Proterozoic reconstruction models. Precambrian Research 184, 43-62.

Howard, K.E., Hand, M., Barovich, K.M., Reid, A., Wade, B.P., Belousova, E.A., 2009. Detrital zircon ages: Improving interpretation via Nd and Hf isotopic data. Chemical Geology 262, 277-292.

Iizuka, T., Komiya, T., Rino, S., Maruyama, S., Hirata, T., 2010. Detrital zircon evidence for Hf isotopic evolution of granitoid crust and continental growth. Geochimica et Cosmochimica Acta 74, 2450-2472.

Jackson, S.E., Pearson, N.J., Griffin, W.L., Belousova, E.A., 2004. The application of laser ablation-inductively coupled plasma-mass spectrometry to in situ U–Pb zircon geochronology. Chemical Geology 211, 47-69.

Jenner, G., Dunning, G., Malpas, J., Brown, M., Brace, T., 1991. Bay of Islands and Little Port complexes, revisited: age, geochemical and isotopic evidence confirm suprasubduction-zone origin. Canadian Journal of Earth Sciences 28, 1635-1652.

Jenner, G., Swinden, H.S., 1993. The Pipestone Pond Complex, central Newfoundland: complex magmatism in an eastern Dunnage Zone ophiolite. Canadian Journal of Earth Sciences 30, 434-448.

Johnson, S.C., Fyffe, L.R., McLeod, M.J., Dunning, G.R., 2012. U–Pb ages, geochemistry, and tectonomagmatic history of the Cambro-Ordovician Annidale Group: a remnant of the Penobscot arc system in southern New Brunswick?1. Canadian Journal of Earth Sciences 49, 166-188.

Kean, B.F., Evans, D., Jenner, G., 1995. Geology and mineralization of the Lushs Bight Group.

Keen, C., Keen, M., Nichols, B., Reid, I., Stockmal, G., Colman-Sadd, S., O'Brien, S., Miller, H., Quinlan, G., Williams, H., 1986. Deep seismic reflection profile across the northern Appalachians. Geology 14, 141-145.

Kellett, D.A., Rogers, N., McNicoll, V., Kerr, A., van Staal, C., McFarlane, C., 2014. New age data refine extent and duration of Paleozoic and Neoproterozoic plutonism at Ganderia–Avalonia boundary, Newfoundland. Canadian Journal of Earth Sciences 51, 943-972.

Kemp, A., Hawkesworth, C., Collins, W., Gray, C., Blevin, P., 2009. Isotopic evidence for rapid continental growth in an extensional accretionary orogen: The Tasmanides, eastern Australia. Earth and Planetary Science Letters 284, 455-466.

Kemp, A., Hawkesworth, C., Foster, G., Paterson, B., Woodhead, J., Hergt, J., Gray, C., Whitehouse, M., 2007. Magmatic and crustal differentiation history of granitic rocks from Hf-O isotopes in zircon. Science 315, 980-983.

Keppie, J.D., Dostal, J., Murphy, J.B., Nance, R.D., 2008. Synthesis and tectonic interpretation of the westernmost Paleozoic Variscan orogen in southern Mexico: From rifted Rheic margin to active Pacific margin. Tectonophysics 461, 277-290.

Keppie, J.D., Nance, R.D., Murphy, J.B., Dostal, J., 2003. Tethyan, Mediterranean, and Pacific analogues for the Neoproterozoic-Paleozoic birth and development of peri-Gondwanan terranes and their transfer to Laurentia and Laurussia. Tectonophysics 365, 195-219.

Kerr, A., Dunning, G., Tucker, R., 1993. The youngest Paleozoic plutonism of the Newfoundland Appalachians: U-Pb ages from the St. Lawrence and François granites. Canadian Journal of Earth Sciences 30, 2328-2333.

Kerr, A., Jenner, G.A., Fryer, B.J., 1995. Sm–Nd isotopic geochemistry of Precambrian to Paleozoic granitoid suites and the deep-crustal structure

of the southeast margin of the Newfoundland Appalachians. Canadian Journal of Earth Sciences 32, 224-245.

Kerr, I., Skulski, T., McNicoll, V., Castonguay, S., Van Staal, C.R., 2008. Flatwater Pond Group: tectonostratigraphy and age constraints of an Ordovician ophiolite cover sequence, Baie Verte Peninsula, Newfoundland. Atlantic Geology 44.

King, T.R., 1997. PTtd evolution paths within the Gander Zone, NE Newfoundland. Oxford Brookes University.

Kurth, M., Sassen, A., Suhr, G., Mezger, K., 1998. Precise ages and isotopic constraints for the Lewis Hills (Bay of Islands Ophiolite): Preservation of an arc-spreading ridge intersection. Geology 26, 1127-1130.

Linnemann, U., Gerdes, A., Hofmann, M., Marko, L., 2014. The Cadomian Orogen: Neoproterozoic to Early Cambrian crustal growth and orogenic zoning along the periphery of the West African Craton—Constraints from U–Pb zircon ages and Hf isotopes (Schwarzburg Antiform, Germany). Precambrian Research.

Lissenberg, C., van Staal, C., 2002. The relationships between the Annieopsquotch ophiolite belt, the Dashwoods Block and the Notre Dame Arc in southwestern Newfoundland. Current Research, Rep. 02 1, 145-153.

MacLachlan, K., Dunning, G., 1998. U-Pb ages and tectono-magmatic evolution of Middle Ordovician volcanic rocks of the Wild Bight Group, Newfoundland Appalachians. Canadian Journal of Earth Sciences 35, 998-1017.

Marillier, F., Keen, C.E., Stockmal, G.S., Quinlan, G., Williams, H., Colman-Sadd, S.P., O'Brien, S.J., 1989. Crustal structure and surface zonation of the Canadian Appalachians: implications of deep seismic reflection data. Canadian Journal of Earth Sciences 26, 305-321.

Matteini, M., Junges, S.L., Dantas, E.L., Pimentel, M.M., Bühn, B., 2010. In situ zircon U–Pb and Lu–Hf isotope systematic on magmatic rocks: Insights on the crustal evolution of the Neoproterozoic Goiás Magmatic Arc, Brasília belt, Central Brazil. Gondwana Research 17, 1-12.

McGee, B., Collins, A.S., Trindade, R.I., Payne, J., 2015. Age and provenance of the Cryogenian to Cambrian passive margin to foreland basin sequence of the northern Paraguay Belt, Brazil. Geological Society of America Bulletin 127, 76-86.

Mišković, A., Schaltegger, U., 2009. Crustal growth along a non-collisional cratonic margin: a Lu–Hf isotopic survey of the Eastern Cordilleran granitoids of Peru. Earth and Planetary Science Letters 279, 303-315.

Mueller, P.A., Kamenov, G.D., Heatherington, A.L., Richards, J., 2008. Crustal Evolution in the Southern Appalachian Orogen: Evidence from Hf Isotopes in Detrital Zircons. Journal of Geology 116, 414-422.

Murphy, J.B., Keppie, J.D., 2005. The Acadian orogeny in the northern Appalachians. International Geology Review 47, 663-687.

Murphy, J.B., Keppie, J.D., Nance, R.D., Dostal, J., 2010. Comparative evolution of the Iapetus and Rheic Oceans: A North America perspective. Gondwana Research 17, 482-499.

Murphy, J.B., Pisarevsky, S., Nance, R.D., 2013. Potential geodynamic relationships between the development of peripheral orogens along the northern margin of Gondwana and the amalgamation of West Gondwana. Mineralogy and Petrology 107, 635-650.

Murphy, J.B., Pisarevsky, S.A., Nance, R.D., Keppie, J.D., 2004. Neoproterozoic—Early Paleozoic evolution of peri-Gondwanan terranes: implications for Laurentia-Gondwana connections. Int J Earth Sci (Geol Rundsch) 93, 659-682.

Murphy, J.B., Strachan, R.A., Nance, R.D., Parker, K.D., Fowler, M.B., 2000. Proto-Avalonia: A 1.2-1.0 Ga tectonothermal event and constraints for the evolution of Rodinia. Geology 28, 1071-1074.

Nance, R.D., Gutiérrez-Alonso, G., Keppie, J.D., Linnemann, U., Murphy, J.B., Quesada, C., Strachan, R.A., Woodcock, N.H., 2012. A brief

history of the Rheic Ocean. Geoscience Frontiers 3, 125-135.

Nance, R.D., Murphy, J.B., 1994. Contrasting basement isotopic signatures and the palinspastic restoration of peripheral orogens: example from the Neoproterozoic Avalonian-Cadomian belt. Geology 22, 617-620.

Nance, R.D., Murphy, J.B., 1996. Basement isotopic signatures and Neoproterozoic paleogeography of Avalonian-Cadomian and related terranes in the circum-North Atlantic, Special Paper of the Geological Society of America, pp. 333-346.

Nance, R.D., Murphy, J.B., Strachan, R.A., Keppie, J.D., Gutiérrez-Alonso, G., Fernández-Suárez, J., Quesada, C., Linnemann, U., D'lemos, R., Pisarevsky, S.A., 2008. Neoproterozoic-early Palaeozoic tectonostratigraphy and palaeogeography of the peri-Gondwanan terranes: Amazonian v. West African connections. Geological Society, London, Special Publications 297, 345-383.

O'Brien, S., O'Brien, B., Dunning, G., Tucker, R., 1996. Late Neoproterozoic Avalonian and related peri-Gondwanan rocks of the Newfoundland Appalachians. SPECIAL PAPERS-GEOLOGICAL SOCIETY OF AMERICA, 9-28.

O'Brien, S., Dickson, W., Blackwood, R., 1986. Geology of the central portion of the Hermitage Flexure area, Newfoundland. Current research. Newfoundland Department of Mines and Energy, Mineral Development Division, Report, 86-81.

Patchett, P.J., Kouvo, O., Hedge, C.E., Tatsumoto, M., 1981. Evolution of continental crust and mantle heterogeneity: evidence from Hf isotopes. Contributions to Mineralogy & Petrology 78, 279-297.

Payne, J.L., Barovich, K.A., Hand, M., 2006. Provenance of metasedimentary rocks in the northern Gawler Craton, Australia: Implications for palaeoproterozoic reconstructions. Precambrian Research 148, 275-291.

Payne, J.L., Ferris, G., Barovich, K.M., Hand, M., 2010. Pitfalls of classifying ancient magmatic suites with tectonic discrimination diagrams: An example from the Paleoproterozoic Tunkillia Suite, southern Australia. Precambrian Research 177, 227-240.

Payne, J.L., Hand, M., Barovich, K.M., Wade, B.P., 2008. Temporal constraints on the timing of high-grade metamorphism in the northern Gawler Craton: implications for assembly of the Australian Proterozoic. Australian Journal of Earth Sciences 55, 623-640.

Percival, J.A., 2007. Geology and metallogeny of the Superior Province, Canada. Mineral Deposits of Canada: A Synthesis of Major Deposit-Types, District Metallogeny, the Evolution of Geological Provinces, and Exploration Methods, 903-928.

Pickett, J., 1987. Geology and geochemistry of the Skidder Basalt. Paper-Geological Survey of Canada 86, 195-218.

Piercey, S.J., Squires, G.C., Brace, T.D., 2014. Lithostratigraphic, Hydrothermal, and Tectonic Setting of the Boundary Volcanogenic Massive Sulfide Deposit, Newfoundland Appalachians, Canada: Formation by Subseafloor Replacement in a Cambrian Rifted Arc. Economic Geology 109, 661-687.

Pimentel, M.M., Rodrigues, J.B., DellaGiustina, M.E.S., Junges, S., Matteini, M., Armstrong, R., 2011. The tectonic evolution of the Neoproterozoic Brasília Belt, central Brazil, based on SHRIMP and LA-ICPMS U–Pb sedimentary provenance data: A review. Journal of South American Earth Sciences 31, 345-357.

Pollock, J., Wilton, D., 2001. Metallogenic studies of the Tally Pond Belt, Victoria Lake Group: trace element geochemistry and lead isotope data from the Exploits Subzone, Newfoundland. Newfoundland and Labrador Department of Natural Resources, Geological Survey, Report, 01-01.

Pollock, J.C., 2007. The Neoproterozoic-early Paleozoic tectonic evolution of the peri-Gondwanan margin of the Appalachian Orogen: An integrated geochronological, geochemical and isotopic study from North Carolina and

Newfoundland. ProQuest.

Pollock, J.C., Hibbard, J.P., van Staal, C.R., 2011. A paleogeographical review of the peri-Gondwanan realm of the Appalachian orogen1 This article is one of a series of papers published in this CJES Special Issue: In honour of Ward Neale on the theme of Appalachian and Grenvillian geology. Canadian Journal of Earth Sciences 49, 259-288.

Pollock, J.C., Sylvester, P.J., Barr, S.M., Murphy, B., 2015. Lu–Hf zircon and Sm–Nd whole-rock isotope constraints on the extent of juvenile arc crust in Avalonia: examples from Newfoundland and Nova Scotia, Canada. Canadian Journal of Earth Sciences 52, 1-21.

Pollock, J.C., Wilton, D.H.C., van Staal, C.R., Morrissey, K.D., 2007. U-Pb detrital zircon geochronological constraints on the Early Silurian collision of Ganderia and Laurentia along the Dog Bay Line: The terminal Iapetan suture in the Newfoundland Appalachians. American Journal of Science 307, 399-433.

Ramos, V.A., 2009. Anatomy and global context of the Andes: Main geologic features and the Andean orogenic cycle. Geological Society of America Memoirs 204, 31-65.

Reimann, C., Bahlburg, H., Kooijman, E., Berndt, J., Gerdes, A., Carlotto, V., Lopez, S., 2010. Geodynamic evolution of the early Paleozoic Western Gondwana margin 14–17 S reflected by the detritus of the Devonian and Ordovician basins of southern Peru and northern Bolivia. Gondwana Research 18, 370-384.

Roberts, N.W., Slagstad, T., Parrish, R., Norry, M., Marker, M., Horstwood, M.A., 2013. Sedimentary recycling in arc magmas: geochemical and U–Pb–Hf–O constraints on the Mesoproterozoic Suldal Arc, SW Norway. Contrib Mineral Petrol 165, 507-523.

Rogers, N., van Staal, C.R., McNicoll, V., Pollock, J., Zagorevski, A., Whalen, J., 2006. Neoproterozoic and Cambrian arc magmatism along the eastern margin of the Victoria Lake Supergroup: A remnant of Ganderian basement in central Newfoundland? Precambrian Research 147, 320-341.

Rosenbaum, G., Lister, G.S., 2004. Neogene and Quaternary rollback evolution of the Tyrrhenian Sea, the Apennines, and the Sicilian Maghrebides. Tectonics 23, n/a-n/a.

Scherer, E., Münker, C., Mezger, K., 2001. Calibration of the Lutetium-Hafnium Clock. Science 293, 683-687.

Schofield, D.I., D'Lemos, R.S., 2000. Granite petrogenesis in the Gander Zone, NE Newfoundland: mixing of melts from multiple sources and the role of lithospheric delamination. Canadian Journal of Earth Sciences 37, 535-547.

Schroetter, J.-M., Tremblay, A., Bédard, J.H., Villeneuve, M.E., 2006. Syncollisional basin development in the Appalachian orogen—The Saint-Daniel Mélange, southern Québec, Canada. Geological Society of America Bulletin 118, 109-125.

Schulz, K.J., Stewart, D.B., Tucker, R.D., Pollock, J.C., Ayuso, R.A., 2008. The Ellsworth terrane, coastal Maine: Geochronology, geochemistry, and Nd-Pb isotopic composition—Implications for the rifting of Ganderia. Geological Society of America Bulletin 120, 1134-1158.

Scotese, C.R., 2004. A Continental Drift Flipbook. Journal of Geology 112, 729-741.

Sevastjanova, I., Clements, B., Hall, R., Belousova, E.A., Griffin, W.L., Pearson, N., 2011. Granitic magmatism, basement ages, and provenance indicators in the Malay Peninsula: Insights from detrital zircon U–Pb and Hf-isotope data. Gondwana Research 19, 1024-1039.

Skulski, T., Castonguay, S., McNicoll, V., van Staal, C., Kidd, W., Rogers, N., Morris, W., Ugalde, H., Slavinski, H., Spicer, W., 2010. Tectonostratigraphy of the Baie Verte oceanic tract and its ophiolite cover sequence on the Baie Verte Peninsula. Newfoundland and Labrador Department of Natural Resources, Geological Survey, Report 1, 315-337.

Sláma, J., Košler, J., Condon, D.J., Crowley,

J.L., Gerdes, A., Hanchar, J.M., Horstwood, M.S.A., Morris, G.A., Nasdala, L., Norberg, N., Schaltegger, U., Schoene, B., Tubrett, M.N., Whitehouse, M.J., 2008. Plešovice zircon - A new natural reference material for U-Pb and Hf isotopic microanalysis. Chemical Geology 249, 1-35.

Smith, I.E., Price, R.C., 2006. The Tonga–Kermadec arc and Havre–Lau back-arc system: their role in the development of tectonic and magmatic models for the western Pacific. Journal of volcanology and geothermal research 156, 315-331.

Stampfli, G., Hochard, C., Vérard, C., Wilhem, C., vonRaumer, J., 2013. The formation of Pangea. Tectonophysics.

Stewart, D., Tucker, R.D., Ayuso, R.A., Lux, R.D., 2001. Minimum age of the Proterozoic Seven Hundred Acre Island Formation and the tectonic setting of the Islesboro Formation, Islesboro block, Maine. Atlantic Geology 37, pp 41-59.

Stockmal, G.S., Colman-Sadd, S.P., Keen, C.E., Marillier, F., O'Brien, S.J., Quinlan, G.M., 1990. Deep seismic structure and plate tectonic evolution of the Canadian Appalachians. Tectonics 9, 45-62.

Strachan, R.A., Nance, R.D., Dallmeyer, R.D., D'Lemos, R.S., Murphy, J.B., Watt, G.R., 1996. Late Precambrian tectonothermal evolution of the Malverns Complex. Journal of the Geological Society 153, 589-600.

Swinden, S., 1996. Geochemistry of volcanic rocks in the Moreton's Harbour-Twillingate area, Notre Dame Bay. Current Research (1996) Newfoundland Department of Mines and Energy Geological Survey, Report, 96-91.

Szybinski, Z.A., 1995. Paleotectonic and structural setting of the western Notre Dame Bay area, Newfoundland Appalachians. Memorial University of Newfoundland.

Teale, W., Collins, A.S., Foden, J., Payne, J.L., Plavsa, D., Chetty, T.R.K., Santosh, M., Fanning, M., 2011. Cryogenian (-830Ma) mafic magmatism and metamorphism in the northern Madurai Block, southern India: A magmatic link between Sri Lanka and Madagascar? Journal of Asian Earth Sciences 42, 223-233.

Tesfai, F.G., 2011. Petrology and Ti-VP Potential of the Lower Coverdale Plutonic Suite, Southeastern New Brunswick, Canada. Acadia University.

Tremblay, A., Meshi, A., Bédard, J.H., 2009. Oceanic core complexes and ancient oceanic lithosphere: insights from Iapetan and Tethyan ophiolites (Canada and Albania). Tectonophysics 473, 36-52.

van Staal, C., Whalen, J., McNicoll, V., Pehrsson, S., Lissenberg, C.J., Zagorevski, A., van Breemen, O., Jenner, G., 2007. The Notre Dame arc and the Taconic orogeny in Newfoundland. Geological Society of America Memoirs 200, 511-552.

van Staal, C.R., 1994. Brunswick subduction complex in the Canadian Appalachians: record of the Late Ordovician to Late Silurian collision between Laurentia and the Gander margin of Avalon. Tectonics 13, 946-962.

van Staal, C.R., Barr, S.M., 2011. Lithospheric architecture and tectonic evolution of the Canadian Appalachians and associated Atlantic margin., In: Percival, J.A., Cook, F.A., Clowes, R.M. (Eds.), Tectonic Styles in Canada Revisited: the LITHOPROBE perspective. Geological Association of Canada

van Staal, C.R., Barr, S.M., Murphy, J.B., 2012. Provenance and tectonic evolution of Ganderia: Constraints on the evolution of the Iapetus and Rheic oceans. Geology 40, 987-990.

van Staal, C.R., Dewey, J., Mac Niocaill, C., McKerrow, W., 1998. The Cambrian-Silurian tectonic evolution of the northern Appalachians and British Caledonides: history of a complex, west and southwest Pacific-type segment of Iapetus. Geological Society, London, Special Publications 143, 197-242.

van Staal, C.R., Sullivan, R.W., Whalen, J.B., 1996. Provenance and tectonic history of the Gander Zone in the Caledonian/Appalachian orogen: Implications for the origin and assembly of Avalon. SPECIAL PAPERS-GEOLOGICAL

SOCIETY OF AMERICA, 347-368.

van Staal, C.R., Whalen, J.B., Valverde-Vaquero, P., Zagorevski, A., Rogers, N., 2009. Pre-Carboniferous, episodic accretion-related, orogenesis along the Laurentian margin of the northern Appalachians. Geological Society, London, Special Publications 327, 271-316.

Waldron, J.W., Schofield, D.I., Dufrane, S.A., Floyd, J.D., Crowley, Q.G., Simonetti, A., Dokken, R.J., Pothier, H.D., 2014. Ganderia–Laurentia collision in the Caledonides of Great Britain and Ireland. Journal of the Geological Society 171, 555-569.

Waldron, J.W.F., van Staal, C.R., 2001. Taconian orogeny and the accretion of the Dashwoods block: A peri-Laurentian microcontinent in the Iapetus Ocean. Geology 29, 811-814.

Whalen, J.B., JENNER, G.A., LONGSTAFFE, F.J., ROBERT, F., GARIÉPY, C., 1996. Geochemical and isotopic (O, Nd, Pb and Sr) constraints on A-type granite petrogenesis based on the Topsails igneous suite, Newfoundland Appalachians. Journal of Petrology 37, 1463-1489.

Whalen, J.B., McNicoll, V.J., van Staal, C.R., Lissenberg, C.J., Longstaffe, F.J., Jenner, G.A., van Breeman, O., 2006. Spatial, temporal and geochemical characteristics of Silurian collision-zone magmatism, Newfoundland Appalachians: An example of a rapidly evolving magmatic system related to slab break-off. Lithos 89, 377-404.

White, C.E., Barr, S.M., Bevier, M.L., Kamo, S., 1994. A revised interpretation of Cambrian and Ordovician rocks in the Bourinot belt of central Cape Breton Island, Nova Scotia. 1994.

White, C.E., Barr, S.M., Miller, B.V., Hamilton, M.A., 2002. Granitoid plutons of the Brookville terrane, southern New Brunswick: Petrology, age, and tectonic setting. Atlantic Geology 38, 53-74.

Whitmeyer, S.J., Karlstrom, K.E., 2007. Tectonic model for the Proterozoic growth of North America. Geosphere 3, 220-259.

Williams, H., 1979. Appalachian orogen in Canada. Canadian Journal of Earth Sciences 16, 792-807.

Williams, H., Colman-Sadd, S., Swinden, H., 1988. Tectonic-stratigraphic subdivisions of central Newfoundland. Current Research, Part B. Geological Survey of Canada, Paper 88, 91-98.

Williams, H., Currie, K., Piasecki, M., 1993. The Dog Bay Line: a major Silurian tectonic boundary in northeast Newfoundland. Canadian Journal of Earth Sciences 30, 2481-2494.

Willner, A., Barr, S., Gerdes, A., Massonne, H.-J., White, C., 2013. Origin and evolution of Avalonia: evidence from U–Pb and Lu–Hf isotopes in zircon from the Mira terrane, Canada, and the Stavelot–Venn Massif, Belgium. Journal of the Geological Society 170, 769-784.

Willner, A.P., Gerdes, A., Massonne, H.J., van Staal, C.R., Zagorevski, A., 2014. Crustal Evolution of the Northeast Laurentian Margin and the Peri-Gondwanan Microcontinent Ganderia Prior to and During Closure of the Iapetus Ocean: Detrital Zircon U-Pb and Hf Isotope Evidence from Newfoundland. Geoscience Canada 41, 345-364.

Zagorevski, A., Lissenberg, C.J., Van Staal, C., 2009. Dynamics of accretion of arc and backarc crust to continental margins: Inferences from the Annieopsquotch Accretionary Tract, Newfoundland Appalachians. Tectonophysics 479, 150-164.

Zagorevski, A., Rogers, N., van Staal, C.R., McNicoll, V., Lissenberg, C.J., Valverde-Vaquero, P., 2006. Lower to Middle Ordovician evolution of peri-Laurentian arc and backarc complexes in Iapetus: Constraints from the Annieopsquotch accretionary tract, central Newfoundland. Geological Society of America Bulletin 118, 324-342.

Zagorevski, A., Van Staal, C., 2011. The record of Ordovician arc–arc and arc–continent collisions in the Canadian Appalachians during the closure of Iapetus, Arc-Continent Collision. Springer, pp. 341-371.

Zagorevski, A., Van Staal, C.R., McNicoll, V., Rogers, N., 2007. Upper Cambrian to Upper Ordovician peri-Gondwanan Island arc activity in the Victoria Lake Supergroup, Central Newfoundland: Tectonic development of the northern Ganderian margin. American Journal of Science 307, 339-370.

Zagorevski, A., van Staal, C.R., Rogers, N., McNicoll, V.J., Pollock, J., 2010. Middle Cambrian to Ordovician arc-backarc development on the leading edge of Ganderia, Newfoundland Appalachians. Geological Society of America Memoirs 206, 367-396.

Zlatkin, O., Avigad, D., Gerdes, A., 2013. Evolution and provenance of Neoproterozoic basement and Lower Paleozoic siliciclastic cover of the Menderes Massif (western Taurides): Coupled U–Pb–Hf zircon isotope geochemistry. Gondwana Research 23, 682-700.

Supporting information

Supplementary Table 1. U-Pb zircon data

Sample	**No.**	**Pb207/Pb206**		**Pb206/U238**		**Pb207/U235**		**Pb208/Th232**		**Concordancy**	**Pb207/Pb206**		**Pb206/U238**		**Pb207/U235**		**Pb208/Th232**	
aco-13-08	1	0.05838	0.00082	0.09571	0.00109	0.77045	0.01102	0.02957	0.00101	102	544.1	30.26	589.2	6.4	580	6.32	589.1	19.79
aco-13-08	2	0.05955	0.00095	0.09579	0.00114	0.78692	0.01273	0.0307	0.00135	100	587.4	34.11	589.7	6.69	589.4	7.23	611.1	26.43
aco-13-08	3	0.05866	0.00077	0.09522	0.00117	0.77007	0.01107	0.02921	0.00084	101	554.5	28.4	586.3	6.88	579.8	6.35	581.9	16.57
aco-13-08	4	0.05897	0.00089	0.09001	0.00104	0.73165	0.01123	0.02773	0.00119	100	565.9	32.45	555.6	6.17	557.5	6.58	552.8	23.44
aco-13-08	5	0.05927	0.00129	0.09043	0.00142	0.73859	0.01723	0.02627	0.0017	99	577.2	46.78	558.1	8.38	561.6	10.06	524.1	33.47
aco-13-08	6	0.05989	0.00094	0.09426	0.00128	0.77841	0.01348	0.02953	0.00143	99	599.6	33.54	580.7	7.56	584.6	7.7	588.3	28.04
aco-13-08	7	0.05851	0.00167	0.09051	0.00151	0.72972	0.02127	0.0268	0.00193	100	548.8	61.29	558.6	8.94	556.4	12.48	534.5	37.98
aco-13-08	8	0.06783	0.00096	0.09984	0.00127	0.93358	0.01443	0.03339	0.00118	92	863.4	29.04	613.5	7.43	669.5	7.58	663.9	23.06
aco-13-08	9	0.05833	0.00084	0.08972	0.00118	0.72153	0.0116	0.02677	0.00112	100	541.5	31.84	553.9	6.98	551.6	6.84	534	22.06
aco-13-08	10	0.05896	0.00098	0.09124	0.0011	0.74132	0.01263	0.02835	0.00141	100	565.5	35.82	562.9	6.5	563.2	7.36	565	27.75
aco-13-08	11	0.0599	0.0017	0.10172	0.00154	0.84017	0.02452	0.03273	0.00333	101	600.1	60.34	624.5	9	619.2	13.53	650.9	65.17
aco-13-08	12	0.05911	0.00098	0.09122	0.00133	0.74346	0.01388	0.02744	0.00123	100	571.2	35.56	562.8	7.87	564.4	8.08	547.1	24.14
aco-13-08	13	0.05971	0.00098	0.09026	0.00125	0.74302	0.01333	0.02737	0.00088	99	593.3	34.82	557.1	7.39	564.2	7.76	545.8	17.27
aco-13-08	14	0.05941	0.00111	0.09409	0.00124	0.76987	0.01478	0.02853	0.00151	100	582.1	39.96	579.7	7.31	579.7	8.48	568.5	29.75
aco-13-08	15	0.06671	0.00103	0.0914	0.00113	0.84016	0.01363	0.02914	0.00137	91	828.7	31.89	563.8	6.67	619.2	7.52	580.6	27
aco-13-08	16	0.05784	0.00112	0.09188	0.0014	0.73257	0.01544	0.02833	0.00155	102	523.3	41.98	566.7	8.28	558.1	9.05	564.7	30.5
aco-13-08	17	0.05828	0.00103	0.09139	0.00124	0.73429	0.01378	0.02818	0.00105	101	539.7	38.85	563.7	7.35	559.1	8.07	561.7	20.74
aco-13-08	18	0.05853	0.00084	0.09175	0.00116	0.74037	0.01156	0.02774	0.00117	101	549.7	30.96	565.9	6.87	562.6	6.74	553.1	22.99
aco-13-08	19	0.0673	0.00103	0.08818	0.00112	0.81818	0.01332	0.03012	0.00145	90	847.1	31.42	544.8	6.62	607	7.44	599.9	28.47
aco-13-08	20	0.05794	0.0011	0.09224	0.00137	0.73695	0.0152	0.02838	0.00165	101	527.2	41.42	568.8	8.09	560.6	8.88	565.6	32.5
aco-13-08	21	0.0594	0.00081	0.09009	0.00121	0.73802	0.01158	0.029	0.00104	99	581.9	29.5	556.1	7.14	561.2	6.77	577.8	20.44
aco-13-08	22	0.06024	0.00098	0.09063	0.0013	0.75282	0.01373	0.02916	0.00138	98	612.4	34.77	559.3	7.7	569.9	7.95	581	27.16
aco-13-08	23	0.05938	0.00471	0.09047	0.00261	0.74101	0.05533	0.02723	0.00839	99	580.9	163.51	558.3	15.46	563	32.27	543.1	165.14
aco-13-08	24	0.0617	0.00102	0.08978	0.00123	0.76387	0.01362	0.02988	0.0013	96	663.8	34.94	554.2	7.26	576.2	7.84	595.1	25.58
aco-13-08	25	0.06009	0.00105	0.08991	0.00129	0.74479	0.01416	0.02906	0.00152	98	606.8	37.22	555	7.63	565.2	8.24	579	29.78
aco-13-08	26	0.05772	0.0011	0.08992	0.00123	0.71577	0.01421	0.02752	0.00122	101	518.9	41.62	555.1	7.28	548.2	8.41	548.8	24.07
aco-13-08	27	0.06425	0.00097	0.09058	0.00125	0.80243	0.01357	0.02816	0.00129	93	749.9	31.43	558.9	7.41	598.2	7.64	561.4	25.45
aco-13-08	28	0.06023	0.00093	0.09054	0.00113	0.75183	0.01213	0.02823	0.00121	98	611.7	32.92	558.7	6.67	569.3	7.03	562.6	23.88
aco-13-08	29	0.07299	0.02103	0.08119	0.00705	0.82574	0.228	-0.198	0.09216	82	1013.8	494.87	503.2	42.03	611.2	126.8	******	2322.76
aco-13-08	30	0.0582	0.00085	0.09029	0.00115	0.72461	0.01147	0.02844	0.00125	101	536.6	32.39	557.3	6.8	553.4	6.75	566.8	24.61
aco-13-08	31	0.06024	0.01348	0.08982	0.00659	0.74365	0.15102	0.03717	0.00661	98	612.1	421.5	554.5	39	564.5	87.94	737.6	128.86
aco-13-08	32	0.0581	0.001	0.09118	0.00124	0.73056	0.01338	0.02784	0.00152	101	533	37.86	562.5	7.31	556.9	7.85	554.9	29.95
aco-13-08	33	0.05942	0.00093	0.08551	0.00114	0.70064	0.0119	0.02745	0.00135	98	582.5	33.77	529	6.75	539.2	7.1	547.3	26.49
aco-13-08	34	0.0681	0.00291	0.07868	0.00139	0.73857	0.02983	0.02777	0.00512	87	871.5	86	488.3	8.33	561.6	17.42	553.6	100.77
aco-13-08	35	0.05999	0.00087	0.09433	0.00118	0.78022	0.01216	0.02812	0.00078	99	603.2	31.16	581.1	6.93	585.6	6.93	560.6	15.42
aco-13-08	36	0.06005	0.00089	0.09047	0.00119	0.74914	0.01224	0.02791	0.00104	98	605.5	31.77	558.3	7.04	567.7	7.11	556.4	20.51
aco-13-08	37	0.05998	0.00091	0.08978	0.00123	0.74243	0.01256	0.02749	0.00106	98	602.7	32.34	554.3	7.26	563.8	7.32	548.2	20.81
aco-13-08	38	0.05954	0.00096	0.09045	0.00125	0.74249	0.01325	0.02916	0.0013	99	586.9	34.7	558.2	7.4	563.9	7.72	581	25.45
aco-13-08	39	0.0598	0.00081	0.09709	0.00121	0.8005	0.01182	0.03048	0.00102	100	596.4	28.93	597.3	7.08	597.1	6.66	606.8	20.07
aco-13-08	40	0.05969	0.00098	0.09014	0.00124	0.74177	0.01334	0.0282	0.0013	99	592.8	34.66	556.4	7.34	563.4	7.78	562.2	25.53
aco-13-08	41	0.05889	0.00103	0.09067	0.00115	0.73621	0.01324	0.03017	0.00159	100	562.9	37.72	559.5	6.8	560.2	7.74	600.8	31.15
aco-13-08	42	0.06145	0.00119	0.09044	0.0013	0.76617	0.0158	0.02853	0.0017	97	654.9	41.04	558.1	7.68	577.6	9.08	568.5	33.45
aco-13-08	43	0.0595	0.00083	0.09681	0.00122	0.79413	0.01212	0.03067	0.0012	100	585.4	30.02	595.7	7.17	593.5	6.86	610.7	23.59
aco-12-16	74	0.13247	0.00222	0.38893	0.00603	7.10239	0.13329	0.10607	0.00444	99	2130.9	29.1	2117.8	27.99	2124.3	16.7	2037.7	81.09
aco-12-16	75	0.092	0.00125	0.24641	0.00354	3.12491	0.05051	0.07174	0.00274	97	1467.2	25.69	1419.9	18.31	1438.8	12.43	1400.3	51.61
aco-12-16	76	0.18551	0.00269	0.31273	0.00464	7.99777	0.13763	0.09063	0.00453	65	2702.8	23.75	1754.1	22.81	2230.8	15.53	1753.6	84.03
aco-12-16	77	0.1059	0.00151	0.25585	0.00372	3.73502	0.06225	0.10853	0.0046	85	1730	25.93	1468.6	19.11	1578.9	13.35	2082.6	83.93
aco-12-16	78	0.05574	0.00121	0.06867	0.00108	0.52777	0.01227	0.02025	0.00087	100	441.6	47.35	428.2	6.54	430.3	8.16	405.2	17.22
aco-12-16	79	0.10712	0.00163	0.31987	0.00485	4.72472	0.08477	0.08942	0.00397	102	1751	27.52	1789.1	23.7	1771.6	15.03	1731.1	73.62
aco-12-16	80	0.05861	0.0012	0.07155	0.00114	0.57814	0.01289	0.02102	0.00111	96	552.7	43.98	445.5	6.84	463.3	8.3	420.4	22.05
aco-12-16	81	0.05557	0.00095	0.06812	0.00099	0.52191	0.00994	0.02148	0.00082	100	434.9	37.26	424.8	5.96	426.4	6.63	429.6	16.28
aco-12-16	82	0.07621	0.00124	0.18372	0.00263	1.93037	0.03501	0.05584	0.00257	99	1100.6	32.22	1087.3	14.31	1091.7	12.13	1098.3	49.21
aco-12-16	83	0.05666	0.00133	0.06688	0.001	0.5224	0.0127	0.02063	0.00102	98	477.6	51.43	417.3	6.06	426.8	8.47	412.7	20.28
aco-12-16	84	0.0558	0.00151	0.06717	0.00105	0.51674	0.01418	0.0223	0.00142	99	444.1	59.1	419.1	6.35	423	9.49	445.7	28.11
aco-12-16	85	0.05838	0.00193	0.06754	0.00111	0.5435	0.01772	0.02197	0.00165	96	543.9	70.76	421.3	6.72	440.7	11.66	439.3	32.54
aco-12-16	86	0.08723	0.00158	0.22968	0.00335	2.76224	0.05419	0.06889	0.00362	98	1365.7	34.35	1332.8	17.59	1345.4	14.62	1346.6	68.42
aco-12-16	87	0.09891	0.00179	0.28311	0.00421	3.86055	0.07658	0.08698	0.00496	100	1603.6	33.3	1607	21.14	1605.5	16	1685.7	92.15
Sample No.	Analysis_ #	Pb207/Pb206		Pb206/U238		Pb207/U235		Pb208/Th232		Concordancy	Pb207/Pb206		Pb206/U238		Pb207/U235		Pb208/Th232	
ACO-12-14B	32	0.06064	0.00138	0.07248	0.00087	0.60594	0.01314	0.02354	0.00087	94	626.6	48.16	451.1	5.25	481	8.31	470.3	17.16
ACO-12-14B	27	0.05858	0.00146	0.07257	0.00089	0.5861	0.01391	0.02516	0.00097	96	551.5	53.42	451.6	5.38	468.4	8.9	502.2	19.22
ACO-12-14B	2	0.06007	0.00136	0.07289	0.00087	0.60359	0.01307	0.02337	0.00068	95	605.9	48.19	453.6	5.25	479.5	8.28	467	13.35
ACO-12-14B	28	0.05551	0.00137	0.07384	0.0009	0.56508	0.01328	0.02311	0.00086	101	432.4	53.55	459.3	5.39	454.8	8.62	461.8	17.08
ACO-12-14B	31	0.06354	0.00126	0.07394	0.00088	0.64774	0.01247	0.02617	0.00083	91	726.4	41.48	459.8	5.27	507.1	7.68	522.1	16.28
ACO-12-14B	48	0.05631	0.0016	0.07412	0.00099	0.57523	0.01567	0.02275	0.00084	100	463.8	62.17	460.9	5.96	461.4	10.1	454.7	16.55
ACO-12-14B	50	0.05987	0.00115	0.07458	0.00095	0.61545	0.01189	0.02376	0.00089	95	598.8	41.02	463.7	5.71	487	7.47	474.6	17.66
ACO-12-14B	45	0.05622	0.00098	0.07474	0.00088	0.57923	0.01003	0.02196	0.00056	100	460.3	38.46	464.7	5.27	464	6.45	439.1	11
ACO-12-14B	62	0.07515	0.00136	0.07501	0.00094	0.77704	0.01404	0.02587	0.00071	80	1072.6	36	466.3	5.62	583.8	8.02	516.3	13.94
ACO-12-14B	52	0.05936	0.00113	0.07506	0.0009	0.6142	0.01145	0.02331	0.00074	96	580.4	40.68	466.6	5.41	486.2	7.2	465.8	14.63
ACO-12-14B	42	0.08149	0.00154	0.07549	0.00097	0.84783	0.01582	0.02186	0.00054	75	1233.2	36.54	469.1	5.83	623.5	8.69	437.1	10.62
ACO-12-14B	10	0.0735	0.00145	0.07556	0.00092	0.7656	0.01462	0.03107	0.00095	81	1027.7	39.37	469.6	5.49	577.2	8.41	618.4	18.64
ACO-12-14B	29	0.05903	0.00088	0.07594	0.00085	0.6181	0.00922	0.02398	0.00062	97	568.3	32.12	471.9	5.11	488.7	5.78	478.9	12.27
ACO-12-14B	1	0.0597	0.00105	0.07597	0.00082	0.62522	0.01048	0.0251	0.00076	96	593.1	37.24	472	4.89	493.1	6.55	501	14.92
ACO-12-14B	7	0.06272	0.00155	0.07643	0.00097	0.66081	0.01574	0.02474	0.00078	92	698.7	51.83	474.7	5.81	515.1	9.62	493.9	15.31
ACO-12-14B	24	0.05602	0.00095	0.07642	0.00088	0.59025	0.00997	0.02248	0.00054	101	452.7	37.09	474.7	5.29	471	6.36	449.3	10.58
ACO-12-14B	26	0.07812	0.00148	0.07649	0.00094	0.82392	0.0152	0.02524	0.00063	78	1150	37.13	475.1	5.63	610.2	8.46	503.8	12.47

ACO-12-14B	36	0.05653	0.00104	0.07667	0.00099	0.5976	0.01126	0.02214	0.00104	100	472.6	40.63	476.2	5.93	475.7	7.16	442.5	20.48
ACO-12-14B	55	0.06004	0.00145	0.07695	0.00105	0.63682	0.01514	0.02302	0.00096	96	604.9	51.42	477.9	6.27	500.3	9.39	460.1	19.05
ACO-12-14B	63	0.06638	0.00184	0.07695	0.00105	0.70399	0.01865	0.0251	0.00089	88	818.3	57.01	477.9	6.27	541.2	11.11	501	17.52
ACO-12-14B	33	0.05851	0.00148	0.07706	0.00098	0.62154	0.01511	0.02625	0.00098	97	548.8	54.44	478.5	5.85	490.8	9.46	523.7	19.3
ACO-12-14B	14	0.06085	0.00199	0.07712	0.0011	0.6469	0.02014	0.02453	0.0011	95	633.8	68.89	478.9	6.58	506.6	12.41	489.8	21.64
ACO-12-14B	46	0.05885	0.0014	0.07716	0.00099	0.6259	0.01442	0.02451	0.00078	97	561.7	51.02	479.2	5.9	493.5	9.01	489.5	15.42
ACO-12-14B	11	0.05396	0.00194	0.07729	0.00113	0.57507	0.0198	0.02474	0.00105	104	369.4	78.96	479.9	6.74	461.3	12.77	493.9	20.67
ACO-12-14B	34	0.05922	0.00173	0.07734	0.00105	0.63138	0.01763	0.02499	0.00108	97	575.2	62.32	480.2	6.26	497	10.97	498.9	21.29
ACO-12-14B	65	0.06114	0.00147	0.07752	0.00104	0.65319	0.01537	0.02311	0.00076	94	644	50.77	481.3	6.24	510.4	9.44	461.8	15.04
ACO-12-14B	37	0.06832	0.00144	0.07762	0.00098	0.73112	0.01503	0.02604	0.00089	86	878.2	43.11	481.9	5.84	557.2	8.82	519.5	17.6
ACO-12-14B	19	0.06129	0.00219	0.07766	0.00127	0.65625	0.02271	0.0259	0.00137	94	649.5	74.94	482.1	7.58	512.3	13.92	516.9	27.03
ACO-12-14B	5	0.05587	0.00111	0.07795	0.00089	0.6004	0.01151	0.02511	0.00073	101	447	43.31	483.9	5.33	477.5	7.3	501.2	14.33
ACO-12-14B	21	0.05671	0.00096	0.07797	0.00088	0.60969	0.0101	0.02424	0.0007	100	479.7	37.29	484	5.25	483.4	6.37	484.1	13.86
ACO-12-14B	39	0.05532	0.0016	0.07811	0.00103	0.59558	0.01651	0.02386	0.00117	102	425.1	62.72	484.8	6.19	474.4	10.51	476.5	23.05
ACO-12-14B	25	0.12147	0.00223	0.07827	0.00099	1.3108	0.02304	0.04675	0.00116	57	1977.9	32.28	485.8	5.9	850.5	10.12	923.5	22.47
ACO-12-14B	58	0.10603	0.0018	0.07839	0.00096	1.14599	0.01907	0.03377	0.00108	63	1732.3	30.84	486.5	5.74	775.3	9.02	671.3	21.03
ACO-12-14B	47	0.05664	0.00166	0.07848	0.00106	0.61243	0.01717	0.0241	0.0009	100	476.7	63.62	487	6.32	485.1	10.81	481.3	17.77
ACO-12-14B	40	0.06154	0.00142	0.07848	0.00106	0.66591	0.01514	0.01872	0.00068	94	658.2	48.71	487.1	6.35	518.2	9.23	374.8	13.57
ACO-12-14B	30	0.05748	0.00122	0.07852	0.00097	0.62227	0.01294	0.02353	0.00066	99	509.6	46.45	487.3	5.78	491.3	8.1	470	13.03
ACO-12-14B	13	0.0585	0.00172	0.07856	0.00108	0.63357	0.01791	0.0228	0.00088	98	548.5	63.07	487.5	6.44	498.3	11.13	455.6	17.38
ACO-12-14B	76	0.05908	0.00115	0.07879	0.00097	0.64149	0.01236	0.02317	0.00074	97	569.9	41.71	488.9	5.82	503.2	7.65	463	14.68
ACO-12-14B	66	0.07312	0.00131	0.07887	0.00097	0.79486	0.01412	0.02379	0.00058	82	1017.3	35.92	489.4	5.79	593.9	7.99	475.2	11.44
ACO-12-14B	15	0.07432	0.00161	0.07901	0.001	0.80951	0.01694	0.03033	0.00101	81	1050.1	43.1	490.2	5.96	602.2	9.51	604	19.88
ACO-12-14B	59	0.07127	0.00205	0.07907	0.00122	0.77666	0.02179	0.01851	0.00082	84	965.2	57.71	490.6	7.28	583.6	12.45	370.6	16.18
ACO-12-14B	77	0.05977	0.00148	0.07936	0.00106	0.65383	0.01575	0.02346	0.00086	96	594.9	53.05	492.3	6.33	510.8	9.67	468.7	17.06
ACO-12-14B	78	0.05966	0.00108	0.07944	0.00095	0.65327	0.0117	0.02548	0.00093	97	591.3	38.63	492.8	5.66	510.5	7.19	508.5	18.4
ACO-12-14B	51	0.06865	0.00157	0.07947	0.00104	0.75215	0.01674	0.02341	0.00071	87	888.2	46.68	493	6.23	569.5	9.7	467.7	14.11
ACO-12-14B	74	0.05668	0.00111	0.0795	0.00101	0.62108	0.01222	0.02169	0.00072	101	478.4	43.23	493.1	6.04	490.5	7.65	433.8	14.19
ACO-12-14B	54	0.05641	0.0012	0.07961	0.00096	0.61896	0.01279	0.0254	0.00089	101	467.9	47	493.8	5.73	489.2	8.02	507	17.54
ACO-12-14B	17	0.0565	0.00158	0.0797	0.00102	0.62085	0.01653	0.02445	0.00122	101	471.5	60.94	494.3	6.11	490.4	10.35	488.2	24.07
ACO-12-14B	75	0.05798	0.00146	0.08	0.0011	0.63931	0.01584	0.023	0.00087	99	528.7	54.64	496.1	6.59	501.9	9.81	459.5	17.12
ACO-12-14B	12	0.05695	0.00146	0.08026	0.00099	0.63018	0.01537	0.02458	0.001	100	488.9	56.03	497.7	5.93	496.2	9.57	490.9	19.76
ACO-12-14B	80	0.06026	0.00139	0.08045	0.00105	0.66819	0.01512	0.0272	0.00118	96	612.8	49.19	498.8	6.24	519.6	9.2	542.5	23.2
ACO-12-14B	38	0.05821	0.0013	0.08072	0.00097	0.64775	0.01384	0.02639	0.00115	99	537.3	48.57	500.4	5.76	507.1	8.53	526.6	22.7
ACO-12-14B	79	0.06913	0.00177	0.08097	0.00118	0.77146	0.01939	0.02447	0.00102	86	902.6	51.91	501.9	7.01	580.6	11.11	488.6	20.2
ACO-12-14B	67	0.05803	0.00168	0.08101	0.00119	0.64798	0.01834	0.02281	0.00082	99	530.6	62.86	502.2	7.1	507.2	11.3	455.9	16.23
ACO-12-14B	4	0.05774	0.00122	0.08109	0.00094	0.64549	0.01308	0.02657	0.00077	99	519.6	45.92	502.6	5.6	505.7	8.07	530.1	15.13
ACO-12-14B	70	0.05777	0.0015	0.08114	0.00109	0.64602	0.01635	0.02607	0.00089	99	520.7	56.34	502.9	6.48	506	10.09	520.2	17.56
ACO-12-14B	56	0.08857	0.00162	0.08119	0.00101	0.99148	0.01772	0.03373	0.00107	72	1394.9	34.58	503.2	6	699.5	9.03	670.5	20.9
ACO-12-14B	69	0.05912	0.00117	0.08155	0.00101	0.66458	0.01305	0.02435	0.00069	98	571.7	42.63	505.4	6.02	517.4	7.96	486.2	13.55
ACO-12-14B	68	0.06162	0.00151	0.0821	0.00106	0.6972	0.0165	0.0264	0.00089	95	660.9	51.69	508.7	6.29	537.1	9.87	526.6	17.49
ACO-12-14B	43	0.05758	0.00081	0.0825	0.00093	0.65477	0.00935	0.02563	0.00056	100	513.3	30.95	511	5.54	511.4	5.74	511.5	10.95
ACO-12-14B	61	0.08475	0.00201	0.08323	0.00116	0.97233	0.02226	0.03259	0.00094	75	1309.8	45.45	515.4	6.89	689.7	11.46	648.2	18.39
ACO-12-14B	71	0.05772	0.00114	0.08392	0.001	0.66755	0.01285	0.02894	0.00097	100	518.8	42.94	519.5	5.94	519.2	7.82	576.6	19.14
ACO-12-14B	9	0.05567	0.00128	0.08485	0.00104	0.65118	0.01448	0.02659	0.00082	103	438.9	49.91	525	6.2	509.2	8.9	530.3	16.08
ACO-12-14B	73	0.05791	0.00089	0.08494	0.00099	0.67803	0.01059	0.02557	0.00073	100	526.1	33.66	525.6	5.9	525.6	6.41	510.3	14.4
ACO-12-14B	20	0.0953	0.00216	0.08617	0.00118	1.13216	0.02481	0.04175	0.00186	69	1534.1	42.01	532.9	7.01	768.8	11.81	826.8	36.17
ACO-12-14B	35	0.05798	0.00134	0.08849	0.00108	0.70738	0.01572	0.02944	0.00113	101	528.8	50.23	546.6	6.42	543.2	9.35	586.5	22.12
ACO-12-14B	8	0.05935	0.00115	0.08871	0.00099	0.72589	0.01344	0.03025	0.00103	99	579.9	41.67	547.9	5.84	554.1	7.91	602.4	20.16
ACO-12-14B	60	0.05919	0.00106	0.09534	0.00112	0.77785	0.01376	0.02607	0.00097	100	574	38.63	587.1	6.61	584.3	7.86	520.1	19.02
ACO-12-14B	16	0.09665	0.00158	0.10385	0.00122	1.38386	0.02219	0.0284	0.00093	72	1560.5	30.4	636.9	7.12	882.1	9.45	566.1	18.18
ACO-12-14B	23	0.11093	0.00174	0.12013	0.00144	1.83743	0.02849	0.05105	0.00129	40	1814.6	28.18	731.3	8.3	1058.9	10.2	1006.5	24.86
ACO-12-14B	53	0.073	0.0018	0.17113	0.00238	1.72206	0.04122	0.04971	0.00177	100	1014	49.05	1018.3	13.09	1016.8	15.38	980.6	34.16
ACO-12-14B	41	0.07811	0.0016	0.17616	0.00207	1.89534	0.0367	0.05181	0.00235	91	1149.6	40.25	1046	11.35	1079.5	12.87	1020.9	45.21
ACO-12-14B	6	0.07387	0.00097	0.18344	0.00199	1.86803	0.02447	0.05584	0.00135	105	1037.9	26.2	1085.7	10.81	1069.8	8.66	1098.3	25.83
ACO-12-14B	57	0.07716	0.00154	0.1909	0.00244	2.03085	0.03969	0.05178	0.00167	100	1125.3	39.23	1126.3	13.23	1125.9	13.3	1020.3	32.02
ACO-12-14B	72	0.08042	0.00256	0.20158	0.00318	2.23423	0.06775	0.06383	0.00277	98	1207.3	61.52	1183.8	17.06	1191.8	21.27	1250.7	52.63
ACO-12-14B	49	0.08367	0.00125	0.21586	0.00261	2.48948	0.03838	0.06497	0.00204	98	1284.7	28.96	1259.9	13.83	1269	11.17	1272.3	38.62
ACO-12-14B	3	0.09257	0.00164	0.23222	0.00261	2.96392	0.04932	0.06374	0.00239	91	1479.1	33.25	1346.1	13.67	1398.4	12.63	1249	45.36
ACO-12-14B	64	0.09048	0.00274	0.24138	0.00386	3.00966	0.08662	0.07136	0.00305	97	1435.5	56.81	1393.9	20.04	1410.1	21.94	1393.3	57.63
ACO-12-14B	22	0.60293	0.0072	0.24169	0.00276	20.092	0.24037	0.47985	0.01025	31	4515.1	17.23	1395.5	14.32	3095.8	11.57	7922	140
ACO-12-14B	18	0.10016	0.00167	0.28235	0.00312	3.89889	0.06186	0.08607	0.00387	99	1627	30.66	1603.2	15.69	1613.5	12.82	1668.8	72.04
ACO-12-14B	44	0.10584	0.00151	0.30315	0.00335	4.42184	0.06123	0.09312	0.00262	99	1728.9	25.89	1706.9	16.56	1716.4	11.47	1799.7	48.49

aco-13-08	44	0.0615	0.00096	0.09004	0.00115	0.76352	0.01269	0.03005	0.00139	96	656.7	33.09	555.8	6.82	576	7.31	598.5	27.35
aco-13-08	45	0.06069	0.00123	0.09088	0.00132	0.76055	0.01625	0.02968	0.00194	98	628.3	43.04	560.7	7.77	574.3	9.37	591.1	38.02
Sample no	Analysis_ #	Pb207/Pb206		Pb206/U238		Pb207/U235		Pb208/Th232		Concordancy	Pb207/Pb206		Pb206/U238		Pb207/U235		Pb208/Th232	
aco-13-13	1	0.05616	0.00156	0.0767	0.00111	0.5936	0.01629	0.02371	0.00088	101	458.3	60.61	476.4	6.63	473.2	10.38	473.7	17.28
aco-13-13	2	0.10828	0.00142	0.30564	0.00388	4.5612	0.06662	0.0861	0.00254	97	1770.7	23.8	1719.2	19.18	1742.2	12.16	1669.5	47.32
aco-13-13	3	0.05796	0.00095	0.07511	0.00093	0.59959	0.01012	0.02372	0.00084	98	527.8	35.9	466.9	5.56	477	6.43	473.8	16.55
aco-13-13	4	0.05857	0.00118	0.07506	0.00098	0.60591	0.01237	0.02311	0.00074	97	551.1	43.31	466.6	5.88	481	7.82	461.8	14.68
aco-13-13	5	0.05978	0.00095	0.07455	0.00094	0.61414	0.01021	0.02243	0.00067	95	595.2	34.5	463.5	5.62	486.2	6.43	448.3	13.2
aco-13-13	6	0.05526	0.00161	0.07197	0.00104	0.54806	0.0157	0.02476	0.00102	101	422.6	63.15	448	6.27	443.7	10.3	494.4	20.21
aco-13-13	7	0.0628	0.00161	0.07387	0.00106	0.63937	0.01619	0.02449	0.00095	92	701.6	53.61	459.5	6.35	501.9	10.03	489.1	18.71
aco-13-13	8	0.06278	0.00192	0.07708	0.00116	0.66679	0.02002	0.02563	0.00116	92	700.7	63.88	478.7	6.91	518.8	12.19	511.6	22.85
aco-13-13	9	0.06158	0.00098	0.07397	0.00093	0.62767	0.01049	0.02366	0.00076	93	659.5	33.8	460	5.57	494.6	6.55	472.6	15.08
aco-13-13	10	0.23797	0.00607	0.10126	0.00141	3.32479	0.08193	0.07538	0.00709	42	3106.4	40.03	621.8	8.26	1486.9	19.24	1468.9	133.26
aco-13-13	11	0.05701	0.00119	0.07628	0.00104	0.59902	0.01276	0.02216	0.00088	99	491.4	45.4	473.9	6.21	476.6	8.1	443	17.44
aco-13-13	12	0.06033	0.00206	0.07872	0.00123	0.65432	0.02191	0.02446	0.00124	96	615.3	72.11	488.5	7.33	511.1	13.45	488.3	24.47
aco-13-13	13	0.06419	0.00188	0.07749	0.0012	0.68542	0.01986	0.02646	0.00138	91	748	60.68	481.1	7.21	530	11.96	527.8	27.17
aco-13-13	14	0.05763	0.0011	0.07513	0.00102	0.59637	0.01182	0.02385	0.00113	98	515.5	41.6	467	6.11	474.9	7.52	476.3	22.27
aco-13-13	15	0.0612	0.00242	0.07663	0.00133	0.64618	0.02484	0.02396	0.00142	94	646.3	82.87	476	7.98	506.1	15.32	478.6	28.01
aco-13-13	16	0.0565	0.00094	0.072	0.00092	0.56047	0.00975	0.02159	0.00064	99	471.2	36.6	448.2	5.53	451.8	6.35	431.8	12.6
aco-13-13	17	0.0625	0.00163	0.07614	0.00112	0.65557	0.01695	0.02336	0.0009	92	691.1	54.59	473.1	6.71	511.9	10.39	466.8	17.78
aco-13-13	18	0.05997	0.00248	0.07462	0.00129	0.61662	0.0248	0.0199	0.00104	95	602.4	87.02	463.9	7.71	487.7	15.58	398.3	20.59
aco-13-13	19	0.05688	0.00078	0.07658	0.00093	0.60016	0.00882	0.02265	0.00072	100	486.1	30.34	475.7	5.54	477.3	5.6	452.6	14.16
aco-13-13	20	0.05894	0.00149	0.07633	0.00106	0.61995	0.01568	0.02276	0.00082	97	564.8	54.18	474.2	6.34	489.8	9.83	454.9	16.12
aco-13-13	21	0.05711	0.00158	0.07805	0.00111	0.61435	0.01683	0.02369	0.00091	100	495.2	60.35	484.4	6.65	486.3	10.59	473.3	18.02
aco-13-13	22	0.05935	0.00145	0.0792	0.00113	0.64764	0.01584	0.02202	0.00088	97	579.8	52.26	491.3	6.73	507	9.76	440.2	17.34
aco-13-13	23	0.06042	0.00185	0.07845	0.00123	0.6533	0.01975	0.02025	0.00104	95	618.6	64.82	486.9	7.35	510.5	12.13	405.2	20.57
aco-13-13	24	0.06464	0.00127	0.07939	0.00096	0.70773	0.01356	0.02307	0.00141	91	762.7	40.77	492.5	5.74	543.4	8.06	461.1	27.77
aco-13-13	25	0.06101	0.00181	0.07775	0.00124	0.65399	0.01925	0.02286	0.0012	94	639.6	62.6	482.7	7.39	510.9	11.82	456.8	23.79
aco-13-13	26	0.05777	0.00259	0.07869	0.00152	0.62679	0.02736	0.02496	0.00181	99	520.7	95.84	488.3	9.11	494.1	17.07	498.2	35.69
aco-13-13	27	0.07998	0.00135	0.19286	0.00259	2.12608	0.03806	0.05567	0.00245	95	1196.4	33.04	1136.9	13.98	1157.3	12.36	1095.1	46.82
aco-13-13	28	0.05873	0.00146	0.07381	0.00102	0.59752	0.0147	0.02228	0.00105	97	556.9	53.26	459.1	6.14	475.7	9.35	445.3	20.75
aco-13-13	29	0.06315	0.00152	0.07712	0.00114	0.67144	0.01629	0.02598	0.0015	92	713.4	50.22	478.9	6.8	521.6	9.9	518.5	29.59
aco-13-13	30	0.05713	0.00108	0.07727	0.00099	0.6085	0.01166	0.02405	0.00109	99	495.8	41.06	479.8	5.91	482.6	7.36	480.3	21.43
aco-13-13	31	0.05867	0.00231	0.07271	0.00121	0.588	0.0226	0.02346	0.00113	96	554.8	83.63	452.5	7.26	469.6	14.45	468.7	22.32
aco-13-13	32	0.05604	0.00089	0.07299	0.00089	0.56365	0.00929	0.02191	0.00066	100	453.6	34.59	454.1	5.35	453.9	6.03	438.1	12.99
aco-13-13	33	0.06411	0.00139	0.07837	0.00102	0.69243	0.01497	0.02879	0.00102	91	745.2	45.26	486.4	6.11	534.3	8.98	573.6	19.98
aco-13-13	34	0.05741	0.00155	0.07465	0.00107	0.5907	0.01586	0.02393	0.00098	98	506.9	58.77	464.1	6.44	471.3	10.12	477.9	19.32
aco-13-13	35	0.05886	0.0024	0.08796	0.00153	0.7136	0.02816	0.03417	0.00226	99	561.8	86.44	543.5	9.07	546.9	16.69	679.1	44.15
aco-13-13	36	0.05751	0.00144	0.07751	0.00102	0.61445	0.015	0.02312	0.00103	99	510.6	54.45	481.3	6.11	486.4	9.44	461.9	20.29
aco-13-13	37	0.05731	0.00127	0.08055	0.00117	0.63646	0.0146	0.02609	0.00141	100	503.1	48.68	499.4	6.95	500.1	9.06	520.5	27.68
aco-13-13	38	0.06659	0.00343	0.07452	0.00156	0.68415	0.03409	0.02705	0.0019	88	825	103.92	463.3	9.37	529.3	20.55	539.4	37.4
aco-13-13	39	0.05629	0.00125	0.08054	0.00109	0.62484	0.01401	0.02543	0.00114	101	462.9	48.94	499.3	6.51	492.9	8.75	507.6	22.39
aco-13-13	41	0.05847	0.00121	0.07889	0.00109	0.63576	0.01359	0.02586	0.00132	98	547.3	44.73	489.5	6.53	499.7	8.44	516.1	26.08
aco-13-13	42	0.05778	0.00249	0.0792	0.00138	0.63078	0.02658	0.02512	0.00148	99	521.3	92.14	491.4	8.27	496.6	16.55	501.4	29.25
aco-13-13	43	0.06027	0.0015	0.07947	0.00105	0.66021	0.01604	0.02551	0.00171	96	613.1	52.91	493	6.3	514.7	9.81	509.1	33.77
aco-13-13	44	0.06029	0.00262	0.0849	0.00144	0.70556	0.02956	0.03135	0.00238	97	614	91.22	525.3	8.56	542.1	17.6	623.9	46.71
aco-13-13	45	0.05649	0.00242	0.07977	0.00142	0.62115	0.02592	0.02572	0.00193	101	470.8	92.88	494.8	8.5	490.6	16.23	513.2	37.98
aco-13-13	46	0.05807	0.0022	0.07793	0.00133	0.62378	0.02314	0.02644	0.00128	98	531.9	81.23	483.7	7.97	492.2	14.47	527.4	25.29
aco-13-13	47	0.08393	0.00155	0.07716	0.00107	0.89272	0.01719	0.03567	0.00135	74	1290.7	35.54	479.2	6.41	647.8	9.22	708.5	26.42
aco-13-13	48	0.05807	0.00101	0.07591	0.001	0.60771	0.01115	0.02411	0.00079	98	532	38.24	471.7	5.98	482.1	7.04	481.6	15.52
aco-13-13	49	0.0575	0.00183	0.07379	0.00119	0.58495	0.01841	0.02675	0.00159	98	510.5	68.95	459	7.13	467.6	11.8	533.6	31.31
aco-13-13	50	0.05709	0.00123	0.07587	0.00108	0.59707	0.01329	0.02673	0.00115	99	494.4	46.74	471.4	6.48	475.4	8.45	533.1	22.66
aco-13-13	51	0.06462	0.00114	0.07399	0.00094	0.6589	0.0119	0.0241	0.00091	90	762.1	36.72	460.1	5.66	513.9	7.29	481.3	17.91
aco-13-13	52	0.05617	0.00198	0.07507	0.00118	0.58124	0.0201	0.02446	0.0013	100	458.6	76.15	466.7	7.08	465.3	12.91	488.4	25.71
aco-13-13	53	0.05814	0.00122	0.07366	0.00098	0.59015	0.0125	0.02317	0.00103	97	534.7	45.87	458.2	5.88	471	7.98	462.9	20.44
aco-13-13	54	0.08116	0.00207	0.07869	0.00124	0.8802	0.02263	0.03112	0.00196	76	1225.4	49.18	488.3	7.38	641.1	12.22	619.5	38.42
aco-13-13	55	0.3757	0.05802	0.14673	0.01498	7.59325	0.95024	0.06471	0.00973	40	3814.6	215.74	882.6	84.21	2184.1	112.28	1267.4	184.77
aco-13-13	56	0.05716	0.00104	0.07554	0.001	0.59516	0.01131	0.02403	0.00096	99	497.3	39.72	469.4	5.97	474.2	7.2	480	18.96
aco-13-13	57	0.0587	0.00179	0.07471	0.00119	0.60459	0.01832	0.02626	0.00161	97	556	65.1	464.5	7.16	480.1	11.59	524	31.74
aco-13-13	58	0.05664	0.00231	0.07419	0.00123	0.57872	0.02306	0.02321	0.00126	100	476.8	88.57	461.3	7.39	463.6	14.83	463.7	24.92
aco-13-13	59	0.13151	0.00237	0.0828	0.00113	1.50086	0.02756	0.05116	0.00209	55	2118.2	31.3	512.8	6.74	930.7	11.19	1008.5	40.23
aco-13-13	60	0.08134	0.00329	0.07163	0.00136	0.80315	0.03106	0.02625	0.00181	75	1229.8	77.27	446	8.15	598.6	17.49	523.7	35.61
aco-13-13	61	0.06565	0.0045	0.07906	0.00179	0.71545	0.04756	0.03012	0.00278	90	795.2	137.58	490.5	10.71	548	28.15	599.7	54.47
aco-13-13	62	0.05787	0.00148	0.0779	0.00106	0.62131	0.0157	0.02749	0.00155	99	524.7	55.36	483.6	6.33	490.7	9.83	548.1	30.48
aco-13-13	63	0.05835	0.00156	0.08115	0.00113	0.65266	0.01718	0.02674	0.00152	99	543	57.28	503	6.76	510.1	10.55	533.4	29.95
aco-13-13	64	0.05789	0.00116	0.08062	0.00102	0.64321	0.01286	0.0274	0.00141	99	525.2	43.48	499.8	6.07	504.3	7.95	546.3	27.79
aco-13-13	65	0.05563	0.00268	0.0771	0.00145	0.59115	0.02768	0.02454	0.00189	102	437.2	103.47	478.8	8.67	471.6	17.66	489.9	37.25
aco-13-13	66	0.05785	0.00229	0.07513	0.00114	0.5991	0.02313	0.02506	0.00143	98	523.9	84.67	467	6.85	476.7	14.69	500.3	28.17
aco-13-13	67	0.0601	0.00197	0.07347	0.00101	0.60869	0.01941	0.0227	0.00132	95	607.2	69.51	457	6.06	482.7	12.25	453.7	26.04
aco-13-13	68	0.05858	0.0011	0.0786	0.00093	0.63476	0.01185	0.02507	0.00123	98	551.6	41.18	487.8	5.57	499.1	7.36	500.6	24.18
aco-13-13	69	0.05942	0.00162	0.07932	0.00111	0.64949	0.01744	0.02864	0.00178	97	582.4	58.23	492	6.65	508.2	10.74	570.7	34.94
aco-13-13	70	0.05787	0.0016	0.08069	0.0012	0.64365	0.01768	0.02531	0.00184	99	524.6	59.83	500.3	7.13	504.6	10.92	505.3	36.26
aco-13-13	71	0.06525	0.00351	0.07698	0.00152	0.69241	0.03604	0.02819	0.00235	89	782.4	109	478	9.08	534.2	21.62	561.9	46.12
aco-13-13	72	0.06033	0.00128	0.07745	0.00097	0.64399	0.0135	0.02608	0.0015	95	615.3	45.02	480.9	5.82	504.8	8.34	520.3	29.6
aco-13-13	73	0.05871	0.00129	0.07847	0.00102	0.63507	0.01385	0.02529	0.00163	98	556.4	47.13	487	6.12	499.3	8.6	504.9	32.16
aco-13-13	74	0.05777	0.00174	0.07693	0.00108	0.61269	0.0181	0.02604	0.00165	98	521	65.11	477.8	6.49	485.3	11.4	519.6	32.57
aco-13-13	75	0.05814	0.00139	0.07597	0.00105	0.60893	0.01453	0.0259	0.0021	98	534.7	52	472	6.32	482.9	9.17	516.8	41.31
aco-13-13	76	0.06052	0.00178	0.07668	0.00112	0.63959	0.01839	0.02497	0.00184	95	622.1	62.05	476.3	6.73	502.1	11.39	498.6	36.23
aco-13-13	77	0.0575	0.00141	0.0758	0.00101	0.6007	0.01453	0.02498	0.00173	99	510.2	53.33	471	6.08	477.7	9.22	498.8	34.21
aco-13-13	78	0.08299	0.00252	0.21085	0.00339	2.41271	0.07276	0.06544	0.00743	97	1269.1	58.14	1233.3	18.07	1246.4	21.65	1281.2	140.91
aco-13-13	79	0.10153	0.00295	0.05997	0.00093	0.83951	0.02365	0.02243	0.00203	61	1652.3	52.91	375.5	5.68	618.9	13.05	448.4	40.22
aco-13-13	80	0.06934	0.00269	0.07561	0.00129	0.72275	0.02709	0.026	0.00226	85	908.9	78.27	469.8	7.73	552.3	15.97	518.8	44.59
aco-13-13	40D	0.05698	0.00119	0.07743	0.00102	0.60818	0.01282	0.02476	0.00103	100	490.2	45.45	480.8	6.08	482.4	8.09	494.4	20.4
Sample No.	Analysis_ #	Pb207/Pb206		Pb206/U238		Pb207/U235		Pb208/Th232		Concordancy	Pb207/Pb206		Pb206/U238		Pb207/U235		Pb208/Th232	

ACO-13-14	1	0.09384	0.00114	0.09238	0.00114	1.19543	0.01631	0.02636	0.0006	71	1504.9	22.81	569.6	6.73	798.5	7.55	525.8	11.87
ACO-13-14	2	0.06016	0.00107	0.08947	0.00127	0.74227	0.01429	0.02529	0.00092	98	609.2	37.96	552.4	7.53	563.7	8.33	504.7	18.16
ACO-13-14	3	0.0583	0.00092	0.08702	0.00106	0.69944	0.01138	0.02556	0.00076	100	540.5	34.9	537.9	6.28	538.5	6.8	510.1	14.95
ACO-13-14	4	0.05885	0.0008	0.08565	0.0011	0.69519	0.01056	0.02498	0.00072	99	561.7	29.39	529.7	6.52	535.9	6.32	498.7	14.17
ACO-13-14	5	0.10617	0.00184	0.30161	0.00424	4.41712	0.08099	0.08472	0.00287	98	1734.7	31.43	1699.3	20.98	1715.6	15.18	1643.6	53.5
ACO-13-14	6	0.06333	0.00098	0.1135	0.00148	0.99131	0.01655	0.03168	0.00098	99	719.3	32.56	693	8.57	699.4	8.44	630.4	19.15
ACO-13-14	7	0.0586	0.00084	0.09119	0.00115	0.73691	0.0115	0.0266	0.0008	100	552.1	31.13	562.6	6.82	560.6	6.72	530.6	15.7
ACO-13-14	8	0.06943	0.00088	0.14685	0.00182	1.40595	0.0198	0.0367	0.00118	99	911.6	25.88	883.3	10.21	891.4	8.36	728.5	22.94
ACO-13-14	9	0.05867	0.0012	0.08703	0.00122	0.70439	0.01491	0.02389	0.00096	99	554.9	44.05	538	7.22	541.4	8.88	477.1	18.87
ACO-13-14	10	0.06298	0.00157	0.08799	0.00134	0.76406	0.01925	0.02863	0.00165	94	707.5	52.18	543.6	7.95	576.3	11.08	570.5	32.51
ACO-13-14	11	0.06078	0.00125	0.09265	0.00121	0.77663	0.01598	0.02607	0.00084	98	631.6	43.56	571.2	7.15	583.6	9.13	520.2	16.58
ACO-13-14	12	0.05792	0.00166	0.08699	0.0014	0.69441	0.01992	0.02499	0.00165	100	526.5	62.1	537.7	8.27	535.4	11.94	498.9	32.6
ACO-13-14	13	0.05854	0.00131	0.0903	0.00138	0.72822	0.01684	0.02591	0.00201	100	549.9	47.96	557.3	8.13	555.5	9.89	517	39.54
ACO-13-14	14	0.05871	0.00085	0.08837	0.00108	0.71538	0.01089	0.0249	0.00089	100	556.3	31.14	545.9	6.42	547.9	6.45	497.2	17.47
ACO-13-14	15	0.06092	0.00137	0.08755	0.0012	0.73557	0.01659	0.0262	0.00107	97	636.5	47.8	541	7.11	559.8	9.71	522.8	21.02
ACO-13-14	16	0.05868	0.00102	0.08811	0.00118	0.71281	0.01314	0.02594	0.00096	100	555.3	37.89	544.3	6.96	546.4	7.79	517.7	18.88
ACO-13-14	17	0.05845	0.00111	0.09063	0.00119	0.73029	0.01425	0.02619	0.00087	100	546.8	41.03	559.2	7	556.7	8.36	522.6	17.21
ACO-13-14	18	0.05864	0.00109	0.08975	0.00114	0.72559	0.01375	0.02546	0.00079	100	553.9	40.1	554	6.77	554	8.09	508.2	15.55
ACO-13-14	19	0.12924	0.0017	0.37004	0.00452	6.59336	0.09389	0.09761	0.00305	97	2087.7	22.99	2029.6	21.26	2058.5	12.55	1882.5	56.16
ACO-13-14	20	0.05893	0.00085	0.09059	0.00108	0.73588	0.01116	0.02626	0.00084	100	564.3	30.75	559	6.37	560	6.53	523.9	16.53
ACO-13-14	21	0.06053	0.00129	0.08801	0.0012	0.73433	0.01586	0.02525	0.001	97	622.5	45.25	543.7	7.1	559.1	9.28	504	19.66
ACO-13-14	22	0.06409	0.00112	0.1131	0.00137	0.99945	0.01758	0.0346	0.00148	98	744.7	36.6	690.7	7.92	703.5	8.93	687.6	28.9
ACO-13-14	23	0.12167	0.00252	0.35477	0.00527	5.94943	0.12929	0.09862	0.0066	99	1980.8	36.47	1957.3	25.05	1968.5	18.89	1901.1	121.48
ACO-13-14	24	0.06332	0.00109	0.10661	0.00138	0.93048	0.01674	0.03106	0.00132	98	718.9	36.13	653	8.03	667.9	8.8	618.3	25.91
ACO-13-14	25	0.05898	0.00123	0.08782	0.00112	0.71404	0.01483	0.02498	0.00104	99	566.2	44.73	542.6	6.63	547.1	8.78	498.7	20.42
ACO-13-14	26	0.06164	0.00128	0.08748	0.00114	0.74345	0.01551	0.02594	0.0011	96	661.8	43.92	540.6	6.78	564.4	9.03	517.6	21.61
ACO-13-14	27	0.05975	0.00104	0.09069	0.0011	0.74696	0.01314	0.02614	0.00114	99	594.3	37.3	559.6	6.52	566.5	7.64	521.6	22.5
ACO-13-14	28	0.06214	0.00165	0.08673	0.00132	0.74303	0.01983	0.02601	0.00176	95	678.9	55.73	536.2	7.81	564.2	11.55	519	34.64
ACO-13-14	29	0.06009	0.00113	0.09207	0.00113	0.76262	0.01431	0.0249	0.00121	99	606.7	40	567.8	6.69	575.5	8.24	497	23.83
ACO-13-14	30	0.19022	0.00302	0.52434	0.00639	13.7492	0.22441	0.13715	0.00647	99	2744.1	25.84	2717.6	27.04	2732.6	15.45	2597.9	115.01
ACO-13-14	31	0.18458	0.00271	0.52556	0.00676	13.3716	0.20359	0.13891	0.00413	101	2694.5	24.01	2722.7	28.55	2706.3	14.38	2629	73.21
ACO-13-14	32	0.07275	0.00088	0.08992	0.00102	0.90171	0.01159	0.02818	0.00074	85	1007	24.4	555.1	6.02	652.6	6.19	561.6	14.63
ACO-13-14	33	0.07646	0.00105	0.18364	0.0022	1.93529	0.02827	0.05347	0.00158	98	1107.1	27.21	1086.8	12	1093.4	9.78	1052.8	30.22
ACO-13-14	34	0.05738	0.00215	0.09134	0.00163	0.72217	0.02664	0.02399	0.00152	102	505.6	80.81	563.5	9.61	551.9	15.71	479.2	29.98
ACO-13-14	35	0.05825	0.00167	0.09142	0.00124	0.73415	0.02026	0.0279	0.00132	101	538.6	62.12	563.9	7.34	559	11.86	556.2	25.96
ACO-13-14	36	0.06932	0.00089	0.08608	0.00101	0.8225	0.01132	0.02857	0.00083	87	908.4	26.16	532.3	6	609.4	6.31	569.4	16.32
ACO-13-14	37	0.05933	0.00111	0.08854	0.00113	0.72401	0.0138	0.02524	0.0009	99	579.3	40.06	546.9	6.72	553	8.13	503.7	17.78
ACO-13-14	38	0.11652	0.00184	0.33359	0.00418	5.35711	0.08693	0.09109	0.00313	97	1903.5	28.13	1855.7	20.19	1878	13.88	1762	57.96
ACO-13-14	39	0.06167	0.00101	0.08868	0.0011	0.75385	0.01284	0.02604	0.00085	96	662.8	34.8	547.7	6.52	570.5	7.43	519.6	16.81
ACO-13-14	40	0.08874	0.0014	0.22928	0.00283	2.8045	0.04584	0.06519	0.00235	95	1398.5	29.91	1330.7	14.85	1356.7	12.23	1276.4	44.63
ACO-13-14	41	0.05919	0.0013	0.093	0.00126	0.7586	0.01682	0.02601	0.00104	100	573.9	47.07	573.2	7.41	573.2	9.71	519	20.43
ACO-13-14	42	0.06144	0.00112	0.0911	0.00122	0.77151	0.01484	0.02566	0.00113	97	654.7	38.71	562.1	7.22	580.6	8.5	512	22.23
ACO-13-14	43	0.06844	0.00133	0.10766	0.00148	1.01552	0.02063	0.03127	0.00143	93	881.8	39.8	659.1	8.6	711.7	10.4	622.4	28.07
ACO-13-14	44	0.08019	0.00199	0.18884	0.00297	2.08712	0.05358	0.04923	0.00341	93	1201.8	48.1	1115.1	16.12	1144.6	17.62	971.3	65.6
ACO-13-14	45	0.071	0.00149	0.15848	0.00211	1.55106	0.03285	0.0434	0.00164	100	957.3	42.45	948.3	11.76	950.9	13.08	858.8	31.68
ACO-13-14	46	0.18252	0.00265	0.09048	0.00114	2.27647	0.03457	0.04298	0.00131	46	2675.9	23.82	558.4	6.76	1205	10.71	850.7	25.48
ACO-13-14	47	0.13197	0.00216	0.38545	0.00527	7.00921	0.12452	0.10073	0.00453	99	2124.3	28.43	2101.7	24.52	2112.6	15.79	1939.9	83.2
ACO-13-14	48	0.06682	0.0025	0.10126	0.0018	0.93265	0.03412	0.03154	0.00188	93	832.1	76.04	621.8	10.55	669	17.92	627.6	36.82
ACO-13-14	49	0.05952	0.00135	0.08388	0.00118	0.68813	0.01588	0.02515	0.00104	98	586.1	48.46	519.3	7.03	531.7	9.55	502	20.59
ACO-13-14	50	0.06385	0.00101	0.08901	0.00115	0.78349	0.01329	0.02839	0.00119	94	736.7	32.98	549.7	6.81	587.5	7.56	565.9	23.43
ACO-13-14	51	0.08351	0.00131	0.20614	0.00265	2.37326	0.03958	0.062	0.00247	94	1281.1	30.31	1208.2	14.14	1234.6	11.92	1215.8	46.93
ACO-13-14	52	0.06158	0.00086	0.08898	0.00107	0.75549	0.01128	0.0271	0.0009	96	659.6	29.6	549.5	6.36	571.4	6.52	540.4	17.71
ACO-13-14	53	0.12265	0.00262	0.34788	0.00516	5.88197	0.13156	0.09645	0.00633	96	1995.1	37.56	1924.5	24.7	1958.6	19.41	1861	116.71
ACO-13-14	54	0.12314	0.00251	0.37621	0.00551	6.38591	0.13639	0.09871	0.00587	103	2002.2	35.82	2058.5	25.81	2030.3	18.75	1902.7	108.07
ACO-13-14	55	0.05943	0.00098	0.08635	0.0011	0.70752	0.01234	0.02776	0.00115	98	583	35.55	533.9	6.54	543.3	7.34	553.5	22.55
ACO-13-14	56	0.10819	0.00163	0.32119	0.00395	4.79109	0.07545	0.08873	0.00339	101	1769	27.26	1795.5	19.28	1783.3	13.23	1718.2	62.85
ACO-13-14	57	0.06858	0.00124	0.0946	0.00128	0.89433	0.01718	0.03515	0.00184	90	886.1	36.96	582.7	7.55	648.7	9.21	698.3	35.89
ACO-13-14	58	0.06209	0.00129	0.0989	0.00133	0.84661	0.01789	0.02874	0.00137	98	677.3	43.7	607.9	7.83	622.8	9.84	572.6	26.89
ACO-13-14	59	0.06322	0.00148	0.08438	0.00106	0.73589	0.01653	0.02585	0.00201	93	715.8	48.79	522.2	6.32	560	9.67	515.9	39.52
ACO-13-14	60	0.05902	0.0011	0.09233	0.00118	0.75135	0.01428	0.0271	0.00121	100	567.8	39.96	569.3	6.95	569	8.28	540.4	23.89
ACO-13-14	61	0.05953	0.00125	0.09179	0.00118	0.75319	0.01579	0.02728	0.00112	99	586.4	44.81	566.1	6.96	570.1	9.15	544	22.04
ACO-13-14	62	0.12643	0.00244	0.36926	0.00509	6.43511	0.12739	0.09519	0.00537	99	2049	33.64	2025.9	23.97	2037.1	17.4	1837.8	99.06
ACO-13-14	63	0.06553	0.00183	0.08978	0.0012	0.81153	0.02178	0.02683	0.0013	92	791.3	57.46	554.2	7.1	603.3	12.21	535.2	25.58
ACO-13-14	64	0.09261	0.0014	0.2403	0.00276	3.06968	0.04628	0.07184	0.00293	94	1479.8	28.43	1388.3	14.34	1425.2	11.55	1402.3	55.26
ACO-13-14	65	0.05935	0.00102	0.08216	0.00099	0.67229	0.01168	0.02496	0.00107	97	580	36.85	509	5.91	522.1	7.09	498.4	21.16
ACO-13-14	66	0.0593	0.00105	0.08004	0.00096	0.65453	0.01166	0.02312	0.00099	97	578.2	38.04	496.4	5.74	511.3	7.15	462	19.57
ACO-13-14	67	0.06097	0.00156	0.08107	0.00111	0.68135	0.0172	0.02459	0.00118	95	638	54.24	502.5	6.6	527.6	10.39	490.9	23.31
ACO-13-14	68	0.06243	0.00121	0.09879	0.00118	0.85086	0.01619	0.03084	0.00143	97	688.8	40.66	607.3	6.95	625.1	8.88	614	28.12
ACO-13-14	69	0.06343	0.00135	0.08386	0.0011	0.73324	0.01558	0.02651	0.00146	93	722.5	44.52	519.1	6.51	558.5	9.13	528.9	28.84
ACO-13-14	70	0.06094	0.00131	0.08143	0.00099	0.68437	0.01429	0.02867	0.00164	95	637	45.64	504.7	5.92	529.4	8.62	571.3	32.32
ACO-13-14	71	0.06734	0.0012	0.09026	0.00106	0.83854	0.01478	0.02829	0.00143	90	848.3	36.76	557.1	6.26	618.3	8.16	564	28.18
ACO-13-14	72	0.064	0.00128	0.11423	0.00139	1.00841	0.01987	0.03778	0.00216	98	741.6	41.87	697.2	8.01	708.1	10.05	749.6	42.15
ACO-13-14	73	0.05803	0.00152	0.09791	0.00139	0.78358	0.02031	0.03094	0.00272	103	530.4	56.96	602.2	8.15	587.5	11.56	615.9	53.34
ACO-13-14	74	0.05992	0.00108	0.08718	0.00106	0.72026	0.01307	0.02628	0.00151	98	600.7	38.71	538.8	6.29	550.8	7.72	524.3	29.71
ACO-13-14	75	0.13078	0.00202	0.35232	0.0041	6.35724	0.09888	0.09793	0.00529	92	2108.4	26.88	1945.7	19.55	2026.4	13.65	1888.3	97.42
ACO-13-14	76	0.05794	0.00147	0.08655	0.00118	0.69135	0.01721	0.02727	0.0018	100	527.1	54.81	535.1	7.01	533.6	10.33	543.9	35.42
ACO-13-14	77	0.06208	0.00105	0.09795	0.00115	0.83896	0.0142	0.03004	0.00173	97	676.9	35.8	602.4	6.75	618.6	7.84	598.3	34
ACO-13-14	78	0.16782	0.00291	0.45644	0.00562	10.5617	0.18449	0.12623	0.00811	96	2536	28.79	2423.8	24.86	2485.4	16.2	2402.8	145.57
ACO-13-14	79	0.16038	0.00312	0.17041	0.00219	3.76783	0.0737	0.05596	0.00422	41	2459.7	32.55	1014.4	12.05	1585.9	15.69	1100.7	80.69
ACO-13-14	80	0.06041	0.00122	0.09355	0.00111	0.77981	0.01526	0.03002	0.00217	98	618.2	42.88	576.5	6.56	585.4	8.71	597.9	42.57
ACO-13-14	81	0.07342	0.00095	0.16875	0.0024	1.70817	0.02702	0.05001	0.00116	98	1025.7	26.09	1005.2	13.22	1011.6	10.13	986.3	22.28
ACO-13-14	82	0.12008	0.00139	0.35032	0.00496	5.79918	0.08635	0.10597	0.00267	99	1957.4	20.47	1936.1	23.67	1946.3	12.9	2035.8	48.78
ACO-13-14	83	0.06397	0.00105	0.10267	0.00149	0.90546	0.01674	0.02658	0.00072	96	740.6	34.51	630.1	8.71	654.6	8.92	530.3	14.24
ACO-13-14	84	0.2234	0.0026	0.58733	0.00821	18.0896	0.26707	0.15758	0.00433	99	3005.4	18.55	2978.6	33.36	2994.5	14.21	2957.7	75.57
ACO-13-14	85	0.06441	0.00082	0.08927	0.00127	0.79263	0.01245	0.02884	0.0008	93	755	26.67	551.2	7.5	592.7	7.05	574.6	15.77
ACO-13-14	86	0.09154	0.00134	0.25035	0.00379	3.15969	0.05612	0.0748	0.00312	99	1457.7	27.63	1440.3	19.52	1447.4	13.7	1458	58.66
ACO-13-14	87	0.128	0.0019	0.37029	0.00552	6.53459	0.1149	0.1086	0.00467	98	2070.7	25.9	2030.8	25.98	2050.6	15.48	2083.8	85.15
ACO-13-14	88	0.11018	0.00147	0.31643	0.00441	4.80679	0.07572	0.09088	0.00304	98	1802.3	24.12	1772.2	21.57	1786.1	13.24	1758.2	56.26

ACO-13-14	89	0.06141	0.00084	0.10227	0.00143	0.86591	0.01394	0.03382	0.00129	99	653.6	28.93	627.7	8.38	633.3	7.59	672.2	25.16
ACO-13-14	90	0.06046	0.00103	0.09814	0.0015	0.81814	0.01596	0.03251	0.00149	99	620.2	36.35	603.5	8.8	607	8.91	646.7	29.24
ACO-13-14	91	0.09194	0.00132	0.25011	0.00344	3.17034	0.05163	0.07919	0.00304	98	1466	27.19	1439	17.74	1450	12.57	1540.5	57.01
ACO-13-14	92	0.13413	0.00166	0.39089	0.00545	7.22845	0.10983	0.10902	0.00352	99	2152.7	21.41	2127	25.25	2140	13.55	2091.5	64.15
ACO-13-14	93	0.0622	0.00088	0.0902	0.0013	0.77351	0.01295	0.0313	0.00121	96	681	29.78	556.7	7.67	581.8	7.41	623	23.81
ACO-13-14	94	0.06371	0.00095	0.09268	0.00129	0.81412	0.0138	0.0294	0.00131	94	732.1	31.3	571.4	7.63	604.8	7.72	585.7	25.68
ACO-13-14	95	0.06098	0.00129	0.09002	0.00144	0.75668	0.01733	0.02869	0.00175	97	638.6	44.77	555.6	8.5	572.1	10.02	571.8	34.45
ACO-13-14	96	0.06217	0.00088	0.08765	0.00123	0.75122	0.01241	0.0289	0.00065	95	680	29.99	541.6	7.26	568.9	7.2	575.9	12.82
ACO-13-14	97	0.05785	0.00081	0.08795	0.00124	0.70142	0.01158	0.02981	0.00075	101	523.8	30.79	543.4	7.32	539.6	6.91	593.8	14.68
ACO-13-14	98	0.06842	0.00115	0.09274	0.00129	0.87455	0.01591	0.03133	0.00145	90	881.3	34.32	571.7	7.61	638	8.62	623.6	28.38
ACO-13-14	99	0.05979	0.00081	0.08737	0.00121	0.72021	0.0115	0.02952	0.00074	98	596	29.02	540	7.17	550.8	6.79	588.1	14.51
ACO-13-14	100	0.06026	0.0008	0.09002	0.00125	0.74794	0.01189	0.0321	0.00082	98	613.1	28.54	555.7	7.41	567	6.91	638.5	16.05
ACO-13-14	101	0.187	0.00256	0.53615	0.00735	13.8232	0.21783	0.15202	0.00571	102	2715.9	22.42	2767.3	30.84	2737.7	14.92	2860.4	100.26
ACO-13-14	102	0.05835	0.00163	0.1027	0.0016	0.82632	0.02327	0.03341	0.00123	103	543.1	59.99	630.2	9.36	611.6	12.94	664.2	24.06
ACO-13-14	103	0.05689	0.00092	0.08927	0.00124	0.70029	0.01247	0.02732	0.00111	102	486.7	35.88	551.2	7.32	539	7.45	544.8	21.8
ACO-13-14	104	0.05787	0.00098	0.08846	0.00123	0.70574	0.013	0.02876	0.00116	101	524.4	37.15	546.4	7.3	542.2	7.74	573	22.73
ACO-13-14	105	0.0598	0.00092	0.1057	0.00149	0.87138	0.01517	0.03608	0.00121	102	596.2	32.99	647.7	8.68	636.3	8.23	716.5	23.55
Sample No	Analysis_ #	Pb207/Pb206		Pb206/U238		Pb207/U235		Pb208/Th232		Concordancy	Pb207/Pb206		Pb206/U238		Pb207/U235		Pb208/Th232	
aco-12-15b	1	0.05727	0.00066	0.07405	0.0009	0.58463	0.00759	0.02218	0.00039	99	501.3	25.27	460.5	5.38	467.4	4.86	443.5	7.74
aco-12-15b	2	0.05675	0.00074	0.07187	0.0009	0.56237	0.0081	0.02091	0.00042	99	481.3	28.78	447.4	5.41	453.1	5.26	418.2	8.38
aco-12-15b	3	0.06858	0.00094	0.0717	0.00093	0.67796	0.01032	0.02145	0.00053	85	886.3	28.2	446.4	5.59	525.5	6.25	429	10.55
aco-12-15b	4	0.05689	0.00076	0.06956	0.00085	0.5456	0.0079	0.0213	0.00038	98	486.8	29.75	433.5	5.11	442.1	5.19	426	7.58
aco-12-15b	5	0.08316	0.0009	0.14696	0.00173	1.68491	0.02059	0.04145	0.00075	88	1272.9	20.89	883.9	9.73	1002.8	7.79	820.9	14.57
aco-12-15b	6	0.06309	0.0008	0.07283	0.00089	0.63345	0.00884	0.02215	0.00042	91	711.1	26.86	453.2	5.34	498.2	5.5	442.8	8.38
aco-12-15b	7	0.07172	0.00118	0.14247	0.00194	1.40877	0.0248	0.04148	0.00121	96	977.9	33.2	858.6	10.93	892.6	10.45	821.6	23.54
aco-12-15b	8	0.05816	0.00076	0.07348	0.00094	0.58916	0.00862	0.02156	0.00054	97	535.1	28.82	457.1	5.64	470.3	5.51	431.1	10.78
aco-12-15b	9	0.06097	0.00089	0.07074	0.00091	0.59457	0.00943	0.02206	0.00057	93	638	31.13	440.6	5.48	473.8	6	441	11.21
aco-12-15b	10	0.05629	0.00069	0.07269	0.00088	0.5641	0.00764	0.02179	0.00046	100	463	27.1	452.3	5.27	454.2	4.96	435.6	9.05
aco-12-15b	11	0.07171	0.00084	0.14263	0.0017	1.41017	0.01824	0.04218	0.00093	96	977.6	23.6	859.5	9.57	893.2	7.69	835	17.95
aco-12-15b	12	0.11407	0.00132	0.07879	0.00092	1.23912	0.0156	0.02735	0.00066	60	1865.2	20.73	488.9	5.47	818.5	7.07	545.4	12.91
aco-12-15b	13	0.10546	0.00118	0.24818	0.003	3.60896	0.04597	0.06568	0.00141	83	1722.4	20.41	1429.1	15.5	1551.5	10.13	1285.7	26.81
aco-12-15b	14	0.06707	0.00084	0.07178	0.00089	0.66375	0.00923	0.01814	0.00049	86	839.9	25.72	446.9	5.33	516.9	5.63	363.4	9.69
aco-12-15b	15	0.0675	0.0009	0.07696	0.00094	0.71632	0.01031	0.02534	0.00059	87	853.3	27.31	477.9	5.65	548.5	6.1	505.9	11.57
aco-12-15b	16	0.07368	0.00091	0.10874	0.00133	1.10467	0.01512	0.02615	0.00046	88	1032.8	24.34	665.4	7.76	755.6	7.29	521.8	9.11
aco-12-15b	17	0.05758	0.00063	0.07207	0.00085	0.57214	0.0071	0.02221	0.00038	98	513.5	23.53	448.6	5.14	459.4	4.58	443.9	7.52
aco-12-15b	18	0.05739	0.0007	0.08018	0.00096	0.63448	0.00851	0.02257	0.00042	100	506.3	26.44	497.2	5.74	498.9	5.29	451	8.2
aco-12-15b	19	0.05786	0.00073	0.07107	0.00085	0.56698	0.00784	0.02104	0.00039	97	524.3	27.78	442.6	5.14	456.1	5.08	420.9	7.79
aco-12-15b	20	0.05764	0.00087	0.06982	0.00089	0.55488	0.00899	0.02152	0.00049	97	515.9	33.12	435.1	5.37	448.2	5.87	430.4	9.75
aco-12-15b	21	0.05672	0.00073	0.07214	0.00087	0.56417	0.0079	0.02213	0.00043	99	480.1	28.51	449	5.21	454.2	5.13	442.5	8.5
aco-12-15b	22	0.05846	0.00069	0.07319	0.00088	0.58995	0.00776	0.02373	0.00047	97	547.1	25.48	455.3	5.27	470.8	4.95	474.1	9.21
aco-12-15b	23	0.05979	0.00067	0.07062	0.00086	0.58225	0.0075	0.0195	0.0004	94	596.1	24.14	439.9	5.15	465.9	4.82	390.4	7.9
aco-12-15b	24	0.05634	0.00069	0.0734	0.00088	0.57018	0.00768	0.02333	0.00049	100	465.2	27.03	456.6	5.27	458.1	4.97	466.2	9.72
aco-12-15b	25	0.05724	0.00071	0.07296	0.00088	0.57576	0.00784	0.02519	0.00056	98	500.1	27.19	454	5.27	461.7	5.05	502.8	11.14
aco-12-15b	26	0.05709	0.00077	0.07195	0.00087	0.5663	0.00823	0.0242	0.00055	98	494.3	29.71	447.9	5.25	455.6	5.33	483.3	10.89
aco-12-15b	27	0.0743	0.00107	0.07454	0.00091	0.76358	0.01163	0.02743	0.00067	80	1049.7	28.88	463.4	5.47	576.1	6.7	547	13.08
aco-12-15b	28	0.06009	0.0008	0.06979	0.00086	0.57823	0.00841	0.02332	0.00058	94	606.8	28.48	434.9	5.19	463.3	5.41	466	11.5
aco-12-15b	29	0.08937	0.00158	0.07345	0.00098	0.90503	0.0165	0.02862	0.00081	70	1412.1	33.42	456.9	5.89	654.4	8.8	570.4	15.85
aco-12-15b	30	0.05757	0.00074	0.07313	0.00089	0.58037	0.00817	0.02275	0.00059	98	512.9	27.71	455	5.32	464.7	5.25	454.7	11.57
aco-12-15b	31	0.07272	0.00092	0.15746	0.00193	1.57829	0.02201	0.04796	0.00082	98	1006.1	25.36	942.6	10.75	961.7	8.67	946.8	15.85
aco-12-15b	32	0.06363	0.00084	0.06839	0.00088	0.59983	0.00894	0.0215	0.00044	89	729.5	27.81	426.4	5.28	477.1	5.67	430	8.64
aco-12-15b	33	0.05869	0.0008	0.06772	0.00084	0.54785	0.0082	0.02185	0.00039	95	555.5	29.56	422.4	5.1	443.6	5.38	436.9	7.67
aco-12-15b	34	0.05656	0.00067	0.07213	0.0009	0.56236	0.00768	0.02301	0.00044	99	473.6	26.22	449	5.4	453.1	4.99	459.9	8.62
aco-12-15b	35	0.05675	0.00083	0.07004	0.00087	0.54799	0.00857	0.02207	0.00042	98	481.3	32.25	436.4	5.25	443.7	5.62	441.3	8.39
aco-12-15b	36	0.09263	0.00116	0.07417	0.00095	0.94719	0.01358	0.03272	0.00067	68	1480.3	23.72	461.2	5.72	676.6	7.08	650.8	13.19
aco-12-15b	37	0.05891	0.00074	0.07168	0.00091	0.58205	0.00833	0.02501	0.00052	96	563.7	27.08	446.3	5.46	465.8	5.34	499.2	10.25
aco-12-15b	38	0.05616	0.00066	0.07406	0.00091	0.57331	0.00767	0.02387	0.00047	100	458.2	25.47	460.6	5.44	460.2	4.95	476.9	9.23
aco-12-15b	39	0.07421	0.00087	0.16595	0.00205	1.69781	0.02277	0.05368	0.00109	98	1047.2	23.46	989.8	11.31	1007.7	8.57	1056.8	20.99
aco-12-15b	40	0.05691	0.00067	0.07295	0.00091	0.57229	0.00778	0.02267	0.00049	99	487.4	25.93	453.9	5.48	459.5	5.03	453	9.71
aco-12-15b	41	0.05898	0.00075	0.07066	0.00087	0.57453	0.00809	0.02322	0.00051	95	566.5	27.42	440.1	5.22	460.9	5.22	464	10.15
aco-12-15b	42	0.06012	0.00072	0.0716	0.00089	0.59336	0.0081	0.02398	0.00052	94	607.7	25.64	445.8	5.33	473	5.16	478.9	10.31
aco-12-15b	43	0.05809	0.00066	0.07036	0.00087	0.56346	0.0074	0.02212	0.00047	97	532.7	24.98	438.3	5.22	453.8	4.8	442.1	9.31
aco-12-15b	44	0.05727	0.00072	0.07148	0.00089	0.56443	0.00799	0.02335	0.00055	98	501.6	27.58	445.1	5.34	454.4	5.18	466.6	10.94
aco-12-15b	45	0.05794	0.00066	0.07324	0.0009	0.58497	0.00778	0.02403	0.00056	97	527	25.27	455.6	5.43	467.6	4.98	480	10.96
aco-12-15b	46	0.06162	0.00086	0.0734	0.00094	0.62348	0.00961	0.02449	0.00062	93	660.9	29.7	456.6	5.63	492	6.01	489	12.33
aco-12-15b	47	0.05607	0.00074	0.07209	0.00091	0.55723	0.00819	0.02357	0.00064	100	454.7	28.64	448.7	5.45	449.7	5.34	470.9	12.69
aco-12-15b	48	0.06231	0.0008	0.07297	0.00092	0.6268	0.00901	0.02488	0.00063	92	684.7	27.08	454	5.5	494.1	5.62	496.6	12.44
aco-12-15b	49	0.0579	0.00076	0.07629	0.00094	0.6091	0.00878	0.02468	0.00074	98	525.8	28.79	474	5.61	483	5.54	492.7	14.64
aco-12-15b	50	0.0579	0.00087	0.07266	0.00093	0.57997	0.00945	0.02217	0.0006	97	525.5	33.03	452.2	5.6	464.4	6.08	443.2	11.86
aco-12-15b	51	0.06034	0.00074	0.0725	0.00088	0.60314	0.00827	0.02351	0.00045	94	615.7	26.28	451.2	5.31	479.2	5.24	469.7	8.85
aco-12-15b	52	0.10972	0.00153	0.07887	0.00101	1.19292	0.01797	0.0401	0.00087	61	1794.8	25.25	489.4	6.02	797.3	8.32	794.8	16.94
aco-12-15b	53	0.05724	0.0008	0.07178	0.0009	0.56644	0.00861	0.02133	0.00046	98	500.4	30.39	446.9	5.43	455.7	5.58	426.5	9.06
aco-12-15b	54	0.05652	0.00083	0.07165	0.00091	0.55828	0.00889	0.0212	0.00051	99	472	32.45	446.1	5.5	450.4	5.79	424	10.05
aco-12-15b	55	0.05787	0.00084	0.06956	0.00086	0.55485	0.00859	0.02257	0.00056	97	524.5	31.83	433.5	5.17	448.2	5.61	451.2	11.1
aco-12-15b	56	0.10285	0.00122	0.20317	0.00244	2.88064	0.03782	0.08247	0.00191	71	1676.1	21.7	1192.3	13.06	1376.9	9.9	1601.7	35.66
aco-12-15b	57	0.06851	0.0008	0.06971	0.00083	0.65832	0.00858	0.02771	0.00068	85	883.9	23.97	434.4	5.01	513.6	5.25	552.5	13.39
aco-12-15b	58	0.0567	0.00075	0.06954	0.00082	0.54347	0.00761	0.02131	0.00058	98	479.1	29.15	433.4	4.94	440.7	5.01	426.2	11.53
aco-12-15b	59	0.08288	0.00131	0.06584	0.00082	0.75224	0.01225	0.02532	0.00071	72	1266.4	30.41	411.1	4.98	569.5	7.1	505.4	13.99
aco-12-15b	60	0.05719	0.00089	0.07233	0.00093	0.57029	0.00944	0.01998	0.00067	98	498.2	33.84	450.2	5.6	458.2	6.11	399.8	13.32
aco-12-15b	61	0.05748	0.00109	0.07812	0.00089	0.61875	0.01138	0.02627	0.00131	99	509.4	41.59	484.9	5.34	489.1	7.14	524.1	25.82
aco-12-15b	62	0.07947	0.00139	0.07423	0.00087	0.81322	0.01398	0.0306	0.00124	76	1183.9	34.26	461.6	5.23	604.3	7.83	609.2	24.3
aco-12-15b	63	0.05943	0.00248	0.07423	0.00116	0.60803	0.02451	0.02556	0.00135	96	583	88.07	461.6	6.94	482.3	15.47	510.2	26.63
aco-12-15b	64	0.05792	0.00114	0.07272	0.00087	0.58064	0.01121	0.02273	0.00095	97	526.5	42.78	452.5	5.23	464.9	7.2	454.3	18.78
aco-12-15b	65	0.06133	0.00129	0.07699	0.00096	0.65088	0.01342	0.02352	0.00101	94	650.9	44.39	478.1	5.75	509	8.25	469.9	19.97
aco-12-15b	66	0.05791	0.00092	0.06769	0.00079	0.54039	0.00864	0.02413	0.00107	96	526	34.64	422.2	4.76	438.7	5.7	482	21.12
aco-12-15b	67	0.05831	0.00179	0.06879	0.00097	0.55245	0.01641	0.02159	0.00128	96	540.7	66.58	428.9	5.87	446.6	10.74	431.7	25.28
aco-12-15b	68	0.07121	0.00265	0.07684	0.00114	0.75408	0.02706	0.03007	0.00169	84	963.5	74.25	477.3	6.84	570.6	15.67	598.9	33.18

aco-12-15b	69	0.05657	0.00109	0.07279	0.00083	0.56768	0.01059	0.0249	0.00146	99	474.1	42.68	452.9	4.99	456.5	6.86	497.1	28.71
aco-12-15b	70	0.05889	0.0013	0.07086	0.00095	0.57481	0.01264	0.0219	0.00134	96	562.9	47.32	441.4	5.71	461.1	8.15	437.9	26.48
aco-12-15b	71	0.05652	0.00187	0.06584	0.00094	0.51309	0.01627	0.02214	0.00142	98	472.2	72.36	411.1	5.67	420.5	10.92	442.7	28.03
aco-12-15b	72	0.05651	0.00118	0.06982	0.00085	0.54379	0.01111	0.02336	0.00114	99	471.9	45.93	435.1	5.14	440.9	7.31	466.7	22.44
aco-12-15b	73	0.05995	0.00216	0.06959	0.00106	0.57511	0.02008	0.02132	0.00107	94	601.9	76.09	433.7	6.42	461.3	12.94	426.4	21.14
aco-12-15b	74	0.05856	0.00141	0.07158	0.00095	0.57791	0.01366	0.02431	0.00131	96	550.8	51.74	445.7	5.69	463.1	8.79	485.5	25.9
aco-12-15b	75	0.05809	0.00257	0.06978	0.00125	0.55871	0.02381	0.022	0.00142	96	532.7	94.46	434.8	7.5	450.7	15.51	439.9	28.1
aco-12-15b	76	0.05603	0.00217	0.06616	0.00098	0.51084	0.01917	0.02388	0.00122	99	453.2	83.64	413	5.9	419	12.88	476.9	24.07
aco-12-15b	77	0.05721	0.00106	0.06964	0.0008	0.54911	0.00995	0.025	0.00109	98	499	40.2	434	4.84	444.4	6.52	499.2	21.43
aco-12-15b	78	0.05987	0.00146	0.07425	0.00099	0.61278	0.01471	0.02123	0.00108	95	598.8	52.02	461.7	5.97	485.3	9.26	424.7	21.33
aco-12-15b	79	0.057	0.00137	0.0725	0.0009	0.5696	0.01336	0.02397	0.00104	99	491	52.93	451.2	5.43	457.8	8.64	478.9	20.6
aco-12-15b	80	0.05702	0.00108	0.07479	0.00091	0.58787	0.01103	0.02459	0.0011	99	491.8	41.18	464.9	5.44	469.5	7.05	491	21.77
Sample No.	Analysis_ #	Pb207/Pb206		Pb206/U238		Pb207/U235		Pb208/Th232			Pb207/Pb206		Pb206/U238		Pb207/U235		Pb208/Th232	
aco-12-16	1	0.07526	0.00138	0.18495	0.00251	1.91846	0.03577	0.0514	0.0015	102	1075.3	36.3	1093.9	13.66	1087.5	12.44	1013.1	28.92
aco-12-16	2	0.09293	0.0013	0.26377	0.00335	3.37957	0.05045	0.07545	0.00221	102	1486.3	26.33	1509.1	17.07	1499.7	11.7	1470.2	41.48
aco-12-16	3	0.05799	0.00151	0.06632	0.00101	0.53021	0.01368	0.02033	0.00079	70	528.9	56.48	414	6.12	432	9.08	406.8	15.64
aco-12-16	4	0.066	0.00132	0.06615	0.00089	0.6019	0.01215	0.0216	0.00069	37	806.4	41.33	412.9	5.4	478.4	7.7	431.9	13.6
aco-12-16	5	0.05603	0.00098	0.06488	0.00084	0.50117	0.00903	0.02054	0.00064	79	453.4	38	405.2	5.11	412.5	6.11	410.9	12.76
aco-12-16	6	0.06062	0.00115	0.06591	0.0009	0.55077	0.01066	0.02154	0.00076	27	625.6	40.37	411.5	5.44	445.5	6.98	430.8	15.09
aco-12-16	7	0.08133	0.00137	0.19637	0.0027	2.20175	0.03874	0.0575	0.00216	94	1229.4	32.64	1155.8	14.53	1181.6	12.29	1130.1	41.32
aco-12-16	8	0.07571	0.00116	0.17458	0.00225	1.82215	0.02939	0.04953	0.00171	95	1087.4	30.44	1037.3	12.32	1053.5	10.57	977	32.96
aco-12-16	9	0.06459	0.00132	0.06088	0.00081	0.54202	0.01095	0.02174	0.00094	40	761.2	42.35	380.9	4.95	439.8	7.21	434.6	18.67
aco-12-16	10	0.05803	0.00137	0.06425	0.00093	0.51405	0.01213	0.02017	0.00084	84	530.6	51.47	401.4	5.61	421.2	8.13	403.7	16.71
aco-12-16	11	0.10094	0.00152	0.27632	0.00358	3.84512	0.06089	0.08616	0.00328	96	1641.5	27.63	1572.8	18.07	1602.2	12.76	1670.5	61.09
aco-12-16	12	0.05755	0.00127	0.07697	0.00105	0.61067	0.01338	0.02583	0.00116	109	512.4	48.17	478	6.31	484	8.44	515.5	22.93
aco-12-16	13	0.05838	0.00239	0.0626	0.00123	0.50353	0.01951	0.02337	0.00236	80	544.2	87.12	391.4	7.43	414.1	13.18	466.9	46.7
aco-12-16	14	0.06104	0.00095	0.06508	0.00084	0.54766	0.00899	0.02147	0.00089	93	640.6	33.14	406.5	5.06	443.5	5.9	429.3	17.69
aco-12-16	15	0.07555	0.00181	0.16357	0.00257	1.70387	0.04061	0.06169	0.00587	252	1083.3	47.38	976.6	14.25	1010	15.25	1209.9	111.72
aco-12-16	16	0.05644	0.00172	0.07769	0.0013	0.6044	0.01805	0.02791	0.00186	116	468.9	66.46	482.3	7.75	480	11.42	556.5	36.63
aco-12-16	17	0.05819	0.0016	0.06483	0.00103	0.52013	0.01412	0.01975	0.00109	99	536.4	59.73	404.9	6.21	425.2	9.43	395.2	21.59
aco-12-16	18	0.05792	0.00099	0.07352	0.00097	0.58704	0.01045	0.02544	0.0012	111	526.5	37.46	457.3	5.81	469	6.69	507.7	23.62
aco-12-16	19	0.10333	0.00183	0.29614	0.00415	4.21873	0.07825	0.08524	0.00479	99	1684.7	32.26	1672.1	20.65	1677.7	15.23	1653.4	89.24
aco-12-16	20	0.06394	0.00115	0.07034	0.00097	0.61999	0.0116	0.02507	0.00138	106	739.6	37.61	438.2	5.82	489.8	7.27	500.4	27.28
aco-12-16	21	0.05887	0.00147	0.0692	0.001	0.56195	0.01367	0.0275	0.00122	106	562.3	53.36	431.3	6.05	452.8	8.89	548.3	23.96
aco-12-16	22	0.08869	0.00139	0.21671	0.00291	2.6475	0.04463	0.085	0.00366	90	1397.5	29.73	1264.5	15.42	1313.9	12.42	1649	68.16
aco-12-16	23	0.05662	0.00119	0.06289	0.00087	0.49072	0.0104	0.02329	0.00087	93	475.9	46.44	393.2	5.27	405.4	7.08	465.3	17.1
aco-12-16	24	0.1051	0.00138	0.24301	0.00297	3.52104	0.04977	0.10271	0.00322	82	1716	23.8	1402.3	15.41	1532	11.18	1976.2	59.02
aco-12-16	25	0.0727	0.00121	0.14633	0.00188	1.46661	0.02511	0.0551	0.00184	207	1005.6	33.5	880.3	10.55	916.7	10.34	1084.1	35.2
aco-12-16	26	0.08684	0.00117	0.17076	0.00209	2.04435	0.0296	0.04979	0.00163	75	1357	25.83	1016.3	11.53	1130.4	9.87	982.1	31.31
aco-12-16	27	0.0921	0.0015	0.21784	0.00267	2.76595	0.0449	0.0815	0.00369	86	1469.3	30.68	1270.5	14.13	1346.4	12.11	1583.6	69.01
aco-12-16	28	0.14415	0.00409	0.17201	0.00318	3.41413	0.09128	0.09359	0.00542	45	2277.7	48.06	1023.2	17.47	1507.7	21	1808.3	100.21
aco-12-16	29	0.08628	0.00149	0.18787	0.00234	2.23482	0.03808	0.06685	0.00308	83	1344.4	32.99	1109.8	12.68	1192	11.95	1308	58.32
aco-12-16	30	0.09578	0.00186	0.07092	0.00096	0.93656	0.01804	0.04184	0.00153	99	1543.4	36.12	441.7	5.75	671.1	9.46	828.4	29.67
aco-12-16	31	0.05723	0.00121	0.05889	0.00077	0.46478	0.00977	0.02148	0.00085	81	499.8	46.5	368.9	4.71	387.6	6.77	429.5	16.84
aco-12-16	32	0.09515	0.00172	0.22363	0.00282	2.93261	0.05181	0.07725	0.00386	85	1531	33.6	1301	14.88	1390.4	13.38	1504	72.51
aco-12-16	33	0.08158	0.00185	0.07031	0.00104	0.79076	0.01775	0.02663	0.00139	91	1235.5	43.74	438	6.28	591.6	10.06	531.1	27.37
aco-12-16	34	0.06899	0.00138	0.10829	0.00142	1.03044	0.02044	0.04127	0.00173	137	898.3	40.82	662.8	8.26	719.1	10.22	817.4	33.58
aco-12-16	35	0.11724	0.0026	0.30791	0.00464	4.97302	0.11041	0.08915	0.00552	90	1914.6	39.29	1730.4	22.88	1814.7	18.77	1726.1	102.53
aco-12-16	36	0.06237	0.00187	0.06246	0.00101	0.53704	0.01564	0.0233	0.00147	54	686.9	62.81	390.6	6.12	436.5	10.33	465.6	28.94
aco-12-16	37	0.05853	0.00111	0.06129	0.00078	0.49493	0.00927	0.02256	0.00102	42	549.8	40.86	383.5	4.72	408.3	6.3	450.9	20.24
aco-12-16	38	0.08818	0.00218	0.2179	0.0033	2.64839	0.06365	0.07633	0.0054	92	1386.5	46.57	1270.8	17.48	1314.2	17.71	1486.7	101.41
aco-12-16	39	0.08381	0.00171	0.13292	0.00184	1.53603	0.0312	0.04897	0.00251	76	1288	39.33	804.5	10.5	944.9	12.49	966.3	48.45
aco-12-16	40	0.11559	0.00239	0.30416	0.00438	4.84617	0.10002	0.09152	0.00512	91	1889.1	36.8	1711.9	21.64	1792.9	17.37	1770	94.81
aco-12-16	41	0.05799	0.00084	0.06886	0.00085	0.55011	0.00839	0.02363	0.00069	39	529	31.64	429.3	5.14	445.1	5.49	472.1	13.63
aco-12-16	42	0.05671	0.00111	0.06294	0.00084	0.49162	0.00972	0.02267	0.00072	34	479.5	43.17	393.5	5.07	406	6.62	453	14.29
aco-12-16	43	0.07492	0.00174	0.06348	0.00095	0.6552	0.01503	0.02961	0.00122	34	1066.4	46.12	396.8	5.78	511.7	9.22	589.8	23.87
aco-12-16	44	0.05998	0.00177	0.06095	0.00094	0.50348	0.01427	0.01859	0.00117	29	602.9	62.54	381.4	5.71	414.1	9.64	372.3	23.24
aco-12-16	45	0.05818	0.00114	0.06252	0.00083	0.50093	0.00987	0.02272	0.00078	30	536	42.79	390.9	5.02	412.3	6.68	454.1	15.46
aco-12-16	46	0.05827	0.00097	0.06443	0.00084	0.51696	0.00891	0.02	0.0007	29	539.1	36.65	402.5	5.07	423.1	5.97	400.3	13.78
aco-12-16	47	0.09217	0.00129	0.23513	0.00292	2.98439	0.04466	0.07315	0.0026	93	1470.7	26.54	1361.3	15.22	1403.6	11.38	1426.9	48.9
aco-12-16	48	0.05834	0.00114	0.06216	0.00083	0.49931	0.00979	0.02055	0.00079	26	541.7	42.68	388.8	5.01	411.2	6.63	411.1	15.61
aco-12-16	49	0.0585	0.00095	0.07569	0.00096	0.60964	0.01027	0.02457	0.00094	29	548.4	35.18	470.3	5.77	483.3	6.48	490.6	18.58
aco-12-16	50	0.09948	0.00157	0.25596	0.00325	3.50503	0.05722	0.07892	0.00332	91	1614.4	29.13	1469.1	16.68	1528.3	12.9	1535.2	62.18
aco-12-16	51	0.07569	0.00126	0.17456	0.00228	1.81969	0.0313	0.05245	0.00233	95	1087	33	1037.2	12.49	1052.6	11.27	1033.2	44.78
aco-12-16	52	0.07984	0.00146	0.18897	0.00246	2.07637	0.0383	0.06059	0.00311	94	1193	35.73	1115.8	13.36	1141	12.64	1189	59.36
aco-12-16	53	0.11462	0.00144	0.13442	0.00183	2.12341	0.03173	0.02734	0.00056	43	1873.9	22.54	813	10.4	1156.4	10.32	545.2	10.95
aco-12-16	54	0.09219	0.00125	0.25231	0.00367	3.20732	0.05299	0.0597	0.00184	99	1471.2	25.6	1450.4	18.9	1458.9	12.79	1172	35.15
aco-12-16	55	0.0647	0.00102	0.06512	0.00091	0.58064	0.01027	0.02031	0.00049	87	764.5	32.97	406.7	5.53	464.9	6.6	406.5	9.62
aco-12-16	56	0.13095	0.00174	0.14357	0.00202	2.59132	0.04058	0.05317	0.00117	41	2110.7	23.12	864.8	11.37	1298.2	11.47	1047.1	22.49
aco-12-16	57	0.18466	0.00217	0.49895	0.0069	12.6976	0.18713	0.11776	0.00278	97	2695.2	19.25	2609.3	29.69	2657.5	13.87	2250.2	50.27
aco-12-16	58	0.06062	0.00098	0.0744	0.00103	0.62166	0.01117	0.02102	0.0006	94	625.7	34.59	462.6	6.21	490.9	6.99	420.5	11.91
aco-12-16	59	0.2238	0.00259	0.52506	0.00727	16.1975	0.23722	0.18744	0.0042	90	3008.2	18.5	2720.6	30.72	2888.5	14.01	3472.5	71.42
aco-12-16	60	0.19658	0.00227	0.48623	0.00678	13.1754	0.19447	0.11209	0.00255	91	2798	18.76	2554.3	29.4	2692.3	13.93	2147.4	46.31
aco-12-16	61	0.0945	0.00138	0.25527	0.00353	3.32588	0.05583	0.06127	0.00242	97	1518.2	27.24	1465.6	18.12	1487.1	13.1	1202	46.02
aco-12-16	62	0.11276	0.00138	0.31572	0.0044	4.90701	0.07501	0.07127	0.00194	96	1844.3	22.05	1768.8	21.54	1803.5	12.89	1391.5	36.51
aco-12-16	63	0.0957	0.0015	0.27305	0.00398	3.60202	0.06349	0.07586	0.00174	101	1541.8	29.17	1556.3	20.16	1550	14.01	1478	32.75
aco-12-16	64	0.09536	0.0012	0.26357	0.00386	3.46506	0.05516	0.06491	0.00159	98	1535.3	23.51	1508.1	19.71	1519.3	12.54	1271.2	30.11
aco-12-16	65	0.07687	0.0015	0.17066	0.00255	1.80799	0.0374	0.03706	0.00114	97	1117.9	38.52	1015.8	14.03	1048.4	13.52	735.5	22.3
aco-12-16	66	0.05541	0.00107	0.06812	0.00099	0.52031	0.01077	0.01933	0.00055	100	428.7	42.09	424.8	5.98	425.4	7.2	386.9	10.95
aco-12-16	67	0.05861	0.00081	0.07922	0.00114	0.6401	0.01059	0.01978	0.00055	98	552.8	29.81	491.5	6.8	502.4	6.56	395.8	10.81
aco-12-16	68	0.06022	0.00131	0.06579	0.00099	0.5462	0.01242	0.01434	0.00053	93	611.7	46.15	410.8	6.01	442.5	8.16	287.9	10.61
aco-12-16	69	0.05606	0.00106	0.07004	0.00103	0.54117	0.0111	0.02056	0.00063	99	454.2	41.31	436.4	6.23	439.2	7.31	411.3	12.4
aco-12-16	70	0.09153	0.00167	0.07408	0.00114	0.93478	0.01861	0.03577	0.00116	69	1457.5	34.33	460.7	6.83	670.1	9.77	710.4	22.71
aco-12-16	71	0.07883	0.00135	0.16555	0.00232	1.79817	0.03307	0.04229	0.00215	95	1168	33.6	987.6	12.84	1044.8	12	837.1	41.62
aco-12-16	72	0.09211	0.00189	0.24901	0.00377	3.16032	0.06699	0.0722	0.00318	98	1469.6	38.57	1433.4	19.45	1447.5	16.35	1409	59.9
aco-12-16	73	0.07581	0.00178	0.16142	0.00249	1.68637	0.04031	0.04842	0.00229	96	1090.1	46.45	964.7	13.81	1003.4	15.23	955.8	44.1

Hafnium isotopic zircon data

							Scherer et al., 2001 - ^{176}Lu decay constant (1.865x10^{-11})						
							Hf_i	epsilon	1se	T(DM)	T(DM)		
Sample N	No.	Hf176/Hf177	1 S.D.	Lu176/Hf177	Yb176/Hf177	U/Pb AGE				(Ga)	(crustal)	Hf Chur (t)	Hf DM (t)
1308	4	0.282341799	3.831E-05	0.0011352	0.0355606	555.6	0.282330	-3.41	1.3	1.29	1.72	0.282426	0.282851
1308	2	0.282366572	6.507E-05	0.0023234	0.0766073	589.7	0.282341	-2.27	2.3	1.30	1.67	0.282405	0.282826
1308	6	0.282347432	5.495E-05	0.0026533	0.0707908	580.7	0.282319	-3.26	1.9	1.34	1.73	0.282410	0.282833
1308	9	0.282342613	2.941E-05	0.0008907	0.0280807	553.9	0.282333	-3.32	1.0	1.28	1.71	0.282427	0.282852
1308	11	0.282347527	4.088E-05	0.0011683	0.0375267	624.5	0.282334	-1.74	1.4	1.28	1.66	0.282383	0.282801
1308	16	0.282323229	5.891E-05	0.001746	0.051703	566.7	0.282305	-4.06	2.1	1.34	1.77	0.282419	0.282843
1308	14	0.282320325	3.564E-05	0.0014416	0.0474056	579.7	0.282305	-3.77	1.2	1.33	1.76	0.282411	0.282834
1308	18	0.282347587	2.544E-05	0.0011656	0.0388096	565.9	0.282335	-2.99	0.9	1.28	1.70	0.282420	0.282844
1308	20	0.282348687	4.296E-05	0.0018846	0.0589922	568.8	0.282329	-3.16	1.5	1.31	1.71	0.282418	0.282841
1308	25	0.282354734	2.996E-05	0.0012971	0.0410724	555	0.282341	-3.02	1.0	1.28	1.69	0.282427	0.282851
1308	26	0.282308799	2.795E-05	0.0006643	0.0222492	555.1	0.282302	-4.41	1.0	1.32	1.78	0.282427	0.282851
1308	33	0.282392431	2.947E-05	0.001795	0.064422	529	0.282375	-2.41	1.0	1.24	1.64	0.282443	0.282870
1308	31	0.282375515	2.825E-05	0.0008653	0.0280029	554.5	0.282367	-2.14	1.0	1.23	1.64	0.282427	0.282852
1308	39	0.282336279	3.484E-05	0.0015337	0.0524009	597.3	0.282319	-2.87	1.2	1.31	1.71	0.282400	0.282821
1308	43	0.28236104	5.193E-05	0.0018446	0.0647801	595.7	0.282340	-2.15	1.8	1.29	1.67	0.282401	0.282822
1308	37	0.282377253	3.585E-05	0.0016431	0.0571868	554.3	0.282360	-2.37	1.3	1.26	1.65	0.282427	0.282852
1308	36	0.282357873	3.039E-05	0.0011529	0.0374078	558.3	0.282346	-2.79	1.1	1.27	1.68	0.282425	0.282849
1314	58	0.282120134	2.763E-05	0.0009629	0.0386815	607.9	0.282109	-10.07	1.0	1.59	2.17	0.282393	0.282813
1314	55	0.282160909	1.867E-05	0.0002756	0.0090326	533.9	0.282158	-9.97	0.7	1.51	2.11	0.282440	0.282867
1314	29	0.282186269	3.664E-05	0.0022468	0.0815325	567.8	0.282162	-9.07	1.3	1.55	2.08	0.282419	0.282842
1314	24	0.282123559	3.797E-05	0.0011517	0.0374317	653	0.282109	-9.06	1.3	1.60	2.14	0.282365	0.282780
1314	60	0.282217696	4.687E-05	0.0019223	0.0672846	569.3	0.282197	-7.81	1.6	1.50	2.00	0.282418	0.282841
1314	49	0.282290313	2.273E-05	0.0012006	0.0472429	519.3	0.282279	-6.03	0.8	1.37	1.85	0.282449	0.282877
1314	4	0.282295426	3.699E-05	0.0013374	0.0429894	529.7	0.282282	-5.67	1.3	1.36	1.84	0.282442	0.282870
1314	20	0.282295885	2.135E-05	0.0005814	0.0143075	559	0.282290	-5.1	0.8	1.34	1.80	0.282433	0.282849
1314	11	0.282298754	3.328E-05	0.001328	0.0434231	571.2	0.282285	-4.67	1.2	1.36	1.81	0.282416	0.282840
1314	18	0.282336904	2.313E-05	0.0012603	0.0327931	554	0.282324	-4.0	0.8	1.30	1.73	0.282436	0.282852
1314	7	0.282317285	2.691E-05	0.0007152	0.0201765	562.6	0.282310	-3.97	0.9	1.31	1.76	0.282422	0.282846
1314	37	0.282363732	2.463E-05	0.0026055	0.068192	546.9	0.282337	-3.7	0.9	1.31	1.71	0.282441	0.282857
1314	17	0.282362217	2.101E-05	0.0012436	0.0325924	559.2	0.282349	-3.0	0.7	1.27	1.67	0.282433	0.282848
1314	13	0.282357031	2.789E-05	0.0006733	0.0270883	557.3	0.282350	-2.66	1.0	1.25	1.67	0.282425	0.282850
1314	12	0.28242204	5.976E-05	0.0034844	0.1231457	537.7	0.282387	-1.79	2.1	1.26	1.60	0.282437	0.282864
1314	41	0.282430379	1.73E-05	0.0019694	0.0521563	573.2	0.282409	-0.5	0.6	1.19	1.53	0.282424	0.282838
1314	16	0.282448833	3.918E-05	0.0010453	0.0341382	544.3	0.282438	0.17	1.4	1.14	1.48	0.282433	0.282859
1314	25	0.282480069	2.877E-05	0.0013443	0.0545336	542.6	0.282466	1.14	1.0	1.10	1.42	0.282434	0.282860
1314	22	0.282439973	3.548E-05	0.0025473	0.0723275	690.7	0.282407	2.32	1.2	1.20	1.46	0.282342	0.282753
1314	9	0.282532063	3.17E-05	0.0008707	0.0322234	538	0.282523	3.05	1.1	1.02	1.30	0.282437	0.282864
1314	6	0.282493883	5.451E-05	0.0012758	0.0379882	693	0.282477	4.86	1.9	1.08	1.30	0.282340	0.282751
1314	8	0.282300189	3.697E-05	0.0006892	0.0253705	883.3	0.282289	2.42	1.3	1.33	1.60	0.282221	0.282613
1314	45	0.281597426	1.545E-05	0.0004144	0.015495	948.3	0.281590	-20.89	0.5	2.28	3.08	0.282180	0.282566
1314	5	0.2815227	2.191E-05	0.000507	0.0208059	1734.7	0.281506	-6.19	0.8	2.39	2.77	0.281680	0.281988
1314	56	0.281368687	1.899E-05	0.0004406	0.0175358	1769	0.281354	-10.81	0.7	2.59	3.08	0.281658	0.281963
1314	88	0.281645178	1.95E-05	0.0008982	0.0246726	1802.3	0.281614	-0.8	0.7	2.25	2.50	0.281636	0.281938
1314	38	0.281539479	3.495E-05	0.0009638	0.0328067	1903.5	0.281505	-2.40	1.2	2.40	2.67	0.281572	0.281863
1314	82	0.281434522	2.057E-05	0.0005722	0.0149875	1957.4	0.281413	-4.4	0.7	2.51	2.83	0.281536	0.281823
1314	23	0.281279644	2.869E-05	0.0007144	0.0251733	1980.8	0.281253	-9.58	1.0	2.73	3.16	0.281523	0.281806
1314	54	0.281433128	2.836E-05	0.0008755	0.031501	2002.2	0.281400	-3.87	1.0	2.54	2.84	0.281509	0.281790
1314	87	0.281690644	2E-05	0.0017801	0.0508137	2070.7	0.281621	5.6	0.7	2.24	2.32	0.281462	0.281739
1314	19	0.281424575	2.537E-05	0.0004116	0.0139753	2087.7	0.281408	-1.62	0.9	2.52	2.77	0.281454	0.281726
1314	47	0.281437849	3.461E-05	0.0014385	0.0467232	2124.3	0.281380	-1.80	1.2	2.57	2.81	0.281430	0.281699
1314	92	0.28165013	1.696E-05	0.0009114	0.0253168	2152.7	0.281613	7.3	0.6	2.24	2.29	0.281409	0.281678
1314	31	0.28112429	3.984E-05	0.0007955	0.0267217	2694.5	0.281083	0.79	1.4	2.95	3.09	0.281061	0.281272
1314	30	0.281004619	3.062E-05	0.0007822	0.0297717	2744.1	0.280964	-2.32	1.1	3.11	3.31	0.281029	0.281235
1314	84	0.280769506	1.605E-05	0.0004827	0.0129527	3005.4	0.280742	-3.8	0.6	3.40	3.68	0.280848	0.281037
13-13	6	0.282839622	4.877E-05	0.0037218	0.1312635	448	0.282808	11.15	1.7	0.63	0.72	0.282493	0.282929
13-13	16	0.282386168	3.543E-05	0.0021501	0.076248	448.2	0.282368	-4.43	1.2	1.26	1.70	0.282493	0.282929
13-13	31	0.282790602	6.311E-05	0.0018435	0.0614156	452.5	0.282775	10.07	2.2	0.67	0.79	0.282491	0.282926
13-13	32	0.282800056	3.855E-05	0.0019592	0.065166	454.1	0.282783	10.40	1.3	0.66	0.77	0.282490	0.282924
13-13	53	0.282836732	5.907E-05	0.0042591	0.1287655	458.2	0.282800	11.08	2.1	0.65	0.73	0.282487	0.282921
13-13	49	0.282851047	7.816E-05	0.0028863	0.0841585	459	0.282826	12.02	2.7	0.60	0.67	0.282487	0.282921
13-13	28	0.282783873	4.843E-05	0.0018204	0.0638989	459.1	0.282768	9.97	1.7	0.68	0.80	0.282487	0.282921
13-13	58	0.282754006	6.053E-05	0.0030399	0.0827781	461.3	0.282728	8.59	2.1	0.75	0.89	0.282485	0.282919
13-13	5	0.282839087	3.698E-05	0.0057063	0.1428436	463.5	0.282790	10.5	1.3	0.67	0.75	0.282493	0.282918
13-13	18	0.282790752	1.788E-05	0.0017671	0.0437655	463.9	0.282775	10.0	0.6	0.67	0.78	0.282493	0.282917
13-13	34	0.282796419	4.651E-05	0.0021889	0.0729885	464.1	0.282777	10.41	1.6	0.67	0.78	0.282483	0.282917
13-13	57	0.282792584	2.871E-05	0.0025422	0.0632393	464.5	0.282770	9.8	1.0	0.68	0.79	0.282493	0.282917
13-13	4	0.282802537	2.122E-05	0.0012804	0.0255632	466.6	0.282791	10.6	0.8	0.64	0.75	0.282491	0.282915
13-13	52	0.282886988	4.86E-05	0.0039114	0.1193169	466.7	0.282853	13.13	1.7	0.56	0.61	0.282482	0.282915
13-13	3	0.28285828	6.021E-05	0.0029096	0.0991373	466.9	0.282833	12.43	2.1	0.59	0.65	0.282482	0.282915
13-13	14	0.282599694	0.0001158	0.0037881	0.1023575	467	0.282567	3.01	4.1	1.00	1.25	0.282482	0.282915
13-13	56	0.282789595	3.404E-05	0.0023891	0.0747698	469.4	0.282769	10.21	1.2	0.68	0.80	0.282480	0.282913
13-13	50	0.28281668	2.733E-05	0.001767	0.0517538	471.4	0.282801	11.41	1.0	0.63	0.72	0.282479	0.282912
13-13	48	0.282849248	8.927E-05	0.0019876	0.0624166	471.7	0.282832	12.50	3.1	0.59	0.65	0.282479	0.282912
13-13	11	0.28289973	0.0001757	0.0053461	0.156524	473.9	0.282852	13.28	6.2	0.57	0.60	0.282477	0.282910
13-13	20	0.282806763	1.966E-05	0.0016246	0.0447796	474.2	0.282792	10.8	0.7	0.64	0.74	0.282487	0.282910
13-13	19	0.282883061	0.0001043	0.0111728	0.4487361	475.7	0.282783	10.88	3.6	0.72	0.76	0.282476	0.282909
13-13	15	0.282788316	1.821E-05	0.0017662	0.0437622	476	0.282773	10.2	0.6	0.67	0.78	0.282485	0.282909
13-13	1	0.282802822	3.557E-05	0.0010008	0.0391316	476.4	0.282794	11.26	1.2	0.64	0.73	0.282476	0.282908
13-13	30	0.282818821	7.553E-05	0.0055494	0.1662889	479.8	0.282769	10.46	2.6	0.70	0.79	0.282474	0.282906
13-13	40	0.282823171	1.88E-05	0.0013941	0.0452136	480.8	0.282811	11.95	0.7	0.61	0.69	0.282473	0.282905
13-13	36	0.282855629	6.487E-05	0.0056758	0.1633093	481.3	0.282804	11.75	2.3	0.64	0.71	0.282473	0.282905

13-13	25	0.282814785	2.225E-05	0.0029167	0.0710929	482.7	0.282788	10.9	0.8	0.65	0.74	0.282481	0.282904
13-13	46	0.282636865	0.0002723	0.0042803	0.1153127	483.7	0.282598	4.49	9.5	0.95	1.17	0.282471	0.282903
13-13	21	0.282839132	3.527E-05	0.0021803	0.0772602	484.4	0.282819	12.34	1.2	0.60	0.67	0.282471	0.282903
13-13	23	0.282810272	2.878E-05	0.0045594	0.1121077	486.9	0.282769	10.3	1.0	0.69	0.78	0.282478	0.282901
13-13	26	0.282706381	0.0001169	0.0061795	0.1740181	488.3	0.282650	6.43	4.1	0.90	1.05	0.282468	0.282900
13-13	12	0.282824541	2.058E-05	0.0020974	0.0528658	488.5	0.282805	11.6	0.7	0.62	0.70	0.282477	0.282900
13-13	41	0.282823355	4.276E-05	0.0043632	0.1468683	489.5	0.282783	11.18	1.5	0.67	0.75	0.282468	0.282899
13-13	22	0.282805003	4.798E-05	0.0043336	0.1026908	491.3	0.282765	10.2	1.7	0.70	0.79	0.282476	0.282898
13-13	42	0.28282409	3.925E-05	0.0017647	0.0505385	491.4	0.282808	12.09	1.4	0.62	0.69	0.282466	0.282897
13-13	43	0.282835233	2.65E-05	0.0034994	0.0826587	493	0.282803	11.6	0.9	0.63	0.70	0.282475	0.282896
13-13	45	0.282837107	3.176E-05	0.0021825	0.0751194	494.8	0.282817	12.49	1.1	0.61	0.67	0.282464	0.282895
13-13	39	0.282764416	6.749E-05	0.0016158	0.0470716	499.3	0.282749	10.19	2.4	0.70	0.82	0.282461	0.282892
13-13	37	0.282844482	6.004E-05	0.0055255	0.204958	499.4	0.282793	11.73	2.1	0.66	0.72	0.282461	0.282892
13-13	44	0.282849378	4.461E-05	0.0017636	0.0598992	525.3	0.282832	13.70	1.6	0.58	0.62	0.282445	0.282873
13-13	35	0.282828897	6.831E-05	0.003347	0.1064116	543.5	0.282795	12.78	2.4	0.64	0.69	0.282434	0.282860
13-13	27	0.282016416	0.0001987	0.0026198	0.0870573	1196.4	0.281957	-2.33	7.0	1.82	2.13	0.282023	0.282385
13-13	2	0.281714546	5.488E-05	0.0015928	0.0469946	1770.7	0.281661	0.13	1.9	2.19	2.42	0.281657	0.281962
ACO-12-15B	33	0.282546562	2.229E-05	0.001211	0.0332588	422.4	0.282537	0.6	0.8	1.00	1.34	0.282519	0.282947
ACO-12-15B	58	0.282457756	2.152E-05	0.0013166	0.0327984	433.4	0.282447	-2.3	0.8	1.13	1.54	0.282512	0.282939
ACO-12-15B	4	0.282257055	2.112E-05	0.0017947	0.0494396	433.5	0.282242	-9.5	0.7	1.44	1.99	0.282512	0.282939
ACO-12-15B	55	0.282158176	2.029E-05	0.0015734	0.0388836	433.5	0.282145	-13.0	0.7	1.57	2.20	0.282512	0.282939
ACO-12-15B	20	0.282374214	1.88E-05	0.00178	0.0426764	435.1	0.282360	-5.4	0.7	1.27	1.73	0.282511	0.282938
ACO-12-15B	35	0.282528952	2.178E-05	0.0012208	0.0346212	436.4	0.282519	0.3	0.8	1.03	1.37	0.282510	0.282937
ACO-12-15B	43	0.282396501	2.3E-05	0.00163	0.043598	438.3	0.282383	-4.5	0.8	1.23	1.67	0.282509	0.282936
ACO-12-15B	41	0.282186916	2.195E-05	0.001723	0.0449153	440.1	0.282173	-11.9	0.8	1.53	2.14	0.282508	0.282935
ACO-12-15B	19	0.282296083	1.895E-05	0.0010381	0.0253317	442.6	0.282287	-7.8	0.7	1.35	1.88	0.282507	0.282933
ACO-12-15B	44	0.281898058	1.611E-05	0.0011602	0.0317131	445.1	0.281888	-21.8	0.6	1.91	2.75	0.282505	0.282931
ACO-12-15B	54	0.282319494	1.764E-05	0.0006782	0.0179897	446.1	0.282314	-6.7	0.6	1.31	1.82	0.282504	0.282930
ACO-12-15B	37	0.282292532	1.561E-05	0.0014789	0.0376893	446.3	0.282280	-7.9	0.6	1.37	1.90	0.282504	0.282930
ACO-12-15B	53	0.282427461	1.923E-05	0.001495	0.0373151	446.9	0.282415	-3.1	0.7	1.18	1.60	0.282504	0.282930
ACO-12-15B	2	0.282242054	1.668E-05	0.0012134	0.0298665	447.4	0.282232	-9.6	0.6	1.43	2.00	0.282503	0.282929
ACO-12-15B	26	0.282393766	1.938E-05	0.001618	0.0410029	447.9	0.282380	-4.4	0.7	1.23	1.67	0.282503	0.282929
ACO-12-15B	17	0.282469728	3.01E-05	0.0030567	0.0742139	448.6	0.282444	-2.1	1.1	1.17	1.53	0.282503	0.282928
ACO-12-15B	47	0.282283846	1.776E-05	0.0011967	0.0298892	448.7	0.282274	-8.1	0.6	1.37	1.91	0.282503	0.282928
ACO-12-15B	21	0.282487785	2.809E-05	0.0012931	0.0355543	449	0.282477	-0.9	1.0	1.09	1.46	0.282502	0.282928
ACO-12-15B	34	0.282248605	1.725E-05	0.0014941	0.0401086	449	0.282236	-9.4	0.6	1.44	1.99	0.282502	0.282928
ACO-12-15B	60	0.282342016	2.456E-05	0.0014121	0.0332093	450.2	0.282330	-6.1	0.9	1.30	1.78	0.282502	0.282927
ACO-12-15B	50	0.282209688	1.857E-05	0.0010994	0.02953	452.2	0.282200	-10.6	0.7	1.47	2.07	0.282500	0.282926
ACO-12-15B	10	0.282422602	1.983E-05	0.0006703	0.0173535	452.3	0.282417	-3.0	0.7	1.16	1.59	0.282500	0.282926
ACO-12-15B	40	0.282435092	1.827E-05	0.000904	0.0228415	453.9	0.282427	-2.5	0.6	1.15	1.57	0.282499	0.282925
ACO-12-15B	25	0.281937199	1.779E-05	0.000547	0.0140358	454	0.281933	-20.1	0.6	1.83	2.65	0.282499	0.282924
ACO-12-15B	30	0.282071077	1.723E-05	0.0011547	0.0268725	455	0.282061	-15.5	0.6	1.67	2.37	0.282499	0.282924
ACO-12-15B	22	0.282398288	2.241E-05	0.0020017	0.0490164	455.3	0.282381	-4.2	0.8	1.24	1.67	0.282498	0.282924
ACO-12-15B	45	0.28227281	1.649E-05	0.000692	0.0172436	455.6	0.282267	-8.2	0.6	1.37	1.92	0.282498	0.282923
ACO-12-15B	24	0.282325523	2.155E-05	0.0005606	0.0151688	456.6	0.282321	-6.3	0.8	1.29	1.80	0.282498	0.282923
ACO-12-15B	8	0.282593057	4.374E-05	0.0032178	0.0779281	457.1	0.282566	2.4	1.5	0.99	1.26	0.282497	0.282922
ACO-12-15B	1	0.282417979	2.153E-05	0.0013694	0.0331295	460.5	0.282406	-3.2	0.8	1.19	1.61	0.282495	0.282920
ACO-12-15B	38	0.282346573	1.878E-05	0.000819	0.0233472	460.6	0.282340	-5.5	0.7	1.27	1.75	0.282495	0.282920
ACO-12-15B	49	0.28231964	2.646E-05	0.0023733	0.0640325	474	0.282299	-6.7	0.9	1.37	1.82	0.282487	0.282910
ACO-12-15B	18	0.282196778	2.407E-05	0.001916	0.0502143	497.2	0.282179	-10.4	0.9	1.53	2.07	0.282472	0.282893
ACO-12-15B	7	0.282201965	1.868E-05	0.00151	0.040529	858.6	0.282178	-2.3	0.7	1.50	1.86	0.282243	0.282631
ACO-12-15B	11	0.282167519	2.419E-05	0.000633	0.0170599	859.5	0.282157	-3.0	0.9	1.52	1.90	0.282242	0.282631
ACO-12-15B	31	0.282037909	1.721E-05	0.0006816	0.0194904	942.6	0.282026	-5.8	0.6	1.70	2.18	0.282189	0.282570
ACO-12-15B	39	0.282178346	1.551E-05	0.0006265	0.0186851	989.8	0.282167	0.3	0.5	1.50	1.83	0.282159	0.282536
aco-12-16	31	0.282498614	4.002E-05	0.0010294	0.0342517	368.9	0.282492	-1.82	1.4	1.07	1.48	0.282543	0.282986
aco-12-16	45	0.28252442	7.109E-05	0.0018851	0.0610335	390.9	0.282511	-0.65	2.5	1.06	1.42	0.282529	0.282970
aco-12-16	13	0.282458122	4.974E-05	0.0015402	0.0552428	391.4	0.282447	-2.90	1.7	1.14	1.56	0.282529	0.282970
aco-12-16	23	0.282479004	4.019E-05	0.0014334	0.0536467	393.2	0.282468	-2.10	1.4	1.11	1.51	0.282528	0.282968
aco-12-16	42	0.2825011	6.109E-05	0.001419	0.0546671	393.5	0.282491	-1.30	2.1	1.07	1.46	0.282527	0.282968
aco-12-16	10	0.282524048	4.732E-05	0.0016281	0.0614607	401.4	0.282512	-0.38	1.7	1.05	1.41	0.282523	0.282962
aco-12-16	46	0.282313281	4.765E-05	0.0011974	0.0462642	402.5	0.282304	-7.70	1.7	1.33	1.87	0.282522	0.282962
aco-12-16	17	0.28241912	5.317E-05	0.0014828	0.0531363	404.9	0.282408	-3.98	1.9	1.19	1.64	0.282520	0.282960
aco-12-16	5	0.282409616	6.625E-05	0.0021246	0.0659279	405.2	0.282393	-4.48	2.3	1.23	1.67	0.282520	0.282960
aco-12-16	3	0.28248976	8.949E-05	0.0019256	0.0677222	414	0.282475	-1.41	3.1	1.11	1.49	0.282515	0.282953
aco-12-16	41	0.282453349	6.928E-05	0.0018099	0.0630354	429.3	0.282439	-2.35	2.4	1.15	1.56	0.282505	0.282942
aco-12-16	21	0.282398835	8.689E-05	0.0028794	0.0948706	431.3	0.282376	-4.54	3.0	1.27	1.69	0.282504	0.282941

aco-12-16	18	0.282073663	6.621E-05	0.0017412	0.072767	457.3	0.282059	-15.18	2.3	1.69	2.37	0.282488	0.282922
aco-12-16	49	0.282290109	9.557E-05	0.0024615	0.0821642	470.3	0.282268	-7.47	3.3	1.41	1.91	0.282480	0.282913
aco-12-16	12	0.282477006	4.224E-05	0.0015399	0.0542675	478	0.282463	-0.41	1.5	1.11	1.47	0.282475	0.282907
aco-12-16	16	0.282598679	4.633E-05	0.0015933	0.0503829	482.3	0.282584	3.97	1.6	0.94	1.20	0.282472	0.282904
aco-12-16	25	0.282198005	4.388E-05	0.0011548	0.0411182	880.3	0.282179	-1.54	1.5	1.49	1.85	0.282222	0.282615
aco-12-16	15	0.282201625	4.4E-05	0.0009379	0.0294689	976.6	0.282184	0.80	1.5	1.48	1.77	0.282162	0.282545
aco-12-16	1	0.282256339	7.94E-05	0.0010833	0.0351293	1075.3	0.282234	4.78	2.8	1.41	1.60	0.282099	0.282473
aco-12-16	51	0.282367149	8.536E-05	0.0043254	0.1616867	1087	0.282279	6.61	3.0	1.37	1.50	0.282092	0.282465
aco-12-16	8	0.282101461	0.0001155	0.0018263	0.0514346	1087.4	0.282064	-0.98	4.0	1.66	1.97	0.282092	0.282464
aco-12-16	2	0.281915125	3.279E-05	0.0009438	0.0303805	1486.3	0.281889	1.77	1.1	1.88	2.10	0.281839	0.282172
aco-12-16	11	0.281715639	6.155E-05	0.0017827	0.0618906	1641.5	0.281660	-2.83	2.2	2.20	2.50	0.281740	0.282057
aco-12-16	19	0.281839638	7.813E-05	0.0017818	0.0621386	1684.7	0.281783	2.50	2.7	2.03	2.21	0.281712	0.282025
ACO-12-14B	14_2	0.2821	0.000013	0.001303	0.0513749	453	0.28208895	-14.548	0.461	1.637	2.309	0.2824835	0.28290642
ACO-12-14B	14_48	0.281947	0.000012	0.000668	0.0249622	460	0.28194125	-19.62	0.426	1.82	2.592	0.28247401	0.28289558
ACO-12-14B	14_36	0.281809	0.000013	0.0012339	0.0539792	476	0.281798	-24.334	0.461	2.04	2.838	0.28174983	0.28206795
ACO-12-14B	14_11	0.281919	0.000011	0.0009139	0.0399875	479	0.2819108	-20.274	0.39	1.871	2.608	0.28249993	0.28292521
ACO-12-14B	14_39	0.282066	0.0000093	0.0008134	0.0342012	484	0.28205863	-14.929	0.33	1.663	2.358	0.28247844	0.28290064
ACO-12-14B	14_30	0.281782	0.000008	0.0014141	0.0611358	487	0.2817691	-25.111	0.284	2.087	2.983	0.28248539	0.28290859
ACO-12-14B	14_17	0.281823	0.000015	0.001099	0.0506622	494	0.28181283	-23.407	0.532	2.013	2.887	0.28248033	0.28290281
ACO-12-14B	14_75	0.282061	0.0000074	0.0009605	0.037022	496	0.28205207	-14.892	0.262	1.676	2.362	0.28168453	0.28199332
ACO-12-14B	14_67	0.28202	0.0000094	0.0006996	0.0275039	502	0.28201342	-16.127	0.333	1.721	2.404	0.28249551	0.28292015
ACO-12-14B	14_70	0.282009	0.000012	0.0011733	0.0324487	502	0.28199796	-16.674	0.426	1.758	2.476	0.28197068	0.28232035
ACO-12-14B	14_73	0.281979	0.00001	0.0009049	0.0373057	525	0.2819701	-17.146	0.355	1.787	2.522	0.28214354	0.2825179
ACO-12-14B	14_9	0.282075	0.0000076	0.0014466	0.0578695	525	0.28206077	-13.936	0.269	1.678	2.258	0.28207258	0.28243681
ACO-12-14B	14_8	0.28203	0.00001	0.0016252	0.0654118	547	0.28201334	-15.123	0.355	1.75	2.386	0.28212885	0.28250111
ACO-12-14B	14_60	0.282004	0.0000088	0.0009933	0.0413381	587	0.28199307	-14.945	0.312	1.757	2.439	0.28241514	0.28282831
ACO-12-14B	14_53	0.282122	0.00001	0.0006706	0.0216766	1014	0.2821092	-1.217	0.354	1.58	1.914	0.28187363	0.28220944
ACO-12-14B	14_6	0.282212	0.000035	0.0014277	0.0610112	1037	0.28218412	1.959	1.24	1.485	1.728	0.28246895	0.2828898
ACO-12-14B	14_57	0.282189	0.0000076	0.0006377	0.0272898	1125	0.28217548	3.648	0.269	1.486	1.71	0.28246895	0.2828898
ACO-12-14B	14_72	0.282149	0.000008	0.0007664	0.0342794	1207	0.28213155	3.953	0.284	1.546	1.758	0.28202007	0.28237679
ACO-12-14B	14_49	0.281713	0.0000097	0.0005937	0.0205276	1284	0.28169861	-9.649	0.344	2.137	2.643	0.2824544	0.28287317
ACO-12-14B	14_64	0.281954	0.00001	0.000396	0.016409	1435	0.28194326	2.47	0.355	1.798	2.032	0.28247275	0.28289414
ACO-12-14B	14_18	0.281953	0.000011	0.0016106	0.0653163	1627	0.28190338	5.45	0.39	1.858	1.997	0.28244047	0.28285726
ACO-12-14B	14_44	0.281819	0.000012	0.0005773	0.0230789	1728	0.28180009	4.103	0.426	1.991	2.152	0.2824544	0.28287317

Chapter 4

The P-T-t evolution of Ganderia in the Paleozoic: the metamorphic record of back-arc basin tectonics and continental ribbon transfer

ABSTRACT

Ganderia is a microcontinental terrane that was transferred from the Gondwanan margin to eastern Laurentia at the expense of the Iapetus Ocean during the Ordovician. Episodes of low-medium grade metamorphism are broadly attributed to events associated with the transfer and accretion of Ganderia and Avalonia to Laurentia; however, the timing and nature of the metamorphism is poorly characterised. In this chapter U-Pb monazite geochronology and mineral phase equilibria modelling are presented from a series of amphibolite facies rocks within the Dover Fault Shear Zone of Newfoundland, Canada in order to provide insight into the timing and conditions of metamorphism in Ganderia.

The metamorphic rocks along the Dover Fault Zone record two major stages of the Ganderian evolution. The first is a low pressure, high temperature (3-4 kbar, 600°C) event recorded by 460 ± 7 Ma monazite within andalusite bearing metamorphic assemblages. This is attributed to an extensional environment, most likely within the Tetagouche-Exploits back-arc basin that separated the active Popelogan-Victoria arc from the passive trailing Gander margin. The second is both a higher pressure event (5-6 kbar, ~600-650°C) and a lower pressure event (3-4 kbar) characterised by migmatisation at 409 ± 6 Ma; interpreted to reflect a short interval of compression along the Dover Fault Shear Zone followed by the emplacement of the Hare Bay Gneiss and other granite suites. Ganderia forms a locus of intermittent extension and contraction events between the early Ordovician-middle Devonian, most likely relating to the opening and closing of back-arc basins, during the consumption of the Iapetus and the Rheic Oceans.

1. INTRODUCTION

The transfer of continental terranes as microcontinents or ribbon terranes is an important part of plate tectonics and continental growth (Moresi et al., 2014), but the process of rifting a continental ribbon from one margin to another are loosely understood. The north-eastern section of the Appalachian-Caledonian Orogen is composed of deformed Laurentian crust and a collage of exotic microcontinental ribbons, collectively termed the 'peri-Gondwanan' terranes (Pollock et al., 2011). Ganderia and Avalonia are two peri-Gondwanan terranes interpreted to originate along the northern margin of Amazonia and North Africa in the Neoproterozoic (Nance and Murphy, 1994; O'Brien et al., 1996; Keppie et al., 2003; Murphy et al., 2004). During the orthogonal opening and closing of the Iapetus and Rheic Oceans, the peri-Gondwana terranes are purported to have been transferred from the Gondwanan margin to the Baltican/Laurussian margin (Van Staal et al., 1998b; Murphy and Keppie, 2005; Pollock et al., 2011). Closure of the Rheic Ocean was accompanied by continental collision between Gondwana and Laurussia forming the Appalachian-Variscan Orogen of North America and western Europe (Scotese, 2004; Hibbard et al., 2010; Stampfli et al., 2013).

Ganderia comprises several distinct, but tectonically related terranes, which form the most inboard of the peri-Gondwanan terranes along the Laurentian margin (van Staal et al., 2009), and are located in New Brunswick, Cape Breton and Newfoundland in Maritime Canada, and New England in the USA (Pollock et al., 2011); and across the Atlantic Ocean, is also recognised in southern Ireland and central Britain, and are interpreted to form parts of the southern Carpathians (Balintoni et al., 2014). Ganderia comprises (broadly) Neoproterozoic arc magmatic and volcanic rocks, Cambrian-Ordovician rifted margin and passive margin sedimentary sequences and Ordovician oceanic-arc rocks

and associated ophiolitic fragments (see Nance et al., 2008 and references therein; Pollock et al., 2011).

The boundary between Ganderia and Avalonia (the next terrane outboard) is marked by the Dover Fault Shear Zone, a major brittle-ductile structure that cuts down to the moho separating two crustal blocks of differing seismic character (Marillier et al., 1989; Stockmal et al., 1990)(Fig. 1a). Its surface expression is a ~25km high strain zone characterised by an eastwards trending increase in metamorphic grade and granite emplacement (Holdsworth, 1994). It forms a region of focused deformation and metamorphism attributed to the mid-Silurian sinistral-oblique collision between Avalonia and Ganderia (Blackwood and Kennedy, 1975; Dallmeyer et al., 1983). The record of structural deformation and metamorphism has been described in some detail by King (1997), where three episodes of metamorphism are proposed, but there are few temporal or calculated pressure-temperature constraints for the metamorphic episodes. In this chapter U-Pb monazite geochronology and mineral phase equilibria modelling are presented from a series of low-medium grade amphibolite facies Gander Group rocks within the Dover Fault Shear Zone. The data are used to characterise the timing and pressure-temperature evolution of metamorphism in Ganderia and to discuss the implications for the tectonic evolution of Ganderia within the Canadian Appalachians.

2. GEOLOGICAL BACKGROUND: GANDERIA

The basement is not exposed anywhere in the Ganderian terrane. The oldest Ganderian rocks are found in New Brunswick and include a 978 ± 7 Ma alkalic anorthosite (Tesfai, 2011), the stromatolite-bearing carbonates and quartzites of the Green Head Group in New Brunswick (Barr et al., 2003a; Barr et al., 2014) and the Seven Hundred Acre Island Formation in coastal Maine (Stewart et al., 2001). The earliest evidence of Ediacaran magmatic arc activity is only found in the Brookville and New River terranes of southern New Brunswick (~652 Ma, Lingley Suite, Currie and McNicoll, 1999; ~622 Ma, Blacks Harbour Granite, Barr et al., 2003b), whereas the younger phase (~580-540 Ma) is more abundant and widespread across Ganderia. In Newfoundland this is represented by the Roti Suite (~578-564 Ma, Kerr et al., 1995) and Cripple Back Intrusive suite (~565 Ma, Rogers et al., 2006), in Cape Breton the plutonic suites of the Bras d'Or terrane (Barr et al., 1990) (~565-555 Ma) and in New Brunswick the Simpsons Island Formation (539 ± 4 Ma, Barr et al., 2003b) and the Golden Grove Plutonic Suite (553-527 Ma, White et al., 2002; Barr et al., 2014). The latter phase of magmatism is also associated with metamorphism and deformation variably dated between ~570-540 Ma (see Nance et al., 2008 and references therein).

The structure of the Ganderian terrane during transfer across the Iapetus Ocean comprises a leading volcanic arc (the Popelogan/Victoria arc) and an associated back arc basin with a trailing passive margin (the "Gander Zone" of Williams, 1979). The evolution of Ganderia during the late Neoproterozoic-early Silurian interval is complex and involves the generation of two magmatic arcs and associated back arc systems, separated by a brief hiatus, and multiple deformation events associated with the docking of Ganderia with Laurentia (see Zagorevski and Van Staal, 2011 and references therein).

The Middle Cambrian to early Ordovician in Ganderia is marked by renewed arc magmatism and the concurrent deposition of clastic sedimentary rocks in a passive margin-type environment (van Staal et al., 1998a; Hibbard et al., 2010; van Staal and Barr, 2011). The juxtaposition of the magmatic activity and clastic sedimentation is explained by the development of an active arc on the outboard edge of Ganderia, with an associated back-arc (Penobscot arc-backarc system), and

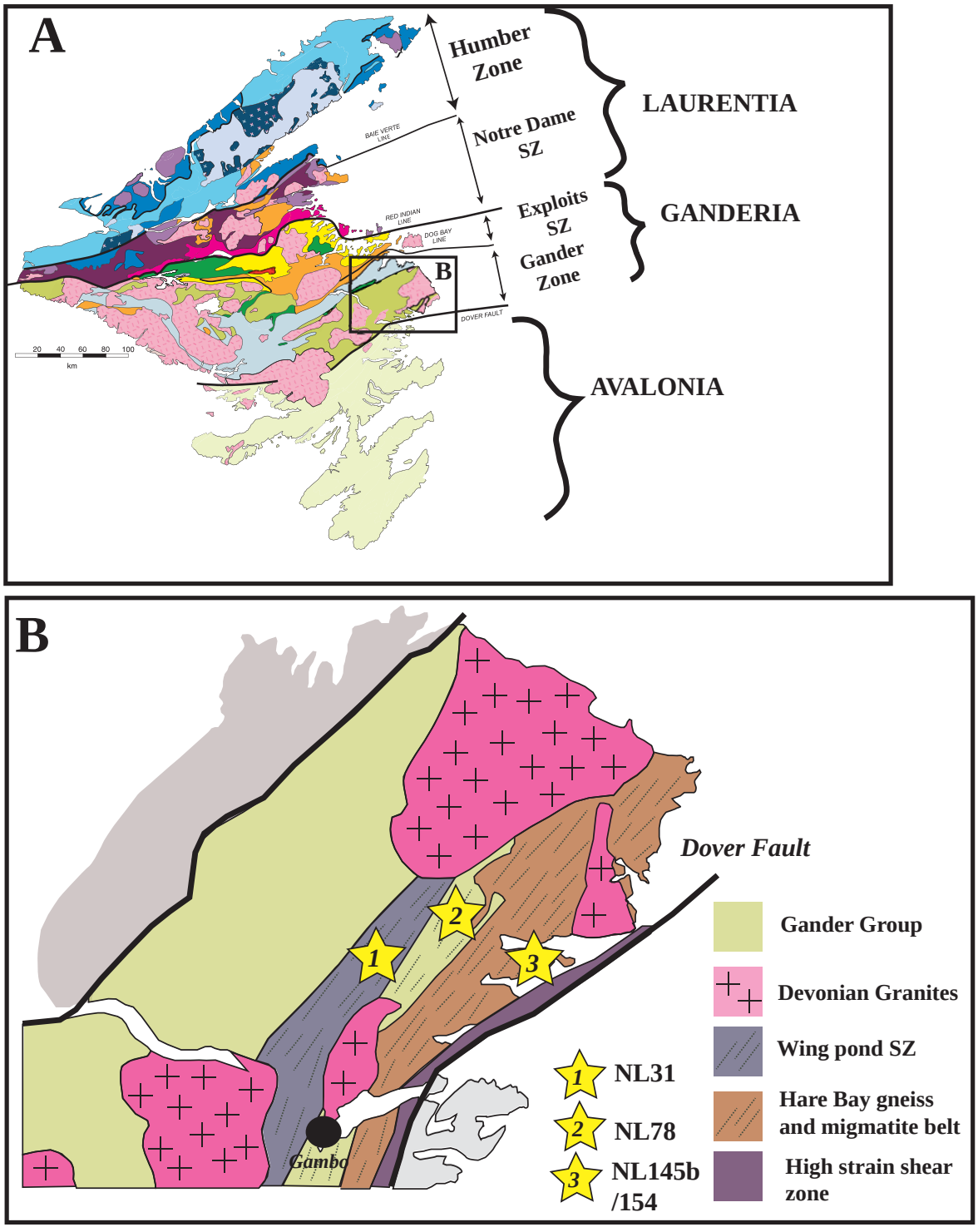

Figure 1

1a) Detailed geology map of Newfoundland, Canada showing the division into the major tectonic terranes of the Appalachian Orogen. Included within "Laurentia" are the Humber Zone and Notre Dame Subzone, and in "Ganderia" the Exploits Subzone and Gander Margin. The Notre Dame Subzone and Exploits Subzones are considered to be the Iapetan Oceanic realms developed on either side of the Iapetus Ocean. The figure is modified after van Staal et al. (2007), van Staal and Barr (2011) and Piercey et al. (2014).

1b) The inset shows the geology of the Gander Zone in northeasetern Newfoundland modified after Schofield and D'Lemos (2000). Sample locations are shown by the yellow stars. The magmatic belt and Wing Pond Shear Zone are based broadly on those defined by King (1997) and Schofield and D'Lemos (2000).

a trailing passive edge known as the 'Gander margin' (van Staal, 1994). The Penobscot arc is interpreted to have formed at ~515 Ma in an intra-oceanic setting outboard of the Gander margin above a west-dipping subduction zone (MacLachlan and Dunning, 1998; van Staal et al., 1998a; Zagorevski et al., 2007a). The ongoing subduction resulted in the collision of the arc system and the obduction of supra-subduction zone ophiolites (Colman-Sadd et al., 1992; Jenner and Swinden, 1993) on to the Gander margin. The apparent collision of the Penobscot arc with the Gander margin is assigned to the Penobscot Orogeny at ~485 Ma (van Staal et al., 1998a). Subduction reversal resulted in subduction beneath the Gander margin heralding the onset of magmatism within the Popelogan-Victoria arc system at ~478 Ma (van Staal et al., 1998a; van Staal et al., 2009) that was active until ~455 Ma, when it was shut down upon arrival to the peri-Laurentian Red Indian Lake arc closing the main Iapetan tract (van Staal and Barr, 2011). Collision of the Gander arc system and trailing edge with the Laurentian margin occurred between ~450-430 Ma, and was followed by the soft collision of Avalonia along the Dover Fault Shear Zone between ~422-408 Ma (Zagorevski et al., 2007b).

Newfoundland is an exceptional natural laboratory for investigating the tectonics of Appalachian geology as a NW-SE transect covers all Laurentian and Gondwanan components involved in the orogenic event (Fig. 1a). From west to east: the Neoproterozoic-early Ordovician Laurentian passive margin (Humber Zone), which includes inliers of the Mesoproterozoic Grenville Province; the Dunnage Zone (Williams, 1979), which preserves rocks of the Iapetan oceanic realm including the peri-Laurentian Notre Dame Subzone and the peri-Ganderian Exploits Subzone; and the Gander margin that is composed of predominantly Cambrian-Silurian metasedimentary rocks of increasing grade, from greenschist to upper amphibolite, towards the eastern boundary, marked by the Dover Fault Shear Zone (DFSZ). The DFSZ is up to 25 km in width and forms a north-northeast to northeast-southwest oriented high strain zone, which marks the surface expression of boundary between Avalonia and Ganderia (D'Lemos et al., 1997). It is defined by seismic-reflection studies as a crustal-scale structure that offsets the moho (Keen et al., 1986; Marillier et al., 1989; Stockmal et al., 1990). The DFSZ is comprised of paragneisses and migmatites of the Square Pond and Hare Bay Gneiss (Schofield and D'Lemos, 2000). The DFSZ is truncated by the Ackley granite suite, which has a U-Pb zircon crystallisation age of 377 ± 3 Ma (O'Brien et al., 1986; Kerr et al., 1993; Kellett et al., 2014).

3. SAMPLE SELECTION

Four samples of different metamorphic grade were selected from the Gander Group within the Dover-Fault Shear Zone (Fig 1b). An eastwards increase in metamorphic grade and deformation occurs towards the DFSZ from lower greenschist facies rocks, through to upper amphibolite bearing assemblages and migmatites associated with the magmatism along the Avalon-Gander boundary (King, 1997). The rocks were sampled on the basis of mineralogical assemblages that indicated an appropriate level of metamorphism to crystallise monazite grains (i.e. amphibolite facies). The samples host aluminous mineral assemblages (i.e. garnet, sillimanite, kyanite, andalusite, staurolite and cordierite) capable of producing meaningful thermodynamic metamorphic models. All four samples were analysed insitu for U-Pb monazite geochronology and three (NL31, NL78, NL145b) were used for metamorphic mineral equilibria modelling.

4. PETROGRAPHY

4.1 Sample NL31

Sample NL31 is from the Wing Pond Shear Zone (Fig. 1b), which is a prominent high strain belt trending NE, and containing a steeply dipping transpressional foliation

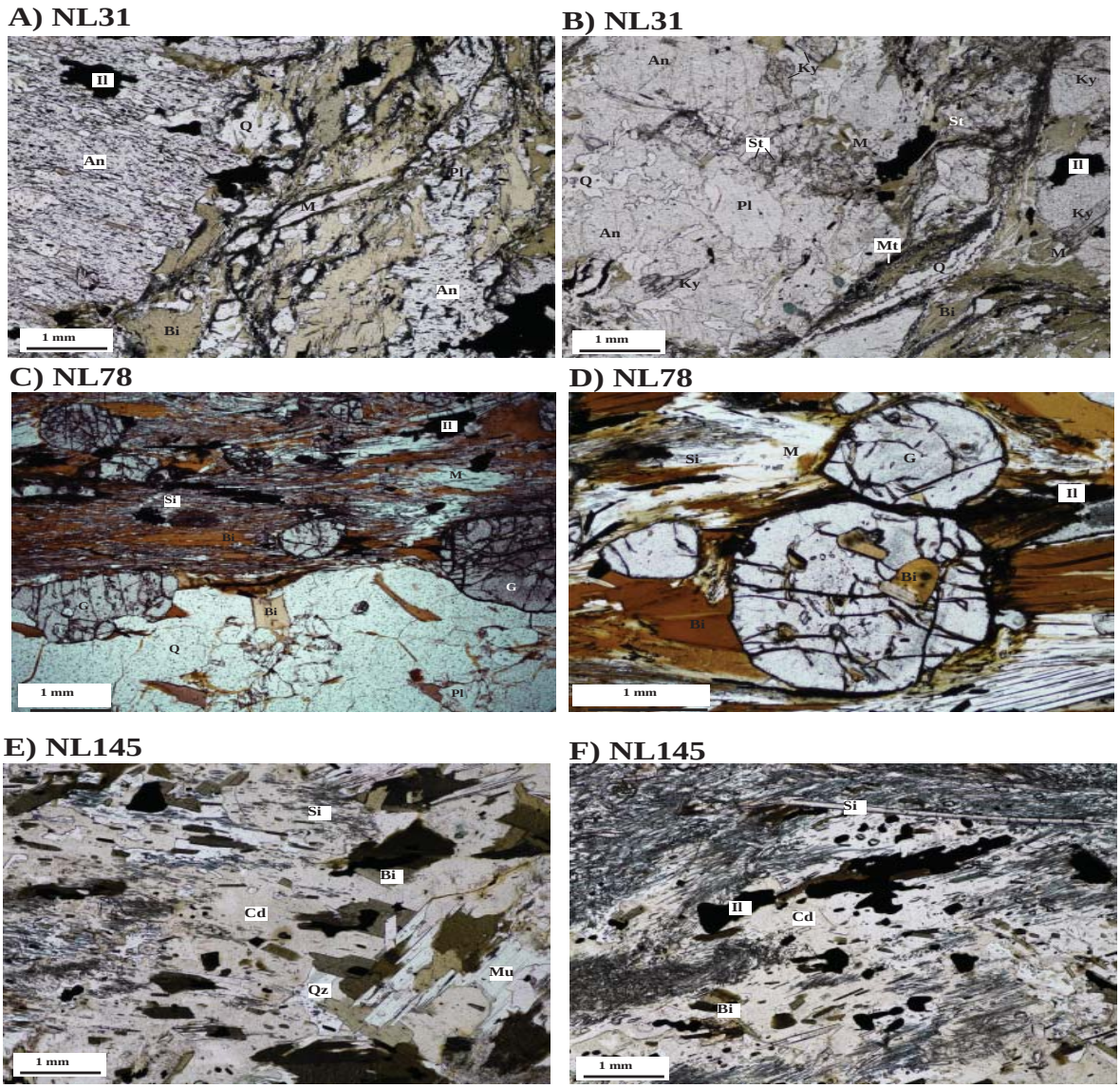

Figure 2

Representative thin section photomicrographs of the Gander Group from the Gander Zone. (a) Sample NL31: coarse poikiloblasts of andalusite contain inclusions of magnetite and ilmenite, which align to a subparallel fabric. Coarse laths of biotite and muscovite wrap around the andalusite grains. (B) Grains of kyanite grains appear as coarse, subhedral laths within and at the edges of andalusite grains. The kyanite is interpreted to be replacing the andalusite. (C) Sample NL78: coarse, equant garnet grains occur sub-parallel to the dominant schistose fabric, which is defined by sillimanite, biotite and ilmenite. Coarse layers of quartz and plagioclase form parallel to the schistose foliation. (D) Garnet grains are zoned with a poikiloblastic core that contains inclusions of quartz, biotite, muscovite and ilmenite, and a rim that is inclusion free. (E) Sample NL1475b: coarse domains of unfoliated crystalline anhedral quartz and plagioclase with minor Perthite and aggregates of biotite and muscovite. Coarse grains of cordierite are rimmed by biotite and muscovite grains and filled with dense sillimanite mats. (F) Cordierite is interpreted to have replaced sillimanite within restricted domains.

(King, 1997). The sample contains andalusite, magnetite, ilmenite, quartz, biotite, muscovite, plagioclase, kyanite and staurolite. Andalusite comprises coarse poikiloblasts that contain inclusions of magnetite and ilmenite, which form a fabric sub-parallel to the external foliation (Fig. 2a). Minor inclusions of muscovite and quartz also appear in andalusite. The matrix fabric consists of staurolite, biotite, muscovite, ilmenite and magnetite and wraps around andalusite poikiloblasts. Staurolite forms fine needles restricted to the

domains around andalusite grains. The later fabric is divided into more quartzofeldspathic domains composed of predominantly quartz and plagioclase. Randomly aligned, coarse grains of muscovite and biotite also form within the quartzofeldspathic domains. Kyanite grains partially replace andalusite and occur as coarse, subhedral laths within and at the edges of andalusite grains (Fig. 2b). Kyanite is restricted to locations adjacent to or within andalusite. The volumetrically dominant assemblage is interpreted to be andalusite, plagioclase, muscovite, quartz, biotite, magnetite and ilmenite. The secondary assemblage, which, although widely distributed in the sample, forms a comparatively minor percentage (~ 10%) of the mineralogy. The secondary assemblage is kyanite, staurolite, plagioclase, quartz, biotite, muscovite, ilmenite and magnetite.

4.2 Sample NL78

Sample NL78 is from a zone defined by King (1997) as the Central Gander Metasedimentary Belt, a sparsely migmatitic section of metapelite and metapsammites invaded by abundant pegmatites. The sample contains garnet, biotite, sillimanite, muscovite, quartz, plagioclase, and ilmenite (Fig. 2c). Garnet appears predominantly as coarse (~1-2 mm) equant grains, and more rarely as elongate grains sub-parallel to the dominant foliation in the rock. Garnet grains are typically zoned with a poikiloblastic core (Fig. 2d) that contains inclusions of quartz, biotite, muscovite and ilmenite, and a rim that is inclusion free. The main fabric in the rock consists of alternating schistose domains of biotite, sillimanite and muscovite and quartzofeldspathic domains composed of predominantly quartz and plagioclase with minor coarse, elongate ilmenite grains that broadly align with the fabric. The peak assemblage is interpreted to be garnet, sillimanite, biotite, muscovite, quartz, plagioclase and ilmenite.

4.3 Sample NL145b

Sample 145b is from the Eastern Gander Migmatite Belt (King, 1997), a high-grade belt dominated by the highly migmatised Gander Group metasedimentary rocks and the intrusion of the Hare Bay Gneiss (Schofield and D'Lemos, 2000) (Fig. 1b). King (1997) described andalusite-cordierite bearing migmatites from within the Eastern Gander Migmatite Belt. The sample contains plagioclase, quartz, muscovite, biotite, magnetite, ilmenite, sillimanite, perthite and cordierite (Fig. 2e). The rock is predominantly composed of unfoliated crystalline anhedral quartz and plagioclase with minor perthite. Aggregates of biotite and muscovite occur throughout the quartz-plagioclase domains. Fine grained magnetite and ilmenite grains are usually in contact with biotite. Coarse grains of cordierite are rimmed by biotite and muscovite grains (Fig. 2f), isolated from the crystalline quartz-plagioclase domains. Dense mats of sillimanite appear throughout the cordierite grains (Fig. 2f). Cordierite is interpreted to have replaced sillimanite within these restricted domains. The early assemblage in this rock is sillimanite, quartz, muscovite, biotite, plagioclase, magnetite and ilmenite. The later peak assemblage is interpreted to be cordierite, plagioclase, K-feldspar (perthite), magnetite, ilmenite, biotite and quartz (+ melt).

5. ANALYTICAL METHODS

5.1 U-Pb monazite geochronology

In-situ U–Pb analysis of monazite was undertaken at Adelaide Microscopy using an Agilent 7500cs ICPMS coupled with the New Wave 213 nm Nd-YAG laser. Analytical techniques for U–Pb isotopic dating of monazite grains follow those of Payne et al., (2008). In-situ monazite grains were identified and imaged on thin, using a Phillips XL30 SEM with a Backscattered Electron detector (BSE). U-Pb isotopic data is shown in supplementary data.

U–Pb fractionation was corrected

using the documented standard Madel (TIMS age 206Pb/238U = 514.8 Ma, Payne et al., 2008), in conjunction with the in-house standard 94-222 (~450 Ma, Payne et al., 2008), which was used to monitor ongoing accuracy of the laser. Data reduction was completed using GLITTER software (Van Achterbergh E., 2001). A ± 5% discordancy threshold was applied to was 516.2 ± 1.5 (n = 53), and the weighted average 206Pb/238U age for 222 was 455.6 ± 5.6 Ma (n = 24).

5.2 Major element chemistry

Mineral compositions of minerals were obtained using a Cameca SXFive electron microrobe at Adelaide Microscopy, University of Adelaide. A beam current of 20 nA, accelerating voltage of 15 kV and a defocussed beam size of 2 μm were used for all point analyses. Representative mineral compositions are shown in supplementary data.

5.3 Bulk composition of rocks

The bulk composition for samples NL31, NL78 and NL145 were measured via whole-rock X-ray fluorescence at Franklin and Marshall College, Philadelphia, USA. Major element concentrations were determined using a Panalytical 2404 XRF unit. Samples were prepared for analysis by fusion of the milled sample with lithium tetraborate. Wet chemistry methods were used to determine the amount of FeO and Fe2O3. The bulk compositions used for P-T pseudosections (wt% oxide) and whole rock geochemistry are presented in supplementary data.

5.4 Mineral equilibria modelling

Metamorphic phase diagram calculations were performed using Theriak-Domino software (de Capitani and Petrakakis, 2010) in the geologically realistic NCKFMASHTO (Na2O–CaO–K2O–FeO–MgO–Al2O3–SiO2–H2O–TiO2–Fe2O3) chemical system for samples NL31 and NL78, and MnNCKFMASHTO (MnO-Na2O–CaO–K2O–FeO–MgO–Al2O3–SiO2–H2O–TiO2–Fe2O3) for sample NL145. The phase diagrams were calculated using the internally consistent thermodynamic dataset of Holland and Powell (1998 ;dataset tcds55 November 2003 update), compiled as tcdb55c2d for use in Theriak-Domino, and the most recently available a–x models: garnet, biotite and silicate melt (White et al., 2007), orthopyroxene, spinel and magnetite (White and Powell, 2002), cordierite (Holland and Powell, 1998), K-feldspar and plagioclase (Holland and Powell, 2003) and ilmenite (White et al., 2000).

6. RESULTS

6.1 U-Pb Monazite geochronology

The results of monazite U-Pb geochronology are shown in Figure 3. Full data tables are included in the supplementary data files. Data was filtered for concordance whereby analyses within 100 ± 10% are considered to be concordant.

6.1.1 Sample NL31

Forty analyses were collected from 40 monazite grains distributed throughout the matrix. Monazite grains are subhedral to subrounded, up to 50 μm long and display no discernable zoning patterns in BSE. Of the forty analyses, six were discounted for discordance. The 238U/206Pb ages of the concordant monazites range from 433 ± 6 Ma to 469 ± 6 Ma, with a weighted mean of all the concordant grains yielding a 238U/206Pb age of 458 ± 2.5 Ma (MSWD=1.4) (Fig. 3a). If the two younger outliers (433 ± 6 Ma, 441 ± 5 Ma) are excluded from the calculation the weighted mean is 459 ± 2 Ma, with an MSWD of 0.64.

6.1.2 Sample NL-78

Thirty analyses were collected from 30 monazite grains in sample NL-78. Monazite grains are subhedral to rounded, up to 100 μm long and are either homogenous in

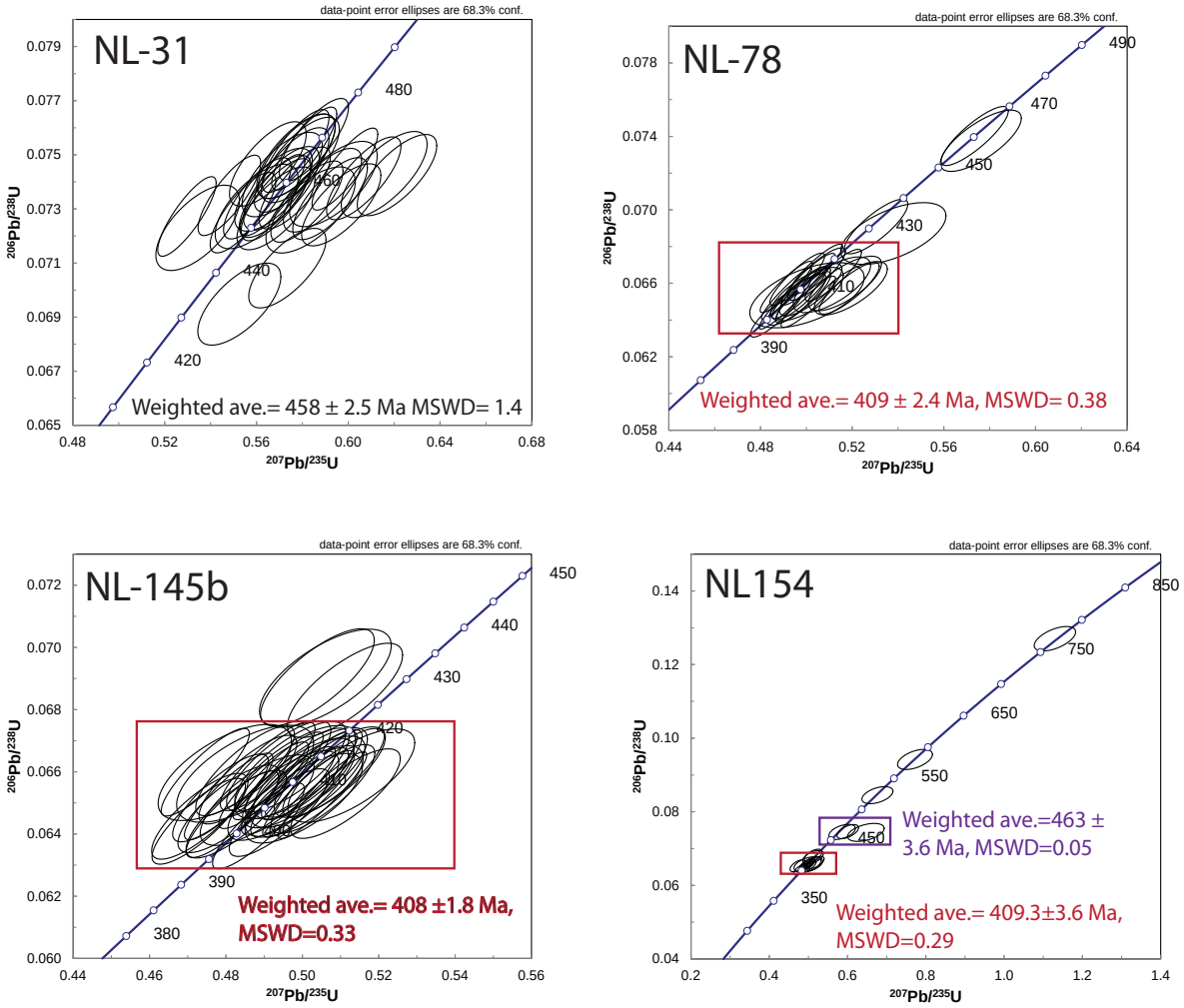

Figure 3

In situ LA–ICP–MS monazite U–Pb geochronology. Data are presented on U–Pb concordia diagrams: (A) Sample NL31 monazite geochronology showing weighted average 206Pb/238U age of the dominant Ordovician population. (B) Sample NL78 monazite geochronology showing weighted average 206Pb/238U age of the dominant Devonian population. (C) Sample NL145b monazite geochronology showing weighted average 206Pb/238U of the dominant Devonian population. (D) Sample NL154 monazite geochronology showing weighted average 206Pb/238U of the dominant Devonian population.

BSE, or rarely display irregular patterns. Of the forty analyses, five were discounted for discordance. The monazites fall into one of three population ranges; ~405-415 Ma, 430 Ma and 460 Ma (Fig. 3b). The dominant monazite population is the ~405-415 Ma (n=21) where the weighted mean 238U/206Pb age is 409 ± 2.4 Ma (MSWD= 0.38). Two analyses yield mid-Ordovician ages (458 ± 6 Ma and 460 ± 6 Ma) and two analyses are mid-Silurian (428 ± 6 Ma and 430 ± 6 Ma).

6.1.3 Sample NL-145b

Forty-eight analyses were collected from 48 monazite grains in sample NL-145b. Monazite grains are subhedral to rounded, up to 50 µm long and do not display any discernable zoning patterns in BSE. Six grains were excluded for discordance. The monazite grains fall into two age populations; a dominant 400-415 Ma population and a much smaller 430 Ma population (Fig. 3c). A weighted mean for the Devonian population yields a 238U/206Pb age is 408 ± 1.8 Ma (MSWD=0.33), and for the Silurian population 429 ± 7 Ma (MSWD= 0.056).

6.1.4 Sample NL-154

Sample NL-154 is petrologically identical to sample NL-145b. Twenty-seven

analyses were collected from 27 monazite grains in sample NL-154, of which 19 are concordant. Monazite grains are subhedral and up to 75 μm long and do not display any discernable zoning patterns in BSE (Fig. 3d). There are two dominant monazite populations at 409 ± 4 Ma (n=11, MSWD= 0.29) and 463 ± 9 Ma (n=3). Two monazites are 422 ± 6 and 424 ± 6 Ma and single monazites at 523 ± 9, 580 ± 10 and 770 ± 12 Ma.

6.2 P-T PSUEDOSECTIONS

6.2.1 Sample NL31

Figure 4 shows the calculated P-T diagram for sample NL31. The presence of secondary kyanite indicates that the abundant andalusite in the sample is metastable. However, the metastability of andalusite provides insight into the early metamorphic evolution of the sample. The early formed andalusite bearing assemblage (andalusite-biotite-muscovite-quartz-plagioclase-ilmenite-magnetite) is assumed to have included a fluid phase, and is modelled to have formed at ~3.5 kbar and 560 °C (Fig. 4).

The secondary assemblage of staurolite-kyanite-muscovite-quartz-plagioclase-ilmenite-magnetite is also interpreted to have contained a fluid phase. Although the secondary assemblage is modally subordinate to the earlier andalusite-bearing assemblage, it is nonetheless distributed consistently throughout the rock, particularly in the foliation that envelopes the andalusite porphyroblasts (Fig. 2b). At the comparatively low P-T conditions recorded by sample NL31, the presence of large relic porphyroblasts that clearly formed at different P-T conditions to the surrounding matrix assemblage means that valid mineral equilibria modelling of the matrix assemblage should "remove" the porphyroblasts from the modelled bulk composition. However, andalusite is the direct compositional equivalent of the later kyanite, which means that the average rock bulk composition used in the modelling should be a realistic estimate of the effective chemical composition of the system. The secondary assemblage of staurolite-kyanite-muscovite-quartz-plagioclase-ilmenite-magnetite is modelled to occupy a narrow temperature range of 580-625 C° at pressures of > 5kbar. The low modal proportion of staurolite in the sample is consistent with the secondary assemblage forming just down-T of the staurolite-out boundary. The maximum pressure of the kyanite-staurolite bearing assemblage is unconstrained in the current model. However it is evident that the formation of this assemblage at the expense of the earlier andalusite bearing assemblage required burial with respect to the early formed assemblage.

6.2.2 Sample NL78

Figure 5 shows the calculated P-T diagram for sample NL78. The sample contains a well foliated assemblage consisting of biotite-muscovite-sillimanite and minor ilmenite within a matrix of quartz and plagioclase, which contains porphyroblasts of garnet. The sampled sequence also contains leucosomes and pegmatite, and is therefore interpreted to have experienced anatectic conditions. In Figure 5, the peak assemblage of garnet-sillimanite-biotite-muscovite-plagioclase-quartz-ilmenite-melt is calculated to occur at approximately 700°C and 6.5 kbar. However, petrologically the assemblage garnet-sillimanite-biotite-muscovite-plagioclase-quartz-ilmenite-melt-H2O would be indistinguishable from the equivalent H2O-absent assemblage, and therefore the peak assemblage could equally fall into the H2O-bearing field at approximately 670°C and 6.5 kbar. Based on Figure 5, the minimum pressure for the assemblage in NL78 is approximately 6 kbar, constrained by the absence of magnetite in the assemblage. However, the stability of magnetite will be influenced by the bulk rock oxidation state, with decreasing Fe3+/Fe2+ decreasing the pressure of the magnetite-out boundary. The Fe3+/Fe2+ ratio was used for modelling was determined by titration. In

all likelihood Fe3+/Fe2+ ratio's determined from surface-derived samples will be greater than those that existed when the rocks were undergoing metamorphism. Therefore the minimum pressure of the assemblage may actually be lower than modelling in Figure 5.

Figure 6 shows XFe contours for garnet overlain on the mineral stability fields. Analysed garnets are all greater than 1000 micron in diameter, and aside from an overall core to rim decrease in Mn and a corresponding increase in Fe, garnet compositions are homogeneous, and show no evidence for a near rim decrease in Mg (Fig. 7), typically associated with retrograde compositional change. The general rimward decrease in Mn suggests that the garnets to at least some extent preserve their growth composition, and therefore their interior compositions may still hold some information about the conditions associated with garnet nucleation. XMn in the garnet cores is around 0.24 and the corresponding XFe is around 0.62 (Fig. 7). Although the contours are not overly P-T sensitive, the area of P-T space corresponding to the garnet core compositions lies at around 550°C and 3.5 kbar, suggesting that the garnet nucleated in the andalusite field (Fig. 6). This logically accounts for the lack of sillimanite inclusions in garnet, in contrast to the presence of biotite-quartz-muscovite-ilmenite-magnetite inclusions, since andalusite typically forms porhyroblasts that are rarely included in other minerals. The inference that garnet nucleated at low pressures is consistent with the comparatively Mn-rich bulk composition of the sample, which would have promoted garnet growth at low pressures (e.g. Mendard and Spear, 1993). The rimward decrease in XMn at a constant, or slightly increasing, XFe is consistent with a pressure increase, an interpretation supported by the predicated P-T stability of the assemblage in the sample. However the modelling does not reproduce the observed XFe values near the garnet rims. This may be because the effective modelled bulk composition does not take into account the Fe compositional reservoirs represented by the garnet interiors.

6.2.3 Sample NL145b

Figure 8 shows the P-T model for sample NL145, which comes from highly migmatitic rocks from the Hare Bay Gneiss and migmatite belt. The peak assemblage in NL145b consists of cordierite-biotite-quartz-plagioclase-ilmenite-magnetite-melt, placing it within a large and poorly constrained P-T field with a minimum-T of 660°C at 3.2 kbar, but extending to temperatures as high as approximately 760°C, which bound the appearance of orthopyroxene. Pressures are poorly constrained to less than approximately 5.7 kbar. King (1997), reported the presence of relic andalusite in migmatised cordierite-bearing Hare Bay Gneiss. If this is considered as a constraint, then the prograde P-T evolution for NL145b must have passed through the andalusite field at pressures high enough to result in the formation of sillimanite, prior to the growth of cordierite, accounting for the presence of dense sillimanite mats within cordierite porphyroblasts. The sillimanite mats may well signify the former presence of andalusite grains. Therefore, the prograde path of NL145b probably passed through the lower pressure section of the biotite-muscovite-sillimanite-ilmenite-magnetite-quartz-H2O field, indicating that peak pressures were probably no more than 4kbar. The presence of coarse-grained muscovite-biotite rimming cordierite is consistent with retrogression associated with melt crystallisation, although the retrograde P-T path is unconstrained.

7. DISCUSSION

7.1 Interpretations of the monazite geochronology

The U-Pb monazite geochronology preserves two main age peaks; an Ordovician population at ~460 Ma and a Devonian population at ~410 Ma, with a small number of monazites that fall in between these

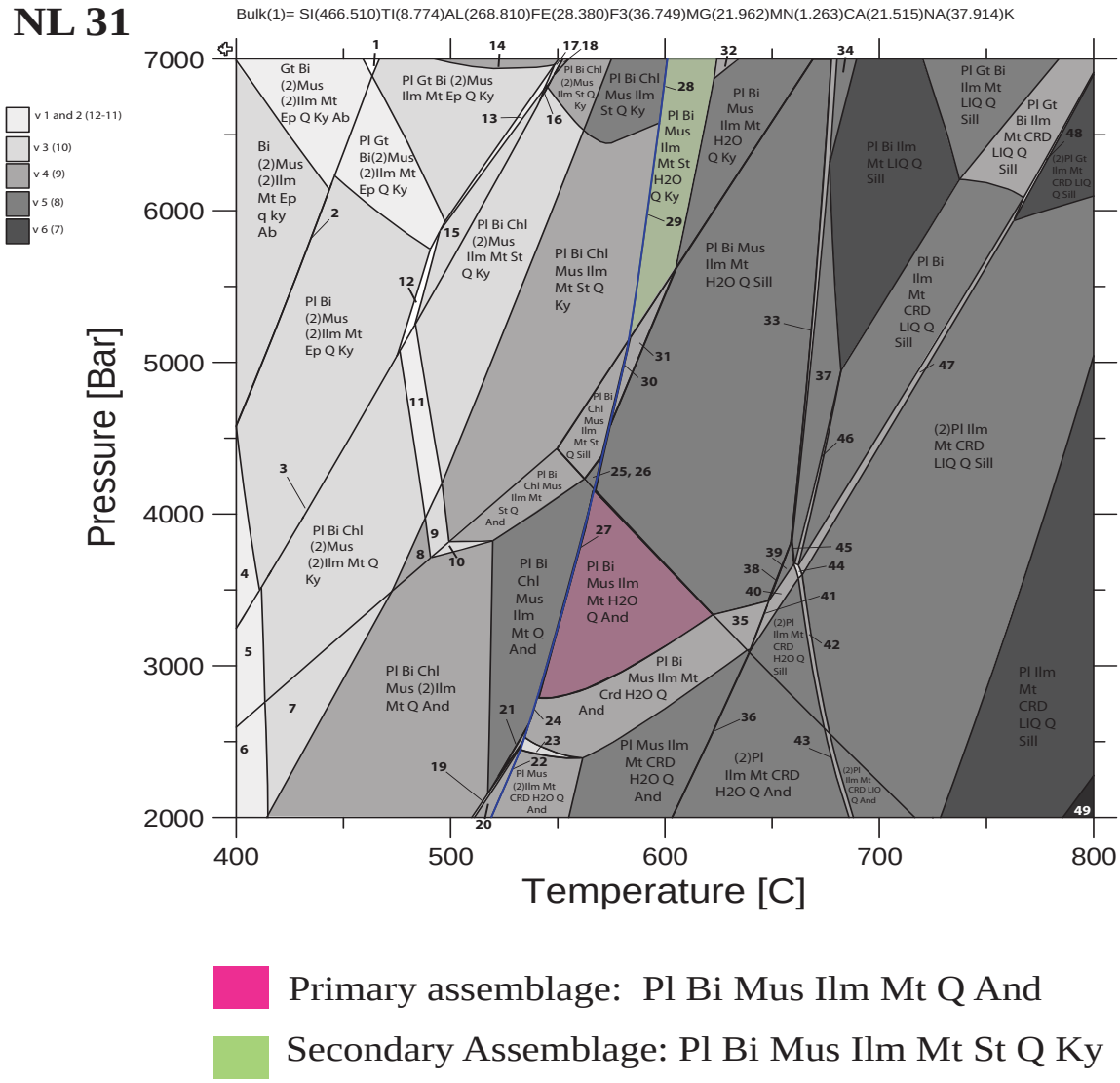

Figure 4

P–T pseudosections constructed for the bulk composition of Sample NL31 in the NCKFMASHTO system. The stability field corresponding to the inferred peak mineral assemblage is outlined in pink.

populations at ~430 Ma (Fig. 3). Sample NL31 preserves only the older population at ~460 Ma, sample NL78 and NL154 preserves a minor population at ~460 Ma and a dominant population at ~410 Ma, and sample NL145 preserves only a single population at ~410 Ma. The preservation of the Ordovician monazite population is apparently related to the distance from the Dover Fault zone; whereby the samples furthest from the Dover Fault Zone (sample NL31) preserve the older monazite population and those closest tend to contain predominantly Devonian monazites (sample NL78, NL145b, NL154).

The dominant Ordovician population (~460 Ma) in sample NL31 is texturally most obviously associated with the main mineral assemblage. The assemblage indicates low pressure and moderate temperature conditions of around 3.5 kbars and 550°C. The development of a subsequent higher pressure assemblage is also evident in sample NL31. As monazite is most commonly reset under granulite facies conditions (Bingen and van Breemen, 1998; Rubatto et al., 2001; Forbes et al., 2007) or during the influx of fluids or melts (Kelly et al., 2006; Bosse et al., 2009; Williams et al., 2011), it seems unlikely that the monazite ages are associated with the development of the later mineral assemblage. Therefore, while the ~460 Ma monazite grains cannot be unambiguously related the volumetrically dominant mineral assemblage,

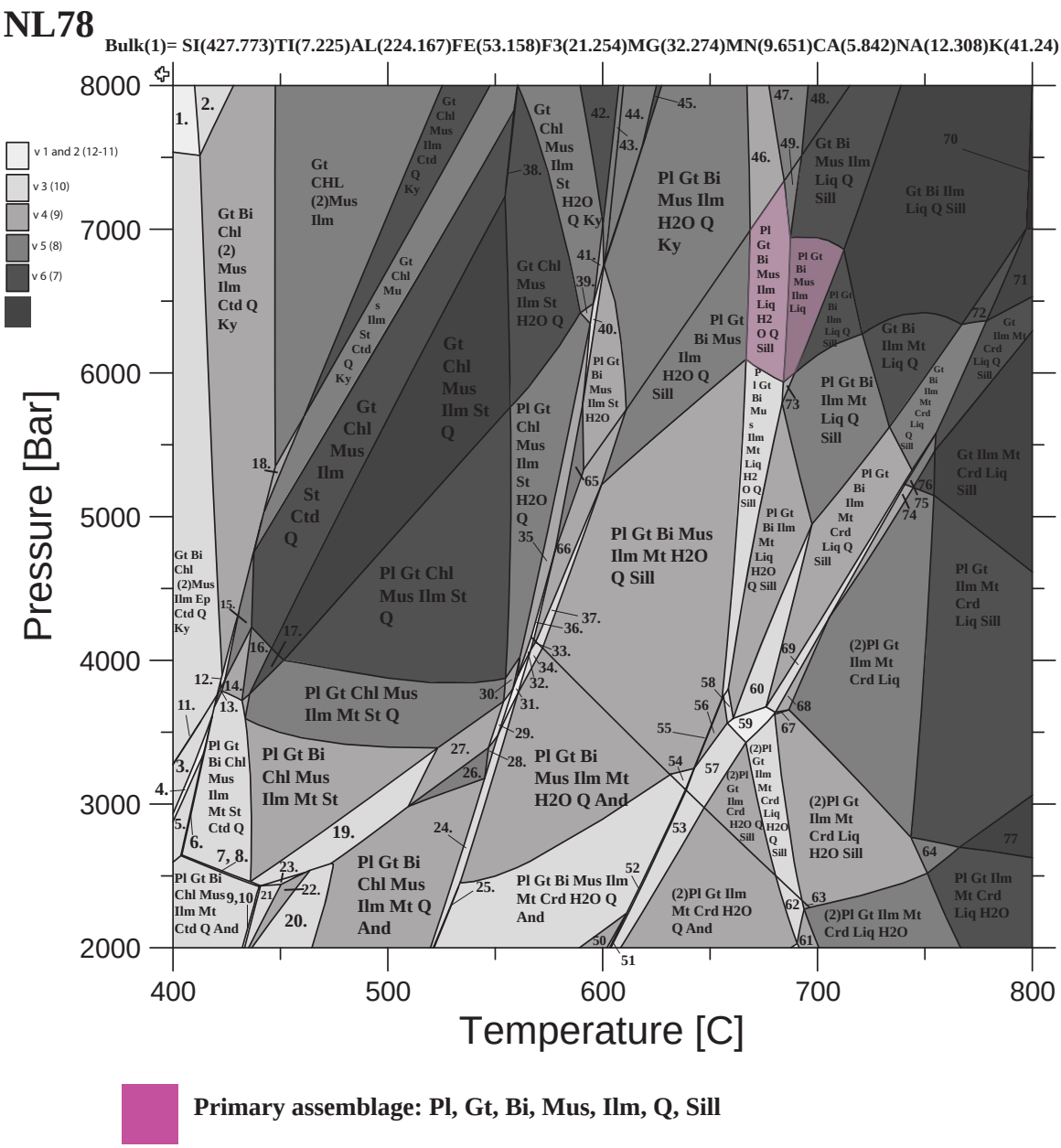

Figure 5

P–T pseudosections constructed for the bulk composition of Sample NL78 in the NCKFMASHTO system. The stability field corresponding to the inferred peak mineral assemblage is outlined in pink and the secondary assemblage in brown.

it is less likely that they were crystallised during the later higher pressure metamorphism, that is recorded by no more than ~10% of the sample.

The Devonian (~410 Ma) monazite populations are found in samples NL78, NL145b and NL154. All three samples preserve peak mineral assemblages that indicate high temperature and medium and low pressure conditions. The inferred evolution for NL78, NL145b and NL154 is similar to that of NL31. NL78 and NL154 contain a dominant monazite population at ~410 Ma and a minor population at 460 Ma, which overlaps with the dominant monazite population (459 ± 2 Ma) in sample NL31. Field based and petrographic observations (Fig. 2) also indicate that NL78, NL145b and NL154 have undergone melting with the formation of leucosomes, whereas NL31 has not. A tentative interpretation of the dual monazite populations is that all the samples in the Gander Zone underwent low P, high T metamorphism at ~460 and then subsequently again at 410 Ma. However, the difference in

the monazite populations preserved between the samples is that NL31 did not experience the high temperatures and melting processes that NL78/NL145/NL154 did, therefore the monazite grains in the rocks were not either reset or recrystallised. In contrast, the proximity of samples NL78/NL145/NL154 to the Dover Fault Shear Zone and the associated Devonian magmatism allowed these rocks to reach temperatures high enough to induce melting and recrystallization of the original ~460 Ma population and possibly the growth of new Devonian (~410 Ma) monazites.

The small number of 429 ± 6 Ma monazites are interpreted to either record partial resetting of ~460 Ma monazites along concordia (see Halpin et al., 2007) as a result of the high temperature event at ~410 Ma, or could possible reflect the final closure of the Tetagouche-Exploits back arc basin (430-423 Ma, Williams et al., 1993; Pollock et al., 2007) during the latter stages of the Salinic Orogeny. As there are only a small number of ~430 Ma monazite grains and few distinct textural constraints, it is not possible to determine which scenario is more plausible.

7.2 Tectonic implications of the P-T-t history of the Gander Zone

The tectonic evolution of Ganderia between ~450-380 Ma is complex as the interval covers the arrival of Ganderia arc to Laurentia (~455-450 Ma), the closure of the Tetagouche-Exploits back-arc basin (~435-422 Ma) and the arrival of Avalonia to Ganderia (~422-408 Ma) (Keppie et al., 2003; Murphy and Keppie, 2005; Zagorevski et al., 2007b; van Staal et al., 2009). However, deformation and metamorphism associated with the ~450-380 Ma interval are normally ascribed to either the ~435-422 Ma Salinic Orogeny (van Staal et al., 2004) or the ~422-408 Ma Acadian Orogeny (Murphy and Keppie, 2005).

Gander Zone rocks preserve peak metamorphic mineral assemblages that indicate an early metamorphic event characterised by low pressures (3-4 kbars) and high temperatures (~550-600°C Ma) and a subsequent mineral assemblage associated with higher pressures (6-6.5 kbar) and temperatures (~650°C). Monazite geochronology and calculated mineral equilibria phase diagrams for metamorphic rocks in the Gander Zone indicate the high temperature, low pressure metamorphism occurred at ~460 Ma and a later comparatively mid-P, high-T event at ~410 Ma. The timing and nature of the metamorphic events have implications for the tectonic evolution of Ganderia during the Paleozoic and will be discussed herein.

Metamorphism at 460 Ma is recorded by andalusite bearing assemblages in NL31 and is recorded by relic andalusite in NL145 and equivalent rocks in the migmatite belt (see King, 1997). The regional low pressure, high temperature event coincides with an interval of oceanic-arc, supra-subduction zone magmatism in the ~475-455 Ma Popelogan-Victoria arc (Evans et al., 1990; Zagorevski et al., 2007a) that is recorded by juvenile hafnium isotopes in zircons (Chapter 3). Ganderia formed a retreating oceanic-arc-back-arc system, similar to the modern day SW pacific (Chapter 3). Coeval with the Popelogan-Victoria arc system is the development of the Tetagouche-Exploits back-arc basin, which separated the passive Gander margin from the leading volcanic arc (van Staal and Barr, 2011; van Staal et al., 2012). Therefore, the ~460 Ma low P, high T metamorphism is interpreted to be associated with an extensional tectonic environment in Ganderia, plausibly the development of the Tetagouche-Exploits back-arc basin (Zagorevski et al., 2007a). Early (pre ~470 Ma) flat lying fabrics and stretching mineral lineation's are documented pervasively across the Gander Zone (Colman-Sadd, 1980; Hanmer, 1981; Colman-Sadd et al., 1992; King, 1997), and have previously been attributed to the obduction of the Dunnage Zone over the Gander Zone (King, 1997). However, given the low P- high T environment and early horizontal fabric, it seems more plausible that these conditions were generated in an extensional environment,

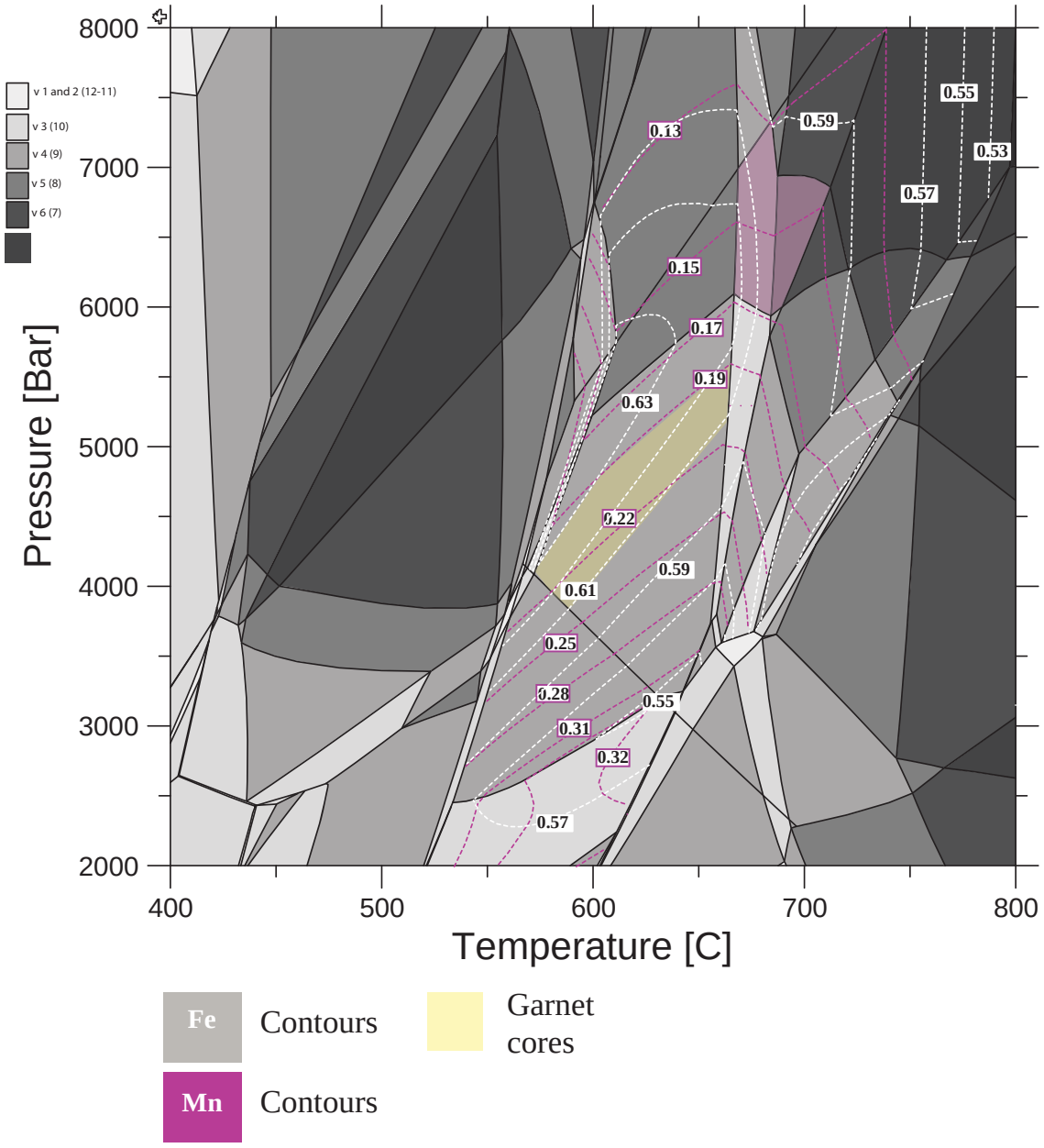

Figure 6

Garnet isopleths for Xfe in sample NL78 with the composition of the garnet cores shown in yellow. The range of the garnet rims overlaps with the field defined for the peak mineral assemblage (shown in pink).

such as a back-arc basin.

All samples from the Gander Zone petrologically preserve evidence for a later mid-pressure, high-temperature metamorphic event that is interpreted to have occurred at ~410 Ma. NL31 records secondary high pressure assemblages requiring near isothermal burial (Fig. 4). Similarly, although not recorded petrographically, the garnet zoning in NL78 also suggests an early low P assemblage was overprinted by a higher temperature assemblage. In NL145, constraints on the maximum pressures are poor. Based on the modelled composition, the presence of cordierite and the absence of garnet suggest that the pressures must be below ~6 kbar. Conceivably, NL145 also experienced pressures as high as ~6kbar, with early andalusite reported by King (1997) as a relic from ~460 Ma metamorphism. However, the preserved assemblage in NL145 doesn't constrain the maximum pressure beyond the general constraints offered by the PT boundaries of the modelled peak field (Fig. 8).

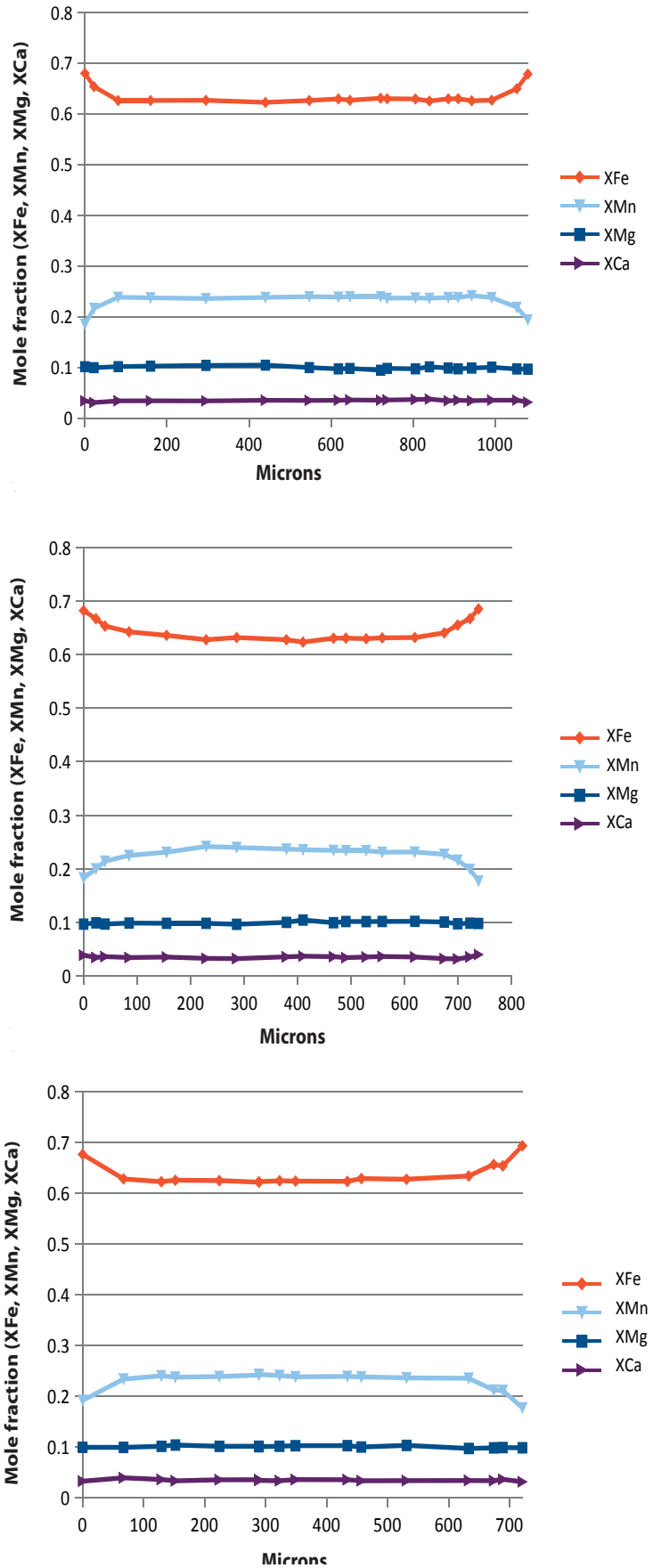

Figure 7

Garnet zoning profiles from sample NL78 that map out the distribution of the mole fraction components of XFe, Xfe, XMg and Xca.

The preferred interpretation that accommodates the geochronology, metamorphism and geological constraints is that a short, compressional event associated with comparatively higher pressure metamorphism occurred at ~410 Ma and was related to transpressional accretion of Avalonia to peri-Laurentia (Ganderia) along the Dover Fault Shear Zone (Holdsworth, 1994; D'Lemos et al., 1997). Upright folds with steep dipping axial planar fabrics are recorded across the Gander Zone, deforming the earlier flat-lying fabrics (Colman-Sadd, 1980; Colman-Sadd et al., 1992; King, 1997), and supporting the compressional nature of the Devonian event. Immediately following, the composite Laurentian margin transitioned towards a largely extensional environment that experienced widespread post-collisional magmatism and exhumation along the Dover Fault Shear Zone. Thus, the ~410 Ma monazites record the up-pressure prograde metamorphic path associated with the accretion of Avalonia and the abundant magmatic products between ~400-380 Ma indicate increased heat-flow in the Ganderian realm.

The 410 Ma monazites record a short compressional metamorphic event that coincides with the latest stages of the ~422-408 Ma Acadian Orogeny (Zagorevski et al., 2007b), whereas the main phase of Devonian magmatism commences ~10 million years later across the Appalachians (Kellett et al., 2014). Devonian magmatism occurs in a broadly linear belt parallel to the orogens strike (Fig. 1a) and is considered to have been emplaced syn to post deformation (D'Lemos et al., 1997) at shallow depths (Whalen, 1980; Tuach, 1987). Schofield and D'Lemos (2000) interpret the granites to have been emplaced during widespread exhumation and uplift, signifying the nature of the magmatism was largely post-collisional.

The transition towards a heat-dominated setting within the Gander Zone is recorded by the emplacement of abundant pegmatites, migmatites and syntectonic granites, particularly in the rocks closest to the Dover Fault Shear Zone (Holdsworth, 1994). The magmatism is dated from ~430 Ma, but the most prominent ages across the Canadian Appalachians occur between ~400-380 Ma (see Kellett et al., 2014 and references therein). Hafnium isotopes from ~430-380 Ma zircons in Gander Zone rocks (Chapter 3) indicates recycling of the Paleoproterozoic-Mesoproterozoic basement with juvenile arc magmas was dominant during the late Silurian-Devonian magmatism. The bimodal magmatism has been interpreted to have been generated during delamination of a thickened orogenic keel (Schofield and D'Lemos, 2000), or slab failure of a subducting plate (Whalen et al., 2006). Given the overlap between the end of the ~435-422 Ma Salinic Orogeny and the onset of the Acadian Orogeny, and the apparent lack of suitable magmatic arc and suture-zone rocks, it seems unlikely that a wide ocean basin existed between Ganderia and Avalonia. An exception to this is the 'Coastal Volcanic belt' (Gates, 1969; Bradley, 1983), a series of predominantly Silurian bimodal, siliciclastic volcanics, granites and minor mafic dyke swarms preserved throughout New Brunswick, Maine and Newfoundland (see van Staal and Barr, 2011 and references therein). However, the successions are contemporaneous with Silurian basin development across Ganderia (Fyffe et al., 2009) and the Coastal Volcanic belt, and its equivalents, are commonly attributed to a back-arc or intra-arc setting (see van Staal and Barr, 2011 and references therein).

Although sufficient heat could be generated in a delamination event (Whalen et al., 2006; van Staal et al., 2014) there is little evidence for significant crustal thickening (hard collision, Zagorevski and Van Staal, 2011) during the late Silurian-early Devonian (~420-400 Ma) and the development of a keel beneath Ganderia. An alternative scenario could be that Ganderia occupied a largely extensional accretionary orogen setting during much of the Silurian, whereby subduction was accommodated

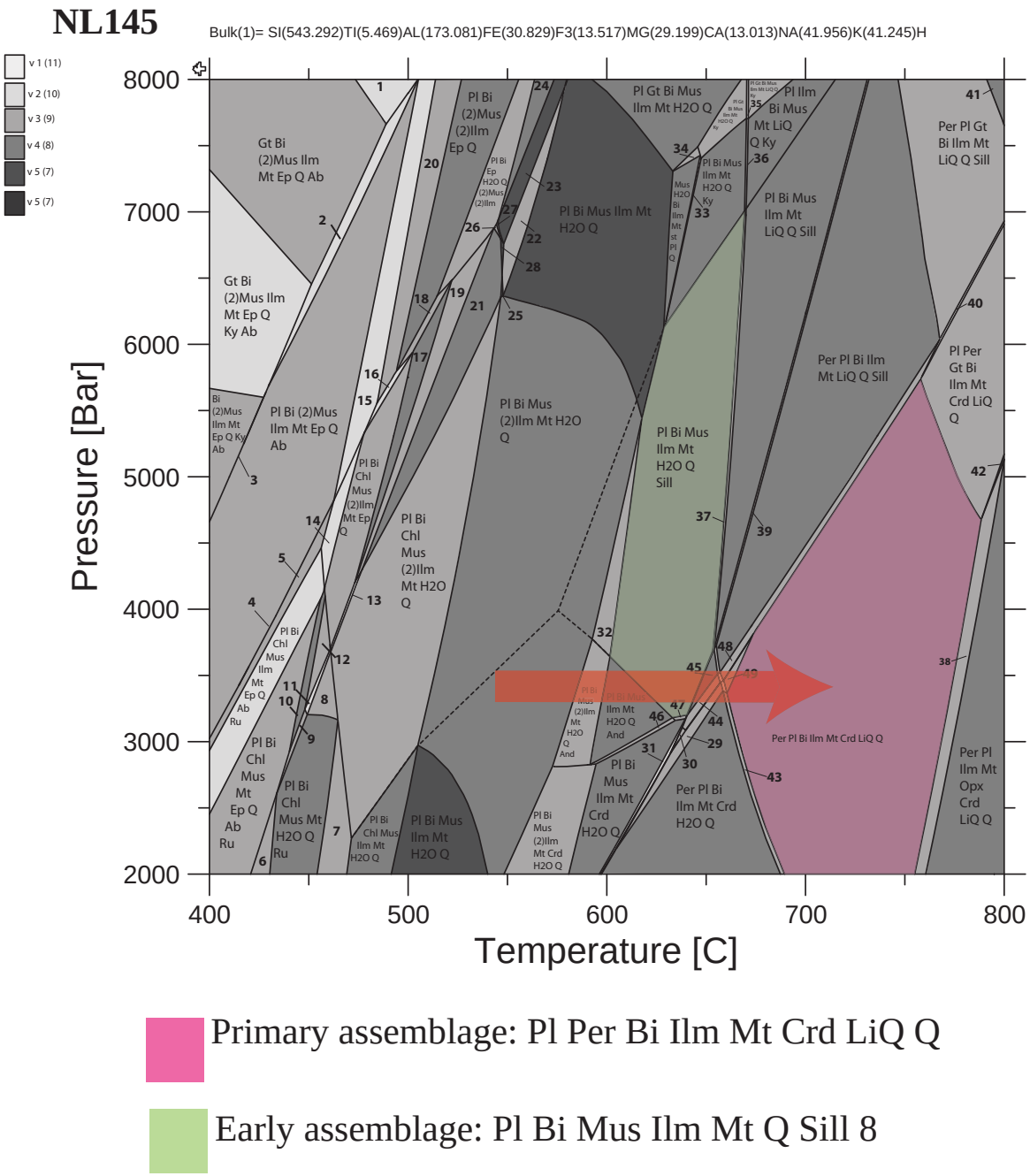

Figure 8

P–T pseudosections constructed for the bulk composition of Sample NL145b in the NCKFMASHTO system. The stability field corresponding to the inferred peak mineral assemblage is outlined in pink. The early low P, low T, and subsequent, later high P and T evolution of sample NL45b is indicated by the red arrow.

outboard of the peri-Laurentian margin, and Ganderia occupied an upper plate location. In this scenario the Coastal Volcanic arc back-arc system and associated extensional basins generated during the Silurian across Ganderia would have been accommodated within an extensional, back-arc setting. Consequently, the arrival of Avalonia represented a short contractional phase whereby the narrow basin between Ganderia and Avalonia was closed, prior to another phase of extension during the mid-Devonian. Ganderian geology satisfies a number of the criteria defined by Collins et al. (2002) for an extensional accretionary setting including 1) sequential rift basins developed throughout the orogenic history dominated by volcanics, volcanoclastics and turbiditic rocks (i.e. the Silurian Mascarene basin, Kingston

Basin and Fredericton Trough; Fyffe et al., 2009 and references therein), 2) the absence of a well-defined magmatic arc chain, and 3) an abundance of granites and silicic volcanics, but an absence of blueschist facies rocks and paired metamorphic belts. The existence of a long term, extensional accretionary orogen on the peri-Laurentian margin will be discussed further in Chapter 5.

8. CONCLUSIONS

- The Dover Fault Zone records metamorphic events that are recorded by the growth of metamorphic mineral assemblages and coeval monazites.

- The first event is a low pressure, high temperature (3-4 kbar, 600°C) event recorded by 460 ± 7 Ma monazite within andalusite bearing metamorphic assemblages. This event is attributed to an extensional environment, most likely within the Tetagouche-Exploits back-arc basin that separated the active Popelogan-Victoria arc from the passive trailing Gander margin.

- The second event is both a higher pressure event (5-6 kbar, ~600-650°C) and a lower pressure event (3-4 kbar) characterised by migmatisation and the formation of garnet-sillimanite bearing metamorphic assemblages at 409 ± 6 Ma; interpreted to reflect a short interval of compression along the Dover Fault Shear Zone followed by the emplacement of the Hare Bay Gneiss and other granite suites.

REFERENCES

Balintoni, I., Balica, C., Ducea, M.N., Hann, H.-P., 2014. Peri-Gondwanan terranes in the Romanian Carpathians: A review of their spatial distribution, origin, provenance, and evolution. Geoscience Frontiers 5, 395-411.

Barr, S.M., Davis, D.W., Kamo, S., White, C.E., 2003a. Significance of U–Pb detrital zircon ages in quartzite from peri-Gondwanan terranes, New Brunswick and Nova Scotia, Canada. Precambrian Research 126, 123-145.

Barr, S.M., Dunning, G.R., Raeside, R.P., Jamieson, R.A., 1990. Contrasting U–Pb ages from plutons in the Bras d'Or and Mira terranes of Cape Breton Island, Nova Scotia. Canadian Journal of Earth Sciences 27, 1200-1208.

Barr, S.M., White, C.E., Davis, D.W., McClelland, W.C., van Staal, C.R., 2014. Infrastructure and provenance of Ganderia: Evidence from detrital zircon ages in the Brookville terrane, southern New Brunswick, Canada. Precambrian Research 246, 358-370.

Barr, S.M., White, C.E., Miller, B.V., 2003b. Age and geochemistry of Late Neoproterozoic and Early Cambrian igneous rocks in southern New Brunswick: similarities and contrasts. Atlantic Geology 39.

Bingen, B., van Breemen, O., 1998. U-Pb monazite ages in amphibolite-to granulite-facies orthogneiss reflect hydrous mineral breakdown reactions: Sveconorwegian Province of SW Norway. Contributions to Mineralogy and Petrology 132, 336-353.

Blackwood, R.F., Kennedy, M.J., 1975. The Dover Fault: Western Boundary of the Avalon Zone in Northeastern Newfoundland. Canadian Journal of Earth Sciences 12, 320-325.

Bosse, V., Boulvais, P., Gautier, P., Tiepolo, M., Ruffet, G., Devidal, J.L., Cherneva, Z., Gerdjikov, I., Paquette, J.L., 2009. Fluid-induced disturbance of the monazite Th-Pb chronometer: In situ dating and element mapping in pegmatites from the Rhodope (Greece, Bulgaria). Chemical Geology 261, 286-302.

Bradley, D.C., 1983. Tectonics of the Acadian orogeny in New England and adjacent Canada. The Journal of Geology, 381-400.

Collins, W.J., 2002. Nature of extensional accretionary orogens. Tectonics 21, 6-1-6-12.

Colman-Sadd, S., 1980. Geology of south-central Newfoundland and evolution of the eastern margin of Iapetus. American Journal of Science 280, 991-

1017.

Colman-Sadd, S., Stone, P., Swinden, H., Barnes, R., 1992. Parallel geological development in the Dunnage Zone of Newfoundland and the Lower Palaeozoic terranes of southern Scotland: an assessment. Transactions of the Royal Society of Edinburgh: Earth Sciences 83, 571-594.

Currie, K., McNicoll, V., 1999. New data on the age and geographic distribution of Neoproterozoic plutons near Saint John, New Brunswick. Atlantic Geology 35.

D'Lemos, R.S., Schofield, D.I., Holdsworth, R.E., King, T.R., 1997. Deep crustal and local rheological controls on the siting and reactivation of fault and shear zones, northeastern Newfoundland. Journal of the Geological Society 154, 117-121.

Dallmeyer, R.D., Hussey, E.M., O'Brien, S.J., O'Driscoll, C.F., 1983. Chronology of tectonothermal activity in the western Avalon Zone of the Newfoundland Appalachians. Canadian Journal of Earth Sciences 20, 355-363.

de Capitani, C., Petrakakis, K., 2010. The computation of equilibrium assemblage diagrams with Theriak/Domino software. American Mineralogist 95, 1006-1016.

Evans, D., Kean, B., Dunning, G., 1990. Geological studies, Victoria Lake Group, central Newfoundland. Current Research. Newfoundland Department of Mines and Energy, Geological Survey Branch, Report, 90-91.

Forbes, C.J., Giles, D., Betts, P.G., Weinberg, R., Kinny, P.D., 2007. Dating Prograde Amphibolite and Granulite Facies Metamorphism Using In Situ Monazite U-Pb SHRIMP Analysis. Journal of Geology 115, 691-705.

Fyffe, L.R., Barr, S.M., Johnson, S.C., McLeod, M.J., McNicoll, V.J., Valverde-Vaquero, P., van Staal, C.R., White, C.E., 2009. Detrital zircon ages from Neoproterozoic and Early Paleozoic conglomerate and sandstone units of New Brunswick and coastal Maine: implications for the tectonic evolution of Ganderia. Atlantic Geology 45, 110-144.

Gates, O., 1969. Lower Silurian-Lower Devonian Volcanic Rocks of New England Coast and Southern New Brunswick: Chapter 37: Central Orogenic Belt.

Halpin, J.A., White, R.W., Clarke, G.L., Kelsey, D.E., 2007. The Proterozoic P-T-t Evolution of the Kemp Land Coast, East Antarctica; Constraints from Si-saturated and Si-undersaturated Metapelites. Journal of Petrology 48, 1321-1321.

Hanmer, S., 1981. Tectonic significance of the northeastern Gander Zone, Newfoundland: an Acadian ductile shear zone. Canadian Journal of Earth Sciences 18, 120-135.

Hibbard, J.P., van Staal, C.R., Rankin, D.W., 2010. Comparative analysis of the geological evolution of the northern and southern Appalachian orogen: Late Ordovician-Permian. Geological Society of America Memoirs 206, 51-69.

Holdsworth, R., 1994. Structural evolution of the Gander-Avalon terrane boundary: a reactivated transpression zone in the NE Newfoundland Appalachians. Journal of the Geological Society 151, 629-646.

Holland, T., Powell, R., 2003. Activity-compositions relations for phases in petrological calculations: An asymetric multicomponent formulation. Contributions to Mineralogy and Petrology 145, 492-501.

Holland, T.J.B., Powell, R., 1998. An internally consistent thermodynamic data set for phases of petrological interest. Journal of Metamorphic Geology 16, 309-343.

Jenner, G., Swinden, H.S., 1993. The Pipestone Pond Complex, central Newfoundland: complex magmatism in an eastern Dunnage Zone ophiolite. Canadian Journal of Earth Sciences 30, 434-448.

Keen, C., Keen, M., Nichols, B., Reid, I., Stockmal, G., Colman-Sadd, S., O'Brien, S., Miller, H., Quinlan, G., Williams, H., 1986. Deep seismic reflection profile across the northern Appalachians. Geology 14, 141-145.

Kellett, D.A., Rogers, N., McNicoll, V., Kerr,

A., van Staal, C., McFarlane, C., 2014. New age data refine extent and duration of Paleozoic and Neoproterozoic plutonism at Ganderia–Avalonia boundary, Newfoundland. Canadian Journal of Earth Sciences 51, 943-972.

Kelly, N.M., Clarke, G.L., Harley, S.L., 2006. Monazite behaviour and age significance in poly-metamorphic high-grade terrains: A case study from the western Musgrave Block, central Australia. Lithos 88, 100-134.

Keppie, J.D., Nance, R.D., Murphy, J.B., Dostal, J., 2003. Tethyan, Mediterranean, and Pacific analogues for the Neoproterozoic-Paleozoic birth and development of peri-Gondwanan terranes and their transfer to Laurentia and Laurussia. Tectonophysics 365, 195-219.

Kerr, A., Dunning, G., Tucker, R., 1993. The youngest Paleozoic plutonism of the Newfoundland Appalachians: U-Pb ages from the St. Lawrence and François granites. Canadian Journal of Earth Sciences 30, 2328-2333.

Kerr, A., Jenner, G.A., Fryer, B.J., 1995. Sm–Nd isotopic geochemistry of Precambrian to Paleozoic granitoid suites and the deep-crustal structure of the southeast margin of the Newfoundland Appalachians. Canadian Journal of Earth Sciences 32, 224-245.

King, T.R., 1997. PTtd evolution paths within the Gander Zone, NE Newfoundland. Oxford Brookes University.

MacLachlan, K., Dunning, G., 1998. U-Pb ages and tectono-magmatic evolution of Middle Ordovician volcanic rocks of the Wild Bight Group, Newfoundland Appalachians. Canadian Journal of Earth Sciences 35, 998-1017.

Marillier, F., Keen, C.E., Stockmal, G.S., Quinlan, G., Williams, H., Colman-Sadd, S.P., O'Brien, S.J., 1989. Crustal structure and surface zonation of the Canadian Appalachians: implications of deep seismic reflection data. Canadian Journal of Earth Sciences 26, 305-321.

Mendard, T., Spear, F.S., 1993. Metamorphism of Calcic Pelitic Schists, Strafford Dome, Vermont: Compositional Zoning and Reaction History. Journal of Petrology 34, 977-1005.

Moresi, L., Betts, P., Miller, M., Cayley, R., 2014. Dynamics of continental accretion. Nature 508, 245-248.

Murphy, J.B., Keppie, J.D., 2005. The Acadian orogeny in the northern Appalachians. International Geology Review 47, 663-687.

Murphy, J.B., Pisarevsky, S.A., Nance, R.D., Keppie, J.D., 2004. Neoproterozoic—Early Paleozoic evolution of peri-Gondwanan terranes: implications for Laurentia-Gondwana connections. International Journal of Earth Sciences 93, 659-682.

Nance, R.D., Murphy, J.B., 1994. Contrasting basement isotopic signatures and the palinspastic restoration of peripheral orogens: example from the Neoproterozoic Avalonian-Cadomian belt. Geology 22, 617-620.

Nance, R.D., Murphy, J.B., Strachan, R.A., Keppie, J.D., Gutiérrez-Alonso, G., Fernández-Suárez, J., Quesada, C., Linnemann, U., D'lemos, R., Pisarevsky, S.A., 2008. Neoproterozoic-early Palaeozoic tectonostratigraphy and palaeogeography of the peri-Gondwanan terranes: Amazonian v. West African connections. Geological Society, London, Special Publications 297, 345-383.

O'Brien, S., O'Brien, B., Dunning, G., Tucker, R., 1996. Late Neoproterozoic Avalonian and related peri-Gondwanan rocks of the Newfoundland Appalachians. SPECIAL PAPERS-GEOLOGICAL SOCIETY OF AMERICA, 9-28.

O'Brien, S., Dickson, W., Blackwood, R., 1986. Geology of the central portion of the Hermitage Flexure area, Newfoundland. Current research. Newfoundland Department of Mines and Energy, Mineral Development Division, Report, 86-81.

Payne, J.L., Hand, M., Barovich, K.M., Wade, B.P., 2008. Temporal constraints on the timing of high-grade metamorphism in the northern Gawler

Craton: implications for assembly of the Australian Proterozoic. Australian Journal of Earth Sciences 55, 623-640.

Pollock, J.C., Hibbard, J.P., van Staal, C.R., 2011. A paleogeographical review of the peri-Gondwanan realm of the Appalachian orogen1 This article is one of a series of papers published in this CJES Special Issue: In honour of Ward Neale on the theme of Appalachian and Grenvillian geology. Canadian Journal of Earth Sciences 49, 259-288.

Pollock, J.C., Wilton, D.H.C., van Staal, C.R., Morrissey, K.D., 2007. U-Pb detrital zircon geochronological constraints on the Early Silurian collision of Ganderia and Laurentia along the Dog Bay Line: The terminal Iapetan suture in the Newfoundland Appalachians. American Journal of Science 307, 399-433.

Rogers, N., van Staal, C.R., McNicoll, V., Pollock, J., Zagorevski, A., Whalen, J., 2006. Neoproterozoic and Cambrian arc magmatism along the eastern margin of the Victoria Lake Supergroup: A remnant of Ganderian basement in central Newfoundland? Precambrian Research 147, 320-341.

Rubatto, D., Williams, I.S., Buick, I.S., 2001. Zircon and monazite response to prograde metamorphism in the Reynolds Range, central Australia. Contributions to Mineralogy and Petrology 140, 458-468.

Schofield, D.I., D'Lemos, R.S., 2000. Granite petrogenesis in the Gander Zone, NE Newfoundland: mixing of melts from multiple sources and the role of lithospheric delamination. Canadian Journal of Earth Sciences 37, 535-547.

Scotese, C.R., 2004. A Continental Drift Flipbook. Journal of Geology 112, 729-741.

Stampfli, G., Hochard, C., Vérard, C., Wilhem, C., vonRaumer, J., 2013. The formation of Pangea. Tectonophysics.

Stewart, D., Tucker, R.D., Ayuso, R.A., Lux, R.D., 2001. Minimum age of the Proterozoic Seven Hundred Acre Island Formation and the tectonic setting of the Islesboro Formation, Islesboro block, Maine. Atlantic Geology 37, pp 41-59.

Stockmal, G.S., Colman□Sadd, S.P., Keen, C.E., Marillier, F., O'Brien, S.J., Quinlan, G.M., 1990. Deep seismic structure and plate tectonic evolution of the Canadian Appalachians. Tectonics 9, 45-62.

Tesfai, F.G., 2011. Petrology and Ti-VP Potential of the Lower Coverdale Plutonic Suite, Southeastern New Brunswick, Canada. Acadia University.

Tuach, J., 1987. The Ackley high-silica magmatic/metallogenic system and associated post-tectonic granites, southeast Newfoundland. Memorial University of Newfoundland.

Van Achterbergh E., R.C.G., JACKSON S. E. & GRIFFIN W. L., 2001. Appendix 3: data reduction software for LA-ICP-MS. in: Sylvester, P. (Ed.), Laser-Ablation-ICPMS in the Earth Sciences Mineralogical Association of Canada, 239-243.

van Staal, C.R., 1994. Brunswick subduction complex in the Canadian Appalachians: record of the Late Ordovician to Late Silurian collision between Laurentia and the Gander margin of Avalon. Tectonics 13, 946-962.

van Staal, C.R., Barr, S.M., 2011. Lithospheric architecture and tectonic evolution of the Canadian Appalachians and associated Atlantic margin., In: Percival, J.A., Cook, F.A., Clowes, R.M. (Eds.), Tectonic Styles in Canada Revisited: the LITHOPROBE perspective. Geological Association of Canada

van Staal, C.R., Barr, S.M., Murphy, J.B., 2012. Provenance and tectonic evolution of Ganderia: Constraints on the evolution of the Iapetus and Rheic oceans. Geology 40, 987-990.

van Staal, C.R., Dewey, J., Mac Niocaill, C., McKerrow, W., 1998a. The Cambrian-Silurian tectonic evolution of the northern Appalachians and British Caledonides: history of a complex, west and southwest Pacific-type segment of Iapetus. Geological Society, London, Special Publications 143, 197-242.

Van Staal, C.R., Dewey, J.F., Niocaill, C.M.,

McKerrow, W.S., 1998b. The Cambrian-Silurian tectonic evolution of the northern Appalachians and British Caledonides: history of a complex, west and southwest Pacific-type segment of Iapetus. Geological Society, London, Special Publications 143, 197-242.

van Staal, C.R., McNicoll, V., Valverde-Vaquero, P., Barr, S.M., Fyffe, L.R., Reusch, D.N., 2004. Ganderia, Avalonia, and the Salinic and Acadian orogenies, Geological Society of America Abstracts with Programs, pp. 128-129.

van Staal, C.R., Whalen, J.B., Valverde-Vaquero, P., Zagorevski, A., Rogers, N., 2009. Pre-Carboniferous, episodic accretion-related, orogenesis along the Laurentian margin of the northern Appalachians. Geological Society, London, Special Publications 327, 271-316.

van Staal, C.R., Zagorevski, A., McNicoll, V.J., Rogers, N., 2014. Time-transgressive Salinic and Acadian orogenesis, magmatism and Old Red Sandstone sedimentation in Newfoundland. Geoscience Canada 41, 138-164.

Whalen, J., 1980. Geology and geochemistry of the molybdenite showings of the Ackley City batholith, southeast Newfoundland. Canadian Journal of Earth Sciences 17, 1246-1258.

Whalen, J.B., McNicoll, V.J., van Staal, C.R., Lissenberg, C.J., Longstaffe, F.J., Jenner, G.A., van Breeman, O., 2006. Spatial, temporal and geochemical characteristics of Silurian collision-zone magmatism, Newfoundland Appalachians: An example of a rapidly evolving magmatic system related to slab break-off. Lithos 89, 377-404.

White, Powell, Holland, Worley, 2000. The effect of TiO2 and Fe2O3 on metapelitic assemblages at greenschist and amphibolite facies conditions: Mineral equilibria calculations in the system K2O-FeO-MgO-Al2O3-SiO2-H2O-TiO2-Fe2O3. Journal of Metamorphic Geology 18, 497-511.

White, C.E., Barr, S.M., Miller, B.V., Hamilton, M.A., 2002. Granitoid plutons of the Brookville terrane, southern New Brunswick: Petrology, age, and tectonic setting. Atlantic Geology 38, 53-74.

White, R.W., Powell, R., 2002. Melt loss and the preservation of granulite facies mineral assemblages. Journal of Metamorphic Geology 20, 621-632.

White, R.W., Powell, R., Holland, T.J.B., 2007. Progress relating to calculation of partial melting equilibria for metapelites. Journal of Metamorphic Geology 25, 511-527.

Williams, H., 1979. Appalachian orogen in Canada. Canadian Journal of Earth Sciences 16, 792-807.

Williams, H., Currie, K., Piasecki, M., 1993. The Dog Bay Line: a major Silurian tectonic boundary in northeast Newfoundland. Canadian Journal of Earth Sciences 30, 2481-2494.

Williams, M.L., Jercinovic, M.J., Harlov, D.E., Budzyń, B., Hetherington, C.J., 2011. Resetting monazite ages during fluid-related alteration. Chemical Geology 283, 218-225.

Zagorevski, A., Van Staal, C., 2011. The record of Ordovician arc–arc and arc–continent collisions in the Canadian Appalachians during the closure of Iapetus, Arc-Continent Collision. Springer, pp. 341-371.

Zagorevski, A., Van Staal, C.R., McNicoll, V., Rogers, N., 2007a. Upper Cambrian to Upper Ordovician peri-Gondwanan Island arc activity in the Victoria Lake Supergroup, Central Newfoundland: Tectonic development of the northern Ganderian margin. American Journal of Science 307, 339-370.

Zagorevski, A., van Staal, C.R., McNicoll, V.J., 2007b. Distinct Taconic, Salinic, and Acadian deformation along the Iapetus suture zone, Newfoundland Appalachians. Canadian Journal of Earth Sciences 44, 1567-1585.

SUPPLEMENTARY DATA

Table 1: U-Pb monazite geochronology data

Analysis_#	Sample	Pb206/U238	Err ± 2σ	Pb207/U235	Err ± 2σ	Concordance	Pb207/Pb206	±2σ	Pb206/U238	±2σ	Pb207/U235	±2σ
M1	NL-31	0.07369	0.00102	0.58879	0.01125	97	527.6	39.17	458.3	6.14	470.1	7.19
M3	NL-31	2.75898	0.05338	230.42567	4.7169	154	4524.8	26.53	8536	91.55	5528	20.7
M4	NL-31	0.07494	0.00103	0.57752	0.01108	101	448.3	39.38	465.8	6.19	462.9	7.13
M5	NL-31	0.07425	0.00099	0.62124	0.01143	94	629.6	37.34	461.7	5.94	490.6	7.16
M6	NL-31	0.07495	0.00103	0.57725	0.01129	101	446.5	40.39	465.9	6.17	462.7	7.27
M7	NL-31	0.07555	0.00101	0.58503	0.00994	100	458.4	33.67	469.5	6.07	467.7	6.37
~~#48~~	NL-31	~~0.48342~~	~~2.41586~~	**********	~~268.64063~~	#VALUE!	~~0.1~~	~~7873.49~~	~~2542.1~~	********	—NaN	********
M9	NL-31	0.07315	0.001	0.59694	0.01139	96	573.7	38.42	455.1	6.03	475.3	7.24
M10	NL-31	3.33377	4.00642	53.3753	182.29942	233	1823.1	2339.49	9453.3	5959.48	4057.4	3404.19
M11	NL-31	0.07286	0.00098	0.55414	0.00944	101	418.7	33.81	453.4	5.86	447.7	6.17
M12	NL-31	0.07338	0.001	0.59208	0.01073	97	549.4	36.19	456.5	5.99	472.2	6.85
M13	NL-31	0.0723	0.00104	0.53438	0.01202	104	355.3	48.93	450	6.26	434.7	7.96
M14	NL-31	0.07327	0.00099	0.58199	0.01037	98	514.6	35.91	455.8	5.96	465.7	6.65
M15	NL-31	0.07392	0.00104	0.59354	0.0126	97	538.2	44.41	459.7	6.26	473.1	8.03
M18	NL-31	0.07302	0.00101	0.56852	0.01121	99	470.1	40.9	454.3	6.08	457.1	7.26
M19	NL-31	0.07427	0.00103	0.57122	0.01152	101	443.4	41.55	461.8	6.2	458.8	7.45
M20	NL-31	0.07376	0.00102	0.57086	0.01089	100	457.1	38.87	458.8	6.09	458.6	7.04
M22	NL-31	0.07413	0.00101	0.60676	0.01069	96	580.1	34.76	461	6.04	481.5	6.76
M23	NL-31	0.07377	0.001	0.57668	0.01025	99	478.7	35.93	458.8	6.03	462.3	6.6
M24	NL-31	0.07427	0.00105	0.61566	0.01235	95	607.6	40.74	461.8	6.29	487.1	7.76
M25	NL-31	0.08556	0.00116	1.2348	0.01927	65	1708.5	24.81	529.2	6.91	816.5	8.75
M26	NL-31	0.07444	0.00103	0.57536	0.01074	100	454.1	37.76	462.8	6.16	461.5	6.92
M27	NL-31	0.07481	0.00104	0.57911	0.01122	100	457.6	39.3	465.1	6.25	463.9	7.22
M28	NL-31	0.07447	0.001	0.59854	0.00945	97	539.6	30.87	463.1	5.98	476.3	6
M28_2	NL-31	0.07523	0.00101	0.58082	0.00935	101	451.5	31.04	467.6	6.03	465	6.01
M29	NL-31	0.07351	0.00099	0.56701	0.00927	100	449.6	31.9	457.2	5.93	456.1	6.01
M30	NL-31	0.07514	0.00101	0.57709	0.00959	101	440	32.28	467	6.05	462.6	6.17
M31	NL-31	0.07339	0.00099	0.56038	0.00971	101	427	34.27	456.6	5.97	451.8	6.32
M32	NL-31	0.06948	0.001	0.55254	0.01194	97	517	45.15	433	6.04	446.7	7.81
M32_2	NL-31	0.07312	0.00103	0.73131	0.01453	82	1001.1	37.79	454.9	6.17	557.3	8.52
M33	NL-31	0.07334	0.001	0.56847	0.01002	100	460.1	35.48	456.2	5.98	457	6.49
M34	NL-31	0.07346	0.001	0.56815	0.01033	100	455.5	36.44	457	6	456.8	6.69

M35	NL-31	0.07296	0.00105	0.58361	0.01284	97	529.7	46.09	454	6.31	466.8	8.23
M36	NL-31	0.0735	0.00098	0.5482	0.009	103	374.6	32.7	457.2	5.89	443.8	5.9
M37	NL-31	0.07272	0.00097	0.52971	0.0084	105	319.4	31.85	452.5	5.83	431.6	5.57
M38	NL-31	0.07466	0.00103	0.56497	0.01103	102	407.5	40.01	464.2	6.19	454.8	7.16
M39	NL-31	0.07309	0.00103	0.56008	0.01192	101	435.4	44.08	454.7	6.18	451.6	7.76
M40	NL-31	0.07028	0.00102	0.69593	0.01573	82	980.7	44.21	437.9	6.17	536.4	9.42
M41	NL-31	0.07081	0.00097	0.57347	0.01111	96	557.5	39.03	441.1	5.85	460.3	7.17
M42	NL-31	0.07371	0.00101	0.56745	0.01117	100	445.7	40.38	458.5	6.09	456.4	7.23
1	NL-78	0.06545	0.00092	0.49887	0.00773	99	423.5	28.15	408.7	5.56	410.9	5.24
1_2	NL-78	0.07376	0.0011	0.57613	0.01166	99	478.7	40.97	458.8	6.63	462	7.51
2	NL-78	0.06599	0.00098	0.51679	0.01055	97	483.9	41.43	412	5.91	423	7.06
3	NL-78	0.0658	0.00092	0.49122	0.00751	101	377.2	27.88	410.8	5.56	405.7	5.12
4	NL-78	0.06524	0.00092	0.4986	0.00798	99	429.2	29.56	407.4	5.58	410.8	5.41
5	NL-78	0.06545	0.00092	0.49132	0.00725	101	389.3	25.89	408.7	5.55	405.8	4.94
6	NL-78	0.06622	0.00093	0.50083	0.00775	100	405.5	28.3	413.4	5.63	412.3	5.24
7	NL-78	0.0649	0.00092	0.49067	0.00744	100	405.4	26.75	405.3	5.54	405.4	5.07
7_2	NL-78	0.06549	0.00093	0.49692	0.00784	100	412.8	29.05	408.9	5.6	409.6	5.32
8	NL-78	0.06535	0.00117	0.50028	0.01648	99	431.7	72.78	408.1	7.1	411.9	11.15
8_2	NL-78	0.06445	0.00091	0.48733	0.00775	100	404.5	29.66	402.6	5.52	403.1	5.29
10	NL-78	0.06917	0.00098	0.57681	0.00911	93	619.9	28.29	431.1	5.9	462.4	5.87
10_2	NL-78	0.07164	0.00103	0.64968	0.01079	88	797.8	29.87	446	6.18	508.3	6.64
10_4	NL-78	0.06592	0.001	0.51115	0.01115	98	461	45.07	411.5	6.04	419.2	7.49
11	NL-78	0.07402	0.00106	0.57347	0.00968	100	458.8	32.2	460.4	6.35	460.3	6.25
11_2	NL-78	0.06622	0.00094	0.49602	0.0079	101	384.3	29.06	413.4	5.71	409	5.36
11_3	NL-78	0.06737	0.00096	0.64246	0.01074	83	903.5	29.45	420.3	5.81	503.8	6.64
13	NL-78	0.06499	0.00092	0.50085	0.00785	98	447.7	27.56	405.9	5.55	412.3	5.31
14	NL-78	0.06512	0.00093	0.49575	0.0084	99	420.4	32.02	406.7	5.61	408.8	5.7
15	NL-78	0.06909	0.00098	0.53043	0.00915	100	439.1	32.83	430.7	5.92	432.1	6.07
15_2	NL-78	0.06565	0.00094	0.50191	0.00899	99	429.9	34.82	409.9	5.68	413	6.08
16	NL-78	0.06573	0.00096	0.51941	0.01051	97	503.1	41.16	410.4	5.8	424.8	7.03
16_2	NL-78	0.06541	0.00096	0.50025	0.01047	99	431	42.34	408.5	5.8	411.9	7.08

17	NL-78	0.06573	0.00093	0.51867	0.00867	97	499.8	30.79	410.4	5.65	424.3	5.8	
18	NL-78	0.0665	0.00094	0.50442	0.00829	100	414.3	30.83	415	5.67	414.7	5.6	
19	NL-78	0.06871	0.00111	0.53794	0.01517	98	484.1	61.53	428.4	6.72	437.1	10.01	
20	NL-78	0.06672	0.00093	0.50398	0.00778	100	403.5	27.75	416.4	5.63	414.4	5.25	
21	NL-78	0.06644	0.00093	0.51176	0.00812	99	447.1	28.69	414.7	5.62	419.6	5.46	
22	NL-78	0.07884	0.00116	1.12932	0.02037	64	1694.7	30	489.2	6.91	767.4	9.71	
23	NL-78	0.09942	0.00191	1.72438	0.0526	60	2039.9	55.42	611	11.23	1017.7	19.6	
3	NL-145	0.06588	0.00099	0.51282	0.01097	98	469.5	44.44	411.3	5.99	420.3	7.36	
4	NL-145	0.06598	0.00102	0.47971	0.01153	104	317.9	52.09	411.9	6.15	397.9	7.91	
5	NL-145	0.06618	0.00096	0.49382	0.00901	101	376.3	35.82	413.1	5.77	407.5	6.12	
4_2	NL-145	0.06594	0.00103	0.48502	0.01184	103	344.2	52.34	411.6	6.2	401.5	8.09	
6	NL-145	0.06599	0.00099	0.49809	0.01045	100	402.3	42.5	411.9	5.96	410.4	7.09	
7	NL-145	0.06901	0.00104	0.50604	0.01139	103	337.4	47.09	430.2	6.29	415.8	7.68	
8	NL-145	0.06616	0.00096	0.49687	0.0096	101	390.9	38.46	413	5.79	409.6	6.51	
9	NL-145	0.06564	0.00095	0.49895	0.00963	100	417.7	38.1	409.8	5.77	411	6.52	
10	NL-145	0.06509	0.00096	0.48817	0.00984	101	387.6	40.46	406.5	5.82	403.7	6.71	
11	NL-145	0.06599	0.00096	0.50718	0.00961	99	442.3	36.94	411.9	5.83	416.5	6.47	
12	NL-145	0.06597	0.00094	0.50817	0.00877	99	446.8	32.31	411.8	5.66	417.2	5.9	
12_2	NL-145	0.0653	0.00095	0.51129	0.00948	97	482.6	35.94	407.8	5.75	419.3	6.37	
13	NL-145	0.06587	0.00093	0.49364	0.00782	101	385.6	28.85	411.2	5.61	407.4	5.31	
14	NL-145	0.06595	0.00096	0.49866	0.00898	100	406.1	34.48	411.7	5.8	410.8	6.09	
14_2	NL-145	0.06537	0.00097	0.50048	0.01019	99	434.3	40.64	408.2	5.87	412	6.89	
15	NL-145	0.06603	0.00095	0.48501	0.00853	103	341	34.11	412.2	5.76	401.5	5.83	
16	NL-145	0.06595	0.00097	0.50214	0.00984	100	421.8	39.16	411.7	5.85	413.2	6.65	
16_3	NL-145	0.06835	0.00142	0.8145	0.033	70	1348.9	78.83	426.2	8.57	605	18.47	
17	NL-145	0.06904	0.00103	0.50395	0.00983	104	326.5	38.75	430.4	6.2	414.4	6.64	
17_2	NL-145	0.06588	0.00094	0.50182	0.00826	100	421.8	29.92	411.3	5.7	412.9	5.59	
17_3	NL-145	0.25692	0.00971	7.12233	0.39438	69	2833.5	98.64	1474.1	49.81	2126.8	49.3	
17_4	NL-145	0.06618	0.00094	0.49093	0.00819	102	362.6	32.26	413.1	5.71	405.5	5.58	
17_5	NL-145	0.06426	0.00091	0.48851	0.00793	99	417.5	29.59	401.5	5.51	403.9	5.41	
18	NL-145	0.06575	0.00094	0.48576	0.00846	102	353.3	33.59	410.5	5.71	402	5.78	
19	NL-145	0.06568	0.00097	0.50142	0.00989	99	426.7	39.26	410.1	5.84	412.7	6.69	

20	NL-145	0.06464	0.00092	0.48168	0.00799	101	372.9	31.5	403.8	5.56	399.2	5.47
21	NL-145	0.0654	0.00093	0.49634	0.00814	100	413.9	30.02	408.4	5.61	409.2	5.52
21_2	NL-145	0.06862	0.001	0.51118	0.00995	102	372.5	39.26	427.8	6.02	419.2	6.68
21_3	NL-145	0.06545	0.00094	0.5054	0.00896	98	452.1	33.7	408.7	5.67	415.4	6.04
23	NL-145	0.06557	0.00092	0.4899	0.00776	101	378.6	29.25	409.4	5.57	404.8	5.29
24	NL-145	0.10875	0.00176	0.82761	0.02185	109	417.8	56.48	665.5	10.22	612.3	12.14
25	NL-145	0.06818	0.00096	0.57949	0.00922	92	661.4	28.13	425.2	5.82	464.1	5.93
26	NL-145	0.06521	0.00092	0.48072	0.00765	102	348.6	29.22	407.3	5.56	398.6	5.25
27	NL-145	0.08185	0.00166	1.40847	0.0447	57	2024.9	58.32	507.2	9.86	892.5	18.84
28	NL-145	0.06469	0.00093	0.49396	0.00864	99	427.4	32.87	404.1	5.64	407.6	5.87
28_2	NL-145	0.06529	0.00092	0.50164	0.00794	99	441.2	28.08	407.7	5.6	412.8	5.37
29	NL-145	0.06595	0.00093	0.50298	0.00839	100	424.5	31.48	411.7	5.65	413.7	5.67
30	NL-145	0.06524	0.00095	0.49502	0.00958	100	413.3	38.34	407.4	5.74	408.3	6.51
31	NL-145	0.06599	0.00093	0.47459	0.00762	104	292.3	30.7	411.9	5.59	394.4	5.25
31_2	NL-145	0.06535	0.00094	0.49927	0.00844	99	428.5	30.82	408.1	5.7	411.2	5.71
32	NL-145	0.06452	0.00094	0.66293	0.01246	78	1055.1	34.25	403.1	5.72	516.4	7.61
33	NL-145	0.06525	0.00092	0.50526	0.00767	98	458.5	26.18	407.5	5.57	415.3	5.17
34	NL-145	0.06516	0.00093	0.47859	0.00828	102	340.3	33.48	406.9	5.6	397.1	5.68
34_2	NL-145	0.06481	0.00093	0.48079	0.00882	102	362.7	37.37	404.8	5.63	398.6	6.05
35	NL-145	0.06515	0.00095	0.50039	0.01015	99	440.2	41.09	406.9	5.76	412	6.87
36	NL-145	0.06441	0.00091	0.47287	0.00807	102	339.4	33.36	402.4	5.48	393.2	5.56
36_2	NL-145	0.06457	0.00091	0.47315	0.00832	103	334.8	34.72	403.4	5.53	393.4	5.73
37	NL-145	0.06464	0.00093	0.48272	0.00868	101	377.7	35.14	403.8	5.64	399.9	5.95
M1	NL-154	0.06425	0.00094	0.47898	0.01075	101	370.2	48.25	401.4	5.72	397.4	7.38
M2	NL-154	0.06531	0.00094	0.50515	0.00975	98	456.4	38.98	407.8	5.7	415.2	6.58
M3	NL-154	0.06593	0.00093	0.50368	0.00863	99	428.8	32.76	411.6	5.64	414.2	5.83
M6	NL-154	0.08452	0.00153	0.67647	0.02621	100	532.1	84.13	523.1	9.12	524.6	15.87
M7	NL-154	0.0656	0.00097	0.49276	0.0104	101	391	43.74	409.6	5.89	406.8	7.08
M8	NL-154	0.07462	0.00126	0.60064	0.01827	97	543.3	65.43	463.9	7.55	477.6	11.59
M9	NL-154	0.08414	0.00226	0.79472	0.05513	88	883.2	142.44	520.8	13.42	593.8	31.19
M10	NL-154	0.06576	0.00098	0.50283	0.00979	99	430.4	37.83	410.6	5.91	413.6	6.62
M11	NL-154	0.06563	0.00101	0.51578	0.01108	97	491.4	42.55	409.8	6.1	422.3	7.42

M12	NL-154	0.07126	0.00111	0.77568	0.01829	76	1167.4	45.33	443.7	6.68	583	10.46
M13	NL-154	0.066	0.00099	0.49807	0.00967	100	401.4	38.26	412	6	410.4	6.55
M14	NL-154	0.06565	0.00101	0.4964	0.01083	100	405.4	44.38	409.9	6.11	409.3	7.35
M15	NL-154	0.06773	0.00169	0.62945	0.03624	85	850	120.02	422.4	10.22	495.8	22.58
M16	NL-154	0.06809	0.00115	0.51247	0.01507	101	395	63.48	424.6	6.92	420.1	10.12
M17	NL-154	0.06624	0.00108	0.51902	0.01398	97	484	56.65	413.5	6.52	424.5	9.34
M18	NL-154	0.08562	0.00232	1.09916	0.06442	70	1489.9	112.46	529.6	13.76	752.9	31.16
M19	NL-154	0.10724	0.00218	1.64771	0.05848	66	1822.7	64.93	656.7	12.68	988.7	22.43
M20	NL-154	0.06766	0.0012	0.51201	0.01747	101	407.2	73.84	422.1	7.27	419.8	11.73
M21	NL-154	0.06582	0.00156	0.58328	0.03283	88	750.5	118.36	410.9	9.45	466.6	21.05
M22	NL-154	0.0744	0.00161	0.64694	0.03095	91	710.2	101.02	462.6	9.67	506.6	19.08
M23	NL-154	0.06567	0.0014	0.49993	0.02412	100	420.5	106.36	410	8.5	411.7	16.33
M24	NL-154	0.08927	0.00173	1.15709	0.04045	71	1508.8	66.3	551.2	10.22	780.6	19.04
M25	NL-154	0.06533	0.00106	0.47258	0.01283	104	305	59.42	408	6.42	393	8.84
M26	NL-154	0.09423	0.0018	0.77245	0.02939	100	583.7	82.19	580.5	10.58	581.2	16.84
M27	NL-154	0.07453	0.00135	0.58636	0.02238	99	493.2	83.4	463.4	8.09	468.5	14.32
M28	NL-154	0.12703	0.00219	1.12987	0.03494	100	757.9	63.96	770.9	12.54	767.7	16.66
M29	NL-154	0.25497	0.00475	4.16107	0.12435	88	1931.4	53.4	1464	24.42	1666.4	24.46

Table 2: mineral chemistry tables for samples 31, 78 and 145

ID number	**31**	**31**	**31**	**31**	**31**	**31**	**31**	**31**	**31**
Mineral	**Bi**	**Qz**	**Pl**	**Mus**	**And**	**Ilm**	**Mt**	**ky**	**St**
SiO2	35.56	99.84	60.14	46.00	35.96	0.05	0.06	35.92	34.88
TiO2	1.93	0.00	0.00	0.80	0.04	45.06	0.18	0.03	0.11
Al2O3	18.69	0.00	24.68	34.52	61.12	0.04	0.42	61.14	59.84
Cr2O3	0.02	0.01	0.01	0.03	0.01	0.00	0.15	0.00	0.01
FeO	16.52	0.06	0.28	2.74	1.19	47.86	89.90	1.16	2.38
MnO	0.25	0.00	0.00	0.01	0.00	0.25	0.07	0.03	0.05
MgO	11.63	0.00	0.00	0.68	0.04	0.01	0.01	0.07	0.59
ZnO	0.01	0.01	0.00	0.00	0.02	0.00	0.02	0.00	0.02
CaO	0.00	0.01	6.74	0.01	0.00	0.02	0.03	0.01	0.02
Na2O	0.34	0.02	8.05	1.03	0.01	0.00	0.00	0.00	0.01
K2O	9.05	0.00	0.07	9.64	0.00	0.01	0.00	0.01	0.00
V2O3	0.05	0.00	0.00	0.10	0.00	0.04	0.34	0.03	0.05
ZrO2	0.00	0.00	0.00	0.02	0.06	0.05	0.00	0.02	0.03
SrO	0.05	0.05	0.05	0.05	0.05	0.05	0.05	0.05	0.05
BaO	0.00	0.00	0.00	0.00	0.00	0.00	0.00	0.00	0.00
NiO	0.00	0.00	0.00	0.00	0.00	0.00	0.00	0.00	0.00
Total	94.09	100.00	100.01	95.62	98.50	93.45	91.22	98.46	98.04
No. Oxygens	11.00	2.00	8.00	11.00	5.00	3.00	4.00	5.00	5.00
Si	2.39	1.00	2.68	3.07	0.99	0.00	0.00	0.99	0.96
Ti	0.10	0.00	0.00	0.04	0.00	0.91	0.01	0.00	0.00
Al	1.48	0.00	1.29	2.71	1.98	0.00	0.02	1.98	1.95
Cr	0.00	0.00	0.00	0.00	0.00	0.00	0.00	0.00	0.00
Fe2+	2.56	0.00	0.05	0.02	0.04	0.17	1.95	0.04	0.12
Mn2+	-1.64	0.00	-0.04	0.13	-0.01	0.91	1.00	-0.02	-0.06
Mg	0.01	0.00	0.00	0.00	0.00	0.01	0.00	0.00	0.00
Zn	1.16	0.00	0.00	0.07	0.00	0.00	0.00	0.00	0.02
Ca	0.00	0.00	0.00	0.00	0.00	0.00	0.00	0.00	0.00
Na	0.00	0.00	0.32	0.00	0.00	0.00	0.00	0.00	0.00
K	0.04	0.00	0.69	0.13	0.00	0.00	0.00	0.00	0.00
V3+	0.78	0.00	0.00	0.82	0.00	0.00	0.00	0.00	0.00
Zr	0.00	0.00	0.00	0.01	0.00	0.00	0.01	0.00	0.00
Sr	0.00	0.00	0.00	0.00	0.00	0.00	0.00	0.00	0.00
Ba	0.00	0.00	0.00	0.00	0.00	0.00	0.00	0.00	0.00
Ni	0.00	0.00	0.00	0.00	0.00	0.00	0.00	0.00	0.00
	0.00	0.00	0.00	0.00	0.00	0.00	0.00	0.00	0.00
Total Cations (S)	6.90	1.00	5.00	7.00	3.00	2.00	3.00	3.00	3.00

ID number	**78**	**78**	**78**	**78**	**78**	**78**	**78**	**78**
Mineral	**Bi**	**Qz**	**Sill**	**Pl**	**Mus**	**Ilm**	**Gt**	**Gt**
							cores	rims
SiO2	35.37	99.81	34.88	59.92	47.83	0.03	36.32	35.84
TiO2	1.56	0.01	0.11	0.01	0.92	52.18	0.15	0.03
Al2O3	19.70	0.01	59.84	23.62	37.30	0.02	20.43	20.57
Cr2O3	0.03	0.00	0.01	0.00	0.01	0.00	0.02	0.02
FeO	17.46	0.00	2.38	0.01	0.91	42.32	28.24	29.34
MnO	0.21	0.00	0.05	0.00	0.02	3.69	10.39	8.53
MgO	10.53	0.00	0.59	0.00	0.62	0.05	2.51	2.98
ZnO	0.12	0.00	0.02	0.08	0.00	0.01	0.03	0.03
CaO	0.00	0.00	0.02	5.91	0.02	0.00	1.22	1.17
Na2O	0.20	0.01	0.01	8.48	1.02	0.00	0.02	0.04
K2O	9.24	0.00	0.00	0.11	9.03	0.03	0.00	0.01
V2O3	0.08	0.01	0.05	0.01	0.05	0.00	0.01	0.01
ZrO2	0.03	0.00	0.03	0.00	0.01	0.00	0.01	0.01
SrO	0.05	0.05	0.05	0.05	0.05	0.05	0.05	0.05
BaO	0.00	0.00	0.00	0.00	0.00	0.00	0.00	0.00
NiO	0.00	0.00	0.00	0.00	0.00	0.00	0.00	0.00
Total	94.59	99.91	98.04	98.20	97.80	98.38	99.41	98.63
No. Oxygens	11.00	2.00	5.00	8.00	11.00	3.00		
Si	2.38	1.00	0.96	2.70	3.11	0.00	1.21	1.19
Ti	0.08	0.00	0.00	0.00	0.04	1.01	0.00	0.00
Al	1.56	0.00	1.95	1.26	2.85	0.00	0.60	0.61
Cr	0.00	0.00	0.00	0.00	0.00	0.00	0.00	0.00
Fe2+	2.54	0.00	0.12	0.08	0.00	0.00	0.39	0.41
Mn2+	-1.56	0.00	-0.06	-0.08	0.05	0.91	0.15	0.12
Mg	0.01	0.00	0.00	0.00	0.00	0.08	0.06	0.07
Zn	1.06	0.00	0.02	0.00	0.06	0.00	0.00	0.00
Ca	0.01	0.00	0.00	0.00	0.00	0.00	0.02	0.02
Na	0.00	0.00	0.00	0.29	0.00	0.00	0.00	0.00
K	0.03	0.00	0.00	0.74	0.13	0.00	0.00	0.00
V3+	0.79	0.00	0.00	0.01	0.75	0.00	0.00	0.00
Zr	0.00	0.00	0.00	0.00	0.00	0.00	0.00	0.00
Sr	0.00	0.00	0.00	0.00	0.00	0.00	0.00	0.00
Ba	0.00	0.00	0.00	0.00	0.00	0.00	0.00	0.00
Ni	0.00	0.00	0.00	0.00	0.00	0.00	0.00	0.00
	0.00	0.00	0.00	0.00	0.00	0.00	0.00	0.00
Total Cations (S)	6.90	1.00	3.00	5.00	7.00	2.00	2.44	2.42

ID number	**145**	**145**	**145**	**145**	**145**	**145**	**145**	**145**	**145**
Analysis No.									
Mineral	**Bi**	**Cd**	**Qz**	**Sill**	**Per**	**Pl**	**Mus**	**Ilm**	**Mt**
SiO2	35.66	48.11	99.72	34.09	63.52	61.69	45.26	0.05	0.05
TiO2	2.49	0.00	0.00	0.01	0.08	0.01	0.95	46.11	0.01
Al2O3	20.51	32.00	0.03	57.49	0.01	23.62	33.74	0.02	0.16
Cr2O3	0.01	0.00	0.00	0.03	17.80	0.02	0.04	0.03	0.41
FeO	15.98	8.00	0.02	1.01	0.01	0.01	3.21	45.53	90.55
MnO	0.26	0.73	0.00	0.00	0.05	0.00	0.03	0.42	0.09
MgO	9.99	7.87	0.00	0.02	0.01	0.00	0.72	0.05	0.00
ZnO	0.08	0.03	0.00	0.01	0.00	0.00	0.00	0.00	0.00
CaO	0.01	0.01	0.01	0.01	0.03	5.11	0.21	0.02	0.01
Na2O	0.21	0.45	0.00	0.00	0.30	8.94	0.71	0.00	0.00
K2O	8.83	0.00	0.02	0.00	2.59	0.28	10.06	0.02	0.00
V2O3	0.13	0.01	0.00	0.01	12.73	0.00	0.00	0.06	0.29
ZrO2	0.00	0.00	0.00	0.00	0.50	0.03	0.00	0.00	0.00
SrO	0.05	0.05	0.05	0.05	0.00	0.05	0.05	0.05	0.05
BaO	0.00	0.00	0.00	0.00	0.00	0.00	0.00	0.00	0.00
NiO	0.00	0.00	0.00	0.00	0.00	0.00	0.00	0.00	0.00
Total	94.20	97.27	99.86	92.73	97.63	99.76	94.99	92.37	91.62
No. Oxygens	11.00	18.00	2.00	5.00		8.00	11.00	3.00	4.00
Si	2.69	5.02	1.00	1.00	3.45	2.75	3.06	0.00	0.00
Ti	0.14	0.00	0.00	0.00	0.00	0.00	0.05	0.96	0.00
Al	1.82	3.94	0.00	1.98	0.00	1.24	2.69	0.00	0.01
Cr	0.00	0.00	0.00	0.00	0.76	0.00	0.00	0.00	0.02
Fe2+	1.01	0.70	0.00	0.02	0.00	0.00	0.18	1.06	3.93
Mn2+	0.02	0.06	0.00	0.00	0.00	0.00	0.00	0.01	0.00
Mg	1.12	1.23	0.00	0.00	0.00	0.00	0.07	0.00	0.00
Zn	0.00	0.00	0.00	0.00	0.00	0.00	0.00	0.00	0.00
Ca	0.00	0.00	0.00	0.00	0.00	0.24	0.01	0.00	0.00
Na	0.03	0.09	0.00	0.00	0.00	0.77	0.09	0.00	0.00
K	0.85	0.00	0.00	0.00	0.03	0.02	0.87	0.00	0.00
V3+	0.01	0.00	0.00	0.00	0.18	0.00	0.00	0.00	0.01
Zr	0.00	0.00	0.00	0.00	0.56	0.00	0.00	0.00	0.00
Sr	0.00	0.00	0.00	0.00	0.01	0.00	0.00	0.00	0.00
Ba	0.00	0.00	0.00	0.00	0.00	0.00	0.00	0.00	0.00
Ni	0.00	0.00	0.00	0.00	0.00	0.00	0.00	0.00	0.00
Total Cations (S)	7.69	11.05	1.00	3.01	5.00	5.02	7.03	2.04	3.98

Sample No.	**NL31**	**145**	**78**
SiO2	53.20	63.52	52.56
TiO2	1.33	0.85	1.18
Al2O3	26.01	17.17	23.37
Fe2O3	5.57	2.10	3.47
FeO	3.87	4.31	7.81
MnO	0.17	0.15	1.40
MgO	1.68	2.29	2.66
CaO	2.29	1.42	0.67
Na2O	2.23	2.53	0.78
K2O	1.77	3.78	3.09
P2O5	0.29	0.14	0.13
LOI	1.51	1.90	3.21
Total	**99.92**	**100.16**	**100.33**
Fe2O3T	9.87	6.89	12.15
Rb	102.9	263.5	203.4
Sr	267	105	67
Y	44.6	31.2	40.9
Zr	306	193	73
V	162	101	139
Ni	28	40	25
Cr	195	132	92
Nb	22.0	18.2	20.9
Ga	28.7	22.1	30.4
Cu	16	19	30
Zn	106	81	124
Co	65	56	89
Ba	349	438	373
La	41	30	40
Ce	80	67	100
U	3.0	1.7	4.8
Th	21.2	8.2	22.1
Sc	20	14	18
Pb	30	4	1

Table 3
Bulk rock chemistry for mineral phase equilibria and whole rock geochemistry for samples NL31, NL78 and NL145.

Chapter 5

The Neoproterozoic to late Paleozoic evolution of Avalonia, Ganderia and Meguma in the northern Appalachians: a hafnium isotopic perspective

ABSTRACT

Since Wilson's 1966 proposal for a proto-Atlantic (Iapetus) Ocean along the eastern margin of Laurentia, geologists have variably constrained the timing of ocean opening to the Late Neoproterozoic, most recently to ~615 Ma. However, based on a compilation of hafnium isotopic arrays of detrital and magmatic zircons from Avalonia, Ganderia and Meguma in the northern Appalachians, and comparisons with Hf data compilations from cratonic Amazonia, Baltica and Laurentia, it is proposed that the opening of proto-Iapetus Ocean began much earlier, at ~750 Ma,. Geological similarities between Ganderia and Avalonia are confirmed by Hf arrays and show that both initiated near the former Grenville suture, likely the Laurentian margin, and not from Gondwana as commonly thought. Moreover, the presence of in situ 750 Ma calc-alkaline granites in Avalonia requires subduction had begun by at least 750 Ma. Indeed, detrital zircons from Avalonia suggest magmatism/subduction began at ~800 Ma, which coincides with the final stages of suprasubduction zone magmatism (~870-740 Ma) in the Valhalla Orogen, to the north.

We suggest that southward propagation of Valhalla subduction initiated a continental-type arc between ~800-750 in the former Grenville Orogen, along the Laurentian margin. Penecontemporaneously, the Asgard Sea progressively opened behind, as Baltica drifted away from Laurentia. A uniform shift in the Hf isotope array toward juvenile values between ~750-650 Ma suggests the Avalonian/Ganderian arc retreated from Laurentia to form a microcontinental ribbon at least by 700 Ma. Extension-related 760-680 Ma alkaline granites in the central Appalachians attests to ongoing subduction retreat. The intervening back-arc basin became the proto-Iapetus Ocean.

Between ~750-650 Ma the ribbon transferred by subduction retreat across the Asgard Sea, closing it and colliding with the Gondwanan margin at ~650 Ma, consistent with paleomagnetic and geological evidence. Accretion of the ribbon is also reflected in the reversal of εHf data to progressively negative values between 650-600 Ma, which is also recorded across other northern peri-Gondwanan terranes, such as Iberia and Cadomia. Avalonia, Ganderia and Meguma separated diachronously from Gondwana as 'composite Avalonia' between 550-500 Ma, forming the Rheic Ocean. Meguma is interpreted to form the trailing passive margin to the retreating continental ribbon during the late Cambrian-Ordovician. All terranes show an εHf isotopic trend toward juvenile values, consistent with the transition from continental to a retreating oceanic-arc. Avalonia and Ganderia migrated northward, initially closing the Tornquist Sea as it collided with Baltica, then closing Iapetus at ~450-440 Ma as it finally re-amalgamated with Laurentia. Thus, proto-Iapetus and Iapetus has a 300 Ma-long history recorded by zircons in the adjacent, retreating arc systems, and did not form by Atlantic-style ocean-opening.

Following the final accretion of composite Avalonia by ~430 Ma, subduction stepped outboard into the trailing Rheic Ocean. Subduction was initiated within the Rheic Ocean, placing the peri-Gondwanan terranes in an upper plate, back-arc setting. The hafnium isotopic array indicates that tectonic switching between retreating (e.g. Salinic and Neoacadian orogenies) and advancing (e.g. Acadian Orogeny) subduction episodes progressively homogenised the crust, exclusively reworking the juvenile (Late Neoproterozoic) and Grenvillian-type basement.

The geological evidence for overall predominantly extensional environment is preserved in the protracted development of pull-apart basins and abundant bimodal and granitic magmatism across composite Avalonia between ~430-350 Ma, which was punctuated by brief intervals of contraction and transpression.

1. INTRODUCTION

A fundamental aspect of plate tectonics is the concept of the Wilson cycle, coined for Tuzo Wilson who first proposed the existence of a proto-Atlantic Ocean (Iapetus Ocean) along the eastern margin of Laurentia during the early Paleozoic (Wilson, 1966). Crucial for recognising the opening and closing of a late Neoproterozoic-Paleozoic ocean was the recognition of a suture zone that ran through Atlantic Canada and into Western Europe, separating rocks of Laurentian affinity from those of Gondwanan affinity (Fig. 1). Over the last four decades, targeted field work, complimented by technological advancements, have further refined the fundamental principles of the Wilson cycle, with much of the work taking place in the type section of Atlantic Canada (Fig. 1). Building on Wilsons (1966) concept, Williams (1979) recognised important contrasts in the lithology, fauna, metamorphic and igneous record of the Neoproterozoic-Paleozoic rocks of Newfoundland (and Nova Scotia), and them into five distinct tectonostratigraphic zones. Williams et al., (1988) further recognised that the centre of Newfoundland (the Dunnage Zone) comprised of two distinct "oceanic" domains that have linkages to Laurentia (Notre Dame Subzone) and Ganderia (Exploits Subzone) and represent vestiges of the Iapetus Ocean. The timing of the opening of Iapetus has been constrained by paleomagnetic, geological and geochronological data since 1966 (Harland and Gayer, 1972; Rankin, 1976; Dalziel, 1992, 1997; Cawood et al., 2001; Waldron and van Staal, 2001) and is now frequently considered to have opened via a triple-junction between Baltica, Amazonia and Laurentia between ~620 Ma and 570 Ma (Harland and Gayer, 1972; Rankin, 1976; Dalziel, 1992, 1997; Cawood et al., 2001; Waldron and van Staal, 2001; Cawood and Pisarevsky, 2006; Pisarevsky et al., 2008).

The transfer of outboard terranes from the northern Gondwanan margin during the early Paleozoic to the Laurentian margin in the late Ordovician-early Silurian, played a fundamental role in the closure of the Iapetus Ocean as well as the birth of the successor Rheic Ocean (Murphy et al., 2010; Pollock et al., 2011; Nance et al., 2012; Willner et al., 2014). These outboard terranes of Atlantic Canada include Ganderia, Avalonia and Meguma, and are generally accepted as having evolved along the Amazonian and/or West African margins of northern Gondwana in the late Neoproterozoic as part of an extensive continental-arc system (Murphy et al., 2013; Linnemann et al., 2014). During the late Cambrian-early Ordovician the peri-Gondwanan terranes are proposed to have rifted from the Gondwanan margin and were transferred across the Iapetus Ocean to the Laurentian margin, opening the Rheic Ocean in their wake (Murphy et al., 2006; Nance et al., 2012). The closure of the Rheic Ocean in the late Devonian-early Carboniferous culminated in the oblique collision of West Africa with Laurentia during final assembly of Pangea (Stampfli and Borel, 2002; Stampfli et al., 2013). Therefore, the geodynamic driving forces behind the transfer of the peri-Gondwanan terranes are tied intrinsically to the timing and evolution of the Iapetus and Rheic Oceans.

New geochronological and isotopic data from Avalonia and Ganderia (Henderson et al., 2016; Henderson, in prep) raise several unresolved issues regarding the early Neoproterozoic history of the peri-Gondwanan terranes and the evolution of Iapetus, which have implications for Neoproterozoic and Paleozoic paleogeography of the northern Appalachian orogen. Isotopic similarities between Ganderia and Avalonia including the nature of the basement, the timing of Neoproterozoic (~650-550 Ma) continental-arc magmatism and the close timing of accretion to the Laurentian margin, suggest the terranes share a common history throughout the late Neoproterozoic-early

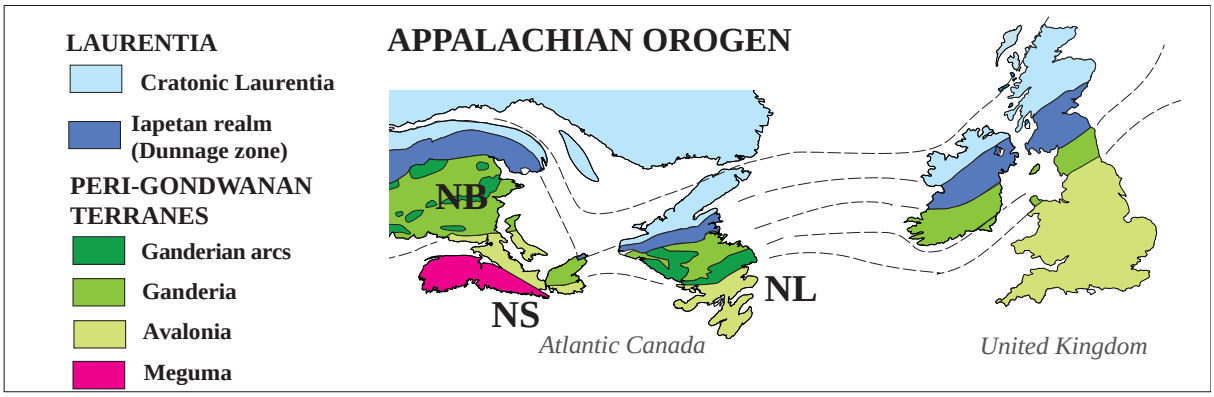

Figure 1

Tectonic map showing the distribution of the Appalachian orogen and the extension into the United Kingdom. Shown are the tectonic-stratigraphic subdivisions within the Appalachian orogen including Laurentia, the Iapetan "Dunnage Zone", Ganderian arcs, Ganderia, Avalonia and Meguma. NL: Newfoundland, NS: Nova Scotia, NB: New Brunswick. The figure is modified from Hibbard et al., (2007), Barreiro et al., (2007), Keppie et al., (2008) and Pollock et al., (2011).

Paleozoic (Henderson et al., 2016). Isotopic data from detrital zircons in Avalonia and Ganderia indicate a comparable magmatic-arc history that commences at ~800-750 Ma (Henderson et al., 2016; Henderson, in prep) outboard of Gondwana, prior to arc accretion and ensuing continental arc-magmatism along the Gondwanan margin between ~650-550 Ma (Murphy et al., 2013; Henderson et al., 2016). Although the basement of Avalonia and Ganderia are not definitively exposed, it has been characterised by geochronological and isotopic methods and is composed of Mesoproterozoic-Paleoproterozoic (~1.0-2.2 Ga) "Grenvillian-type" crust (Henderson et al., 2016; Henderson, in prep). Crust of this age is abundant in areas assigned to the Grenvillian orogeny, such as the Grenville Province in Laurentia (Dickin et al., 1990; Daly and McLelland, 1991; Dickin, 2000), the Sveconorwegian Orogen in Sweden (Andersen et al., 2007 and references therein) and the SW Amazon craton (Sunsas Belt, Tohver et al., 2006 and references therein). However, the Grenville regions are generally interpreted to be 'locked' up within the interior of the Rodinian supercontinent until final break-up during the opening of Iapetus at ~620-570 Ma (Cawood et al., 2001; Cawood and Pisarevsky, 2006).

The present constraints on the timing of Iapetus opening make it impossible to reconcile a Grenville origin for the basement to the Neoproterozoic Avalonia and Ganderia arcs, as suggested by the geochronological and isotopic data. Ganderian and Avalonian arc magmatism occurs virtually continuously between ~650-450 Ma suggesting they developed along a single active plate margin (Henderson et al., Submitted); with the subducted plate generally considered to be Iapetus in most reconstructions (Pollock et al., 2011; van Staal et al., 2012). However, the timing of the continental arc-magmatism is inconsistent with Iapetus opening between ~620-570 Ma and cannot be reconciled with the destruction of Iapetus. Therefore, either the peri-Gondwanan terranes occupied a location away from the Iapetan margins during the mid-late Neoproterozoic (e.g. Keppie et al., 2003; Linnemann et al., 2008; Murphy et al., 2013) or Iapetus opened earlier in the Neoproterozoic (see Chew et al., 2008).

Consistent with existing geological constraints, Avalonia and Ganderia (± Meguma) formed part of series of continental arcs along the northern Gondwana margin by ~650 Ma (Von Raumer et al., 2002; Pollock et al., 2011). The rifting of the peri-Gondwana terranes from the Gondwanan margin occurred variably between ~510-480 Ma (Murphy et al., 2006; Pollock et al., 2009; van Staal et

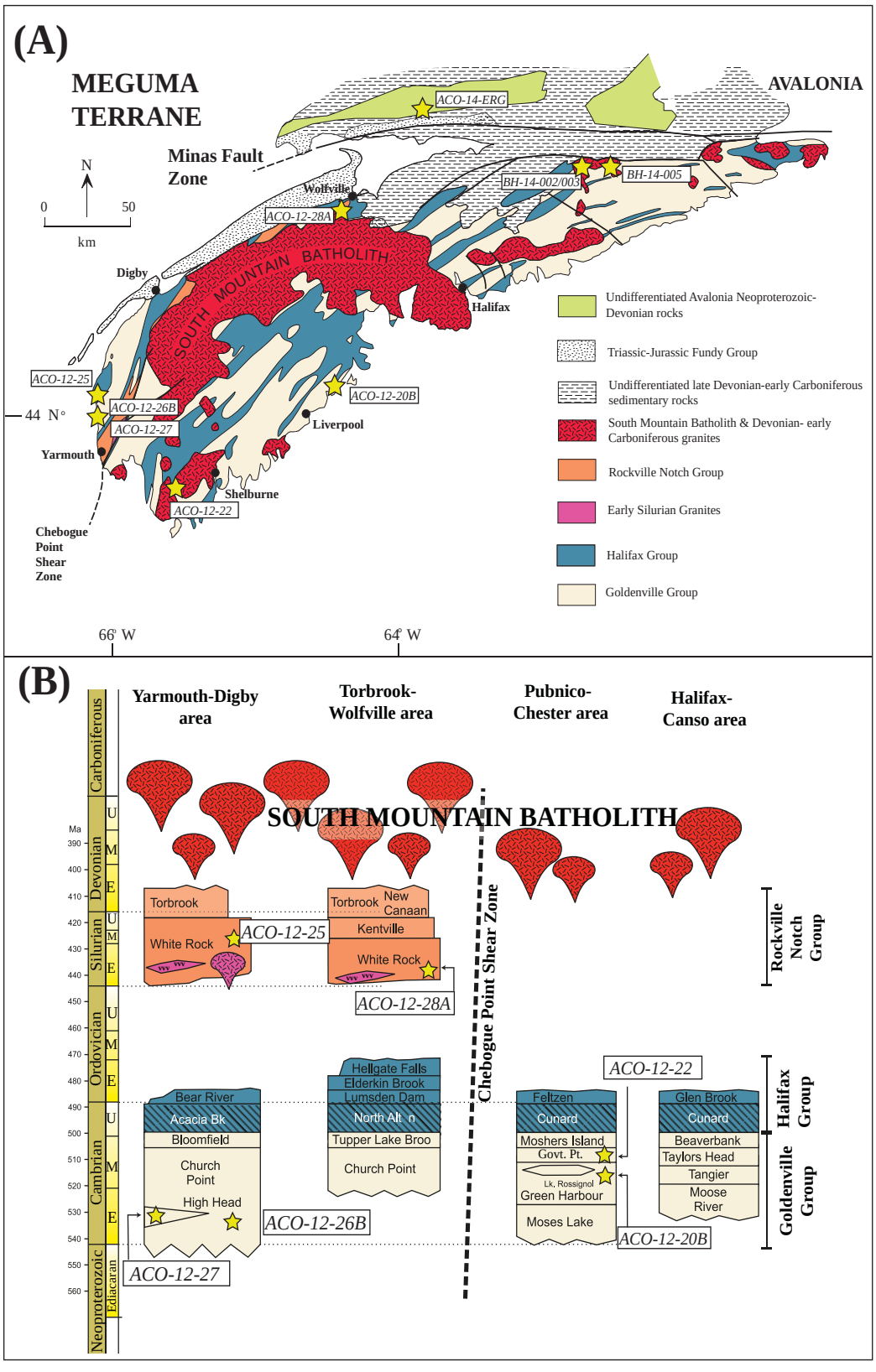

Figure 2

A) Simplified geology map of the Meguma terrane in Nova Scotia showing the location of the major geologic units and structural zones. The yellow stars show the location of the new samples taken for U-Pb-Hf analysis. The figure is modified from Pothier et al. (2015) and reference. B) Time-space plot showing the major episodes of sedimentation, deformation and magmatism throughout the Meguma terrane. The plot is divided into NE and SW zone by a major structural feature, the Chebogue Point Shear Zone. The plot is modified after White et al. (2012) and references therein.

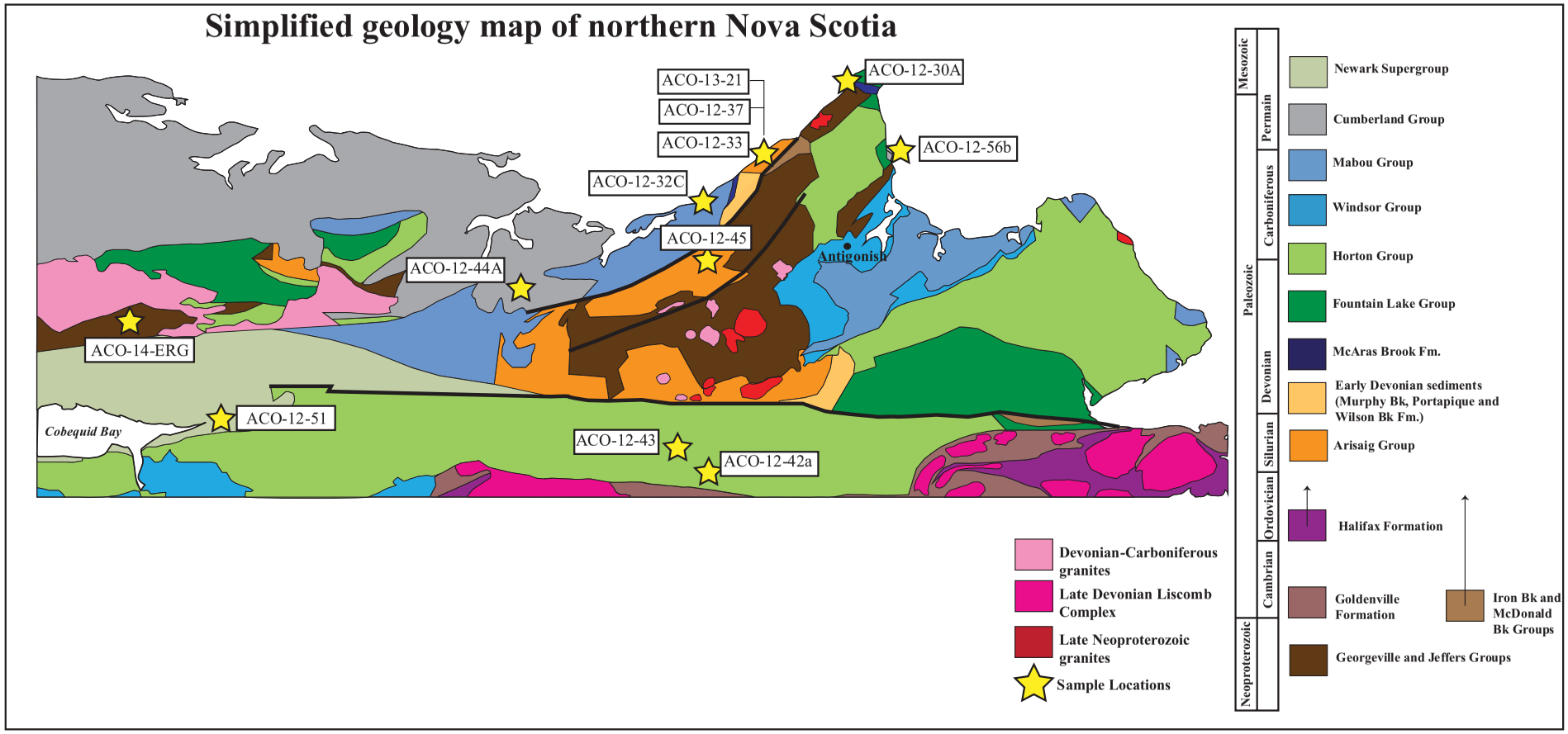

Figure3

A) Simplified geological subdivision of Nova Scotia and Newfoundland. B) Detailed geology of northern Nova Scotia (Avalonia) with the sample locations represented by yellow stars. Map modi-fied from Murphy et al., (1991), Keppie (2000) and White et al. (2012).

al., 2012), either as a more or less contiguous ribbon (e.g. Avalonia sensu lato, O'Brien et al., 1996; Nance et al., 2002; Nance et al., 2010) or as separate entities requiring several ocean basins to open (Barr and White, 1996; van Staal et al., 1996; van Staal et al., 1998; Barr et al., 2003). Between the late Ordovician to early Devonian the terranes progressively accreted to the Laurentian margin. If the terranes are considered to have been individual fragments then subduction is required to step outboard following the collision of each terrane, establishing a continental arc on the upper plate during each ocean closure event (van Staal et al., 2009; Zagorevski and Van Staal, 2011). A common issue in the Appalachians is the paucity of Silurian-early Carboniferous calc-alkaline rocks indicative of continental arc magmatism, making the reconstruction of wide ocean basins between the peri-Gondwanan terranes less feasible.

In this chapter we present a comprehensive compilation of new and existing U-Pb-Hf isotopic data from magmatic and detrital zircons from Neoproterozoic-Silurian rocks of Avalonia, Ganderia and Meguma. We use hafnium isotopes to reassess the evolution of the peri-Gondwana Avalonia, Ganderia and Meguma terranes. Hafnium isotopic arrays are sensitive to long and short term changes within a tectonic framework, such as the establishment or destruction of an oceanic basin (Henderson et al., Submitted), and thus can be used to test the existing tectonic reconstruction models for the Appalachians. Based on this data, we propose an alternative model for the evolution for the Iapetus Ocean and the Paleozoic assembly of the composite Laurentian margin prior to the amalgamation of Pangea.

2. Sample selection and geological framework

The present study follows on from Henderson et al., (2016) and Henderson et al., (submitted) that focused on the hafnium isotopic signatures of the basement rocks in Avalonia and Ganderia (respectively) in the northern Canadian Appalachians. In order to obtain a full hafnium isotopic array for the peri-Gondwanan terranes of the northern Appalachians it is essential to characterise Meguma, and the clastic sedimentary rocks deposited on Avalonia and Meguma during the complex Ordovician-Carboniferous interval. In order to 'tie' the detrital zircons to the magmatic record in Avalonia, Ganderia and Meguma we also sampled six igneous rocks (five granites and one rhyolite) from across Nova Scotia and Newfoundland (Fig. 2, 3).

2.1 Meguma terrane

The late Neoproterozoic-Paleozoic evolution of Meguma is under ongoing debate (Murphy et al., 2004b; Waldron et al., 2009; Waldron et al., 2011; White and Barr, 2012) as there is no exposed arc-related basement like Avalonia and Ganderia and preserves unique Paleozoic stratigraphy. Meguma comprises a thick sequence of early Cambrian-early Ordovician turbiditic sandstones and shales that are collectively referred to as the Meguma Group (Stevenson, 1959), and subdivided into the metasandstones-dominated Goldenville and slate-dominated Halifax groups (White and Barr, 2012). Systematic mapping, geochronology and faunal age constraints conducted in the last decade or so have resulted in further subdivision of the Goldenville and Halifax groups and the establishment of regional stratigraphy (White, 2010 and references therein). A significant advancement was the recognition of a major high-strain zone, the Chebogue Point shear zone, which divides Meguma into northwestern and southeastern parts (Fig. 2a). Silurian metasedimentary sequences and two series of mafic dykes only occur northwest of the shear zone (White, 2010; White and Barr, 2012).

Early limited detrital zircon data provided an initial maximum deposition age of 566 ± 8 Ma for the Goldenville Group (Krogh and Keppie, 1990). Analysis of the stratigraphically lowest and highest members

Sample No.	Stratigraphic name	Tectonic affiliation	Depositional age	Youngest population	No. of U-Pb analyses	Coordinates	
ACO-12-44A	Stellarton Formation	Avalonia/Meguma	Carboniferous	410 ± 5 Ma	71/139	45°34'50.83"N	62°40'8.12"W
ACO-12-56B	Cribbons Pt Formation	Avalonia/Meguma	late Carboniferous	623 ± 6 Ma	28/70	45°45'24.41"N	61°53'43.47"W
ACO-12-51	Graham Hill Formation	Avalonia/Meguma	Carboniferous	380 ± 5 Ma	65/80	45°21'10.27"N	63°16'19.99"W
ACO-12-32C	Lismore Formation	Avalonia/Meguma	Carboniferous	413 ± 4 Ma	78/96	45°43'30.02"N	62°13'27.25"W
ACO-12-42B	Cross River Fm.	Avalonia/Meguma	late Devonian-early Carboniferous	362 ± 5 Ma	53/80	45°16'54.85"N	62°23'35.61"W
ACO-12-43	Barrans Fm.	Avalonia/Meguma	late Devonian-early Carboniferous	362 ± 3 Ma	74/80	45°20'32.36"N	62°25'17.64"W
ACO-12-30A	McArras Brook Fm.	Avalonia	late Devonian	403 ± 4 Ma	60/60	45°51'47.77"N	61°59'1.32"W
ACO-12-33	Knoydart Fm.	Avalonia	lower Devonian	413 ± 6 Ma	35/47	45°43'56.69"N	62°12'35.29"W
ACO-12-37	MacAdam Fm.	Avalonia	Wenlock-Ludlow	440 ± 7 Ma	73/80	45°44'51.90"N	62°10'4.09"W
ACO-12-45	Beechill Cove Fm.	Avalonia	Llandovery	543 ± 8 Ma	45/60	45°35'45.67"N	62°15'47.56"W
ACO-12-28a	White Rock Fm.	Meguma	early Silurian	514 ± 6 Ma	56/85	45° 3'34.19"N	64°27'1.10"W
ACO-12-25	White Rock Fm.	Meguma	early Silurian	539 ± 7 Ma	41/80	44° 5'26.65"N	66°12'3.02"W
ACO-12-22A	Government Point Fm.	Meguma	mid-Cambrian	535 ± 5 Ma	70/80	43°34'32.15"N	65°34'28.67"W
ACO-12-20B	Green Harbour Fm.	Meguma	early-mid Cambrian	591 ± 6 Ma	51/80	44°12'46.98"N	64°26'12.28"W
ACO-12-27	High Head Member	Meguma	early Cambrian	551 ± 8 Ma	65/71	43°57'26.49"N	66° 9'42.91"W
ACO-12-26B	Church Point Fm.	Meguma	early Cambrian	579 ± 7 Ma	76/80	44° 0'50.00"N	66° 9'28.53"W

Table 1

Full list of sedimentary rocks sampled in this study with relevant sample details and key analytical results.

of the Goldenville Group northwest of the Chebogue Point shear zone yielded maximum deposition ages from detrital zircon of 544 ± 18 Ma and 529 ± 19 Ma, respectively (Waldron et al., 2009). The detrital zircon spectra of the lowest points in the Goldenville Group stratigraphy (High Head and Church Point members) comprise solely of Neoproterozoic zircons (~750-540 Ma), whereas higher in the stratigraphy the detrital zircon spectra becomes more complex yielding Neoproterozoic populations (~550-620 Ma), scattered Mesoproterozoic (~1000-1200 Ma, ~1500 Ma), Paleoproterozoic (1900-2200 Ma) and Archean populations (~2500-3000 Ma) (Waldron et al., 2009). Further age constraints were established by the documentation of Cambrian ichnofossils in the Church Point Formation that constrain the group to the Lower Cambrian (Gingras et al., 2011); and are also similar to trace fossils found in northwest Argentina and south-eastern Newfoundland. The deposition of the Goldenville Formation post-dates the ~650-550 Ma magmatic arc activity that dominated along the northern Gondwanan margin (Murphy et al., 2013), and coincides with the onset of rifting and bimodal volcanism in the Avalonia terrane (Keppie et al., 2003).

To expand on the previous geochronology undertaken in the Goldenville Group, four samples were selected for U-Pb-Hf detrital zircon analysis; two from the northwest of the Chebogue Point shear zone (ACO-12-26b, Church Point Fm.; ACO-12-27, High Head) and two from southeast of the shear zone (ACO-12-20b, Government Point Fm.; ACO-12-22, Government Point Fm.). Hafnium isotopes from Meguma detrital zircons have not been assessed before and will allow the source terrane to be constrained with much more confidence.

The Silurian Rockville Notch Group occurs only in the northwest of the shear zone, where it disconformably overlies the Halifax Group. The Rockville Notch Group consists of quartzites, metasiltstones and slates and interlayered mafic and felsic metavolcanic rocks (White et al., 2011, 2012a), divided into the White Rock Formation, Kentville and New Canaan/Torbrook Groups (Fig. 2b). The interpreted depositional environment for the protolith rocks is a shallow marine environment (MacDonald et al., 2002 and references therein). The geochemistry of the mafic volcanic rocks is predominantly alkaline

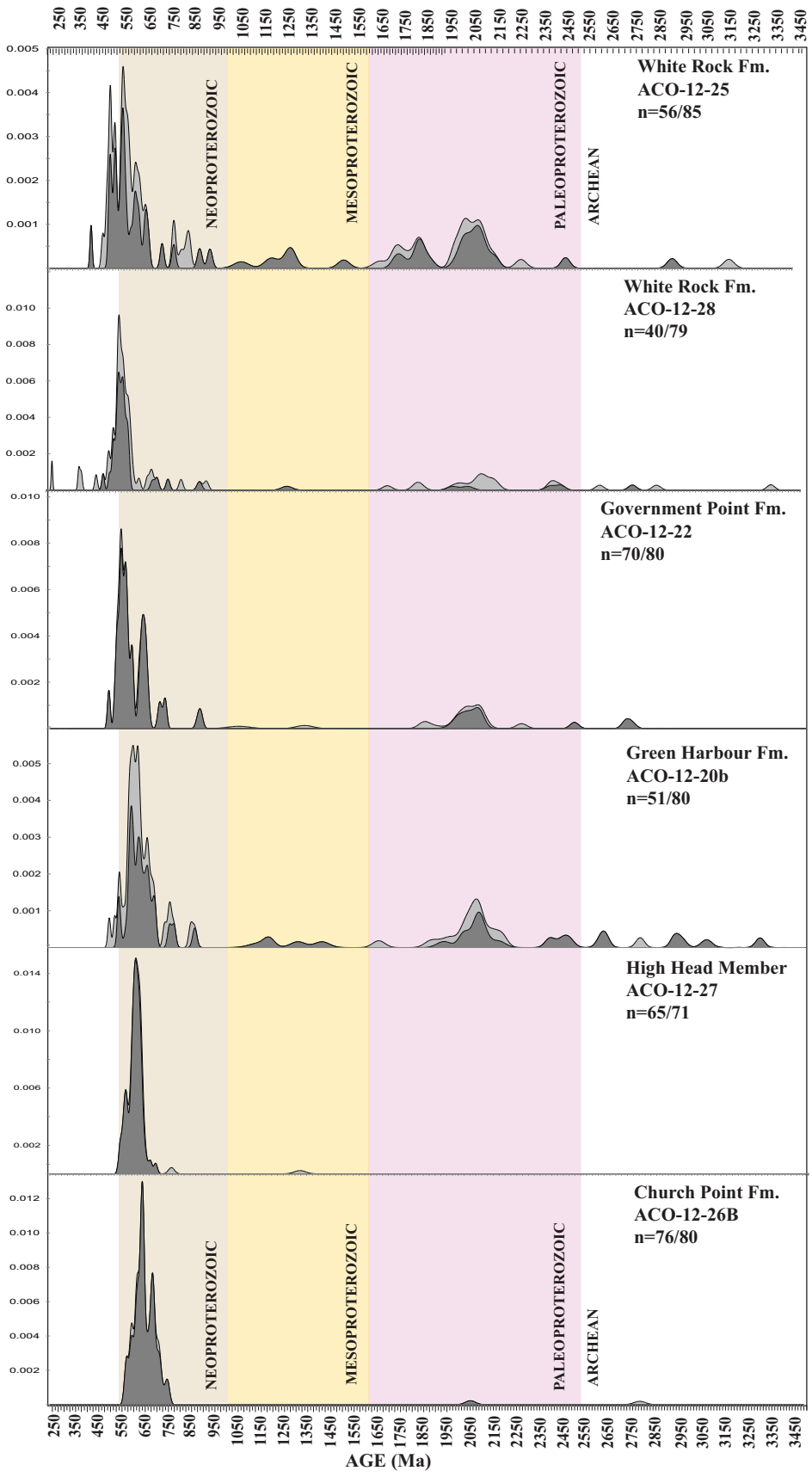

Figure 4

Detrital zircon age probability density distribution plots for sedimentary rocks from Meguma. Lighter grey fields represent zircon grains that are > 10% discordant. n =xxx/xxx equals number of > 90–110% concordant analyses/number of < 90% or > 110% concordant analyses.

and indicates a within-plate setting that has been previously associated with rifting from the Gondwanan margin (MacDonald et al., 2002; White and Barr, 2003; White et al., 2012b).

Two samples were taken from the metasedimentary layers of the Silurian White Rock Formation; the first from the cliffs at Cape Saint Marys (ACO-12-25) and the second from Kentville (ACO-12-28A). U-Pb zircon age constraints for the felsic volcanics in the White Rock Formation are constrained to 438 ± 3 Ma (MacDonald et al., 2002), which is coeval to the Brenton Pluton that yielded an age of 439 ± 3 Ma (Krogh and Keppie, 1990) and thus these bodies are interpreted to be co-magmatic (MacDonald et al., 2002). Previous detrital zircon provenance studies have been conducted on the White Rock and Torbrook Formations (Murphy et al., 2004b), where the detrital zircon spectra comprised late Neoproterozoic-early Paleozoic (~520-640 Ma, 390-440 Ma), minor Tonian (~830, 980 Ma), Mesoproterozoic (~1000-1200 Ma, ~1400 Ma) and Paleoproterozoic (~1950-2200 Ma) populations. The presence of early Neoproterozoic and Mesoproterozoic zircons are comparable to the Silurian-early Devonian Arisaig Group in Avalonia, and Murphy et al., (2004b) suggest a shared Paleozoic history for Meguma and Avalonia to account for the similarities.

2.2 Silurian-Carboniferous sedimentary rocks

During the Silurian-Carboniferous Avalonia and Meguma underwent a complex evolution during in which they were progressively accreted to the Laurentian margin and subsequently underwent a number of compressional and extensional events associated with internal interactions with one another and the composite Laurentian margin (e.g. the Salinic, Acadian, Neoacadian, Alleghenian orogenies, Murphy et al., 1999; van Staal et al., 2004; Murphy and Keppie, 2005; Zagorevski et al., 2007b; van Staal et al., 2009). Obtaining geochronological and isotopic data from the sedimentary sequences deposited during late Ordovician-Carboniferous are fundamental to understanding the geodynamic framework of the Appalachian orogen and the Iapetus and Rheic oceans.

Late Neoproterozoic arc rocks of Avalonia (~630-540 Ma) are overlain by a sequence of Cambrian-Lower Ordovician volcanic and terrestrial to shallow marine clastic rocks and limestones that preserve Acado-Baltic fauna commonly attributed to a northern Gondwanan affinity (Landing and Murphy, 1991). A thick succession of late Ordovician-Early Devonian siliciclastic rocks (the Arisaig Group) unconformably overly the Cambrian-Ordovician platformal sequences (Waldron et al., 1996). The Arisaig Group consists of a ~80-200 m base of bimodal volcanic rocks, known variably as the Dunn Point or Bears Brook Formations, which are disconformably overlain by a ~1800-1900 m continuous sequence of shallow-marine, fossiliferous siliciclastic rocks (Waldron et al., 1996; Murphy et al., 2004a; Braid and Murphy, 2006). Fossils constrain the deposition of the formations within the Arisaig Group to the Lower Llandoverian to Lochkovian (see Boucot, 1974; Waldron et al., 1996). On the basis of contrasting Sm-Nd whole rock isotopic and the detrital zircon record Murphy et al. (2004a) determined that the Arisaig Group was unlikely to have been derived from the underlying Avalonian arc rocks and instead are likely to have been derived from Baltica in the latest Ordovician, and subsequently Laurentia by the Middle Silurian. Three samples were collected from the Arisaig Group (Fig. 3); from the 439 Ma Beechill Cove Formation (ACO-12-45), the 424 Ma MacAdam Formation (ACO-12-37) and the 405 Ma Knoydart Formation (ACO-12-33).

Unconformably overlying the Arisaig

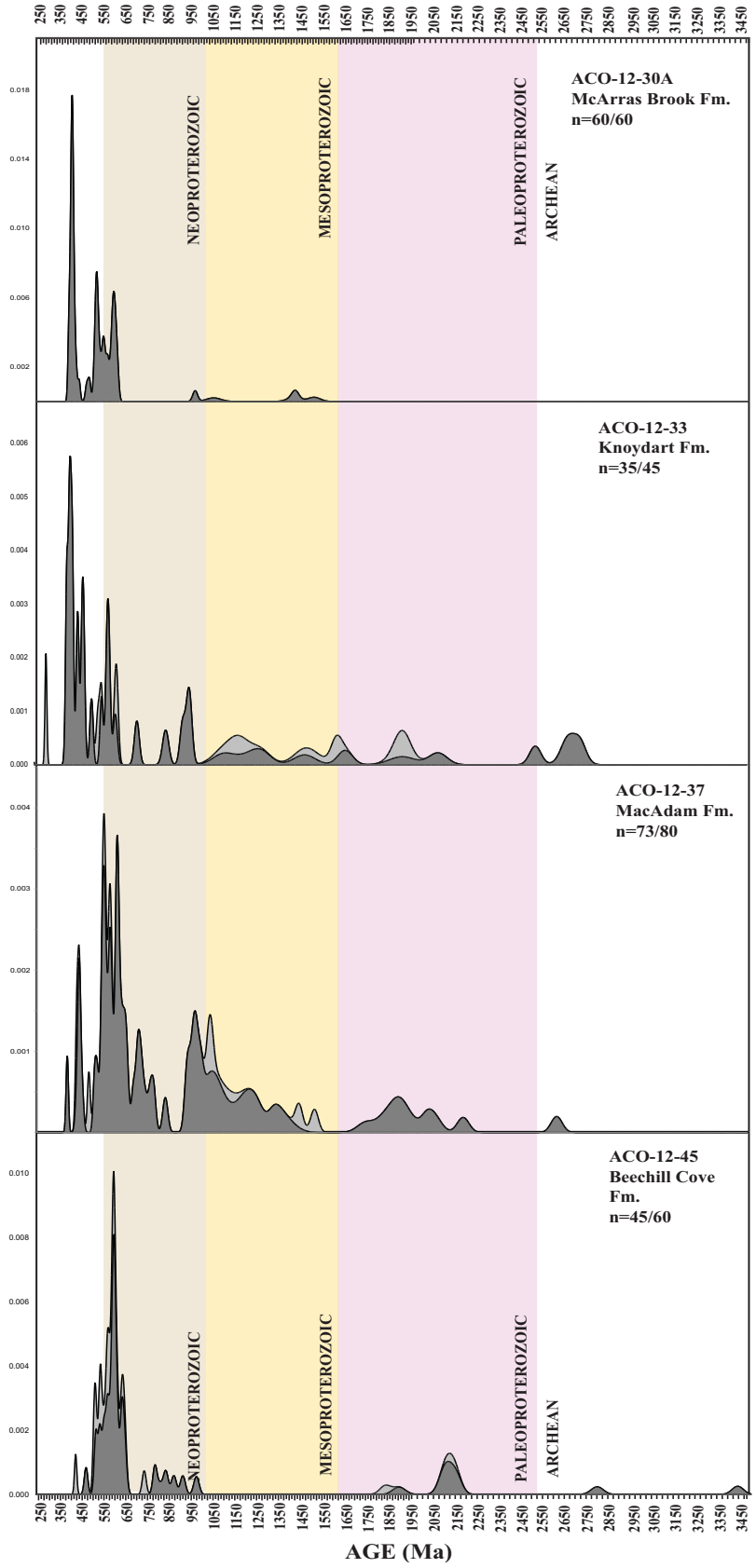

Figure 5

Detrital zircon age probability density distribution plots for Silurian to lower Devonian sedimentary rocks from Avalonia. Lighter grey fields represent zircon grains that are > 10% discordant. n =xxx/xxx equals number of > 90–110% concordant analyses/number of < 90% or > 110% concord-ant analyses.

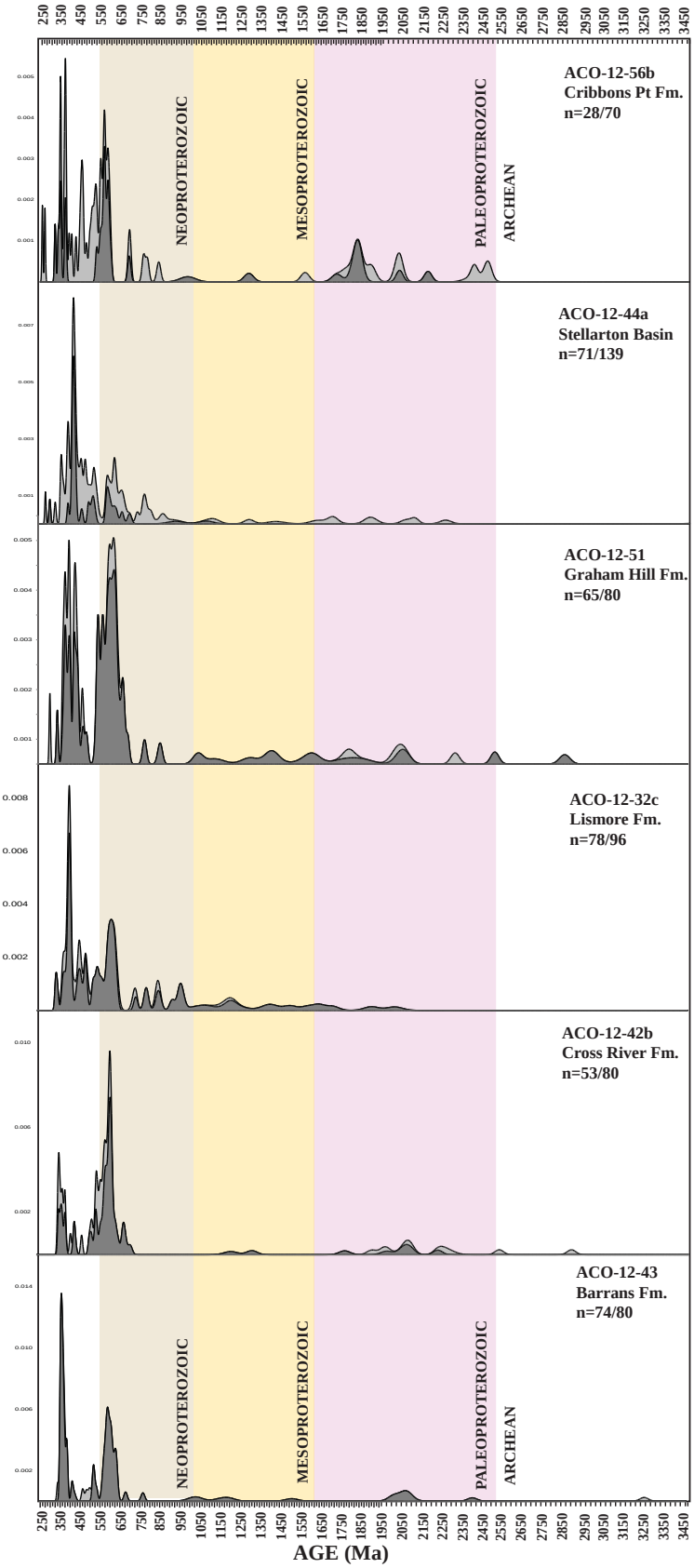

Figure 6

Detrital zircon age probability density distribution plots for lower Devonian to Permian sedimentary rocks from Avalonia. Lighter grey fields represent zircon grains that are > 10% discordant. n =xxx/xxx equals number of > 90–110% concordant analyses/number of < 90% or > 110% concord-ant analyses.

Sample No.	Name	Tectonic affiliation	Crystallisation age	Youngest inherited population	Coordinates	
ACO-ERG-14	Economy River Gneiss	Avalonia	735 ± 3 Ma		45°26'38.19"N	63°54'54.69"W
ACO-13-17	Clarenville granite	Avalonia	607 ± 3 Ma		48° 7'42.62"N	53°55'59.55"W
ACO-13-21	Dunn Pt rhyolite	Avalonia	466 ± 6 Ma		45°45'43.83"N	62°10'19.13"W
ACO-13-16	Deadmans Bay granite	Ganderia	393 ± 2 Ma		49°21'1.47"N	53°41'27.19"W
BH-002/003	South Mountain Batholith	Meguma		401 ± 6 Ma	45°15'30.92"N	62°34'37.36"W
BH-005	South Mountain Batholith	Meguma		457 ± 7 Ma	45°15'52.23"N	62°32'2.93"W

Table 2
Full list of igneous rocks sampled in this study with relevant sample details and key analytical results.

Group is the Middle to Late Devonian McArras Brook Formation, which comprises interbedded mafic volcanics and continental redbeds interpreted to have been deposited during an episode of regional intracrustal extension, associated with the dextral transpression between Avalonia and Meguma (Murphy et al., 2011) during the latest stages of the Acadian orogeny (Murphy and Keppie, 2005). A sample of the McArras Brook Formation was collected for hafnium isotope analysis (ACO-12-30A). During the late Devonian- Carboniferous a series of rift basins developed on the composite Laurentian margin, overstepping the Avalonia-Meguma boundary (Murphy and Keppie, 1998; Murphy and Hamilton, 2000; Piper and Pe-Piper, 2001). Clastic sequences sourced locally from uplifted Neoproterozoic arc rocks and the Meguma terrane (Murphy and Hamilton, 2000) were deposited and deformed during progressive dextral shear during the convergence between Laurentia and Gondwana and the final assembly of Pangea.

We collected six late Devonian-late Carboniferous samples from the Barrens Formation (ACO-12-43), Cross River Formation (ACO-12-42B) and the Graham Hill Formation (ACO-12-51), a sample from the Namurian Lismore Formation (AOC-12-32c), a sample from the Stellarton Formation (ACO-12-44a) and a sample from the Cribbons Point Formation (ACO-12-56b). Previous detrital zircon data has been collected from the Graham Hill, Barrens and Cross River Formations (Murphy and Hamilton 2000).

2.3 Igneous rocks

Unequivocal basement of Avalonia is not exposed anywhere in the terrane (Murphy et al., 2000), which means there are no ways to directly test the composition of the basement rocks. However, isotopic analysis of Neoproterozoic igneous rocks enables the characterisation of the nature of the lower crust (Murphy et al., 2000). Previous studies have used Sm-Nd whole rock isotopes to estimate the age of the basement (Nance and Murphy, 1994; Kerr et al., 1995; Nance and Murphy, 1996; Samson et al., 2000; Murphy and Nance, 2002) and generally found whole rock models ages of ~1.0-1.2 Ga for western Avalonia, with the exception of the Simmons Brook Intrusive Suite and the Seal Cove granite in Newfoundland (Tucker and Corfu, 1993; Kerr et al., 1995) that record Nd TDM model ages of ~1.6 Ga; indicating the presence of an older basement in Avalonia. Pollock et al. (Pollock et al., 2015) recently presented hafnium isotopes from zircons in a suite of late Neoproterozoic igneous rocks from the Avalon terrane in Nova Scotia and Newfoundland and found the majority of Neoproterozoic zircons (~570-650 Ma) record TDM of 0.84-1.30 Ga, with minor populations preserving significantly older TDM of ~1.4-3.10 Ga. Henderson et al. (2016) also analysed detrital zircons from Neoproterozoic arc-related sequences in Avalonian Nova Scotia and concluded the early Avalonia arc was likely built on Mesoproterozoic-Paleoproterozoic "Grenvillian-type" (2.0-1.0 Ga) crust.

To strengthen the ties between the

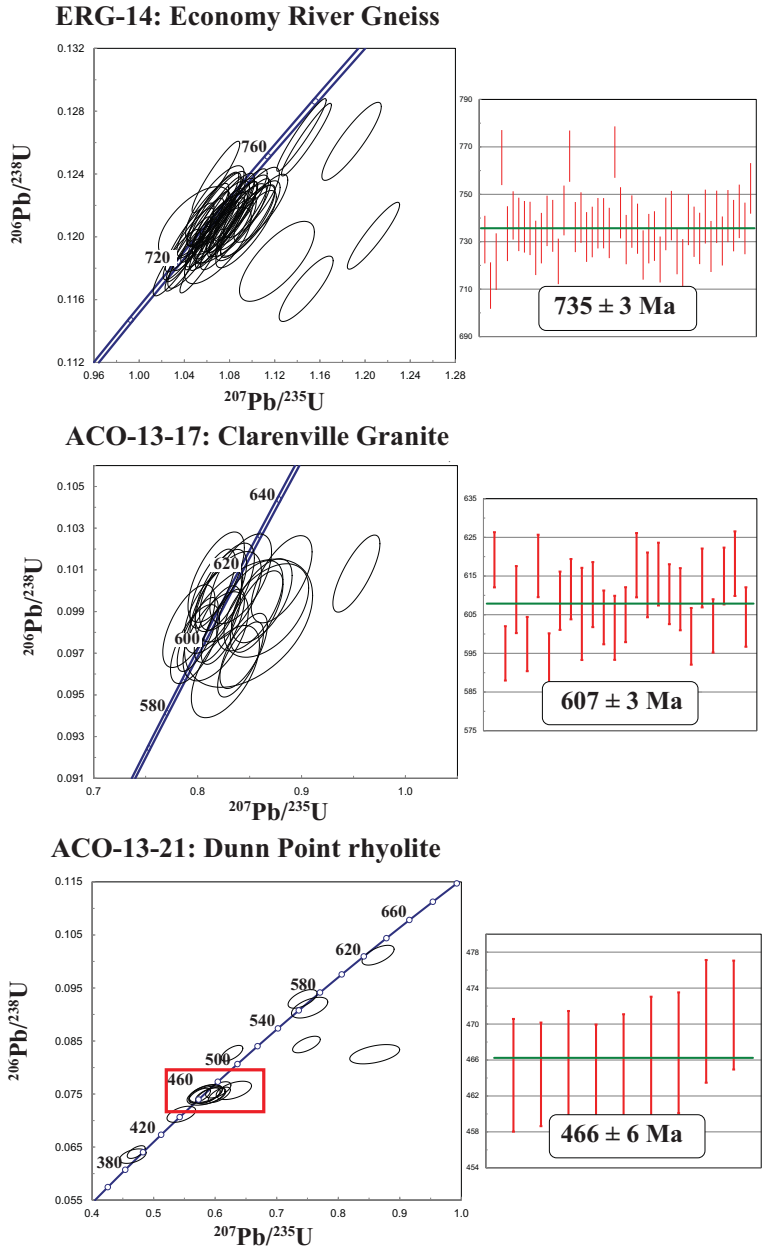

Figure 7

Concordia plots for zircon grains from the Economy River Gneiss, Clarenville Granite and Dunn Point Rhyolite. Mean ages displayed are 206Pb/238U ages with mean errors quoted at the one standard deviation level.

hafnium isotope array defined by detrital zircons with the Neoproterozoic magmatic record of Avalonia, two granites from western Avalonia were sampled for hafnium isotopic analysis. The first from the 734 Ma Economy River Gneiss (Doig et al., 1993), which is one of the oldest magmatic rocks exposed in Nova Scotia. The Economy River Gneiss (sample ACO-14-ERG) intrudes the oldest metasedimentary rock (Gamble Brook Formation) that was recently analysed for detrital zircon hafnium isotopic analysis (Henderson et al., 2016) and contained almost exclusively Mesoproterozoic-Paleoproterozoic detritus (~2.0-1.0 Ga) isotopically compatible with Baltica. The second sample is the Clarenville Granite from the Avalon Zone in Newfoundland (ACO-13-17). Based on undeformed nature of the granite it had previously been assumed to be Devonian in age (Kerr et al., 1993), but has been potentially considered to be Neoproterozoic based on other field constraints (Normore, 2012). No geochronological constraints currently exist for the Clarenville Granite.

Igneous rocks are scarce in the early Paleozoic in Avalonia and Meguma, but become increasingly abundant throughout the mid-Silurian- late Devonian (Keppie and Krogh, 2000; MacDonald et al., 2002; Murphy and Dostal, 2007). The Dunn Point Formation in Avalonia (Fig. 3) records an important interval of mid-Ordovician bimodal volcanism interpreted to reflect extension and basin development during the oblique collision between Avalonia and Laurentia (Hamilton and Murphy, 2004). A sample of flow-banded rhyolite was collected from the Dunn Point Formation for U-Pb zircon and Hf analysis (sample ACO-13-21, Fig. 3). Previously, a rhyolite from the Dunn Point Formation has been yielded a U-Pb zircon age of 460 ± 3 Ma (Hamilton and Murphy, 2004). Silurian-early Devonian magmatism throughout Ganderia is generally attributed to the closure of an ocean basin (van Staal et al., 2009; van Staal and Barr, 2011) between Ganderia and Avalonia and subsequent post-collisional orogenic collapse (Schofield and D'Lemos, 2000) and/or delamination (Whalen et al., 2006). Although magmatism occurs from ~430 Ma, it is most prevalent between ~400-380 Ma (Kellett et al., 2014). We present U-Pb-Hf isotopic data from the Deadmans Bay Granite in Ganderia (sample ACO-13-16), which has previously been dated at 390 ± 4 Ma (Kellett et al., 2014).

Peraluminous mid-to late Devonian granites are a definitive characteristic of the Meguma terrane (Clarke et al., 1997); of which the largest plutonic suite is the granodioritic to leucogranitic South Mountain Batholith ("SMB") (Fig. 2, Shellnutt and Dostal, 2015). Plutons exposed towards the boundary of the SMB are often more 'mafic' in character (e.g. Barrington Passage, Shelburne and Port Mouton, White et al., 2012a). The SMB is considered to have been generated by predominantly melting of the unexposed basement, with contamination from the Goldenville and Halifax Groups and mixing with mantle derived mafic magmas (Tate et al., 1997; Clarke et al., 2000). Given the S-type nature and abundance of inherited zircons within the SMB, it has been notoriously difficult to obtain a precise crystallisation age (Tate and Clarke, 1997; MacLean et al., 2003; Moran et al., 2007). However, various monazite, zircon and titanite ages have yielded populations between ~380-370 Ma (Clarke and Halliday, 1980; Clarke et al., 2000; MacLean et al., 2003; Moran et al., 2007), indicating SMB magmatism occurred over a ~10 million year period. Generally, the age of the granites young towards the southeast in the Meguma terrane (White and Barr, 2012 and references therein). Two samples were collected from the SMB; one is a granite from the Long John Lake pluton (BH-002/003) and the second is a quartz diorite from the Ten Mile Lake pluton (BH005) (Fig. 2). 40Ar/39Ar ages from hornblende, muscovite and biotite indicate that most of the Meguma terrane cooled through 300 °C by ~368-345 Ma, which indicates rapid denudation of up to 10 km following the emplacement of the SMB (Keppie and Dallmeyer 1995).

3. RESULTS ZIRCON GEOCHRONOLOGY

A total of 1268 detrital zircon and 226 igneous zircon analyses were conducted on samples from across Avalonia, Ganderia and Meguma. A summary of the samples analysed for U-Pb and Hafnium analyses are presented in Tables 1 and 2. Detrital zircon age spectra for the Cambrian-Silurian Meguma metasedimentary rocks are presented in Figure 4, for early Silurian to early Devonian Avalonia sedimentary rocks in Figure 5 and Devonian-Carboniferous sedimentary rocks deposited on the boundary of Avalonia and Meguma in Figure 6. Concordia and weighted age diagrams are presented for the Neoproterozoic-Devonian igneous rocks in Figures 7 and 8.

3.1 Meguma U-Pb zircon geochronology

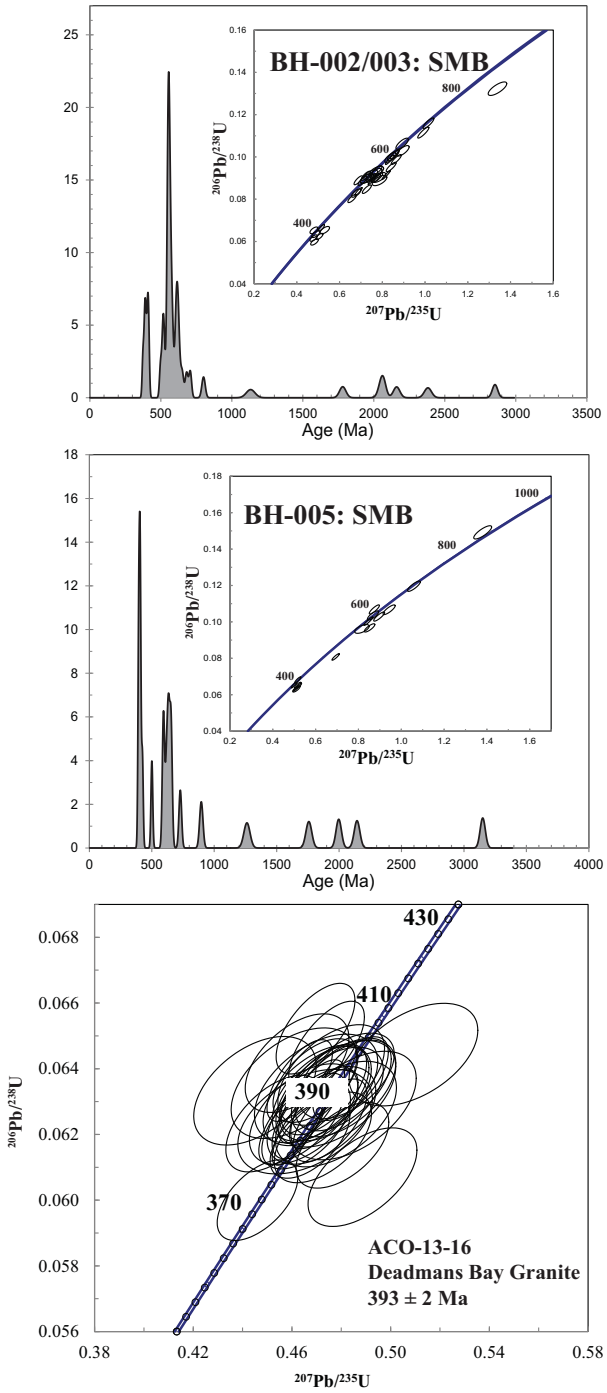

Figure 8

Concordia plots for zircon grains from the South Mountain Batholith and Deadmans Bay granite. Mean ages displayed are 206Pb/238U ages with mean errors quoted at the one standard deviation level.

3.1.1 ACO-12-26b (Church Point Formation)

Sample ACO-12-26b is taken from a medium grained sandstone of the early Cambrian Church Point Formation (Fig. 4). ACO-12-26b had 80 analyses conducted on 80 detrital zircon grains, of which 76 are 90-110 % concordant (Fig. 4). All but one of the concordant grains are Neoproterozoic, with a single zircon recording a Paleoproterozoic age of 2063 ± 21 Ma. The Neoproterozoic zircons cover a broad population spanning 577- 760 Ma, with 69% of zircons falling into the Cryogenian (760-635 Ma) and 29% being Ediacaran (635-577 Ma). The youngest detrital zircon population is 579 ± 7 Ma (n=4, MSWD=0.43).

3.1.2 ACO-12-27 (High Head Member)

Sample ACO-12-27 is taken from a gritty, medium grained sandstone of the early Cambrian High Head Member (Fig. 4). ACO-12-27 had 71 analyses conducted on 71 detrital zircon grains, of which 65 are 90-110% concordant. All of the grains are restricted to Neoproterozoic ages covering a continuous population between 702-549 Ma. The dominant population are Ediacaran (81%) falling between 635-549 Ma. the remainder of the zircons are 635-702 Ma. The youngest detrital zircon population is 551 ± 8 Ma (n=3, MSWD=0.076).

3.1.3 ACO-12-20b (Green Harbour Formation)

Sample ACO-12-20b is taken from a feldspathic, fine grained greywacke of the Cambrian Green Harbour Formation (Fig. 4). ACO-12-20b had 80 analyses conducted on 80 detrital zircon grains, of which 51 are 90-110 % concordant (Fig. 4). The sample is dominated by Neoproterozoic zircons (54%), of which 31% span the Ediacaran (542-635 Ma) and 24% are Cryogenian (635-780 Ma). Paleoproterozoic zircons are 24% of the total concordant grains and form two major populations; one at 1950-2180 Ma and the second at 2400-2800 Ma. There are minor Archean populations (11%) at 2620-2640 Ma, 2970-3075 Ma and a single zircon at 3305 ± 19 Ma. A single zircon records a Tonian age (870 ± 9 Ma). The youngest detrital zircon population is 591 ± 6 Ma (n=4, MSWD= 0.44).

3.1.4 ACO-12-22a (Government Point Formation)

Sample ACO-12-22 is taken from medium grained quartz sandstone of the middle Cambrian Government Point Formation (Fig. 4). ACO-12-22a had had 80 analyses conducted on 80 detrital zircon grains, of which 70 are 90-110 % concordant (Fig. 4). The dominant population of detrital zircons are Ediacaran (44%) spanning a continuous spread between 548 and 632 Ma. Cryogenian zircon grains are 24% of the total concordant population and define minor peaks at 640-670 Ma and 720-745 Ma. Minor populations of Cambrian (11%) and Paleoproterozoic (11%) zircons define peaks at 530-540 Ma and 2000-2100 Ma. Individual Archean zircons records ages at 2505 ± 18 Ma, 2725 ± 17 and 2751 ± 19 Ma. Individual Tonian zircons are recorded at 887 ± 10 and 898 ± 9 Ma. The youngest detrital zircon population is 535 ± 5 Ma (n=6, MSWD=0.64).

3.1.5 ACO-12-28a (White Rock Formation)

ACO-12-28a is take from a pebbly conglomerate of the Silurian White Rock Formation. ACO-12-28a had 80 analyses conducted on 80 detrital grains, of which 41 are 90-110% concordant (Fig. 4). The sample contains zircon populations that are Cambrian (12%), Ediacaran (34%) and Paleoproterozoic (12%). Within these populations the zircon distribution patterns define major peaks at 550-580 Ma, minor peaks at 525-540 Ma and 2000-2100 Ma. Single Mesoproterozoic zircons are recorded at 1043 ± 26 and 1288 ± 23 Ma as well as a single Archean zircon (2777 ± 17 Ma). The youngest detrital zircon population is 539 ± 7 Ma (n=3, MSWD=0.068).

3.1.6 ACO-12-25 (White Rock Formation)

ACO-12-25 is taken from a medium grained sandstone of the Silurian White Rock Formation. ACO-12-25 had 85 analyses conducted on 85 detrital grains, of which 56 are 90-110% concordant (Fig. 4). The sample contains zircon populations that are Cambrian (14%), Ediacaran (24%), Cryogenian (12%), Mesoproterozoic (11%) and Paleoproterozoic (30%). Within these populations the zircon distribution patterns defines a major peak at 550-620 Ma, and minor peaks at 510-540 Ma, 640-680 Ma, 1760-1900 Ma and 2030-2200

Ma. Single Tonian zircons are recorded at 905 ± 10 and 950 ± 10 Ma, as well as single Archean zircons at 2507 ± 19 Ma and 2974 ± 21 Ma and a single Silurian zircon at 430 ± 4 Ma. The youngest detrital zircon population is 514 ± 6 Ma (n=4, MSWD=0.37).

3.2 U-Pb zircon geochronology for Silurian-early Devonian Avalonian rocks

3.2.1 ACO-12-45 (Beechill Cove Formation)

Sample ACO-12-45 is fine-grained sandstone taken from the Silurian Beechill Cove Formation (Fig. 5). Sixty analyses were conducted on sixty detrital zircons; of these forty-five are concordant. The sample is dominated by Neoproterozoic (71%) grains with minor Paleoproterozoic (20%) and Cambrian populations (11%). The zircon distribution patterns define a broad peak at 520-650 Ma and minor peaks at 800-850 Ma and 2100-2150 Ma. Singular zircons are dated at 2800 ± 27 Ma, 3439 ± 26 and 487 ± 8 Ma. The youngest detrital zircon population is 543 ± 8 Ma (n=4, MSWD=0.43).

3.2.2 ACO-12-37 (MacAdam Formation)

Sample ACO-12-37 is fine-grained sandstone taken from the Silurian MacAdam Formation (Fig. 5). Eighty analyses were conducted on eighty detrital zircons; of these seventy-three are concordant. The sample is dominated by Neoproterozoic (53%) grains with large Mesoproterozoic (23%) and Paleoproterozoic (12%). Two Cambrian (513, 525 Ma), two Silurian (444, 453 Ma) and three Devonian (387, 433, 440 Ma) zircon grains were also analysed. The zircon distribution patterns define a broad peak at 520-670 Ma and narrow peaks at 430-450 Ma, 700-760 Ma, 950-1080 Ma, 1150-1250 Ma and 1850-1950 Ma. Single zircons are scattered in the Mesoproterozoic (1330 ± 27 Ma, 1362 ± 35, 1396 ± 46 Ma), Paleoproterozoic (1755 ± 39 Ma, 2034 ± 27, 2073 ± 31 and 2199 ± 26 Ma). The youngest detrital zircon population is 440 ± 7 Ma (n=3, MSWD=0.61).

3.2.3 ACO-12-33 (Knoydart Formation)

Sample ACO-12-33 is a medium-grained, red sandstone taken from the Devonian Knoydart Formation (Fig. 5). Forty-seven analyses were conducted on forty-seven detrital zircons; of these thirty-five are concordant. The detrital zircon spectra from the sample is complex covering the Devonian through to the Archean (Fig. 5). The largest population comes from Neoproterozoic zircons (28%) whereby zircons fall broadly into two peaks at 560-620 Ma and 930-950 Ma. Single zircons are also dated at 718 ± 11 Ma and 850 ± 14 Ma. Devonian and Ordovician zircons both form 15% of the detrital zircon spectra with peaks at 397-413 Ma and 447-477 Ma, respectively. Three Silurian zircons were also analysed (418 ± 6, 425 ±6, 425 ± 6 Ma) as well as one Cambrian zircon (511 ± 7 Ma). Mesoproterozoic zircons (11%) are scattered between 1012 and 1483 Ma. Paleoproterozoic zircons (9%) are scattered between 1688 and 2093 Ma. Archean zircons (11%) are dated at 2536 ± 26, 2700-2740 and 2683 ± 29 Ma. The youngest detrital zircon population is 413 ± 6 Ma (n=4, MSWD=0.44).

3.2.4 ACO-12-30A (McArras Brook Formation)

Sample ACO-12-30a is a gritty, sandstone taken from the early Devonian McArras Brook Formation (Fig. 5). Sixty analyses were conducted on sixty detrital zircon grains; of these all sixty are concordant. The detrital zircon spectrum is dominated by Ediacaran (28%), Cambrian (18%) and Devonian grains (27%). Minor populations of Silurian (10%) and Mesoproterozoic (7%) are also documented. There are two Ordovician zircons dated at 444 ± 5 and 480 ± 6 Ma. The zircon distribution patterns define peaks at 397-430 Ma, 520-560 Ma and 590-620 Ma. The youngest detrital zircon population is 403 ± 4 Ma (n=7, NSWD=0.84).

3.3 U-Pb zircon geochronology Devonian-Carboniferous sedimentary rocks

3.3.1 ACO-12-43 (Barrens Formation)

Sample ACO-12-43 is a quartzite from the late Devonian-early Carboniferous Barrens Formation in the St Marys Basin. Eighty analyses were conducted on eighty detrital zircons, of which seventy-four are concordant (Fig. 6). The sample is dominated by Devonian (36%) and Ediacaran zircons (32%), with minor populations of Cambrian (5%), Cryogenian (6%) Mesoproterozoic (5%), Paleoproterozoic (9%). The zircon distribution patterns define peaks at 360-395 Ma, 520-540 Ma, 570-640 Ma, 1160-1210 Ma and 2020-2100 Ma. Single zircons are also analysed at 772 ± 9 Ma, 915 ± 10 Ma, 1029 ± 3 Ma, 1520 ± 31 ad 2426 ± 23 Ma. The youngest detrital zircon population is 362 ± 3 Ma (n=14, MSWD=0.54).

3.3.2 ACO-12-42b (Cross River Formation)

Sample ACO-12-42b is a conglomerate from the late Devonian-early Carboniferous Cross River Formation in the St Marys Basin. Eighty analyses were conducted on eighty detrital zircons, of which fifty-three are concordant (Fig. 6). The sample is dominated by Ediacaran zircons (49%) that form a broad peak between 530-620 Ma. Devonian (15%) and Cryogenian (13%) zircons form moderate populations between 360-400 Ma and 640-715 Ma, respectively. Scattered Paleoproterozoic zircons are dated at 1785 ± 27 Ma, 1995 ± 29 Ma, 2070-2110 Ma, and 2249 ± 23 Ma. Two Silurian (438 ± 5, 441 ± 7 Ma) and two Cambrian (514 ± 6, 525 ± 6 Ma) were also analysed. The youngest detrital zircon population is 362 ± 5 Ma (n=3, MSWD=0.6).

3.3.3 ACO-12-32c (Lismore Formation)

Sample ACO-12-32c is coarse-grained sandstone taken from the Carboniferous Lismore Formation. Ninety-Six analyses were conducted on ninety-six detrital zircon grains; of these seventy-eight zircons are concordant (Fig. 6). The detrital zircon spectra is complex, ranging from the Carboniferous (343 Ma) to the Paleoproterozoic (2040 Ma). The largest populations are Devonian (20%), Ediacaran (23%) and Mesoproterozoic (18%). Minor populations of Cambrian (13%), Cryogenian (9%) and Paleoproterozoic (13%) are also noted. Accessory Carboniferous (343 ± 5 Ma, 351 ± 5 Ma), Silurian (420 Ma), Ordovician (450-475 Ma) and Tonian (850 Ma, 933 ± 10 Ma) zircons complete the complex signature. Within the major detrital zircon distribution patterns are the following defined peaks; 400-425 Ma, 470-540 Ma, 550 Ma and 600-650 Ma. The youngest detrital zircon population is 413 ± 4 Ma (n=9, MSWD= 0.14).

3.3.4 ACO-12-51 (Graham Hill Formation)

Sample ACO-12-51 is a fine grained sandstone from the Carboniferous Horton Group. Eighty analyses were conducted on eighty detrital zircons; of these sixty-five are concordant (Fig. 6). The detrital zircon spectrum is complex and covers the Carboniferous to the Archean. The largest population is Ediacaran (35%), with smaller Carboniferous (13%), Cryogenian (13%), Mesoproterozoic (9%) and Paleoproterozoic (7%) populations. Accessory Silurian and Ordovician populations were also analysed (5%). The detrital zircon patterns form peaks at 370-410 Ma, 430-450 Ma, 540-650 Ma, 660-700 Ma, 1420 Ma, 1620 Ma and 2060-2080 Ma. Single zircons are also date at 780 ± 10 Ma, 858 ± 11 Ma, 1048 ± 24, 1131 ± 40 Ma, 1306 ± 40 Ma, 1777 ± 55, 2533 ± 20 and 2882 ± 26 Ma. The youngest detrital zircon population is 380 ± 5 Ma (n=3, MSWD=0.95).

3.3.5 ACO-12-44a (Stellarton Basin Group)

Sample ACO-12-44a is coal-bearing sandstone taken from the Carboniferous

Stellarton Basin Group. One hundred and thirty-nine analyses were conducted on one hundred and thirty-nine detrital zircon grains; of these only seventy-one zircons are concordant (Fig. 6). The detrital zircon spectra is complex but is limited to a wide interval covering the Carboniferous (308 Ma) to mid-Mesoproterozoic (1377 Ma). One Paleoproterozoic zircon (2364 ± 30 Ma) was analysed. The largest detrital population is Cryogenian (23%), which forms a broad peak at 640-750 Ma. There are also minor Ordovician (17%), Silurian (14%), Devonian (14%), Carboniferous (12%), Ediacaran (12%) and Mesoproterozoic (10%) populations. The zircon distribution patterns define a broad peak at 380-460 Ma, 520-570 Ma, 630-660 Ma, 730-750 Ma, 1035 Ma and 1330-1380 Ma. The youngest detrital zircon population is 410 ± 5 Ma (n=4, MSWD=0.92).

3.3.6 ACO-12-56b (Cribbons Point Formation)

Sample ACO-12-56b is coal-bearing sandstone taken from the late Carboniferous Cribbons Point Formation. Seventy analyses were conducted on seventy detrital zircon grains; of these only twenty-eight zircons are concordant (Fig. 6). The small percentage of zircons that are concordant are scattered between the Carboniferous (338 Ma) and the late Paleoproterozoic (2492 Ma). Paleoproterozoic zircons form the largest percentage of concordant grains (28%) and form a peak at 1965-2100 Ma and single ages at 2328 ± 20 and 2492 ± 22 Ma. Ediacaran and Cryogenian zircons form a broad peak at 580-660 Ma. Devonian and Carboniferous zircons are scattered between 338-400 Ma. Two Mesoproterozoic zircons are dated at 1104 ± 45 and 1457 ± 27 Ma. The youngest detrital population (n=>3) is 623 ± 6 Ma (n=4, MSWD=0.089).

3.4 U-Pb zircon geochronology for igneous rocks

3.4.1 ERG-14 (Economy River Gneiss)

Sample ERG-14 is a K-feldspar, biotite bearing granitic gneiss from the Cryogenian Economy River Gneiss. A total of fifty analyses were obtained from prismatic, euhedral zircons (Fig. 7) extracted from the sample, with 48 in totally that are concordant. The 206Pb/238U weighted average age of the dominant population is 735 ± 3 Ma (MSWD=0.47).

3.4.2 ACO-13-17 (Clarenville Granite)

Sample ACO-13-17 is porphyryblastic K-feldspar bearing granite from the Clarenville suite. A total of 30 analyses were obtained from subhedral zircons extracted from the sample, with twenty-four that are concordant (Fig. 7). The 206Pb/238U weighted average age of the dominant population is 607 ± 3 Ma (MSWD=0.99).

3.4.3 ACO-13-21 (Dunn Pt. Formation)

Sample ACO-13-21 is a fine grained, pink rhyolite from the Dunn Point Formation (Fig.7). Only twenty zircons were extracted from the sample, and twenty analyses were obtained from these zircon grains. Of the twenty grains nineteen are concordant. Previous age constraints indicate the Dunn Pt. rhyolite crystallised at 460Ma (Hamilton and Murphy, 2004), and the dominant zircon population (n=9) overlaps with this (466 ± 6 Ma, MSWD= 0.17). Three zircons are younger than 466 Ma (395 ± 5 Ma, 400 ± 5 Ma, 443 ± 6 Ma). The remainder of the zircons are a single Cambrian (512 ± 6 Ma), three Ediacaran (563 ± 7, 572 ± 7 and 621 ± 7 Ma) and a single Mesoproterozoic grain (1592 ± 17 Ma). As the youngest zircons do not form a statistically significant population they cannot be considered the crystallisation age of the rhyolite.

3.4.4 ACO-13-16 (Deadmans Bay)

Sample ACO-13-16 is a megacrystic

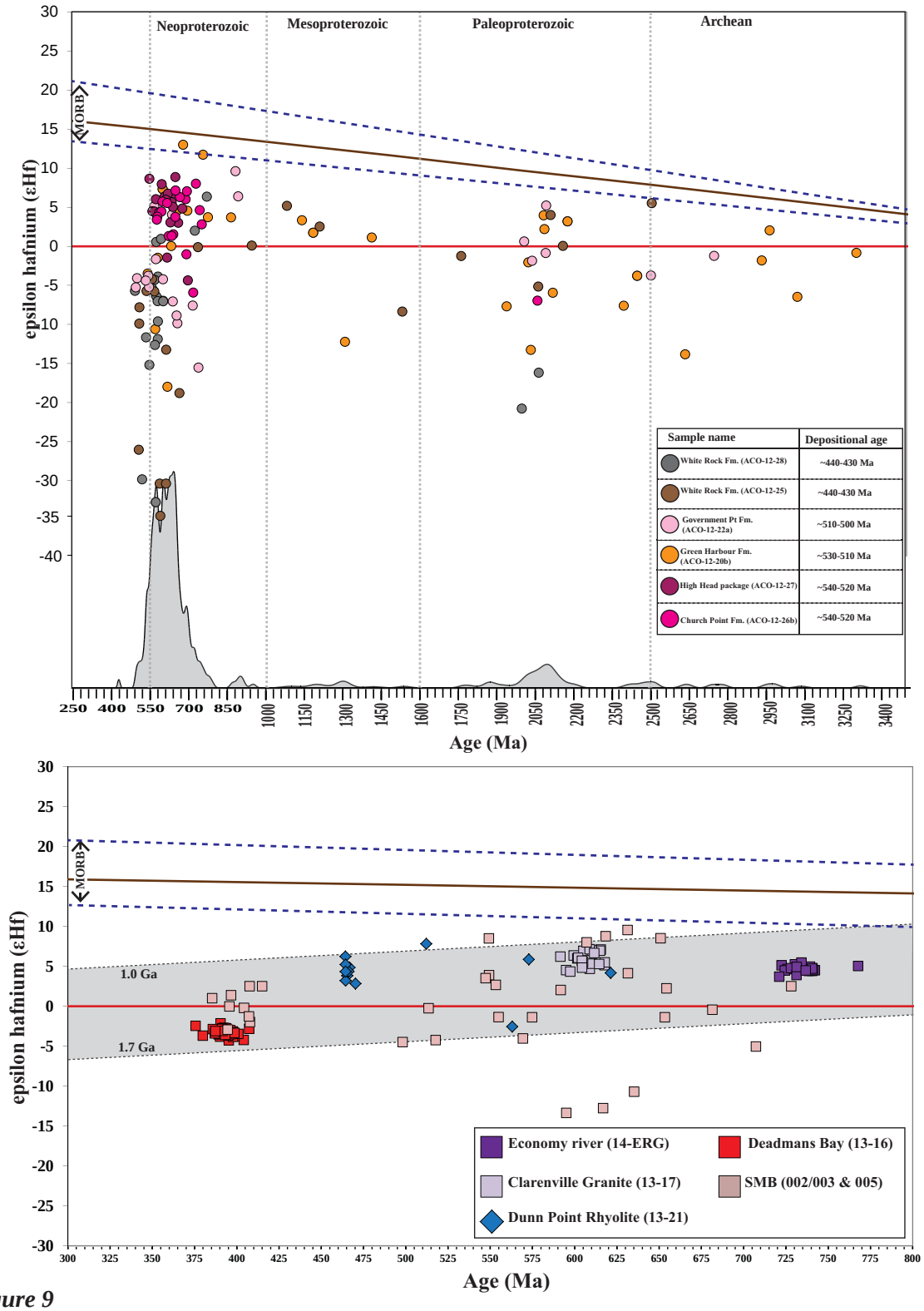

Figure 9

A) εHf values plotted against the U-Pb ages for individual zircon grains from the Meguma Cambrian-Silurian sedimentary rock. The crustal evolution limits were projected to the depleted mantle curve using Lu/Hf ratio of average crust (0.015, Griffin et al., 2004), CHUR= chondritic uniform reservoir. The field defined for the depleted mantle array and MORB is from Dhuime et al., (2011) and Griffin et al., (2004), and are also illustrated in Figures 10, 11 and 15. The grey field defines the cumulative detrital zircon spectra. B) εHf values plotted against the U-Pb ages for magmatic zircon grains from the Economy River Gneiss, Clarenville Granite, Deadmans Bay granite, Dunn Point Rhyolite and two samples from the South Mountain Batholith.

granite from the Devonian Deadmans Bay suite. A total of forty analyses were conducted on the zircons extracted from the sample, with thirty-seven that are concordant (Fig. 8). The weighted average of the dominant population is 393 ± 2 Ma (MSWD=0.56), with a small population of outliers at ~375 Ma and ~405 Ma.

3.4.5 BH-002/003 and BH-005 (South Mountain Batholith)

Sample BH-002/003 and Sample BH-005 are from the Devonian South Mountain Batholith (Fig. 8). A total of twenty-seven analyses were conducted on sample BH002/003 and of these twenty-one were concordant. The recorded age for the South Mountain Batholith is ~380-360 Ma (Clarke and Halliday, 1980; Tate and Clarke, 1997; Clarke et al., 2000; MacLean et al., 2003; Moran et al., 2007), but no zircons of this age were extracted from the sample. Therefore, it is likely that all the zircons in the granite (BH-002/003) are inherited. The youngest population is 401 ± 6 Ma (n=5, MSWD=0.99). There are scattered zircons that record Cambrian, (500 Ma), Ediacaran (590-635 Ma) and Cryogenian (650 Ma, 730 Ma) ages. Paleoproterozoic zircons were dated at 1757 ± 23 Ma, 1997 ± 21 Ma and 2143 ± 22 Ma. A single Tonian (896 ± 13 Ma), Mesoproterozoic (1262 ± 24 Ma) and Archean (3150 ± 20 Ma) zircon were also analysed.

In sample BH-005 sixty analyses were conducted on sixty zircons; of which forty-five are concordant (Fig. 8). The youngest zircon grains analysed do not form a statistical population and are dated at 374 ± 6 Ma, 385 ± 6 Ma, 390 ± 5 Ma and 396 ± 6 Ma. The remainder of the inherited zircon grains are dominated by Ediacaran zircons (38%) that form a broad population between 547-630 Ma. Minor populations of Cambrian (498-520 Ma), Cryogenian (650-800 Ma) and Paleoproterozoic (1780 Ma, 2050-2150 and 2380 Ma) zircons are noted. Single Mesoproterozoic (1132 ± 30 Ma) and Archean zircons (2853 ± 20 Ma) are also analysed.

4. RESULTS HAFNIUM ISOTOPES

A total of 531 Lu-Hf isotopic analyses were obtained from the early Cambrian-Silurian clastic sequences from Meguma, Ordovician-Carboniferous clastic sequences from Avalonia and the Avalonia-Meguma boundary and the Neoproterozoic- Devonian igneous rocks. Full data tables are presented in the supplementary data. Hafnium data for Meguma rocks and igneous rocks is presented in Figure 9, and for the Ordovician-Carboniferous Avalonia/Meguma rocks in Figure 10.

4.1 Meguma hafnium isotopic array

4.1.1 Church Point and High Head hafnium results

Sample ACO-12-26b and ACO-12-27 are from the Church Point and High Head members, respectively. The detrital zircon spectra range from ~750-550 Ma, with one Paleoproterozoic zircon analysed in the Church Point member (2063 Ma, εHf= -7). Of the ~750-550 Ma zircons 89% record a positive epsilon hafnium value (i.e. above 0), with only four zircons returning a negative epsilon hafnium value (Fig. 9a). The εHf value of the ~750-550 Ma zircons ranges between +9 and -5, with an average εHf value of +5. The crustal depleted mantle model ages for the ~750-550 Ma range from 1.9 to 0.95 Ga, with the majority of the ~750-550 Ma zircons recording a TDMc of 1.0-1.3 Ga. The hafnium isotopic data for the Church Point and High Head members indicate the magmatic source for the zircons was predominantly juvenile with contamination from a Mesoproterozoic-early Neoproterozoic crustal source.

4.1.2 Government Point and Green Harbour Formations hafnium results

Sample ACO-12-20b and ACO-12-22 are from the Green Harbour Formation and Government Point Formation, respectively. The Neoproterozoic zircons fall broadly into three populations; a dominant peak at 550-680 Ma and smaller peaks at 750-780 Ma and 860-880 Ma. The Neoproterozoic zircons record wide range of εHf values between -32 and +12. Of these, 60% record negative εHf values (Fig. 9a). The hafnium isotopic array from the ~870-550 Ma zircons records an interval of progressively increased crustal recycling. The early-mid Neoproterozoic zircons ~880-700 Ma are predominantly juvenile (εHf= +10 to +5) with the exception of 2 grains at ~750 Ma (εHf= -10 to -15). Zircons crystallised in the interval between ~650-550 Ma record mixing between juvenile and ancient crust (εHf= +4 to -32), but the majority are evolved. Extremely negative zircons (εHf= -32) indicate the recycling of Archean crust (TDMc= 3.3 Ga).

The majority of the zircons in the ~650-550 Ma population indicate recycling of Paleoproterozoic-Mesoproterozoic (TDMc= 2.1- 1.0 Ga) crust with variable juvenile input. Government Point Formation records a population of Mesoproterozoic-early Paleoproterozoic zircons (~1150-1450 Ma) that are not recorded in the Green Harbour Formation. The ~1000-1450 Ma zircons are juvenile (εHf= 0 to +5) and indicate recycling of Paleoproterozoic crust (TDMc= 2.1- 1.8 Ga). Both the Government Point and Green Harbour Formations record a large Paleoproterozoic population (~1950-2150 Ma). The ~1950-2150 Ma form a vertical mixing array that indicates recycling of Archean and juvenile Paleoproterozoic crust (εHf= +5 to -13). Scattered late Paleoproterozoic-Archean zircons (2350-3300 Ma) record highly variable εHf values that are predominantly evolved (εHf= +2 to -15) and all indicate the recycling of ancient Mesoarchean-Paleoarchean crust (TDMc= 3.1- 3.9 Ga).

4.1.3 White Rock Formation hafnium results

Sample ACO-12-25 and sample ACO-12-28a are from the Silurian White Rock Formation. The detrital zircon spectra from both samples are complex; dominated by early Cambrian and Neoproterozoic (~500-750 Ma) zircons with minor populations of Mesoproterozoic (~1000-1500 Ma), Paleoproterozoic (2000-2150 Ma) and Archean (~2500-2900 Ma) grains (Fig. 9a). The populations are similar to those recorded in the Government Point and Green Harbour Formations, although εHf values extend to much greater negative values (-25 to -35). The mid-late Neoproterozoic (~550-750 Ma) and Cambrian (~500-540 Ma) zircon populations are overwhelmingly evolved (90%) with a range of εHf values between -35 and +6. The majority of the ~500-750 Ma zircons record εHf values between -20 and 0, which correspond to TDMc of 2.7- 1.3 Ga. Two zircons at 905 and 950 Ma record contrasting εHf values of -27 and 0, respectively. Late Mesoproterozoic zircons (1000-1200 Ma) straddle CHUR (εHf= 0 to +5) and an early Mesoproterozoic zircon at 1536 Ma is evolved (εHf= -10). Paleoproterozoic zircons (2000-2150 Ma) form a vertical mixed array between juvenile and Archean crust (εHf= +5 to -23), which correspond to TDMc of 1.6- 3.9 Ga.

4.3 Hafnium isotopic data for igneous rocks

4.3.1 Neoproterozoic granite results

Sample ACO-14-ERG is from the 735 ± 3 Ma Cryogenian Economy River Gneiss, located in Avalonia (Fig.3). All the zircon grains analysed yield a consistent measured 176Hf/177Hf ratios of 0.282441 - 0.282498 and initial 176Hf/177Hf ratios of 0.282434-0.282442, which correspond to εHf values of 3.9 to 5.5. The TDMc for the zircon grains is 1.25-1.38 Ga.

Sample ACO-13-17, the Clarenville Granite from the Avalon terrane,

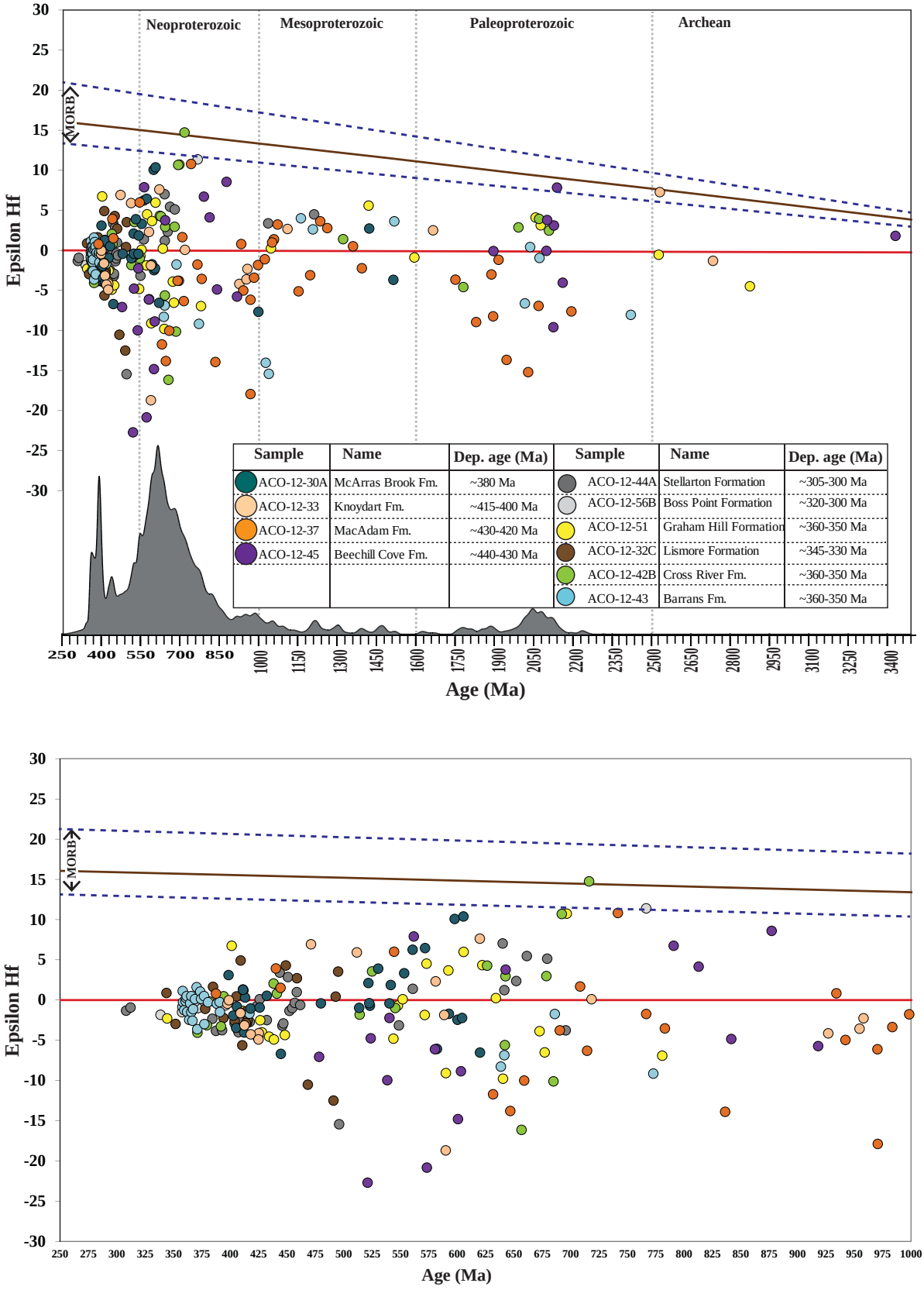

Figure 10

A) εHf values plotted against the U-Pb ages for individual zircon grains from the Paleozoic sedimentary rocks from the northern Appalachians. The grey field defines the cumulative detrital zircon spectra. B) εHf values plotted against the U-Pb ages for individual zircon grains showing only zircons 1000-250 Ma from the Paleozoic sedimentary rocks from the northern Appalachians.

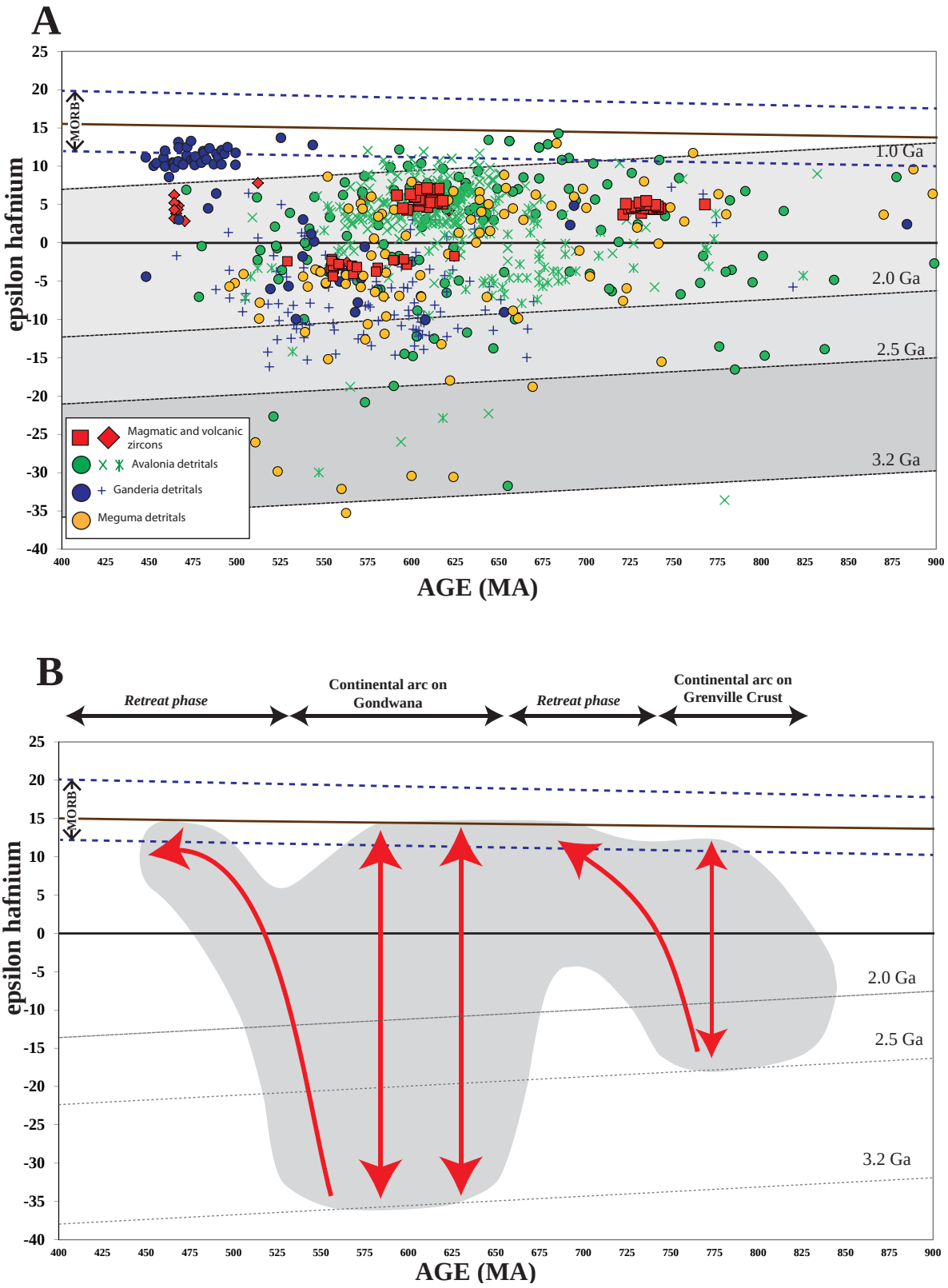

Figure 11

A) εHf values plotted against the U-Pb ages for all available ~900-450 Ma zircons from Avalonia, Ganderia and Meguma. Included are published zircon data Willner et al. (2013, 2014) and Pollock et al. (2015). The grey fields define the crustal evolution projected to the depleted mantle curve using Lu/Hf ratio of average crust (0.015, Griffin et al., 2004). B) The grey field defines the shape of the evolutionary array during the Neoproterozoic-early Paleozoic evolution of Avalonia, Meguma and Ganderia. The red arrays indicate the evolving trend of the hafnium array during an evolving tectonic regime.

Newfoundland, has a crystallisation age of 607 ± 3 Ma. Zircon grains yield a very consistent measured 176Hf/177Hf ratios of 0.282545-0.282650 and initial 176Hf/177Hf ratios of 0.282531- 0.282603, which correspond to εHf values of 4.3 to 7.1 (Fig. 9b). The TDMc for the zircon grains is 1.08-1.25 Ga.

4.3.2 Ordovician to Devonian igneous rocks

A rhyolite from the Ordovician Dunn Point Formation (ACO-13-21), from Avalonia, has a crystallisation age of 466 ± 6 Ma. Zircons from the dominant ~465-460 Ma population yield εHf values between +6 and +3 (Fig. 9b), corresponding to the TDMc of 1.0 to 1.25 Ga. Cambrian-Ediacaran zircons (~515-620 Ma) yield variable εHf values between -2 and -8.
The Deadmans Bay granite (ACO-13-16), in the Gander Zone has a crystallisation age of 393 ± 2 Ma. All the zircon grains have a consistent measured 176Hf/177Hf ratios of 0.282427-0.282492 and initial 176Hf/177Hf ratios of 0.282416- 0.282478, which correspond to εHf values of -2.2 to -4.3 (Fig. 9b). The T(DM)c for the ~395 Ma population is 1.51 to 1.63 Ga. It has no measured inherited cores.

The Carboniferous South Mountain Batholith samples (BH-002/003 and BH-005) from Meguma did not yield a statistically sufficient population that can be considered the crystallisation age of the rocks. The youngest zircons are ~385-400 Ma, similar to the Deadmans Bay granite, and record very consistent εHf values of -2.9 to +2.5 (Fig. 9b). The T(DM)c for the ~400-385 Ma population is 1.20-1.55 Ga .Ediacaran- Cryogenian (~590-730 Ma) inherited zircons in the SMB yield variable εHf values of -13 to +10, corresponding to T(DM)c of 0.95-2.3 Ga. Single Tonian and Mesoproterozoic zircons (896 Ma, 1262 Ma) yield εHf values of +8 and +1, respectively. Paleoproterozoic zircons (~1780-2380 Ma) are variable recording εHf values of -14 to +5, and a single Archean zircon (2853 ± 20 Ma) straddles CHUR at εHf= 0.

4.4 Paleozoic hafnium isotopic results

The Silurian-Carboniferous rocks from Avalonia (and composite Avalonia/Meguma) comprise similar detrital populations, so the hafnium isotopic array is considered as a single entity (Fig. 10). The dominant zircon populations (Figs. 5, 6) include broad Neoproterozoic (~800-550Ma), Ordovician ~470-450 Ma, Devonian 400-360 Ma and Paleoproterozoic ~1950-2150 Ma peaks. Minor Mesoproterozoic (~1000-1150 Ma, ~1200-1350 Ma and ~1450-1550 Ma), Paleoproterozoic (~1750-1900 Ma) and Archean (~2500-2750 Ma) peaks are also noted.

Paleoproterozoic zircons (~1950-2150 Ma) form a vertical array with εHf values of +9 to -17 and corresponding model ages of 2.2 to 3.6 Ga, similar to Paleoproterozoic zircons in the Neoproterozoic sedimentary rocks (Fig. 10). The entire Mesoproterozoic is defined by reworking of Paleoproterozoic crust, as the hafnium data lie along a typical crustal reworking array (Lu/Hf=0.015), with model ages (TDMc) constrained between 1.7-2.2 Ga. At the Neoproterozoic-Mesoproterozoic boundary, a few zircons are very evolved (εHf= -17 to -15) and have Archean model ages. There are also a small percentage of zircons between ~1000-900 Ma that form a continuation of the dominant Mesoproterozoic crustal reworking array.

Neoproterozoic zircons (~800-550 Ma) yield a variable hafnium isotopic array. Zircons dated at ~850-775 Ma are a mix from Paleoproterozoic and juvenile crustal sources (εHf= -15 to +10), that corresponds to model ages of ~2.0 to 0.95 Ga. In the ~775-680 Ma interval, zircons are generally more juvenile recording εHf values of 0 to +14, with a small number of zircons recording negative εHf values of 0 to -10. Between ~650-525 Ma zircon grains record a mixing array between Archean crust (TDMc= 2.6-2.8 Ga) and

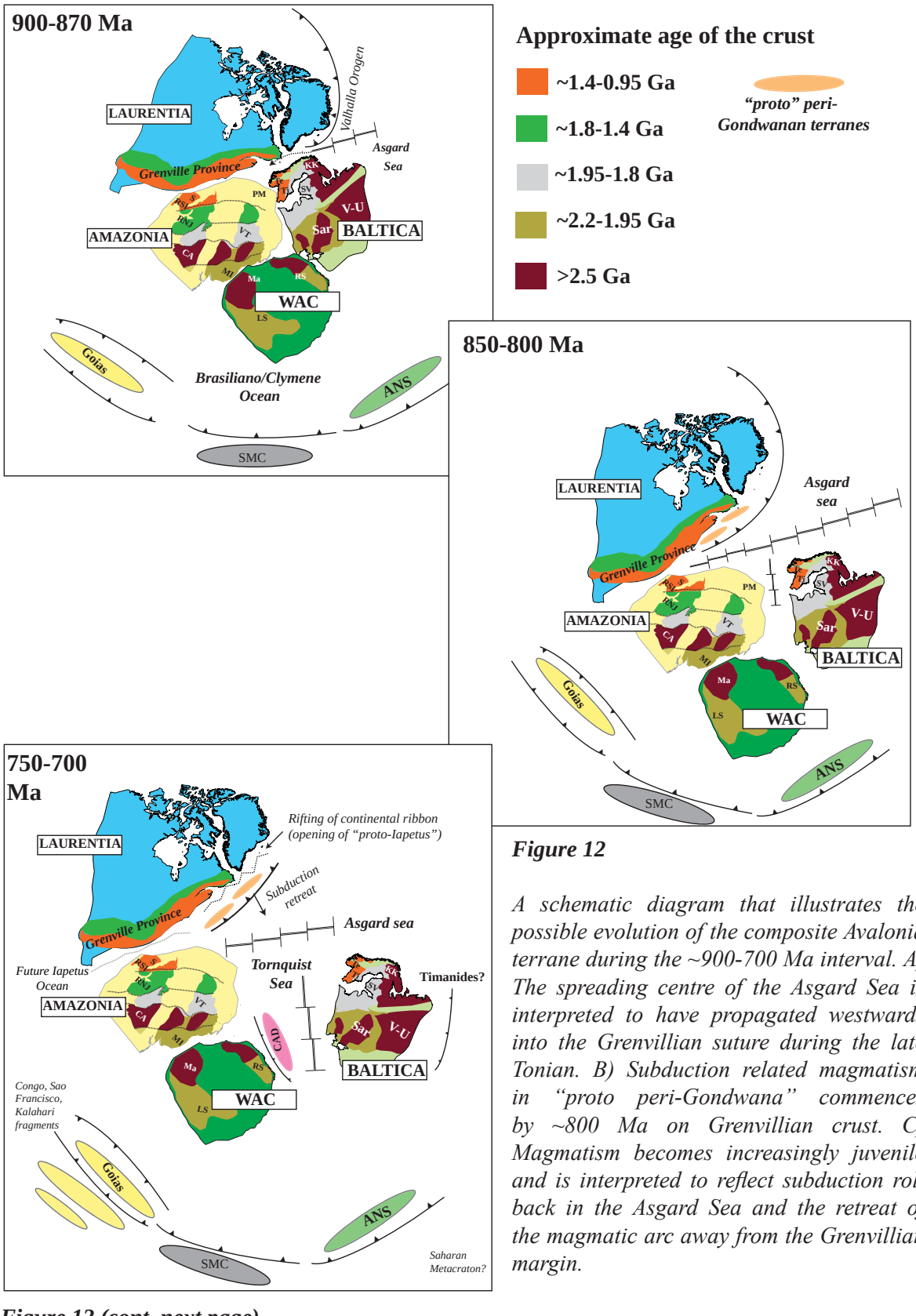

Figure 12

A schematic diagram that illustrates the possible evolution of the composite Avalonia terrane during the ~900-700 Ma interval. A) The spreading centre of the Asgard Sea is interpreted to have propagated westwards into the Grenvillian suture during the late Tonian. B) Subduction related magmatism in "proto peri-Gondwana" commences by ~800 Ma on Grenvillian crust. C) Magmatism becomes increasingly juvenile and is interpreted to reflect subduction roll back in the Asgard Sea and the retreat of the magmatic arc away from the Grenvillian margin.

Figure 13 (cont. next page)

A schematic diagram that illustrates the possible evolution of the composite Avalonia terrane during the ~650-450 Ma interval. A) By ~650 Ma the peri-Gondwanan ribbon had arrived at the northern Gondwanan margin closing the Asgard Sea. The hafnium isotopic array is interpreted to indicate the accretion of the continental ribbon to the Gondwanan margin and the stepping outboard of subduction into the ocean.

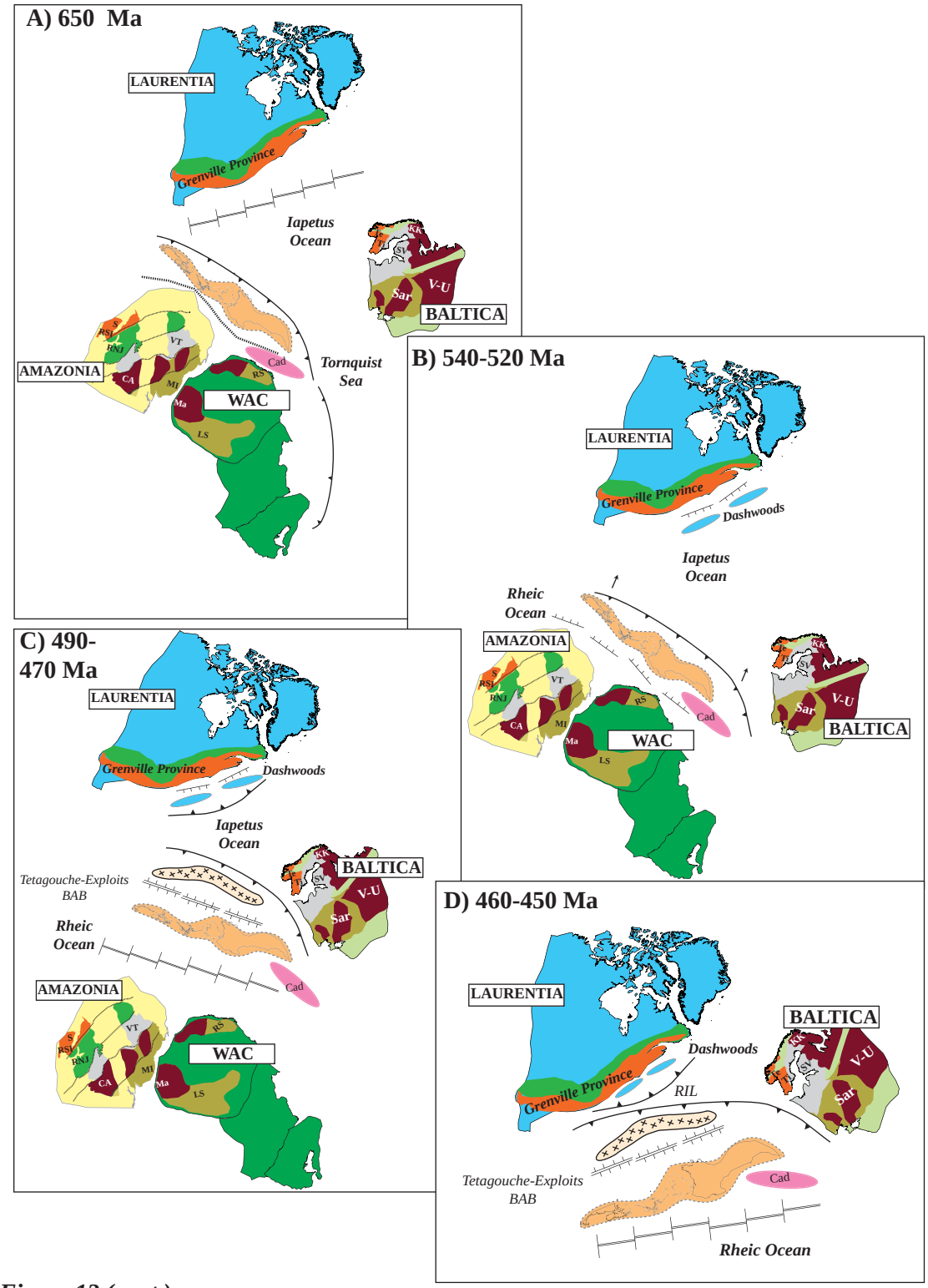

Figure 13 (cont.)

B) Hafnium isotopes record a transition towards increasingly positive εHf values between ~550-500 Ma, which is interpreted to indicate a retreating subduction zone. The composite Avalonian terrane is rifted away from the Gondwanan margin, opening the Rheic Ocean in its wake. C) During the transfer of composite Avalonia across the Iapetus Ocean magmatism was ongoing in the leading arc system, best represented by the exclusively juvenile Popelogan-Victoria arc in Ganderia. D) The arrival of the leading edge of the peri-Gondwanan ribbon (Ganderia) is recorded in late Ordovician (~450 Ma) overstep sequences in the Exploits Subzone of Newfoundland. Magmatism in the Notre Dame and Popelogan-Victoria arcs largely shuts down by ~450 Ma during the final closure of Iapetus.

juvenile material (TDMc=0.9-1.0 Ga).

From the late Cambrian to late Carboniferous the hafnium isotopic array records a contraction towards CHUR. The hafnium isotopic data shifts from mixing between quite juvenile (εHf= +7) and Archean crust (εHf= -25 to -15) at ~525 Ma to simultaneously reducing the ancient crustal and juvenile input between ~525-300 Ma. The overall effect is a very restricted hafnium isotopic array in the late Paleozoic, which forms an "arrowhead" pattern . During the ~425-300 Ma interval, all data falls in a band that yields εHf values between -5 and +5, corresponding to model ages of 1.7 to 1.0 Ga.

5. DISCUSSION

5.1 Interpretation of the hafnium isotopic arrays

5.1.1 Meguma hafnium isotopic array

The Meguma detrital zircon spectra is dominated by a broad Cryogenian-Ediacaran population (~500-800 Ma) and minor populations at ~850-950 Ma, 1150-1300 Ma, 1750-1850 Ma, 2000-2200 Ma, 2400-2550 Ma, 2750 Ma, 2950 Ma and 3000 Ma. The early Cambrian Church Point Formation and High Head Member are dominated almost exclusively by Cryogenian-Ediacaran zircons (750-550 Ma), whereas the early-mid Cambrian Green Harbour and Government Point Formations contain a much more complex detrital zircon spectra that includes the Mesoproterozoic, Paleoproterozoic and Archean populations (Fig. 9). The Silurian White Rock Formation contains zircon populations similar to the Green Harbour and Government Point samples, suggesting it has been recycled directly from the Cambrian Meguma rocks, without any younger zircon input. Overall, the detrital zircon data are consistent with previous studies of the Meguma metasedimentary rocks (Krogh and Keppie, 1990; Murphy et al., 2004b; Waldron et al., 2009).

Neoproterozoic detrital zircons in Meguma are interpreted to have been derived from either peri-Gondwanan arc terranes, such as Avalonia or Cadomia, or internal pan-African orogens that formed during the assembly of Gondwana (Waldron et al., 2009). The hafnium isotopic array produced by these zircons enables a comparison to be made with the potential sources. Cryogenian (~775-650 Ma) zircons predominantly record the recycling of Mesoproterozoic crust (TDMc = 1.0-1.6 Ga) with the majority of the zircons recording εHf values between 0 and +10. A small percentage of Cryogenian zircons also record mixing with Paleoproterozoic crust (εHf = -18 to -5, TDMc =2.0 Ga). Ediacaran-Cambrian zircons are significantly more evolved (εHf = -12 to -35) and indicate recycling of Archean crust (TDMc =2.5 to 3.2 Ga). The shift in the hafnium isotopic array suggest a change in the tectonic environment at ~650 Ma, leading to the introduction of an Archean crustal source into the magmatic system.

The Neoproterozoic Meguma hafnium array is similar to that of Avalonia and Ganderia (Willner et al., 2013; Willner et al., 2014; Pollock et al., 2015; Henderson et al., 2016; Henderson, in prep), indicating mixing between Archean and juvenile crust between ~650-525 Ma. The vertical mixing array in Avalonia and Ganderia is interpreted to indicate the onset of continental arc magmatism following the accretion of the terranes onto the northern Gondwanan margin (Murphy et al., 2013; Henderson et al., 2016). The similarities between the Neoproterozoic zircons from Meguma and those recorded in the Avalonian/Ganderian rocks indicate that they are all derived from the same continental-arc system of Avalonia and Ganderia.

Although Mesoproterozoic zircons form a minor percentage of the Meguma detritus (~5%) they persist throughout the Cambrian and Silurian rocks (Fig. 9a). The Mesoproterozoic isotopic array indicates

The 393 ±2 Ma Deadmans Bay Granite of Ganderia records restricted εHf values of -4 to -2 that also require a Mesoproterozoic crustal source. - The isotopic data are consistent with the Deadmans Bay granite being derived from the same source as the 565 Ma Cripple Back granite (Henderson et al., Submitted), confirming that the basement to Ganderia is composed of Mesoproterozoic-Paleoproterozoic crust.

The hafnium isotopic arrays for the inherited populations in the ~380-360 Ma South Mountain Batholith in the Meguma terrane are consistent with recycling from the late Neoproterozoic Avalonian basement. The youngest(~400-385Ma)populationofinherited zircons from the SMB record homogenous εHf values of -2 to +2, which correspond to model ages of 1.5 to 1.3 Ga. Neoproterozoic (~750-500 Ma) and Mesoproterozoic (~1100-1200 Ma) zircons. Neoproterozoic (~750-500 Ma) inherited zircons in the SMB also yield Mesoproterozoic- model ages (Fig. 9b). The exception are three zircons (~600, 625, 650 Ma) that all record Paleoproterozoic model ages (TDMc= 2.4-2.1 Ga). The model ages are all consistent with the isotopic record of ~750-500 Ma arc magmatism in Avalonia and Ganderia, including the excursion at~650-525 Ma during continental-arc magmatism (Henderson et al. 2016, Henderson et al. in prep). The SMB hafnium array supports the hypothesis that the SMB is generated from partial melting of Avalonian crust with minor assimilation from the Goldenville and Halifax Groups (Shellnutt and Dostal, 2015).

5.1.3 Paleozoic hafnium isotopic array

Broadly, the Ordovician-Carboniferous rocks from Avalonia/Meguma/Ganderia all have similar detrital zircon populations to each other, so the hafnium isotopic array is considered as a single entity (Fig. 10). A broad zircon population dominates the Neoproterozoic-early Paleozoic, spanning ~800-550 Ma. The hafnium isotopic record of ~800-500 Ma arc-magmatism is similar to that seen in the late Neoproterozoic Georgeville Group and the Cambrian clastic sequences of the Antigonish Highlands (Henderson et al., 2016). The Paleoproterozoic and Mesoproterozoic populations in the mid-late Paleozoic rocks are also similar to the hafnium isotopic array from the late Neoproterozoic-Cambrian Avalonian clastic sequences (Pollock et al., 2015; Henderson et al., 2016), suggesting recycling from the late Neoproterozoic zircons throughout much of the Paleozoic.

After ~550-525 Ma, a sharp excursion of negative εHf values towards CHUR is evident, coinciding with an excursion of positive εHf values towards CHUR yielding an "arrowhead" isotopic array at 430-300 Ma. It indicates that the~400-300 Ma magmas, and possibly the magma sources, were increasingly homogenised around CHUR values. The arrowhead array is intriguing as it coincides with the collision of the Gander margin, Avalonia and Meguma to the Laurentian margin (van Staal et al., 2009), yet none of these events create a disturbance in the hafnium isotopic record. The 'arrowhead' array does not fit with the hypothesis that the peri-Gondwanan terranes arrived separately to the Laurentian margin and were isolated from one another by individual ocean basins (Hibbard et al., 2007b; van Staal et al., 2009; Pollock et al., 2011). If this were the case, the hafnium isotopic array would record the development of continental-type arc mixing arrays along the composite Laurentian margin during each ocean closure event.

5.2 Neoproterozoic- Paleozoic evolutionary model for the Appalachians

The hafnium isotopic data presented here (Figs. 9, 10), as well as recently published compilations from Henderson et al. (2016, submitted), Pollock et al.(2015), Willner et al. (2013; 2014) allow the geological evolution of the Canadian Appalachians to be revaluated.

Previous studies have focused on the Sm-Nd whole rock isotopic data and U-Pb detrital zircon data to distinguish between the peri-Gondwanan terranes. However, the hafnium isotopic data from zircons provides a much more detailed insight into the relationship between the terranes. It indicates that the differences between Avalonia and Ganderia are minimal and suggest they may have shared a common history from the early-mid Neoproterozoic (Henderson et al., submitted). The following two sections will discuss a possible alternative evolutionary model for the Canadian Appalachians that covers the Neoproterozoic to early Paleozoic (part one) and the mid-late Paleozoic (part two). The models attempt to reconcile the existing geological framework with the hafnium isotopic array.

5.2.1 Part one: Neoproterozoic-early Paleozoic evolutionary model for the Canadian Appalachians

900-870 Ma- propagation of the Asgard Sea

The earliest paleogeography of the peri-Gondwanan terranes is inferred from the isotopic and geochronological record of the oldest sedimentary in Avalonia rocks (Gamble Brook Fm., Henderson et al. 2016), and from the crustal model ages of the mid-Neoproterozoic magmatism recorded in the detrital and magmatic zircon record of Avalonia, Ganderia and Meguma (Fig. 11). The ~800-675 Ma detrital and magmatic zircons persistently record model ages that indicate recycling of ~1.0 to 2.0 Ga "Grenvillian" crust (Fig. 11). Previous studies have used Sm-Nd whole rock data to suggest "proto" Avalonian crust was generated in a series of primitive island arcs in the peri-Rodinian ocean at ~1.0-1.2 Ga (Murphy et al., 2000; Murphy and Nance, 2002), which is in contrast to the apparent continental nature of the Avalonian basement (Henderson et al., 2016). The hafnium array requires that the early Avalonian/Ganderian Cryogenian arcs (~800-750 Ma) were nucleated on ~1.0-2.0 Ga "Grenvillian-type crust" (Fig. 11a), and not on peri-Rodinian oceanic crust. Regions that host crust of an appropriate age are the located near the Grenville suture, such as the Grenville Province in Laurentia, the Sveconorwegian orogen in Baltica and Sunsas orogen in Amazonia. Traditionally, these areas are "locked up" within the interior of the Rodinia supercontinent until the late Neoproterozoic (Cawood et al., 2001; Cawood and Pisarevsky, 2006) and are normally not considered as hosts for the peri-Gondwanan magmatic arcs. The hafnium isotopic array for the Gamble Brook Formation has recently been interpreted to share an affinity with the Mesoproterozoic-Paleoproterozoic rocks of Baltica, suggesting a location proximal to the Grenville suture in the early-mid Neoproterozoic (Thompson et al., 2012; Henderson et al., 2016). The mixed provenance (ancient and juvenile crust) and the geochemistry of the Gamble Brook Formation (Murphy, 2002) are interpreted to indicate deposition in a rifted basin environment.

Given the geochemical, isotopic and geochronological constraints, the most plausible area for deposition of the Gamble Brook Formation is within the extensive basin system generated during a 95° rotation of Baltica from Greenland towards Amazonia, which opened the Asgard Sea in the late Mesoproterozoic (Fig. 12a) (Cawood et al., 2007; Cawood et al., 2010). The basin also hosted the thick, siliciclastic successions now preserved in Scotland, Greenland, Svalbard and Norway (see Cawood et al., 2010), which record similar detrital zircon spectra to the Gamble Brook Formation and are also interpreted to have been sourced predominantly from the Grenville-Sveconorwegian orogenic belt (see Cawood et al., 2015 and references therein).

Latest Mesoproterozoic-mid Neoproterozoic (~1030-710 Ma) sedimentation and orogenic activity preserved in Scotland, Shetland, Svalbard and Norway is assigned to the Valhalla Orogen; an external

accretionary orogen on the northern margin of the Asgard Sea (Cawood et al., 2010). The spreading centre of the Asgard Sea is interpreted to have propagated westwards into the Grenvillian suture during the late Tonian (Cawood et al., 2010)(Fig 12a), exposing Grenvillian crust along the eastern Laurentian margin to an open ocean. There is evidence for rifting preserved in a wide spread pulse of mafic and felsic magmatism at ~870 Ma across the Scottish Highlands including the 880-840 Glen Doe and 862 ± 11 Ma Sgurr Dhomhnuill granitic gneisses (Friend et al., 1997; Millar, 1999; Rogers et al., 2001; Cawood et al., 2015). Coeval granites and gabbros in the Seve Napper Complex yielded an age of 845 ± 14 Ma (Paulsson and Andreasson, 2002) and are used to suggest that rifting extended into the Scandinavian Caledonides during an early Rodinian break-up attempt (Paulsson and Andreasson, 2002). The bimodal nature and MORB geochemistry of the mafic rocks in the Scottish Highlands have been interpreted to indicate mafic underplating of the crust (Ryan and Soper, 2001; Fowler et al., 2013) and an overall extensional environment in eastern Laurentia (Millar, 1999) at ~870 Ma.

The propagation of the Asgard Sea ridge into eastern Laurentia and Baltica (and possibly part of Amazonia) during the early-mid Neoproterozoic is possibly driven by opposing geodynamic forces related to subduction zones to the north and the south of the Rodinian supercontinent (Fig. 12a). South-east of Amazonia and West Africa subduction-related magmatism and accretionary processes dominated the early-late Neoproterozoic evolution of the Arabian-Nubian Shield, Oaxaquia terrane, Tocantins province, Saharan Metacraton and the central and southern South American terranes during the protracted assembly of Gondwana (Ramos, 1988; Tohver et al., 2006; Cawood and Buchan, 2007; Johnson et al., 2011) . A second major subduction zone also surrounded the northern continents of Rodinia (India, South China, and East Antarctica) (see Torsvik et al., 2001; Cawood and Buchan, 2007). Essentially, opposing subduction zones along the periphery of Rodinia and could have contributed in "pulling" apart the core of Rodinia and allowing for the continuation of the Asgard Sea into the interior of the continent.

850-800 Ma- initiation of continental arc magmatism

Following the propagation of the Asgard Sea occurred between ~880-840 Ma along the Grenvillian regions of northeastern Laurentia and Baltica, subduction related magmatism commenced by ~800 Ma; as indicated by the presence of 800 Ma zircons in Avalonian, Ganderian and Meguma rocks. The hafnium isotopic record indicates mixing between juvenile and Paleoproterozoic crust (~2.0 -2.1 Ga), with minor zircons suggesting contamination from Archean crust (~2.5 Ga) (Fig. 11a). The magmatic arc is likely to have formed on the Laurentia side of the Asgard margin, but subduction may have also been active on the Baltican side (Cawood et al., 2010; Cawood et al., 2015). The evidence for the active margin could presently be preserved thrust beneath Laurentia during the Caledonian (Gee et al., 2015). Recycling of Paleoproterozoic crust in a vertical isotopic array that is typical of continental arcs occurred at ~800-750 Ma along the Grenvillian margin, forming the earliest arc magmatism in 'composite Avalonia' (Fig. 12b).

750-700 Ma- subduction roll back and a retreating arc

The hafnium isotopic array in the peri-Gondwanan terranes shows a contraction towards mantle-derived magmatism between ~750-650 Ma (Fig. 11b). Magmatism becomes increasingly juvenile as the influence of the Paleoproterozoic (and minor Archean) crust diminishes. The shift in the isotopic array is interpreted to reflect subduction roll back in the Asgard Sea and the retreat of the magmatic arc away from the Grenvillian margin (Fig. 12c), opening the proto-Iapetus

ocean between Baltica and the northeastern Laurentian margin. During subduction retreat a continental ribbon, which will later become the basement to Avalonia and Ganderia (and likely Meguma), is rifted away from the Grenvillian margin. The 734 Ma calc-alkaline Economy River Gneiss (among others, see Murphy et al., 2013) is testament to active subduction beneath Avalonia (Doig et al., 1993).

The eastern Laurentian margin preserves geological evidence for a Cryogenian rifting event (known variably as the pre-Iapetus event), which is interpreted here to be associated with the retreat of the peri-Gondwanan continental ribbon. The Blue Ridge Province in the southern and central Appalachians is host to numerous A-type plutons and bimodal volcanics dated between ~760-700 Ma (Tollo and Aleinikoff, 1996; Ernst and Bleeker, 2010; McClellan and Gazel, 2014), which have been variably attributed to 'failed' intracontinental rifting (Rankin, 1993; Aleinikoff et al., 1995) and mantle plume activity (McClellan and Gazel, 2014). The geochemistry of the bimodal igneous rocks within the Blue Ridge inlier is typically of a mixed origin between mantle derived melts and interaction with the lower crust (Tollo and Aleinikoff, 1996; Novak and Rankin, 2004; Tollo et al., 2004; Tollo et al., 2012; McClellan and Gazel, 2014), and can be attributed to distal extensional activity. The ~750 Ma rifting event coincides with the culmination of the Valhalla orogenesis (Cawood et al., 2010) and is marked by an extensive unconformity in the Grampians, Shetlands, east Greenland and Svalbard (Cawood et al., 2015) that could be related to the departure of the composite Avalonia terrane. On the basis of Cryogenian-Ediacaran zircon populations in proto-Andean sedimentary rocks Chew et al. (2008) also proposed that Amazonia and Laurentia were separated prior between ~770-680 Ma, to allow for the establishment of an magmatic arc only the pro-Andean margin prior to ~700 Ma.

Outboard of the West African Craton an oceanic arc is established that represents the earliest components of Cadomian magmatic activity (Fig. 12c). The hafnium isotopic signature of the ~750-700 Ma magmatism in Cadomia is juvenile (McClellan and Gazel, 2014; Henderson et al., 2016) prior to a marked shift towards a vertical mixing array following accretion of the arc to the West African margin (Walsh et al., 2012).

650 Ma: accretion to the Gondwanan margin

By ~650 Ma the peri-Gondwanan ribbon had arrived at the northern Gondwanan margin closing the Asgard Sea (Fig. 13a). All the hafnium isotopic data from Avalonia, Meguma and Ganderia (Fig. 11a) records a shift towards more evolved epsilon hafnium values, forming a vertical mixing array at ~650 Ma (Fig 11b) whereby arc magmas derived from the depleted mantle are mixed with predominantly Paleoproterozoic-early Archean crust (TDMc = 1.6-2.5 Ga). Some extremely evolved zircons also indicate contamination by Mesoarchean crust (~2.8-3.2 Ga), possibly from the cratonic margin that the continental ribbon accreted to. The record of ~650 Ma arc accretion onto Gondwana is much clearer in Avalonia than Ganderia, where instances of high-intermediate grade metamorphism at ~650 Ma are preserved in east Avalonia (Malverns Plutonic Complex, Strachan et al., 1996) and west Avalonia (southern Maine, Cape Breton Island, southern Newfoundland; O'Brien et al., 1996).

The hafnium isotopic shift is considered to represent the accretion of the continental ribbon to the Gondwanan margin and the stepping outboard of subduction into the ocean. The lack of appreciable magmatic gap in Ganderia and Avalonia between ~750-500 Ma (Fig. 11a) supports the immediate establishment of a continental magmatic arc on the northern Gondwanan margin that was active between ~650-540 Ma (Nance et al., 2002; Murphy et al., 2013).

540-520 Ma: opening of the Rheic Ocean

The hafnium isotopic array for the peri-Gondwanan terranes records a second shift towards the depleted mantle between ~540-500 Ma. Epsilon hafnium values record a progressively increased input from of juvenile crust and an inversely proportional decrease in the contribution of Paleoproterozoic-Archean crust (Fig. 11a). The transition towards increasingly positive (depleted mantle) εHf values between ~550-500 Ma is indicative of a retreating subduction zone analogous to the Tasmanides of Australia (Kemp et al., 2009). The interval coincides with the emplacement of bimodal volcanics of the ~510 Ma, Ellsworth Schist and Castine Volcanics (Schulz et al., 2008) in Ganderia and the ~500-490 Ma McDonalds Brook Group in Avalonia (Murphy and Dostal, 2007), however minor volcanism is recorded throughout the Cambrian in Avalonia suggesting that rifting may have been protracted across the terrane (Nance et al., 2010).

Faunal data from Avalonia is somewhat contradictory as it suggests isolation from Gondwana in the early Cambrian (Landing, 2005; Keppie and Keppie, 2014), but connection with Gondwana by the Middle Cambrian (Landing, 2004; Landing, 2005). The hafnium array suggests that by ~500 Ma the peri-Gondwanan terranes had migrated outboard of Gondwana and the Rheic Ocean had opened in its wake (Fig. 13b). The model is in agreement with Murphy et al. (2006) who suggested that the Rheic Ocean opened along a Neoproterozoic suture where the composite Avalonian arc terranes had previously accreted to the Gondwanan margin. Given the likely weak and hot state of the lithosphere in the accreted continental ribbons by comparison to the thick, stable cratonic margin they were accreted to, the Neoproterozoic is a feasible location for the Rheic Ocean to have opened up (e.g. Hyndman et al., 2005).

490-470 Ma: closing Iapetus

There is no demonstrable gap in the detrital zircon record between ~550-450 Ma (Fig. 11a) suggesting that magmatism did not cease in the peri-Gondwanan realm, but rather stepped outboard during subduction retreat. During ongoing subduction-related magmatism (together with roll-back) the arc system on the peri-Gondwanan ribbon would progressively remove the lower crust and SCLM (Collins et al., 2011), leading to increasingly positive εHf values that reflect the increasing but continual input of juvenile material from the underlying mantle wedge. This is best represented by the hafnium isotopic record of the mid-Ordovician Outflow Formation in Ganderia, where exclusively juvenile zircons are sourced from the proximal Popelogan-Victoria arc (Henderson et al., submitted). In Avalonia a similar trend is recorded by the hafnium isotopic data from the Dunn Point rhyolite whereby juvenile (εHf = +7 to +2) ~470-460 Ma zircons represent an excursion away from the typical crustal evolution of Avalonian rocks (Fig. 9b), indicating an important contribution from depleted mantle derived melts during this time.

The structure of the drifting composite Avalonian ribbon cannot be clarified from this data alone. It is likely to have been an extensive continental ribbon that was led by an oceanic-arc back-arc complex, best represented by the rocks of Exploits Subzone in Ganderia (Fig. 13c). The Gander margin, Avalonia and Meguma comprised the remainder of the continental ribbon and are likely to have undergone degrees of crustal extension and thinning during ribbon transfer. The vast size of the composite terrane led to the development of a diverse range of sedimentary environments (e.g. Hibbard et al., 2007a; Hibbard et al., 2007b), which in the geological record have been interpreted as entirely separate continental entities (van Staal et al., 2009). In reality, all three terranes are likely to have been hosted on the same plate analogous to the continental ribbons of

northern New Zealand, New Caledonia and the Lord Howe Rise (Gaina et al., 2003). Given the configuration of the terranes on the Laurentian margin, it is likely that Meguma formed the trailing edge of the ribbon. The stratigraphic record of Meguma preserves the transition from a shallow continental shelf to a deeper water environment coeval with the protracted development of the Rheic Ocean (Waldron et al., 2009), and thus could reflect deposition during the separation of the peri-Gondwanan ribbon away from Gondwana.

460-450 Ma: closure of Iapetus Ocean

The arrival of the leading edge of the peri-Gondwanan ribbon (Ganderia) is recorded in late Ordovician (~450 Ma) overstep sequences in the Exploits Subzone of Newfoundland. The peri-Laurentian Notre Dame Arc formed the upper plate during the soft collision (Zagorevski et al., 2007a; Zagorevski and Van Staal, 2011) leading to the drowning of the lower plate Popelogan-Victoria arc, which is marked by the deposition of a transgressive sequence of black-shales and manganese-rich sediments (Colman-Sadd et al., 1992). Magmatism in the Notre Dame and Popelogan-Victoria arcs largely shuts down by ~450 Ma coinciding with the subduction of the main Iapetus Ocean tract along the Red Indian line (Fig. 13d, Zagorevski et al., 2006; van Staal et al., 2009).

5.2.2 Part two: late Ordovician to Carboniferous evolution of the Canadian Appalachians

The timing and geodynamic framework for the accretion of the peri-Gondwanan terranes remains an ongoing debate. Broadly, there are two competing hypotheses. The first considers the peri-Gondwanan terranes to be separate entities (Ganderia + Carolinia, Avalonia, Meguma) that arrive at different times to the Laurentia margin (van Staal et al., 1998; Hibbard et al., 2007a; van Staal et al., 2009), each requiring a distinct accretion event (the Salinic, Acadian and Neoacadian, van Staal et al., 2004) upon closure of the ocean basins that separate the terranes (Iapetus Ocean, Rheic Ocean, Acadian Seaway, Theic Ocean). The other school of thought considers Ganderia, Avalonia and Meguma to be part of a single composite terrane (Avalonia) whereby Ganderia forms the leading edge and Meguma the trailing (Cocks and Torsvik, 2002; Murphy et al., 2004b; Murphy and Keppie, 2005). In the latter scenario, the closure of the Iapetus Ocean leads to the accretion of the composite peri-Gondwana terrane to Laurentia, and the subsequent subduction of the Rheic Ocean outboard of the composite Laurentian margin is the cause of the late Silurian-Devonian magmatic and deformational events assigned to the Acadian Orogeny; prior to terminal continent-continent collision during the Alleghenian orogeny (Murphy et al., 1999; Murphy and Keppie, 2005).

Either evolutionary model is able to be tested by investigating the hafnium isotopic array of the igneous zircons crystallised during the Paleozoic: If the terranes arrived as separate crustal blocks there should be a record of the individual Wilson cycles associated with the accretion of each terrane (Fig. 14a). Subduction-related magmatism is restricted to periods of ocean closure (Collins et al., 2011) and records an initial excursion towards the depleted mantle reflecting juvenile arc magmas derived from the mantle wedge, followed by mixing with evolved magmas that mirror the composition of the crust of the upper plate. Following the arrival of each terrane, subduction should step outboard into the next ocean basin and the same process should start again with an arc developing on the margin of the newly accreted terrane. The result of a long-lived accretionary system is a ‘saw-tooth’ type pattern in the Hf isotopic array (Fig. 14a).

In the case of a single continental ribbon model, the hafnium isotopic array should record the development of a single

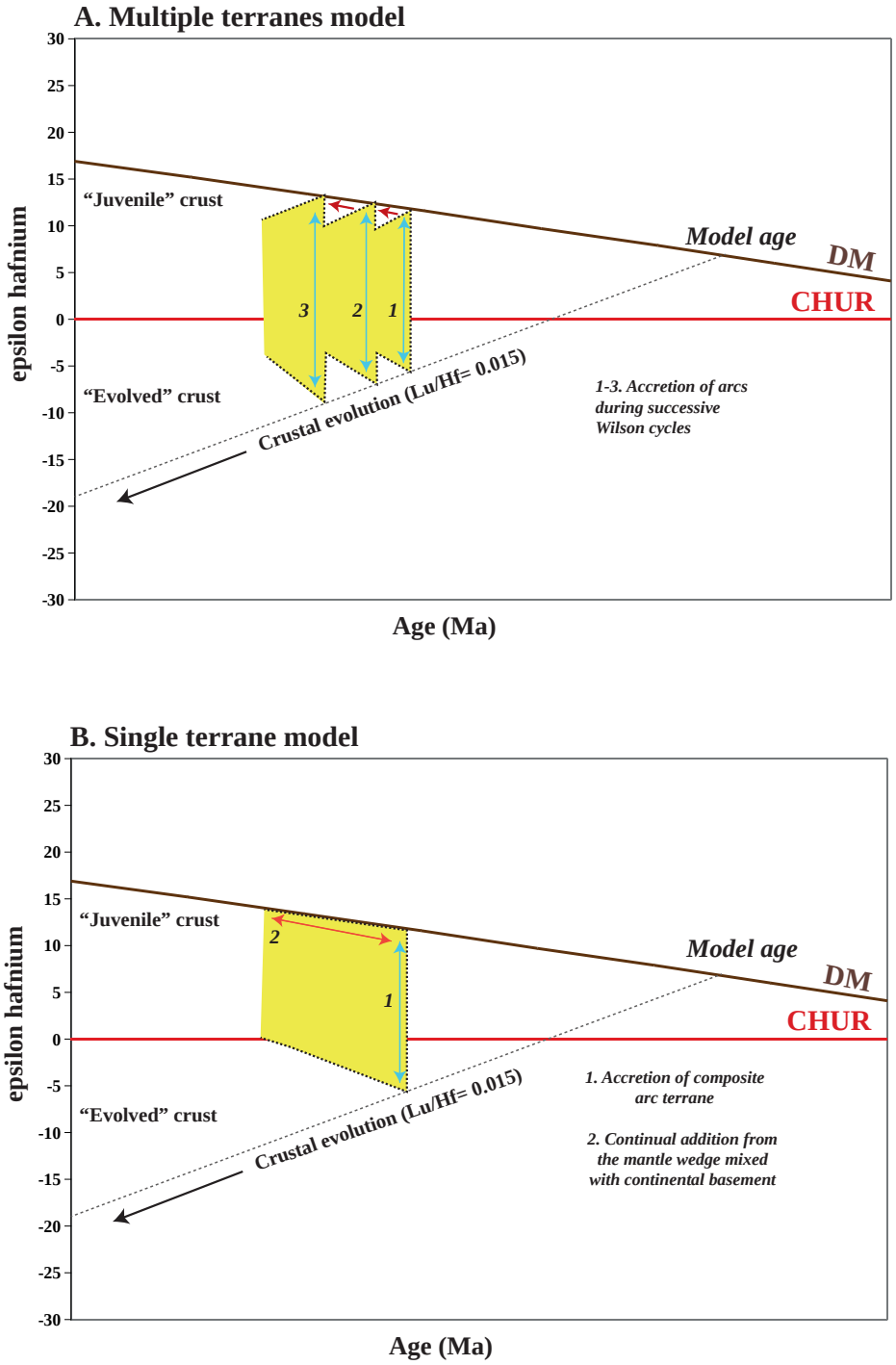

Figure 14

The figure represents the expected hafnium isotopic record of the two main competing theories for the evolution of the northern Appalachian orogen during the Paleozoic. A) The first model considers the peri-Gondwanan terranes to be separate entities that arrived at the Laurentian margin via the closure of multiple oceanic basins (e.g. during consecutive Wilson cycles, see van Staal et al. 2009). The overall effect of this evolutionary model is a "saw-tooth" type pattern in the hafnium array. B) The second model considers the peri-Gondwanan terranes represented a single composite terrane that was accreted to Laurentia in during the Silurian (e.g. Murphy and Keppie 2005). An Andean style continental arc was then built upon the Laurentian margin during the closure of the Rheic Ocean, resulting in a fanning isotopic array that represents the ongoing recycling of juvenile arc magmas with the basement of the continental terrane. As subduction continues it strips the SCLM and replaces it with increasingly juvenile arc magmas, leading to an overall increasingly juvenile arc (see Collins et al., 2011).

continental arc that was active from ~450 to 360 Ma (Fig. 14b), following the arrival of the leading Ganderian arc system (Penobscot/ Popelogan-Victoria arcs). The array should reflect the ongoing recycling of the Avalonia/ Ganderia/Meguma basement (~1.0-2.0 Ga) mixed with juvenile arc magmas from the down-going Rheic slab. This should be represented by a long-lived magmatic arc in the hafnium isotopic record, reflecting ongoing mantle contributions (Fig. 14b).

The Appalachian hafnium isotopic array for the Paleozoic (Fig. 15) does not fit with either of the predicted hafnium isotopic models described in Figure 14. Rather than record the development of one, or a number of, magmatic arcs during the mid-late Paleozoic (Fig. 14a, b), the isotopic array instead records continuous recycling of Mesoproterozoic-Paleoproterozoic crust between ~450-320 Ma. During the ~130 million year interval, there is no recorded contamination from older crust, nor a significant input from the juvenile depleted mantle. The hafnium data does not support the existence of a continental-arc on the composite Laurentian margin after ~440-430 Ma, but rather indicates a tectonic environment dominated by recycling of the Avalonian basement crust leading to progressive homogenisation during ongoing magmatism.

The following section discusses an evolutionary model (Fig. 16) that accommodates the Paleozoic hafnium isotopic array within the existing geological constraints for the Canadian Appalachians.

440-415 Ma: retreating orogenic system

The hafnium isotopic array (Fig. 15) indicates that the Popelogan-Victoria juvenile arc was active until ~445 Ma (Henderson et al., Submitted), shutting off just shortly after the proposed collision with the Notre Dame arc (Zagorevski and Van Staal, 2011). Immediately following the collision of the arcs, the peri-Gondwanan hafnium isotopic array begins to trend towards CHUR (Fig. 15a). The most primitive zircons change from > +10 (εHf) at 445 Ma to 0 (CHUR) by 350 Ma, and the most evolved zircons change from -7 (εHf) at 435 Ma to -2 ε(Hf) by 320 Ma. This "isotopic contraction" reflects an extensive period of crustal homogenisation and recycling of the composite Avalonian terrane and its Mesoproterozoic basement (Fig. 15a). The shift in the hafnium isotopic record demands a change in the geodynamic environment at ~440 Ma in the Canadian Appalachians.

The geological record of the northern Appalachians indicates that the peri-Gondwanan realm was characterised by predominantly an extensional tectonic environment during the Silurian, consistent with an upper plate continental, back-arc setting (Fig. 16a). Testament to the extensional nature is the coeval development of the ~440-430 Ma Mascarene and Kingston basins and the Coastal volcanic province in Maine, New Brunswick and Nova Scotia (Robinson et al., 1998; Barr et al., 2002; Fyffe et al., 2012), and the La Poile basin in Newfoundland (O'Brien et al., 1991; Kerr et al., 1995). The early Silurian basins are all associated with bimodal plutonic and coeval volcanics that are interbedded with clastic sedimentary rocks (see Hogan and Sinha, 1989; Lin et al., 2007; Fyffe et al., 2012; van Staal et al., 2014). In the ~425 Ma Maine Coastal volcanic province, early granitic magmatism yields low-temperature metaluminous (I-type) granites before progressively becoming increasingly high-temperature, anhydrous and peralkaline (A-type) in nature (see Hogan and Sinha, 1989), consistent with an rift-setting whereby mantle-derived magmas provide sufficient heat to progressively melt lower crustal rocks at increasingly higher temperatures. A similar transition from I- to A- type magmatism is recorded in the Lachlan orogen of Australia during the transition towards a retreating (slab-roll back) subduction system (Kemp et al., 2009). The 429 Ma Topsails igneous suite in Newfoundland (Whalen et al., 1987)

also comprises bimodal volcanic and plutonic rocks that are predominantly A-type (Whalen et al., 1996), providing further evidence for the widespread extensional environment across the Appalachians during the early Silurian. The presence of A-type granites across the Appalachians at ~430-425 Ma is consistent with emplacement in the distal back-arc region, with the magmatic arc located outboard, to the southeast (present day coordinates).

In Avalonia, evidence for early Silurian extension is represented by the mafic and felsic volcanics of the Dunn Point Formation (Keppie et al., 1979; Murphy, 1987) and in Meguma, by the bimodal volcanics of the White Rock Formation and the coeval Brenton pluton (Keppie and Krogh, 2000; MacDonald et al., 2002). Mafic rocks from the Bears Brook Formation are tholeitic, having geochemical signatures consistent with emplacement in an extensional environment (Murphy et al., 1991; Murphy and Dostal, 2007), similar to the modern day Taupo volcanic zone (Murphy et al., 2008). Early Silurian mafic volcanic rocks and coeval mafic intrusions in Meguma all record alkalic affinities suggesting emplacement within an extensional, within-plate setting (MacDonald et al., 2002).

415-390 Ma: advancing orogenic system

The tectonic framework of the (~415-390 Ma) Acadian orogeny is controversial. Two contrasting models persist, with the first attributing the deformation and magmatism to the closure of the Acadian seaway and the accretion of Avalonia to composite Laurentia (van Staal et al., 1998; Zagorevski et al., 2007b; van Staal et al., 2009), and the second envisaging an Andean-type margin and interaction with a mantle plume (Murphy and Keppie, 2005). The hafnium isotopic array for the Acadian orogenic interval continues the homogeneous recycling of Mesoproterozoic crust recorded during the Silurian.

The start of the Acadian orogeny is marked by the late Silurian inversion of the early Silurian volcanic basins across the composite Avalonian terrane realm. The La Poile and Mascarene basins were inverted at ~420 Ma (O'Brien et al., 1991; van Staal et al., 2004) in Newfoundland and Maine/New Brunswick.

The final closure of the Tetagouche-Exploits basin in the late Silurian (van Staal et al., 2009) could also be considered to have resulted from the short term switch towards a compressional tectonic environment. An Acadian orogenic front, represented by migrating deformation and an Acadian foredeep, is preserved throughout Maine, New Brunswick and into Quebec (Robinson et al., 1998; Murphy and Keppie, 2005). The earliest evidence of the deformation front is in the central Maine Basin at ~415 Ma, prior to progressively moving northwest until ~385 Ma in Quebec (Fig. 16b).

The earliest Acadian structural deformation in the Avalonia terrane is the development of upright folds in early Silurian rocks of the Fredericton Trough, which are intruded by 406 Ma granites (Murphy and Keppie, 2005). In Avalonian Nova Scotia, the start of the Acadian orogeny is locally marked by a pervasive unconformity between early and late Devonian strata (Braid and Murphy, 2006). Acadian deformation and metamorphism commences in the Meguma terrane at ~415 Ma with regional greenschist facies metamorphism and polyphase deformation (Keppie and Dallmeyer 1995) that continued until the late Devonian (see Murphy and Keppie 2005). In Newfoundland, Acadian deformation is evident along major tectonostratigraphic boundaries: along the Dog Bay Line, it commenced at ~415-410 Ma (Whalen et al., 2006), along the Red Indian Line at ~408 Ma (Elliot et al., 1991), and along the Dover Fault Zone dextral-transpression is recorded at ~410-400 Ma (Schofield and D'Lemos, 2000 ,Chapter 4 within), synchronous with granite emplacement and migmatisation (Kellett et al., 2014, Chapters 3

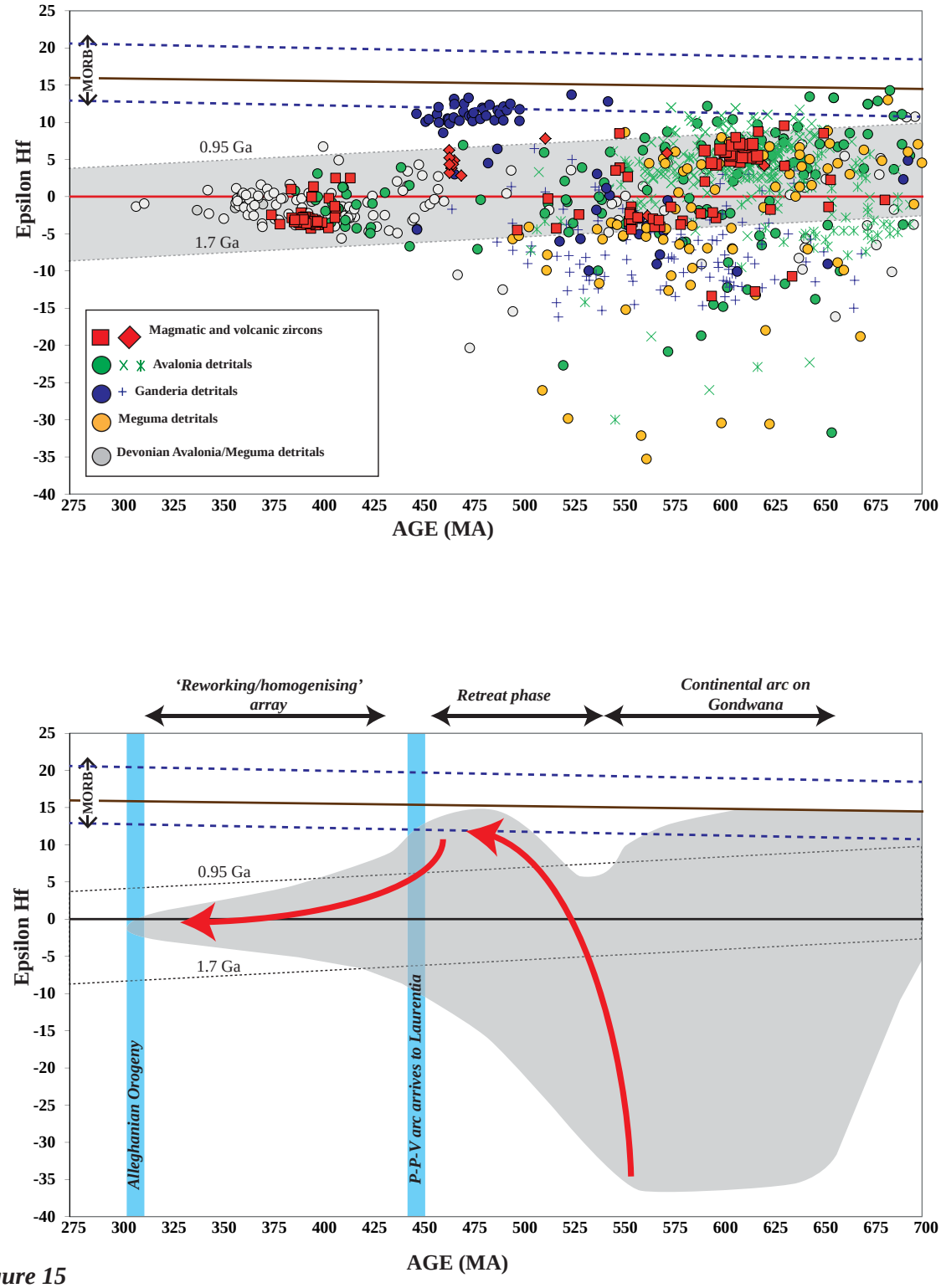

Figure 15

A) εHf values plotted against the U-Pb ages for all available ~700-300 Ma zircons from Avalonia, Ganderia and Meguma. Included are published zircon data Willner et al., (2013, 2014) and Pollock et al., (2015). B) The grey field defines the shape of the evolutionary array during the late Neoproterozoic-late Paleozoic evolution of Avalonia, Meguma and Ganderia. The red arrays indicate the evolving trend of the hafnium array during transition from a continental arc, to a retreating oceanic arc and the collision with the Laurentian margin. The final stage is one of homogenous recycling of late Neoproterozoic arc crust. Also shown is the timing of the arrival of the Popelogan-Victoria arc to the Laurentian margin and the timing of the Alleghenian Orogeny.

and 4 within). The Central Maine Belt records the emplacement of syntectonic granites during dextral-transpressive deformation and peak metamorphism at ~408-404 Ma (Solar et al., 1998).

The hafnium isotopic record during the ~410-380 Ma Acadian orogeny is potentially compatible with the plume-modified subduction model proposed by Murphy and Keppie (2005), whereby the arrival of an oceanic plateau above a mantle plume to the Appalachian trench led to flattening of the subducting slab and the inboard migration of deformation and magmatism. The hafnium array is similar to the Silurian, as it shows ongoing contraction toward CHUR (Fig. 15). This indicates that no new material was being processed in the arc-back-arc environment, and requires that the same subduction zone operated throughout the Silurian-Devonian. If the mantle-plume model is correct, no zircons from the plume-derived magmas have been recorded in the analysed Devonian-Carboniferous rocks.

The switch towards an advancing subduction system also could have been caused by the arrival of a seamount or oceanic plateau to the trench (see Collins, 2002; Collins and Richards, 2008). The arrival of a buoyant oceanic anomaly, such as a seamount or plateau, to the trench forces the slab hinge to migrate inboard, causing the upper-plate to undergo deformation and metamorphism typically associated with crustal thickening in a compressional regime (see Murphy et al., 1999; Collins, 2002; Collins and Richards, 2008). The evolutionary model that is more consistent with the hafnium isotopic array and the Acadian geologic record is that the subduction zone outboard of Meguma/Avalonia transitions from retreating to advancing in the late Silurian (Fig. 16b).

380-300 Ma: retreating orogenic system

The mid-late Devonian (~380-350 Ma) geological record of the composite Avalonian margin is compatible with the transition towards an overall extensional environment. The interval marks the development of suite of linear, fault bounded half-grabens across the onshore and offshore Maritime Canada and Maine. The basins are predominantly linked to extension-related master faults that are oriented E-W to NE-SW (see Bradley, 1982; Pe-Piper and Piper, 2003) and extend across terrane boundaries, including the Avalonia/Meguma boundary in Nova Scotia (see Murphy et al., 1996; Murphy and Hamilton, 2000). Volcanic rocks are present throughout the mid-late Devonian basins across the Appalachians. In Cape Breton rhyolites from the Fisset Brook Formation are dated to 373 ± 4 Ma (Dunning et al., 2002), and the Sunnyville Formation in mainland Nova Scotia comprises a thick succession of mafic and felsic flows (389 ± 2 Ma) and pyroclastic rocks and coeval gabbroic plutons (Cormier et al., 1995). Coeval rhyolitic and basaltic volcanism and intrusions in the Narragansett Basin of Maine at ~380 Ma preserves transitional alkalic geochemistry (Thompson and Hermes, 2003). Bimodal magmatism in Maine provides further evidence for a tectonic switch towards a retreating subduction system and extensional environment following the Acadian orogeny, at least in the northern Appalachians. In Meguma, the age of the granites appear too young towards the SE between ~380-370 Ma (Moran et al., 2007), indicative of a subduction retreat model.

Perhaps the most noticeable geological evidence for the transition towards an extensional regime is the emplacement of the voluminous S-type South Mountain Batholith at ~380-370 Ma in Nova Scotia (Shellnutt and Dostal, 2015). Collins and Richards (2008) described the relationship between extension and S-type magmatism in the Lachlan Orogen in eastern Australia. They described a process whereby sediment-filled, turbiditic back-arc basins were thickened during short-lived contractional events associated with slab

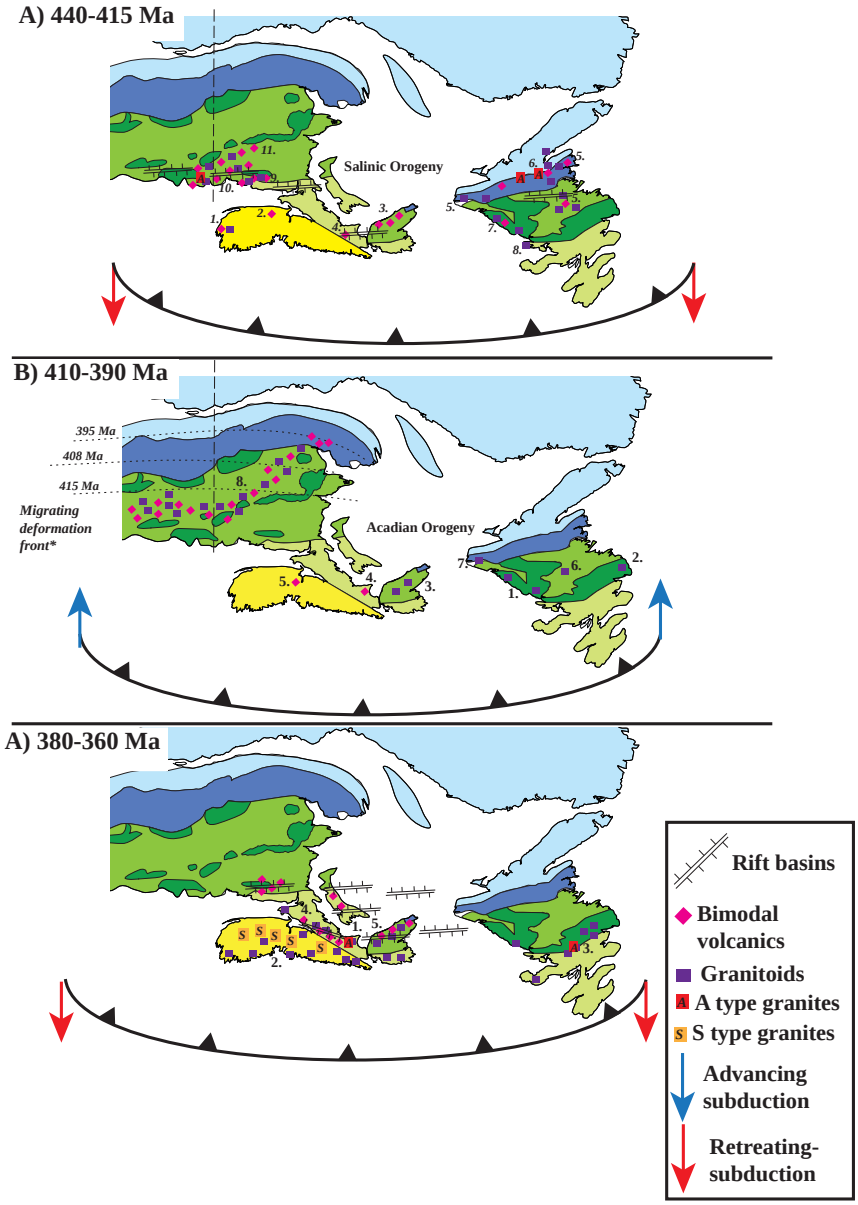

Figure 16

The figure illustrates the magmatic history of the northern Canadian Appalachians during the mid-late Paleozoic. Shown is the migrating distribution of bimodal volcanism, granite magmatism, A and S-type magmatism and rift basin development. A) 440-415 Ma 1. White Rock Formation volcanics and Brenton Pluton (Keppie and Krogh, 2000; MacDonald et al., 2002). 2) White Rock Formation volcanics (Keppie and Krogh, 2000). 3) Money Point Group rhyolite (Keppie and Krogh, 2000). 4) Bears Brook Formation (Keppie et al., 2000). 5) Silurian plutonic and volcanic rocks of Ganderia in Newfoundland (see Kellett et al., 2014 and references therein; van Staal et al., 2014). 6) Topsails A-type igneous suite (Whalen et al., 1996). 7) La Poile Group and Burgeo pluton (van Staal et al., 2014). 8) Pass Island granite (Kellett et al., 2014). 9) Kingston terrane (see Barr et al., 2002 and references therein). 10) Mascarene Basin granites and volcanics (see Barr et al., 2002 and references therein). 11) Fredericton Trough (see Barr et al., 2002 and references therein). B) 410-390 Ma 1) North Bay granite suite, Chetwynd granite (see Kellett et al., 2014 and references therein). 2) Deadmans Bay granite (this study). 3) Neils Harbour orthogneiss, West Branch North River pluton and Cameron Brook pluton (Dunning et al., 1990). 4) Sunnyvale Formation, McArras Brook basalts and Wilson Brook felsics (Cormier et al., 1995). 5) New Canaan volcanics (White et al., 2011). 6) Middle range granite (Kellett et al., 2014). 7) Rose Blanche granite (Kellett et al., 2014). 8) Maine magmatic province (Schoonmaker et al., 2005). C) 380-360 Ma 1) West Moose river pluton (A-type granite), (Pe Piper et al., 1991). 2) Liscomb Complex (South Mountain Batholith) (Shellnutt and Dostal, 2015 and references therein). 3) Newfoundland Devonian granites (Kellett et al., 2014). Ackely granite (A-type) (Tuach, 1987). 4) Devonian-Carboniferous volcanic rocks across Magdalen Basin (Dunning et al., 2002).

advance, as with the early-middle Devonian Acadian orogeny. In that model, slab advance was associated with ocean plateau subduction, where eclogitisation of the slab was delayed by the presence of abundant plagioclase. However, on eclogitisation occurred, the slab sinks rapidly, inducing slab rollback and extension in the overlying plate as arc magmatism re-initiated (Collins and Richards, 2008).

Applied to Meguma, the sedimentary basin contains the Halifax and Goldenville groups, which was thickened during the Acadian slab advance. However, once the thick slab transforms to eclogite, it rapidly retreated and arc magmatism re-initiated below the Meguma Group in Nova Scotia. The resultant burst of magmatism was associated with lamprophyric mafic dykes (Clarke et al., 1997; Tate et al., 1997), representing mantle melting in the metasomatised subcontinental lithospheric mantle, associated with melting of the buried Meguma Group metasediments and the Avalonian basement in the middle to deep crust, producing the coeval South Mountain S-type batholith (Clarke et al., 1997; Tate et al., 1997). Mid-late Devonian A-type granites across the Appalachians, such as the Ackley granite in Newfoundland (Tuach, 1987) and the West Moose River pluton in the Cobequid Highlands (Pe-Piper and Piper, 2003), are testament to the retreating extensional nature of the orogen.

The combined U-Pb-Hf detrital zircon data set (Fig. 15a) indicates that magmatism continued in the northern Appalachians until the latest Carboniferous. The "arrow-head" hafnium isotopic array (Fig. 15) indicates that magmatism continued to homogenise the crust, with εHf values of the youngest (315-310 Ma) zircons close to CHUR. Hence, the late Devonian-Carboniferous interval of extension only continued to rework the crust of the composite Avalonian terrane. Associated mafic dykes, such as the lamprophyres of the South Mountain Batholith ("Weekend dykes", Tate et al., 1997), and the Late Devonian-Carboniferous tholeiitic basalts that intrude the Maritimes Basins across Nova Scotia (Dessureau et al., 2000), New Brunswick (Fyffe and Barr, 1986) and Quebec (Fleche et al., 1998) presumably produced too few zircons to have been represented in the analysed sample set. It appears that the sweeping migration of magmatic belts back and forth across the composite terrane was the necessary process to homogenise the crust.

Another key result, implicit from the Hf isotope array, is that Gondwanan cratonic crust did not interact with the (composite) Avalonian terrane, prior to, or during the Pangean assembly in the late Carboniferous (Stampfli et al., 2013). However, it is worth noting that the late Carboniferous was dominated by dextral strike-slip tectonics in the northern Appalachians (Murphy 2003) and therefore it seems unlikely that Gondwanan crust would have been introduced in the magmatic system during the final Pangean assembly. Late Carboniferous zircons record only the continuous recycling of juvenile Neoproterozoic arc crust (~750 Ma) and Grenvillian-aged basement. Interestingly, a similar contraction and accordingly, lack of Gondwanan cratonic involvement, is evident from the 550-300 Ma Hf isotopic array of Variscan Europe (See Chapter 6), suggesting it formed from a similar tectono-magmatic process.

REFERENCES

Albert, R., Arenas, R., Gerdes, A., Martínez, S.S., Fernández-Suárez, J., Fuenlabrada, J., 2014. Provenance of the Variscan Upper Allochthon (Cabo Ortegal Complex, NW Iberian Massif). Gondwana Research.

Aleinikoff, J.N., Zartman, R.E., Walter, M., Rankin, D.W., Lyttle, P.T., Burton, W.C., 1995. U-Pb ages of metarhyolites of the Catoctin and Mount Rogers Formations, central and southern Appalachians: Evidence for two pulses of Iapetan

rifting. American Journal of Science 295, 428-454.

Andersen, T., Griffin, W.L., Sylvester, A.G., 2007. Sveconorwegian crustal underplating in southwestern Fennoscandia: LAM-ICPMS U–Pb and Lu–Hf isotope evidence from granites and gneisses in Telemark, southern Norway. Lithos 93, 273-287.

Barr, S.M., White, C.E., 1996. Contrasts in Late Precambrian-Early Paleozoic tectonothermal history between Avalon composite terrane sensu stricto and other possible peri-Gondwanan terranes in southern New Brunswick and Cape Breton Island, Canada. SPECIAL PAPERS-GEOLOGICAL SOCIETY OF AMERICA, 95-108.

Barr, S.M., White, C.E., Miller, B.V., 2002. The Kingston terrane, southern New Brunswick, Canada: evidence for an Early Silurian volcanic arc. Geological Society of America Bulletin 114, 964-982.

Barr, S.M., White, C.E., Miller, B.V., 2003. Age and geochemistry of Late Neoproterozoic and Early Cambrian igneous rocks in southern New Brunswick: similarities and contrasts. Atlantic Geology 39.

Barreiro, J.G., Catalán, J.R.M., Arenas, R., Castiñeiras, P., Abati, J., García, F.D., Wijbrans, J.R., 2007. Tectonic evolution of the upper allochthon of the Órdenes Complex (northwestern Iberian Massif): structural constraints to a polyorogenic peri-Gondwanan terrane. Geological Society of America Special Papers 423, 315-332.

Boucot, A.J., 1974. Geology of the Arisaig area, Antigonish County, Nova Scotia. Geological Society of America.

Bradley, D., 1982. Subsidence in late Paleozoic basins in the northern Appalachians. Tectonics.

Braid, J.A., Murphy, J.B., 2006. Acadian deformation in the shallow crust: An example from the Siluro-Devonian Arisaig Group, Avalon terrane, mainland Nova Scotia. Canadian Journal of Earth Sciences 43, 71-81.

Cawood, P.A., Buchan, C., 2007. Linking accretionary orogenesis with supercontinent assembly. Earth-Science Reviews 82, 217-256.

Cawood, P.A., McCausland, P.J.A., Dunning, G.R., 2001. Opening Iapetus: Constraints from the Laurentian margin in Newfoundland. Geological Society of America Bulletin 113, 443-453.

Cawood, P.A., Nemchin, A.A., Strachan, R., Prave, T., Krabbendam, M., 2007. Sedimentary basin and detrital zircon record along East Laurentia and Baltica during assembly and breakup of Rodinia. Journal of the Geological Society 164, 257-275.

Cawood, P.A., Pisarevsky, S.A., 2006. Was Baltica right-way-up or upside-down in the Neoproterozoic? Journal of the Geological Society 163, 753-759.

Cawood, P.A., Strachan, R., Cutts, K., Kinny, P.D., Hand, M., Pisarevsky, S., 2010. Neoproterozoic orogeny along the margin of Rodinia: Valhalla orogen, North Atlantic. Geology 38, 99-102.

Cawood, P.A., Strachan, R.A., Merle, R.E., Millar, I.L., Loewy, S.L., Dalziel, I.W., Kinny, P.D., Jourdan, F., Nemchin, A.A., Connelly, J.N., 2015. Neoproterozoic to early Paleozoic extensional and compressional history of East Laurentian margin sequences: The Moine Supergroup, Scottish Caledonides. Geological Society of America Bulletin 127, 349-371.

Chew, D.M., Magna, T., Kirkland, C.L., Mišković, A., Cardona, A., Spikings, R., Schaltegger, U., 2008. Detrital zircon fingerprint of the Proto-Andes: Evidence for a Neoproterozoic active margin? Precambrian Research 167, 186-200.

Clarke, D., Halliday, A., 1980. Strontium isotope geology of the South Mountain batholith, Nova Scotia. Geochimica et Cosmochimica Acta 44, 1045-1058.

Clarke, D.B., Fallon, R., Heaman, L.M., 2000. Interaction among upper crustal, lower crustal,

and mantle materials in the Port Mouton pluton, Meguma Lithotectonic Zone, southwest Nova Scotia. Canadian Journal of Earth Sciences 37, 579-600.

Clarke, D.B., MacDonald, M.A., Tate, M.C., 1997. Late Devonian mafic-felsic magmatism in the Meguma zone, Nova Scotia. MEMOIRS-GEOLOGICAL SOCIETY OF AMERICA, 107-128.

Cocks, L.R.M., Torsvik, T.H., 2002. Earth geography form 500 to 400 million years ago: A faunal and palaeomagnetic review. Journal of the Geological Society 159, 631-644.

Collins, W., 2002. Hot orogens, tectonic switching, and creation of continental crust. Geology 30, 535-538.

Collins, W., Richards, S., 2008. Geodynamic significance of S-type granites in circum-Pacific orogens. Geology 36, 559-562.

Collins, W.J., Belousova, E.A., Kemp, A.I.S., Murphy, J.B., 2011. Two contrasting Phanerozoic orogenic systems revealed by hafnium isotope data. Nature Geoscience 4, 333-337.

Colman-Sadd, S., Stone, P., Swinden, H., Barnes, R., 1992. Parallel geological development in the Dunnage Zone of Newfoundland and the Lower Palaeozoic terranes of southern Scotland: an assessment. Transactions of the Royal Society of Edinburgh: Earth Sciences 83, 571-594.

Cormier, C.F.M., Barr, S.M., Dunning, G.R., 1995. Geological setting and petrochemistry of early Middle Devonian volcanic and gabbroic rocks in the Guysborough area, Nova Scotia Atlantic Geology 31.

Daly, J., McLelland, J., 1991. Juvenile middle Proterozoic crust in the Adirondack highlands, Grenville province, northeastern North America. Geology 19, 119-122.

Dalziel, I.W.D., 1992. On the organization of American plates in the Neoproterozoic and the breakout of Laurentia. GSA Today 2, 237,240-241.

Dalziel, I.W.D., 1997. Neoproterozoic-Paleozoic geography and tectonics: Review, hypothesis, environmental speculation. Geological Society of America Bulletin 109, 16-42.

Dessureau, G., Piper, D.J.W., Pe Piper, G., 2000. Geochemical evolution of earliest Carboniferous continental tholeiitic basalts along a crustal-scale shear zone, South western Maritimes basin, eastern Canada. Lithos.

Dhuime, B., Hawkesworth, C., Cawood, P., 2011. When continents formed. Science 331, 154-155.

Dickin, A., 2000. Crustal formation in the Grenville Province: Nd-isotope evidence. Canadian Journal of Earth Sciences 37, 165-181.

Dickin, A., McNutt, R., Clifford, P., 1990. A neodymium isotope study of plutons near the Grenville Front in Ontario, Canada. Chemical Geology 83, 315-324.

Doig, R., Murphy, J.B., Nance, R.D., 1993. Tectonic significance of the late Proterozoic Economy River gneiss, Cobequid Highlands, Avalon composite terrane, Nova Scotia. Canadian Journal of Earth Sciences 30, 474-479.

Dunning, G.R., Barr, S.M., Giles, P.S., McGregor, D.C., Pe Piper, G., Piper, D.J.W., 2002. Chronology of Devonian to early Carboniferous rifting and igneous activity in southern Magdalen Basin based on U-Pb (Zircon) dating. Canadian Journal of Earth Sciences 39.

Dunning, G.R., Barr, S.M., Raeside, R.P., 1990. U-Pb zircon, titanite and monazite ages in the Bras d'Or and Aspy terranes of Cape Breton Islad, Nova Scotia: Implications for igneous and metamorphic history. Geological Society of America Bulletin 102.

Elliot, C.G., Duninng, G.R., Williams, P.F., 1991. New U/Pb zircon age constraints on the timing of deformation in north-central Newfoundland and implications for early Paleozoic Appalachian orogenesis. Geological Society of America

Bulletin 103, 125-135.

Ernst, R., Bleeker, W., 2010. Large igneous provinces (LIPs), giant dyke swarms, and mantle plumes: significance for breakup events within Canada and adjacent regions from 2.5 Ga to the Present. Canadian Journal of Earth Sciences 47, 695-739.

Fleche, M.R., Camire, G., Jenner, G., 1998. Geochemistry of post-Acadian, Carboniferous continental intraplate basalts from the Maritimes Basin, Magdalen islands, Quebec, Canada. Chemical Geology.

Fowler, M., Millar, I., Strachan, R., Fallick, A., 2013. Petrogenesis of the Neoproterozoic West Highland Granitic Gneiss, Scottish Caledonides: cryptic mantle input to S-type granites? Lithos 168, 173-185.

Friend, C., Kinny, P., Rogers, G., Strachan, R., Paterson, B., 1997. U-Pb zircon geochronological evidence for Neoproterozoic events in the Glenfinnan Group (Moine Supergroup): the formation of the Ardgour granite gneiss, north-west Scotland. Contributions to Mineralogy and Petrology 128, 101-113.

Fyffe, L.R., Barr, S.M., 1986. Petrochemistry and tectonic significance of Carboniferous volcanic rocks in New Brunswick. Canadian Journal of Earth Sciences.

Fyffe, L.R., Johnson, S.C., van Staal, C.R., 2012. A Review of Proterozoic to Early Paleozoic Lithotectonic Terranes in New Brunswick, Canada and their Tectonic Evolution during Penobscot, Taconic, Salinic and Acadian Orogenesis. 2012, 38.

Gaina, c., MÜLLER, R.D., BROWN, B.J., ISHIHARA, T., 2003. Microcontinent formation around Australia. Geological Society of America Special Papers 372, 405-416.

Gee, D.G., Andréasson, P.-G., Lorenz, H., Frei, D., Majka, J., 2015. Detrital zircon signatures of the Baltoscandian margin along the Arctic Circle Caledonides in Sweden: The Sveconorwegian connection. Precambrian Research 265, 40-56.

Gingras, M.K., Waldron, J.W.F., White, C.E., Barr, S.M., 2011. The evolutionary significance of a Lower Cambrian trace-fossil assemblage from the Meguma terrane, Nova Scotia. Canadian Journal of Earth Sciences 48, 71-85.

Griffin, W.L., Belousova, E.A., Shee, S.R., Pearson, N.J., O'Reilly, S.Y., 2004. Archean crustal evolution in the northern Yilgarn Craton: U–Pb and Hf-isotope evidence from detrital zircons. Precambrian Research 131, 231-282.

Hamilton, M.A., Murphy, J.B., 2004. Tectonic significance of a Llanvirn age for the Dunn Point volcanic rocks, Avalon terrane, Nova Scotia, Canada: Implications for the evolution of the Iapetus and Rheic Oceans. Tectonophysics 379, 199-209.

Harland, W., Gayer, R., 1972. The Arctic Caledonides and earlier oceans. Geological Magazine 109, 289-314.

Henderson, B., in prep. The P-T-t evolution of Ganderia in the Paleozoic: the metamorphic record of back-arc basin tectonics and continental ribbon transfer The University of Adelaide.

Henderson, B., Collins, W.J., Murphy, B., Hand, M., Submitted. A hafnium isotopic record of magmatic arcs and continental growth in the Iapetus Ocean: the contrasting evolution of Ganderia and the peri-Laurentian margin Gondwana Research.

Henderson, B., Collins, W.J., Murphy, B.J., Gutiérrez-Alonso, G., Hand, M., 2016. Gondwanan basement terranes of the Variscan-Appalachian orogen: Baltican, Saharan and West African hafnium isotopic fingerprints in Avalonia, Iberia and the Armorican Terranes. Tectonophysics.

Hibbard, J.P., van Staal, C.R., Miller, B.V., 2007a. Links among Carolinia, Avalonia, and Ganderia in the Appalachian peri-Gondwanan realm. Geological Society of America Special Papers 433, 291-311.

Hibbard, J.P., Van Staal, C.R., Rankin, D.W., 2007b. A comparative analysis of pre-Silurian crustal building blocks of the northern and the southern Appalachian orogen. American Journal of Science 307, 23-45.

Hogan, J.P., Sinha, A.K., 1989. Compositional variation of plutonism in the coastal Maine magmatic province: mode of origin and tectonic setting. Studies in Maine geology 4, 1-33.

Hyndman, R.D., Currie, C.A., Mazzotti, S.P., 2005. Subduction zone backarcs, mobile belts, and orogenic heat. GSA Today 15, 4-10.

Johnson, P., Andresen, A., Collins, A.S., Fowler, A., Fritz, H., Ghebreab, W., Kusky, T., Stern, R., 2011. Late Cryogenian–Ediacaran history of the Arabian–Nubian Shield: a review of depositional, plutonic, structural, and tectonic events in the closing stages of the northern East African Orogen. Journal of African Earth Sciences 61, 167-232.

Kellett, D.A., Rogers, N., McNicoll, V., Kerr, A., van Staal, C., McFarlane, C., 2014. New age data refine extent and duration of Paleozoic and Neoproterozoic plutonism at Ganderia–Avalonia boundary, Newfoundland. Canadian Journal of Earth Sciences 51, 943-972.

Kemp, A., Hawkesworth, C., Collins, W., Gray, C., Blevin, P., 2009. Isotopic evidence for rapid continental growth in an extensional accretionary orogen: The Tasmanides, eastern Australia. Earth and Planetary Science Letters 284, 455-466.

Keppie, D., Dallmeyer, R.D., 1995. Late Paleozoic collision, delamination, short-lived mgmatism, and rapid denudation in the Meguma Terrane (Nova Scotia, Canada): constraints from 40Ar/39Ar isotopic data Canadian Journal of Earth Sciences 32.

Keppie, J.D., Dostal, J., Dallmeyer, R.D., Doig, R., 2000. Superposed Neoproterozoic and Silurian magmatic arcs in central Cape Breton Island, Canada: Geochemical and geochronological constraints. Geological Magazine 137, 137-153.

Keppie, J.D., Dostal, J., Murphy, J.B., Nance, R.D., 2008. Synthesis and tectonic interpretation of the westernmost Paleozoic Variscan orogen in southern Mexico: From rifted Rheic margin to active Pacific margin. Tectonophysics 461, 277-290.

Keppie, J.D., Dostal, J., Zentilli, M., 1979. Early Silurian volcanic rocks at Arisaig, Nova Scotia. Canadian Journal of Earth Sciences 16, 1635-1640.

Keppie, J.D., Keppie, D.F., 2014. Ediacaran–Middle Paleozoic Oceanic Voyage of Avalonia from Baltica via Gondwana to Laurentia: Paleomagnetic, Faunal and Geological Constraints. Geoscience Canada 41, 5-18.

Keppie, J.D., Krogh, T.E., 2000. 440 Ma igneous activity in the Meguma Terrane, Nova Scotia, Canada; part of the Appalachian overstep sequence? American Journal of Science 300, 528-538.

Keppie, J.D., Nance, R.D., Murphy, J.B., Dostal, J., 2003. Tethyan, Mediterranean, and Pacific analogues for the Neoproterozoic-Paleozoic birth and development of peri-Gondwanan terranes and their transfer to Laurentia and Laurussia. Tectonophysics 365, 195-219.

Kerr, A., Dunning, G., Tucker, R., 1993. The youngest Paleozoic plutonism of the Newfoundland Appalachians: U-Pb ages from the St. Lawrence and François granites. Canadian Journal of Earth Sciences 30, 2328-2333.

Kerr, A., Jenner, G.A., Fryer, B.J., 1995. Sm–Nd isotopic geochemistry of Precambrian to Paleozoic granitoid suites and the deep-crustal structure of the southeast margin of the Newfoundland Appalachians. Canadian Journal of Earth Sciences 32, 224-245.

Krogh, T., Keppie, J.D., 1990. Age of detrital zircon and titanite in the Meguma Group, southern Nova Scotia, Canada: clues to the origin of the Meguma Terrane. Tectonophysics 177, 307-323.

Landing, E., 2004. Precambrian–Cambrian

boundary interval deposition and the marginal platform of the Avalon microcontinent. Journal of Geodynamics 37, 411-435.

Landing, E., 2005. Early Paleozoic Avalon–Gondwana unity: an obituary—response to "Palaeontological evidence bearing on global Ordovician–Silurian continental reconstructions" by R.A. Fortey and L.R.M. Cocks. Earth-Science Reviews 69, 169-175.

Landing, E., Murphy, J.B., 1991. Uppermost Precambrian(?)-lower Cambrian of mainland Nova Scotia: faunas, depositional environments, and stratigraphic revision. Journal of Paleontology 65, 382-396.

Lin, S., Davis, D.W., Barr, S.M., Van Staal, C.R., Chen, Y., Constantin, M., 2007. U-Pb geochronological constraints on the evolution of the Aspy terrane, Cape Breton Island: implications for relationships between Aspy and Bras d'Or terranes and Ganderia in the Canadian Appalachians. American Journal of Science 307, 371-398.

Linnemann, U., Gerdes, A., Hofmann, M., Marko, L., 2014. The Cadomian Orogen: Neoproterozoic to Early Cambrian crustal growth and orogenic zoning along the periphery of the West African Craton—Constraints from U–Pb zircon ages and Hf isotopes (Schwarzburg Antiform, Germany). Precambrian Research 244, 236-278.

Linnemann, U., Pereira, F., Jeffries, T.E., Drost, K., Gerdes, A., 2008. The Cadomian Orogeny and the opening of the Rheic Ocean: the diacrony of geotectonic processes constrained by LA-ICP-MS U–Pb zircon dating (Ossa-Morena and Saxo-Thuringian Zones, Iberian and Bohemian Massifs). Tectonophysics 461, 21-43.

MacDonald, L.A., Barr, S.M., White, C.E., Ketchum, J.W., 2002. Petrology, age, and tectonic setting of the White Rock Formation, Meguma terrane, Nova Scotia: evidence for Silurian continental rifting. Canadian Journal of Earth Sciences 39, 259-277.

MacLean, N.J., Barr, S.M., White, C.E., Ketchum, J.W., 2003. New U-Pb (zircon) age and geochemistry of the Wedgeport pluton, Meguma terrane, Nova Scotia. Atlantic Geology 39.

McClellan, E., Gazel, E., 2014. The Cryogenian intra-continental rifting of Rodinia: Evidence from the Laurentian margin in eastern North America. Lithos 206, 321-337.

Millar, I.L., 1999. Neoproterozoic extensional basic magmatism associated with the West Highland granite gneiss in the Moine Supergroup of NW Scotland. Journal of the Geological Society 156, 1153-1162.

Moran, P.C., Barr, S.M., White, C.E., Hamilton, M.A., 2007. Petrology, age, and tectonic setting of the Seal Island Pluton, offshore southwestern Nova Scotia. Canadian Journal of Earth Sciences 44, 1467-1478.

Murphy, B., Keppie, D.J., Hynes, A.J., 1991. Geology, Antigonish Highlands, Nova Scotia, In: Canada, G.S.o. (Ed.).

Murphy, B.J., van Staal, C.R., Duncan Keppie, J., 1999. Middle to late Paleozoic Acadian orogeny in the northern Appalachians: A Laramide-style plume-modified orogeny? Geology 27, 653-656.

Murphy, J.B., 1987. Petrology of Upper Ordovician-Lower Silurian rocks of the Antigonish Highlands, Nova Scotia. Canadian Journal of Earth Sciences 24, 752-759.

Murphy, J.B., 2002. Geochemistry of the Neoproterozoic metasedimentary Gamble Brook Formation, Avalon Terrane, Nova Scotia: Evidence for a rifted-arc environment along the West Gondwanan margin of Rodinia. Journal of Geology 110, 407-419.

Murphy, J.B., Dostal, J., 2007. Continental mafic magmatism of different ages in the same terrane: Constraints on the evolution of an enriched mantle source. Geology 35, 335-338.

Murphy, J.B., Dostal, J., Keppie, J.D., 2008.

Neoproterozoic-Early Devonian magmatism in the Antigonish Highlands, Avalon terrane, Nova Scotia: Tracking the evolution of the mantle and crustal sources during the evolution of the Rheic Ocean. Tectonophysics 461, 181-201.

Murphy, J.B., Fernández-Suárez, J., Jeffries, T.E., 2004a. Lithogeochemical and Sm-Nd and U-Pb isotope data from the Silurian-Lower Devonian Arisaig Group clastic rocks, Avalon terrane, Nova Scotia: A record of terrane accretion in the Appalachian-Caledonide orogen. Bulletin of the Geological Society of America 116, 1183-1201.

Murphy, J.B., Fernández-Suárez, J., Keppie, J.D., Jeffries, T.E., 2004b. Contiguous rather than discrete Paleozoic histories for the Avalon and Meguma terranes based on detrital zircon data. Geology 32, 585-588.

Murphy, J.B., Gutierrez-Alonso, G., Nance, R.D., Fernandez-Suarez, J., Keppie, J.D., Quesada, C., Strachan, R.A., Dostal, J., 2006. Origin of the Rheic Ocean: Rifting along a Neoproterozoic suture? Geology 34, 325-328.

Murphy, J.B., Hamilton, M.A., 2000. Orogenesis and Basin development: U-Pb detrital zircon age constraints on evolution of the Late Paleozoic St. Marys Basin, Central Mainland Nova Scotia. Journal of Geology 108, 53-71.

Murphy, J.B., Keppie, J.D., 1998. Late Devonian palinspastic reconstruction of the Avalon-Meguma terrane boundary: Implications for terrane accretion and basin development in the Appalachian orogen. Tectonophysics 284, 221-231.

Murphy, J.B., Keppie, J.D., 2005. The Acadian orogeny in the northern Appalachians. International Geology Review 47, 663-687.

Murphy, J.B., Keppie, J.D., Dostal, J., Waldron, J.W.F., Cude, M.P., 1996. Geochemical and isotopic characteristics of early Silurian clastic sequences in Antigonish Highlands, Nova Scotia, Canada: Constraints on the accretion of Avalonia in the Appalachian - Caledonide Orogen. Canadian Journal of Earth Sciences 33, 379-388.

Murphy, J.B., Keppie, J.D., Nance, R.D., Dostal, J., 2010. Comparative evolution of the Iapetus and Rheic Oceans: A North America perspective. Gondwana Research 17, 482-499.

Murphy, J.B., Nance, R.D., 2002. Sm-Nd isotopic systematics as tectonic tracers: An example from West Avalonia in the Canadian Appalachians. Earth-Science Reviews 59, 77-100.

Murphy, J.B., Pisarevsky, S., Nance, R.D., 2013. Potential geodynamic relationships between the development of peripheral orogens along the northern margin of Gondwana and the amalgamation of West Gondwana. Mineralogy and Petrology 107, 635-650.

Murphy, J.B., Strachan, R.A., Nance, R.D., Parker, K.D., Fowler, M.B., 2000. Proto-Avalonia: A 1.2-1.0 Ga tectonothermal event and constraints for the evolution of Rodinia. Geology 28, 1071-1074.

Murphy, J.B., Waldron, J.W.F., Kontak, D.J., Pe-Piper, G., Piper, D.J.W., 2011. Minas Fault Zone: Late Paleozoic history of an intra-continental orogenic transform fault in the Canadian Appalachians. Journal of Structural Geology 33, 312-328.

Nance, R.D., Gutiérrez-Alonso, G., Keppie, J.D., Linnemann, U., Murphy, J.B., Quesada, C., Strachan, R.A., Woodcock, N.H., 2010. Evolution of the Rheic Ocean. Gondwana Research 17, 194-222.

Nance, R.D., Gutiérrez-Alonso, G., Keppie, J.D., Linnemann, U., Murphy, J.B., Quesada, C., Strachan, R.A., Woodcock, N.H., 2012. A brief history of the Rheic Ocean. Geoscience Frontiers 3, 125-135.

Nance, R.D., Murphy, J.B., 1994. Contrasting basement isotopic signatures and the palinspastic restoration of peripheral orogens: example from the Neoproterozoic Avalonian-Cadomian belt. Geology 22, 617-620.

Nance, R.D., Murphy, J.B., 1996. Basement isotopic signatures and Neoproterozoic paleogeography

of Avalonian-Cadomian and related terranes in the circum-North Atlantic, Special Paper of the Geological Society of America, pp. 333-346.

Nance, R.D., Murphy, J.B., Keppie, J.D., 2002. A Cordilleran model for the evolution of Avalonia. Tectonophysics 352, 11-31.

Normore, L.S., 2012. Geology of the Random Island map area (NTS 2C/04), Newfoundland, In: Government of Newfoundland and Labrador, D.o.N.R., Geological Survey. (Ed.), Map 2012-06. Scale 1:50,000.

Novak, S.W., Rankin, D.W., 2004. Compositional zoning of a Neoproterozoic ash-flow sheet of the Mount Rogers Formation, southwestern Virginia Blue Ridge, and the aborted rifting of Laurentia. Geological Society of America Memoirs 197, 571-600.

O'Brien, B., O'Brien, S., Dunning, G., 1991. Silurian cover, late Precambrian-Early Ordovician basement, and the chronology of Silurian orogenesis in the Hermitage Flexure (Newfoundland Appalachians). American Journal of Science 291, 760-799.

O'Brien, S., O'Brien, B., Dunning, G., Tucker, R., 1996. Late Neoproterozoic Avalonian and related peri-Gondwanan rocks of the Newfoundland Appalachians. SPECIAL PAPERS-GEOLOGICAL SOCIETY OF AMERICA, 9-28.

Paulsson, O., Andreasson, P.-G., 2002. Attempted break-up of Rodinia at 850 Ma: geochronological evidence from the Seve–Kalak Superterrane, Scandinavian Caledonides. Journal of the Geological Society 159, 751-761.

Pe-Piper, G., Piper, D.J., 2003. A synopsis of the geology of the Cobequid Highlands, Nova Scotia. Atlantic Geology 38.

Pe Piper, G., Cormier, C.F.M., Piper, D.J.W., 1991. The age and significance of Carboniferous plutons of the western Cobequid Highlands, Nova Scotia. Canadian Journal of Earth Sciences 26.

Piper, D.J.W., Pe-Piper, G., 2001. Tectonic deformation and magmatism along the southern flank of the Maritimes Basin: the northeastern Cobequid Highlands, Nova Scotia. Canadian Journal of Earth Sciences 38, 43-58.

Pisarevsky, S.A., Murphy, J.B., Cawood, P.A., Collins, A.S., 2008. Late Neoproterozoic and Early Cambrian palaeogeography: models and problems. Geological Society, London, Special Publications 294, 9-31.

Pollock, J.C., Hibbard, J.P., Sylvester, P.J., 2009. Early Ordovician rifting of Avalonia and birth of the Rheic Ocean: U–Pb detrital zircon constraints from Newfoundland. Journal of the Geological Society 166, 501-515.

Pollock, J.C., Hibbard, J.P., van Staal, C.R., 2011. A paleogeographical review of the peri-Gondwanan realm of the Appalachian orogen1 This article is one of a series of papers published in this CJES Special Issue: In honour of Ward Neale on the theme of Appalachian and Grenvillian geology. Canadian Journal of Earth Sciences 49, 259-288.

Pollock, J.C., Sylvester, P.J., Barr, S.M., Murphy, B., 2015. Lu–Hf zircon and Sm–Nd whole-rock isotope constraints on the extent of juvenile arc crust in Avalonia: examples from Newfoundland and Nova Scotia, Canada. Canadian Journal of Earth Sciences 52, 1-21.

Ramos, V.A., 1988. Late Proterozoic-early Paleozoic of South America - a collisional history. Episodes 11, 168-174.

Rankin, D.W., 1976. Appalachian salients and recesses: Late Precambrian continental breakup and the opening of the Iapetus Ocean. Journal of Geophysical Research 81, 5605-5619.

Rankin, D.W., 1993. The volcanogenic Mount Rogers Formation and the overlying glaciogenic Konnarock Formation; two late Proterozoic units in southwestern Virginia. USGPO; US Geological Survey, Map Distribution.

Reynolds, P.H., White, C.E., Barr, S.M., Muir, C.M., 2012. 40Ar–39Ar ages for detrital white

mica in Meguma terrane, Nova Scotia, Canada: implications for provenance of the Goldenville and Halifax groups. Canadian Journal of Earth Sciences 49, 781-795.

Robinson, P., Tucker, R.D., Bradley, D., Berry IV, H.N., Osberg, P.H., 1998. Paleozoic orogens in New England, USA. GFF 120, 119-148.

Rogers, G., Kinny, P., Strachan, R., Friend, C., Paterson, B., 2001. U–Pb geochronology of the Fort Augustus granite gneiss: constraints on the timing of Neoproterozoic and Palaeozoic tectonothermal events in the NW Highlands of Scotland. Journal of the Geological Society 158, 7-14.

Ryan, P.D., Soper, N., 2001. Modelling anatexis in intra-cratonic rift basins: an example from the Neoproterozoic rocks of the Scottish Highlands. Geological Magazine 138, 577-588.

Samson, S.D., Barr, S.M., White, C.E., 2000. Nd isotopic characteristics of terranes within the Avalon Zone, southern New Brunswick. Canadian Journal of Earth Sciences 37, 1039-1052.

Schofield, D.I., D'Lemos, R.S., 2000. Granite petrogenesis in the Gander Zone, NE Newfoundland: mixing of melts from multiple sources and the role of lithospheric delamination. Canadian Journal of Earth Sciences 37, 535-547.

Schoonmaker, A., Kidd, W., Bradley, D., 2005. Foreland-forearc collisional granitoid and mafic magmatism caused by lowerplate lithospheric slab break-off: The Acadian of Maine, and other orogens. . Geology 33.

Schulz, K.J., Stewart, D.B., Tucker, R.D., Pollock, J.C., Ayuso, R.A., 2008. The Ellsworth terrane, coastal Maine: Geochronology, geochemistry, and Nd-Pb isotopic composition—Implications for the rifting of Ganderia. Geological Society of America Bulletin 120, 1134-1158.

Shellnutt, J.G., Dostal, J., 2015. Granodiorites of the South Mountain Batholith (Nova Scotia, Canada) derived by partial melting of Avalonia granulite rocks beneath the Meguma terrane: Implications for the heat source of the Late Devonian granites of the Northern Appalachians. Tectonophysics 655, 206-212.

Solar, S.G., Pressley, R.A., Brown, M., Tucker, R.D., 1998. Granite ascent in convergent orogenic belts: testing a model. Geology 26.

Stampfli, G., Borel, G., 2002. A plate tectonic model for the Paleozoic and Mesozoic constrained by dynamic plate boundaries and restored synthetic oceanic isochrons. Earth and Planetary Science Letters 196, 17-33.

Stampfli, G., Hochard, C., Vérard, C., Wilhem, C., vonRaumer, J., 2013. The formation of Pangea. Tectonophysics.

Stevenson, I.M., 1959. Shubenacadie and Kennetcook Map-areas, Colchester, Hants and Halifax Counties, Nova Scotia. Department of Mines and Technical Surveys.

Strachan, R.A., Nance, R.D., Dallmeyer, R.D., D'Lemos, R.S., Murphy, J.B., Watt, G.R., 1996. Late Precambrian tectonothermal evolution of the Malverns Complex. Journal of the Geological Society 153, 589-600.

Tate, M., Clarke, D., 1997. Compositional diversity among Late Devonian peraluminous granitoid intrusions in the Meguma Zone of Nova Scotia, Canada. Lithos 39, 179-194.

Tate, M.C., Clarke, D.B., Heaman, L.M., 1997. Progressive hybridisation between Late Devonian mafic-intermediate and felsic magmas in the Meguma Zone of Nova Scotia, Canada. Contributions to Mineralogy and Petrology 126, 401-415.

Thompson, M.D., Barr, S.M., Grunow, A.M., 2012. Avalonian perspectives on Neoproterozoic paleogeography: Evidence from Sm-Nd isotope geochemistry and detrital zircon geochronology in SE New England, USA. Bulletin of the Geological Society of America 124, 517-531.

Thompson, M.D., Hermes, O.D., 2003. Early rifting in the Narragansett Basin, Massachusetts-

Rhodes Island: evidence from late Devonian bimodal volcanic rocks. The Journal of Geology.

Tohver, E., D'Agrella-Filho, M.S., Trindade, R.I.F., 2006. Paleomagnetic record of Africa and South America for the 1200–500 Ma interval, and evaluation of Rodinia and Gondwana assemblies. Precambrian Research 147, 193-222.

Tollo, R.P., Aleinikoff, J.N., 1996. Petrology and U-PB geochronology of the Robertson River Igneous Suite, Blue Ridge province, Virginia-Evidence for multistage magmatism associated witn an early episode of Laurentian rifting. American Journal of Science 296, 1045-1090.

Tollo, R.P., Aleinikoff, J.N., Bartholomew, M.J., Rankin, D.W., 2004. Neoproterozoic A-type granitoids of the central and southern Appalachians: intraplate magmatism associated with episodic rifting of the Rodinian supercontinent. Precambrian Research 128, 3-38.

Tollo, R.P., Aleinikoff, J.N., Mundil, R., Southworth, C.S., Cosca, M.A., Rankin, D.W., Rubin, A.E., Kentner, A.E., Parendo, C.A., Ray, M.S., 2012. Igneous activity, metamorphism, and deformation in the Mount Rogers area of SW Virginia and NW North Carolina: A geologic record of Precambrian tectonic evolution of the southern Blue Ridge Province. Field Guides 29, 1-66.

Torsvik, T.H., Carter, L.M., Ashwal, L.D., Bhushan, S.K., Pandit, M.K., Jamtveit, B., 2001. Rodinia refined or obscured: palaeomagnetism of the Malani igneous suite (NW India). Precambrian Research 108, 319-333.

Tuach, J., 1987. The Ackley high-silica magmatic/metallogenic system and associated post-tectonic granites, southeast Newfoundland. Memorial University of Newfoundland.

Tucker, R., Corfu, F., 1993. Late Precambrian magmatic record of the Avalon Zone, Newfoundland: age and source inferences from U–Pb and Lu–Hf isotopic measurements of zircon, Geological Society of America, Abstracts with Programs, p. 86.

van Staal, C.R., Barr, S.M., 2011. Lithospheric architecture and tectonic evolution of the Canadian Appalachians and associated Atlantic margin., In: Percival, J.A., Cook, F.A., Clowes, R.M. (Eds.), Tectonic Styles in Canada Revisited: the LITHOPROBE perspective. Geological Association of Canada

van Staal, C.R., Barr, S.M., Murphy, J.B., 2012. Provenance and tectonic evolution of Ganderia: Constraints on the evolution of the Iapetus and Rheic oceans. Geology 40, 987-990.

van Staal, C.R., Dewey, J., Mac Niocaill, C., McKerrow, W., 1998. The Cambrian-Silurian tectonic evolution of the northern Appalachians and British Caledonides: history of a complex, west and southwest Pacific-type segment of Iapetus. Geological Society, London, Special Publications 143, 197-242.

van Staal, C.R., McNicoll, V., Valverde-Vaquero, P., Barr, S.M., Fyffe, L.R., Reusch, D.N., 2004. Ganderia, Avalonia, and the Salinic and Acadian orogenies, Geological Society of America Abstracts with Programs, pp. 128-129.

van Staal, C.R., Sullivan, R.W., Whalen, J.B., 1996. Provenance and tectonic history of the Gander Zone in the Caledonian/Appalachian orogen: Implications for the origin and assembly of Avalon. SPECIAL PAPERS-GEOLOGICAL SOCIETY OF AMERICA, 347-368.

van Staal, C.R., Whalen, J.B., Valverde-Vaquero, P., Zagorevski, A., Rogers, N., 2009. Pre-Carboniferous, episodic accretion-related, orogenesis along the Laurentian margin of the northern Appalachians. Geological Society, London, Special Publications 327, 271-316.

van Staal, C.R., Zagorevski, A., McNicoll, V.J., Rogers, N., 2014. Time-transgressive Salinic and Acadian orogenesis, magmatism and Old Red Sandstone sedimentation in Newfoundland. Geoscience Canada 41, 138-164.

Von Raumer, J., Stampfli, G., Borel, G., Bussy, F., 2002. Organization of pre-Variscan basement areas at the north-Gondwanan margin. International Journal of Earth Sciences 91, 35-52.

Waldron, J.W., Schofield, D.I., White, C.E., Barr, S.M., 2011. Cambrian successions of the Meguma Terrane, Nova Scotia, and Harlech Dome, North Wales: dispersed fragments of a peri-Gondwanan basin? Journal of the Geological Society 168, 83-98.

Waldron, J.W., White, C.E., Barr, S.M., Simonetti, A., Heaman, L.M., 2009. Provenance of the Meguma terrane, Nova Scotia: rifted margin of early Paleozoic Gondwana. Canadian Journal of Earth Sciences 46, 1-8.

Waldron, J.W.F., Murphy, J.B., Melchin, M.J., Davis, G., 1996. Silurian tectonics of western Avalonia: Strain-corrected subsidence history of the Arisaig Group, Nova Scotia. Journal of Geology 104, 677-694.

Waldron, J.W.F., van Staal, C.R., 2001. Taconian orogeny and the accretion of the Dashwoods block: A peri-Laurentian microcontinent in the Iapetus Ocean. Geology 29, 811-814.

Walsh, G.J., Benziane, F., Aleinikoff, J.N., Harrison, R.W., Yazidi, A., Burton, W.C., Quick, J.E., Saadane, A., 2012. Neoproterozoic tectonic evolution of the Jebel Saghro and Bou Azzer—El Graara inliers, eastern and central Anti-Atlas, Morocco. Precambrian Research 216–219, 23-62.

Whalen, J.B., Currie, K.L., Chappell, B.W., 1987. A-type granites: geochemical characteristics, discrimination and petrogenesis. Contributions to Mineralogy and Petrology 95, 407-419.

Whalen, J.B., JENNER, G.A., LONGSTAFFE, F.J., ROBERT, F., GARIÉPY, C., 1996. Geochemical and isotopic (O, Nd, Pb and Sr) constraints on A-type granite petrogenesis based on the Topsails igneous suite, Newfoundland Appalachians. Journal of Petrology 37, 1463-1489.

Whalen, J.B., McNicoll, V.J., van Staal, C.R., Lissenberg, C.J., Longstaffe, F.J., Jenner, G.A., van Breeman, O., 2006. Spatial, temporal and geochemical characteristics of Silurian collision-zone magmatism, Newfoundland Appalachians: An example of a rapidly evolving magmatic system related to slab break-off. Lithos 89, 377-404.

White, C., Barr, S., 2003. Age and petrochemistry of mafic sills on the northwestern margin of the Meguma terrane in the Bear River–Yarmouth area of southwestern Nova Scotia. Mineral Resources Branch, Report of Activities, 2004-2001.

White, C., Palacios, T., Jensen, S., Barr, S., 2011. The Meguma terrane of southern Nova Scotia: insights on its pre-Carboniferous stratigraphy.

White, C., Palacios, T., Jensen, S., Barr, S., 2012a. Cambrian–Ordovician acritarchs in the Meguma terrane, Nova Scotia, Canada: Resolution of early Paleozoic stratigraphy and implications for paleogeography. Geological Society of America Bulletin 124, 1773-1792.

White, C.E., 2010. Stratigraphy of the Lower Paleozoic Goldenville and Halifax groups in the western part of southern Nova Scotia. 2010, 19.

White, C.E., Barr, S.M., 2012. Meguma terrane revisited: Stratigraphy, metamorphism, paleontology, and provenance. Geoscience Canada 39.

White, C.E., Barr, S.M., Archibald, D.B., Drummond, J., Voy, K., Escarraga, E.A., MacFarlane, C.R.M., 2012b. A new geological interpretation of the Antigonish Highlands, Northern Nova Scotia. Nova Scotia Mineral Resources Branch, Natural Resources, Geology matters 2012.

Williams, H., 1979. Appalachian orogen in Canada. Canadian Journal of Earth Sciences 16, 792-807.

Williams, H., Colman-Sadd, S., Swinden, H., 1988. Tectonic-stratigraphic subdivisions of

central Newfoundland. Current Research, Part B. Geological Survey of Canada, Paper 88, 91-98.

Willner, A., Barr, S., Gerdes, A., Massonne, H.-J., White, C., 2013. Origin and evolution of Avalonia: evidence from U–Pb and Lu–Hf isotopes in zircon from the Mira terrane, Canada, and the Stavelot–Venn Massif, Belgium. Journal of the Geological Society 170, 769-784.

Willner, A.P., Gerdes, A., Massonne, H.J., van Staal, C.R., Zagorevski, A., 2014. Crustal Evolution of the Northeast Laurentian Margin and the Peri-Gondwanan Microcontinent Ganderia Prior to and During Closure of the Iapetus Ocean: Detrital Zircon U-Pb and Hf Isotope Evidence from Newfoundland. Geoscience Canada 41, 345-364.

Wilson, J.T., 1966. Did the Atlantic close and then re-open? Nature.

Zagorevski, A., Rogers, N., van Staal, C.R., McNicoll, V., Lissenberg, C.J., Valverde-Vaquero, P., 2006. Lower to Middle Ordovician evolution of peri-Laurentian arc and backarc complexes in Iapetus: Constraints from the Annieopsquotch accretionary tract, central Newfoundland. Geological Society of America Bulletin 118, 324-342.

Zagorevski, A., Van Staal, C., 2011. The record of Ordovician arc–arc and arc–continent collisions in the Canadian Appalachians during the closure of Iapetus, Arc-Continent Collision. Springer, pp. 341-371.

Zagorevski, A., Van Staal, C.R., McNicoll, V., Rogers, N., 2007a. Upper Cambrian to Upper Ordovician peri-Gondwanan Island arc activity in the Victoria Lake Supergroup, Central Newfoundland: Tectonic development of the northern Ganderian margin. American Journal of Science 307, 339-370.

Zagorevski, A., van Staal, C.R., McNicoll, V.J., 2007b. Distinct Taconic, Salinic, and Acadian deformation along the Iapetus suture zone, Newfoundland Appalachians. Canadian Journal of Earth Sciences 44, 1567-1585.

Supporting data

Supplementary Table 1. U-Pb detrital zircon data

Sample		Pb207/Pb206		Pb206/U238		Pb207/U235		Conc.	Pb207/Pb206		Pb206/U238		Pb207/U235	
ACO-12-26B	26b-01	0.06324	0.00144	0.11371	0.00142	0.9914	0.02178	101	716.3	47.77	694.3	8.2	699.4	11.11
ACO-12-26B	26b-02	0.061	0.00115	0.10225	0.00124	0.86004	0.01604	100	639.3	40.05	627.6	7.25	630.1	8.75
ACO-12-26B	26b-03	0.06563	0.00122	0.10475	0.0013	0.94788	0.0175	105	794.6	38.41	642.2	7.56	677	9.12
ACO-12-26B	26b-04	0.06358	0.00166	0.1052	0.00153	0.92216	0.02369	103	727.7	54.31	644.8	8.94	663.5	12.51
ACO-12-26B	26b-05	0.06449	0.00125	0.10548	0.00143	0.93785	0.01859	104	757.8	40.38	646.4	8.34	671.8	9.74
ACO-12-26B	26b-06	0.0686	0.00097	0.10413	0.00127	0.98488	0.01471	109	886.7	28.87	638.6	7.44	696.1	7.52
ACO-12-26B	26b-07	0.06413	0.00111	0.10214	0.00134	0.9031	0.01625	104	745.9	36.17	626.9	7.85	653.4	8.67
ACO-12-26B	26b-08	0.06328	0.00122	0.12459	0.0015	1.08701	0.02051	99	717.7	40.31	756.9	8.62	747.1	9.98
ACO-12-26B	26b-09	0.06227	0.00143	0.10634	0.00136	0.91294	0.02037	101	683.5	48.3	651.4	7.91	658.6	10.81
ACO-12-26B	26b-10	0.05952	0.00087	0.0969	0.00122	0.79516	0.01245	100	586.1	31.48	596.2	7.17	594.1	7.04
ACO-12-26B	26b-11	0.06375	0.00113	0.11335	0.0014	0.9963	0.01782	101	733.4	37.24	692.1	8.1	701.9	9.06
ACO-12-26B	26b-12	0.07701	0.00112	0.09779	0.00117	1.03842	0.0155	120	1121.5	28.67	601.5	6.85	723.1	7.72
ACO-12-26B	26b-13	0.06288	0.00088	0.09376	0.0012	0.81295	0.01243	105	704.3	29.46	577.8	7.05	604.1	6.96
ACO-12-26B	26b-14	0.06849	0.00115	0.10979	0.00136	1.03679	0.01757	108	883.5	34.2	671.5	7.87	722.3	8.76
ACO-12-26B	26b-15	0.0598	0.00087	0.09746	0.00115	0.80355	0.01211	100	596.2	31.25	599.5	6.77	598.8	6.82
ACO-12-26B	26b-16	2.49645	0.03361	0.11727	0.00134	40.36353	0.53698	529	6494.4	18.02	714.8	7.76	3779.7	13.18
ACO-12-26B	26b-17	0.06205	0.00097	0.10593	0.0013	0.90625	0.01462	101	675.8	32.98	649.1	7.56	655.1	7.79
ACO-12-26B	26b-18	0.06303	0.0014	0.10988	0.00145	0.9549	0.02092	101	709.2	46.46	672.1	8.43	680.6	10.87
ACO-12-26B	26b-19	0.06409	0.00143	0.1111	0.00139	0.98181	0.02129	102	744.5	46.57	679.1	8.08	694.5	10.91
ACO-12-26B	26b-20	0.05893	0.00085	0.10223	0.00121	0.83064	0.01247	98	564.6	30.56	627.5	7.1	614	6.91
ACO-12-26B	26b-21	0.06555	0.0011	0.11211	0.00138	1.01317	0.0172	104	792	34.81	685	7.98	710.5	8.68
ACO-12-26B	26b-22	0.06278	0.0008	0.11823	0.00138	1.02339	0.01381	99	700.9	26.92	720.4	7.94	715.6	6.93
ACO-12-26B	26b-23	0.06196	0.00112	0.11411	0.00142	0.97483	0.0177	99	672.8	38.18	696.6	8.22	690.9	9.1
ACO-12-26B	26b-24	0.06304	0.00083	0.09993	0.00122	0.8685	0.01231	103	709.6	27.71	614	7.13	634.8	6.69
ACO-12-26B	26b-25	0.06255	0.00091	0.11265	0.00134	0.9715	0.01464	100	693	30.83	688.1	7.76	689.2	7.54
ACO-12-26B	26b-26	0.06482	0.00198	0.11555	0.00169	1.03278	0.03037	102	768.6	63.08	704.9	9.78	720.3	15.17
ACO-12-26B	26b-27	0.0629	0.00092	0.11355	0.00139	0.98472	0.01513	100	704.9	30.86	693.3	8.05	696	7.74
ACO-12-26B	26b-28	0.06181	0.00096	0.10599	0.00127	0.90323	0.0144	101	667.5	33.07	649.4	7.43	653.5	7.68
ACO-12-26B	26b-29	0.05912	0.00097	0.10665	0.00126	0.86927	0.01435	97	571.4	35.44	653.3	7.33	635.2	7.8
ACO-12-26B	26b-30	0.06747	0.0014	0.1252	0.00157	1.16467	0.02358	103	852.2	42.59	760.4	8.99	784.1	11.06
ACO-12-26B	26b-31	0.06359	0.00105	0.09866	0.00123	0.86504	0.01462	104	728.1	34.48	606.6	7.23	632.9	7.96
ACO-12-26B	26b-32	0.0622	0.00078	0.10587	0.00122	0.90792	0.01204	101	681	26.55	648.7	7.14	655.9	6.41

ACO-12-26B	26b-33	0.06175	0.00086	0.11406	0.00126	0.97111	0.01351	99	665.5	29.44	696.3	7.31	689	6.96
ACO-12-26B	26b-34	0.06473	0.00144	0.12313	0.00163	1.09883	0.02401	101	765.5	46.09	748.5	9.37	752.8	11.62
ACO-12-26B	26b-35	0.06106	0.00098	0.10669	0.00132	0.89812	0.01487	100	641.3	34.17	653.5	7.71	650.7	7.95
ACO-12-26B	26b-36	0.06136	0.00136	0.09621	0.00126	0.81396	0.01777	102	651.8	46.98	592.2	7.39	604.7	9.95
ACO-12-26B	26b-37	0.06345	0.00169	0.11826	0.00163	1.03464	0.02661	100	723.5	55.35	720.5	9.42	721.2	13.28
ACO-12-26B	26b-38	0.06386	0.00124	0.11345	0.00151	0.99899	0.01959	102	737.1	40.43	692.8	8.73	703.3	9.95
ACO-12-26B	26b-39	0.07355	0.00125	0.10157	0.00125	1.0299	0.01762	115	1029	34.08	623.6	7.34	718.9	8.81
ACO-12-26B	26b-40	0.06788	0.00125	0.10308	0.0012	0.96472	0.01718	108	864.8	37.68	632.5	7.01	685.7	8.88
ACO-12-26B	26b-41	0.06186	0.00091	0.1098	0.0013	0.93628	0.01421	100	669.4	31.3	671.6	7.54	670.9	7.45
ACO-12-26B	26b-42	0.0646	0.00168	0.12049	0.00166	1.07304	0.02709	101	761.4	53.84	733.4	9.57	740.2	13.27
ACO-12-26B	26b-43	0.06435	0.00174	0.10234	0.00147	0.90789	0.02392	104	753	56.11	628.1	8.57	655.9	12.73
ACO-12-26B	26b-44	0.06431	0.00139	0.10804	0.00148	0.95791	0.02066	103	752	44.91	661.4	8.58	682.2	10.72
ACO-12-26B	26b-45	0.06154	0.00111	0.10528	0.00126	0.89314	0.01595	100	658.3	38.2	645.3	7.35	648.1	8.55
ACO-12-26B	26b-46	0.06396	0.00155	0.11263	0.00149	0.99299	0.02336	102	740.3	50.4	688	8.64	700.2	11.9
ACO-12-26B	26b-47	0.06029	0.00086	0.1069	0.00127	0.88852	0.01322	99	614.2	30.54	654.7	7.42	645.6	7.11
ACO-12-26B	26b-48	0.05867	0.00098	0.09473	0.00112	0.76622	0.01282	99	555.1	35.93	583.5	6.62	577.6	7.37
ACO-12-26B	26b-49	0.05991	0.00093	0.11166	0.00129	0.92215	0.01441	97	600.4	33.25	682.4	7.51	663.5	7.61
ACO-12-26B	26b-50	0.06213	0.00123	0.11445	0.00151	0.98028	0.01962	99	678.6	41.87	698.5	8.74	693.8	10.06
ACO-12-26B	26b-51	0.06244	0.00103	0.10575	0.00123	0.91024	0.0149	101	689.4	34.75	648	7.17	657.2	7.92
ACO-12-26B	26b-52	0.06148	0.00091	0.11596	0.00137	0.9827	0.01488	98	656	31.3	707.3	7.91	695	7.62
ACO-12-26B	26b-53	0.06174	0.00141	0.10508	0.00136	0.89429	0.01995	101	665	48.13	644.1	7.93	648.7	10.69
ACO-12-26B	26b-54	0.06101	0.00116	0.10161	0.00125	0.85454	0.0161	101	639.5	40.36	623.8	7.3	627.1	8.82
ACO-12-26B	26b-55	0.19613	0.00307	0.47984	0.0053	12.96726	0.19671	111	2794.2	25.43	2526.5	23.11	2677.3	14.3
ACO-12-26B	26b-56	0.06009	0.00168	0.09807	0.00142	0.81243	0.02217	100	606.8	59.33	603.1	8.37	603.8	12.42
ACO-12-26B	26b-57	0.05969	0.00098	0.11357	0.0013	0.93429	0.01522	97	592.8	34.8	693.4	7.52	669.9	7.99
ACO-12-26B	26b-58	0.06139	0.00088	0.09912	0.00119	0.83886	0.01261	102	652.9	30.6	609.3	6.97	618.5	6.96
ACO-12-26B	26b-59	0.05997	0.00099	0.10928	0.00132	0.90337	0.01504	98	602.5	35.2	668.6	7.65	653.5	8.02
ACO-12-26B	26b-60	0.0637	0.00157	0.10675	0.00138	0.93705	0.02225	103	731.7	51.49	653.8	8.05	671.3	11.66
ACO-12-26B	26b-61	0.06165	0.00108	0.10118	0.00123	0.85988	0.01509	101	662	36.99	621.3	7.22	630.1	8.24
ACO-12-26B	26b-62	0.05984	0.00079	0.10595	0.0012	0.87407	0.01191	98	597.9	28.23	649.2	7.02	637.8	6.46
ACO-12-26B	26b-63	0.07089	0.00164	0.11885	0.00155	1.16149	0.02598	108	954.2	46.73	723.9	8.92	782.7	12.2
ACO-12-26B	26b-64	0.06362	0.00095	0.11344	0.00127	0.99491	0.01478	101	729	31.37	692.7	7.36	701.2	7.52
ACO-12-26B	26b-65	0.06207	0.00087	0.10162	0.00118	0.86952	0.01263	102	676.6	29.77	623.9	6.93	635.3	6.86
ACO-12-26B	26b-66	0.06204	0.00102	0.10703	0.00129	0.91543	0.01526	101	675.6	34.89	655.5	7.5	659.9	8.09
ACO-12-26B	26b-67	0.06252	0.00091	0.11881	0.00139	1.024	0.01529	99	691.8	30.66	723.7	8.03	715.9	7.67
ACO-12-26B	26b-68	0.06132	0.00098	0.10114	0.00115	0.855	0.01351	101	650.4	33.93	621.1	6.72	627.4	7.4

ACO-12-26B	26b-69	0.06471	0.00109	0.11635	0.00138	1.03807	0.01744	102	765	35.14	709.5	7.96	723	8.69
ACO-12-26B	26b-70	0.12749	0.00159	0.36662	0.00432	6.44385	0.08589	102	2063.7	21.82	2013.5	20.37	2038.3	11.72
ACO-12-26B	26b-71	0.06817	0.00135	0.10683	0.0014	1.00398	0.01993	108	873.7	40.4	654.3	8.15	705.8	10.1
ACO-12-26B	26b-72	0.06074	0.00109	0.09801	0.00117	0.82084	0.01459	101	630.2	38.17	602.7	6.85	608.5	8.13
ACO-12-26B	26b-73	0.06522	0.00135	0.09296	0.00124	0.83577	0.01738	108	781.3	43.05	573	7.33	616.8	9.61
ACO-12-26B	26b-74	0.06229	0.00086	0.10626	0.00123	0.91252	0.01301	101	684.1	29.12	651	7.18	658.4	6.91
ACO-12-26B	26b-75	0.06439	0.00146	0.10552	0.00144	0.93679	0.02105	104	754.6	47.08	646.7	8.41	671.2	11.03
ACO-12-26B	26b-76	0.06088	0.00107	0.10428	0.00127	0.87536	0.01549	100	635.2	37.52	639.4	7.42	638.5	8.39
ACO-12-26B	26b-77	0.05956	0.00086	0.09436	0.0011	0.77495	0.01151	100	587.8	31.02	581.3	6.49	582.6	6.59
ACO-12-26B	26b-78	0.06225	0.00144	0.1048	0.00138	0.89944	0.02046	101	682.7	48.72	642.5	8.08	651.4	10.94
ACO-12-26B	26b-79	0.06182	0.00088	0.10525	0.00123	0.89711	0.01319	101	667.9	30.25	645.1	7.16	650.2	7.06
ACO-12-26B	26b-80	0.06055	0.001	0.10293	0.0013	0.85924	0.01475	100	623.3	35.36	631.5	7.61	629.7	8.05
ACO-12-27	1	0.05966	0.0019	0.0894	0.00131	0.73519	0.02256	101	591.3	67.43	552	7.74	559.6	13.2
ACO-12-27	2	0.06087	0.00186	0.09366	0.00134	0.78579	0.02311	102	634.8	64.47	577.2	7.88	588.8	13.14
ACO-12-27	3	0.06428	0.00137	0.10675	0.00128	0.94564	0.01938	103	750.8	44.26	653.8	7.45	675.8	10.11
ACO-12-27	4	0.06489	0.00198	0.10625	0.0015	0.94996	0.0277	104	770.7	63.04	650.9	8.75	678.1	14.43
ACO-12-27	5	0.05956	0.00088	0.10411	0.00116	0.85463	0.01264	98	587.6	31.77	638.5	6.8	627.2	6.92
ACO-12-27	6	0.06206	0.00145	0.10149	0.00125	0.86794	0.01943	102	676.3	49.01	623.1	7.31	634.4	10.56
ACO-12-27	7	0.06742	0.0012	0.098	0.00114	0.91065	0.0159	109	850.8	36.64	602.7	6.7	657.4	8.45
ACO-12-27	8	0.10244	0.0016	0.09623	0.00115	1.35896	0.02118	147	1668.9	28.57	592.3	6.78	871.4	9.11
ACO-12-27	9	0.06086	0.00109	0.09584	0.00114	0.80402	0.01426	102	634.3	38.04	590	6.72	599.1	8.03
ACO-12-27	10	0.05836	0.00102	0.09159	0.00108	0.73679	0.01276	99	543.4	37.62	564.9	6.39	560.5	7.46
ACO-12-27	11	0.06479	0.0017	0.10369	0.00142	0.92608	0.02354	105	767.6	54.37	636	8.27	665.6	12.41
ACO-12-27	12	0.06441	0.00145	0.10131	0.00129	0.89946	0.01962	105	755.1	46.77	622.1	7.55	651.4	10.49
ACO-12-27	13	0.06404	0.00159	0.10136	0.00139	0.89489	0.02158	104	742.8	51.52	622.4	8.12	649	11.57
ACO-12-27	14	0.05925	0.0012	0.09278	0.00112	0.75777	0.01495	100	576.2	43.3	572	6.63	572.7	8.64
ACO-12-27	15	0.06705	0.00107	0.1151	0.00133	1.06403	0.0169	105	839.4	32.92	702.3	7.68	735.8	8.31
ACO-12-27	16	0.06014	0.00103	0.10019	0.00116	0.83063	0.0141	100	608.5	36.77	615.5	6.79	614	7.82
ACO-12-27	17	0.06036	0.00177	0.09906	0.00143	0.82444	0.02338	100	616.5	61.99	608.9	8.37	610.5	13.01
ACO-12-27	18	0.55773	0.01447	0.22744	0.00472	17.48399	0.37838	224	4401.6	37.38	1321.1	24.8	2961.8	20.79
ACO-12-27	19	0.05996	0.00103	0.09766	0.00114	0.80736	0.01369	100	602.1	36.66	600.7	6.68	601	7.69
ACO-12-27	20	0.06195	0.00133	0.09721	0.00127	0.83044	0.01771	103	672.3	45.43	598	7.44	613.9	9.82
ACO-12-27	21	0.06123	0.00138	0.10311	0.00128	0.87048	0.01902	101	647.3	47.76	632.6	7.49	635.8	10.33
ACO-12-27	22	0.06061	0.00148	0.09721	0.00134	0.81236	0.01954	101	625.5	51.94	598.1	7.88	603.8	10.95
ACO-12-27	23	0.06178	0.00102	0.11138	0.00122	0.94852	0.0152	99	666.6	34.94	680.8	7.1	677.3	7.92
ACO-12-27	24	0.06052	0.00139	0.1051	0.0013	0.87684	0.01947	99	622.1	48.81	644.2	7.59	639.3	10.53
ACO-12-27	25	0.06094	0.00154	0.09217	0.00119	0.77445	0.01891	102	637.2	53.59	568.4	7.02	582.3	10.82
ACO-12-27	26	0.06127	0.00158	0.10027	0.00131	0.84692	0.02099	101	648.6	54.29	616	7.69	623	11.54
ACO-12-27	27	0.06275	0.00169	0.10006	0.00142	0.86574	0.02275	103	699.6	56.48	614.8	8.32	633.3	12.38
ACO-12-27	28	0.06235	0.00142	0.10433	0.00126	0.89666	0.01957	102	686.3	47.98	639.7	7.34	649.9	10.48
ACO-12-27	29	0.06352	0.0012	0.10098	0.00127	0.88474	0.01662	104	725.8	39.47	620.2	7.46	643.5	8.96
ACO-12-27	30	0.06618	0.00159	0.10053	0.00139	0.91763	0.0216	107	811.9	49.52	617.5	8.13	661.1	11.44

ACO-12-27	31	0.06071	0.00147	0.10328	0.00129	0.86441	0.02015	100	628.8	51.47	633.6	7.55	632.5	10.97
ACO-12-27	32	0.06425	0.00192	0.10862	0.00158	0.96259	0.02769	103	750	61.87	664.7	9.18	684.6	14.33
ACO-12-27	33	0.20069	0.00539	0.12691	0.00225	3.51264	0.08621	199	2831.8	43.11	770.2	12.88	1530.1	19.4
ACO-12-27	34	0.08645	0.00312	0.10356	0.00178	1.2345	0.04205	129	1348.2	67.98	635.3	10.41	816.4	19.11
ACO-12-27	35	0.06148	0.00143	0.10283	0.00131	0.8717	0.01966	101	655.9	49.04	631	7.68	636.5	10.67
ACO-12-27	36	0.06412	0.00114	0.09485	0.00112	0.83874	0.01467	106	745.5	37.06	584.2	6.61	618.5	8.1
ACO-12-27	37	0.06682	0.00144	0.10153	0.00129	0.93567	0.01969	108	832.1	44.36	623.4	7.53	670.6	10.33
ACO-12-27	38	0.06058	0.00171	0.10126	0.0014	0.84591	0.02298	100	624.5	59.58	621.8	8.19	622.4	12.64
ACO-12-27	39	0.05748	0.00115	0.10152	0.00123	0.8047	0.01582	96	509.6	43.83	623.3	7.21	599.5	8.9
ACO-12-27	40	0.06379	0.00119	0.0995	0.00119	0.87529	0.0161	104	734.8	39.16	611.5	6.96	638.4	8.72
ACO-12-27	41	0.06145	0.00102	0.09717	0.00113	0.82344	0.01351	102	654.9	35.06	597.8	6.64	610	7.52
ACO-12-27	42	0.06109	0.00097	0.1027	0.0012	0.86542	0.01368	100	642.5	33.6	630.2	6.99	633.1	7.45
ACO-12-27	43	0.06035	0.00125	0.09946	0.00123	0.82784	0.01684	100	616.3	44.23	611.3	7.23	612.4	9.35
ACO-12-27	44	0.05862	0.00106	0.09948	0.00117	0.80407	0.01437	98	552.9	39.01	611.3	6.88	599.1	8.09
ACO-12-27	45	0.06197	0.00137	0.10311	0.00127	0.88101	0.01888	101	673	46.72	632.6	7.44	641.5	10.19
ACO-12-27	46	0.06157	0.00161	0.08969	0.00121	0.76155	0.01922	104	659.3	54.99	553.7	7.18	574.9	11.08
ACO-12-27	47	0.06035	0.00089	0.10258	0.00114	0.8536	0.01257	100	616.2	31.56	629.5	6.68	626.6	6.88
ACO-12-27	48	0.06233	0.00145	0.09895	0.00128	0.85041	0.01928	103	685.3	48.98	608.3	7.54	624.9	10.58
ACO-12-27	49	0.06587	0.00126	0.0982	0.0012	0.89198	0.01674	107	802.3	39.49	603.8	7.07	647.4	8.98
ACO-12-27	50	0.06354	0.00167	0.10166	0.00139	0.89071	0.0226	104	726.4	54.65	624.1	8.13	646.7	12.14
ACO-12-27	51	0.06033	0.00105	0.10167	0.00118	0.84567	0.01451	100	615.3	37.17	624.2	6.89	622.3	7.98
ACO-12-27	52	0.05735	0.00213	0.09994	0.00159	0.79027	0.0283	96	504.6	80.33	614.1	9.32	591.3	16.05
ACO-12-27	53	0.06528	0.00156	0.09823	0.00138	0.88403	0.02084	106	783.4	49.54	604	8.09	643.2	11.23
ACO-12-27	54	0.06106	0.00105	0.10338	0.00121	0.87032	0.01488	100	641.2	36.72	634.2	7.05	635.7	8.08
ACO-12-27	55	0.2108	0.00369	0.10596	0.0013	3.08009	0.05039	220	2911.7	28.1	649.3	7.57	1427.7	12.54
ACO-12-27	56	0.06015	0.00119	0.09329	0.00107	0.77375	0.01469	101	609	42.12	574.9	6.32	581.9	8.41
ACO-12-27	57	0.06094	0.00148	0.09888	0.00128	0.83075	0.01951	101	637	51.27	607.8	7.51	614	10.82
ACO-12-27	58	0.06148	0.00188	0.09471	0.00139	0.80283	0.02368	103	656.1	64.11	583.4	8.16	598.4	13.34
ACO-12-27	59	0.07046	0.00164	0.10451	0.00136	1.01526	0.02278	111	941.7	46.89	640.8	7.93	711.5	11.48
ACO-12-27	60	0.06148	0.00122	0.1042	0.00129	0.88328	0.01731	101	656.1	42.03	639	7.54	642.8	9.33
ACO-12-27	61	0.06027	0.00125	0.09978	0.00134	0.82844	0.01725	100	613.2	44.34	613.1	7.84	612.7	9.58
ACO-12-27	62	0.06052	0.00105	0.10034	0.00117	0.83703	0.01429	100	622.3	36.96	616.4	6.84	617.5	7.9
ACO-12-27	63	0.06171	0.00107	0.10515	0.00121	0.89456	0.01517	101	664.2	36.58	644.5	7.09	648.8	8.13
ACO-12-27	64	0.06161	0.00177	0.08901	0.00125	0.75583	0.0209	104	660.5	60.36	549.7	7.4	571.6	12.08
ACO-12-27	65	0.06009	0.00104	0.09155	0.00108	0.75815	0.013	101	606.7	36.94	564.7	6.38	572.9	7.51
ACO-12-27	66	0.06679	0.00125	0.09313	0.00111	0.85734	0.01565	110	831.3	38.49	574	6.57	628.7	8.55
ACO-12-27	67	0.06651	0.00185	0.10358	0.00146	0.94947	0.02542	107	822.4	57.11	635.4	8.53	677.8	13.24
ACO-12-27	68	0.06153	0.00125	0.09858	0.00119	0.83619	0.01654	102	657.7	43.12	606.1	6.99	617	9.15
ACO-12-27	69	0.06125	0.00157	0.10434	0.00139	0.88084	0.02176	100	647.9	54.01	639.8	8.11	641.4	11.74
ACO-12-27	70	0.06791	0.00176	0.09967	0.00138	0.93285	0.02333	109	865.9	52.87	612.4	8.08	669.1	12.26
ACO-12-27	71	0.06581	0.00105	0.09375	0.00106	0.85058	0.01334	108	800.3	33.18	577.7	6.22	625	7.32
ACO-12-20B	20B-01	0.06943	0.00089	0.14448	0.00167	1.38289	0.0186	101	911.7	26.09	870	9.39	881.7	7.93
ACO-12-20B	20B-02	0.07334	0.001	0.09121	0.00111	0.9222	0.01347	118	1023.4	27.42	562.7	6.57	663.5	7.11
ACO-12-20B	20B-03	0.09278	0.00128	0.09939	0.00114	1.27121	0.0178	136	1483.3	26	610.8	6.7	832.9	7.96
ACO-12-20B	20B-04	0.06013	0.00138	0.10336	0.00124	0.85675	0.01876	99	608.4	48.86	634.1	7.24	628.3	10.26

ACO-12-20B	20B-05	0.13409	0.00161	0.35225	0.00386	6.51155	0.08019	111	2152.2	20.81	1945.3	18.4	2047.5	10.84
ACO-12-20B	20B-06	0.17663	0.00229	0.45536	0.00563	11.08921	0.157	108	2621.4	21.4	2419	24.93	2530.7	13.19
ACO-12-20B	20B-07	0.07798	0.00169	0.19212	0.00264	2.06542	0.04446	101	1146.4	42.57	1132.9	14.3	1137.4	14.73
ACO-12-20B	20B-08	0.12054	0.0022	0.08093	0.00104	1.34492	0.02367	172	1964.2	32.13	501.7	6.19	865.4	10.25
ACO-12-20B	20B-09	0.11548	0.00181	0.2049	0.00243	3.26145	0.0509	157	1887.5	28.02	1201.6	13	1471.9	12.13
ACO-12-20B	20B-10	0.06277	0.00103	0.09796	0.00106	0.84755	0.01338	103	700.5	34.56	602.4	6.23	623.3	7.35
ACO-12-20B	20B-11	0.06326	0.00258	0.09343	0.00158	0.81463	0.03161	105	717	84.17	575.8	9.32	605	17.68
ACO-12-20B	20B-12	0.08496	0.00141	0.2141	0.00271	2.50787	0.04271	105	1314.4	31.97	1250.6	14.37	1274.3	12.36
ACO-12-20B	20B-13	0.09434	0.00194	0.08872	0.00109	1.15369	0.02246	142	1515	38.28	547.9	6.46	779	10.59
ACO-12-20B	20B-14	0.06151	0.00087	0.09643	0.0011	0.81789	0.01176	102	657.2	30.06	593.5	6.45	606.9	6.57
ACO-12-20B	20B-15	0.12732	0.00169	0.27821	0.00325	4.88394	0.06765	130	2061.4	23.2	1582.4	16.4	1799.5	11.67
ACO-12-20B	20B-16	0.11327	0.00159	0.09513	0.00109	1.4858	0.02096	158	1852.5	25.12	585.8	6.41	924.6	8.56
ACO-12-20B	20B-17	0.11934	0.00175	0.14134	0.00152	2.32516	0.03308	143	1946.4	25.94	852.2	8.59	1220	10.1
ACO-12-20B	20B-18	0.06567	0.0013	0.10184	0.00124	0.92203	0.0178	106	796	41.02	625.2	7.25	663.4	9.4
ACO-12-20B	20B-19	0.12489	0.00164	0.38022	0.00435	6.54663	0.08846	98	2027.2	23.03	2077.3	20.34	2052.2	11.9
ACO-12-20B	20B-20	0.08245	0.00214	0.09598	0.00146	1.091	0.02765	127	1256.2	49.8	590.8	8.56	749	13.43
ACO-12-20B	20B-21	0.21407	0.00242	0.55856	0.00631	16.48424	0.19633	103	2936.6	18.16	2860.7	26.08	2905.3	11.4
ACO-12-20B	20B-22	0.06064	0.00079	0.0967	0.00109	0.80836	0.01084	101	626.6	27.8	595	6.41	601.5	6.08
ACO-12-20B	20B-23	0.12858	0.0017	0.27742	0.00344	4.91768	0.06999	132	2078.6	23.08	1578.4	17.37	1805.3	12.01
ACO-12-20B	20B-24	0.05904	0.00173	0.10759	0.00147	0.87552	0.02454	97	568.7	62.66	658.7	8.55	638.6	13.29
ACO-12-20B	20B-25	0.0608	0.00168	0.10138	0.00145	0.84973	0.02282	100	632.3	58.42	622.5	8.46	624.5	12.53
ACO-12-20B	20B-26	0.07044	0.00094	0.10137	0.00119	0.98444	0.01366	112	941.3	27.06	622.5	6.95	695.9	6.99
ACO-12-20B	20B-27	0.07974	0.00094	0.20479	0.00228	2.251	0.02766	99	1190.5	23.02	1201	12.19	1197.1	8.64
ACO-12-20B	20B-28	0.19553	0.00224	0.36277	0.00401	9.77746	0.1176	140	2789.2	18.66	1995.3	18.96	2414	11.08
ACO-12-20B	20B-29	0.11914	0.00205	0.33206	0.00419	5.45174	0.09281	105	1943.4	30.5	1848.4	20.26	1893	14.61
ACO-12-20B	20B-30	0.05937	0.00117	0.09835	0.00118	0.80496	0.01551	99	580.8	42.21	604.8	6.94	599.6	8.72
ACO-12-20B	20B-31	0.06702	0.00094	0.09609	0.00102	0.88758	0.01214	109	838.4	28.96	591.4	6	645.1	6.53
ACO-12-20B	20B-32	0.15957	0.00245	0.44317	0.00554	9.74857	0.15269	104	2451.2	25.71	2364.8	24.74	2411.3	14.42
ACO-12-20B	20B-33	0.10211	0.0015	0.23386	0.00276	3.29167	0.04903	123	1662.8	26.96	1354.7	14.41	1479.1	11.6
ACO-12-20B	20B-34	0.12987	0.0017	0.37743	0.00442	6.75758	0.0919	102	2096.2	22.85	2064.3	20.7	2080.2	12.03
ACO-12-20B	20B-35	0.12166	0.00184	0.28374	0.00309	4.75701	0.06911	123	1980.7	26.69	1610.2	15.5	1777.3	12.19
ACO-12-20B	20B-36	0.15475	0.00191	0.44825	0.00502	9.56037	0.12193	100	2399.1	20.8	2387.5	22.33	2393.4	11.72
ACO-12-20B	20B-37	0.12653	0.00165	0.33126	0.0038	5.7759	0.07828	111	2050.2	22.85	1844.5	18.38	1942.8	11.73
ACO-12-20B	20B-38	0.13735	0.00179	0.32845	0.00374	6.21826	0.08285	120	2194	22.45	1830.9	18.14	2007	11.65
ACO-12-20B	20B-39	0.06056	0.00121	0.10827	0.0013	0.90366	0.01758	99	623.8	42.6	662.7	7.56	653.7	9.38
ACO-12-20B	20B-40	0.06394	0.001	0.12871	0.00146	1.13421	0.01755	99	739.8	32.75	780.5	8.33	769.8	8.35

ACO-12-20B	20B-41	0.11426	0.00141	0.10866	0.00124	1.71174	0.02191	152	1868.2	22.14	665	7.21	1012.9	8.2
ACO-12-20B	20B-42	0.17842	0.00211	0.46009	0.00525	11.31651	0.14021	108	2638.2	19.51	2440	23.16	2549.6	11.56
ACO-12-20B	20B-43	0.05838	0.00205	0.08822	0.0014	0.71	0.02404	100	544	74.96	545	8.29	544.7	14.27
ACO-12-20B	20B-44	0.07355	0.00128	0.10248	0.00126	1.03916	0.01806	115	1029	34.89	628.9	7.39	723.5	9
ACO-12-20B	20B-45	0.12942	0.00161	0.37644	0.0045	6.71669	0.08992	101	2090.1	21.72	2059.6	21.05	2074.8	11.83
ACO-12-20B	20B-46	0.10792	0.00163	0.09848	0.00118	1.46525	0.02216	151	1764.6	27.36	605.5	6.95	916.2	9.13
ACO-12-20B	20B-47	0.06161	0.00076	0.11364	0.00128	0.96528	0.01248	99	660.7	26.33	693.9	7.43	686	6.45
ACO-12-20B	20B-48	0.23338	0.00346	0.6145	0.00659	19.7697	0.28175	100	3075.4	23.5	3088	26.31	3080.2	13.77
ACO-12-20B	20B-49	0.0626	0.00184	0.1028	0.0015	0.88708	0.02517	102	694.5	61.41	630.8	8.77	644.8	13.54
ACO-12-20B	20B-50	0.08966	0.00153	0.2603	0.00299	3.21731	0.05289	95	1418.3	32.15	1491.4	15.27	1461.3	12.73
ACO-12-20B	20B-51	0.06177	0.0009	0.10603	0.0012	0.90288	0.01326	101	666.2	30.95	649.6	6.97	653.3	7.08
ACO-12-20B	20B-52	0.07445	0.00288	0.10439	0.00187	1.07152	0.03944	116	1053.4	76.45	640.1	10.89	739.5	19.33
ACO-12-20B	20B-53	0.06324	0.0012	0.11001	0.00134	0.95906	0.01789	101	716.2	39.68	672.8	7.76	682.8	9.27
ACO-12-20B	20B-54	0.07292	0.00141	0.11195	0.00132	1.12549	0.02097	112	1011.8	38.69	684.1	7.67	765.6	10.02
ACO-12-20B	20B-55	0.07752	0.00144	0.08479	0.00102	0.90609	0.0164	125	1134.4	36.57	524.7	6.07	655	8.74
ACO-12-20B	20B-56	0.2954	0.00467	0.1256	0.00148	5.11526	0.0768	241	3446.3	24.3	762.7	8.47	1838.6	12.75
ACO-12-20B	20B-57	0.13041	0.00208	0.10136	0.00127	1.82222	0.02942	169	2103.5	27.71	622.4	7.44	1053.5	10.59
ACO-12-20B	20B-58	0.13193	0.00178	0.38916	0.00448	7.07835	0.09806	100	2123.8	23.41	2118.9	20.81	2121.3	12.32
ACO-12-20B	20B-59	0.1256	0.00174	0.37079	0.00421	6.42043	0.09017	100	2037.2	24.25	2033.1	19.8	2035.1	12.34
ACO-12-20B	20B-60	0.05946	0.00103	0.10388	0.00124	0.85158	0.01469	98	584	37.01	637.1	7.24	625.5	8.06
ACO-12-20B	20B-61	0.07434	0.00087	0.12167	0.00136	1.24655	0.01529	111	1050.8	23.3	740.2	7.81	821.8	6.91
ACO-12-20B	20B-62	0.06468	0.00121	0.12533	0.00146	1.11728	0.02027	100	763.9	38.97	761.2	8.37	761.7	9.72
ACO-12-20B	20B-63	0.06346	0.00122	0.11471	0.00139	1.0032	0.01888	101	723.6	40.22	700.1	8.01	705.4	9.57
ACO-12-20B	20B-64	0.12923	0.00178	0.37297	0.00405	6.64423	0.08951	102	2087.6	24.03	2043.4	19.04	2065.2	11.89
ACO-12-20B	20B-65	0.06318	0.00159	0.11176	0.00149	0.97307	0.02364	101	714.3	52.46	683	8.66	690	12.17
ACO-12-20B	20B-66	0.26995	0.00331	0.67086	0.00735	24.95881	0.31215	100	3305.7	19.1	3309.2	28.37	3306.6	12.21
ACO-12-20B	20B-67	0.06312	0.00133	0.09913	0.00118	0.86255	0.01742	104	712.3	44.07	609.3	6.95	631.5	9.5
ACO-12-20B	20B-68	0.05654	0.00117	0.09757	0.00122	0.76031	0.01552	96	473	45.63	600.2	7.16	574.2	8.95
ACO-12-20B	20B-69	0.1296	0.0018	0.36487	0.00448	6.51604	0.09517	104	2092.5	24.17	2005.2	21.18	2048.1	12.86
ACO-12-20B	20B-70	0.05849	0.001	0.10115	0.00121	0.8153	0.01399	97	548	37.06	621.1	7.07	605.4	7.82
ACO-12-20B	20B-71	0.07308	0.00237	0.09876	0.00149	0.99463	0.03057	115	1016.1	64.35	607.1	8.74	701.1	15.56
ACO-12-20B	20B-72	0.05969	0.00108	0.09506	0.00107	0.78208	0.01361	100	592.8	38	585.4	6.3	586.7	7.75
ACO-12-20B	20B-73	0.07453	0.00136	0.09413	0.00116	0.96688	0.01737	118	1055.6	36.47	579.9	6.81	686.9	8.97
ACO-12-20B	20B-74	0.21817	0.00287	0.5871	0.00681	17.65335	0.2396	100	2967.2	21.04	2977.6	27.65	2971	13.04
ACO-12-20B	20B-75	0.06125	0.00118	0.08776	0.00104	0.74082	0.01394	104	647.9	40.92	542.3	6.17	562.9	8.13
ACO-12-20B	20B-76	0.059	0.00204	0.10533	0.00159	0.85656	0.02831	97	567.2	73.57	645.6	9.27	628.2	15.48

ACO-12-20B	20B-77	0.1625	0.0023	0.43264	0.00495	9.68764	0.13859	107	2481.8	23.65	2317.6	22.29	2405.5	13.17
ACO-12-20B	20B-78	0.13627	0.00227	0.42225	0.00503	7.92972	0.12978	96	2180.3	28.74	2270.7	22.81	2223.1	14.76
ACO-12-20B	20B-79	0.0591	0.00117	0.10919	0.00136	0.88935	0.01737	97	570.7	42.35	668	7.92	646	9.34
ACO-12-20B	20B-80	0.08206	0.00225	0.10022	0.00148	1.13355	0.02977	125	1247.1	52.62	615.7	8.7	769.4	14.17
ACO-12-22A	22A-01	0.05948	0.001	0.09274	0.00108	0.76033	0.01265	100	584.7	36.05	571.7	6.37	574.2	7.3
ACO-12-22A	22A-02	0.19109	0.00223	0.53483	0.00587	14.08875	0.16888	100	2751.6	19.08	2761.8	24.67	2755.7	11.36
ACO-12-22A	22A-03	0.05836	0.00102	0.0888	0.00096	0.71444	0.01199	100	543.4	37.93	548.4	5.7	547.4	7.1
ACO-12-22A	22A-04	0.12377	0.00192	0.3728	0.00441	6.36069	0.09616	102	2011.3	27.21	2042.6	20.69	2026.9	13.26
ACO-12-22A	22A-05	0.06156	0.00119	0.09253	0.00112	0.78528	0.01489	97	658.8	40.98	570.5	6.61	588.5	8.47
ACO-12-22A	22A-06	0.06176	0.00088	0.11837	0.00135	1.00772	0.01455	102	665.6	30.29	721.2	7.76	707.7	7.36
ACO-12-22A	22A-07	0.06872	0.00121	0.14764	0.00187	1.39876	0.02494	100	890.5	35.91	887.7	10.52	888.4	10.56
ACO-12-22A	22A-08	0.05859	0.00109	0.08704	0.00103	0.70308	0.01284	100	551.8	40.09	538	6.13	540.6	7.66
ACO-12-22A	22A-09	0.05884	0.00092	0.10315	0.00118	0.83673	0.01307	103	561.1	33.55	632.8	6.87	617.3	7.23
ACO-12-22A	22A-10	0.06365	0.00209	0.11843	0.00173	1.03923	0.0324	100	730.1	67.95	721.5	9.97	723.5	16.13
ACO-12-22A	22A-11	0.05875	0.00099	0.08143	0.0009	0.65951	0.01078	98	558	36.32	504.6	5.34	514.3	6.6
ACO-12-22A	22A-12	0.07473	0.00185	0.09139	0.00125	0.94162	0.02238	53	1061.3	49.1	563.7	7.37	673.7	11.7
ACO-12-22A	22A-13	0.06289	0.00143	0.10451	0.00127	0.90609	0.01974	98	704.4	47.8	640.8	7.42	655	10.52
ACO-12-22A	22A-14	0.061	0.00205	0.09329	0.00137	0.78448	0.02505	98	639.2	70.66	574.9	8.05	588	14.26
ACO-12-22A	22A-15	0.06243	0.00237	0.09291	0.00151	0.7997	0.02891	96	689	78.97	572.7	8.88	596.7	16.31
ACO-12-22A	22A-16	0.06098	0.00142	0.09084	0.00113	0.76363	0.01702	97	638.5	49.16	560.5	6.67	576.1	9.8
ACO-12-22A	22A-17	0.06426	0.00172	0.08969	0.00119	0.79463	0.02027	93	750.3	55.52	553.7	7.01	593.8	11.47
ACO-12-22A	22A-18	0.06202	0.00117	0.10809	0.00122	0.92422	0.01663	100	674.9	39.66	661.6	7.07	664.6	8.78
ACO-12-22A	22A-19	0.06192	0.00167	0.0948	0.00124	0.8092	0.02079	97	671.3	56.69	583.8	7.3	602	11.67
ACO-12-22A	22A-20	0.12599	0.00183	0.30908	0.00349	5.36863	0.07712	85	2042.8	25.5	1736.2	17.17	1879.9	12.3
ACO-12-22A	22A-21	0.06226	0.00138	0.09755	0.00123	0.83722	0.01798	97	683.1	46.62	600	7.22	617.6	9.94
ACO-12-22A	22A-22	0.12597	0.00147	0.37312	0.0044	6.48098	0.08187	100	2042.5	20.52	2044.1	20.64	2043.3	11.11
ACO-12-22A	22A-23	0.0591	0.00162	0.09371	0.00132	0.76299	0.02037	100	570.7	58.62	577.4	7.76	575.7	11.73
ACO-12-22A	22A-24	0.06404	0.00107	0.10662	0.00115	0.94084	0.01502	97	743	34.85	653.1	6.73	673.3	7.86
ACO-12-22A	22A-25	0.0608	0.00132	0.08645	0.00114	0.7247	0.01556	97	632.3	46.05	534.5	6.74	553.4	9.16
ACO-12-22A	22A-26	0.05985	0.00137	0.09849	0.00121	0.81232	0.01784	100	598.1	48.7	605.6	7.11	603.8	10
ACO-12-22A	22A-27	0.12997	0.00155	0.38737	0.00454	6.94012	0.08838	101	2097.5	20.85	2110.6	21.09	2103.8	11.3
ACO-12-22A	22A-28	0.16483	0.00184	0.43863	0.00436	9.9615	0.10717	94	2505.8	18.69	2344.5	19.54	2431.2	9.93
ACO-12-22A	22A-29	0.06326	0.00117	0.10917	0.00122	0.95163	0.01675	98	717.1	38.64	667.9	7.07	678.9	8.72
ACO-12-22A	22A-30	0.05835	0.00138	0.10559	0.00128	0.84888	0.01916	104	542.8	50.9	647.1	7.46	624	10.52

ACO-12-22A	22A-31	0.06584	0.00125	0.10502	0.00118	0.95271	0.01714	95	801.3	39.2	643.7	6.86	679.5	8.91
ACO-12-22A	22A-32	0.06002	0.00103	0.09748	0.00105	0.80616	0.01323	100	604.2	36.83	599.6	6.16	600.3	7.44
ACO-12-22A	22A-33	0.06139	0.00089	0.09827	0.00104	0.83126	0.01176	98	652.9	30.98	604.3	6.11	614.3	6.52
ACO-12-22A	22A-34	0.06779	0.0013	0.14953	0.00174	1.3967	0.02578	101	862.2	39.41	898.3	9.76	887.5	10.92
ACO-12-22A	22A-35	0.06101	0.00149	0.1054	0.00133	0.88602	0.0207	100	639.4	51.58	646	7.77	644.2	11.15
ACO-12-22A	22A-36	0.05922	0.00212	0.09769	0.00149	0.79713	0.02723	101	575.2	76.13	600.8	8.74	595.2	15.38
ACO-12-22A	22A-37	0.18806	0.00199	0.46441	0.00495	12.03959	0.13181	90	2725.3	17.29	2459	21.8	2607.5	10.26
ACO-12-22A	22A-38	0.07225	0.00157	0.10215	0.00121	1.01689	0.02087	88	992.9	43.68	627	7.07	712.3	10.51
ACO-12-22A	22A-39	0.06252	0.00077	0.08711	0.00094	0.75079	0.0094	95	692	26.11	538.4	5.59	568.7	5.45
ACO-12-22A	22A-40	0.06213	0.00091	0.10599	0.0011	0.90736	0.01267	99	678.6	30.84	649.4	6.41	655.7	6.74
ACO-12-22A	22A-41	0.05856	0.00086	0.10755	0.00116	0.86811	0.01248	104	550.9	31.76	658.5	6.73	634.5	6.78
ACO-12-22A	22A-42	0.11359	0.00148	0.18853	0.00211	2.95128	0.0386	60	1857.6	23.31	1113.4	11.47	1395.2	9.92
ACO-12-22A	22A-43	0.12273	0.00247	0.35855	0.00426	6.06317	0.11485	99	1996.3	35.32	1975.3	20.22	1985	16.51
ACO-12-22A	22A-44	0.06057	0.00091	0.0902	0.00107	0.75274	0.01156	98	623.9	31.92	556.7	6.34	569.8	6.7
ACO-12-22A	22A-45	0.12972	0.0018	0.36447	0.0045	6.51309	0.09479	96	2094.2	24.23	2003.3	21.26	2047.7	12.81
ACO-12-22A	22A-46	0.05858	0.00106	0.08736	0.00103	0.70518	0.01258	100	551.7	39.17	539.9	6.09	541.9	7.49
ACO-12-22A	22A-47	0.12685	0.0016	0.3703	0.0041	6.47086	0.08302	99	2054.8	22.09	2030.8	19.28	2041.9	11.28
ACO-12-22A	22A-48	0.06414	0.0009	0.12218	0.00136	1.07967	0.01521	100	746.3	29.42	743.1	7.82	743.5	7.42
ACO-12-22A	22A-49	0.06261	0.00117	0.10809	0.0013	0.93234	0.01704	99	695.1	39.25	661.7	7.54	668.9	8.95
ACO-12-22A	22A-50	0.05724	0.00159	0.09184	0.00121	0.72417	0.01921	102	500.3	60.49	566.4	7.13	553.1	11.31
ACO-12-22A	22A-51	0.05511	0.00119	0.08061	0.00093	0.61198	0.01263	103	416.6	47.01	499.7	5.56	484.8	7.96
ACO-12-22A	22A-52	0.0635	0.00145	0.08679	0.00117	0.75919	0.01708	94	725.2	47.58	536.5	6.97	573.5	9.86
ACO-12-22A	22A-53	0.06287	0.00158	0.10462	0.00139	0.90592	0.02198	98	703.9	52.61	641.4	8.14	654.9	11.71
ACO-12-22A	22A-54	0.06584	0.00192	0.09245	0.0014	0.83822	0.0237	92	801.1	59.87	570	8.27	618.2	13.09
ACO-12-22A	22A-55	0.12349	0.00161	0.36858	0.00411	6.26787	0.08275	101	2007.2	23.03	2022.7	19.35	2014	11.56
ACO-12-22A	22A-56	0.05984	0.00089	0.08524	0.00093	0.70219	0.01024	98	597.8	31.77	527.3	5.54	540.1	6.11
ACO-12-22A	22A-57	0.05925	0.00182	0.09563	0.00138	0.78027	0.02302	101	576.4	65.33	588.8	8.13	585.6	13.13
ACO-12-22A	22A-58	0.07006	0.00145	0.1029	0.00125	0.9925	0.01968	90	930	41.79	631.4	7.28	700	10.03
ACO-12-22A	22A-59	0.06359	0.00135	0.09403	0.00123	0.82319	0.01723	95	727.9	44.28	579.3	7.22	609.8	9.59
ACO-12-22A	22A-60	0.11581	0.0025	0.27547	0.00398	4.39527	0.09413	83	1892.5	38.4	1568.5	20.09	1711.5	17.72
ACO-12-22A	22A-61	0.06237	0.00082	0.12255	0.00134	1.05316	0.0139	102	686.9	27.7	745.2	7.7	730.4	6.87
ACO-12-22A	22A-62	0.06441	0.00108	0.0891	0.00098	0.79078	0.01281	93	755.3	35.15	550.2	5.81	591.6	7.27
ACO-12-22A	22A-63	0.06005	0.00082	0.08961	0.00098	0.74164	0.01012	98	605.3	29.28	553.2	5.78	563.4	5.9
ACO-12-22A	22A-64	0.06002	0.00086	0.09044	0.00097	0.74807	0.0105	98	604.2	30.61	558.1	5.76	567.1	6.1
ACO-12-22A	22A-65	0.06058	0.00217	0.09088	0.00156	0.75775	0.02645	98	624.5	75.27	560.7	9.23	572.7	15.28

ACO-12-22A	22A-66	0.06969	0.00201	0.08984	0.0014	0.86253	0.02419	88	919.1	58.07	554.6	8.27	631.5	13.19
ACO-12-22A	22A-67	0.06094	0.00162	0.0902	0.00117	0.75764	0.01916	97	637.3	56.11	556.7	6.9	572.6	11.07
ACO-12-22A	22A-68	0.07106	0.00099	0.08835	0.00098	0.86535	0.01205	86	959.3	28.29	545.8	5.83	633	6.56
ACO-12-22A	22A-69	0.06177	0.00129	0.09331	0.00111	0.79449	0.01595	97	666	44.15	575.1	6.53	593.7	9.03
ACO-12-22A	22A-70	0.08627	0.00168	0.10338	0.00122	1.22956	0.02266	47	1344.3	37.08	634.2	7.14	814.1	10.32
ACO-12-22A	22A-71	0.06159	0.00166	0.09411	0.00135	0.79867	0.02109	97	660	56.86	579.8	7.96	596.1	11.91
ACO-12-22A	22A-72	0.06147	0.00088	0.1075	0.00119	0.91103	0.01301	100	655.9	30.38	658.2	6.94	657.6	6.91
ACO-12-22A	22A-73	0.06195	0.00191	0.09394	0.00132	0.80225	0.02351	97	672.2	64.59	578.8	7.76	598.1	13.24
ACO-12-22A	22A-74	0.0589	0.00144	0.08934	0.00122	0.72508	0.0175	100	563.3	52.56	551.6	7.23	553.7	10.3
ACO-12-22A	22A-75	0.1298	0.00174	0.37689	0.0042	6.74424	0.09058	98	2095.3	23.32	2061.7	19.64	2078.4	11.88
ACO-12-22A	22A-76	0.14422	0.00197	0.3379	0.00379	6.71856	0.09204	82	2278.5	23.38	1876.6	18.26	2075.1	12.11
ACO-12-22A	22A-77	0.05971	0.00138	0.11009	0.00131	0.9063	0.0199	103	593.4	48.97	673.3	7.63	655.1	10.6
ACO-12-22A	22A-78	0.12879	0.00192	0.35391	0.0042	6.28166	0.09585	94	2081.5	25.94	1953.2	20.02	2015.9	13.37
ACO-12-22A	22A-79	0.05684	0.00132	0.09015	0.00107	0.70657	0.01554	103	484.8	50.46	556.4	6.31	542.7	9.25
ACO-12-22A	22A-80	0.13176	0.00181	0.31627	0.00349	5.74641	0.07896	84	2121.5	23.84	1771.5	17.1	1938.4	11.88
ACO-12-25	25-1	0.11456	0.00139	0.31461	0.00368	4.9678	0.06478	106	1872.9	21.65	1763.3	18.05	1813.9	11.02
ACO-12-25	25-2	0.07675	0.00155	0.08329	0.00118	0.88104	0.0183	80	1114.6	39.84	515.7	7.01	641.5	9.88
ACO-12-25	25-3	0.09319	0.0011	0.0831	0.00098	1.06736	0.01384	70	1491.7	22.2	514.6	5.81	737.4	6.8
ACO-12-25	25-4	0.07412	0.00112	0.07751	0.00102	0.79169	0.01303	81	1044.6	30.21	481.2	6.08	592.1	7.38
ACO-12-25	25-5	0.06997	0.00109	0.09179	0.00123	0.88519	0.0151	88	927.4	31.68	566.1	7.26	643.8	8.13
ACO-12-25	25-6	0.05995	0.00094	0.09414	0.00112	0.778	0.01253	99	601.9	33.66	580	6.63	584.3	7.16
ACO-12-25	25-7	0.08448	0.00139	0.09717	0.00123	1.13157	0.01911	78	1303.6	31.64	597.8	7.23	768.5	9.1
ACO-12-25	25-8	0.06337	0.00086	0.10406	0.00125	0.90896	0.01316	97	720.6	28.44	638.2	7.27	656.5	7
ACO-12-25	25-9	0.06315	0.00081	0.09295	0.00112	0.80913	0.01131	95	713.3	26.93	573	6.59	602	6.35
ACO-12-25	25-10	0.06546	0.00088	0.09527	0.00114	0.85965	0.01241	93	789.2	28.03	586.6	6.7	629.9	6.78
ACO-12-25	25-11	0.2192	0.00296	0.55133	0.00624	16.66057	0.2253	105	2974.8	21.57	2830.7	25.94	2915.5	12.95
ACO-12-25	25-12	0.06636	0.0012	0.12184	0.00146	1.11464	0.01986	97	817.7	37.29	741.2	8.36	760.4	9.54
ACO-12-25	25-13	0.06083	0.00092	0.09262	0.00112	0.77666	0.01224	98	633.3	32.32	571	6.6	583.6	7
ACO-12-25	25-14	0.10781	0.00142	0.2416	0.00295	3.59083	0.05111	126	1762.7	23.85	1395	15.33	1547.5	11.3
ACO-12-25	25-15	0.05787	0.00143	0.0875	0.00117	0.69809	0.01691	101	524.7	53.69	540.7	6.91	537.6	10.11
ACO-12-25	25-16	0.08572	0.00132	0.14097	0.00171	1.66589	0.0262	85	1331.8	29.63	850.2	9.65	995.6	9.98
ACO-12-25	25-17	0.12645	0.00204	0.2344	0.00325	4.08284	0.07242	151	2049.3	28.26	1357.5	16.99	1650.9	14.47
ACO-12-25	25-18	0.11722	0.00225	0.09392	0.00124	1.51791	0.02831	62	1914.3	34.08	578.7	7.31	937.6	11.42
ACO-12-25	25-19	0.0714	0.00111	0.1308	0.00153	1.28754	0.02007	94	968.8	31.28	792.4	8.7	840.2	8.91
ACO-12-25	25-20	0.06488	0.00137	0.1047	0.00151	0.93639	0.0204	96	770.3	43.72	641.9	8.83	671	10.7
ACO-12-25	25-21	0.12432	0.00136	0.23056	0.00274	3.95216	0.04922	151	2019.1	19.27	1337.4	14.37	1624.4	10.09
ACO-12-25	25-22	0.0726	0.00143	0.09556	0.00137	0.95612	0.01965	86	1002.8	39.45	588.4	8.07	681.3	10.2
ACO-12-25	25-23	0.06229	0.00083	0.08665	0.00104	0.74429	0.01061	95	684.2	28.07	535.7	6.17	564.9	6.17
ACO-12-25	25-24	0.06248	0.00072	0.09796	0.00113	0.84418	0.01056	97	690.5	24.3	602.5	6.61	621.5	5.82
ACO-12-25	25-25	0.13122	0.00157	0.37235	0.00429	6.74067	0.08543	104	2114.4	20.79	2040.5	20.15	2078	11.21
ACO-12-25	25-26	0.13486	0.00185	0.37891	0.0042	7.04475	0.09684	104	2162.2	23.73	2071.2	19.66	2117.1	12.22

ACO-12-25	25-27	0.08282	0.00191	0.19803	0.00274	2.26545	0.05066	109	1264.9	44.32	1164.7	14.73	1201.6	15.75
ACO-12-25	25-28	0.13782	0.00169	0.36791	0.00444	6.99429	0.0934	109	2199.9	21.18	2019.6	20.93	2110.7	11.86
ACO-12-25	25-29	0.11702	0.00156	0.32213	0.00396	5.20082	0.07422	106	1911.1	23.7	1800.1	19.33	1852.8	12.15
ACO-12-25	25-30	0.06154	0.00305	0.08962	0.0018	0.76082	0.03606	96	658.1	102.83	553.3	10.64	574.5	20.79
ACO-12-25	25-31	0.31811	0.00361	0.14288	0.00163	6.27262	0.07671	43	3560.7	17.34	860.9	9.2	2014.6	10.71
ACO-12-25	25-32	0.12722	0.00144	0.35549	0.00421	6.23973	0.0789	105	2059.9	19.82	1960.8	20.01	2010	11.07
ACO-12-25	25-33	0.07031	0.00087	0.15084	0.00188	1.46221	0.02046	99	937.4	25.3	905.7	10.55	914.9	8.44
ACO-12-25	25-34	0.11402	0.00147	0.32935	0.00408	5.18053	0.07288	102	1864.5	23.15	1835.2	19.8	1849.4	11.97
ACO-12-25	25-35	0.06278	0.00124	0.08622	0.00107	0.74764	0.01452	94	700.7	41.48	533.1	6.33	566.9	8.44
ACO-12-25	25-36	0.06101	0.00094	0.09216	0.00112	0.77598	0.01234	97	639.5	32.72	568.3	6.6	583.2	7.05
ACO-12-25	25-37	0.10985	0.00154	0.30658	0.00386	4.64682	0.06929	104	1796.9	25.29	1723.9	19.04	1757.7	12.46
ACO-12-25	25-38	0.12766	0.00156	0.36825	0.00429	6.49168	0.08476	102	2066	21.42	2021.1	20.19	2044.8	11.49
ACO-12-25	25-39	0.12527	0.00166	0.35148	0.00399	6.08814	0.08229	105	2032.6	23.28	1941.7	19.03	1988.5	11.79
ACO-12-25	25-40	0.05751	0.00087	0.08287	0.00099	0.65804	0.01025	100	511	33.17	513.2	5.9	513.4	6.28
ACO-12-25	25-41	0.07557	0.00097	0.15888	0.00194	1.65609	0.02321	96	1083.7	25.47	950.6	10.8	991.9	8.87
ACO-12-25	25-42	0.06024	0.00094	0.08245	0.00104	0.68504	0.01129	96	612.1	33.45	510.7	6.18	529.8	6.8
ACO-12-25	25-43	0.05742	0.00163	0.0863	0.00121	0.68402	0.01877	101	507.1	61.53	533.6	7.16	529.2	11.32
ACO-12-25	25-44	0.16503	0.00194	0.47625	0.00562	10.84174	0.13866	100	2507.9	19.62	2510.9	24.54	2509.7	11.89
ACO-12-25	25-45	0.12817	0.00162	0.30239	0.00372	5.34503	0.07426	122	2073	22.06	1703.1	18.42	1876.1	11.88
ACO-12-25	25-46	0.08463	0.00104	0.20862	0.00255	2.43474	0.03329	107	1307.1	23.65	1221.5	13.62	1252.9	9.84
ACO-12-25	25-47	0.0844	0.00103	0.22352	0.00264	2.60173	0.03458	100	1301.6	23.56	1300.4	13.92	1301.1	9.75
ACO-12-25	25-48	0.06313	0.00106	0.10045	0.0014	0.8742	0.01612	97	712.7	35.45	617.1	8.19	637.8	8.73
ACO-12-25	25-49	0.06701	0.0009	0.10167	0.00134	0.93884	0.01444	93	838.2	27.81	624.2	7.83	672.3	7.56
ACO-12-25	25-50	0.07254	0.0011	0.10244	0.00138	1.02398	0.01716	88	1001.2	30.52	628.7	8.06	715.9	8.61
ACO-12-25	25-51	0.10387	0.00168	0.2377	0.00324	3.4036	0.0594	123	1694.4	29.46	1374.7	16.86	1505.2	13.7
ACO-12-25	25-52	0.09955	0.00226	0.09904	0.0016	1.35914	0.03205	70	1615.6	41.62	608.8	9.37	871.5	13.79
ACO-12-25	25-53	0.06714	0.00099	0.08579	0.00117	0.79402	0.01327	89	842.3	30.26	530.6	6.94	593.4	7.51
ACO-12-25	25-54	0.06387	0.00108	0.10903	0.00136	0.96014	0.01668	98	737.2	35.43	667.1	7.89	683.4	8.64
ACO-12-25	25-55	0.06317	0.00142	0.10163	0.00136	0.88521	0.01972	97	714	47	624	7.95	643.8	10.62
ACO-12-25	25-56	0.09916	0.00174	0.10535	0.00141	1.44011	0.02602	71	1608.3	32.33	645.7	8.24	905.8	10.83
ACO-12-25	25-57	0.09114	0.00192	0.13651	0.00203	1.71518	0.03749	81	1449.3	39.66	824.9	11.49	1014.2	14.02
ACO-12-25	25-58	0.09543	0.0013	0.26433	0.00318	3.47759	0.05034	102	1536.6	25.4	1512	16.2	1522.1	11.42
ACO-12-25	25-59	0.13156	0.00178	0.39547	0.00461	7.17249	0.10129	99	2118.9	23.5	2148.2	21.31	2133.1	12.59
ACO-12-25	25-60	0.0628	0.0011	0.10941	0.00141	0.94717	0.01725	99	701.4	36.96	669.3	8.19	676.6	9
ACO-12-25	25-61	0.05855	0.00082	0.08392	0.00104	0.67734	0.01023	99	550.3	30.14	519.5	6.16	525.2	6.19
ACO-12-25	25-62	0.08073	0.00115	0.21029	0.00262	2.34031	0.03557	99	1214.8	27.67	1230.4	13.96	1224.6	10.81
ACO-12-25	25-63	0.11146	0.00156	0.2194	0.00306	3.37219	0.05454	143	1823.4	25.13	1278.7	16.16	1498	12.67
ACO-12-25	25-64	0.06014	0.0021	0.0828	0.00128	0.68638	0.02304	97	608.6	73.9	512.8	7.6	530.6	13.87
ACO-12-25	25-65	0.08783	0.00105	0.09638	0.00112	1.167	0.01513	76	1378.8	22.86	593.2	6.57	785.2	7.09
ACO-12-25	25-66	0.0622	0.00077	0.11146	0.00132	0.95581	0.01292	100	681.1	26.15	681.2	7.67	681.1	6.71
ACO-12-25	25-67	0.13254	0.00151	0.41864	0.00508	7.64945	0.0994	95	2131.9	19.8	2254.3	23.09	2190.7	11.67
ACO-12-25	25-68	0.12951	0.00171	0.35871	0.00485	6.40533	0.09815	106	2091.3	22.97	1976.1	23.03	2033	13.46
ACO-12-25	25-69	0.05883	0.00095	0.09119	0.00112	0.73958	0.0123	100	560.7	34.23	562.6	6.59	562.2	7.18
ACO-12-25	25-70	0.10803	0.00129	0.31975	0.00391	4.76204	0.06412	99	1766.3	21.74	1788.5	19.1	1778.2	11.3
ACO-12-25	25-71	0.13416	0.00264	0.10671	0.0015	1.9736	0.03814	59	2153.1	33.93	653.6	8.76	1106.5	13.03
ACO-12-25	25-72	0.07572	0.00124	0.18513	0.00237	1.9325	0.03285	99	1087.7	32.37	1094.9	12.9	1092.4	11.37

ACO-12-25	25-73	0.13391	0.00226	0.33977	0.00504	6.27305	0.11667	114	2149.9	29.2	1885.5	24.25	2014.7	16.29
ACO-12-25	25-74	0.1139	0.00136	0.34098	0.00414	5.3544	0.07168	98	1862.6	21.44	1891.4	19.9	1877.6	11.45
ACO-12-25	25-75	0.06189	0.00153	0.09041	0.00121	0.77145	0.01856	96	670.5	51.93	558	7.16	580.6	10.64
ACO-12-25	25-76	0.06069	0.001	0.09252	0.00115	0.77413	0.01318	98	628.3	35.07	570.4	6.79	582.1	7.54
ACO-12-25	25-77	0.12953	0.00193	0.37809	0.00536	6.75276	0.11467	101	2091.6	26	2067.4	25.08	2079.6	15.02
ACO-12-25	25-78	0.14712	0.00205	0.35469	0.0048	7.19448	0.11379	118	2312.6	23.72	1957	22.86	2135.8	14.1
ACO-12-25	25-79	0.25616	0.0038	0.52398	0.00618	18.50185	0.27359	119	3223.2	23.2	2716	26.13	3016.2	14.24
ACO-12-25	25-80	0.07892	0.00127	0.08027	0.00105	0.87344	0.01484	78	1170.2	31.56	497.8	6.25	637.4	8.05
ACO-12-25	25-81	0.06054	0.00084	0.06901	0.0008	0.5759	0.0083	93	622.8	29.68	430.2	4.81	461.8	5.35
ACO-12-25	25-82	0.13351	0.00161	0.36294	0.00448	6.6807	0.09118	107	2144.6	20.93	1996.1	21.17	2070.1	12.05
ACO-12-25	25-83	0.08884	0.0013	0.1308	0.00151	1.60201	0.02374	82	1400.7	27.62	792.4	8.62	971	9.26
ACO-12-25	25-84	0.0796	0.00112	0.08073	0.00097	0.88594	0.01316	78	1187.1	27.59	500.5	5.81	644.2	7.08
ACO-12-25	25-85	0.07006	0.00114	0.09562	0.00125	0.92355	0.01589	89	930	32.95	588.7	7.34	664.2	8.39
ACO-12-28A	28A-01	0.06403	0.00104	0.08999	0.00118	0.79388	0.01373	94	742.7	33.9	555.5	6.98	593.4	7.77
ACO-12-28A	28A-02	0.13609	0.00154	0.3501	0.00418	6.56792	0.0832	89	2178.1	19.56	1935.1	19.97	2055.1	11.16
ACO-12-28A	28A-03	0.06469	0.00098	0.09077	0.00118	0.80918	0.01329	93	764.3	31.6	560.1	6.95	602	7.46
ACO-12-28A	28A-04	0.1032	0.00123	0.11513	0.00131	1.63795	0.02067	71	1682.4	21.86	702.5	7.6	984.9	7.96
ACO-12-28A	28A-05	0.13351	0.00169	0.34769	0.00447	6.39751	0.09152	90	2144.6	21.99	1923.5	21.36	2031.9	12.56
ACO-12-28A	28A-06	0.06175	0.00084	0.09399	0.00104	0.80019	0.01102	97	665.4	28.82	579.1	6.16	596.9	6.22
ACO-12-28A	28A-07	0.12779	0.00177	0.36296	0.00477	6.39056	0.09797	97	2067.9	24.26	1996.2	22.58	2031	13.46
ACO-12-28A	28A-08	0.06693	0.00101	0.09377	0.00117	0.86489	0.01387	91	835.5	31.25	577.8	6.91	632.8	7.55
ACO-12-28A	28A-09	0.06393	0.00113	0.09193	0.00104	0.81054	0.01384	94	739.2	36.84	566.9	6.16	602.8	7.76
ACO-12-28A	28A-10	0.06321	0.00093	0.09732	0.00123	0.84772	0.01348	96	715.3	31.04	598.7	7.23	623.4	7.41
ACO-12-28A	28A-11	0.08382	0.00103	0.19803	0.0023	2.28826	0.03005	90	1288.2	23.77	1164.7	12.36	1208.7	9.28
ACO-12-28A	28A-12	0.12314	0.0017	0.3575	0.00475	6.06674	0.09329	98	2002.2	24.35	1970.3	22.56	1985.5	13.4
ACO-12-28A	28A-13	0.07538	0.00089	0.08664	0.00103	0.9003	0.01174	82	1078.6	23.43	535.7	6.1	651.9	6.27
ACO-12-28A	28A-14	0.06546	0.00076	0.12783	0.00145	1.15345	0.01437	100	789.1	24.1	775.5	8.29	778.9	6.77
ACO-12-28A	28A-15	0.20687	0.00235	0.46914	0.00585	13.37611	0.17754	86	2881.2	18.37	2479.8	25.68	2706.6	12.54
ACO-12-28A	28A-16	0.0574	0.00081	0.09507	0.00117	0.75219	0.01147	103	506.5	30.64	585.5	6.87	569.5	6.65
ACO-12-28A	28A-17	0.06111	0.00074	0.09492	0.00108	0.79967	0.01032	98	643.1	25.92	584.6	6.34	596.6	5.82
ACO-12-28A	28A-18	0.1941	0.00211	0.49693	0.00585	13.29606	0.16361	94	2777.2	17.73	2600.6	25.2	2700.9	11.62
ACO-12-28A	28A-19	0.06366	0.00088	0.08719	0.00095	0.76537	0.0105	93	730.4	28.94	538.9	5.62	577.1	6.04
ACO-12-28A	28A-20	0.059	0.00075	0.08764	0.00097	0.71283	0.00933	99	566.9	27.3	541.6	5.75	546.4	5.53
ACO-12-28A	28A-21	0.06214	0.00087	0.0939	0.00105	0.80449	0.01138	97	678.9	29.6	578.6	6.21	599.4	6.4
ACO-12-28A	28A-22	0.06243	0.0009	0.097	0.00119	0.83475	0.0128	97	688.9	30.53	596.8	7.01	616.2	7.09
ACO-12-28A	28A-23	0.07498	0.00084	0.10043	0.00114	1.03817	0.01259	85	1068	22.32	616.9	6.66	723	6.27
ACO-12-28A	28A-24	0.10539	0.00118	0.17824	0.00214	2.5893	0.0328	61	1721.1	20.43	1057.3	11.7	1297.6	9.28
ACO-12-28A	28A-25	0.0611	0.00067	0.0912	0.00103	0.76824	0.00919	97	642.8	23.46	562.6	6.07	578.8	5.28

ACO-12-28A	28A-26	0.11288	0.00131	0.28184	0.00315	4.3862	0.05332	87	1846.3	20.79	1600.6	15.84	1709.7	10.05
ACO-12-28A	28A-27	0.06446	0.00087	0.09277	0.00116	0.82422	0.01218	94	756.7	28.08	571.9	6.87	610.4	6.78
ACO-12-28A	28A-28	0.06164	0.00076	0.09847	0.00109	0.83685	0.01075	98	661.8	26.37	605.4	6.4	617.4	5.94
ACO-12-28A	28A-29	0.11388	0.00141	0.25339	0.00315	3.97712	0.05475	78	1862.2	22.14	1455.9	16.22	1629.5	11.17
ACO-12-28A	28A-30	0.06148	0.00073	0.0846	0.00092	0.71706	0.00881	95	656	25.18	523.5	5.5	548.9	5.21
ACO-12-28A	28A-31	0.06343	0.00099	0.0985	0.00116	0.86141	0.01368	96	722.8	32.89	605.6	6.83	630.9	7.46
ACO-12-28A	28A-32	0.0608	0.0007	0.09115	0.00102	0.764	0.00939	98	632	24.57	562.4	6.04	576.3	5.4
ACO-12-28A	28A-33	0.06	0.00088	0.09483	0.00111	0.78436	0.01182	99	603.4	31.48	584	6.51	588	6.73
ACO-12-28A	28A-34	0.06556	0.00102	0.09129	0.00117	0.82493	0.01369	92	792.4	32.44	563.2	6.93	610.8	7.62
ACO-12-28A	28A-35	0.14264	0.00186	0.09931	0.00126	1.95238	0.02779	56	2259.5	22.31	610.4	7.38	1099.3	9.56
ACO-12-28A	28A-36	0.09606	0.00108	0.04367	0.0005	0.57826	0.0071	59	1549	20.89	275.5	3.11	463.3	4.57
ACO-12-28A	28A-37	0.06073	0.00071	0.08722	0.00103	0.73012	0.0095	97	629.7	25.15	539.1	6.11	556.6	5.58
ACO-12-28A	28A-38	0.13515	0.00154	0.15712	0.0018	2.92736	0.03597	68	2166	19.71	940.7	10.05	1389	9.3
ACO-12-28A	28A-39	0.07491	0.00108	0.10612	0.00131	1.09583	0.01671	87	1066.1	28.74	650.2	7.63	751.3	8.1
ACO-12-28A	28A-40	0.10823	0.00119	0.13772	0.0015	2.05479	0.02378	73	1769.8	19.93	831.7	8.5	1133.9	7.9
ACO-12-28A	28A-41	0.20705	0.00222	0.06258	0.00072	1.78625	0.0212	38	2882.6	17.27	391.3	4.35	1040.5	7.73
ACO-12-28A	28A-42	0.15803	0.0018	0.38736	0.00443	8.43922	0.10287	87	2434.7	19.14	2110.6	20.58	2279.4	11.07
ACO-12-28A	28A-43	0.08141	0.00108	0.09987	0.00126	1.12075	0.01646	80	1231.4	25.85	613.6	7.41	763.3	7.88
ACO-12-28A	28A-44	0.06326	0.001	0.06428	0.00084	0.56048	0.00952	89	717.1	33.35	401.6	5.08	451.8	6.19
ACO-12-28A	28A-45	0.06213	0.00083	0.08945	0.00107	0.76613	0.01096	96	678.4	28.25	552.3	6.33	577.5	6.3
ACO-12-28A	28A-46	0.07407	0.00098	0.15182	0.00192	1.55012	0.02277	96	1043.4	26.34	911.2	10.77	950.5	9.07
ACO-12-28A	28A-47	0.0658	0.00077	0.11973	0.00138	1.08611	0.01385	98	800.1	24.38	729	7.96	746.6	6.74
ACO-12-28A	28A-48	0.06925	0.00083	0.08374	0.00096	0.79942	0.01027	87	906.3	24.49	518.4	5.71	596.5	5.79
ACO-12-28A	28A-49	0.07414	0.00126	0.10185	0.00137	1.04082	0.01874	86	1045.4	33.97	625.3	8.03	724.3	9.33
ACO-12-28A	28A-50	0.06532	0.00114	0.09663	0.00125	0.86994	0.01569	94	784.6	36.35	594.6	7.32	635.5	8.52
ACO-12-28A	28A-51	0.13187	0.00157	0.25391	0.00302	4.61633	0.05996	69	2123.1	20.67	1458.6	15.54	1752.2	10.84
ACO-12-28A	28A-52	0.07101	0.00113	0.09532	0.00119	0.93314	0.01541	88	957.7	32.31	586.9	6.98	669.3	8.09
ACO-12-28A	28A-53	0.10761	0.00127	0.11233	0.00129	1.66631	0.02105	69	1759.3	21.29	686.2	7.5	995.8	8.02
ACO-12-28A	28A-54	0.13412	0.00195	0.16926	0.00227	3.12827	0.04987	47	2152.6	25.14	1008	12.53	1439.7	12.27
ACO-12-28A	28A-55	0.12538	0.00154	0.17543	0.00223	3.03157	0.04268	51	2034.2	21.57	1042	12.21	1415.6	10.75
ACO-12-28A	28A-56	0.07445	0.00127	0.0989	0.00135	1.01479	0.01843	85	1053.5	34.4	608	7.91	711.3	9.29
ACO-12-28A	28A-57	0.17819	0.00197	0.32136	0.0038	7.89442	0.09858	68	2636.1	18.2	1796.4	18.53	2219	11.25
ACO-12-28A	28A-58	0.07453	0.00133	0.09122	0.00112	0.93726	0.01658	84	1055.6	35.78	562.7	6.59	671.4	8.69
ACO-12-28A	28A-59	0.05811	0.00078	0.07996	0.00094	0.64052	0.00907	99	533.2	29.43	495.9	5.62	502.6	5.61
ACO-12-28A	28A-60	0.13724	0.00181	0.29339	0.00378	5.54959	0.08184	76	2192.6	22.74	1658.4	18.83	1908.3	12.69
ACO-12-28A	28A-61	0.07307	0.00101	0.09649	0.00122	0.97138	0.01463	86	1016	27.84	593.8	7.15	689.2	7.54

ACO-12-28A	28A-62	0.07403	0.00105	0.09136	0.00115	0.93189	0.01422	84	1042.3	28.43	563.6	6.77	668.6	7.47
ACO-12-28A	28A-63	0.07748	0.00096	0.0924	0.00109	0.98663	0.01315	82	1133.8	24.21	569.7	6.43	697	6.72
ACO-12-28A	28A-64	0.06221	0.00077	0.09507	0.00112	0.8151	0.01095	97	681.4	26.26	585.4	6.6	605.3	6.12
ACO-12-28A	28A-65	0.15703	0.00198	0.40447	0.00529	8.74758	0.12634	90	2424	21.24	2189.6	24.29	2312	13.16
ACO-12-28A	28A-66	0.08328	0.00104	0.09115	0.00112	1.04587	0.01455	77	1275.5	24.39	562.3	6.64	726.8	7.22
ACO-12-28A	28A-67	0.28201	0.00304	0.25597	0.00298	9.94868	0.12022	44	3374.1	16.74	1469.2	15.29	2430	11.15
ACO-12-28A	28A-68	0.42435	0.00457	0.36848	0.00428	21.54998	0.26012	51	3997.7	16	2022.2	20.14	3163.7	11.71
ACO-12-28A	28A-69	0.13033	0.00164	0.30365	0.00395	5.45028	0.07879	81	2102.4	21.94	1709.4	19.52	1892.8	12.4
ACO-12-28A	28A-70	0.07482	0.00128	0.09278	0.00128	0.95592	0.01748	84	1063.6	34.08	572	7.56	681.2	9.07
ACO-12-28A	28A-71	0.06175	0.00089	0.09307	0.00117	0.79188	0.0123	97	665.5	30.58	573.6	6.89	592.2	6.97
ACO-12-28A	28A-72	0.06456	0.00094	0.09098	0.00117	0.80924	0.0128	93	760	30.42	561.3	6.89	602	7.19
ACO-12-28A	28A-73	0.16127	0.00188	0.4205	0.0052	9.34453	0.12472	92	2469	19.51	2262.7	23.6	2372.4	12.24
ACO-12-28A	28A-74	0.07136	0.0013	0.11631	0.00162	1.14317	0.02194	92	967.7	36.66	709.3	9.38	774	10.4
ACO-12-28A	28A-75	0.06232	0.00107	0.09285	0.00121	0.79746	0.0143	96	685.1	36.34	572.4	7.12	595.4	8.08
ACO-12-28A	28A-76	0.06429	0.00087	0.09014	0.00113	0.79854	0.01191	93	751	28.38	556.4	6.69	596	6.72
ACO-12-28A	28A-77	0.06967	0.00097	0.07494	0.00099	0.71939	0.01126	85	918.7	28.34	465.9	5.91	550.3	6.65
ACO-12-28A	28A-78	0.06894	0.00113	0.09755	0.00129	0.92666	0.01616	90	896.9	33.43	600.1	7.6	665.9	8.52
ACO-12-28A	28A-79	0.1317	0.00157	0.31757	0.00363	5.76557	0.07331	84	2120.8	20.8	1777.8	17.74	1941.3	11
ACO-12-28A	28A-80	0.08151	0.00166	0.08313	0.00123	0.93291	0.01989	77	1233.9	39.35	514.8	7.32	669.2	10.45
ACO-12-33	1	0.05708	0.001	0.06818	0.00091	0.53669	0.0099	97	494	38.15	425.2	5.49	436.2	6.54
ACO-12-33	2	0.06046	0.00141	0.09582	0.00141	0.79865	0.01901	99	620.1	49.59	589.9	8.32	596.1	10.73
ACO-12-33	3	0.05565	0.00165	0.06362	0.00105	0.48837	0.01456	98	438	64.37	397.6	6.34	403.8	9.93
ACO-12-33	4	0.11181	0.00216	0.10211	0.00145	1.57416	0.03082	65	1829.1	34.65	626.7	8.46	960.1	12.16
ACO-12-33	5	0.05503	0.00086	0.06382	0.00081	0.48426	0.00803	99	413.6	34.36	398.8	4.89	401	5.49
ACO-12-33	6	0.05644	0.00105	0.07225	0.001	0.56216	0.01102	99	468.9	41	449.7	5.99	452.9	7.16
ACO-12-33	7	0.06093	0.001	0.09433	0.00128	0.79249	0.01408	98	636.8	34.97	581.1	7.52	592.6	7.97
ACO-12-33	8	0.06582	0.00106	0.09031	0.00121	0.81967	0.01433	92	800.7	33.43	557.3	7.16	607.9	7.99
ACO-12-33	9	0.07938	0.00162	0.17163	0.00232	1.87903	0.03872	0	1181.5	39.73	1021.1	12.77	1073.7	13.66
ACO-12-33	10	0.05596	0.0013	0.06609	0.00095	0.50997	0.01203	99	450.6	50.57	412.5	5.76	418.4	8.09
ACO-12-33	11	0.14763	0.00399	0.08767	0.0015	1.78455	0.04654	52	2318.6	45.65	541.7	8.9	1039.8	16.97
ACO-12-33	12	0.08109	0.00257	0.17013	0.00299	1.90203	0.05987	94	1223.7	60.85	1012.8	16.47	1081.8	20.95
ACO-12-33	13	0.1834	0.00325	0.51626	0.00726	13.05422	0.24876	100	2683.9	29.03	2683.3	30.88	2683.6	17.97
ACO-12-33	14	0.07213	0.0014	0.15467	0.00217	1.53812	0.03112	98	989.5	38.88	927.1	12.1	945.8	12.45
ACO-12-33	15	0.20132	0.00471	0.03778	0.00065	1.04813	0.02421	33	2836.9	37.64	239	4.04	728	12
ACO-12-33	16	0.1002	0.0013	0.21505	0.00266	2.9708	0.04213	77	1627.9	23.89	1255.7	14.09	1400.2	10.77
ACO-12-33	17	0.07095	0.00167	0.15962	0.00242	1.56123	0.0374	100	956	47.32	954.7	13.45	955	14.83
ACO-12-33	18	0.07184	0.00235	0.14095	0.00248	1.39576	0.04519	96	981.4	65.31	850	14	887.1	19.15
ACO-12-33	19	0.05858	0.00124	0.067	0.00091	0.54111	0.01159	95	551.5	45.54	418.1	5.5	439.2	7.63
ACO-12-33	20	0.05701	0.00109	0.07689	0.00108	0.60432	0.01215	99	491.3	41.56	477.5	6.46	480	7.69
ACO-12-33	21	0.16789	0.00265	0.47	0.00645	10.87862	0.18483	98	2536.7	26.23	2483.6	28.29	2512.8	15.8

ACO-12-33	22	0.07662	0.00187	0.17948	0.00285	1.89554	0.04756	96	1111.3	48.09	1064.1	15.55	1079.5	16.68
ACO-12-33	23	0.06129	0.00174	0.10095	0.00164	0.85287	0.02442	99	649.3	59.81	620	9.61	626.2	13.38
ACO-12-33	24	0.11874	0.00232	0.26844	0.00385	4.39441	0.0875	79	1937.3	34.61	1532.9	19.55	1711.3	16.47
ACO-12-33	25	0.77983	0.01449	0.85345	0.01331	91.75896	1.72833	81	4885.3	26.24	3977.8	46.28	4599.7	18.92
ACO-12-33	26	0.06038	0.0017	0.066	0.00102	0.5494	0.01541	93	617.1	59.6	412	6.18	444.6	10.1
ACO-12-33	27	0.07224	0.00159	0.16026	0.0022	1.59603	0.03525	99	992.6	44.22	958.2	12.25	968.7	13.79
ACO-12-33	28	0.06148	0.00126	0.09561	0.00127	0.81016	0.01675	98	656	43.34	588.7	7.49	602.5	9.4
ACO-12-33	29	0.06318	0.00176	0.07169	0.00107	0.62436	0.01706	91	714.4	58.13	446.3	6.41	492.6	10.66
ACO-12-33	30	0.06101	0.00197	0.07518	0.0012	0.63223	0.01991	94	639.4	67.81	467.3	7.22	497.5	12.39
ACO-12-33	31	0.0837	0.00198	0.20197	0.00289	2.33056	0.05487	92	1285.5	45.48	1185.9	15.51	1221.6	16.73
ACO-12-33	32	0.12964	0.0031	0.35789	0.00573	6.39581	0.15501	94	2093	41.5	1972.2	27.2	2031.7	21.28
ACO-12-33	33	0.07444	0.00159	0.04823	0.00071	0.49483	0.01101	74	1053.2	42.88	303.6	4.36	408.2	7.48
ACO-12-33	34	0.09279	0.00244	0.23522	0.0035	3.00969	0.07747	92	1483.5	49.16	1361.8	18.26	1410.1	19.62
ACO-12-33	35	0.06476	0.0019	0.11791	0.00192	1.0529	0.03086	98	766.6	60.69	718.5	11.1	730.3	15.26
ACO-12-33	36	0.11748	0.00247	0.19006	0.00273	3.07834	0.06666	58	1918.2	37.26	1121.7	14.79	1427.3	16.6
ACO-12-33	37	0.11823	0.00405	0.3121	0.00604	5.08712	0.16967	91	1929.6	60.14	1751	29.66	1834	28.3
ACO-12-33	39	0.05707	0.00139	0.06814	0.00096	0.53612	0.01301	97	493.6	53.26	425	5.78	435.9	8.6
ACO-12-33	40	0.18987	0.00317	0.50774	0.00646	13.29104	0.22993	97	2741.1	27.17	2647	27.63	2700.5	16.34
ACO-12-33	41	0.10244	0.00189	0.298	0.00404	4.20975	0.08038	101	1668.8	33.79	1681.4	20.08	1675.9	15.67
ACO-12-33	42	0.05898	0.00131	0.07584	0.001	0.61683	0.01363	97	566.3	47.75	471.2	5.97	487.9	8.56
ACO-12-33	43	0.0785	0.00285	0.17417	0.00323	1.88539	0.06755	89	1159.5	70.25	1035	17.74	1076	23.77
ACO-12-33	44	0.05899	0.00157	0.0826	0.00124	0.67188	0.0179	98	566.9	56.94	511.6	7.39	521.9	10.87
ACO-12-33	45	0.09426	0.00329	0.23299	0.00425	3.02917	0.10443	89	1513.3	64.57	1350.1	22.24	1415	26.32
ACO-12-33	46	0.05703	0.00161	0.06549	0.001	0.51512	0.01441	97	492.3	61.56	409	6.02	421.9	9.66
ACO-12-33	47	0.18516	0.00498	0.47566	0.0069	12.13814	0.3148	93	2699.6	43.75	2508.3	30.13	2615.1	24.33
ACO-12-30A	1	0.06059	0.00078	0.10043	0.0012	0.83901	0.01166	100	624.8	27.49	616.9	7.03	618.6	6.44
ACO-12-30A	2	0.05698	0.00104	0.06616	0.00087	0.51973	0.00984	97	490.3	39.94	413	5.28	425	6.57
ACO-12-30A	3	0.05858	0.00092	0.09898	0.00124	0.79942	0.01318	102	551.4	33.81	608.4	7.29	596.5	7.44
ACO-12-30A	4	0.0558	0.00085	0.06589	0.00085	0.50687	0.00832	99	444.3	33.06	411.3	5.16	416.3	5.6
ACO-12-30A	5	0.06403	0.00154	0.09718	0.00138	0.85794	0.0207	95	742.8	50.11	597.9	8.1	629	11.31
ACO-12-30A	6	0.05468	0.00073	0.06378	0.00078	0.48085	0.00694	100	399.2	29.37	398.6	4.7	398.7	4.76
ACO-12-30A	7	0.05608	0.00073	0.06625	0.0008	0.51226	0.00725	98	455.1	28.5	413.5	4.82	420	4.87
ACO-12-30A	8	0.05849	0.00103	0.08962	0.00116	0.72274	0.01318	100	548.1	37.92	553.3	6.85	552.3	7.77
ACO-12-30A	9	0.0558	0.00106	0.06725	0.00091	0.51731	0.01021	99	444	41.27	419.6	5.51	423.4	6.84
ACO-12-30A	10	0.06018	0.00159	0.09821	0.00144	0.81483	0.02139	100	610.1	55.94	603.9	8.45	605.2	11.97
ACO-12-30A	11	0.05541	0.00118	0.06726	0.00094	0.51378	0.0112	100	428.3	46.27	419.6	5.67	421	7.51
ACO-12-30A	12	0.05862	0.00149	0.08433	0.00114	0.68158	0.01708	99	552.9	54.66	521.9	6.77	527.7	10.31
ACO-12-30A	13	0.05873	0.00094	0.09761	0.00127	0.79037	0.01347	102	557.2	34.38	600.4	7.48	591.4	7.64
ACO-12-30A	14	0.05846	0.00107	0.0668	0.00091	0.53838	0.01032	95	547.1	39.31	416.8	5.49	437.4	6.81
ACO-12-30A	15	0.05563	0.00098	0.06708	0.0009	0.51445	0.00957	99	437.3	38.34	418.5	5.42	421.4	6.42

ACO-12-30A	16	0.06395	0.00106	0.09319	0.00113	0.82137	0.01381	94	740	34.55	574.4	6.66	608.8	7.7
ACO-12-30A	17	0.06096	0.00184	0.09719	0.00141	0.81671	0.02385	99	637.7	63.5	597.9	8.26	606.2	13.33
ACO-12-30A	18	0.07465	0.00121	0.17854	0.00226	1.8375	0.03108	100	1058.7	32.71	1059	12.36	1059	11.12
ACO-12-30A	19	0.05825	0.00096	0.08453	0.00106	0.6789	0.01166	99	538.7	36.41	523.1	6.3	526.1	7.05
ACO-12-30A	20	0.05278	0.00144	0.06617	0.00098	0.48149	0.01316	103	319.1	60.82	413	5.95	399.1	9.02
ACO-12-30A	21	0.05754	0.00127	0.06698	0.00095	0.53143	0.01197	97	512	47.98	418	5.74	432.8	7.94
ACO-12-30A	22	0.05902	0.00145	0.09037	0.00124	0.73522	0.01799	100	567.8	52.63	557.7	7.3	559.6	10.53
ACO-12-30A	23	0.08993	0.00144	0.23722	0.00307	2.94112	0.04996	96	1423.9	30.18	1372.2	16	1392.6	12.87
ACO-12-30A	24	0.06137	0.0016	0.09829	0.00146	0.83162	0.02172	98	652.2	55.03	604.4	8.58	614.5	12.04
ACO-12-30A	25	0.05831	0.00173	0.07729	0.0011	0.6212	0.01784	98	540.8	64.26	480	6.58	490.6	11.17
ACO-12-30A	26	0.05593	0.00196	0.06497	0.00112	0.50061	0.01737	98	449.1	76.08	405.8	6.75	412.1	11.76
ACO-12-30A	27	0.05935	0.00152	0.08293	0.00111	0.6783	0.01686	98	579.8	54.55	513.6	6.62	525.7	10.2
ACO-12-30A	28	0.06043	0.00168	0.06645	0.00103	0.55362	0.01545	93	619.2	58.96	414.7	6.25	447.4	10.1
ACO-12-30A	29	0.05735	0.00116	0.08764	0.00115	0.69286	0.01422	101	504.5	44.41	541.6	6.82	534.5	8.53
ACO-12-30A	30	0.06166	0.00143	0.0989	0.00143	0.84073	0.01989	98	662.4	48.9	607.9	8.42	619.6	10.97
ACO-12-30A	31	0.05515	0.00073	0.06831	0.00081	0.51945	0.00733	100	418.3	28.95	426	4.91	424.8	4.9
ACO-12-30A	32	0.05978	0.00106	0.09088	0.00117	0.74895	0.01367	99	595.1	38.33	560.8	6.91	567.6	7.94
ACO-12-30A	33	0.05988	0.00097	0.0899	0.00113	0.74211	0.01253	98	599.3	34.72	554.9	6.69	563.6	7.3
ACO-12-30A	34	0.05858	0.00109	0.08489	0.00114	0.68542	0.01325	99	551.4	40.17	525.2	6.75	530	7.99
ACO-12-30A	35	0.09445	0.0014	0.26323	0.00323	3.4279	0.05275	99	1517.2	27.78	1506.4	16.49	1510.8	12.1
ACO-12-30A	36	0.05893	0.00111	0.08561	0.00111	0.69551	0.01339	99	564.5	40.56	529.5	6.6	536.1	8.02
ACO-12-30A	37	0.0562	0.0009	0.06595	0.00082	0.51095	0.00851	98	459.4	35.15	411.7	4.98	419.1	5.72
ACO-12-30A	38	0.06116	0.00126	0.08413	0.00112	0.7093	0.01481	96	644.9	43.82	520.7	6.68	544.3	8.8
ACO-12-30A	39	0.09476	0.0013	0.24855	0.003	3.24681	0.04723	94	1523.3	25.66	1431	15.48	1468.4	11.29
ACO-12-30A	40	0.05466	0.00104	0.06554	0.00087	0.49381	0.00972	100	398.2	41.96	409.2	5.28	407.5	6.61
ACO-12-30A	41	0.05592	0.00095	0.06444	0.00083	0.49676	0.00881	98	448.8	36.86	402.6	5.05	409.5	5.98
ACO-12-30A	42	0.05588	0.00085	0.06619	0.00085	0.50976	0.00834	99	447.1	33.15	413.1	5.14	418.3	5.61
ACO-12-30A	43	0.0572	0.00107	0.07141	0.00091	0.56305	0.01069	98	498.8	40.42	444.6	5.51	453.5	6.94
ACO-12-30A	44	0.0555	0.00136	0.06607	0.00096	0.50559	0.01249	99	432	53.37	412.4	5.8	415.5	8.42
ACO-12-30A	45	0.05392	0.00143	0.06489	0.00096	0.48243	0.01275	101	367.6	58.45	405.3	5.81	399.7	8.73
ACO-12-30A	46	0.05955	0.0009	0.08578	0.00105	0.70419	0.01117	98	587.2	32.42	530.5	6.25	541.3	6.66
ACO-12-30A	47	0.05791	0.00088	0.08538	0.00103	0.6816	0.01075	100	526	33.15	528.2	6.12	527.7	6.49
ACO-12-30A	48	0.05568	0.00082	0.06587	0.0008	0.50561	0.00785	99	439.4	31.96	411.2	4.85	415.5	5.3
ACO-12-30A	49	0.06409	0.00103	0.07931	0.00096	0.70081	0.01152	91	744.7	33.66	492	5.74	539.3	6.88
ACO-12-30A	50	0.06065	0.00092	0.09632	0.00122	0.80538	0.01309	99	627	32.38	592.8	7.2	599.9	7.36
ACO-12-30A	51	0.0574	0.00081	0.06936	0.00084	0.54879	0.00823	97	506.3	30.56	432.3	5.07	444.2	5.4

ACO-12-30A	52	0.07252	0.00094	0.16316	0.00195	1.6313	0.02282	97	1000.6	26.06	974.3	10.83	982.4	8.81
ACO-12-30A	53	0.05946	0.00089	0.08442	0.00103	0.69204	0.01094	98	583.9	32.29	522.5	6.15	534	6.56
ACO-12-30A	54	0.05624	0.00079	0.06351	0.00077	0.49247	0.00738	98	461.2	31.13	397	4.66	406.6	5.02
ACO-12-30A	55	0.06187	0.00103	0.09452	0.00123	0.80615	0.01411	97	669.7	35.16	582.2	7.23	600.3	7.93
ACO-12-30A	56	0.06009	0.00117	0.08742	0.00112	0.72423	0.01428	98	606.8	41.7	540.3	6.66	553.2	8.41
ACO-12-30A	57	0.06098	0.00179	0.09849	0.00146	0.82802	0.02381	99	638.4	61.83	605.6	8.54	612.5	13.23
ACO-12-30A	58	0.06083	0.00093	0.10096	0.0012	0.84674	0.0133	100	633.3	32.62	620.1	7.03	622.9	7.31
ACO-12-30A	59	0.06038	0.001	0.09273	0.00114	0.77189	0.01304	98	617.3	35.3	571.7	6.7	580.8	7.47
ACO-12-30A	60	0.05821	0.00141	0.06536	0.00096	0.52452	0.01291	95	537.2	52.84	408.1	5.82	428.2	8.6
ACO-12-32C	1	0.08087	0.0011	0.22689	0.00314	2.52884	0.03949	92	1218.4	26.49	1318.2	16.5	1280.4	11.36
ACO-12-32C	2	0.09733	0.00171	0.07004	0.00108	0.93991	0.01809	154	1573.6	32.55	436.4	6.54	672.8	9.47
ACO-12-32C	3	0.05409	0.00144	0.06669	0.00116	0.49734	0.01341	98	374.5	58.6	416.2	7.02	409.9	9.1
ACO-12-32C	4	0.0944	0.00163	0.2542	0.00369	3.30671	0.05987	104	1516.1	32.2	1460.1	18.97	1482.6	14.12
ACO-12-32C	5	0.08748	0.00573	0.06374	0.00186	0.76874	0.04662	145	1371.2	121.07	398.3	11.28	579	26.76
ACO-12-32C	6	0.05588	0.00195	0.06645	0.00118	0.51155	0.01757	101	447.3	75.94	414.7	7.11	419.5	11.81
ACO-12-32C	7	0.05466	0.00155	0.06576	0.00108	0.49508	0.01396	99	398.2	61.38	410.6	6.53	408.4	9.48
ACO-12-32C	8	0.06047	0.00096	0.10609	0.00148	0.88397	0.01522	99	620.6	33.76	650	8.63	643.1	8.2
ACO-12-32C	9	0.07026	0.0014	0.14207	0.00221	1.37513	0.02872	103	936	40.35	856.4	12.45	878.4	12.28
ACO-12-32C	10	0.05729	0.00198	0.06303	0.00112	0.49702	0.01669	104	502.1	74.69	394	6.79	409.7	11.32
ACO-12-32C	11	0.06272	0.00309	0.09394	0.00193	0.8113	0.03851	104	698.7	101.49	578.8	11.37	603.2	21.59
ACO-12-32C	12	0.06022	0.00099	0.10166	0.00143	0.84337	0.01488	99	611.6	35	624.2	8.35	621	8.2
ACO-12-32C	13	0.0557	0.00201	0.06151	0.00117	0.47239	0.0167	102	440.1	78.57	384.8	7.13	392.8	11.52
ACO-12-32C	14	0.06139	0.00185	0.08884	0.00149	0.75118	0.02218	104	652.8	63.26	548.7	8.82	568.9	12.86
ACO-12-32C	15	0.06728	0.00147	0.08191	0.00129	0.75832	0.01697	113	846.6	44.64	507.5	7.72	573	9.8
ACO-12-32C	16	0.0683	0.00119	0.13139	0.00189	1.23604	0.02297	103	877.6	35.74	795.8	10.78	817.1	10.43
ACO-12-32C	17	0.05943	0.0013	0.08564	0.0013	0.70104	0.01565	102	582.8	46.82	529.7	7.73	539.4	9.34
ACO-12-32C	18	0.05634	0.00131	0.07914	0.0012	0.61424	0.01452	99	465.1	51.22	491	7.19	486.2	9.13
ACO-12-32C	19	0.07437	0.00141	0.06442	0.001	0.65964	0.01319	128	1051.5	37.75	402.4	6.03	514.4	8.07
ACO-12-32C	20	0.0615	0.00281	0.09845	0.00209	0.83424	0.03669	102	656.9	94.98	605.3	12.27	616	20.31
ACO-12-32C	21	0.07982	0.00176	0.17091	0.00279	1.88056	0.04298	117	1192.5	43.02	1017.1	15.36	1074.3	15.15
ACO-12-32C	22	0.05964	0.00123	0.06493	0.00096	0.53354	0.01124	107	590.4	44.27	405.5	5.79	434.2	7.45
ACO-12-32C	23	0.06071	0.00176	0.09815	0.00159	0.82113	0.02353	101	628.9	61.33	603.6	9.35	608.7	13.12
ACO-12-32C	24	0.05658	0.00108	0.07376	0.00106	0.57514	0.01136	101	474.5	42.18	458.8	6.38	461.3	7.32
ACO-12-32C	25	0.07495	0.00174	0.1612	0.00253	1.66504	0.03847	103	1067.3	45.89	963.4	14.05	995.3	14.66
ACO-12-32C	26	0.07328	0.00162	0.16163	0.0025	1.63211	0.03635	102	1021.6	44.22	965.8	13.88	982.7	14.02

ACO-12-32C	27	0.12561	0.00284	0.35051	0.00571	6.06844	0.13894	105	2037.3	39.46	1937	27.24	1985.7	19.96
ACO-12-32C	28	0.06648	0.00154	0.10022	0.00148	0.91816	0.02069	107	821.6	47.63	615.7	8.68	661.4	10.95
ACO-12-32C	29	0.07724	0.00216	0.16356	0.0027	1.74135	0.04691	105	1127.5	54.74	976.6	14.99	1024	17.38
ACO-12-32C	30	0.05669	0.00127	0.07538	0.00111	0.58911	0.01314	100	478.8	49.1	468.5	6.66	470.3	8.39
ACO-12-32C	31	0.05338	0.00152	0.0664	0.00108	0.48857	0.01358	97	345.1	63.12	414.4	6.52	403.9	9.26
ACO-12-32C	32	0.08428	0.00237	0.12052	0.00207	1.39986	0.03831	121	1298.9	53.77	733.5	11.91	888.9	16.21
ACO-12-32C	33	0.0825	0.00181	0.23026	0.00364	2.61583	0.0579	94	1257.3	42.26	1335.8	19.09	1305.1	16.26
ACO-12-32C	34	0.0605	0.00111	0.10374	0.00149	0.86492	0.01658	99	621.5	39.14	636.3	8.7	632.8	9.03
ACO-12-32C	35	0.10195	0.00154	0.28067	0.00397	3.94052	0.06571	104	1660	27.71	1594.7	20	1622	13.5
ACO-12-32C	36	0.08952	0.00169	0.25966	0.00395	3.20051	0.06333	95	1415.2	35.72	1488.1	20.23	1457.3	15.31
ACO-12-32C	37	0.07415	0.0023	0	0	0	0	#####	1045.6	61.31	0	0	0	0
ACO-12-32C	38	0.09888	0.00178	0.29045	0.00426	3.94978	0.0742	98	1603.1	33.13	1643.8	21.29	1623.9	15.22
ACO-12-32C	39	0.06917	0.00224	0.14239	0.00259	1.35519	0.04254	101	903.8	65.45	858.1	14.64	869.8	18.34
ACO-12-32C	40	0.05436	0.00217	0.08665	0.00169	0.64777	0.02492	95	385.9	86.63	535.7	10.04	507.1	15.36
ACO-12-32C	41	0.06156	0.00108	0.10397	0.00146	0.88154	0.01621	101	658.9	37.06	637.6	8.55	641.8	8.75
ACO-12-32C	42	0.0683	0.00121	0.12227	0.00173	1.15015	0.02131	105	877.6	36.21	743.6	9.97	777.3	10.07
ACO-12-32C	43	0.05465	0.00124	0.07985	0.0012	0.6008	0.01367	96	398	49.59	495.2	7.18	477.7	8.67
ACO-12-32C	44	0.06019	0.00112	0.10465	0.00151	0.86698	0.01669	99	610.4	39.63	641.6	8.8	633.9	9.08
ACO-12-32C	45	0.11768	0.00247	0.33975	0.00529	5.49228	0.11717	102	1921.3	37.11	1885.5	25.46	1899.4	18.32
ACO-12-32C	46	0.06387	0.00131	0.08938	0.00132	0.78585	0.01644	107	737.5	42.89	551.9	7.83	588.8	9.35
ACO-12-32C	47	0.05653	0.00187	0.06612	0.00121	0.51495	0.01649	102	472.3	72.4	412.8	7.31	421.8	11.05
ACO-12-32C	48	0.05605	0.00183	0.09144	0.00165	0.70343	0.02229	96	453.9	70.99	564	9.73	540.8	13.29
ACO-12-32C	49	0.05277	0.00123	0.05479	0.00083	0.39828	0.0094	99	319	52.15	343.9	5.08	340.4	6.82
ACO-12-32C	50	0.07622	0.00143	0.18519	0.00272	1.94526	0.03801	101	1100.8	37.06	1095.3	14.79	1096.8	13.1
ACO-12-32C	51	0.05212	0.00166	0.05611	0.00096	0.40262	0.01262	98	290.6	71.24	351.9	5.88	343.5	9.13
ACO-12-32C	52	0.07991	0.00169	0.207	0.00319	2.28034	0.04905	99	1194.9	41.17	1212.8	17.04	1206.2	15.18
ACO-12-32C	53	0.06234	0.00223	0.09852	0.00192	0.84747	0.02925	103	685.8	74.51	605.8	11.28	623.3	16.07
ACO-12-32C	54	0.07285	0.00151	0.15446	0.00234	1.55119	0.03295	103	1009.7	41.48	925.9	13.07	951	13.11
ACO-12-32C	55	0.06531	0.00152	0.06567	0.00101	0.59039	0.01382	115	784.3	48.27	410	6.11	471.1	8.82
ACO-12-32C	56	0.06299	0.00122	0.0669	0.00098	0.58048	0.01167	111	707.8	40.57	417.5	5.9	464.8	7.5
ACO-12-32C	57	0.05836	0.00147	0.10296	0.00164	0.82813	0.02091	97	543.4	54.25	631.7	9.58	612.6	11.62
ACO-12-32C	58	0.06158	0.00261	0.07947	0.00163	0.6745	0.02757	106	659.7	88.5	492.9	9.74	523.4	16.72
ACO-12-32C	59	0.05965	0.00156	0.10153	0.0017	0.83466	0.02179	99	590.9	55.6	623.4	9.97	616.2	12.06
ACO-12-32C	60	0.05397	0.00112	0.06553	0.00098	0.48749	0.0105	99	369.5	46.26	409.2	5.94	403.2	7.17
ACO-12-32C	61	0.10561	0.00188	0.28249	0.00413	4.11174	0.07811	108	1725	32.3	1603.9	20.74	1656.6	15.52
ACO-12-32C	62	0.07755	0.00153	0.07393	0.00111	0.78948	0.01629	129	1135.3	38.84	459.8	6.67	590.9	9.24

ACO-12-32C	63	0.05649	0.00215	0.06038	0.00115	0.46961	0.01733	103	470.9	82.72	378	6.99	390.9	11.98
ACO-12-32C	64	0.05385	0.00158	0.07215	0.00125	0.53499	0.01551	97	364.8	64.52	449.1	7.51	435.1	10.26
ACO-12-32C	65	0.05557	0.00144	0.06467	0.00105	0.49537	0.01284	101	434.9	56.47	403.9	6.36	408.6	8.72
ACO-12-32C	66	0.05642	0.00231	0.06802	0.00126	0.52911	0.02095	102	468	88.86	424.2	7.58	431.2	13.91
ACO-12-32C	67	0.05664	0.00117	0.06655	0.00099	0.51953	0.01107	102	476.8	45.5	415.3	5.97	424.8	7.4
ACO-12-32C	68	0.10163	0.00188	0.14099	0.00215	1.97511	0.03881	130	1654.2	33.95	850.3	12.17	1107.1	13.25
ACO-12-32C	69	0.05775	0.00155	0.06631	0.0011	0.52793	0.01413	104	520.2	57.96	413.9	6.66	430.4	9.39
ACO-12-32C	70	0.17981	0.0061	0.07567	0.00173	1.87555	0.057	228	2651.2	55.16	470.2	10.37	1072.5	20.13
ACO-12-32C	71	0.0605	0.00383	0.07639	0.00203	0.63663	0.0383	105	621.4	130.9	474.5	12.18	500.2	23.76
ACO-12-32C	72	0.12059	0.00325	0.10697	0.00192	1.77714	0.04721	158	1965	47.25	655.1	11.2	1037.1	17.26
ACO-12-32C	73	0.06262	0.00173	0.09929	0.00165	0.85681	0.02345	103	695.4	57.65	610.3	9.67	628.4	12.82
ACO-12-32C	74	0.05762	0.00278	0.0932	0.00186	0.74004	0.03459	98	515.2	102.72	574.4	10.98	562.4	20.19
ACO-12-32C	75	0.06102	0.00152	0.10165	0.00164	0.8546	0.02145	100	640	52.82	624.1	9.58	627.2	11.75
ACO-12-32C	76	0.06669	0.00205	0.13148	0.00229	1.20826	0.03639	101	828	62.91	796.3	13.04	804.4	16.73
ACO-12-32C	77	0.06549	0.00213	0.09802	0.00176	0.88444	0.02793	107	790.2	66.82	602.8	10.36	643.4	15.05
ACO-12-32C	78	0.08921	0.00285	0.24232	0.00463	2.979	0.09238	101	1408.7	59.8	1398.8	24.01	1402.3	23.57
ACO-12-32C	79	0.0739	0.00158	0.17349	0.00264	1.76663	0.0387	101	1038.9	42.53	1031.3	14.53	1033.3	14.2
ACO-12-32C	80	0.11533	0.00487	0.06093	0.00147	0.96823	0.03758	180	1885	74.11	381.3	8.93	687.6	19.39
ACO-12-44A	44a-01	0.17364	0.0034	0.20059	0.00294	4.78493	0.0977	45	2593.1	32.3	1178.5	15.77	1782.3	17.15
ACO-12-44A	44a-02	0.05691	0.00193	0.07345	0.00126	0.57563	0.01956	99	487.3	73.8	456.9	7.59	461.6	12.61
ACO-12-44A	44a-03	0.15638	0.00212	0.30852	0.00398	6.21252	0.08211	72	2416.9	22.86	1733.4	19.59	2006.2	11.56
ACO-12-44A	44a-04	-0.00378	0.00235	0.07352	0.0013	-0.03822	0.02381	-1155	0.1	0	457.3	7.8	-39.6	25.14
ACO-12-44A	44a-05	0.07557	0.00196	0.11178	0.00168	1.16102	0.03068	87	1083.8	50.88	683.1	9.77	782.4	14.41
ACO-12-44A	44a-06	0.13251	0.00241	0.135	0.00187	2.2996	0.04084	67	2131.5	31.51	816.3	10.6	1212.2	12.57
ACO-12-44A	44a-07	0.08961	0.00294	0.07521	0.00129	0.92483	0.0295	70	1417.2	61.34	467.5	7.71	664.9	15.56
ACO-12-44A	44a-08	5.75428	0.07721	0.14161	0.00207	105.0522	1.27729	18	7604.4	17.5	853.8	11.72	4735.7	12.23
ACO-12-44A	44a-09	0.46446	0.02865	0.50164	0.01666	30.10272	1.58012	63	4132.2	88.54	2620.8	71.53	3490.2	51.58
ACO-12-44A	44a-10	0.06159	0.00156	0.07163	0.00107	0.5704	0.01394	97	659.9	53.31	446	6.42	458.3	9.01
ACO-12-44A	44a-100	0.10678	0.00185	0.07166	0.00105	1.05278	0.01955	61	1745.1	31.31	446.2	6.32	730.3	9.67
ACO-12-44A	44a-11	-0.01264	0.00021	-0.25252	0.0032	0.41339	0.00711	#####	0.1	0	******	27.63	351.3	5.11
ACO-12-44A	44a-12	-0.01134	0.0017	0.08291	0.00122	-0.12188	0.01829	-389	0.1	0	513.5	7.26	-132	21.15
ACO-12-44A	44a-13	0.0568	0.00122	0.07124	0.00098	0.5254	0.0111	103	483.1	46.9	443.6	5.92	428.8	7.39
ACO-12-44A	44a-14	0.09973	0.0015	0.08311	0.0011	1.07792	0.01623	69	1619.1	27.67	514.7	6.56	742.6	7.93
ACO-12-44A	44a-15	0.07455	0.00122	0.04552	0.0006	0.44196	0.00725	77	1056.2	32.88	286.9	3.72	371.6	5.1
ACO-12-44A	44a-16	0.05031	0.00111	0.06083	0.00085	0.39923	0.00871	112	209.5	50.56	380.7	5.15	341.1	6.32

ACO-12-44A	44a-17	0.05868	0.00326	0.04962	0.00079	0.3804	0.02087	95	555.3	116.7	312.2	4.84	327.3	15.35
ACO-12-44A	44a-18	0.08178	0.00134	0.11334	0.00152	1.2127	0.01987	86	1240.2	31.68	692.1	8.81	806.4	9.12
ACO-12-44A	44a-19	0.05811	0.00095	0.22173	0.00293	1.68845	0.028	242	533.5	35.77	1291	15.46	1004.2	10.58
ACO-12-44A	44a-20	0.0535	0.00112	0.1116	0.00154	0.78362	0.01625	116	350	46.62	682	8.95	587.5	9.25
ACO-12-44A	44a-21	0.13556	0.00285	0.31012	0.00466	5.7867	0.12353	80	2171.2	36.19	1741.3	22.92	1944.4	18.48
ACO-12-44A	44a-22	0.07086	0.00148	0.10825	0.00153	1.05678	0.02243	90	953.3	42.27	662.6	8.89	732.2	11.07
ACO-12-44A	44a-23	0.0702	0.00119	0.0916	0.00119	0.88603	0.01557	88	934.1	34.4	565	7.02	644.2	8.38
ACO-12-44A	44a-24	0.05821	0.00149	0.07309	0.00107	0.5861	0.01492	97	537.2	56	454.7	6.41	468.4	9.55
ACO-12-44A	44a-25	0.05607	0.00135	0.07246	0.00105	0.55972	0.01355	100	454.7	52.41	450.9	6.33	451.3	8.82
ACO-12-44A	44a-26	0.15162	0.00272	0.39295	0.0057	8.20773	0.15518	90	2364.2	30.25	2136.5	26.39	2254.2	17.11
ACO-12-44A	44a-27	0.05745	0.00161	0.06686	0.00094	0.52927	0.0147	97	508.3	60.71	417.2	5.69	431.3	9.76
ACO-12-44A	44a-28	0.06276	0.00134	0.11114	0.00155	0.96108	0.02075	99	700.3	44.72	679.4	8.97	683.9	10.74
ACO-12-44A	44a-29	0.09167	0.00136	0.21536	0.00279	2.72075	0.04328	86	1460.4	28.11	1257.3	14.81	1334.1	11.81
ACO-12-44A	44a-30	0.06181	0.00148	0.10806	0.00152	0.92065	0.02185	100	667.4	50.43	661.4	8.83	662.7	11.55
ACO-12-44A	44a-31	0.07805	0.00183	0.06797	0.00097	0.7312	0.01691	76	1148.1	45.96	423.9	5.84	557.3	9.92
ACO-12-44A	44a-32	0.08268	0.00177	0.06178	0.00091	0.70407	0.01536	71	1261.8	41.2	386.5	5.52	541.2	9.15
ACO-12-44A	44a-33	0.0625	0.00164	0.07043	0.00099	0.60673	0.01557	91	691.4	55.09	438.8	5.95	481.5	9.84
ACO-12-44A	44a-34	0.06086	0.00137	0.07241	0.001	0.60747	0.01367	93	634.5	47.62	450.6	5.99	482	8.64
ACO-12-44A	44a-35	0.05492	0.00134	0.07178	0.00106	0.54333	0.01342	101	408.8	52.82	446.9	6.38	440.6	8.83
ACO-12-44A	44a-36	0.07359	0.00181	0.06479	0.00098	0.65714	0.01619	79	1030.3	49.04	404.7	5.96	512.9	9.92
ACO-12-44A	44a-37	0.07146	0.00171	0.0931	0.00139	0.91693	0.02202	87	970.6	48	573.8	8.22	660.7	11.67
ACO-12-44A	44a-38	0.06552	0.00212	0.09263	0.00157	0.83639	0.02663	93	790.9	66.43	571.1	9.26	617.2	14.73
ACO-12-44A	44a-39	0.65825	0.01022	0.3012	0.00455	27.32364	0.45018	37	4642.2	22.22	1697.3	22.53	3395.1	16.14
ACO-12-44A	44a-40	0.07385	0.00175	0.17334	0.00259	1.76435	0.04206	99	1037.3	47.1	1030.5	14.25	1032.4	15.45
ACO-12-44A	44a-41	0.09181	0.00232	0.07614	0.00121	0.96414	0.02419	69	1463.3	47.38	473.1	7.26	685.4	12.5
ACO-12-44A	44a-42	0.18566	0.00353	0.07804	0.00119	1.99865	0.03917	43	2704.1	31.04	484.4	7.11	1115.1	13.26
ACO-12-44A	44a-43	0.05955	0.0012	0.10645	0.00155	0.87427	0.01855	102	587.2	43.17	652.1	9.04	637.9	10.05
ACO-12-44A	44a-44	0.06575	0.00161	0.10441	0.00148	0.94624	0.02282	95	798.5	50.47	640.2	8.66	676.1	11.91
ACO-12-44A	44a-45	0.05683	0.00132	0.07122	0.00107	0.55819	0.01332	98	484.2	50.5	443.5	6.44	450.3	8.68
ACO-12-44A	44a-46	0.11925	0.00178	0.2495	0.00324	4.09819	0.06577	74	1945	26.49	1435.9	16.72	1653.9	13.1
ACO-12-44A	44a-47	6.59688	0.21019	0.09744	0.00314	88.64926	1.59946	13	7783.6	41.04	599.4	18.42	4565.1	18.12
ACO-12-44A	44a-48	0.08264	0.00146	0.24995	0.00322	2.84755	0.05125	114	1260.8	33.95	1438.2	16.62	1368.2	13.53
ACO-12-44A	44a-49	0.09916	0.00178	0.11664	0.00158	1.59387	0.02931	73	1608.4	33.13	711.2	9.15	967.8	11.47
ACO-12-44A	44a-50	0.06455	0.0011	0.0864	0.00111	0.76888	0.01353	92	759.6	35.55	534.2	6.57	579.1	7.77
ACO-12-44A	44a-51	0.08065	0.00177	0.21063	0.00314	2.34259	0.05232	102	1212.8	42.66	1232.2	16.71	1225.3	15.89
ACO-12-44A	44a-52	0.25641	0.00608	0.14216	0.00257	5.02679	0.11124	47	3224.8	36.94	856.9	14.5	1823.8	18.74

ACO-12-44A	44a-53	0.05483	0.00122	0.07375	0.00105	0.55761	0.0127	102	405.2	48.8	458.7	6.32	450	8.28
ACO-12-44A	44a-54	0.06584	0.00132	0.10464	0.00141	0.94966	0.01932	95	801.2	41.54	641.6	8.24	677.9	10.06
ACO-12-44A	44a-55	0.06551	0.00181	0.0847	0.00126	0.76492	0.02068	91	790.8	57.01	524.1	7.46	576.8	11.9
ACO-12-44A	44a-56	0.06299	0.00133	0.06736	0.00095	0.58511	0.0126	90	707.9	44.19	420.2	5.73	467.7	8.07
ACO-12-44A	44a-57	0.06004	0.00181	0.05469	0.0009	0.45286	0.01364	91	604.9	63.83	343.3	5.48	379.3	9.53
ACO-12-44A	44a-58	0.14273	0.00354	0.12042	0.00202	2.37013	0.05684	59	2260.5	42.18	733	11.64	1233.6	17.13
ACO-12-44A	44a-59	0.0726	0.00185	0.06952	0.00111	0.69593	0.01796	81	1002.9	50.65	433.2	6.71	536.4	10.76
ACO-12-44A	44a-60	0.13406	0.00259	0.20808	0.00312	3.84675	0.07578	57	2151.8	33.41	1218.6	16.65	1602.6	15.87
ACO-12-44A	44a-61	0.06193	0.00138	0.06607	0.00093	0.56451	0.01276	91	671.8	46.96	412.4	5.6	454.5	8.28
ACO-12-44A	44a-62	0.10505	0.00334	0.06675	0.00119	0.9673	0.02975	61	1715.2	57.28	416.5	7.17	687.1	15.35
ACO-12-44A	44a-63	0.0649	0.00251	0.08107	0.00146	0.72531	0.02734	91	771.1	79.34	502.5	8.69	553.8	16.09
ACO-12-44A	44a-64	0.08558	0.00179	0.06025	0.00082	0.71035	0.01483	69	1328.6	40.12	377.2	4.98	545	8.8
ACO-12-44A	44a-65	0.1183	0.00296	0.20207	0.0032	3.29443	0.08059	61	1930.7	44.1	1186.4	17.14	1479.7	19.06
ACO-12-44A	44a-66	0.25172	0.00412	0.08821	0.00123	3.06263	0.05197	38	3195.6	25.67	544.9	7.3	1423.4	12.99
ACO-12-44A	44a-67	0.08196	0.00149	0.06295	0.00084	0.71106	0.01341	72	1244.7	35.07	393.5	5.11	545.4	7.96
ACO-12-44A	44a-68	0.15004	0.00475	0.16098	0.0031	3.33152	0.09948	65	2346.4	53.13	962.2	17.19	1488.5	23.32
ACO-12-44A	44a-69	0.0852	0.00295	0.10428	0.00191	1.22639	0.04144	79	1320.1	65.8	639.5	11.18	812.7	18.9
ACO-12-44A	44a-70	0.11294	0.00255	0.17454	0.0025	2.71434	0.05956	56	1847.3	40.25	1037.1	13.7	1332.4	16.28
ACO-12-44A	44a-71	0.21481	0.95415	1.41595	2.9431	41.97012	184.8352	193	2942.2		5686.3	7853	3818.4	
ACO-12-44A	44a-72	0.09952	0.00283	0.21128	0.00334	2.88917	0.07881	77	1615.1	52.08	1235.6	17.8	1379.1	20.58
ACO-12-44A	44a-73	0.09528	0.00219	0.14841	0.00227	1.95067	0.04528	81	1533.7	42.65	892	12.73	1098.7	15.58
ACO-12-44A	44a-74	0.06264	0.00184	0.0668	0.00107	0.57693	0.01694	90	695.9	61.46	416.9	6.44	462.5	10.91
ACO-12-44A	44a-75	0.06349	0.00143	0.11398	0.00163	0.99796	0.02288	99	724.7	46.96	695.8	9.45	702.8	11.63
ACO-12-44A	44a-76	0.14349	0.00382	0.11788	0.00209	2.33292	0.06076	59	2269.8	45.16	718.3	12.03	1222.4	18.51
ACO-12-44A	44a-77	0.07429	0.0019	0.12286	0.0019	1.25895	0.03232	90	1049.5	50.73	747	10.89	827.4	14.53
ACO-12-44A	44a-78	0.12903	0.00262	0.07886	0.00121	1.40312	0.02941	55	2084.8	35.33	489.3	7.24	890.3	12.43
ACO-12-44A	44a-79	0.07148	0.00182	0.1196	0.00171	1.17691	0.02939	92	971.2	51.17	728.3	9.82	789.9	13.71
ACO-12-44A	44a-80	0.06285	0.00146	0.09091	0.00126	0.78756	0.01828	95	703.3	48.66	560.9	7.44	589.8	10.38
ACO-12-44A	44a-81	0.06856	0.00119	0.20074	0.00278	1.89591	0.03481	133	885.6	35.45	1179.3	14.92	1079.7	12.21
ACO-12-44A	44a-82	0.17749	0.00314	0.09496	0.00142	2.31805	0.04202	48	2629.5	29.12	584.8	8.37	1217.8	12.86
ACO-12-44A	44a-83	0.0961	0.00142	0.07975	0.0011	1.05405	0.01709	68	1549.7	27.45	494.6	6.55	730.9	8.45
ACO-12-44A	44a-84	0.08958	0.00183	0.07669	0.00114	0.94494	0.01966	71	1416.6	38.48	476.3	6.84	675.5	10.26
ACO-12-44A	44a-85	0.05669	0.00158	0.07998	0.0013	0.62307	0.01746	101	478.9	60.37	496	7.79	491.8	10.92
ACO-12-44A	44a-86	0.05318	0.0015	0.07425	0.00121	0.54264	0.01542	105	336.6	62.61	461.7	7.26	440.2	10.15
ACO-12-44A	44a-87	0.07187	0.00178	0.19177	0.00288	1.89785	0.04643	115	982.2	49.55	1130.9	15.6	1080.3	16.27
ACO-12-44A	44a-88	0.12285	0.00192	0.0598	0.00078	1.01078	0.01635	53	1998.1	27.52	374.4	4.75	709.3	8.26

ACO-12-44A	44a-89	0.08431	0.00153	0.0725	0.00104	0.84089	0.01599	73	1299.5	34.96	451.2	6.24	619.6	8.82
ACO-12-44A	44a-90	0.15525	0.00317	0.14272	0.00226	3.04825	0.06208	61	2404.5	34.29	860	12.74	1419.8	15.57
ACO-12-44A	44a-91	0.07194	0.00203	0.12714	0.00206	1.25632	0.03496	93	984.4	56.47	771.5	11.79	826.3	15.73
ACO-12-44A	44a-92	0.08387	0.00136	0.07419	0.00102	0.85692	0.01488	73	1289.4	31.37	461.4	6.13	628.4	8.14
ACO-12-44A	44a-93	0.0625	0.00129	0.07184	0.00106	0.61756	0.01323	92	691.3	43.27	447.3	6.35	488.3	8.3
ACO-12-44A	44a-94	0.08501	0.0013	0.11204	0.00154	1.31063	0.02196	81	1315.7	29.51	684.6	8.96	850.4	9.65
ACO-12-44A	44a-95	0.10051	0.00214	0.08376	0.00127	1.1585	0.02491	66	1633.5	39.05	518.6	7.58	781.3	11.72
ACO-12-44A	44a-96	0.06178	0.00163	0.07248	0.00113	0.61569	0.01626	93	666.5	55.45	451.1	6.77	487.1	10.22
ACO-12-44A	44a-97	0.10169	0.00175	0.07097	0.00101	0.9932	0.01806	63	1655.2	31.6	442	6.09	700.4	9.2
ACO-12-44A	44a-98	0.05915	0.00174	0.08884	0.00147	0.72321	0.02129	99	572.8	62.63	548.7	8.71	552.6	12.55
ACO-12-44A	44a-99	0.67749	0.01053	0.40688	0.0064	37.9222	0.65517	47	4683.7	22.19	2200.7	29.32	3717.9	17.09
ACO-12-44A	121	0.06128	0.00149	0.10011	0.00136	0.84553	0.01976	99	649.2	51.52	615.1	7.95	622.2	10.87
ACO-12-44A	122	0.06479	0.00091	0.06208	0.00076	0.55443	0.00823	87	767.5	29.21	388.2	4.61	447.9	5.38
ACO-12-44A	123	0.05652	0.001	0.06141	0.00082	0.4785	0.00878	97	471.9	39.04	384.2	4.99	397	6.03
ACO-12-44A	124	0.06238	0.00124	0.08829	0.00113	0.75878	0.01472	95	687	42.03	545.4	6.7	573.3	8.5
ACO-12-44A	125	0.05906	0.00103	0.06583	0.00082	0.53578	0.00935	94	569.3	37.43	411	4.97	435.6	6.18
ACO-12-44A	126	0.09653	0.00144	0.0589	0.00074	0.78382	0.01216	63	1558.2	27.79	368.9	4.48	587.7	6.92
ACO-12-44A	127	0.06305	0.00262	0.07274	0.00134	0.63231	0.0252	91	709.8	86.07	452.7	8.05	497.5	15.68
ACO-12-44A	128	0.05606	0.00116	0.06285	0.00081	0.48534	0.0099	98	454.5	45.26	392.9	4.93	401.7	6.77
ACO-12-44A	129	0.06013	0.00165	0.06466	0.00096	0.5355	0.01402	93	608.1	58.16	403.9	5.78	435.5	9.27
ACO-12-44A	130	0.06133	0.00206	0.06308	0.00104	0.53341	0.01699	91	650.7	70.59	394.4	6.3	434.1	11.25
ACO-12-44A	131	0.06659	0.00109	0.13075	0.00165	1.20026	0.02023	99	825	33.88	792.2	9.41	800.7	9.33
ACO-12-44A	132	0.05845	0.00252	0.06522	0.00124	0.52563	0.02187	95	546.6	91.68	407.3	7.5	428.9	14.56
ACO-12-44A	133	0.06537	0.00176	0.11362	0.00179	1.02393	0.02686	97	786.2	55.43	693.8	10.34	715.9	13.47
ACO-12-44A	134	0.0881	0.00136	0.21476	0.00277	2.60886	0.04195	91	1384.7	29.38	1254.2	14.71	1303.1	11.8
ACO-12-44A	135	0.05838	0.00128	0.07266	0.00102	0.58506	0.01267	97	544.1	47.11	452.2	6.16	467.7	8.11
ACO-12-44A	136	0.06441	0.00121	0.11569	0.00159	1.02705	0.01966	98	755	39.09	705.7	9.22	717.5	9.85
ACO-12-44A	137	0.08775	0.00122	0.24133	0.00298	2.91997	0.04293	101	1377	26.41	1393.6	15.46	1387.1	11.12
ACO-12-44A	138	0.05766	0.00186	0.06935	0.00116	0.55108	0.01725	97	516.5	69.62	432.2	7	445.7	11.29
ACO-12-44A	139	0.06527	0.00132	0.123	0.00178	1.10677	0.02284	99	783.2	41.87	747.8	10.19	756.6	11.01
ACO-12-44A	140	0.05582	0.00156	0.06831	0.00111	0.52564	0.01451	99	445	60.99	426	6.67	428.9	9.66
ACO-12-44A	141	0.12565	0.00225	0.29139	0.00376	5.04609	0.08939	81	2038	31.33	1648.5	18.75	1827.1	15.01
ACO-12-44A	142	0.05838	0.00164	0.06587	0.00105	0.52997	0.01463	95	544.1	60.38	411.3	6.33	431.8	9.71
ACO-12-44A	143	0.08269	0.00172	0.19921	0.0028	2.27145	0.0468	93	1261.9	40.12	1171.1	15.07	1203.5	14.53
ACO-12-44A	144	0.06043	0.00182	0.10383	0.00169	0.86502	0.02504	101	619.1	63.85	636.8	9.89	632.9	13.63
ACO-12-44A	145	0.06184	0.00215	0.06715	0.00112	0.57117	0.01884	91	668.5	72.74	419	6.79	458.8	12.18

ACO-12-44A	146	0.05901	0.00155	0.06793	0.00098	0.55262	0.01427	95	567.6	56.16	423.6	5.89	446.7	9.33
ACO-12-44A	147	0.06504	0.00093	0.12225	0.00153	1.09615	0.01669	99	775.5	29.81	743.5	8.8	751.5	8.09
ACO-12-44A	148	0.08564	0.00113	0.2216	0.00278	2.61618	0.03776	97	1329.9	25.48	1290.3	14.67	1305.2	10.6
ACO-12-44A	149	0.06077	0.00093	0.1022	0.00128	0.85629	0.01368	100	631.2	32.75	627.3	7.47	628.1	7.48
ACO-12-44A	150	0.05483	0.00127	0.04898	0.0007	0.37012	0.00855	96	405.1	50.63	308.2	4.32	319.7	6.34
ACO-12-44A	151	0.07379	0.00114	0.17906	0.00226	1.82153	0.02905	103	1035.6	30.78	1061.8	12.34	1053.2	10.45
ACO-12-44A	152	0.06051	0.00089	0.08851	0.0011	0.73842	0.01144	97	621.9	31.29	546.7	6.54	561.5	6.68
ACO-12-44A	153	0.06488	0.00167	0.06255	0.00094	0.55941	0.014	87	770.3	53.24	391.1	5.73	451.1	9.11
ACO-12-44A	154	0.07501	0.00104	0.06315	0.00078	0.65311	0.00966	77	1068.7	27.73	394.8	4.73	510.4	5.93
ACO-12-44A	155	0.0679	0.0016	0.08377	0.00124	0.78401	0.0182	88	865.5	48	518.6	7.41	587.8	10.36
ACO-12-44A	156	0.13942	0.00176	0.3333	0.00416	6.40612	0.08912	84	2220	21.71	1854.4	20.13	2033.1	12.22
ACO-12-44A	157	0.08063	0.00115	0.06091	0.00079	0.67682	0.01051	73	1212.5	27.9	381.1	4.83	524.8	6.37
ACO-12-44A	158	0.05684	0.00102	0.06195	0.00081	0.48542	0.00889	96	484.6	39.66	387.5	4.92	401.8	6.08
ACO-12-44A	159	0.06145	0.00124	0.10683	0.00139	0.90481	0.01784	100	655	42.73	654.3	8.08	654.3	9.51
ACO-12-44A	160	0.06057	0.00138	0.09863	0.00133	0.82353	0.0183	99	624.1	48.36	606.3	7.79	610	10.19
ACO-12-45	1	0.07406	0.00118	0.16419	0.00216	1.67296	0.02782	102	1043	31.82	980	11.95	998.3	10.57
ACO-12-45	2	0.06763	0.00108	0.09581	0.00116	0.89266	0.01451	110	857.3	32.78	589.8	6.85	647.8	7.78
ACO-12-45	3	0.06328	0.00115	0.09749	0.00122	0.84973	0.01556	104	717.7	38.18	599.7	7.17	624.5	8.54
ACO-12-45	4	0.071	0.00142	0.06917	0.00088	0.67651	0.0134	122	957.4	40.24	431.2	5.32	524.7	8.11
ACO-12-45	5	0.06587	0.00172	0.08342	0.00118	0.7567	0.0194	111	802.3	53.81	516.5	7.05	572.1	11.22
ACO-12-45	6	0.06174	0.00106	0.09422	0.00117	0.80123	0.01393	103	665.2	36.47	580.5	6.88	597.5	7.85
ACO-12-45	7	0.06508	0.00201	0.10143	0.00147	0.90932	0.02746	105	777	63.77	622.8	8.62	656.7	14.61
ACO-12-45	8	0.0649	0.00127	0.10029	0.00136	0.89587	0.01772	105	771	40.8	616.1	7.99	649.5	9.49
ACO-12-45	9	0.29416	0.00499	0.67094	0.00915	27.16931	0.48387	104	3439.8	26.08	3309.5	35.29	3389.6	17.44
ACO-12-45	10	0.08471	0.00213	0.106	0.00165	1.23623	0.03031	126	1308.8	48.06	649.5	9.6	817.2	13.76
ACO-12-45	11	0.07449	0.00102	0.09808	0.00117	1.00629	0.01446	117	1054.4	27.59	603.2	6.87	707	7.32
ACO-12-45	12	0.13253	0.00281	0.38546	0.00574	7.03371	0.15056	101	2131.8	36.58	2101.7	26.71	2115.7	19.03
ACO-12-45	13	0.05845	0.00135	0.09811	0.00139	0.78961	0.01819	98	546.7	49.62	603.3	8.13	590.9	10.32
ACO-12-45	14	0.0663	0.00123	0.10432	0.00141	0.95237	0.01805	106	815.8	38.16	639.7	8.25	679.3	9.39
ACO-12-45	15	0.1163	0.00189	0.33923	0.00447	5.43259	0.09276	101	1900.1	28.99	1883	21.52	1890	14.64
ACO-12-45	16	0.06029	0.00138	0.10485	0.00152	0.87047	0.0199	99	614.1	48.68	642.8	8.85	635.8	10.8
ACO-12-45	17	0.06751	0.00176	0.10713	0.00162	0.99597	0.02548	107	853.4	53.11	656	9.44	701.8	12.96
ACO-12-45	18	0.13291	0.00188	0.35063	0.00429	6.41785	0.09604	110	2136.8	24.51	1937.6	20.46	2034.7	13.15
ACO-12-45	19	0.05836	0.00179	0.09768	0.00144	0.78499	0.02376	98	543.1	65.79	600.8	8.44	588.3	13.52
ACO-12-45	20	0.07779	0.00302	0.10158	0.00186	1.08824	0.04061	120	1141.4	75.33	623.6	10.86	747.6	19.75
ACO-12-45	21	0.11233	0.00155	0.26226	0.00327	4.05933	0.06033	122	1837.4	24.82	1501.4	16.7	1646.2	12.11
ACO-12-45	22	0.06867	0.00147	0.14578	0.00202	1.37929	0.02946	100	888.9	43.56	877.3	11.39	880.1	12.57
ACO-12-45	23	0.13514	0.00185	0.39525	0.00489	7.3628	0.10706	101	2165.9	23.63	2147.1	22.59	2156.5	13
ACO-12-45	24	0.06252	0.00119	0.09858	0.00128	0.84964	0.01632	103	692.1	39.96	606.1	7.53	624.4	8.96
ACO-12-45	25	0.06064	0.00136	0.0842	0.00121	0.70375	0.01566	104	626.4	47.48	521.1	7.22	541	9.33
ACO-12-45	26	0.06293	0.00117	0.10663	0.00143	0.92468	0.01754	102	705.8	39.18	653.1	8.35	664.8	9.26

ACO-12-45	27	0.06176	0.00087	0.09302	0.00114	0.79192	0.01189	103	666	30.01	573.4	6.72	592.3	6.73
ACO-12-45	28	0.06347	0.0012	0.09852	0.00126	0.86212	0.01643	104	724.1	39.72	605.7	7.37	631.3	8.96
ACO-12-45	29	0.0656	0.00138	0.09855	0.00128	0.89125	0.01862	107	793.6	43.42	605.9	7.53	647	10
ACO-12-45	30	0.06637	0.0011	0.088	0.0011	0.80528	0.01358	110	818.1	34.16	543.7	6.52	599.8	7.64
ACO-12-45	31	0.06881	0.00148	0.09304	0.00122	0.88261	0.01865	112	892.9	43.9	573.5	7.22	642.4	10.06
ACO-12-45	32	0.07062	0.00107	0.13054	0.00157	1.27113	0.01984	105	946.5	30.85	790.9	8.97	832.9	8.87
ACO-12-45	33	0.07198	0.00185	0.09439	0.00141	0.93641	0.02343	115	985.3	51.43	581.5	8.3	671	12.29
ACO-12-45	34	0.06376	0.00141	0.09646	0.00133	0.84752	0.01858	105	733.5	46.31	593.6	7.84	623.3	10.21
ACO-12-45	35	0.06007	0.00121	0.08743	0.00113	0.72408	0.01448	102	606.1	42.88	540.3	6.7	553.1	8.53
ACO-12-45	36	0.06298	0.0024	0.09063	0.00149	0.78673	0.02912	105	707.5	79.12	559.3	8.83	589.3	16.55
ACO-12-45	37	0.05897	0.00165	0.08466	0.00122	0.68819	0.01889	101	565.9	59.96	523.9	7.24	531.7	11.36
ACO-12-45	39	0.05841	0.00151	0.09106	0.00122	0.73335	0.01851	99	545.1	55.35	561.8	7.2	558.5	10.85
ACO-12-45	40	0.06544	0.00185	0.08337	0.00115	0.75234	0.02072	110	788.5	58.36	516.2	6.87	569.6	12
ACO-12-45	41	0.11741	0.00158	0.12209	0.00157	1.97649	0.02885	149	1917.1	23.97	742.6	9	1107.5	9.84
ACO-12-45	42	0.06645	0.00091	0.10058	0.00126	0.92153	0.01374	107	820.6	28.48	617.8	7.39	663.2	7.26
ACO-12-45	43	0.06108	0.00093	0.09351	0.00123	0.78754	0.01288	102	642.1	32.47	576.3	7.25	589.8	7.31
ACO-12-45	44	0.07547	0.00152	0.0884	0.00121	0.91981	0.01831	121	1081.1	39.79	546.1	7.17	662.3	9.68
ACO-12-45	45	0.06034	0.00219	0.08712	0.00156	0.7248	0.02511	103	615.7	76.42	538.5	9.23	553.5	14.78
ACO-12-45	46	0.13038	0.00198	0.37104	0.00478	6.66955	0.10503	103	2103	26.39	2034.3	22.48	2068.6	13.9
ACO-12-45	47	0.0683	0.0017	0.09783	0.0014	0.92078	0.02231	110	877.8	50.67	601.7	8.22	662.8	11.79
ACO-12-45	48	0.06266	0.0013	0.0996	0.00141	0.86003	0.01792	103	696.8	43.67	612	8.29	630.1	9.78
ACO-12-45	49	0.06315	0.00256	0.08948	0.00171	0.77878	0.03005	106	713.4	83.78	552.5	10.09	584.8	17.15
ACO-12-45	50	0.0681	0.00374	0.1344	0.00324	1.26249	0.06553	102	871.7	109.67	812.9	18.42	829	29.41
ACO-12-45	51	0.13058	0.00191	0.37642	0.0049	6.77691	0.10633	102	2105.7	25.48	2059.5	22.95	2082.7	13.88
ACO-12-45	52	0.19692	0.00338	0.48932	0.00617	13.26975	0.22844	109	2800.9	27.83	2567.7	26.69	2699	16.25
ACO-12-45	53	0.06997	0.00132	0.13945	0.00185	1.34556	0.02566	103	927.6	38.26	841.6	10.48	865.6	11.11
ACO-12-45	54	0.07014	0.00193	0.09498	0.00152	0.91803	0.02437	113	932.5	55.28	584.9	8.97	661.3	12.9
ACO-12-45	55	0.06124	0.0013	0.09812	0.00138	0.82834	0.0175	102	647.7	44.99	603.4	8.1	612.7	9.72
ACO-12-45	56	0.06043	0.00219	0.07704	0.00133	0.64116	0.0221	105	619.2	76.26	478.4	7.94	503	13.67
ACO-12-45	57	0.06662	0.001	0.10455	0.00132	0.9605	0.01512	107	825.9	30.97	641	7.68	683.6	7.83
ACO-12-45	58	0.13244	0.00219	0.39362	0.00516	7.18821	0.12217	100	2130.6	28.71	2139.6	23.87	2135	15.15
ACO-12-45	59	0.07121	0.00141	0.15308	0.00205	1.50301	0.02963	101	963.5	40.03	918.2	11.46	931.6	12.02
ACO-12-45	60	0.06404	0.00109	0.09814	0.00124	0.86655	0.01493	105	743	35.67	603.5	7.28	633.7	8.12
ACO-12-45	38D	0.1334	0.00225	0.37973	0.0048	6.98426	0.11797	103	2143.2	29.15	2075	22.42	2109.4	15
ACO12-56B	56b-1	0.10528	0.00174	0.09227	0.00104	1.33921	0.02105	66	1719.2	30.01	568.9	6.14	862.9	9.14
ACO12-56B	56b-2	0.1187	0.00196	0.07748	0.00098	1.2677	0.021	58	1936.7	29.26	481.1	5.83	831.4	9.4
ACO12-56B	56b-3	0.05697	0.00136	0.05931	0.00086	0.46584	0.01129	96	489.9	51.89	371.4	5.25	388.3	7.82
ACO12-56B	56b-4	0.05962	0.00085	0.10133	0.00113	0.83295	0.01196	101	590	30.51	622.2	6.64	615.2	6.63
ACO12-56B	56b-5	0.05624	0.00088	0.0589	0.00065	0.45662	0.00705	97	461	34.56	369	3.96	381.9	4.91
ACO12-56B	56b-6	0.0621	0.00122	0.10755	0.00133	0.92076	0.01788	99	677.4	41.44	658.5	7.72	662.8	9.45
ACO12-56B	56b-7	0.10066	0.00153	0.07377	0.00086	1.02376	0.01544	64	1636.4	27.94	458.8	5.16	715.8	7.75
ACO12-56B	56b-8	0.14822	0.00242	0.27431	0.00314	5.60617	0.08711	67	2325.5	27.73	1562.6	15.88	1917	13.39

ACO12-56B	56b-9	0.13026	0.00162	0.39304	0.00436	7.05794	0.09023	102	2101.4	21.69	2136.9	20.18	2118.8	11.37
ACO12-56B	56b-10	0.26437	0.00429	0.05912	0.00069	2.15474	0.03268	32	3272.9	25.29	370.2	4.2	1166.6	10.52
ACO12-56B	56b-11	0.1055	0.00148	0.10655	0.00125	1.54988	0.02227	69	1723.1	25.58	652.7	7.3	950.4	8.87
ACO12-56B	56b-12	0.06477	0.00131	0.10115	0.00118	0.90336	0.01753	95	767	41.91	621.2	6.93	653.5	9.35
ACO12-56B	56b-13	0.07929	0.00138	0.09756	0.00112	1.06631	0.01802	81	1179.3	34.08	600.1	6.59	736.9	8.85
ACO12-56B	56b-14	0.25121	0.0035	0.12687	0.00149	4.39366	0.06123	45	3192.4	21.88	770	8.53	1711.1	11.53
ACO12-56B	56b-15	0.13442	0.00248	0.32756	0.00378	6.07014	0.1077	85	2156.5	31.89	1826.5	18.34	1986	15.47
ACO12-56B	56b-16	0.09152	0.00133	0.25176	0.00286	3.17623	0.04632	99	1457.3	27.41	1447.5	14.7	1451.4	11.26
ACO12-56B	56b-17	0.08627	0.00128	0.09806	0.00114	1.16625	0.01755	77	1344.1	28.4	603	6.72	784.9	8.23
ACO12-56B	56b-18	0.06041	0.00086	0.09873	0.00111	0.82218	0.01182	100	618.2	30.28	607	6.52	609.3	6.59
ACO12-56B	56b-19	0.1242	0.00169	0.20689	0.00231	3.54224	0.04892	60	2017.4	24.02	1212.2	12.36	1536.7	10.94
ACO12-56B	56b-20	0.06837	0.00112	0.08876	0.00104	0.83658	0.01371	89	879.8	33.62	548.2	6.13	617.3	7.58
ACO12-56B	56b-21	0.12724	0.0018	0.38233	0.00472	6.70631	0.0989	101	2060.3	24.7	2087.2	22.01	2073.5	13.03
ACO12-56B	56b-22	0.19208	0.00223	0.39974	0.00434	10.58411	0.12673	79	2760.1	18.9	2167.8	19.99	2487.3	11.11
ACO12-56B	56b-23	0.0619	0.001	0.097	0.00115	0.82762	0.01352	97	670.5	34.1	596.8	6.78	612.3	7.51
ACO12-56B	56b-24	0.05995	0.0009	0.10174	0.00119	0.84078	0.01288	101	601.7	32.05	624.6	6.96	619.6	7.11
ACO12-56B	56b-25	0.16054	0.00211	0.0638	0.00075	1.41177	0.01931	45	2461.4	22.01	398.7	4.54	893.9	8.13
ACO12-56B	56b-26	0.09238	0.00134	0.09377	0.00108	1.19414	0.01741	72	1475.1	27.33	577.8	6.37	797.9	8.05
ACO12-56B	56b-27	0.12586	0.00176	0.04197	0.00049	0.72818	0.0104	48	2041	24.57	265	3.05	555.5	6.11
ACO12-56B	56b-28	0.12577	0.0018	0.06402	0.00076	1.10993	0.01631	53	2039.6	25.15	400.1	4.62	758.1	7.85
ACO12-56B	56b-29	0.25974	0.00474	0.15645	0.00209	5.6022	0.09354	49	3245.1	28.48	937	11.63	1916.4	14.39
ACO12-56B	56b-30	0.12631	0.0028	0.0789	0.00107	1.37387	0.02847	56	2047.2	38.6	489.6	6.41	877.8	12.18
ACO12-56B	56b-31	0.05694	0.00112	0.05705	0.00072	0.44774	0.00881	95	488.6	43	357.6	4.37	375.7	6.18
ACO12-56B	56b-32	0.059	0.00119	0.09392	0.00115	0.76388	0.01515	100	567.1	43.27	578.7	6.8	576.2	8.72
ACO12-56B	56b-33	0.12878	0.00172	0.38139	0.00436	6.77073	0.09234	100	2081.4	23.28	2082.8	20.35	2081.9	12.07
ACO12-56B	56b-34	0.13453	0.00211	0.10092	0.00122	1.87169	0.02903	58	2158	27.17	619.8	7.12	1071.1	10.27
ACO12-56B	56b-35	0.08248	0.00151	0.08691	0.001	0.98825	0.01742	77	1257	35.22	537.3	5.92	697.8	8.9
ACO12-56B	56b-36	0.17713	0.0027	0.14466	0.00177	3.5318	0.05433	57	2626.2	25.09	871	9.97	1534.4	12.17
ACO12-56B	56b-37	0.09485	0.00144	0.06979	0.00081	0.91255	0.01388	66	1525.1	28.43	434.9	4.88	658.4	7.37
ACO12-56B	56b-38	0.07913	0.00159	0.0838	0.00102	0.9142	0.01773	79	1175.4	39.29	518.7	6.05	659.3	9.41
ACO12-56B	56b-39	0.1293	0.00182	0.04435	0.00051	0.79051	0.01127	47	2088.4	24.59	279.7	3.15	591.5	6.39
ACO12-56B	56b-40	0.05884	0.00096	0.06332	0.00073	0.51365	0.00834	94	561.2	35.05	395.8	4.43	420.9	5.6
ACO12-56B	56b-41	0.17733	0.00246	0.062	0.00073	1.51574	0.02084	41	2628.1	22.85	387.8	4.42	936.8	8.41
ACO12-56B	56b-42	0.12944	0.00232	0.35201	0.0046	6.28016	0.11126	93	2090.4	31.14	1944.2	21.95	2015.7	15.52
ACO12-56B	56b-43	0.19087	0.00546	0.1848	0.00338	4.86203	0.12613	40	2749.7	46.29	1093.1	18.41	1795.7	21.85
ACO12-56B	56b-44	0.30456	0.00397	0.06722	0.00079	2.82222	0.03674	31	3493.5	20.01	419.4	4.78	1361.5	9.76

ACO12-56B	56b-45	0.10897	0.0015	0.2172	0.00244	3.26263	0.04479	71	1782.2	24.86	1267	12.93	1472.2	10.67
ACO12-56B	56b-46	0.14844	0.00176	0.39155	0.00431	8.01223	0.0985	91	2328	20.15	2130	19.98	2232.4	11.1
ACO12-56B	56b-47	0.06365	0.00133	0.12627	0.00157	1.10788	0.02261	101	729.9	43.63	766.6	8.99	757.2	10.89
ACO12-56B	56b-48	0.13513	0.00193	0.25411	0.00288	4.73358	0.06688	67	2165.7	24.71	1459.6	14.79	1773.2	11.84
ACO12-56B	56b-49	0.12065	0.00205	0.35728	0.0044	5.94256	0.09853	100	1965.9	29.96	1969.3	20.89	1967.5	14.41
ACO12-56B	56b-50	0.06057	0.00092	0.10517	0.00122	0.87807	0.01352	101	623.9	32.27	644.6	7.14	639.9	7.31
ACO12-56B	56b-51	0.0549	0.00126	0.05392	0.00066	0.40806	0.00905	97	408	50.26	338.6	4.02	347.5	6.52
ACO12-56B	56b-52	0.06196	0.00079	0.10192	0.00117	0.87059	0.01177	98	672.8	27.14	625.6	6.86	635.9	6.39
ACO12-56B	56b-53	0.20155	0.00249	0.33333	0.00399	9.26111	0.12521	65	2838.8	19.98	1854.5	19.29	2364.2	12.39
ACO12-56B	56b-54	0.07461	0.00152	0.09009	0.0011	0.92655	0.01826	84	1057.8	40.75	556	6.53	665.8	9.63
ACO12-56B	56b-55	0.07635	0.00176	0.19197	0.0026	2.02049	0.04545	103	1104.2	45.48	1132	14.04	1122.4	15.28
ACO12-56B	56b-56	0.07511	0.00148	0.06313	0.00076	0.65368	0.01248	77	1071.5	39.1	394.7	4.61	510.7	7.66
ACO12-56B	56b-57	0.16351	0.00218	0.45657	0.00536	10.29139	0.14246	97	2492.2	22.24	2424.4	23.72	2461.3	12.81
ACO12-56B	56b-58	0.10946	0.00192	0.05928	0.00076	0.89461	0.01558	57	1790.5	31.62	371.2	4.59	648.8	8.35
ACO12-56B	56b-59	0.06189	0.00121	0.10512	0.00128	0.89686	0.01726	99	670.1	41.19	644.3	7.49	650	9.24
ACO12-56B	56b-60	0.05999	0.00091	0.10469	0.00123	0.86591	0.01346	101	603.4	32.47	641.8	7.18	633.3	7.33
ACO12-56B	56b-61	0.10004	0.00144	0.08062	0.00089	1.11171	0.01577	66	1624.9	26.48	499.8	5.32	759	7.58
ACO12-56B	56b-62	0.08331	0.00225	0.09135	0.00142	1.05101	0.02765	77	1276.2	51.97	563.5	8.38	729.4	13.69
ACO12-56B	56b-63	0.26194	0.00324	0.10362	0.00118	3.74148	0.04755	40	3258.4	19.36	635.6	6.88	1580.3	10.18
ACO12-56B	56b-64	0.09041	0.00199	0.08038	0.00115	1.00348	0.02187	71	1434.1	41.42	498.4	6.85	705.6	11.08
ACO12-56B	56b-65	0.129	0.00159	0.38372	0.00441	6.82615	0.08871	100	2084.4	21.48	2093.6	20.55	2089.1	11.51
ACO12-56B	56b-66	0.14752	0.0021	0.19077	0.00239	3.88601	0.05859	49	2317.4	24.2	1125.6	12.92	1610.8	12.18
ACO12-56B	56b-67	0.06731	0.00103	0.07922	0.00093	0.73525	0.01138	88	847.5	31.41	491.5	5.57	559.6	6.66
ACO12-56B	56b-68	0.06	0.00161	0.06419	0.00084	0.53085	0.01368	93	603.7	57.14	401.1	5.12	432.4	9.08
ACO12-56B	56b-69	0.20104	0.00343	0.44973	0.00607	12.51744	0.22027	84	2834.7	27.58	2394	26.98	2644	16.55
ACO12-56B	56b-70	0.21462	0.00275	0.14076	0.00159	4.16652	0.05489	51	2940.8	20.54	849	9.01	1667.5	10.79
ACO-12-37	1	0.06356	0.00111	0.10002	0.00131	0.87635	0.01606	96	726.9	36.64	614.5	7.66	639	8.69
ACO-12-37	2	0.0738	0.00171	0.16753	0.00237	1.70488	0.03957	99	1036.1	46.11	998.5	13.1	1010.4	14.85
ACO-12-37	3	0.07741	0.00145	0.16997	0.00227	1.8144	0.03493	89	1131.9	36.94	1011.9	12.52	1050.7	12.6
ACO-12-37	4	0.0625	0.00132	0.10096	0.00136	0.86993	0.01862	98	691.1	44.28	620	7.95	635.5	10.11
ACO-12-37	5	0.06137	0.00093	0.10024	0.00127	0.84809	0.0138	99	652.3	32.1	615.8	7.46	623.6	7.58
ACO-12-37	6	0.05979	0.00273	0.06956	0.00131	0.57328	0.02544	94	596.1	95.99	433.5	7.88	460.1	16.42
ACO-12-37	7	0.12539	0.00197	0.3722	0.00494	6.43377	0.10777	100	2034.3	27.58	2039.7	23.22	2036.9	14.72
ACO-12-37	8	0.06985	0.00103	0.16245	0.0021	1.56411	0.02522	101	923.8	30.01	970.4	11.62	956.1	9.99
ACO-12-37	9	0.08162	0.00141	0.20233	0.00269	2.27649	0.04135	96	1236.3	33.57	1187.8	14.43	1205	12.81
ACO-12-37	10	0.06651	0.00125	0.11922	0.00158	1.09314	0.02124	97	822.5	38.86	726.1	9.12	750	10.3
ACO-12-37	11	0.08275	0.00128	0.21194	0.00272	2.41801	0.04005	98	1263.4	29.92	1239.1	14.46	1248	11.9
ACO-12-37	12	0.06142	0.00154	0.10112	0.00139	0.85636	0.0213	99	654	52.95	620.9	8.13	628.1	11.65

ACO-12-37	13	0.06526	0.00168	0.11306	0.00161	1.01718	0.02598	97	782.7	53.1	690.5	9.34	712.5	13.08
ACO-12-37	14	0.06337	0.00189	0.09982	0.00149	0.87211	0.0255	96	720.5	62.2	613.3	8.72	636.7	13.83
ACO-12-37	15	0.07828	0.00178	0.19323	0.00277	2.08477	0.04799	99	1154.1	44.55	1138.8	14.98	1143.8	15.8
ACO-12-37	16	0.06347	0.00159	0.10296	0.00148	0.90113	0.02268	97	724	52.16	631.7	8.64	652.3	12.11
ACO-12-37	17	0.07339	0.00155	0.16868	0.00243	1.70701	0.0371	98	1024.8	42.04	1004.8	13.41	1011.2	13.92
ACO-12-37	18	0.06681	0.00132	0.12916	0.00178	1.19006	0.02437	98	831.8	40.77	783.1	10.15	796	11.3
ACO-12-37	19	0.08012	0.00207	0.17555	0.00277	1.93896	0.05033	87	1200	50.05	1042.6	15.17	1094.6	17.39
ACO-12-37	20	0.06328	0.00171	0.08929	0.00137	0.77919	0.0211	94	717.7	56.35	551.3	8.09	585	12.04
ACO-12-37	21	0.06084	0.00093	0.09961	0.00128	0.83569	0.01382	99	633.6	32.65	612.1	7.52	616.8	7.64
ACO-12-37	22	0.08566	0.00122	0.20988	0.00268	2.47892	0.03878	92	1330.5	27.38	1228.2	14.28	1265.9	11.32
ACO-12-37	23	0.0633	0.00218	0.10765	0.00181	0.93979	0.03198	98	718.2	71.58	659.1	10.53	672.8	16.74
ACO-12-37	24	0.06206	0.00146	0.09073	0.00134	0.77648	0.0187	96	676	49.66	559.9	7.91	583.5	10.69
ACO-12-37	25	0.06437	0.00152	0.06909	0.00097	0.61325	0.0146	89	753.8	48.99	430.7	5.85	485.6	9.19
ACO-12-37	26	0.07536	0.00145	0.17105	0.00233	1.77746	0.03533	94	1078.1	38.02	1017.9	12.82	1037.3	12.92
ACO-12-37	27	0.06826	0.00153	0.13852	0.00205	1.30395	0.03021	99	876.4	45.85	836.3	11.6	847.5	13.31
ACO-12-37	28	0.06205	0.00172	0.09396	0.00147	0.804	0.02239	97	676	58.14	578.9	8.64	599.1	12.6
ACO-12-37	29	0.12819	0.00229	0.36249	0.00479	6.40627	0.12032	96	2073.4	31.13	1994	22.66	2033.1	16.5
ACO-12-37	30	0.06391	0.00188	0.12194	0.00196	1.07449	0.03166	100	738.6	60.9	741.7	11.26	740.9	15.5
ACO-12-37	31	0.16172	0.00217	0.26572	0.00346	5.92453	0.08823	61	2473.8	22.44	1519	17.62	1964.8	12.94
ACO-12-37	32	0.06573	0.00219	0.09025	0.00144	0.81776	0.02681	92	797.7	68.18	557	8.5	606.8	14.97
ACO-12-37	33	0.06195	0.00111	0.09442	0.00129	0.80637	0.01523	97	672.5	37.85	581.6	7.58	600.4	8.56
ACO-12-37	34	0.13775	0.00216	0.40759	0.00556	7.73975	0.13259	100	2199.1	26.98	2203.9	25.47	2201.2	15.4
ACO-12-37	35	0.05519	0.00135	0.06195	0.00087	0.47132	0.01167	99	419.7	53.16	387.4	5.29	392.1	8.06
ACO-12-37	36	0.06341	0.00143	0.09159	0.00132	0.80069	0.01844	95	722.1	47.24	564.9	7.82	597.2	10.4
ACO-12-37	37	0.06751	0.00163	0.09014	0.00131	0.83881	0.02037	90	853.4	49.24	556.3	7.77	618.5	11.25
ACO-12-37	38	0.06892	0.00155	0.1039	0.00153	0.98718	0.02268	91	896.4	45.82	637.2	8.91	697.3	11.59
ACO-12-37	39	0.10736	0.00235	0.31256	0.00468	4.62584	0.10404	100	1755	39.54	1753.3	22.98	1753.9	18.78
ACO-12-37	40	0.06063	0.0012	0.09655	0.00134	0.80706	0.01659	99	626.2	42.13	594.2	7.86	600.8	9.32
ACO-12-37	41	0.11214	0.00217	0.32048	0.00454	4.95477	0.10048	98	1834.4	34.71	1792.1	22.14	1811.6	17.13
ACO-12-37	42	0.1158	0.00235	0.34294	0.00486	5.47461	0.11507	100	1892.4	36.07	1900.8	23.33	1896.6	18.05
ACO-12-37	43	0.07056	0.00182	0.16252	0.0025	1.58098	0.04098	101	944.6	52.05	970.8	13.84	962.8	16.12
ACO-12-37	44	0.05637	0.00124	0.07069	0.00099	0.54934	0.01237	99	466.2	48.34	440.3	5.95	444.6	8.1
ACO-12-37	45	0.07358	0.00133	0.17932	0.00243	1.81907	0.03447	103	1029.9	36.11	1063.3	13.27	1052.3	12.42
ACO-12-37	46	0.06197	0.00116	0.11616	0.0016	0.99224	0.01958	101	673.2	39.7	708.4	9.25	699.9	9.98
ACO-12-37	47	0.06095	0.00131	0.08814	0.00125	0.74067	0.01634	97	637.6	45.53	544.5	7.4	562.8	9.53
ACO-12-37	48	0.10822	0.0014	0.25192	0.00328	3.75844	0.05568	82	1769.5	23.48	1448.3	16.91	1583.9	11.88
ACO-12-37	49	0.0692	0.00101	0.15596	0.00205	1.48789	0.02397	101	904.7	29.85	934.3	11.44	925.5	9.78
ACO-12-37	50	0.07371	0.00189	0.16484	0.00255	1.67504	0.04314	98	1033.4	50.95	983.6	14.1	999.1	16.37
ACO-12-37	51	0.06308	0.00147	0.10731	0.00157	0.93335	0.02218	98	711	48.83	657.1	9.14	669.4	11.65
ACO-12-37	52	0.06392	0.00122	0.10554	0.00151	0.92939	0.01866	97	739.1	39.78	646.8	8.81	667.3	9.82
ACO-12-37	53	0.06218	0.00107	0.11723	0.00158	1.00492	0.01846	101	680.3	36.47	714.6	9.1	706.3	9.35
ACO-12-37	54	0.0623	0.00181	0.08495	0.00128	0.72963	0.02087	94	684.3	60.9	525.6	7.63	556.3	12.25
ACO-12-37	55	0.07841	0.00169	0.20438	0.00303	2.20789	0.04913	104	1157.3	42.19	1198.8	16.21	1183.5	15.55
ACO-12-37	56	0.08124	0.00145	0.2193	0.00305	2.45625	0.04637	104	1227.3	34.58	1278.2	16.14	1259.3	13.62
ACO-12-37	57	0.06462	0.00165	0.1263	0.00188	1.12459	0.02878	100	762.1	52.94	766.7	10.77	765.2	13.76
ACO-12-37	58	0.17724	0.00272	0.51281	0.00685	12.53012	0.20999	102	2627.2	25.33	2668.6	29.2	2645	15.76

ACO-12-37	59	0.10095	0.00206	0.07839	0.00111	1.09092	0.02286	65	1641.6	37.46	486.5	6.66	749	11.1
ACO-12-37	60	0.07517	0.00161	0.18018	0.00262	1.86716	0.04119	100	1073.1	42.5	1068	14.3	1069.5	14.59
ACO-12-37	61	0.056	0.00093	0.07136	0.00098	0.55085	0.00986	100	451.8	36.06	444.4	5.89	445.6	6.46
ACO-12-37	62	0.08005	0.00129	0.20451	0.00275	2.2569	0.03901	100	1198.2	31.35	1199.5	14.74	1198.9	12.16
ACO-12-37	63	0.14239	0.00368	0.09433	0.00153	1.85155	0.04637	55	2256.4	43.96	581.1	9.02	1064	16.51
ACO-12-37	64	0.06102	0.00144	0.08286	0.00123	0.69672	0.01665	96	640.1	49.78	513.2	7.35	536.8	9.96
ACO-12-37	65	0.07467	0.00169	0.17208	0.00258	1.77092	0.04091	97	1059.6	45.01	1023.5	14.16	1034.9	14.99
ACO-12-37	66	0.07361	0.00172	0.15739	0.00239	1.59549	0.03791	97	1030.9	46.43	942.3	13.33	968.4	14.83
ACO-12-37	67	0.06185	0.00206	0.0902	0.00147	0.76905	0.0253	96	668.8	69.76	556.7	8.71	579.2	14.52
ACO-12-37	68	0.07379	0.00142	0.17821	0.0025	1.8127	0.03633	102	1035.6	38.46	1057.2	13.68	1050.1	13.12
ACO-12-37	69	0.07441	0.0019	0.17475	0.00271	1.79248	0.04586	99	1052.7	50.59	1038.2	14.86	1042.7	16.67
ACO-12-37	70	0.06123	0.00252	0.07292	0.00133	0.61507	0.02447	93	647.4	85.88	453.7	7.97	486.8	15.39
ACO-12-37	71	0.08863	0.00219	0.24315	0.0038	2.9701	0.07381	101	1396.1	46.55	1403.1	19.71	1400	18.88
ACO-12-37	72	0.0601	0.00124	0.09458	0.00135	0.78349	0.01667	99	607	43.99	582.6	7.94	587.5	9.49
ACO-12-37	73	0.08709	0.00161	0.23434	0.00328	2.81238	0.05461	100	1362.5	35.15	1357.2	17.12	1358.8	14.54
ACO-12-37	74	0.11626	0.00261	0.33674	0.00503	5.39596	0.1241	98	1899.5	39.85	1870.9	24.28	1884.2	19.7
ACO-12-37	75	0.06029	0.00179	0.09573	0.00148	0.79558	0.02343	99	614	62.8	589.3	8.69	594.3	13.25
ACO-12-37	76	0.08392	0.00161	0.17492	0.00242	2.02364	0.04018	81	1290.6	36.86	1039.2	13.28	1123.5	13.49
ACO-12-37	77	0.07553	0.00209	0.16005	0.00248	1.66636	0.04579	96	1082.6	54.53	957.1	13.8	995.8	17.44
ACO-12-37	78	0.11758	0.00314	0.345	0.00549	5.59106	0.14949	100	1919.8	47.17	1910.7	26.32	1914.7	23.03
ACO-12-37	79	0.05947	0.00153	0.08912	0.00132	0.73052	0.01878	99	584.4	54.84	550.3	7.83	556.9	11.02
ACO-12-37	80	0.11967	0.00299	0.3405	0.00517	5.61781	0.1415	97	1951.3	44.02	1889.1	24.85	1918.8	21.71
ACO-12-43	12-43-01	0.06071	0.00093	0.09963	0.00121	0.83394	0.01319	99	628.9	32.57	612.3	7.11	615.8	7.3
ACO-12-43	12-43-02	0.08525	0.00202	0.079	0.00117	0.92858	0.02183	73	1321.3	45.39	490.1	7.01	666.9	11.49
ACO-12-43	12-43-03	0.05819	0.00233	0.05973	0.00111	0.47835	0.01866	94	536.2	85.99	374	6.73	396.9	12.81
ACO-12-43	12-43-04	0.05366	0.00091	0.05769	0.00071	0.42683	0.00739	100	356.8	37.9	361.6	4.34	360.9	5.26
ACO-12-43	12-43-05	0.12584	0.00176	0.36263	0.00454	6.29187	0.09482	98	2040.7	24.58	1994.6	21.47	2017.3	13.2
ACO-12-43	12-43-06	0.0549	0.00084	0.05719	0.00069	0.43293	0.00686	98	408.3	33.62	358.5	4.22	365.3	4.86
ACO-12-43	12-43-07	0.05567	0.00083	0.05838	0.00073	0.44811	0.00706	97	438.8	32.39	365.8	4.42	376	4.95
ACO-12-43	12-43-08	0.05421	0.00096	0.0589	0.00073	0.44025	0.00791	100	379.6	39.31	369	4.46	370.4	5.58
ACO-12-43	12-43-09	0.05347	0.00089	0.05753	0.0007	0.42406	0.00715	100	348.5	37	360.6	4.25	359	5.1
ACO-12-43	12-43-10	0.0623	0.00154	0.09756	0.00136	0.83799	0.02036	97	684.4	51.96	600.1	7.97	618	11.25
ACO-12-43	12-43-11	0.06255	0.00087	0.09761	0.00117	0.84175	0.01233	97	692.9	29.38	600.4	6.86	620.1	6.8
ACO-12-43	12-43-12	0.05639	0.00122	0.05713	0.00074	0.44409	0.00954	96	466.8	47.79	358.1	4.53	373.1	6.71
ACO-12-43	12-43-13	0.06104	0.00115	0.09353	0.00119	0.78709	0.01492	98	640.7	39.94	576.4	7.03	589.5	8.48
ACO-12-43	12-43-14	0.05845	0.00109	0.08485	0.00106	0.68378	0.01279	99	546.7	40.25	525	6.3	529.1	7.71
ACO-12-43	12-43-15	0.08209	0.00147	0.08166	0.00104	0.92424	0.01664	76	1247.7	34.45	506	6.21	664.6	8.78
ACO-12-43	12-43-16	0.05965	0.00106	0.09624	0.00121	0.79138	0.01425	100	590.8	37.99	592.3	7.1	592	8.08
ACO-12-43	12-43-17	0.06135	0.00104	0.09924	0.00123	0.83931	0.01451	99	651.4	35.93	609.9	7.23	618.8	8.01
ACO-12-43	12-43-18	0.05907	0.0012	0.08503	0.00109	0.69254	0.014	98	569.8	43.65	526.1	6.47	534.3	8.4
ACO-12-43	12-43-19	0.07355	0.00141	0.17048	0.00217	1.72867	0.03305	99	1029	38.37	1014.8	11.94	1019.3	12.3
ACO-12-43	12-43-20	0.05584	0.00105	0.05821	0.00074	0.44815	0.00849	97	445.8	40.9	364.7	4.49	376	5.95
ACO-12-43	12-43-21	0.13079	0.00183	0.34664	0.00433	6.25032	0.09328	91	2108.6	24.4	1918.5	20.74	2011.5	13.06
ACO-12-43	12-43-22	0.05429	0.00097	0.06207	0.00078	0.46454	0.00844	100	382.9	39.43	388.2	4.75	387.4	5.85
ACO-12-43	12-43-23	0.06109	0.00095	0.09686	0.00118	0.81573	0.01313	98	642.2	33.19	596	6.94	605.7	7.34

ACO-12-43	12-43-24	0.06052	0.00094	0.09583	0.00117	0.79957	0.01286	99	622.1	33.27	589.9	6.86	596.6	7.25
ACO-12-43	12-43-25	0.05928	0.00124	0.09521	0.00124	0.77816	0.01627	100	577.3	44.96	586.3	7.33	584.4	9.29
ACO-12-43	12-43-26	0.05491	0.00168	0.05836	0.00089	0.44182	0.01323	98	408.5	66.35	365.7	5.41	371.5	9.32
ACO-12-43	12-43-27	0.05423	0.00096	0.0576	0.0007	0.43066	0.00768	99	380.4	39.36	361	4.27	363.6	5.45
ACO-12-43	12-43-28	0.06122	0.00117	0.09653	0.00123	0.8148	0.01563	98	647.1	40.51	594	7.24	605.1	8.74
ACO-12-43	12-43-29	0.06229	0.00182	0.10072	0.00153	0.86497	0.02469	98	684.1	61.12	618.6	8.98	632.8	13.44
ACO-12-43	12-43-30	0.05617	0.00158	0.05777	0.00085	0.44735	0.01235	96	458.8	61.19	362.1	5.21	375.4	8.66
ACO-12-43	12-43-31	0.05871	0.00145	0.09878	0.00136	0.79963	0.0194	102	556.4	52.91	607.3	7.96	596.6	10.94
ACO-12-43	12-43-32	0.06138	0.0009	0.10406	0.00125	0.88065	0.01339	100	652.7	31.06	638.2	7.29	641.3	7.23
ACO-12-43	12-43-33	0.07861	0.00134	0.19416	0.00246	2.10419	0.03658	98	1162.2	33.39	1143.9	13.29	1150.2	11.96
ACO-12-43	12-43-34	0.05949	0.00106	0.09374	0.00116	0.76892	0.01377	100	585.2	38.09	577.6	6.83	579.1	7.91
ACO-12-43	12-43-35	0.06058	0.00108	0.10363	0.00128	0.86552	0.01556	100	624.2	38.02	635.7	7.5	633.1	8.47
ACO-12-43	12-43-36	0.07502	0.00129	0.05494	0.0007	0.5682	0.00999	75	1069	34.27	344.8	4.25	456.9	6.47
ACO-12-43	12-43-37	0.12842	0.00189	0.3712	0.00443	6.57216	0.09973	98	2076.4	25.66	2035.1	20.82	2055.6	13.37
ACO-12-43	12-43-38	0.06562	0.00118	0.12738	0.00162	1.15238	0.02112	99	794.3	37.4	772.9	9.29	778.4	9.96
ACO-12-43	12-43-39	0.05498	0.0012	0.0598	0.00078	0.45334	0.00979	99	411.4	47.21	374.4	4.76	379.6	6.84
ACO-12-43	12-43-40	0.05484	0.00111	0.0608	0.00077	0.45975	0.00928	99	405.9	44.43	380.5	4.69	384.1	6.46
ACO-12-43	12-43-41	0.08206	0.00158	0.06064	0.00078	0.68609	0.01306	72	1247	37	379.5	4.75	530.5	7.86
ACO-12-43	12-43-42	0.06001	0.00188	0.09659	0.00148	0.79915	0.02435	100	604	66.38	594.4	8.69	596.3	13.74
ACO-12-43	12-43-43	0.05647	0.00298	0.06842	0.00144	0.53264	0.02706	98	470	113.6	426.7	8.68	433.6	17.93
ACO-12-43	12-43-44	0.06024	0.00104	0.09986	0.00124	0.82933	0.01454	100	612.1	36.88	613.6	7.24	613.2	8.07
ACO-12-43	12-43-45	0.06111	0.00121	0.09999	0.00127	0.84249	0.01665	99	643.1	42.05	614.4	7.45	620.5	9.18
ACO-12-43	12-43-46	0.05457	0.00101	0.05915	0.00073	0.44498	0.00824	99	394.6	40.6	370.4	4.43	373.8	5.79
ACO-12-43	12-43-47	0.05405	0.00103	0.06021	0.00075	0.44867	0.00859	100	372.8	42.5	376.9	4.55	376.3	6.02
ACO-12-43	12-43-48	0.05656	0.00109	0.06251	0.0008	0.48744	0.00947	97	473.8	42.43	390.9	4.88	403.2	6.47
ACO-12-43	12-43-49	0.05361	0.00133	0.05967	0.00081	0.44107	0.01076	101	354.7	55.01	373.6	4.92	371	7.58
ACO-12-43	12-43-50	0.05569	0.00092	0.06249	0.00076	0.47975	0.00808	98	439.6	36.01	390.7	4.58	397.9	5.54
ACO-12-43	12-43-51	0.06279	0.00121	0.11231	0.00145	0.97217	0.01884	99	701.1	40.45	686.1	8.41	689.6	9.7
ACO-12-43	12-43-52	0.05417	0.001	0.06028	0.00075	0.45012	0.00836	100	377.8	40.87	377.3	4.58	377.4	5.85
ACO-12-43	12-43-53	0.0582	0.00132	0.09223	0.00122	0.74003	0.01658	101	536.7	49.5	568.7	7.2	562.4	9.67
ACO-12-43	12-43-54	0.05965	0.00145	0.1031	0.0014	0.84793	0.02028	101	591	51.94	632.5	8.21	623.5	11.14
ACO-12-43	12-43-55	0.17857	0.00357	0.07575	0.00104	1.86485	0.03619	44	2639.6	32.79	470.7	6.26	1068.7	12.83
ACO-12-43	12-43-56	0.06373	0.00115	0.10465	0.00133	0.91947	0.01684	97	732.7	37.76	641.6	7.78	662.1	8.91
ACO-12-43	12-43-57	0.15729	0.00218	0.44769	0.00533	9.70816	0.13987	98	2426.7	23.28	2385	23.72	2407.5	13.26
ACO-12-43	12-43-58	0.05459	0.0011	0.05863	0.00074	0.44128	0.00882	99	395.5	44.09	367.3	4.51	371.2	6.21
ACO-12-43	12-43-59	0.06191	0.00119	0.09431	0.00119	0.80497	0.01541	97	671	40.5	581	7.02	599.6	8.67
ACO-12-43	12-43-60	0.0946	0.0016	0.26138	0.00332	3.40898	0.05885	98	1520.1	31.6	1496.9	16.94	1506.5	13.55
ACO-12-43	12-43-61	0.06068	0.00105	0.09808	0.00121	0.82061	0.01441	99	628.1	36.97	603.1	7.1	608.4	8.04
ACO-12-43	12-43-62	0.0544	0.00098	0.05807	0.00071	0.43554	0.00789	99	387.8	39.8	363.9	4.32	367.1	5.58
ACO-12-43	12-43-63	0.13082	0.00246	0.36216	0.00492	6.53253	0.12479	94	2109.1	32.61	1992.4	23.27	2050.3	16.82
ACO-12-43	12-43-64	0.05742	0.00108	0.06683	0.00084	0.52904	0.00995	97	507.1	41.11	417	5.05	431.2	6.61
ACO-12-43	12-43-65	0.05632	0.00088	0.05854	0.0007	0.45455	0.00727	96	464.1	34.38	366.8	4.29	380.5	5.08
ACO-12-43	12-43-66	0.26717	0.00358	0.5472	0.0064	20.15569	0.28216	86	3289.5	20.9	2813.5	26.66	3098.9	13.54
ACO-12-43	12-43-67	0.12447	0.00189	0.34681	0.00421	5.95122	0.09208	95	2021.2	26.71	1919.3	20.16	1968.7	13.45
ACO-12-43	12-43-68	0.08048	0.00127	0.2051	0.00248	2.27556	0.03656	99	1208.7	30.81	1202.6	13.26	1204.7	11.33
ACO-12-43	12-43-69	0.05451	0.00132	0.05709	0.00076	0.42904	0.01021	99	392.1	53.19	357.9	4.63	362.5	7.25

ACO-12-43	12-43-70	0.0604	0.00109	0.09628	0.0012	0.8018	0.01461	99	618	38.55	592.6	7.06	597.8	8.23
ACO-12-43	12-43-71	0.05694	0.0009	0.05923	0.00071	0.46497	0.00751	96	488.5	34.81	371	4.34	387.7	5.21
ACO-12-43	12-43-72	0.06337	0.00102	0.08747	0.00106	0.76423	0.0126	94	720.7	33.95	540.6	6.29	576.4	7.25
ACO-12-43	12-43-73	0.06177	0.00118	0.08476	0.00108	0.72185	0.01384	95	666.1	40.4	524.5	6.4	551.8	8.16
ACO-12-43	12-43-74	0.06392	0.00164	0.10413	0.00149	0.9177	0.02313	97	739	53.33	638.6	8.7	661.1	12.25
ACO-12-43	12-43-75	0.06254	0.00098	0.10069	0.00122	0.86819	0.01401	97	692.6	33.21	618.5	7.13	634.6	7.62
ACO-12-43	12-43-76	0.05421	0.00082	0.05735	0.00069	0.42857	0.00667	99	379.5	33.67	359.5	4.18	362.2	4.74
ACO-12-43	12-43-77	0.0621	0.00117	0.10227	0.00129	0.87555	0.0165	98	677.5	39.63	627.7	7.55	638.6	8.93
ACO-12-43	12-43-78	0.12927	0.0019	0.35477	0.00426	6.32283	0.09618	94	2088.1	25.64	1957.3	20.25	2021.6	13.34
ACO-12-43	12-43-79	0.07399	0.00124	0.15253	0.00189	1.55608	0.0266	96	1041.3	33.37	915.1	10.59	952.9	10.57
ACO-12-43	12-43-80	0.05695	0.00101	0.06305	0.00077	0.495	0.00885	97	488.8	39.09	394.2	4.68	408.3	6.01
ACO-12-42B	12-42b-01	0.08087	0.00143	0.1964	0.0024	2.18986	0.03824	95	1218.3	34.4	1155.9	12.91	1177.8	12.17
ACO-12-42B	12-42b-02	0.06111	0.00137	0.09675	0.00129	0.81515	0.018	98	642.9	47.33	595.3	7.57	605.3	10.07
ACO-12-42B	12-42b-03	0.06158	0.00091	0.10036	0.00117	0.85211	0.01283	99	659.4	31.23	616.5	6.87	625.8	7.03
ACO-12-42B	12-42b-04	0.05805	0.00084	0.06268	0.00072	0.50168	0.00741	95	531.3	31.96	391.9	4.36	412.8	5.01
ACO-12-42B	12-42b-05	0.13108	0.00191	0.37693	0.00463	6.81261	0.10261	98	2112.5	25.37	2061.9	21.7	2087.4	13.34
ACO-12-42B	12-42b-06	0.06309	0.00094	0.09962	0.00115	0.86659	0.01303	97	711.2	31.23	612.2	6.75	633.7	7.09
ACO-12-42B	12-42b-07	0.06212	0.00115	0.08484	0.00105	0.72672	0.01341	95	678.4	39.1	525	6.22	554.6	7.88
ACO-12-42B	12-42b-08	0.08538	0.00117	0.2151	0.00244	2.53202	0.03535	95	1324	26.49	1256	12.93	1281.3	10.16
ACO-12-42B	12-42b-09	0.07314	0.00172	0.08535	0.00114	0.86073	0.01961	84	1018	46.83	528	6.8	630.5	10.7
ACO-12-42B	12-42b-10	0.15427	0.00228	0.05792	0.00066	1.23199	0.01805	45	2393.8	24.95	363	4.05	815.2	8.21
ACO-12-42B	12-42b-11	0.05443	0.00084	0.05723	0.00067	0.42945	0.00669	99	388.8	33.99	358.7	4.08	362.8	4.75
ACO-12-42B	12-42b-12	0.22632	0.00394	0.06083	0.00073	1.89808	0.03185	35	3026.2	27.66	380.7	4.44	1080.4	11.16
ACO-12-42B	12-42b-13	0.06095	0.00107	0.09525	0.00115	0.80038	0.01399	98	637.4	37.26	586.5	6.75	597	7.89
ACO-12-42B	12-42b-14	0.1283	0.0019	0.35757	0.00428	6.32508	0.09533	95	2074.9	25.82	1970.7	20.32	2021.9	13.21
ACO-12-42B	12-42b-15	0.12186	0.00162	0.29922	0.00342	5.02717	0.06871	85	1983.6	23.43	1687.4	16.99	1823.9	11.58
ACO-12-42B	12-42b-16	0.13722	0.00188	0.0985	0.00113	1.8636	0.0261	57	2192.4	23.59	605.6	6.66	1068.3	9.25
ACO-12-42B	12-42b-17	0.14425	0.00227	0.24665	0.00283	4.90587	0.07653	62	2278.9	26.89	1421.2	14.64	1803.3	13.16
ACO-12-42B	12-42b-18	0.06115	0.00103	0.09803	0.00117	0.82649	0.01397	99	644.6	35.9	602.9	6.88	611.7	7.76
ACO-12-42B	12-42b-19	0.06142	0.00127	0.08302	0.00106	0.70303	0.01433	95	654	43.86	514.1	6.29	540.6	8.55
ACO-12-42B	12-42b-20	0.06227	0.00133	0.09685	0.00128	0.83155	0.01757	97	683.5	45.06	595.9	7.5	614.5	9.74
ACO-12-42B	12-42b-21	0.08785	0.00188	0.06267	0.00081	0.75905	0.01563	68	1379.2	40.61	391.9	4.9	573.5	9.02
ACO-12-42B	12-42b-22	0.06196	0.00119	0.09482	0.00115	0.80997	0.01529	97	672.9	40.56	584	6.77	602.4	8.58
ACO-12-42B	12-42b-23	0.12268	0.00209	0.34699	0.00447	5.86803	0.10183	96	1995.6	29.95	1920.2	21.4	1956.5	15.05
ACO-12-42B	12-42b-24	0.06955	0.00119	0.09214	0.00107	0.88337	0.0148	88	915.1	34.68	568.2	6.31	642.8	7.98
ACO-12-42B	12-42b-25	0.0636	0.00099	0.09981	0.00119	0.87525	0.0139	96	728.5	32.75	613.3	6.99	638.4	7.53
ACO-12-42B	12-42b-26	0.11756	0.00158	0.12347	0.00142	2.00101	0.02756	39	1919.4	23.9	750.5	8.13	1115.9	9.32

ACO-12-42B	12-42b-27	0.06243	0.002	0.1012	0.00158	0.87098	0.02697	98	688.8	66.85	621.4	9.28	636.1	14.64
ACO-12-42B	12-42b-28	0.11208	0.00182	0.09379	0.00115	1.44925	0.02335	64	1833.4	29.19	577.9	6.8	909.6	9.68
ACO-12-42B	12-42b-29	0.05541	0.00122	0.05792	0.00078	0.44249	0.00968	98	428.4	47.86	363	4.73	372	6.82
ACO-12-42B	12-42b-30	0.0611	0.00144	0.08828	0.00115	0.74368	0.01709	97	642.9	49.93	545.4	6.82	564.6	9.95
ACO-12-42B	12-42b-31	0.14179	0.00192	0.37798	0.00431	7.38876	0.10233	92	2249.2	23.22	2066.9	20.18	2159.6	12.39
ACO-12-42B	12-42b-32	0.12657	0.00248	0.09547	0.0012	1.66545	0.03139	59	2050.8	34.16	587.8	7.05	995.5	11.96
ACO-12-42B	12-42b-33	0.10103	0.00145	0.08929	0.00104	1.24367	0.01815	67	1643.1	26.45	551.4	6.17	820.5	8.21
ACO-12-42B	12-42b-34	0.12965	0.00207	0.34057	0.00396	6.08678	0.09629	90	2093.3	27.83	1889.4	19.05	1988.4	13.8
ACO-12-42B	12-42b-35	0.06158	0.00132	0.09782	0.00125	0.83049	0.01742	98	659.5	45.14	601.6	7.34	613.9	9.66
ACO-12-42B	12-42b-36	0.14705	0.00306	0.37252	0.00501	7.54989	0.15615	88	2311.9	35.29	2041.2	23.55	2178.9	18.54
ACO-12-42B	12-42b-37	0.06488	0.00145	0.09605	0.0013	0.85912	0.01895	94	770.4	46.45	591.2	7.62	629.6	10.35
ACO-12-42B	12-42b-38	0.05922	0.00244	0.07084	0.0013	0.57833	0.02305	95	575.3	87.17	441.2	7.84	463.4	14.83
ACO-12-42B	12-42b-39	0.06106	0.00126	0.09985	0.00126	0.84056	0.01701	99	641.4	43.59	613.5	7.41	619.5	9.39
ACO-12-42B	12-42b-40	0.06049	0.00109	0.09298	0.00113	0.77535	0.01388	98	621	38.34	573.1	6.68	582.8	7.94
ACO-12-42B	12-42b-41	0.06117	0.00092	0.09985	0.00115	0.84209	0.01271	99	645.3	31.89	613.6	6.74	620.3	7.01
ACO-12-42B	12-42b-42	0.17295	0.00253	0.07658	0.0009	1.8262	0.02618	45	2586.4	24.19	475.7	5.39	1054.9	9.41
ACO-12-42B	12-42b-43	0.06134	0.00112	0.05828	0.00072	0.49284	0.00901	90	651.3	38.82	365.1	4.41	406.8	6.13
ACO-12-42B	12-42b-44	0.05862	0.00093	0.08838	0.00103	0.7142	0.01135	100	552.9	34.23	545.9	6.09	547.2	6.72
ACO-12-42B	12-42b-45	0.05869	0.00096	0.09651	0.00113	0.78089	0.01277	101	555.6	35.22	593.9	6.67	586	7.28
ACO-12-42B	12-42b-46	0.0599	0.00205	0.08896	0.00137	0.7346	0.02425	98	599.8	72.46	549.4	8.09	559.3	14.19
ACO-12-42B	12-42b-47	0.06016	0.00103	0.0919	0.00109	0.76227	0.01303	99	609.4	36.66	566.8	6.46	575.3	7.51
ACO-12-42B	12-42b-48	0.11984	0.00224	0.0569	0.00071	0.94001	0.0169	53	1953.9	32.99	356.7	4.35	672.9	8.84
ACO-12-42B	12-42b-49	0.06582	0.00107	0.11211	0.00136	1.01737	0.01677	96	800.7	33.81	685	7.87	712.6	8.44
ACO-12-42B	12-42b-50	0.06034	0.0014	0.10018	0.00131	0.83345	0.01884	100	615.9	49.17	615.5	7.68	615.5	10.43
ACO-12-42B	12-42b-51	0.06913	0.00109	0.08895	0.00106	0.84786	0.0135	88	902.7	32.14	549.3	6.28	623.5	7.42
ACO-12-42B	12-42b-52	0.06162	0.00108	0.10205	0.00127	0.86705	0.01541	99	660.9	37.28	626.4	7.45	634	8.38
ACO-12-42B	12-42b-53	0.08564	0.0018	0.09174	0.00121	1.08325	0.02218	76	1330	40.21	565.8	7.12	745.2	10.81
ACO-12-42B	12-42b-54	0.06608	0.00235	0.11752	0.0019	1.07043	0.03639	97	808.9	72.66	716.3	10.93	739	17.85
ACO-12-42B	12-42b-55	0.05587	0.00107	0.05928	0.00073	0.45664	0.00873	97	446.7	41.88	371.2	4.45	381.9	6.09
ACO-12-42B	12-42b-56	0.05542	0.00187	0.06305	0.00099	0.48187	0.01579	99	428.7	73.4	394.2	6.01	399.4	10.82
ACO-12-42B	12-42b-57	0.10915	0.00167	0.32109	0.00383	4.83246	0.07498	101	1785.3	27.65	1795.1	18.71	1790.6	13.05
ACO-12-42B	12-42b-58	0.05781	0.00139	0.06063	0.00079	0.48312	0.01133	95	522.3	52.08	379.4	4.82	400.2	7.75
ACO-12-42B	12-42b-59	0.06042	0.00101	0.10117	0.00121	0.84275	0.01419	100	618.6	35.65	621.2	7.09	620.7	7.82
ACO-12-42B	12-42b-60	0.06016	0.001	0.10176	0.00122	0.84419	0.0142	101	609.4	35.6	624.7	7.14	621.5	7.82
ACO-12-42B	12-42b-61	0.06196	0.00101	0.10482	0.00127	0.89551	0.01488	99	672.6	34.55	642.6	7.43	649.3	7.97
ACO-12-42B	12-42b-62	0.067	0.00093	0.10175	0.00119	0.93988	0.01357	93	837.7	28.78	624.6	6.95	672.8	7.1

ACO-12-42B	12-42b-63	0.05593	0.00109	0.07035	0.00087	0.54252	0.01049	100	449.2	42.26	438.3	5.27	440.1	6.9
ACO-12-42B	12-42b-64	0.06164	0.00096	0.10472	0.00129	0.89013	0.01441	99	661.8	33.09	642	7.55	646.4	7.74
ACO-12-42B	12-42b-65	0.06428	0.00123	0.10032	0.00131	0.88934	0.01721	95	750.9	40.02	616.3	7.65	646	9.25
ACO-12-42B	12-42b-66	0.13057	0.00175	0.26514	0.00302	4.77213	0.06586	72	2105.6	23.32	1516.1	15.41	1780	11.59
ACO-12-42B	12-42b-67	0.21123	0.00284	0.28288	0.00342	8.23946	0.1148	55	2915	21.62	1605.8	17.2	2257.7	12.62
ACO-12-42B	12-42b-68	0.43785	0.00531	0.23095	0.00267	13.9424	0.1793	33	4044.5	17.97	1339.5	13.96	2745.8	12.18
ACO-12-42B	12-42b-69	0.12767	0.00185	0.1006	0.00122	1.77089	0.02617	60	2066.2	25.3	617.9	7.16	1034.8	9.59
ACO-12-42B	12-42b-70	0.07899	0.00162	0.09042	0.0012	0.98485	0.01992	80	1171.9	39.96	558	7.1	696.1	10.19
ACO-12-42B	12-42b-71	0.06481	0.00147	0.11338	0.00149	1.01305	0.0225	97	768.2	47	692.3	8.65	710.4	11.35
ACO-12-42B	12-42b-72	0.08216	0.00145	0.06725	0.00084	0.76177	0.01341	73	1249.4	33.94	419.6	5.08	575	7.73
ACO-12-42B	12-42b-73	0.06196	0.00122	0.10725	0.00134	0.91615	0.01783	99	672.6	41.46	656.8	7.81	660.3	9.45
ACO-12-42B	12-42b-74	0.16976	0.0022	0.22948	0.00266	5.37098	0.07327	52	2555.3	21.5	1331.8	13.96	1880.2	11.68
ACO-12-42B	12-42b-75	0.06252	0.00141	0.10137	0.00132	0.87368	0.01932	98	691.9	47.43	622.4	7.74	637.6	10.47
ACO-12-42B	12-42b-76	0.06038	0.00213	0.05991	0.00098	0.49875	0.01705	91	617.3	74.43	375.1	5.99	410.9	11.55
ACO-12-42B	12-42b-77	0.06198	0.00105	0.11102	0.00135	0.94868	0.0163	100	673.4	35.97	678.7	7.84	677.4	8.49
ACO-12-42B	12-42b-78	0.07339	0.00185	0.09552	0.00133	0.96646	0.02359	86	1024.7	50.11	588.1	7.85	686.6	12.18
ACO-12-42B	12-42b-79	0.08501	0.00126	0.09966	0.00117	1.16805	0.01766	78	1315.7	28.47	612.4	6.86	785.7	8.27
ACO-12-42B	12-42b-80	0.08495	0.00151	0.10067	0.00122	1.17896	0.02082	78	1314.3	34.19	618.3	7.16	790.8	9.7
ACO-12-51	12-51-01	0.14899	0.00195	0.31734	0.00388	6.517	0.09146	76	2334.3	22.25	1776.7	18.97	2048.2	12.35
ACO-12-51	12-51-02	0.07702	0.00162	0.09838	0.00134	1.04473	0.02182	83	1121.8	41.4	604.9	7.84	726.3	10.83
ACO-12-51	12-51-03	0.07424	0.00092	0.17073	0.00197	1.74758	0.02307	97	1048.1	24.88	1016.1	10.87	1026.3	8.53
ACO-12-51	12-51-04	0.06038	0.001	0.09623	0.00117	0.80112	0.01347	99	617.4	35.36	592.3	6.87	597.5	7.59
ACO-12-51	12-51-05	0.06359	0.00088	0.10192	0.00123	0.89352	0.01302	96	728.1	28.93	625.6	7.18	648.3	6.98
ACO-12-51	12-51-06	0.08461	0.00179	0.20593	0.00292	2.40125	0.05074	92	1306.4	40.66	1207.1	15.6	1243	15.15
ACO-12-51	12-51-07	0.06152	0.00122	0.09205	0.00121	0.78061	0.0156	97	657.4	42.03	567.7	7.14	585.8	8.9
ACO-12-51	12-51-08	0.16753	0.00208	0.46958	0.00549	10.84614	0.14281	98	2533.1	20.68	2481.7	24.06	2510	12.24
ACO-12-51	12-51-09	0.06514	0.00126	0.11412	0.00148	1.0247	0.0199	97	778.8	40.03	696.6	8.59	716.3	9.98
ACO-12-51	12-51-10	0.06155	0.00088	0.11076	0.00131	0.93997	0.01393	101	658.7	30.36	677.2	7.58	672.9	7.29
ACO-12-51	12-51-11	0.05899	0.00097	0.06838	0.00085	0.55606	0.00941	95	566.7	35.36	426.4	5.13	449	6.14
ACO-12-51	12-51-12	0.05948	0.00112	0.07039	0.00089	0.57717	0.01096	95	584.6	40.36	438.5	5.38	462.6	7.05
ACO-12-51	12-51-13	0.05721	0.0008	0.06867	0.00081	0.54163	0.00789	97	499.2	30.47	428.1	4.9	439.5	5.19
ACO-12-51	12-51-14	0.05518	0.00115	0.06195	0.00081	0.47119	0.00986	99	419.2	45.4	387.5	4.95	392	6.8
ACO-12-51	12-51-15	0.06214	0.00132	0.08959	0.0012	0.76752	0.01626	96	679.1	44.78	553.1	7.11	578.3	9.34
ACO-12-51	12-51-16	0.05358	0.0014	0.05489	0.00075	0.40544	0.01038	100	353.3	57.99	344.5	4.57	345.6	7.5
ACO-12-51	12-51-17	0.05616	0.00112	0.06099	0.0008	0.47218	0.00945	97	458.3	43.57	381.6	4.85	392.7	6.52
ACO-12-51	12-51-18	0.06988	0.00158	0.06443	0.00088	0.6207	0.01381	82	924.8	45.69	402.5	5.36	490.3	8.65
ACO-12-51	12-51-19	0.07298	0.00147	0.06999	0.00092	0.70421	0.01412	81	1013.5	39.82	436.1	5.55	541.3	8.41
ACO-12-51	12-51-20	0.06351	0.00115	0.10901	0.00138	0.9545	0.01752	98	725.5	37.91	667	8.04	680.4	9.1
ACO-12-51	12-51-21	0.06223	0.00179	0.09702	0.00139	0.83228	0.02295	97	682.1	60.28	596.9	8.16	614.9	12.72

ACO-12-51	12-51-22	0.0654	0.0021	0.06937	0.00105	0.62547	0.01915	88	787.3	66.09	432.3	6.34	493.3	11.96
ACO-12-51	12-51-23	0.06151	0.00216	0.09837	0.00158	0.83413	0.02797	98	657.2	73.69	604.9	9.3	615.9	15.49
ACO-12-51	12-51-24	0.10871	0.00339	0.28463	0.0044	4.26457	0.126	91	1777.9	55.95	1614.7	22.08	1686.6	24.3
ACO-12-51	12-51-25	0.11431	0.00358	0.30883	0.00488	4.86683	0.14366	93	1869	55.5	1734.9	24.05	1796.5	24.86
ACO-12-51	12-51-26	0.06883	0.00247	0.0648	0.00106	0.61487	0.02087	83	893.7	72.39	404.7	6.43	486.6	13.12
ACO-12-51	12-51-27	0.05822	0.00248	0.0716	0.00128	0.57467	0.02322	97	537.5	91.28	445.8	7.68	461	14.97
ACO-12-51	12-51-28	0.06317	0.00206	0.09862	0.0015	0.85902	0.02663	96	714	67.96	606.3	8.78	629.6	14.54
ACO-12-51	12-51-29	0.09926	0.00231	0.05927	0.00076	0.81112	0.01779	62	1610.3	42.72	371.2	4.62	603.1	9.97
ACO-12-51	12-51-30	0.0597	0.00255	0.06353	0.00115	0.52322	0.02099	93	593.1	89.71	397.1	6.95	427.3	13.99
ACO-12-51	12-51-31	0.08955	0.00153	0.25316	0.00303	3.12571	0.05246	103	1415.8	32.29	1454.7	15.58	1439	12.91
ACO-12-51	12-51-32	0.05157	0.00122	0.06487	0.00086	0.46122	0.01055	105	266.2	53.3	405.2	5.22	385.1	7.33
ACO-12-51	12-51-33	0.05784	0.00101	0.08869	0.00105	0.70713	0.01212	101	523.4	38.15	547.8	6.19	543	7.21
ACO-12-51	12-51-34	0.05164	0.00191	0.06153	0.00102	0.43795	0.01555	104	269.4	82.79	384.9	6.17	368.8	10.98
ACO-12-51	12-51-35	0.05249	0.00199	0.05963	0.00101	0.43129	0.01566	103	306.6	84.28	373.4	6.12	364.1	11.11
ACO-12-51	12-51-36	0.0567	0.00112	0.072	0.00087	0.56266	0.01082	99	479.1	43.41	448.2	5.26	453.3	7.03
ACO-12-51	12-51-37	0.05443	0.00113	0.06584	0.00082	0.49381	0.01005	101	388.8	45.87	411	4.97	407.5	6.83
ACO-12-51	12-51-38	0.05766	0.00103	0.09407	0.00113	0.74744	0.01316	102	516.6	39.03	579.5	6.64	566.7	7.65
ACO-12-51	12-51-39	0.20704	0.00342	0.55581	0.00663	15.85921	0.2596	99	2882.5	26.56	2849.3	27.47	2868.4	15.63
ACO-12-51	12-51-40	0.05991	0.00125	0.09852	0.00123	0.81332	0.01654	100	600.2	44.38	605.7	7.2	604.3	9.26
ACO-12-51	12-51-41	0.05685	0.00111	0.08801	0.00108	0.68941	0.01325	102	484.9	42.74	543.8	6.41	532.4	7.97
ACO-12-51	12-51-42	0.05719	0.00125	0.08941	0.00114	0.70473	0.01515	102	498.5	48.05	552.1	6.72	541.6	9.02
ACO-12-51	12-51-43	0.06099	0.00189	0.0759	0.00117	0.63758	0.01908	94	638.8	65.15	471.6	7.01	500.8	11.83
ACO-12-51	12-51-44	0.1256	0.00228	0.31864	0.00393	5.51531	0.09976	88	2037.3	31.76	1783.1	19.23	1903	15.55
ACO-12-51	12-51-45	0.09987	0.002	0.29155	0.00371	4.01247	0.08004	102	1621.6	36.81	1649.3	18.51	1636.7	16.21
ACO-12-51	12-51-46	0.05433	0.00142	0.06424	0.00087	0.48105	0.01227	101	384.8	57.34	401.4	5.3	398.8	8.41
ACO-12-51	12-51-47	0.07757	0.00262	0.10577	0.00175	1.13061	0.03699	84	1135.8	65.9	648.2	10.21	768	17.63
ACO-12-51	12-51-48	0.06182	0.00167	0.09586	0.00136	0.8169	0.02159	97	668	56.72	590.1	7.98	606.3	12.06
ACO-12-51	12-51-49	0.06158	0.00146	0.09271	0.00124	0.78701	0.01841	97	659.6	50.02	571.5	7.29	589.5	10.46
ACO-12-51	12-51-50	0.06524	0.00248	0.09723	0.00167	0.87458	0.03214	94	782.1	77.93	598.2	9.83	638.1	17.41
ACO-12-51	12-51-51	0.06382	0.00143	0.10217	0.00133	0.89903	0.0197	96	735.8	46.84	627.1	7.79	651.2	10.53
ACO-12-51	12-51-52	0.06485	0.00233	0.08739	0.00147	0.78131	0.02695	92	769.6	73.75	540.1	8.74	586.2	15.36
ACO-12-51	12-51-53	0.09968	0.00416	0.06284	0.00123	0.8636	0.03356	62	1618.1	75.66	392.9	7.49	632.1	18.28
ACO-12-51	12-51-54	0.11018	0.00174	0.2421	0.00292	3.67812	0.05828	78	1802.3	28.42	1397.6	15.14	1566.6	12.65
ACO-12-51	12-51-55	0.07416	0.00112	0.04882	0.00057	0.49909	0.00758	75	1045.7	30.14	307.2	3.49	411.1	5.13
ACO-12-51	12-51-56	0.06102	0.00128	0.10338	0.0013	0.86973	0.01783	100	640	44.4	634.2	7.62	635.4	9.68
ACO-12-51	12-51-57	0.05983	0.00114	0.10023	0.00123	0.82682	0.01554	101	597.5	40.73	615.8	7.2	611.8	8.63
ACO-12-51	12-51-58	0.06131	0.00333	0.09927	0.0022	0.83883	0.04354	99	650	112.43	610.1	12.91	618.5	24.04
ACO-12-51	12-51-59	0.07	0.00183	0.14246	0.00207	1.37478	0.03514	98	928.3	52.7	858.6	11.69	878.2	15.02
ACO-12-51	12-51-60	0.07803	0.00167	0.07536	0.001	0.8107	0.01713	78	1147.7	41.94	468.4	6.01	602.8	9.61
ACO-12-51	12-51-61	0.06159	0.00147	0.10378	0.00139	0.88134	0.02051	99	659.9	50.4	636.5	8.09	641.7	11.07
ACO-12-51	12-51-62	0.08258	0.00189	0.10166	0.00138	1.15755	0.02582	80	1259.3	44.1	624.1	8.05	780.8	12.15
ACO-12-51	12-51-63	0.05951	0.00228	0.07901	0.00135	0.64825	0.02389	97	585.9	81	490.2	8.06	507.4	14.71
ACO-12-51	12-51-64	0.07608	0.00198	0.0607	0.00087	0.63663	0.01618	76	1097.1	51.35	379.9	5.27	500.2	10.04
ACO-12-51	12-51-65	0.08983	0.00213	0.25141	0.00348	3.11348	0.07229	102	1421.8	44.7	1445.7	17.92	1436	17.84
ACO-12-51	12-51-66	0.0774	0.00188	0.19893	0.00269	2.12245	0.04959	103	1131.4	47.52	1169.5	14.44	1156.1	16.12

ACO-12-51	12-51-67	0.09859	0.0029	0.27015	0.00414	3.67186	0.10449	96	1597.6	53.94	1541.6	21.01	1565.3	22.71
ACO-12-51	12-51-68	0.06156	0.00125	0.10398	0.00128	0.88242	0.01747	99	658.7	42.96	637.7	7.49	642.3	9.43
ACO-12-51	12-51-69	0.06612	0.00323	0.10463	0.00214	0.95391	0.04453	94	810.3	99.01	641.5	12.49	680.1	23.14
ACO-12-51	12-51-70	0.05805	0.00195	0.0697	0.0011	0.55782	0.0181	96	531.3	72.3	434.3	6.65	450.1	11.8
ACO-12-51	12-51-71	0.06084	0.00213	0.10444	0.00168	0.87599	0.02959	100	633.4	73.52	640.4	9.81	638.8	16.02
ACO-12-51	12-51-72	0.06087	0.00143	0.10133	0.00135	0.85043	0.0196	100	634.8	49.83	622.2	7.89	624.9	10.76
ACO-12-51	12-51-73	0.06493	0.00167	0.10018	0.00142	0.89681	0.02257	95	772	53.15	615.5	8.34	650	12.08
ACO-12-51	12-51-74	0.05948	0.00172	0.09297	0.00133	0.76237	0.02136	100	584.8	61.55	573.1	7.87	575.4	12.3
ACO-12-51	12-51-75	0.05958	0.00139	0.09219	0.00124	0.75722	0.01742	99	588.2	49.89	568.5	7.3	572.4	10.07
ACO-12-51	12-51-76	0.0628	0.0014	0.10658	0.00139	0.92278	0.02018	98	701.6	46.73	652.8	8.09	663.8	10.66
ACO-12-51	12-51-77	0.06227	0.00131	0.10999	0.0014	0.94424	0.01955	100	683.3	44.26	672.7	8.15	675.1	10.21
ACO-12-51	12-51-78	0.06316	0.00156	0.12876	0.00178	1.12135	0.02724	102	713.8	51.7	780.8	10.18	763.6	13.04
ACO-12-51	12-51-79	0.12876	0.00228	0.38425	0.00479	6.82106	0.12115	101	2081.1	30.89	2096.1	22.31	2088.5	15.73
ACO-12-51	12-51-80	0.12733	0.00244	0.37337	0.00481	6.55398	0.12514	99	2061.4	33.45	2045.3	22.58	2053.2	16.82

Supplementary Table 2. U-Pb igneous zircon data

Sample no.	No._#	Pb207/Pb206		Pb206/U238		Pb207/U235		Conc	Pb207/Pb206		Pb206/U238		Pb207/U235	
BH-14-ERG	1	0.06	0.00	0.12	0.00	1.04	0.02	100	733.3	26.42	722.5	9.68	725.3	8.09
BH-14-ERG	2	0.06	0.00	0.12	0.00	1.04	0.02	100	724.4	26.07	726	9.72	725.8	8.01
BH-14-ERG	3	0.06	0.00	0.12	0.00	1.06	0.02	99	761.5	24.93	721.7	9.59	731.7	7.87
BH-14-ERG	4	0.07	0.00	0.12	0.00	1.15	0.02	92	965.9	28.96	711.5	9.8	776.2	9.23
BH-14-ERG	5	0.07	0.00	0.12	0.00	1.21	0.02	91	1011.2	24.51	730.9	10.03	804	8.69
BH-14-ERG	6	0.06	0.00	0.12	0.00	1.05	0.02	100	737.8	30.17	724.4	10.39	727.9	9.16
BH-14-ERG	7	0.06	0.00	0.12	0.00	1.07	0.02	98	771.3	42.31	727.4	11.47	738.6	11.85
BH-14-ERG	8	0.06	0.00	0.12	0.00	1.03	0.02	100	718.3	28.08	721.1	9.99	720.6	8.53
BH-14-ERG	9	0.06	0.00	0.12	0.00	1.07	0.02	99	758.1	30.06	733.7	10.62	740	9.31
BH-14-ERG	10	0.06	0.00	0.12	0.00	1.04	0.02	101	712.8	28.16	730.3	10.33	726.3	8.73
BH-14-ERG	11	0.08	0.00	0.12	0.00	1.32	0.02	87	1158.4	27.43	740	10.25	852.7	9.79
BH-14-ERG	12	0.06	0.00	0.12	0.00	1.06	0.02	100	744.4	28.61	732.4	10.47	735.5	8.98
BH-14-ERG	13	0.06	0.00	0.12	0.00	1.05	0.03	101	706.5	49.15	735.6	10.88	728.5	13
BH-14-ERG	14	0.07	0.00	0.12	0.00	1.08	0.02	99	775.2	29.14	731.5	10.65	742.5	9.29
BH-14-ERG	15	0.06	0.00	0.12	0.00	1.08	0.02	99	763.5	39.88	734.1	10.67	741.3	11.31
BH-14-ERG	16	0.06	0.00	0.12	0.00	1.04	0.02	100	719	28.95	728	10.76	725.7	9.07
BH-14-ERG	17	0.06	0.00	0.12	0.00	1.07	0.02	101	723.7	29.22	740.8	11	736.4	9.25
BH-14-ERG	18	0.06	0.00	0.12	0.00	1.07	0.02	100	736	26.77	739.3	10.74	738.4	8.77
BH-14-ERG	19	0.06	0.00	0.12	0.00	1.07	0.02	100	732.9	32.3	740.6	11.36	738.7	9.98
BH-14-ERG	20	0.06	0.00	0.12	0.00	1.08	0.02	99	756.9	29.13	738.5	11.06	743	9.39
BH-14-ERG	21	0.06	0.00	0.12	0.00	1.06	0.02	100	729.4	25.95	734.2	10.6	732.9	8.56
BH-14-ERG	22	0.07	0.00	0.13	0.00	1.19	0.02	96	879.1	29.07	765.5	11.6	795.1	9.97
BH-14-ERG	23	0.06	0.00	0.12	0.00	1.06	0.02	100	745.3	25.42	731.3	10.45	734.7	8.45
BH-14-ERG	24	0.06	0.00	0.12	0.00	1.05	0.02	100	726.1	28.53	731.4	10.83	730	9.07
BH-14-ERG	25	0.07	0.00	0.12	0.00	1.11	0.02	98	807	31.34	741.1	10.18	757.1	9.38
BH-14-ERG	26	0.07	0.00	0.12	0.00	1.09	0.02	98	802.8	33.9	733.4	11.58	750.8	10.61
BH-14-ERG	27	0.06	0.00	0.12	0.00	1.07	0.02	99	763.1	26.61	732	10.51	739.5	8.71
BH-14-ERG	28	0.07	0.00	0.13	0.00	1.15	0.02	99	806.5	24.13	766.1	10.81	776.3	8.54
BH-14-ERG	29	0.07	0.00	0.13	0.00	1.14	0.02	99	793.5	23.81	767.8	10.84	774.3	8.47
BH-14-ERG	30	0.07	0.00	0.12	0.00	1.12	0.03	94	889.9	44.1	721.6	11.96	763.9	12.97
BH-14-ERG	31	0.06	0.00	0.12	0.00	1.08	0.02	99	765.5	28.12	737.8	10.61	744.5	9.01
BH-14-ERG	32	0.06	0.00	0.12	0.00	1.09	0.02	99	767.2	29.56	742.2	10.81	748.4	9.37
BH-14-ERG	33	0.06	0.00	0.12	0.00	1.08	0.02	100	752	30.38	741	10.44	743.1	9.24
BH-14-ERG	34	0.07	0.00	0.12	0.00	1.10	0.02	98	797.2	29.75	736.3	10.89	751.5	9.54
BH-14-ERG	35	0.08	0.00	0.13	0.00	1.44	0.03	86	1217.9	27.39	781.5	11.15	904.2	10.42
BH-14-ERG	36	0.06	0.00	0.12	0.00	1.08	0.02	99	771.7	26.25	736.2	10.57	744.9	8.71
BH-14-ERG	37	0.06	0.00	0.12	0.00	1.07	0.02	102	693.9	25.93	752.5	10.68	737.7	8.47
BH-14-ERG	38	0.07	0.00	0.12	0.00	1.10	0.02	99	783.3	33.04	743.2	10.5	753.1	9.73
BH-14-ERG	39	0.06	0.00	0.12	0.00	1.07	0.02	100	726.3	30.74	740.5	11.05	736.9	9.56
BH-14-ERG	40	0.07	0.00	0.12	0.00	1.09	0.02	98	794.9	33.8	735.6	11.25	750.4	10.4
BH-14-ERG	41	0.06	0.00	0.12	0.00	1.06	0.02	101	717.4	29.77	736.8	10.86	732	9.31
BH-14-ERG	42	0.07	0.00	0.12	0.00	1.10	0.02	98	798.6	33.82	737.3	11.26	752.6	10.44
BH-14-ERG	43	0.06	0.00	0.12	0.00	1.07	0.02	99	751.9	28.77	735.5	10.56	739.5	9.05
BH-14-ERG	44	0.06	0.00	0.12	0.00	1.08	0.02	99	766.2	28	737.8	10.63	744.8	9.02
BH-14-ERG	45	0.06	0.00	0.12	0.00	1.07	0.02	99	755.9	27.3	730.9	10.39	737	8.74
BH-14-ERG	46	0.07	0.00	0.12	0.00	1.09	0.02	99	783.5	29.24	738.8	10.63	749.9	9.27
BH-14-ERG	47	0.06	0.00	0.12	0.00	1.07	0.02	100	747.2	33.49	737.5	11.1	739.9	10.14
BH-14-ERG	48	0.06	0.00	0.12	0.00	1.09	0.02	99	774	31.91	740.2	10.65	748.6	9.69
BH-14-ERG	49	0.06	0.00	0.12	0.00	1.07	0.02	101	720.6	35.03	742.8	11.27	737.3	10.4
BH-14-ERG	50	0.07	0.00	0.12	0.00	1.09	0.02	99	779.3	32.68	736.7	10.94	747.3	10.06
ACO-13-17	1	0.07	0.00	0.10	0.00	0.95	0.01	91	885.7	31	619.2	7.13	679.5	7.76
ACO-13-17	2	0.06	0.00	0.10	0.00	0.82	0.02	102	564.9	46.08	618.2	8.35	606.9	9.99
ACO-13-17	3	0.06	0.00	0.10	0.00	0.83	0.02	100	600.9	44.08	615.5	8.11	612.6	9.68
ACO-13-17	4	0.13	0.02	0.07	0.00	1.17	0.21	53	2080.7	291.82	418.9	27.58	788.8	98.55

ACO-13-17	5	0.06	0.00	0.10	0.00	0.83	0.02	97	688.8	55.23	591.6	8.57	611.8	12.02
ACO-13-17	6	0.09	0.00	0.10	0.00	1.23	0.02	79	1324.9	32.64	639.5	7.65	813.5	9.69
ACO-13-17	7	0.06	0.00	0.10	0.00	0.81	0.02	101	590.6	47.76	609	8.04	605	10.21
ACO-13-17	8	0.06	0.00	0.10	0.00	0.84	0.01	96	712.2	35.73	595	7.02	619.9	8.02
ACO-13-17	9	0.06	0.00	0.10	0.00	0.80	0.02	101	580.7	41.69	599.4	7.33	595.4	8.79
ACO-13-17	10	0.06	0.00	0.10	0.00	0.86	0.02	97	700.6	40.74	608.6	7.54	628.4	9.15
ACO-13-17	11	0.06	0.00	0.10	0.00	0.85	0.04	97	694.2	103.08	605.2	11.91	624.1	22.34
ACO-13-17	12	0.06	0.00	0.10	0.00	0.82	0.02	99	624.8	54.73	601.6	8.28	606.6	11.58
ACO-13-17	13	0.06	0.00	0.10	0.00	0.81	0.01	102	567.6	36.99	615	7.34	604.9	8.04
ACO-13-17	14	0.06	0.00	0.10	0.00	0.80	0.01	101	577.2	34.13	602.1	6.89	596.9	7.34
ACO-13-17	15	0.06	0.00	0.10	0.00	0.82	0.02	101	594.3	43.41	610.3	7.74	607	9.36
ACO-13-17	16	0.06	0.00	0.10	0.00	0.82	0.01	100	617	37.82	605	7.11	607.5	8.19
ACO-13-17	17	0.06	0.00	0.10	0.00	0.82	0.01	99	633.1	34.76	604.3	6.96	610.4	7.63
ACO-13-17	18	0.06	0.00	0.10	0.00	0.88	0.02	96	726.3	45.54	617.6	8.07	641.4	10.44
ACO-13-17	19	0.06	0.00	0.10	0.00	0.84	0.02	100	628.9	49.25	617.8	8.32	619.9	10.82
ACO-13-17	20	0.18	0.00	0.09	0.00	2.31	0.04	48	2631.5	25.19	580	6.76	1214.4	11.04
ACO-13-17	21	0.06	0.00	0.10	0.00	0.84	0.02	96	710.2	37.08	597.4	7.01	621.5	8.29
ACO-13-17	22	0.14	0.00	0.11	0.00	2.00	0.04	58	2197.9	32.5	646.4	8.18	1116.1	13.06
ACO-13-17	23	0.08	0.00	0.10	0.00	1.08	0.02	80	1218.2	30.78	596.5	6.91	744.2	8.56
ACO-13-17	24	0.08	0.00	0.08	0.00	0.94	0.02	78	1216.2	33.64	521.4	6.28	672.1	8.67
ACO-13-17	25	0.06	0.00	0.10	0.00	0.79	0.02	102	545.1	44.65	604.4	7.69	592.1	9.39
ACO-13-17	26	0.06	0.00	0.10	0.00	0.85	0.02	98	678.3	51.88	610.2	8.41	624.8	11.53
ACO-13-17	27	0.06	0.00	0.10	0.00	0.87	0.03	96	720.8	66.33	608.9	8.67	633.5	14.63
ACO-13-17	28	0.06	0.00	0.10	0.00	0.82	0.02	101	590.1	42.09	614.5	7.61	609.4	9.11
ACO-13-17	29	0.06	0.00	0.10	0.00	0.83	0.02	100	615.7	54.25	612.7	8.37	613.3	11.68
ACO-13-17	30	0.06	0.00	0.10	0.00	0.86	0.02	97	700.9	47.17	611.6	7.79	631.1	10.49
ACO-13-21	1	0.05	0.00	0.06	0.00	0.47	0.01	102	345.9	45.87	400.3	4.77	392.3	6.63
ACO-13-21	2	0.06	0.00	0.07	0.00	0.61	0.01	97	559.2	41.97	465.4	5.69	481.5	7.49
ACO-13-21	3	0.06	0.00	0.08	0.00	0.58	0.02	100	471	67.1	466.8	6.72	467.5	11.3
ACO-13-21	4	0.06	0.00	0.07	0.00	0.58	0.02	100	471.9	68.59	466.2	6.84	467.3	11.54
ACO-13-21	5	0.06	0.00	0.07	0.00	0.55	0.02	100	433.6	62.53	443.3	6.03	441.7	10.1
ACO-13-21	6	0.06	0.00	0.07	0.00	0.59	0.02	98	512.8	60.77	464.3	6.27	472.6	10.37
ACO-13-21	7	0.05	0.00	0.06	0.00	0.47	0.01	102	346.2	69.86	395.6	5.45	388.5	9.91
ACO-13-21	8	0.06	0.00	0.09	0.00	0.75	0.02	99	598.3	55.58	563.1	7.64	570.2	11.27
ACO-13-21	9	0.06	0.00	0.08	0.00	0.61	0.01	98	525.9	48.74	471	6.06	480.4	8.58
ACO-13-21	10	0.10	0.00	0.28	0.00	3.79	0.07	100	1587.2	33.49	1592.7	17.51	1590.2	14.73
ACO-13-21	11	0.06	0.00	0.08	0.00	0.75	0.01	92	752.9	41.62	522	6.15	567.2	8.62
ACO-13-21	12	0.06	0.00	0.09	0.00	0.74	0.02	102	526	46	572.9	6.87	563.6	9.06
ACO-13-21	13	0.06	0.00	0.08	0.00	0.63	0.01	104	412.7	41.54	512.2	5.77	494.4	7.25
ACO-13-21	14	0.06	0.00	0.07	0.00	0.59	0.02	99	483.6	77.21	464.4	7.05	467.7	12.98
ACO-13-21	15	0.06	0.00	0.10	0.00	0.86	0.02	98	673.7	43.03	621.3	7.21	632.7	9.37
ACO-13-21	16	0.06	0.00	0.07	0.00	0.57	0.01	101	444.7	44.23	464.4	5.54	461.1	7.45
ACO-13-21	17	0.08	0.00	0.08	0.00	0.86	0.03	81	1082.9	64.41	511.1	7.15	629.7	14.62
ACO-13-21	18	0.06	0.00	0.08	0.00	0.63	0.02	95	618.3	64.97	470.3	6.83	496.3	11.8
ACO-13-21	19	0.06	0.00	0.07	0.00	0.59	0.01	99	498	47.83	464.4	5.76	470.1	8.12
ACO-13-16	1	0.06	0.00	0.04	0.00	0.30	0.00	85	641.6	32.81	226.5	2.91	267.1	3.88
ACO-13-16	2	0.05	0.00	0.06	0.00	0.47	0.01	103	335.9	46.19	404.1	5.46	394	6.97
ACO-13-16	3	0.05	0.00	0.06	0.00	0.47	0.01	101	366.7	40.1	393.8	5.11	389.8	6.1
ACO-13-16	4	0.06	0.00	0.06	0.00	0.48	0.01	99	413.7	63.46	396.3	5.9	398.7	9.58
ACO-13-16	5	0.05	0.00	0.06	0.00	0.48	0.01	101	375.4	66.32	398.8	6.09	395.3	9.82
ACO-13-16	6	0.05	0.00	0.06	0.00	0.47	0.01	101	377.3	45.71	391.1	5.19	389	6.81
ACO-13-16	7	0.05	0.00	0.06	0.00	0.47	0.02	101	374.7	86.86	390.1	6.38	388	12.47
ACO-13-16	8	0.06	0.00	0.06	0.00	0.48	0.01	99	421.7	44.48	390.4	5.07	394.9	6.82
ACO-13-16	9	0.05	0.00	0.06	0.00	0.47	0.01	101	375.5	60.56	395.3	5.76	392.3	8.93

ACO-13-16	10	0.05	0.00	0.06	0.00	0.48	0.02	100	404.6	73.2	395.3	6.48	396.6	11.01
ACO-13-16	11	0.06	0.00	0.06	0.00	0.48	0.01	99	416.5	44.57	398.1	5.11	400.7	6.9
ACO-13-16	12	0.05	0.00	0.06	0.00	0.46	0.01	101	353.4	43.49	390	5.15	384.7	6.46
ACO-13-16	13	0.05	0.00	0.06	0.00	0.47	0.01	102	352.1	54.49	397.7	5.06	390.9	7.84
ACO-13-16	14	0.05	0.00	0.06	0.00	0.46	0.01	103	320.2	41.13	397.7	4.96	386.4	6.07
ACO-13-16	15	0.06	0.00	0.06	0.00	0.49	0.01	87	733	28.27	353.2	4.14	408.1	4.83
ACO-13-16	16	0.06	0.00	0.06	0.00	0.49	0.01	94	543.7	64.08	379.9	5.99	404	9.93
ACO-13-16	17	0.05	0.00	0.06	0.00	0.46	0.01	101	368.6	33.12	389.2	4.65	386.3	5.03
ACO-13-16	18	0.05	0.00	0.07	0.00	0.47	0.01	104	294.5	49.61	407.3	5.51	390.9	7.29
ACO-13-16	19	0.05	0.00	0.06	0.00	0.46	0.01	104	294.8	67.49	400.9	6.01	385.7	9.63
ACO-13-16	20	0.05	0.00	0.06	0.00	0.47	0.02	101	360.3	78.72	396.2	6.59	391	11.39
ACO-13-16	21	0.05	0.00	0.06	0.00	0.47	0.01	101	369.2	68.42	395	6.12	391.4	9.99
ACO-13-16	22	0.05	0.00	0.06	0.00	0.47	0.01	101	375.3	53.22	396.1	5.52	393.2	7.91
ACO-13-16	23	0.05	0.00	0.06	0.00	0.47	0.01	100	396.7	42.13	392.5	4.82	393.2	6.31
ACO-13-16	24	0.05	0.00	0.06	0.00	0.48	0.01	100	395.5	64.41	395.2	5.71	395.3	9.58
ACO-13-16	25	0.05	0.00	0.06	0.00	0.46	0.01	101	363.5	69.78	391.5	6.1	387.6	10.07
ACO-13-16	26	0.05	0.00	0.06	0.00	0.46	0.02	103	310.9	82.7	397.2	6.71	384.8	11.68
ACO-13-16	27	0.05	0.00	0.06	0.00	0.45	0.02	106	238.9	84.66	395.9	6.63	373.8	11.51
ACO-13-16	28	0.06	0.00	0.06	0.00	0.51	0.02	96	503	74.72	402.5	6.21	417.9	11.59
ACO-13-16	29	0.05	0.00	0.06	0.00	0.45	0.01	103	316.2	64.86	389.8	5.89	379.4	9.13
ACO-13-16	30	0.05	0.00	0.06	0.00	0.48	0.01	100	407.4	58.71	397	5.66	398.6	8.82
ACO-13-16	31	0.05	0.00	0.06	0.00	0.48	0.01	100	405	59.37	398.6	5.21	399.5	8.78
ACO-13-16	32	0.06	0.00	0.06	0.00	0.48	0.01	97	471.6	57.1	385.8	5.24	398.4	8.51
ACO-13-16	33	0.07	0.00	0.06	0.00	0.58	0.01	84	843.8	34.37	389.8	4.67	462.8	6.35
ACO-13-16	34	0.05	0.00	0.06	0.00	0.47	0.01	100	380.1	56.2	389.6	5.43	388.3	8.22
ACO-13-16	35	0.05	0.00	0.06	0.00	0.47	0.01	99	403.3	50.32	387	4.85	389.3	7.38
ACO-13-16	36	0.05	0.00	0.06	0.00	0.47	0.01	100	400.1	67.47	391.3	5.93	392.6	10.03
ACO-13-16	37	0.06	0.00	0.06	0.00	0.48	0.02	98	449.9	76.64	393.1	6.58	401.5	11.47
ACO-13-16	38	0.06	0.00	0.06	0.00	0.48	0.02	99	426.2	74.8	391.6	6.44	396.6	11.12
ACO-13-16	39	0.05	0.00	0.06	0.00	0.45	0.01	100	367.9	54.08	375.6	4.95	374.5	7.57
ACO-13-16	40	0.06	0.00	0.06	0.00	0.47	0.01	99	426.3	60.65	387.3	5.5	392.9	8.97
BH002/003	1	0.06	0.00	0.06	0.00	0.51	0.01	95	535.8	26.57	395.7	5.96	417	5.62
BH002/003	2	0.06	0.00	0.12	0.00	1.06	0.02	99	749	32.43	728.2	10.75	733.3	9.73
BH002/003	3	0.06	0.00	0.10	0.00	0.85	0.01	99	643.7	26.4	616.8	9.01	622.6	7.66
BH002/003	4	0.06	0.00	0.06	0.00	0.51	0.01	94	553.6	40.44	394.6	6.66	418.4	7.6
BH002/003	5	0.12	0.00	0.35	0.01	5.89	0.09	96	1997.1	21.7	1925.5	24.36	1960.1	13.68
BH002/003	6	0.06	0.00	0.07	0.00	0.52	0.01	100	413.1	31.29	424.7	6.68	422.9	6.36
BH002/003	7	0.08	0.00	0.22	0.00	2.53	0.04	102	1262	24.78	1291.8	18.42	1280.6	12.41
BH002/003	8	0.13	0.00	0.39	0.01	7.20	0.12	99	2143.6	22.82	2130.2	26.76	2137	14.5
BH002/003	9	0.07	0.00	0.06	0.00	0.60	0.01	79	999.6	29.69	378.1	5.44	479.5	6.66
BH002/003	10	0.13	0.00	0.34	0.01	6.27	0.10	87	2155.4	20.01	1878.5	24.66	2013.8	13.8
BH002/003	11	0.06	0.00	0.08	0.00	0.69	0.01	94	684.3	27.27	500.6	7.12	534.8	6.77
BH002/003	12	0.07	0.00	0.15	0.00	1.38	0.03	102	841.3	34.95	896.4	13.47	880.6	11.76
BH002/003	13	0.06	0.00	0.10	0.00	0.85	0.02	95	738.1	34.25	595.1	8.79	625.8	8.91
BH002/003	14	0.06	0.00	0.11	0.00	0.94	0.02	97	745.4	34.25	653.4	10.25	674.6	9.79
BH002/003	15	0.24	0.00	0.58	0.01	19.50	0.33	93	3150.2	20.77	2942	35.91	3067.1	16.13
BH002/003	16	0.09	0.00	0.10	0.00	1.28	0.02	76	1416	22.08	637.2	9.07	838.1	8.9
BH002/003	17	0.09	0.00	0.07	0.00	0.78	0.01	69	1359.6	22.55	406.4	5.98	585.5	7.07
BH002/003	18	0.06	0.00	0.10	0.00	0.82	0.02	98	659.7	55.93	591.7	9.38	605.9	12.44
BH002/003	19	0.16	0.00	0.19	0.00	4.11	0.06	47	2417.2	19.36	1124	15.77	1655.7	12.9
BH002/003	20	0.06	0.00	0.06	0.00	0.52	0.01	95	537.5	33.17	404.3	6.53	424.7	6.63
BH002/003	21	0.06	0.00	0.07	0.00	0.50	0.01	99	430.3	28.77	407.8	6.31	411.1	5.9
BH002/003	22	0.06	0.00	0.11	0.00	0.87	0.02	103	580.1	31.49	654.4	9.67	637.9	8.5
BH002/003	23	0.06	0.00	0.07	0.00	0.52	0.01	96	510.6	34.04	407.2	6.55	422.8	6.69
BH002/003	24	0.06	0.00	0.10	0.00	0.87	0.02	100	632.8	36.69	635.2	9.56	634.5	9.41

BH002/003	25	0.06	0.00	0.10	0.00	0.90	0.02	97	715.4	31.47	631.5	9.71	650	8.96
BH002/003	26	0.11	0.00	0.31	0.00	4.64	0.08	100	1757.7	23.58	1756.4	23.49	1756.7	13.96
BH002/003	27	0.07	0.01	0.00	0.00	0.04	0.00	69	848.8	223.96	26.3	0.86	37.9	4.2
BH-005	1	0.13	0.00	0.36	0.01	6.26	0.10	96	2052.2	22.63	1976.6	24.99	2013	14.05
BH-005	2	0.06	0.00	0.10	0.00	0.86	0.01	99	656.5	29.83	621.9	8.35	629.4	7.76
BH-005	3	0.08	0.00	0.10	0.00	1.05	0.02	84	1114.4	41.44	607.8	8.7	727.2	11.41
BH-005	4	0.06	0.00	0.09	0.00	0.78	0.02	99	603.8	37.34	577.8	8.19	583.1	8.64
BH-005	5	0.06	0.00	0.12	0.00	1.02	0.02	99	725.4	29.45	707.3	9.46	711.8	8.47
BH-005	6	0.06	0.00	0.09	0.00	0.77	0.01	96	682	31.26	554.2	7.88	579.8	7.78
BH-005	7	0.07	0.00	0.10	0.00	0.97	0.02	89	954.5	31.88	610.5	8.99	688.8	9.31
BH-005	8	0.06	0.00	0.09	0.00	0.77	0.02	99	607.5	58.71	574.8	8.9	581.6	12.48
BH-005	9	0.08	0.00	0.07	0.00	0.83	0.03	72	1308	71.95	444.9	8.34	616.3	17.01
BH-005	10	0.06	0.00	0.10	0.00	0.84	0.02	99	636.6	39.38	612.9	9.08	617.9	9.6
BH-005	11	0.06	0.00	0.06	0.00	0.48	0.01	97	465.3	50.36	385.5	6.05	397.2	8.04
BH-005	12	0.06	0.00	0.10	0.00	0.85	0.02	99	647.6	38.16	618.4	8.97	624.8	9.4
BH-005	13	0.06	0.00	0.08	0.00	0.73	0.01	94	684	33.76	524.3	7.89	555.2	8.17
BH-005	14	0.06	0.00	0.09	0.00	0.77	0.02	98	621.1	48.58	569.4	8.66	579.9	10.72
BH-005	15	0.08	0.00	0.07	0.00	0.74	0.02	72	1254	36.9	406.7	6.59	561.8	9.46
BH-005	16	0.06	0.00	0.06	0.00	0.48	0.01	94	550.5	48.35	374.4	6	399.9	8.05
BH-005	17	0.05	0.00	0.07	0.00	0.48	0.01	102	344.5	54.31	407.6	6.31	398.3	8.46
BH-005	18	0.06	0.00	0.06	0.00	0.51	0.01	94	559.5	41	390.1	5.81	415.7	7.28
BH-005	19	0.06	0.00	0.07	0.00	0.52	0.01	98	458.9	33.7	415	6	421.8	6.33
BH-005	20	0.06	0.00	0.08	0.00	0.68	0.01	98	578.3	40.86	513.5	7.81	525.6	8.81
BH-005	21	0.06	0.00	0.07	0.00	0.53	0.01	94	564.9	54.76	408.2	6.92	432.6	9.56
BH-005	22	0.06	0.00	0.09	0.00	0.75	0.01	97	649.4	24.91	549.2	7.95	569.1	6.9
BH-005	23	0.09	0.00	0.08	0.00	1.08	0.02	70	1498.4	22.97	519.1	7.61	744.3	8.54
BH-005	24	0.06	0.00	0.10	0.00	0.84	0.01	98	653.6	26.27	606.5	8.68	616.5	7.46
BH-005	25	0.12	0.00	0.11	0.00	1.76	0.03	63	1948.7	25.1	654.6	9.79	1031.2	11.35
BH-005	26	0.06	0.00	0.08	0.00	0.69	0.01	97	593.1	27.24	517.7	7.5	531.8	6.85
BH-005	27	0.09	0.00	0.08	0.00	1.04	0.02	72	1409.5	25.4	523.3	7.84	724.2	8.9
BH-005	28	0.06	0.00	0.09	0.00	0.78	0.01	95	700.3	29.47	557.2	8.1	586.1	7.73
BH-005	29	0.06	0.00	0.09	0.00	0.75	0.02	100	571.5	58.33	564.2	9.39	565.7	12.39
BH-005	30	0.06	0.00	0.10	0.00	0.90	0.02	97	714.2	40.67	631.3	9.59	649.7	10.34
BH-005	31	0.11	0.00	0.32	0.00	4.82	0.08	101	1780.9	22.63	1795.8	24.25	1788.8	13.97
BH-005	32	0.09	0.00	0.06	0.00	0.77	0.02	67	1422.1	53.59	391.1	6.8	582.5	12.74
BH-005	33	0.06	0.00	0.09	0.00	0.75	0.01	98	614	35.56	555.8	8.11	567.4	8.33
BH-005	34	0.06	0.00	0.09	0.00	0.69	0.01	103	455.3	34.97	549.3	8.21	531.4	7.91
BH-005	35	0.06	0.00	0.10	0.00	0.84	0.02	95	744.2	31.06	586.4	8.63	619.8	8.4
BH-005	36	0.06	0.00	0.09	0.00	0.79	0.02	93	750.2	56.81	548.7	9.52	589.5	12.83
BH-005	37	0.10	0.00	0.21	0.00	2.88	0.05	77	1605.5	27.23	1234.5	17.62	1377	13.59
BH-005	38	0.13	0.00	0.20	0.00	3.61	0.06	56	2110.5	21.67	1176.5	16.52	1552.7	13.11
BH-005	39	0.06	0.00	0.06	0.00	0.49	0.01	98	445.2	50.81	396.6	6.4	403.8	8.36
BH-005	40	0.08	0.00	0.10	0.00	1.11	0.02	78	1279.1	38.7	594.4	9.29	758.7	11.8
BH-005	41	0.06	0.00	0.09	0.00	0.72	0.02	100	552.3	45.61	553.3	8.62	553.1	9.93
BH-005	42	0.09	0.00	0.08	0.00	0.96	0.02	71	1410.7	22.87	481.8	7.15	680.9	8.08
BH-005	43	0.06	0.00	0.09	0.00	0.72	0.01	102	514.1	36.41	561.9	8.45	552.5	8.33
BH-005	44	0.06	0.00	0.06	0.00	0.50	0.01	89	670.6	37.91	370.6	5.73	415.1	7.02
BH-005	45	0.06	0.00	0.08	0.00	0.66	0.01	97	585.1	36.84	498.2	7.62	513.9	8.08
BH-005	46	0.06	0.00	0.09	0.00	0.82	0.01	93	771.4	23.93	563.8	8.19	606.9	7.22
BH-005	47	0.13	0.00	0.37	0.01	6.55	0.10	99	2066.4	20.21	2040	26.75	2053.1	14.02
BH-005	48	0.06	0.00	0.09	0.00	0.73	0.02	100	556.9	54.84	555	8.98	555.3	11.57
BH-005	49	0.20	0.00	0.55	0.01	15.33	0.25	99	2853.2	18.98	2811.5	34.93	2835.8	15.3
BH-005	50	0.06	0.00	0.10	0.00	0.87	0.02	96	726.7	30.39	607.1	9.11	633	8.52
BH-005	51	0.06	0.00	0.09	0.00	0.71	0.01	101	526.7	36.12	547.3	8.22	543.3	8.19
BH-005	52	0.06	0.00	0.09	0.00	0.78	0.02	95	703.8	55.9	557.3	9.27	587	12.49

BH-005	53	0.08	0.00	0.11	0.00	1.11	0.02	85	1111.4	33.94	646.1	9.55	759.8	10.49
BH-005	54	0.06	0.00	0.11	0.00	0.99	0.02	97	758.5	28.94	681.5	9.97	699.7	8.81
BH-005	55	0.15	0.00	0.44	0.01	9.21	0.17	98	2380.9	25.17	2335.1	32.41	2359.4	17.15
BH-005	56	0.07	0.00	0.09	0.00	0.90	0.02	88	928.9	48.55	577.5	9.42	654.2	12.37
BH-005	57	0.06	0.00	0.11	0.00	0.89	0.02	100	638	39.92	650.9	10.05	647.8	10.25
BH-005	58	0.07	0.00	0.13	0.00	1.34	0.03	93	1025.9	38.57	800.8	11.99	862.7	12.44
BH-005	59	0.13	0.00	0.40	0.01	7.39	0.13	100	2160.5	22.98	2159.1	28.92	2159.7	15.45
BH-005	60	0.08	0.00	0.19	0.00	2.07	0.04	101	1132.4	30.59	1141.9	17.02	1138.5	13.1

Hafnium data tables for detrital zircons

							Scherer et al., 2001 - ^{176}Lu decay constant (1.865x10^{-11})						
							Hf_i	epsilon	1se	T(DM)	T(DM)		
Sample No.	No.	Hf176/Hf177	1 S.D.	Lu176/ Hf177	Yb176/Hf177	U/Pb AGE				(Ga)	(crustal)	Hf Chur (t)	Hf DM (t)
12-37	35	0.2825856	7.981E-05	0.0029951	0.0997791	387	0.282564	0.8	2.8	1.00	1.30	0.282541	0.282973
12-37	44	0.2826322	9.413E-05	0.0016552	0.0556247	440	0.282619	3.9	3.3	0.89	1.15	0.282508	0.282934
12-37	61	0.2825632	0.0001161	0.0018234	0.0542532	444	0.282548	1.5	4.1	1.00	1.30	0.282505	0.282931
12-37	47	0.2826205	4.941E-05	0.0009037	0.0343452	545	0.282611	6.0	1.7	0.89	1.10	0.282442	0.282859
12-37	16	0.2820735	0.0001087	0.0014947	0.0418492	632	0.282056	-11.7	3.9	1.68	2.27	0.282387	0.282796
12-37	52	0.2820017	7.399E-05	0.0011434	0.0363569	647	0.281988	-13.8	2.6	1.77	2.41	0.282377	0.282785
12-37	23	0.2821081	0.0001438	0.001696	0.051276	659	0.282087	-10.0	5.1	1.64	2.18	0.282369	0.282776
12-37	13	0.2822526	3.048E-05	0.0007244	0.0269286	691	0.282243	-3.8	1.1	1.40	1.82	0.282350	0.282753
12-37	46	0.2824167	7.666E-05	0.0023693	0.0755185	708	0.282385	1.7	2.7	1.23	1.50	0.282338	0.282740
12-37	53	0.2821758	5.722E-05	0.0014772	0.0548852	715	0.282156	-6.3	2.0	1.54	2.00	0.282334	0.282736
12-37	10	0.2817076	3.421E-05	0.0009724	0.0327839	726	0.281694	-22.4	1.2	2.17	2.99	0.282327	0.282727
12-37	30	0.2826385	0.0002794	0.0011784	0.0303714	742	0.282622	10.8	9.9	0.87	0.95	0.282317	0.282716
12-37	57	0.282277	6.158E-05	0.0017163	0.0691772	767	0.282252	-1.7	2.2	1.40	1.75	0.282301	0.282698
12-37	18	0.2822038	9.017E-05	0.0008782	0.0284439	783	0.282191	-3.5	3.2	1.47	1.87	0.282291	0.282686
12-37	27	0.2818901	9.461E-05	0.0016283	0.0480548	836	0.281864	-13.9	3.4	1.95	2.55	0.282257	0.282647
12-37	49	0.2822332	4.725E-05	0.0008581	0.0341794	934	0.282218	0.8	1.7	1.43	1.72	0.282194	0.282576
12-37	66	0.2820974	0.0001241	0.0027113	0.0657186	942	0.282049	-5.0	4.4	1.70	2.09	0.282189	0.282570
12-37	8	0.2820138	5.263E-05	0.0008288	0.0236877	970	0.281999	-6.1	1.9	1.74	2.18	0.282171	0.282550
12-37	43	0.2817112	0.0001666	0.0024479	0.0567934	971	0.281666	-17.9	5.9	2.25	2.90	0.282171	0.282549
12-37	50	0.2820816	6.074E-05	0.0007384	0.0256841	984	0.282068	-3.4	2.2	1.64	2.02	0.282163	0.282540
12-37	2	0.2821574	5.609E-05	0.0028822	0.0857217	999	0.282103	-1.8	2.0	1.62	1.94	0.282153	0.282529
12-37	17	0.2821307	0.0001087	0.0012453	0.0351811	1025	0.282107	-1.1	3.9	1.59	1.91	0.282137	0.282510
12-37	69	0.2821656	7.664E-05	0.0008726	0.025402	1053	0.282148	1.0	2.7	1.53	1.80	0.282119	0.282490
12-37	65	0.2821996	0.0001785	0.0022554	0.0718219	1060	0.282155	1.4	6.3	1.54	1.78	0.282114	0.282485
12-37	60	0.2822217	0.0001014	0.0011641	0.0341615	1073	0.282198	3.3	3.6	1.46	1.68	0.282106	0.282475
12-37	15	0.2819757	0.0001399	0.0029399	0.0781258	1154	0.281912	-5.0	5.0	1.89	2.25	0.282054	0.282416
12-37	62	0.2819657	0.000139	0.0011324	0.0333941	1198	0.281940	-3.0	4.9	1.82	2.17	0.282026	0.282383
12-37	9	0.2821171	2.508E-05	0.0005065	0.0202562	1236	0.282105	3.7	0.9	1.58	1.78	0.282001	0.282355
12-37	11	0.2820873	3.676E-05	0.0009608	0.0390489	1263	0.282064	2.9	1.3	1.64	1.86	0.281984	0.282335
12-37	73	0.2819785	0.0001426	0.0016287	0.049164	1363	0.281937	0.6	5.1	1.82	2.07	0.281920	0.282263
12-37	71	0.2818856	6.956E-05	0.0018123	0.0538361	1396	0.281838	-2.2	2.5	1.96	2.26	0.281899	0.282238
12-37	39	0.2816207	7.066E-05	0.0016185	0.0642186	1755	0.281567	-3.6	2.5	2.32	2.63	0.281667	0.281973
12-37	41	0.2814016	8.438E-05	0.000997	0.023563	1834	0.281367	-8.8	3.0	2.59	3.01	0.281616	0.281915
12-37	42	0.2815411	9.068E-05	0.0012423	0.0334185	1892	0.281496	-2.9	3.2	2.41	2.70	0.281578	0.281872
12-37	74	0.2814903	0.00025	0.0040276	0.1096635	1900	0.281345	-8.1	8.9	2.68	3.01	0.281573	0.281866
12-37	78	0.2815821	7.201E-05	0.0014207	0.0467033	1920	0.281530	-1.1	2.6	2.37	2.61	0.281560	0.281851
12-37	80	0.281271	0.0002264	0.0030422	0.0904847	1951	0.281158	-13.5	8.0	2.92	3.37	0.281540	0.281828
12-37	7	0.2810818	3.167E-05	0.0005171	0.0206381	2034	0.281062	-15.1	1.1	2.98	3.52	0.281486	0.281766
12-37	29	0.2812939	0.0001045	0.0006337	0.0133956	2073	0.281269	-6.8	3.7	2.71	3.14	0.281460	0.281737
12-37	34	0.2812742	0.0001111	0.0025329	0.072259	2199	0.281168	-7.5	3.9	2.88	3.28	0.281378	0.281643
33	**1**	0.2824297	6.774E-05	0.0035835	0.1272305	**425**	0.282401	-4.1	2.4	1.25	1.64	0.282517	0.282945
33	**3**	0.2825509	0.0003375	0.0039141	0.1117401	**398**	0.282522	-0.5	11.9	1.08	1.39	0.282535	0.282965
33	**5**	0.2825533	8.714E-05	0.0026801	0.084479	**399**	0.282533	0.0	3.1	1.04	1.37	0.282534	0.282964
33	**2**	0.2819027	0.0005727	0.0015714	0.0457829	**590**	0.281885	-18.7	20.3	1.93	2.68	0.282413	0.282826
33	10	0.2824547	8.416E-05	0.0024098	0.0739736	413	0.282436	-3.2	3.0	1.17	1.57	0.282526	0.282954
33	6	0.2820637	0.000156	0.0024456	0.0746209	450	0.282043	-16.2	5.5	1.74	2.38	0.282502	0.282928
33	7	0.2825134	0.0003562	0.0026938	0.0786544	581	0.282484	2.3	12.6	1.09	1.35	0.282419	0.282833
33	14	0.2821249	0.0001225	0.00247	0.0670815	927	0.282082	-4.2	4.3	1.65	2.05	0.282199	0.282581
33	17	0.2820966	0.0001242	0.0008961	0.0289597	955	0.282081	-3.6	4.4	1.62	2.02	0.282181	0.282561
33	19	0.2824263	0.0001929	0.0031622	0.0955676	418	0.282402	-4.3	6.8	1.24	1.62	0.282522	0.282950
33	23	0.2826389	0.0003908	0.002554	0.0744258	620	0.282609	7.6	13.8	0.91	1.03	0.282394	0.282804

33	22	0.2821718	8.139E-05	0.0006462	0.0199949	1111	0.282158	2.7	2.9	1.51	1.76	0.282082	0.282447
33	21	0.2814352	8.713E-05	0.0014267	0.041265	2537	0.281366	7.4	3.1	2.57	2.59	0.281157	0.281391
33	28	0.2823711	4.585E-05	0.0008495	0.0308568	589	0.282362	-1.9	1.6	1.24	1.62	0.282414	0.282827
33	27	0.2821297	5.681E-05	0.0008306	0.0232187	958	0.282115	-2.3	2.0	1.58	1.95	0.282179	0.282559
33	35	0.2823647	5.373E-05	0.0022428	0.0745749	719	0.282334	0.1	1.9	1.30	1.55	0.282332	0.282733
33	39	0.2823878	4.072E-05	0.0011376	0.037509	425	0.282379	-4.9	1.4	1.23	1.69	0.282518	0.282945
33	40	0.2810425	6.434E-05	0.0009749	0.0326384	2741	0.280991	-1.1	2.3	3.07	3.29	0.281023	0.281237
33	42	0.2827043	6.086E-05	0.0023041	0.0732871	471	0.282684	6.9	2.2	0.80	0.97	0.282488	0.282912
33	44	0.2826514	0.0001926	0.0022363	0.0574611	512	0.282630	5.9	6.8	0.88	1.08	0.282463	0.282883
33	41	0.2818612	5.602E-05	0.0020491	0.0696303	1669	0.281796	2.6	2.0	2.01	2.22	0.281723	0.282037
33	46	0.2824905	3.52E-05	0.0011419	0.0398389	409	0.282482	-1.6	1.2	1.08	1.49	0.282528	0.282957
30	6	0.2826401	2.661E-05	0.0024625	0.1045134	399	0.282622	3.1	0.9	0.90	1.17	0.282534	0.282964
30	12	0.282524	1.873E-05	0.0008416	0.0298796	522	0.282516	2.1	0.7	1.03	1.32	0.282456	0.282875
30	8	0.2825439	2.169E-05	0.0012892	0.0440071	553	0.282530	3.3	0.8	1.01	1.26	0.282436	0.282853
30	13	0.282361	2.662E-05	0.0021094	0.0789118	600	0.282337	-2.5	0.9	1.30	1.68	0.282407	0.282819
30	18	0.2821647	2.086E-05	0.0005302	0.0190976	1059	0.282154	1.4	0.7	1.52	1.80	0.282115	0.282485
30	**19**	0.282441	1.792E-05	0.000569	0.0187288	**523**	0.282435	-0.7	0.6	1.13	1.48	0.282456	0.282875
30	**17**	0.2827047	2.914E-05	0.0011023	0.0363789	**598**	0.282692	10.1	1.0	0.78	0.89	0.282408	0.282820
30	**23**	0.2819812	2.461E-05	0.0007827	0.0302303	**1424**	0.281960	2.8	0.9	1.78	2.00	0.281881	0.282218
30	**21**	0.2825004	3.012E-05	0.0010672	0.0424465	**418**	0.282492	-1.1	1.1	1.07	1.44	0.282522	0.282950
30	**25**	0.2824818	3.805E-05	0.0012357	0.0484932	**480**	0.282471	-0.4	1.3	1.10	1.46	0.282483	0.282906
30	**24**	0.2823495	1.916E-05	0.0007534	0.0299405	**604**	0.282341	-2.2	0.7	1.27	1.66	0.282404	0.282816
30	**26**	0.2825122	3.093E-05	0.0007147	0.029527	**406**	0.282507	-0.8	1.1	1.04	1.42	0.282530	0.282959
30	**27**	0.282451	3.215E-05	0.0017652	0.0656534	**514**	0.282434	-1.0	1.1	1.16	1.52	0.282462	0.282881
30	29	0.2825066	3.586E-05	0.0009877	0.035062	542	0.282497	1.9	1.3	1.06	1.36	0.282444	0.282861
30	31	0.2824979	2.894E-05	0.0009278	0.036595	426	0.282490	-0.9	1.0	1.07	1.41	0.282517	0.282945
30	32	0.2826355	4.486E-05	0.0025936	0.0899304	561	0.282608	6.2	1.6	0.91	1.10	0.282432	0.282847
30	35	0.2817361	2.991E-05	0.0005757	0.0212614	1517	0.281720	-3.6	1.1	2.10	2.48	0.281821	0.282149
30	37	0.2825669	3.131E-05	0.0009633	0.0378136	412	0.282560	1.2	1.1	0.97	1.30	0.282526	0.282955
30	40	0.282492	2.86E-05	0.0012602	0.0495163	409	0.282482	-1.6	1.0	1.08	1.47	0.282528	0.282957
30	41	0.282487	4.162E-05	0.0013103	0.0459693	403	0.282477	-1.9	1.5	1.09	1.49	0.282532	0.282962
30	42	0.2825564	6.07E-05	0.0029204	0.1085791	413	0.282534	0.3	2.1	1.04	1.36	0.282525	0.282954
30	45	0.2824436	4.731E-05	0.001545	0.0585551	405	0.282432	-3.5	1.7	1.16	1.59	0.282530	0.282960
30	44	0.2824187	2.672E-05	0.0009447	0.036491	412	0.282411	-4.0	0.9	1.18	1.62	0.282526	0.282955
30	43	0.2823217	2.706E-05	0.0006517	0.0255239	445	0.282316	-6.7	1.0	1.30	1.82	0.282505	0.282931
30	46	0.2825782	3.303E-05	0.0017268	0.0517582	531	0.282561	3.9	1.2	0.97	1.22	0.282451	0.282869
30	48	0.2825703	2.827E-05	0.0010876	0.0405102	411	0.282562	1.3	1.0	0.97	1.29	0.282526	0.282955
30	51	0.2825448	4.215E-05	0.0020757	0.0642072	432	0.282528	0.5	1.5	1.03	1.34	0.282513	0.282940
30	50	0.2823739	4.088E-05	0.0009897	0.0328075	593	0.282363	-1.7	1.4	1.24	1.62	0.282411	0.282824
30	52	0.2819501	2.32E-05	0.0006775	0.0261812	1001	0.281937	-7.6	0.8	1.82	2.31	0.282152	0.282528
30	53	0.2824601	3.097E-05	0.0015835	0.0528907	523	0.282445	-0.4	1.1	1.14	1.48	0.282456	0.282875
30	55	0.2822698	5.307E-05	0.0021391	0.0790059	582	0.282246	-6.1	1.9	1.43	1.88	0.282418	0.282832
30	56	0.2824445	2.914E-05	0.0011564	0.0436265	540	0.282433	-0.4	1.0	1.15	1.50	0.282445	0.282862
30	57	0.2827017	2.055E-05	0.0004612	0.0159023	606	0.282696	10.4	0.7	0.77	0.87	0.282403	0.282815
30	58	0.2822243	4.404E-05	0.0012464	0.0503542	620	0.282210	-6.5	1.6	1.46	1.97	0.282394	0.282804
30	59	0.2826274	4.305E-05	0.0018844	0.0716595	572	0.282607	6.5	1.5	0.91	1.10	0.282425	0.282839
32c	**6**	0.2824529	3.958E-05	0.001270	0.041905	**415**	0.282443	-2.9	1.4	1.14	1.56	0.282524	0.282953
32c	**7**	0.2823988	0.0003494	0.0040054	0.1198388	**411**	0.282368	-5.6	12.4	1.31	1.73	0.282527	0.282956
32c	**10**	0.2824822	5.488E-05	0.0011201	0.0390365	**394**	0.282474	-2.2	1.9	1.09	1.50	0.282537	0.282968
32c	**13**	0.2825985	7.559E-05	0.0012473	0.0509967	**385**	0.282589	1.6	2.7	0.93	1.25	0.282543	0.282974
32c	**18**	0.2821346	3.756E-05	0.0012571	0.0497288	**491**	0.282123	-12.5	1.3	1.59	2.21	0.282476	0.282898
32c	**22**	0.2825579	7.496E-05	0.0020075	0.0775694	**406**	0.282543	0.5	2.7	1.01	1.34	0.282530	0.282959
32c	**24**	0.2825806	3.859E-05	0.0009078	0.0298567	**459**	0.282573	2.7	1.4	0.95	1.24	0.282496	0.282921

32c	**30**	0.2821985	4.654E-05	0.0006154	0.0247523	**469**	0.282193	-10.5	1.6	1.47	2.07	0.282490	0.282914
32c	**31**	0.2824979	7.9E-05	0.0016208	0.0568091	**414**	0.282485	-1.4	2.8	1.09	1.46	0.282524	0.282953
32c	**43**	0.2825882	4.484E-05	0.0016644	0.054329	**495**	0.282573	3.5	1.6	0.96	1.22	0.282473	0.282895
32c	**49**	0.2826083	9.879E-05	0.0022788	0.0913216	**344**	0.282594	0.9	3.5	0.94	1.26	0.282569	0.283004
32c	**51**	0.2824892	4.001E-05	0.0014039	0.0565105	**352**	0.282480	-3.0	1.4	1.09	1.51	0.282564	0.282998
32c	**58**	0.2824969	5.437E-05	0.0010896	0.0423448	**493**	0.282487	0.4	1.9	1.07	1.41	0.282475	0.282896
32c	**60**	0.2826767	0.0001057	0.0013859	0.0551691	**409**	0.282666	4.9	3.7	0.82	1.06	0.282528	0.282957
32c	**63**	0.2825196	5.515E-05	0.000484	0.0155892	**378**	0.282516	-1.1	2.0	1.02	1.42	0.282547	0.282979
32c	**64**	0.2826314	3.845E-05	0.0009202	0.0344334	**449**	0.282624	4.3	1.4	0.88	1.13	0.282502	0.282928
32c	**65**	0.2824665	4.55E-05	0.0012133	0.0534593	**404**	0.282457	-2.6	1.6	1.12	1.53	0.282531	0.282961
32c	**66**	0.2824035	5.916E-05	0.0022279	0.0828057	**424**	0.282386	-4.7	2.1	1.24	1.68	0.282518	0.282946
32c	**67**	0.282462	4.755E-05	0.0011195	0.0420789	**415**	0.282453	-2.5	1.7	1.12	1.53	0.282524	0.282952
32c	**69**	0.2824501	3.911E-05	0.0008202	0.0333939	**414**	0.282444	-2.9	1.4	1.13	1.57	0.282525	0.282953
32c	**71**	0.2819221	6.662E-05	0.0011578	0.0383817	**475**	0.281912	-20.3	2.4	1.88	2.71	0.282486	0.282910
12-42b	12-42b-11	0.2825521	3.056E-05	0.0013454	0.057242	359	0.282543	-0.6	1.1	1.00	1.37	0.282559	0.282993
12-42b	12-42b-29	0.2825745	3.784E-05	0.0016606	0.0714702	363	0.282563	0.2	1.3	0.98	1.32	0.282557	0.282990
12-42b	12-42b-55	0.2824456	2.553E-05	0.0012345	0.0513587	371	0.282437	-4.1	0.9	1.15	1.60	0.282552	0.282984
12-42b	12-42b-58	0.2824661	2.397E-05	0.0011953	0.0501488	379	0.282458	-3.1	0.8	1.12	1.55	0.282546	0.282978
12-42b	12-42b-04	0.2824525	3.155E-05	0.0008754	0.0323315	392	0.282446	-3.3	1.1	1.13	1.56	0.282539	0.282969
12-42b	12-42b-56	0.2825638	3.727E-05	0.0018428	0.0734481	394	0.282550	0.5	1.3	1.00	1.33	0.282537	0.282968
12-42b	12-42b-63	0.2825754	3.076E-05	0.0010074	0.0450742	438	0.282567	2.0	1.1	0.96	1.26	0.282509	0.282936
12-42b	12-42b-38	0.2825356	2.85E-05	0.0006865	0.0290194	441	0.282530	0.8	1.0	1.01	1.34	0.282507	0.282934
12-42b	12-42b-19	0.282432	4.92E-05	0.0022804	0.0886253	514	0.282410	-1.8	1.7	1.20	1.57	0.282461	0.282881
12-42b	12-42b-07	0.2825605	2.679E-05	0.0005756	0.0228553	525	0.282555	3.6	0.9	0.97	1.24	0.282454	0.282873
12-42b	12-42b-30	0.2824238	2.603E-05	0.0009972	0.0399082	545	0.282414	-1.0	0.9	1.17	1.54	0.282441	0.282858
12-42b	12-42b-52	0.2825259	2.763E-05	0.0012976	0.0493442	626	0.282511	4.3	1.0	1.04	1.27	0.282390	0.282800
12-42b	12-42b-64	0.2822291	3.064E-05	0.0005968	0.0181137	642	0.282222	-5.6	1.1	1.43	1.90	0.282380	0.282788
12-42b	12-42b-61	0.2824781	3.705E-05	0.0012106	0.0471776	643	0.282463	3.0	1.3	1.10	1.37	0.282380	0.282788
12-42b	12-42b-73	0.2819245	2.575E-05	0.0007724	0.029689	657	0.281915	-16.1	0.9	1.86	2.56	0.282371	0.282778
12-42b	12-42b-77	0.2824495	2.287E-05	0.0006764	0.0259873	679	0.282441	3.0	0.8	1.13	1.39	0.282357	0.282762
12-42b	12-42b-49	0.2820927	9.468E-05	0.0019644	0.0717356	685	0.282067	-10.1	3.4	1.68	2.21	0.282353	0.282757
12-42b	12-42b-71	0.2826649	2.949E-05	0.0011577	0.0365817	692	0.282650	10.7	1.0	0.84	0.92	0.282348	0.282752
12-42b	12-42b-54	0.2827573	2.724E-05	0.0005746	0.0250506	716	0.282750	14.7	1.0	0.69	0.68	0.282333	0.282735
12-42b	12-42b-08	0.2820145	2.998E-05	0.0011297	0.0437012	1324	0.281986	1.5	1.1	1.75	1.98	0.281945	0.282291
12-42b	12-42b-57	0.2815415	2.294E-05	0.0005914	0.0218227	1785	0.281521	-4.5	0.8	2.37	2.70	0.281647	0.281951
12-42b	12-42b-23	0.2816329	2.416E-05	0.000995	0.0378976	1996	0.281595	3.0	0.9	2.27	2.42	0.281511	0.281795
12-42b	12-42b-14	0.2815903	1.968E-05	0.000416	0.0150941	2075	0.281574	4.1	0.7	2.29	2.44	0.281459	0.281736
12-42b	12-42b-05	0.2815115	2.038E-05	8.249E-05	0.0042988	2113	0.281508	2.6	0.7	2.38	2.57	0.281435	0.281708
12-43	12-43-69	0.2825423	1.916E-05	0.0009526	0.036789	358	0.282536	-0.9	0.7	1.00	1.39	0.282560	0.282994

12-43	12-43-12	0.2826	2.834E-05	0.0012636	0.051024	358	0.282592	1.1	1.0	0.93	1.26	0.282560	0.282994
12-43	12-43-06	0.282566	3.265E-05	0.002032	0.081173	359	0.282552	-0.3	1.2	1.00	1.35	0.282560	0.282993
12-43	12-43-76	0.2825365	2.803E-05	0.0019385	0.0723395	360	0.282523	-1.3	1.0	1.04	1.41	0.282559	0.282993
12-43	12-43-09	0.2825604	2.762E-05	0.0008835	0.0412907	361	0.282554	-0.1	1.0	0.98	1.34	0.282558	0.282992
12-43	12-43-27	0.2825775	3.123E-05	0.0018025	0.0711035	361	0.282565	0.3	1.1	0.98	1.32	0.282558	0.282992
12-43	12-43-04	0.2825818	5.526E-05	0.00151	0.0695244	362	0.282572	0.5	2.0	0.96	1.30	0.282558	0.282991
12-43	12-43-30	0.2825381	7.025E-05	0.0032952	0.0968719	362	0.282516	-1.5	2.5	1.08	1.43	0.282557	0.282991
12-43	12-43-62	0.2824901	1.985E-05	0.0004538	0.0193406	364	0.282487	-2.4	0.7	1.06	1.49	0.282556	0.282990
12-43	12-43-20	0.2825533	3.065E-05	0.0014114	0.0554213	365	0.282544	-0.4	1.1	1.00	1.36	0.282556	0.282989
12-43	12-43-26	0.2825815	3.273E-05	0.0018662	0.072707	366	0.282569	0.5	1.2	0.97	1.31	0.282555	0.282988
12-43	12-43-07	0.2825165	2.963E-05	0.0006001	0.0241728	366	0.282512	-1.5	1.0	1.03	1.43	0.282555	0.282988
12-43	12-43-65	0.2824958	7.148E-05	0.002063	0.0642689	367	0.282482	-2.6	2.5	1.10	1.50	0.282554	0.282987
12-43	12-43-58	0.2825323	2.96E-05	0.0015565	0.060853	367	0.282522	-1.1	1.0	1.03	1.41	0.282554	0.282987
12-43	12-43-08	0.2825652	2.349E-05	0.0013267	0.0529026	369	0.282556	0.1	0.8	0.98	1.33	0.282553	0.282986
12-43	12-43-46	0.2826158	8.186E-05	0.0026544	0.1186753	370	0.282597	1.6	2.9	0.94	1.24	0.282552	0.282985
12-43	12-43-71	0.2824636	4.119E-05	0.0020504	0.0827773	371	0.282449	-3.6	1.5	1.15	1.57	0.282552	0.282984
12-43	12-43-49	0.2825909	3.013E-05	0.0016539	0.0644561	374	0.282579	1.0	1.1	0.95	1.28	0.282550	0.282983
12-43	12-43-39	0.2825693	3.186E-05	0.0022628	0.0903718	374	0.282553	0.1	1.1	1.00	1.34	0.282550	0.282982
12-43	12-43-47	0.2825722	3.138E-05	0.0014827	0.0612297	377	0.282562	0.5	1.1	0.98	1.32	0.282548	0.282980
12-43	12-43-52	0.2824716	2.367E-05	0.0011756	0.0482343	377	0.282463	-3.0	0.8	1.11	1.53	0.282548	0.282980
12-43	12-43-40	0.2825476	3.182E-05	0.0013903	0.0558277	381	0.282538	-0.3	1.1	1.01	1.37	0.282546	0.282978
12-43	12-43-22	0.2825414	3.241E-05	0.0018552	0.0679882	388	0.282528	-0.5	1.1	1.03	1.38	0.282541	0.282972
12-43	12-43-50	0.2825439	3.271E-05	0.0015851	0.068896	391	0.282532	-0.2	1.2	1.02	1.37	0.282539	0.282970
12-43	12-43-48	0.2825004	2.101E-05	0.0004431	0.016658	391	0.282497	-1.5	0.7	1.05	1.45	0.282539	0.282970
12-43	12-43-64	0.2824793	2.621E-05	0.0005943	0.0262569	417	0.282475	-1.7	0.9	1.08	1.48	0.282523	0.282951
12-43	12-43-43	0.2816623	2.107E-05	0.0003284	0.0116583	427	0.281660	-30.3	0.7	2.19	3.24	0.282517	0.282944
12-43	12-43-74	0.2821589	3.026E-05	0.0008473	0.0265994	639	0.282149	-8.3	1.1	1.54	2.06	0.282382	0.282791
12-43	12-43-56	0.2822049	3.477E-05	0.0015042	0.0635734	642	0.282187	-6.9	1.2	1.50	1.97	0.282381	0.282789
12-43	12-43-51	0.2823218	3.672E-05	0.0014522	0.0560219	686	0.282303	-1.7	1.3	1.33	1.68	0.282352	0.282756
12-43	12-43-38	0.2820545	2.684E-05	0.0010682	0.0434346	773	0.282039	-9.1	1.0	1.69	2.21	0.282297	0.282693
12-43	12-43-19	0.2817503	1.972E-05	0.0005483	0.0207839	1029	0.281740	-14.0	0.7	2.08	2.70	0.282134	0.282507
12-43	12-43-79	0.2817265	3.503E-05	0.0017049	0.0591774	1041	0.281693	-15.3	1.2	2.18	2.79	0.282126	0.282498
12-43	12-43-33	0.2821655	2.411E-05	0.0001006	0.0044722	1162	0.282163	4.1	0.9	1.50	1.70	0.282049	0.282410
12-43	12-43-68	0.2821061	1.748E-05	0.0004998	0.0191364	1209	0.282095	2.7	0.6	1.59	1.81	0.282019	0.282376
12-43	12-43-60	0.2819443	2.764E-05	0.0007215	0.0287589	1520	0.281924	3.7	1.0	1.83	2.00	0.281819	0.282147

12-43	12-43-67	0.2813283	1.783E-05	0.0004408	0.0167825	2021	0.281311	-6.5	0.6	2.65	3.01	0.281494	0.281776
12-43	12-43-05	0.2815128	1.753E-05	0.0004109	0.0113389	2041	0.281497	0.5	0.6	2.40	2.60	0.281482	0.281761
12-43	12-43-37	0.2814496	1.678E-05	0.0003561	0.0135396	2076	0.281436	-0.8	0.6	2.48	2.76	0.281458	0.281735
12-43	12-43-57	0.2810356	2.481E-05	0.0006025	0.0257557	2427	0.281008	-7.9	0.9	3.05	3.48	0.281229	0.281473
12-51	12-51-16	0.2825111	8.082E-05	0.0011443	0.0399261	345	0.282504	-2.3	2.9	1.05	1.46	0.282568	0.283003
12-51	12-51-17	0.2825492	4.206E-05	0.0013823	0.0554469	382	0.282539	-0.2	1.5	1.01	1.36	0.282545	0.282977
12-51	12-51-46	0.2827297	4.188E-05	0.0008941	0.0322719	401	0.282723	6.7	1.5	0.74	0.94	0.282533	0.282962
12-51	12-51-37	0.2824972	3.833E-05	0.0011204	0.044199	411	0.282489	-1.3	1.4	1.07	1.46	0.282526	0.282956
12-51	12-51-11	0.2824601	4.358E-05	0.0018173	0.0602294	426	0.282446	-2.5	1.5	1.15	1.54	0.282517	0.282944
12-51	12-51-13	0.2824124	5.297E-05	0.0013086	0.0470046	428	0.282402	-4.0	1.9	1.20	1.64	0.282516	0.282943
12-51	12-51-70	0.2823881	4.271E-05	0.0006508	0.0259856	434	0.282383	-4.6	1.5	1.21	1.68	0.282512	0.282939
12-51	12-51-12	0.2823818	5.789E-05	0.0013473	0.0536086	439	0.282371	-4.9	2.1	1.24	1.70	0.282509	0.282936
12-51	12-51-36	0.2823941	4.646E-05	0.0016457	0.0596044	448	0.282380	-4.3	1.6	1.23	1.67	0.282503	0.282929
12-51	12-51-41	0.2823197	4.926E-05	0.0012456	0.0466191	544	0.282307	-4.8	1.7	1.33	1.77	0.282442	0.282860
12-51	12-51-33	0.2824413	8.93E-05	0.00201	0.0632337	548	0.282421	-0.7	3.2	1.18	1.52	0.282440	0.282857
12-51	12-51-42	0.2824502	4.097E-05	0.0010114	0.0403602	552	0.282440	0.1	1.5	1.13	1.48	0.282437	0.282854
12-51	12-51-49	0.2823945	4.186E-05	0.0020775	0.0780237	572	0.282372	-1.9	1.5	1.25	1.61	0.282425	0.282840
12-51	12-51-74	0.2825631	5.588E-05	0.0010806	0.034822	573	0.282552	4.5	2.0	0.98	1.21	0.282424	0.282838
12-51	12-51-48	0.2821647	4.793E-05	0.0007048	0.0233007	590	0.282157	-9.1	1.7	1.52	2.07	0.282413	0.282826
12-51	12-51-04	0.2825244	4.635E-05	0.0007952	0.0296996	592	0.282516	3.7	1.6	1.02	1.28	0.282412	0.282824
12-51	12-51-40	0.282593	7.285E-05	0.0018261	0.0555071	606	0.282572	6.0	2.6	0.95	1.15	0.282403	0.282815
12-51	12-51-72	0.2825331	5.349E-05	0.0015327	0.0502911	622	0.282515	4.3	1.9	1.03	1.26	0.282393	0.282803
12-51	12-51-56	0.2824102	4.515E-05	0.0015429	0.0522308	634	0.282392	0.2	1.6	1.21	1.53	0.282385	0.282794
12-51	12-51-71	0.2821113	8.428E-05	0.0005407	0.015541	640	0.282105	-9.8	3.0	1.59	2.16	0.282381	0.282790
12-51	12-51-77	0.2822596	4.324E-05	0.0006528	0.0219865	673	0.282251	-3.9	1.5	1.39	1.82	0.282361	0.282766
12-51	12-51-10	0.2821817	8.992E-05	0.0005854	0.0169935	677	0.282174	-6.5	3.2	1.49	1.98	0.282358	0.282763
12-51	12-51-09	0.2826515	3.926E-05	0.0002186	0.0067066	697	0.282649	10.7	1.4	0.83	0.92	0.282346	0.282749
12-51	12-51-78	0.2821091	3.432E-05	0.0008502	0.0282811	781	0.282097	-6.9	1.2	1.60	2.06	0.282292	0.282688
12-51	12-51-03	0.2821331	3.622E-05	0.0001523	0.0055969	1048	0.282130	0.3	1.3	1.54	1.83	0.282122	0.282493
12-51	12-51-65	0.2820818	9.547E-05	0.0014745	0.0546495	1422	0.282042	5.7	3.4	1.67	1.80	0.281882	0.282219
12-51	12-51-67	0.2817766	4.547E-05	0.000985	0.0380987	1598	0.281747	-0.8	1.6	2.07	2.33	0.281769	0.282090
12-51	12-51-80	0.2816177	5.584E-05	0.0007777	0.0226398	2061	0.281587	4.2	2.0	2.28	2.40	0.281468	0.281746
12-51	12-51-79	0.2815541	4.114E-05	0.0001753	0.0066096	2081	0.281547	3.3	1.5	2.33	2.47	0.281455	0.281731
12-51	12-51-08	0.2811729	4.517E-05	0.0004918	0.0183225	2533	0.281149	-0.4	1.6	2.86	3.09	0.281160	0.281393

12-51	12-51-39	0.2808941	5.968E-05	0.0015482	0.0496382	2883	0.280809	-4.3	2.1	3.32	3.61	0.280929	0.281130
56b	56B_3	0.2825352	5.045E-05	0.0018402	0.0701485	371	0.282522	-1.0	1.8	1.04	1.41	0.282551	0.282984
56b	56B_5	0.2825555	3.111E-05	0.0011613	0.0402477	369	0.282548	-0.2	1.1	0.99	1.35	0.282553	0.282986
56b	56B_31	0.2825362	4.769E-05	0.0028041	0.0880515	358	0.282517	-1.5	1.7	1.06	1.41	0.282560	0.282994
56b	56B_40	0.2825265	2.222E-05	0.0012632	0.0498223	396	0.282517	-0.7	0.8	1.03	1.41	0.282536	0.282966
56b	56B_47	0.2826306	1.948E-05	0.0005605	0.0198809	767	0.282623	11.4	0.7	0.87	0.94	0.282301	0.282698
56b	56B_51	0.2825267	2.47E-05	0.0010297	0.0380795	339	0.282520	-1.8	0.9	1.03	1.44	0.282572	0.283008
44a	**150**	0.2825563	2.147E-05	0.0004488	0.0150873	**308**	0.282554	-1.3	0.8	0.97	1.38	0.282591	0.283030
44a	**44a-17**	0.282569	3.953E-05	0.0011653	0.0506029	**312**	0.282562	-0.9	1.4	0.97	1.35	0.282589	0.283027
44a	**123**	0.2824852	3.057E-05	0.0010826	0.0522473	**384**	0.282477	-2.3	1.1	1.09	1.50	0.282543	0.282975
44a	**158**	0.2824382	2.372E-05	0.0007007	0.0263178	**388**	0.282433	-3.8	0.8	1.14	1.59	0.282541	0.282972
44a	**128**	0.2824448	4.12E-05	0.0017445	0.0680236	**393**	0.282432	-3.7	1.5	1.17	1.59	0.282538	0.282969
44a	**129**	0.2824597	5.745E-05	0.0014724	0.0506813	**404**	0.282449	-2.9	2.0	1.14	1.55	0.282531	0.282961
44a	**132**	0.282429	5.652E-05	0.001736	0.0584825	**407**	0.282416	-4.0	2.0	1.19	1.62	0.282529	0.282958
44a	**125**	0.2824633	2.313E-05	0.0008535	0.0289998	**411**	0.282457	-2.5	0.8	1.11	1.53	0.282526	0.282956
44a	**142**	0.2825721	2.984E-05	0.0011285	0.0493624	**411**	0.282563	1.3	1.1	0.97	1.29	0.282526	0.282955
44a	**44a-27**	0.2824536	2.564E-05	0.0010683	0.0375311	**417**	0.282445	-2.7	0.9	1.13	1.55	0.282523	0.282951
44a	**146**	0.2825202	6.747E-05	0.0028957	0.0944666	**424**	0.282497	-0.8	2.4	1.09	1.43	0.282519	0.282946
44a	**140**	0.2825357	5.544E-05	0.0020145	0.0654373	**426**	0.282520	0.1	2.0	1.04	1.38	0.282517	0.282945
44a	**138**	0.2824496	2.002E-05	0.0008777	0.0302981	**432**	0.282443	-2.5	0.7	1.13	1.55	0.282513	0.282940
44a	**44a-45**	0.2825578	2.089E-05	0.0013302	0.0498722	**444**	0.282547	1.4	0.7	0.99	1.31	0.282506	0.282932
44a	**44a-13**	0.282631	0.0001033	0.0034933	0.1142507	**444**	0.282602	3.4	3.7	0.94	1.18	0.282506	0.282932
44a	**44a-10**	0.2824253	3.45E-05	0.001387	0.0445208	**446**	0.282414	-3.2	1.2	1.18	1.60	0.282504	0.282930
44a	**44a-35**	0.2824311	2.792E-05	0.001115	0.0451092	**447**	0.282422	-2.9	1.0	1.16	1.58	0.282504	0.282930
44a	**44a-25**	0.2825852	2.306E-05	0.0003885	0.0153255	**451**	0.282582	2.9	0.8	0.93	1.22	0.282501	0.282927
44a	**135**	0.2824723	2.268E-05	0.0011485	0.0431066	**452**	0.282463	-1.3	0.8	1.11	1.49	0.282500	0.282926
44a	**44a-24**	0.282478	4.686E-05	0.0008633	0.0302654	**455**	0.282471	-1.0	1.7	1.09	1.47	0.282499	0.282924
44a	**44a-2**	0.282499	3.755E-05	0.0013774	0.0613203	**457**	0.282487	-0.4	1.3	1.08	1.43	0.282497	0.282922
44a	**44a-53**	0.2825343	2.672E-05	0.0012225	0.050086	**459**	0.282524	1.0	0.9	1.02	1.35	0.282496	0.282921
44a	**44a-86**	0.2824824	1.973E-05	0.0006808	0.0259442	**462**	0.282477	-0.6	0.7	1.08	1.45	0.282494	0.282919
44a	**44a-85**	0.2820447	2.061E-05	0.0008862	0.0273531	**496**	0.282036	-15.4	0.7	1.70	2.39	0.282473	0.282894
44a	**44a-98**	0.2823607	2.421E-05	0.0010402	0.0415272	**549**	0.282350	-3.2	0.9	1.26	1.67	0.282439	0.282856
44a	**44a-80**	0.2824926	5.163E-05	0.0020713	0.0819737	**561**	0.282471	1.4	1.8	1.11	1.40	0.282432	0.282847
44a	**44a-44**	0.2825907	2.211E-05	0.0009065	0.0348091	**640**	0.282580	7.0	0.8	0.93	1.11	0.282381	0.282790
44a	**44a-54**	0.2824262	1.755E-05	0.000916	0.0313219	**642**	0.282415	1.2	0.6	1.17	1.47	0.282381	0.282789
44a	**44a-43**	0.2824526	2.178E-05	0.0009928	0.0305516	**652**	0.282440	2.4	0.8	1.13	1.41	0.282374	0.282781
44a	**44a-30**	0.2825565	3.626E-05	0.0027469	0.1003992	**661**	0.282522	5.5	1.3	1.03	1.22	0.282368	0.282774
44a	**44a-28**	0.282529	3.235E-05	0.0021483	0.0716141	**679**	0.282502	5.1	1.1	1.06	1.25	0.282357	0.282761
44a	**44a-75**	0.2822557	3.63E-05	0.0012456	0.0404308	**696**	0.282239	-3.8	1.3	1.42	1.81	0.282346	0.282749
44a	**44a-40**	0.282238	2.29E-05	0.0006651	0.0276169	**1037**	0.282225	3.4	0.8	1.42	1.67	0.282129	0.282501
44a	**44a-51**	0.2821598	2.015E-05	0.0006465	0.0244492	**1213**	0.282145	4.6	0.7	1.53	1.73	0.282016	0.282373
20	20_43	0.282352	0.000011	0.000905	0.0396092	545	0.2823428	-3.505	0.39	1.269	1.612	0.2824417	0.2828587
20	20_11	0.282135	0.000016	0.0011401	0.0538385	575	0.2821227	-10.624	0.567	1.581	2.159	0.2824227	0.282837
20	20_72	0.282389	0.0000069	0.001317	0.0633386	585	0.2823746	-1.482	0.244	1.231	1.553	0.2824164	0.2828298
20	20_14	0.282226	0.0000095	0.0009449	0.0384846	593	0.2822155	-6.935	0.337	1.446	1.854	0.2824113	0.282824
20	20_30	0.282631	0.000011	0.001746	0.0794413	604	0.2826112	7.325	0.389	0.898	1.038	0.2824044	0.282816
20	20_30	0.282631	0.000011	0.001746	0.0794413	604	0.2826112	7.325	0.389	0.898	1.038	0.2824044	0.282816
20	20_25	0.28189	0.0000073	0.0004092	0.0184138	622	0.2818852	-17.98	0.259	1.886	2.613	0.282393	0.282803
20	20_60	0.282405	0.0000088	0.0017336	0.0716185	637	0.2823843	0.029	0.312	1.222	1.544	0.2823835	0.2827921
20	20_24	0.282503	0.00001	0.0005072	0.0228132	658	0.2824967	4.484	0.354	1.047	1.274	0.2823701	0.2827769
20	20_65	0.282731	0.000009	0.0007791	0.0359503	683	0.282721	12.989	0.318	0.735	0.766	0.2823543	0.2827587
20	20_63	0.282478	0.0000092	0.0004656	0.0204897	700	0.2824719	4.548	0.326	1.08	1.313	0.2823435	0.2827464

20	20_62	0.282686	0.000013	0.0035294	0.149497	761	0.2826356	11.719	0.46	0.86	0.904	0.2823047	0.2827021
20	20_40	0.282407	0.000011	0.0006458	0.031024	780	0.2823975	3.716	0.39	1.184	1.431	0.2822926	0.2826883
20	20_1	0.282347	0.0000088	0.0004763	0.0205508	870	0.2823392	3.679	0.312	1.262	1.491	0.2822354	0.2826229
20	20_7	0.28219	0.000013	0.0017224	0.088791	1146	0.2821528	3.32	0.461	1.528	1.706	0.2820591	0.2824214
20	20_27	0.282086	0.0000071	0.0002778	0.0128902	1190	0.2820798	1.73	0.252	1.613	1.855	0.282031	0.2823892
20	20_27	0.282086	0.0000071	0.0002778	0.0128902	1190	0.2820798	1.73	0.252	1.613	1.882	0.282031	0.2823892
20	20_12	0.281614	0.0000086	0.0002988	0.0137735	1314	0.2816066	-12.23	0.305	2.254	2.784	0.2819514	0.2822983
20	20_50	0.281944	0.000011	0.0010428	0.0518586	1418	0.2819161	1.117	0.39	1.842	2.073	0.2818846	0.2822219
20	20_29	0.281333	0.0000078	0.0001235	0.0055409	1943	0.2813284	-7.696	0.277	2.62	3.068	0.2815451	0.281834
20	20_19	0.281467	0.000009	0.0008977	0.0410314	2027	0.2814324	-2.063	0.32	2.491	2.783	0.2814905	0.2817716
20	20_59	0.281127	0.0000075	0.0004235	0.020411	2037	0.2811106	-13.265	0.267	2.917	3.481	0.281484	0.2817641
20	20_64	0.281601	0.0000095	0.0009665	0.0491946	2087	0.2815626	3.952	0.337	2.311	2.427	0.2814514	0.2817269
20	20_45	0.281543	0.00001	0.0007996	0.0382364	2090	0.2815112	2.194	0.355	2.381	2.556	0.2814495	0.2817247
20	20_58	0.281288	0.000015	0.000682	0.0315074	2123	0.2812605	-5.952	0.533	2.719	3.102	0.281428	0.2817001
20	20_78	0.281503	0.0000074	0.0005519	0.0253342	2180	0.2814801	3.174	0.263	2.42	2.578	0.2813908	0.2816576
20	20_78	0.281503	0.0000074	0.0005519	0.0253342	2180	0.2814801	3.174	0.263	2.42	2.576	0.2813908	0.2816576
20	20_36	0.281089	0.000014	0.0012124	0.0520354	2399	0.2810335	-7.61	0.498	3.029	3.365	0.2812476	0.2814939
20	20_32	0.281117	0.0000084	0.0002191	0.0101138	2451	0.2811068	-3.795	0.299	2.915	3.188	0.2812135	0.281455
20	20_32	0.281117	0.0000084	0.0002191	0.0101138	2451	0.2811068	-3.795	0.299	2.915	3.225	0.2812135	0.281455
20	20_42	0.280741	0.000008	0.0007815	0.0321756	2638	0.2807016	-13.839	0.285	3.462	3.941	0.2810906	0.2813145
20	20_21	0.280916	0.00001	0.0013024	0.0577142	2936	0.2808427	-1.822	0.356	3.272	3.489	0.2808939	0.2810897
20	20_74	0.280948	0.0000063	0.0003154	0.0139847	2967	0.2809301	2.019	0.224	3.147	3.258	0.2808734	0.2810663
20	20_48	0.280706	0.000012	0.0014615	0.0645937	3075	0.2806197	-6.482	0.427	3.571	3.853	0.2808018	0.2809844
20	20_66	0.280713	0.0000085	0.0013828	0.0668241	3305	0.2806251	-0.845	0.303	3.554	3.719	0.2806488	0.2808096
22a	22A_1	0.282598	0.000016	0.0026603	0.120504	571	0.2825695	5.107	0.566	0.969	1.178	0.2824253	0.2828399
22a	22A_10	0.282127	0.0000064	0.00083	0.0361996	721	0.2821158	-7.593	0.227	1.579	2.086	0.2823301	0.2827312
22a	22A_11	0.282366	0.0000065	0.0014615	0.068088	504	0.2823522	-4.089	0.23	1.268	1.698	0.2824677	0.2828884
22a	22A_13	0.28251	0.000016	0.0011613	0.0482818	640	0.2824961	4.055	0.566	1.055	1.296	0.2823815	0.2827899
22a	22A_16	0.281551	0.000014	0.0025251	0.116302	560	0.2815245	-32.141	0.497	2.481	3.281	0.2824322	0.2828478
22a	22A_18	0.282102	0.000008	0.0009944	0.041332	661	0.2820897	-9.865	0.284	1.621	2.18	0.2823682	0.2827747
22a	22A_2	0.281025	0.0000076	0.0008309	0.0373544	2751	0.2809813	-1.241	0.27	3.085	3.283	0.2810161	0.2812294
22a	22A_21	0.281551	0.0000075	0.0003498	0.0123125	600	0.2815471	-30.447	0.266	2.342	3.39	0.2824069	0.2828189
22a	22A_22	0.281461	0.000012	0.0008458	0.0369657	2042	0.2814282	-1.867	0.426	2.495	2.784	0.2814807	0.2817604
22a	22A_23	0.282392	0.000012	0.0016346	0.0705182	577	0.2823743	-1.67	0.425	1.237	1.56	0.2824215	0.2828355
22a	22A_26	0.282312	0.000012	0.002455	0.105331	605	0.2822841	-4.235	0.425	1.381	1.722	0.2824037	0.2828153
22a	22A_27	0.281617	0.0000099	0.0006428	0.0296524	2097	0.2815914	5.204	0.352	2.27	2.385	0.2814449	0.2817195
22a	22A_28	0.281104	0.000014	0.000654	0.0266154	2505	0.2810727	-3.745	0.498	2.965	3.267	0.281178	0.2814145
22a	22A_3	0.282359	0.000014	0.0025497	0.116153	548	0.2823328	-3.79	0.496	1.316	1.703	0.2824398	0.2828565
22a	22A_31	0.282197	0.000011	0.0014144	0.0596014	643	0.2821799	-7.072	0.39	1.505	1.938	0.2823796	0.2827877
22a	22A_34	0.282431	0.00001	0.0019687	0.0880662	898	0.2823978	6.386	0.354	1.192	1.355	0.2822175	0.2826025
22a	22A_4	0.28157	0.0000054	0.001364	0.0590018	2011	0.2815179	0.603	0.192	2.379	2.607	0.2815009	0.2817835
22a	22A_48	0.281908	0.000021	0.0021993	0.105509	743	0.2818773	-15.545	0.745	1.952	2.58	0.2823162	0.2827152
22a	22A_51	0.282355	0.000013	0.0035321	0.159324	499	0.282322	-5.27	0.46	1.359	1.764	0.2824708	0.282892
22a	22A_7	0.282516	0.0000054	0.0012283	0.0501874	887	0.2824955	9.601	0.191	1.048	1.145	0.2822245	0.2826105
22a	22A_72	0.282132	0.0000092	0.0010137	0.0344522	658	0.2821195	-8.877	0.326	1.58	2.054	0.2823701	0.2827769
22a	22A_74	0.282318	0.0000084	0.0026961	0.121046	551	0.2822902	-5.233	0.298	1.382	1.808	0.2824379	0.2828544
22a	22A_75	0.281429	0.0000097	0.0001879	0.0077613	2095	0.2814215	-0.877	0.345	2.496	2.765	0.2814462	0.2817209
22a	22A_8	0.282332	0.00001	0.0009892	0.0377156	538	0.282322	-4.395	0.354	1.3	1.742	0.2824462	0.2828638
26b	26B_15	0.282541	0.000011	0.0007251	0.0274714	599	0.2825329	4.437	0.389	1	1.239	0.2824075	0.2828196
26b	26B_2	0.282437	0.0000083	0.000876	0.0373079	627	0.2824267	1.307	0.294	1.149	1.456	0.2823898	0.2827993
26b	26B_27	0.282525	0.0000097	0.0005312	0.0197765	693	0.2825181	6.027	0.343	1.017	1.213	0.2823479	0.2827515
26b	26B_33	0.282347	0.0000092	0.0022984	0.0979101	696	0.282317	-1.029	0.326	1.325	1.658	0.282346	0.2827493
26b	26B_34	0.282456	0.00001	0.0009011	0.0352025	748	0.2824433	4.617	0.354	1.123	1.347	0.282313	0.2827116
26b	26B_35	0.282503	0.0000087	0.0019283	0.0762958	653	0.2824794	3.756	0.308	1.087	1.324	0.2823733	0.2827805

26b	26B_41	0.282549	0.000011	0.0007793	0.0314111	671	0.2825392	6.279	0.389	0.99	1.181	0.2823619	0.2827674
26b	26B_42	0.28256	0.0000095	0.0008178	0.0354636	733	0.2825487	8.013	0.336	0.976	1.122	0.2823225	0.2827225
26b	26B_45	0.28243	0.0000077	0.0006946	0.0288292	645	0.2824216	1.53	0.273	1.154	1.46	0.2823784	0.2827863
26b	26B_47	0.282587	0.00001	0.0010361	0.0377395	654	0.2825743	7.14	0.354	0.943	1.113	0.2823727	0.2827798
26b	26B_48	0.282537	0.000011	0.0011783	0.0508252	583	0.2825241	3.769	0.389	1.017	1.269	0.2824177	0.2828312
26b	26B_50	0.282564	0.0000086	0.0015713	0.0397375	698	0.2825434	7.036	0.304	0.99	1.154	0.2823447	0.2827479
26b	26B_56	0.282585	0.0000091	0.0016578	0.0659294	603	0.2825663	5.71	0.322	0.962	1.163	0.282405	0.2828167
26b	26B_67	0.282182	0.00001	0.001536	0.069177	723	0.2821611	-5.941	0.354	1.531	1.933	0.2823289	0.2827297
26b	26B_68	0.282589	0.000022	0.003349	0.106873	621	0.28255	5.538	0.779	1.002	1.188	0.2823936	0.2828037
26b	26B_70	0.281317	0.000014	0.001175	0.05451	2063	0.2812709	-6.968	0.498	2.714	3.119	0.2814671	0.2817448
26b	26B_76	0.282429	0.0000085	0.0008025	0.0348144	639	0.2824194	1.317	0.301	1.158	1.464	0.2823822	0.2827906
26b	26B_77	0.282535	0.0000091	0.0018152	0.0822422	581	0.2825152	3.409	0.322	1.038	1.291	0.2824189	0.2828326
26b	26B_8	0.282401	0.00001	0.0010007	0.0379294	756	0.2823868	2.794	0.354	1.204	1.47	0.2823079	0.2827057
27	27_1	0.282689	0.000009	0.0007453	0.0309136	552	0.2826813	8.638	0.318	0.793	0.939	0.2824373	0.2828536
27	27_10	0.282567	0.000013	0.0010414	0.0475767	564	0.282556	4.471	0.46	0.971	1.208	0.2824297	0.282845
27	27_14	0.282559	0.000012	0.0008191	0.0344214	572	0.2825502	4.446	0.425	0.977	1.218	0.2824246	0.2828392
27	27_15	0.28223	0.00001	0.0008754	0.0387902	702	0.2822185	-4.383	0.354	1.438	1.874	0.2823422	0.282745
27	27_19	0.282637	0.0000088	0.0004889	0.0204326	600	0.2826315	7.953	0.311	0.86	1.019	0.2824069	0.2828189
27	27_2	0.2826	0.0000078	0.0007655	0.0332957	577	0.2825917	6.028	0.276	0.918	1.122	0.2824215	0.2828355
27	27_23	0.282497	0.000009	0.0003562	0.0127221	680	0.2824925	4.827	0.319	1.051	1.28	0.2823562	0.2827609
27	27_28	0.282576	0.00001	0.0005667	0.0259661	639	0.2825692	6.623	0.354	0.947	1.134	0.2823822	0.2827906
27	27_3	0.282629	0.0000086	0.00048	0.0207907	653	0.2826231	8.847	0.304	0.871	1.006	0.2823733	0.2827805
27	27_32	0.282457	0.000012	0.0004849	0.0223858	664	0.282451	2.997	0.425	1.11	1.382	0.2823663	0.2827725
27	27_38	0.28236	0.0000095	0.0006419	0.0271885	621	0.2823525	-1.454	0.336	1.249	1.626	0.2823936	0.2828037
27	27_43	0.282585	0.000011	0.0005059	0.0232185	611	0.2825792	6.348	0.389	0.933	1.129	0.2823999	0.2828109
27	27_51	0.282587	0.0000097	0.00047	0.0201725	624	0.2825815	6.721	0.343	0.929	1.116	0.2823917	0.2828015
27	27_60	0.282547	0.000011	0.0004662	0.0212967	639	0.2825414	5.639	0.389	0.985	1.196	0.2823822	0.2827906
27	27_62	0.282569	0.0000053	0.0003245	0.0139085	616	0.2825653	5.966	0.188	0.951	1.157	0.2823968	0.2828073
27	27_63	0.282532	0.0000092	0.0008969	0.0403576	644	0.2825212	5.034	0.326	1.017	1.239	0.282379	0.282787
27	27_64	0.28248	0.0000095	0.0007516	0.0331456	634	0.2824711	3.035	0.336	1.086	1.332	0.2823854	0.2827943
27	27_9	0.28254	0.0000081	0.0004146	0.0124612	590	0.2825354	4.326	0.287	0.993	1.219	0.2824132	0.2828261
25	25-41	0.2817376	3.118E-05	0.0010819	0.0367957	511	0.281727	-26.1	1.1	2.13	3.06	0.282463	0.282884
25	25-64	0.2821903	3.239E-05	0.0008469	0.0322144	513	0.282182	-9.9	1.1	1.49	2.07	0.282462	0.282882
25	25-40	0.2822468	3.061E-05	0.0006035	0.0206499	513	0.282241	-7.8	1.1	1.40	1.94	0.282462	0.282882
25	25-15	0.282296	4.881E-05	0.0013309	0.0539476	541	0.282282	-5.7	1.7	1.36	1.83	0.282444	0.282862
25	25-69	0.2823212	4.323E-05	0.0009231	0.0362112	563	0.282311	-4.2	1.5	1.31	1.75	0.282431	0.282846
25	25-12	0.2822744	3.597E-05	0.0011669	0.0432241	571	0.282262	-5.8	1.3	1.39	1.85	0.282425	0.282840
25	25-47	0.2820324	2.545E-05	0.0009006	0.035812	617	0.282022	-13.2	0.9	1.71	2.35	0.282396	0.282807
25	25-55	0.281539	5.04E-05	0.0009354	0.0281402	624	0.281528	-30.6	1.8	2.39	3.40	0.282392	0.282802
25	25-58	0.2818433	3.144E-05	0.0008985	0.0347334	669	0.281832	-18.8	1.1	1.97	2.72	0.282363	0.282769
25	25-13	0.2823267	3.368E-05	0.0009047	0.0323827	741	0.282314	-0.1	1.2	1.30	1.63	0.282317	0.282716
25	25-32	0.2814609	3.224E-05	0.0007871	0.0272463	906	0.281447	-27.1	1.1	2.49	3.40	0.282213	0.282597
25	25-42	0.2822086	3.554E-05	0.0012624	0.0400963	951	0.282186	0.1	1.3	1.48	1.78	0.282184	0.282564
25	25-72	0.2822611	2.177E-05	0.0009182	0.0353216	1088	0.282242	5.2	0.8	1.40	1.57	0.282096	0.282464
25	25-62	0.2821022	2.198E-05	0.0007031	0.0266185	1215	0.282086	2.5	0.8	1.61	1.83	0.282015	0.282371
25	25-48	0.2824969	5.415E-05	0.0007766	0.0278231	1302	0.282478	18.4	1.9	1.06	0.93	0.281959	0.282307
25	25-59	0.2815947	4.113E-05	0.0007635	0.0312284	1537	0.281573	-8.4	1.5	2.31	2.73	0.281808	0.282135
25	25-70	0.281661	3.28E-05	0.0010883	0.0386378	1766	0.281625	-1.2	1.2	2.24	2.49	0.281660	0.281965
25	25-33	0.281915	3.298E-05	0.0008084	0.0314895	2060	0.281883	14.7	1.2	1.87	1.77	0.281469	0.281747
25	25-38	0.2813324	2.123E-05	0.000327	0.0111458	2066	0.281320	-5.2	0.8	2.63	2.97	0.281465	0.281743
25	25-25	0.2815791	3.648E-05	0.0008305	0.0293893	2114	0.281546	4.0	1.3	2.33	2.46	0.281434	0.281706
25	25-60	0.2823717	2.344E-05	0.0006551	0.0241322	2119	0.282345	32.5	0.8	1.23	0.74	0.281431	0.281703
25	25-26	0.2814527	4.77E-05	0.0012014	0.046961	2162	0.281403	0.0	1.7	2.53	2.77	0.281402	0.281671
25	25-44	0.2813459	3.01E-05	0.0003032	0.0108809	2508	0.281331	5.5	1.1	2.62	2.69	0.281176	0.281412

28	28A-6	0.2822538	4.105E-05	0.0013784	0.0440118	579	0.282239	-6.4	1.5	1.42	1.85	0.282420	0.282834
28	28A-7	0.2810445	6.605E-05	0.0009153	0.0252906	2068	0.281009	-16.2	2.4	3.07	3.69	0.281464	0.281741
28	28A-12	0.280961	5.499E-05	0.0010423	0.0374533	2002	0.280921	-20.8	2.0	3.19	3.91	0.281507	0.281790
28	28A-16	0.2821629	6.816E-05	0.0016722	0.0488575	586	0.282145	-9.6	2.4	1.56	2.11	0.282416	0.282829
28	28A-14	0.2824884	2.956E-05	0.0009483	0.0385023	776	0.282475	6.3	1.0	1.08	1.26	0.282296	0.282692
28	28A-17	0.2820962	6.579E-05	0.0014109	0.0377022	585	0.282081	-11.9	2.3	1.65	2.24	0.282417	0.282830
28	28A-21	0.2824606	4.21E-05	0.0022475	0.0923838	579	0.282436	0.6	1.5	1.16	1.47	0.282420	0.282834
28	28A-22	0.2824606	4.21E-05	0.0022475	0.0923838	597	0.282435	0.9	1.5	1.16	1.46	0.282409	0.282821
28	28A-25	0.2814362	3.565E-05	0.0002194	0.0071607	563	0.281434	-35.3	1.3	2.49	3.66	0.282431	0.282846
28	28A-28	0.2822318	6.599E-05	0.0022463	0.0605991	605	0.282206	-7.0	2.3	1.49	1.96	0.282403	0.282815
28	28A-30	0.281618	3.137E-05	0.000597	0.0196391	524	0.281612	-29.9	1.1	2.27	3.29	0.282455	0.282874
28	28A-32	0.2822909	3.367E-05	0.0011533	0.0400465	562	0.282279	-5.4	1.2	1.36	1.82	0.282431	0.282846
28	28A-33	0.2822227	2.245E-05	0.0003651	0.0143037	584	0.282219	-7.0	0.8	1.43	1.95	0.282417	0.282830
28	28A-31	0.2822179	3.43E-05	0.0012145	0.035095	606	0.282204	-7.1	1.2	1.47	1.96	0.282403	0.282815
28	28A-37	0.2821326	6.213E-05	0.0016331	0.072664	539	0.282116	-11.7	2.2	1.61	2.19	0.282445	0.282863
28	28A-45	0.2820248	5.43E-05	0.0016279	0.0388248	552	0.282008	-15.2	1.9	1.76	2.43	0.282437	0.282853
28	28A-47	0.2823923	3.382E-05	0.0008016	0.0288504	729	0.282381	2.0	1.2	1.21	1.50	0.282325	0.282725
28	28A-59	0.2823241	5.193E-05	0.001336	0.0559831	496	0.282312	-5.7	1.8	1.32	1.79	0.282473	0.282894
28	28A-64	0.2823134	2.938E-05	0.0006514	0.0216322	585	0.282306	-3.9	1.0	1.31	1.75	0.282416	0.282829
28	28A-71	0.2820754	7.16E-05	0.0007983	0.0236334	574	0.282067	-12.6	2.5	1.65	2.31	0.282424	0.282838
28	28A-75	0.2823095	6.74E-05	0.0006636	0.0224479	572	0.282302	-4.3	2.4	1.32	1.79	0.282424	0.282839

Hafnium data tables for igneous zircons

							Scherer et al., 2001 - ^{176}Lu decay constant (1.865x10^{-11})						
							Hf_i	epsilon	1se	T(DM)	T(DM)		
Sample No.	**no.**	**Hf176/Hf177**	**1 S.D.**	**Lu176/Hf177**	**Yb176/Hf177**	**U / P b AGE**				**(Ga)**	**(crustal)**	**Hf Chur (t)**	**Hf DM (t)**
BH-14-002/003	4	0.28246877	5.442E-05	0.0020283	0.0712019	395	0.282454	-2.9	1.9	1.14	1.54	0.282537	0.282967
BH-14-002/003	1	0.282546596	3.155E-05	0.0015489	0.0571944	396	0.282535	0.0	1.1	1.01	1.36	0.282536	0.282967
BH-14-002/003	20	0.282544813	7.199E-05	0.0026721	0.0976674	404	0.282525	-0.2	2.5	1.05	1.38	0.282531	0.282960
BH-14-002/003	23	0.282520794	8.31E-05	0.003725	0.128221	407	0.282492	-1.3	2.9	1.12	1.45	0.282529	0.282958
BH-14-002/003	21	0.282500368	6.493E-05	0.0036627	0.1408421	408	0.282472	-2.0	2.3	1.14	1.49	0.282528	0.282958
BH-14-002/003	18	0.282474329	2.152E-05	0.0004511	0.0148831	592	0.282469	2.0	0.8	1.08	1.39	0.282412	0.282825
BH-14-002/003	13	0.282040984	3.08E-05	0.0007484	0.0295474	595	0.282033	-13.4	1.1	1.69	2.34	0.282410	0.282822
BH-14-002/003	3	0.282048592	3.728E-05	0.0011278	0.0443292	617	0.282036	-12.8	1.3	1.70	2.32	0.282396	0.282807
BH-14-002/003	25	0.282517108	3.663E-05	0.0011443	0.0401757	632	0.282504	4.1	1.3	1.04	1.28	0.282387	0.282796
BH-14-002/003	24	0.282090335	2.183E-05	0.0006948	0.0234097	635	0.282082	-10.7	0.8	1.62	2.21	0.282385	0.282793
BH-14-002/003	14	0.28235576	3.627E-05	0.0017697	0.0544743	653	0.282334	-1.4	1.3	1.29	1.64	0.282373	0.282780
BH-14-002/003	22	0.282447229	2.619E-05	0.0009406	0.0290952	654	0.282436	2.2	0.9	1.14	1.42	0.282372	0.282779
BH-14-002/003	2	0.282404218	2.173E-05	0.0006114	0.0210157	728	0.282396	2.5	0.8	1.19	1.45	0.282326	0.282726
BH-14-002/003	12	0.282451345	2.241E-05	0.0005277	0.0158732	896	0.282442	7.9	0.8	1.12	1.25	0.282219	0.282604
BH-14-002/003	7	0.282022771	3.63E-05	0.0008917	0.0324296	1262	0.282002	0.6	1.3	1.73	1.98	0.281985	0.282336
BH-14-002/003	26	0.28179333	2.521E-05	0.0007342	0.0238285	1758	0.281769	3.7	0.9	2.03	2.19	0.281665	0.281971
BH-14-002/003	5	0.281680582	2.605E-05	0.0008142	0.0293144	1997	0.281650	5.0	0.9	2.19	2.33	0.281510	0.281794
BH-14-002/003	8	0.281560369	2.191E-05	0.0007437	0.0245394	2144	0.281530	4.1	0.8	2.35	2.50	0.281415	0.281685
BH-14-005	11	0.282576719	2.414E-05	0.0008525	0.0306114	386	0.282571	1.0	0.9	0.95	1.29	0.282543	0.282974
BH-14-005	39	0.282576171	1.853E-05	0.0002987	0.0124062	397	0.282574	1.4	0.7	0.94	1.28	0.282536	0.282966
BH-14-005	17	0.282599485	1.365E-05	6.058E-05	0.0028756	408	0.282599	2.5	0.5	0.90	1.21	0.282529	0.282958
BH-14-005	19	0.282605548	3.329E-05	0.0014215	0.0541433	415	0.282595	2.5	1.2	0.93	1.22	0.282524	0.282953
BH-14-005	45	0.28236691	4.578E-05	0.0024436	0.0940887	498	0.282344	-4.5	1.6	1.30	1.72	0.282471	0.282893
BH-14-005	20	0.282467434	2.157E-05	0.0013609	0.0499056	514	0.282454	-0.3	0.8	1.12	1.47	0.282462	0.282881
BH-14-005	26	0.282345951	2.862E-05	0.000711	0.0271398	518	0.282339	-4.2	1.0	1.27	1.72	0.282459	0.282878
BH-14-005	51	0.282556759	2.173E-05	0.0016696	0.0581954	547	0.282540	3.5	0.8	1.00	1.26	0.282440	0.282857
BH-14-005	22	0.282694164	2.866E-05	0.0014894	0.055846	549	0.282679	8.5	1.0	0.80	0.95	0.282439	0.282856
BH-14-005	34	0.282560771	1.698E-05	0.0011923	0.0456013	549	0.282548	3.9	0.6	0.98	1.24	0.282439	0.282856
BH-14-005	41	0.282523192	2.829E-05	0.001113	0.0417397	553	0.282512	2.7	1.0	1.04	1.32	0.282436	0.282853
BH-14-005	48	0.282416744	2.107E-05	0.0019015	0.0672456	555	0.282397	-1.4	0.7	1.21	1.57	0.282435	0.282851
BH-14-005	14	0.282325708	2.26E-05	0.0012919	0.0480178	569	0.282312	-4.0	0.8	1.32	1.75	0.282426	0.282841

BH-14-005	8	0.282396741	3.775E-05	0.0012112	0.0364746	575	0.282384	-1.4	1.3	1.22	1.58	0.282423	0.282837
BH-14-005	50	0.282640337	2.181E-05	0.0010833	0.0340992	607	0.282628	8.0	0.8	0.87	1.02	0.282402	0.282814
BH-14-005	12	0.282655107	2.217E-05	0.001112	0.0303919	618	0.282642	8.7	0.8	0.85	0.98	0.282395	0.282806
BH-14-005	30	0.282666383	2.56E-05	0.0008554	0.0296271	631	0.282656	9.5	0.9	0.83	0.94	0.282387	0.282796
BH-14-005	57	0.282622155	2.387E-05	0.0005904	0.0207279	651	0.282615	8.5	0.8	0.88	1.02	0.282375	0.282782
BH-14-005	54	0.282357875	2.495E-05	0.0011837	0.0440573	682	0.282343	-0.4	0.9	1.27	1.58	0.282355	0.282760
BH-14-005	5	0.282209149	2.256E-05	0.0009497	0.0343598	707	0.282197	-5.0	0.8	1.47	1.87	0.282339	0.282741
BH-14-005	31	0.281720293	2.85E-05	0.0007994	0.0257234	1781	0.281693	1.5	1.0	2.14	2.34	0.281650	0.281954
BH-14-005	1	0.281976456	3.512E-05	0.0004634	0.0156218	2052	0.281958	17.2	1.2	1.77	1.61	0.281474	0.281753
BH-14-005	47	0.281367571	1.841E-05	0.0004709	0.0152723	2066	0.281349	-4.1	0.7	2.60	2.90	0.281465	0.281742
BH-14-005	59	0.281313357	2.448E-05	0.0003749	0.013404	2161	0.281298	-3.8	0.9	2.66	2.94	0.281403	0.281672
BH-14-005	55	0.280889626	1.691E-05	0.0005007	0.0183288	2381	0.280867	-14.0	0.6	3.24	3.83	0.281259	0.281507
BH-14-005	49	0.280961262	2.177E-05	0.0004326	0.0136132	2853	0.280938	-0.4	0.8	3.14	3.34	0.280949	0.281152
ACO-14-ERG	23	0.282441051	1.584E-05	0.0005343	0.0123081	731	0.282434	3.9	0.6	1.13	1.38	0.282324	0.282724
ACO-14-ERG	8	0.28244221	1.891E-05	0.0005987	0.0153939	721	0.282434	3.7	0.7	1.13	1.38	0.282330	0.282731
ACO-14-ERG	19	0.282453195	2.592E-05	0.0008032	0.0197209	741	0.282442	4.4	0.9	1.12	1.35	0.282318	0.282717
ACO-14-ERG	29	0.282498457	3.294E-05	0.0038913	0.0945103	768	0.282442	5.0	1.2	1.16	1.34	0.282300	0.282697
ACO-14-ERG	32	0.282452467	2.136E-05	0.0006546	0.0155099	742	0.282443	4.5	0.8	1.12	1.35	0.282317	0.282716
ACO-14-ERG	20	0.282454431	2.248E-05	0.0007924	0.0192353	739	0.282443	4.4	0.8	1.12	1.35	0.282319	0.282718
ACO-14-ERG	33	0.282451199	1.844E-05	0.0004437	0.0100357	741	0.282445	4.5	0.7	1.12	1.35	0.282317	0.282717
ACO-14-ERG	41	0.282455334	2.283E-05	0.0006597	0.0153801	737	0.282446	4.5	0.8	1.12	1.35	0.282320	0.282720
ACO-14-ERG	13	0.282454367	1.901E-05	0.0005416	0.013939	736	0.282447	4.5	0.7	1.12	1.35	0.282321	0.282721
ACO-14-ERG	39	0.282458524	2.291E-05	0.0005899	0.0134336	741	0.282450	4.7	0.8	1.11	1.33	0.282318	0.282717
ACO-14-ERG	12	0.282463238	1.722E-05	0.0008804	0.0228736	732	0.282451	4.5	0.6	1.11	1.34	0.282323	0.282723
ACO-14-ERG	17	0.282462691	2.152E-05	0.000773	0.0184857	741	0.282452	4.8	0.8	1.11	1.33	0.282318	0.282717
ACO-14-ERG	6	0.282462439	1.946E-05	0.0005878	0.0136044	724	0.282454	4.5	0.7	1.11	1.34	0.282328	0.282729
ACO-14-ERG	2	0.282468056	1.978E-05	0.000745	0.0180962	726	0.282458	4.6	0.7	1.10	1.33	0.282327	0.282728
ACO-14-ERG	18	0.282468157	2.287E-05	0.000716	0.0164231	739	0.282458	4.9	0.8	1.10	1.32	0.282319	0.282718
ACO-14-ERG	16	0.282468524	2.698E-05	0.0006103	0.0151616	728	0.282460	4.8	1.0	1.10	1.32	0.282326	0.282726
ACO-14-ERG	24	0.282476587	2.428E-05	0.0010414	0.0231352	731	0.282462	4.9	0.9	1.10	1.31	0.282324	0.282724
ACO-14-ERG	9	0.282473111	1.907E-05	0.0007316	0.0182691	734	0.282463	5.0	0.7	1.09	1.31	0.282322	0.282722
ACO-14-ERG	10	0.282484207	1.733E-05	0.0008691	0.0225349	730	0.282472	5.2	0.6	1.08	1.29	0.282324	0.282724
ACO-14-ERG	1	0.282482395	1.867E-05	0.0006729	0.0167643	723	0.282473	5.1	0.7	1.08	1.31	0.282329	0.282730
ACO-14-ERG	21	0.282492984	1.814E-05	0.0012174	0.0321889	734	0.282476	5.5	0.6	1.08	1.29	0.282322	0.282722

ACO-13-17	21	0.282578645	5.681E-05	0.0042918	0.1444085	597	0.282531	4.3	2.0	1.05	1.25	0.282409	0.282821
ACO-13-17	7	0.282545706	2.417E-05	0.0010639	0.0382309	609	0.282534	4.7	0.9	1.00	1.23	0.282401	0.282812
ACO-13-17	8	0.282570976	7.642E-05	0.0029984	0.0864642	595	0.282538	4.5	2.7	1.02	1.23	0.282410	0.282823
ACO-13-17	18	0.282563109	3.026E-05	0.0019597	0.0715375	618	0.282540	5.1	1.1	1.00	1.21	0.282396	0.282806
ACO-13-17	25	0.282558075	3.199E-05	0.0015451	0.0555505	604	0.282541	4.8	1.1	1.00	1.22	0.282404	0.282816
ACO-13-17	28	0.28256603	2.821E-05	0.0016912	0.059185	615	0.282547	5.3	1.0	0.99	1.20	0.282398	0.282808
ACO-13-17	15	0.282570664	3.543E-05	0.0017682	0.0538505	610	0.282550	5.3	1.3	0.99	1.19	0.282400	0.282811
ACO-13-17	19	0.28257761	3.658E-05	0.0023323	0.0826645	618	0.282551	5.5	1.3	0.99	1.19	0.282396	0.282806
ACO-13-17	16	0.28258589	3.501E-05	0.0023304	0.0851454	605	0.282559	5.5	1.2	0.98	1.18	0.282404	0.282815
ACO-13-17	17	0.282582196	3.248E-05	0.0015088	0.049275	604	0.282565	5.7	1.1	0.96	1.17	0.282404	0.282816
ACO-13-17	12	0.282586719	2.452E-05	0.0010881	0.0391013	602	0.282574	6.0	0.9	0.94	1.15	0.282406	0.282818
ACO-13-17	14	0.282590566	3.418E-05	0.00125	0.0432152	602	0.282576	6.1	1.2	0.94	1.14	0.282406	0.282817
ACO-13-17	9	0.28260173	3.144E-05	0.001335	0.0495904	599	0.282587	6.4	1.1	0.93	1.12	0.282407	0.282819
ACO-13-17	5	0.28260664	8.461E-05	0.001755	0.0716805	592	0.282587	6.2	3.0	0.93	1.12	0.282412	0.282825
ACO-13-17	30	0.282601246	2.557E-05	0.0011957	0.0421267	612	0.282588	6.7	0.9	0.93	1.11	0.282400	0.282810
ACO-13-17	13	0.282612947	4.808E-05	0.0016943	0.0488585	615	0.282593	6.9	1.7	0.92	1.10	0.282397	0.282808
ACO-13-17	3	0.282616844	4.712E-05	0.0017218	0.053675	616	0.282597	7.1	1.7	0.92	1.09	0.282397	0.282808
ACO-13-17	26	0.282619241	3.835E-05	0.0019266	0.0690638	610	0.282597	7.0	1.4	0.92	1.09	0.282400	0.282812
ACO-13-17	10	0.282618483	4.49E-05	0.0018529	0.0720897	609	0.282597	6.9	1.6	0.92	1.09	0.282401	0.282813
ACO-13-17	11	0.28261505	2.652E-05	0.0014158	0.0506481	605	0.282599	6.9	0.9	0.91	1.10	0.282404	0.282815
ACO-13-17	27	0.282650481	7.701E-05	0.0041864	0.1459285	609	0.282603	7.1	2.7	0.93	1.09	0.282401	0.282812
13-21	6	0.282683206	3.074E-05	0.0016495	0.0722398	464	0.282669	6.2	1.1	0.82	1.02	0.282493	0.282917
13-21	14	0.282655942	4.062E-05	0.0018238	0.0631101	464	0.282640	5.2	1.4	0.86	1.09	0.282493	0.282917
13-21	16	0.282612734	0.0001744	0.0034009	0.0837601	464	0.282583	3.2	6.2	0.97	1.21	0.282493	0.282917
13-21	19	0.282674699	0.0001529	0.0068789	0.2310536	464	0.282615	4.3	5.4	0.97	1.14	0.282493	0.282917
13-21	2	0.282621998	5.21E-05	0.0025382	0.104588	465	0.282600	3.8	1.8	0.93	1.18	0.282492	0.282916
13-21	4	0.282672394	0.0003269	0.0066443	0.259078	466	0.282614	4.3	11.6	0.97	1.14	0.282492	0.282916
13-21	3	0.28264522	3.435E-05	0.0019442	0.0868046	467	0.282628	4.9	1.2	0.88	#REF!	0.282491	0.282915
13-21	18	0.282606591	8.791E-05	0.0042953	0.1522636	470	0.282569	2.8	3.1	1.00	1.24	0.282489	0.282913
13-21	13	0.282722375	5.787E-05	0.0040998	0.1978198	512	0.282683	7.8	2.0	0.82	0.96	0.282462	0.282882
13-21	8	0.282371801	5.269E-05	0.0013088	0.0428268	563	0.282358	-2.6	1.9	1.25	1.65	0.282430	0.282846
13-21	12	0.282644163	6.441E-05	0.0051014	0.2062816	573	0.282589	5.9	2.3	0.97	1.11	0.282424	0.282839
13-21	15	0.282551585	0.0001074	0.0034802	0.1058276	621	0.282511	4.2	3.8	1.06	1.29	0.282393	0.282803
13-21	10	0.282644134	0.000118	0.0039271	0.1603535	1587	0.282526	26.6	4.2	0.93	0.60	0.281776	0.282097
13-16	31	0.282498614	4.002E-05	0.0010294	0.0342517	369	0.282492	-1.82	1.4	1.07	1.48	0.282543	0.282986
13-16	45	0.28252442	7.109E-05	0.0018851	0.0610335	391	0.282511	-0.65	2.5	1.06	1.42	0.282529	0.282970
13-16	13	0.282458122	4.974E-05	0.0015402	0.0552428	391	0.282447	-2.90	1.7	1.14	1.56	0.282529	0.282970
13-16	23	0.282479004	4.019E-05	0.0014334	0.0536467	393	0.282468	-2.10	1.4	1.11	1.51	0.282528	0.282968
13-16	42	0.2825011	6.109E-05	0.001419	0.0546671	394	0.282491	-1.30	2.1	1.07	1.46	0.282527	0.282968
13-16	10	0.282524048	4.732E-05	0.0016281	0.0614607	401	0.282512	-0.38	1.7	1.05	1.41	0.282523	0.282962
13-16	46	0.282313281	4.765E-05	0.0011974	0.0462642	403	0.282304	-7.70	1.7	1.33	1.87	0.282522	0.282962

13-16	17	0.28241912	5.317E-05	0.0014828	0.0531363	405	0.282408	-3.98	1.9	1.19	1.64	0.282520	0.282960
13-16	5	0.282409616	6.625E-05	0.0021246	0.0659279	405	0.282393	-4.48	2.3	1.23	1.67	0.282520	0.282960
13-16	3	0.28248976	8.949E-05	0.0019256	0.0677222	414	0.282475	-1.41	3.1	1.11	1.49	0.282515	0.282953
13-16	41	0.282453349	6.928E-05	0.0018099	0.0630354	429	0.282439	-2.35	2.4	1.15	1.56	0.282505	0.282942
13-16	21	0.282398835	8.689E-05	0.0028794	0.0948706	431	0.282376	-4.54	3.0	1.27	1.69	0.282504	0.282941
13-16	18	0.282073663	6.621E-05	0.0017412	0.072767	457	0.282059	-15.18	2.3	1.69	2.37	0.282488	0.282922
13-16	49	0.282290109	9.557E-05	0.0024615	0.0821642	470	0.282268	-7.47	3.3	1.41	1.91	0.282480	0.282913
13-16	12	0.282477006	4.224E-05	0.0015399	0.0542675	478	0.282463	-0.41	1.5	1.11	1.47	0.282475	0.282907
13-16	16	0.282598679	4.633E-05	0.0015933	0.0503829	482	0.282584	3.97	1.6	0.94	1.20	0.282472	0.282904
13-16	25	0.282198005	4.388E-05	0.0011548	0.0411182	880	0.282179	-1.54	1.5	1.49	1.85	0.282222	0.282615
13-16	15	0.282201625	4.4E-05	0.0009379	0.0294689	977	0.282184	0.80	1.5	1.48	1.77	0.282162	0.282545
13-16	1	0.282256339	7.94E-05	0.0010833	0.0351293	1075	0.282234	4.78	2.8	1.41	1.60	0.282099	0.282473
13-16	51	0.282367149	8.536E-05	0.0043254	0.1616867	1087	0.282279	6.61	3.0	1.37	1.50	0.282092	0.282465
13-16	8	0.282101461	0.0001155	0.0018263	0.0514346	1087	0.282064	-0.98	4.0	1.66	1.97	0.282092	0.282464
13-16	2	0.281915125	3.279E-05	0.0009438	0.0303805	1486	0.281889	1.77	1.1	1.88	2.10	0.281839	0.282172
13-16	11	0.281715639	6.155E-05	0.0017827	0.0618906	1642	0.281660	-2.83	2.2	2.20	2.50	0.281740	0.282057
13-16	19	0.281839638	7.813E-05	0.0017818	0.0621386	1685	0.281783	2.50	2.7	2.03	2.21	0.281712	0.282025

Chapter 6

Statement of Authorship

Title of Paper	Evolution of Variscan Europe from a Hf isotope perspective: implications for Wilson and supercontinental cycles
Publication Status	☐ Published ☐ Accepted for Publication ☐ Submitted for Publication ☒ Unpublished and Unsubmitted work written in manuscript style
Publication Details	Henderson, B., Collins, W.J., Murphy, B.J., Gutierrez, G.A., Hand, M., Evolution of Variscan Europe from a Hf isotope perspective: implications for Wilson and supercontinental cycles

Principal Author

Name of Principal Author (Candidate)	Bonnie Henderson
Contribution to the Paper	Sample collection, U-Pb and Hafnium zircon analysis, data interpretation, manuscript and figure composition
Overall percentage (%)	85%
Certification:	This paper reports on original research I conducted during the period of my Higher Degree by Research candidature and is not subject to any obligations or contractual agreements with a third party that would constrain its inclusion in this thesis. I am the primary author of this paper.
Signature	Date: 05/04/2016

Co-Author Contributions

By signing the Statement of Authorship, each author certifies that:

i. the candidate's stated contribution to the publication is accurate (as detailed above);
ii. permission is granted for the candidate in include the publication in the thesis; and
iii. the sum of all co-author contributions is equal to 100% less the candidate's stated contribution.

Name of Co-Author	W.J Collins
Contribution to the Paper	Project design, data interpretation and manuscript revisions
Signature	Date: 5/4/2016

Name of Co-Author	J. Brendan Murphy
Contribution to the Paper	Assistance with sample collection and manuscript revisions
Signature	Date: April 5 2016

Name of Co-Author	Gabriel Gutierrez-Alonso
Contribution to the Paper	Assistance with sample collection and manuscript revisions
Signature	Date: 05/04/2016

Name of Co-Author	Martin Hand
Contribution to the Paper	Manuscript revisions
Signature	Date: 6-4-2016

Evolution of Variscan Europe from a Hf isotope perspective: implications for Wilson and supercontinental cycles

ABSTRACT

Combined U-Pb-Hf isotope studies of zircons provide new insights into the evolution of large-scale, long-term orogenic systems. The distinct inverted U-shape of some Hf evolutionary arrays has been interpreted as the ocean-closure phase of a Wilson cycle. A compilation of new and existing Hf isotope data from the Variscan-Mediterranean orogenic system of Phanerozoic Europe is used to test the sensitivity of the hafnium isotopic array against a successive Wilson cycles. Remarkably, an inverted U-shaped εHf "reworking" array extends from 600 Ma to present-day, not at the 150-200 Ma time-scales expected for consecutive Wilson cycles associated with evolution of presumed Atlantic-type Paleozoic oceans. The hafnium isotopic array does not record the Variscan orogenic events that resulted in the amalgamation of Pangea; instead the event recycles the Neoproterozoic arc crust that dominates the "peri-Gondwanan" terranes. Geological constraints, as well as a comparison with circum-Pacific Hf isotopic arrays, indicate that the northern peri-Gondwanan margin was part of a vast retreating accretionary orogen between 600-450 Ma. The hafnium isotopic record of 450-300 Ma magmatism in Variscan Europe indicates continuous recycling of ~1.8 Ga Paleoproterozoic and juvenile peri-Gondwanan crust (0.75-0.55 Ga) along a typical crustal evolution path (Lu/Hf=0.015). The hafnium array was generated via back-arc opening-closing events on the Laurussian upper plate that have continued until the present-day, including the events that produced the Variscan Orogeny. The protracted opening-closing events generated the dominantly supra-subduction-related ophiolites that now comprise the Paleozoic allochthonous terranes in the Variscan belt of Europe. A strong negative εHf excursion at 30 Ma indicates subduction and melting of Gondwanan cratonic lithosphere for the first time since 600 Ma.

The ~600-300 Ma isotopic record of the Canadian Appalachians is remarkably similar to the European array. Both regions record a similar transition towards increasingly radiogenic hafnium values between ~600-450 Ma, indicating subduction roll back and retreat of amagmatic arc from the northern Gondwanan margin. Tectonic switching between retreating and advancing subduction episodes led to the homogenisation of the juvenile Late Neoproterozoic arc crust and Grenvillian-type basement in the Appalachians, whereas Variscan Europe has been dominated by the closure of ephemeral basins during slow northward convergence of the African plate.

The inverted U-shaped European εHf isotopic array records the 600 million year closure phase of a supercontinental cycle. Lower and upper εHf model age limits on the post-450 Ma Phanerozoic array corresponds to Nuna and Rodinia breakup events, suggesting that Hf isotopic arrays provide temporal and spatial constraints on supercontinental cycles, which can be reconstructed at a cratonic scale.

1. INTRODUCTION

The Wilson cycle is typically cast in terms of opening and closing of wide ocean basins, based on actualistic models of the Atlantic Ocean, rather than of (marginal) back-arc basins (Worsley et al., 1984). The opening and closing of the Iapetus, Rheic and two Tethyan oceans between Laurentia, Baltica and Gondwana are considered classic Wilson cycles involving successive rifting of Gondwanan ribbons, which then migrated across large oceans (Stampfli et al., 2013). Such models require that each ocean-opening event generates rifts that bite deeper into the continental interior, and the ribbons ultimately accrete to the opposing continental margin during ocean closure. Underthrust ancient

Gondwanan crust should then either exhume or partially melt during each ensuing post-collisional magmatic stage. Thus, post-collisional Variscan magmatism following Pangean amalgamation should produce a significant negative εHf excursion at ~300 Ma (Fig. 1a), which would rapidly terminate after slab breakoff. Repeated Wilson cycles produce a strongly fanning εHf evolutionary array (Fig. 1b), as recorded by the complex Mesozoic collisional orogens of east Asia, driven by the semi-continuous under thrusting and partial melting of Gondwanan fragments beneath Eurasia (Collins et al., 2011). In this contribution, it shown that the European εHf isotopic array does not fan as predicted during a classical Wilson cycle, instead defining an inverted "U-shaped" array and a trajectory of crustal reworking (Fig. 1b), for almost the entire Phanerozoic.

The data presented here have implications for understanding Phanerozoic European geology, classical Wilson cycles, and the broader implications for cyclicity of tectonic cycles. An alternative evolutionary model for Phanerozoic Europe is proposed that meets the existing geological constraints and accommodates the hafnium isotopic array presented here.

2. GEOLOGICAL EVOLUTION OF PHANEROZOIC EUROPE AND NORTHERN AFRICA

Neoproterozoic arc-back-arc systems that fringed West Gondwana, collectively termed the "peri-Gondwanan" terranes, are presently scattered throughout the Paleozoic Caledonian, Variscan and Appalachian orogens (Murphy et al., 2006). They include the massifs of Variscan Europe (Iberian, Armorican, Massif Central and Bohemian; (Linnemann et al., 2013; Ballèvre et al., 2014), the Pontides of eastern Europe,, and "composite Avalonia" in North America. Vestiges of oceanic arc magmatism are recognised between ~750-650 Ma in most of the terranes (Murphy et al., 2006), followed by a major phase of continental arc magmatism between ~650-550 Ma with subduction directed beneath the periphery of West Gondwana (Murphy et al., 2006). Composite Avalonia separated from Gondwana by the early Ordovician opening the Rheic Ocean in its wake, and by the late Ordovician, had docked with Baltica consuming the Tornquist Ocean (Cocks and Torsvik, 2005). This collage then collided with Laurentia in the Silurian, consuming the Iapetus Ocean to form Laurussia during the Salinic-Scandian-Caledonide Orogeny (Cocks and Torsvik, 2005; Chapter 4, this thesis). In the Devonian, the Rheic Ocean lay between Laurussia and Gondwana, and Devonian ophiolites in central and Western Europe are commonly linked to its closure phase (Murphy et al., 2006; Martínez et al., 2011; Arenas et al., 2014).

The Mid Devonian-Carboniferous Variscan Orogeny involved the accretion of the peri-Gondwanan passive margin to the Laurussian continent (Stampfli et al., 2013). By the late Carboniferous, Gondwana collided with Laurussia assembling the Pangean supercontinent. Some workers (Stampfli et al., 2013) propose that the closure of a second Paleozoic ocean, Paleo-Tethys, preceded the major continent-continent collision in western Europe, but others suggest it was, at most, a narrow, ephemeral basin (Robardet, 2003). Subsequently, Neo-Tethys opened in the Early Permian-mid Triassic separating the Cimmerian ribbon from northern Gondwana (Stampfli et al., 2013). Triassic-Jurassic ophiolites in central and eastern Europe record supra-subduction signatures (Robertson et al., 2012), suggesting formation in oceanic arc or back-arc settings (Table 1).

Late Cretaceous to Recent events in the Mediterranean are associated with N-dipping subduction of Africa beneath Europe (Jolivet and Brun, 2010). Back-arc extension, bimodal volcanism and exhumation occurred during southward retreat at the leading edge of the

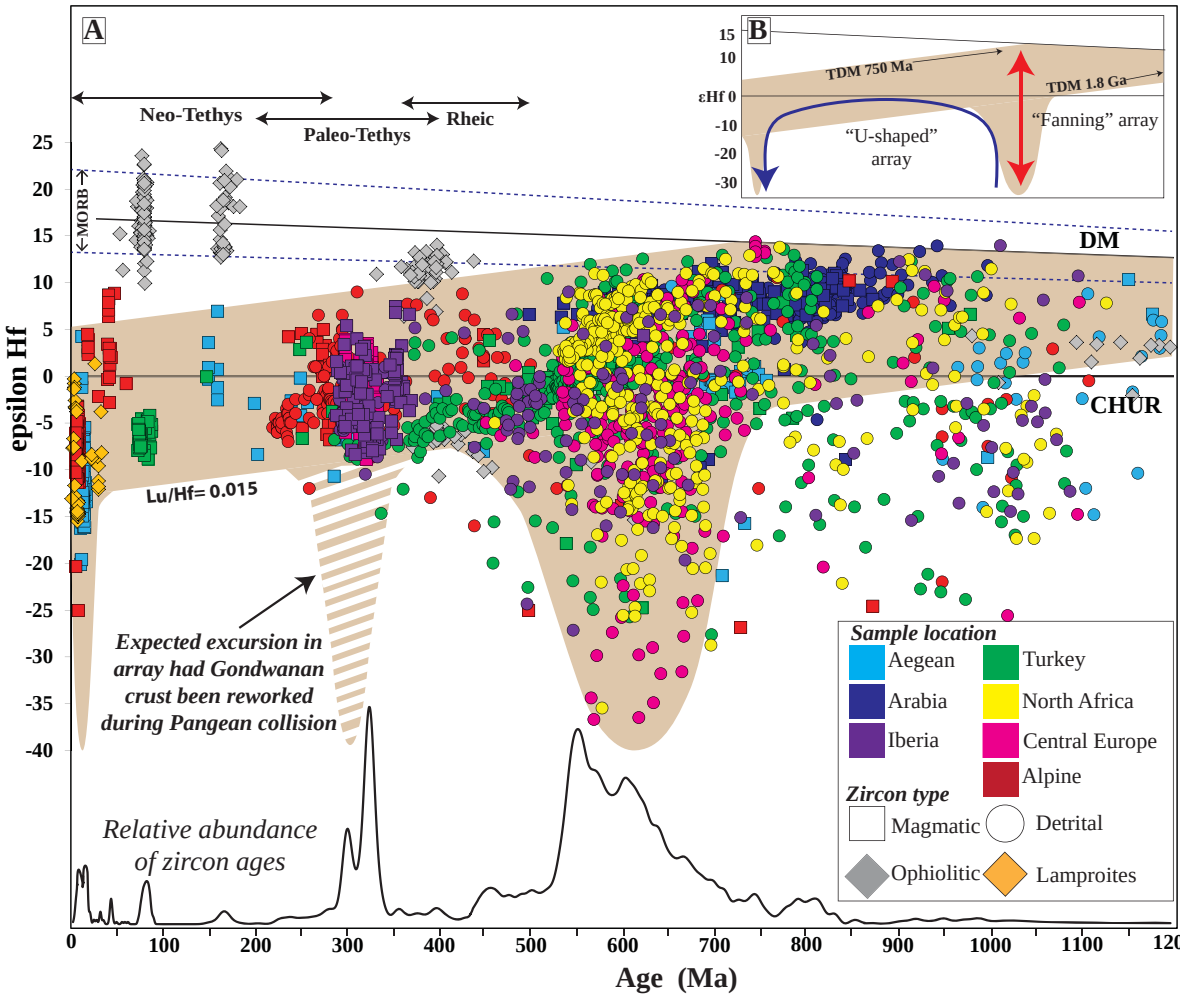

Figure 1

A) Hafnium array (εHf) and U-Pb spectra of detrital, magmatic, ophiolitic and lamproitic zircon grains from Phanerozoic Europe (supplementary data file A). For TDM constraints, we use the most evolved point within the array during the U-shaped excursion (600-550 Ma) for the older TDM limit, and the least evolved portion as the younger limit. These limits were projected to the depleted mantle using Lu/Hf ratio of average crust (0.015, Griffin et al., 2004), CHUR= chondritic uniform reservoir. The field defined for the depleted mantle array and MORB is from Dhuime et al. (2011) and Griffin et al. (2004). B) A schematic overview of the typical "fanning" (Collins et al., 2011) and inverted "U-shaped" hafnium isotopic arrays.

slow-moving African plate (Rosenbaum et al., 2002)

The northern African margin was mostly passive throughout the Phanerozoic, preserving a broadly conformable sequence of mostly clastic Paleozoic strata (e.g. Guiraud et al., 2005 and references therein). Some fault reactivation in the Devonian produced intra-platform highs, but no evidence exists for Paleo-Tethys opening. A Variscan-aged unconformity separates the Gondwanan and Tethyan supercycles, with the latter characterised by Permian-Carboniferous continental deposits overlain by an onlapping sequence of Mesozoic continental clastics, evaporites and carbonates (Guiraud et al., 2005).

3. EUROPEAN OPHIOLITES

A review of >35 Ordovician-Cretaceous putative ophiolite occurrences across Europe and Turkey (Table 1) indicates that the vast majority have supra-subduction (SSZ) signatures; few have MORB-like affinities. This geochemical variety is typical of modern-day oceanic back-arc systems (e.g. Pearce et al., 1984; Ewart et al., 1998), not

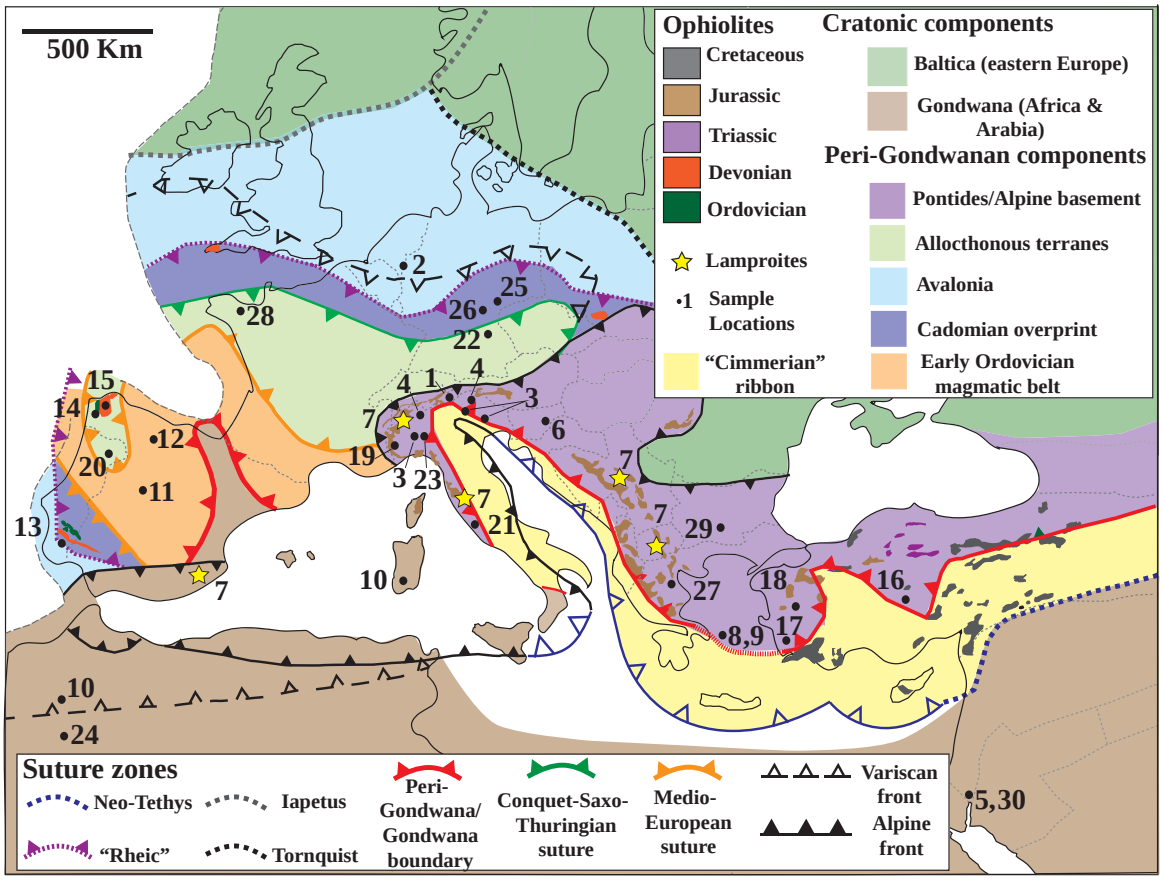

Figure 2

Simplified map of Europe and northern Africa showing the location of samples used for the Hf isotope array in Fig. 1, and the location and ages of Phanerozoic ophiolites in Europe. A review of >35 Ordovician-Cretaceous ophiolite occurrences across Europe and Turkey (Table 1) indicates that the majority have supra-subduction (SSZ) signatures; few have MORB-like affinities. Following Ballevre et al., (2014), peri-Gondwana in Western Europe is divided into four terranes, but the "external thrust belt" is included in Avalonia (4). Also, the "Early Ordovician magmatic belt" is included within the peri-Gondwanan realm, as all measured Ordovician zircons are significantly more juvenile (εHf >-10) than evolved Neoproterozoic grains.

the MORB-like signatures expected if the ophiolites were preserved Rheic or Tethyan ocean floor. Paleozoic ophiolites are typically restricted to regional-scale domains, and are commonly grouped as "allochthonous" terranes (Fig. 2), but with Gondwanan lithostratigraphic units containing Cambrian-Ordovician rocks on either side of the inferred ocean, including the Early Ordovician Armorican quartzite (Ballèvre et al., 2009; Ballèvre et al., 2014). This suggests a back-arc, or peripheral narrow oceanic tract, origin for the ophiolites, consistent with their SSZ signatures.

Intracontinental basins were common on the southern margin of the eastern Europe and Turkey in the Jurassic and Cretaceous, and are interpreted to have been rooted in coeval Neo-Tethyan oceanic basins separated by continental fragments (Robertson, 2002). However, the typical SSZ signature of the ophiolites generated in these basins also suggests a dominant back-arc, rather than a classic Neo-Tethyan origin.

4. THE EUROPEAN ZIRCON HAFNIUM ISOTOPE ARRAY

A compilation (n=3660) of new detrital and magmatic U-Pb-Hf zircon data is presented in conjunction with published data from

No.	Name	Location	Ocean	Geochemistry	Age	Reference
1	Careon ophiolite	Spain	Rheic	SSZ	395	(Martínez et al., 2007)
2	Internal Ossa-Morena Zone ophiolite Sequences	Spain/Portugal	Rheic	N-MORB/E-MORB	479 +/- 5	(Ribeiro et al., 2010)
3	Beja-Acebuches Complex	Spain-Portugal	Rheic or Paleo-Tethys	SSZ	380	(Azor et al., 2008; Ribeiro et al., 2010)
4	Moeche Ophiolite	Spain	Rheic	SSZ	400	(Arenas et al., 2013)
5	Purrido Ophiolite	Spain	Rheic	SSZ	400	(Martínez et al., 2011)
6	Montgenevre ophiolite (Chenaillat)	France	Alpine Tethys	embryonic MOR	165	(Costa and Caby, 2001; Li et al., 2013)
7	Krivaja-Konjuh Ophiolite	Bosnia	Neo-Tethys	SSZ	160	(Lanphere et al., 1975)
8	Mt Kalnik	Bosnia/Montenegro	Neo-Tethys	MORB	185	(Pamić and Jurković, 1997)
9	Zlatibor	Serbia	Paleo-Tethys	SSZ	175	(Lanphere et al., 1975) (Bazylev et al., 2009)
10	W. Albanian ophiolites	Albania	Pindos (Neo-Tethys)	MOR	170	(Robertson and Shallo, 2000)
11	Pindos	Greece	Neo-Tethys	MOR and SSZ	170	(Thuizat et al., 1981) (Spray and Roddick, 1980); (Roddick et al., 1979)
12	Lycian Nappes (Muglya ophiolite)	Turkey	Neo-Tethys	MOR trans to SSZ	88	(Thuizat et al., 1981) (Uysal et al., 2012)
13	Antalya (Godene and Tekirova)	Turkey	Neo-Tethys	MORB	100	(Bağcı and Parlak, 2009; Robertson and Waldron, 1990)
14	Pozanti-Karsanti	Turkey	Neo-Tethys	SSZ	90	(Thuizat et al., 1981)
15	Mersin	Turkey	Neo-Tethys	SSZ	95	(Thuizat et al., 1981) (PARLAK and ROBERTSON, 2004)
16	Bear Bassit	Turkey	Neo-Tethys	SSZ	90	(Thuizat et al., 1981)
17	Troodos	Cyprus	Neo-Tethys?	SSZ	90	(Rautenschlein et al., 1985), (Robinson et al., 1983)
18	E.Albanian ophiolites	Albania	Pindos (Neo-Tethys)	intraoceanic subduction	160	(Robertson and Shallo, 2000)
19	Vourinos ophiolite	Greece	Neo-Tethys	intraoceanic subduction	160	(Jones and Robertson, 1991)
21	Pontides ophiolites	Turkey	Neo-Tethys	SSZ	65	(Elmas and Yiğitbaş, 2001)
22	Kure Ophiolite	Turkey	Paleo-Tethys	SSZ	230	(Ustaomer and Robertson, 1997)
23	Elekdag ophiolite	Turkey	Paleo-Tethys	SSZ	230	(Ustaomer and Robertson, 1997)
24	Guvgueli ophiolite	Greece	Neo-Tethys	SSZ	160	(Robertson, 2002)
25	Lizard Ophiolite	England	Rheic	MOR	397	(Kirby, 1984; Roberts et al., 1993)
26	Sleza Ophiolite	Poland	Rheic	MOR	400	(Kryza et al., 2011)
27	Internal Liguride Ophiolite	Italy	Alpine Tethys	MOR	165	(Rampone et al., 1998)
28	Bazar Ophiolite	Spain/Portugal	Rheic	N-MORB/E-MORB	495 +/- 2	(Martínez et al., 2012)
29	Ybbsitz zone	Austria	Alpine Tethys	MORB?	160	(Ozvoldova and Faupl, 1993)
30	Izmir-Ankara zone	Turkey	Paleo-Tethys	MOR to SSZ	228	(Göncüoglu et al., 2010)
31	Eastern Pontide Ophiolitic Melanges	Turkey	Neo-Tethys	SSZ	100	(Eyuboglu et al., 2007)
32	Apuseni mountains	Romania	Neo-Tethys		140	(Nicolae et al., 1992)
33	Kizildag	Turkey	Neo-Tethys	SSZ	90	(Dilek and Thy, 2009), (KARAOĞLAN et al., 2013)
34	Sarikaraman ophiolite	Turkey	Paleo-Tethys	SSZ to MORB	65	(Alinz et al., 1996)
35	Mirdita Ophiolite Complex	Serbia	Pindos (Neo-Tethys)	SSZ	165	(Dilek et al., 2008)
36	Mt. Medvednica	Croatia	Vardar (Paleo-Tethys)	MORB	165	(Slovenec and Lugović, 2012)

Table 1

Compilation of ophiolites from Variscan Europe including the name, age and tectonic and geochemical affinities.

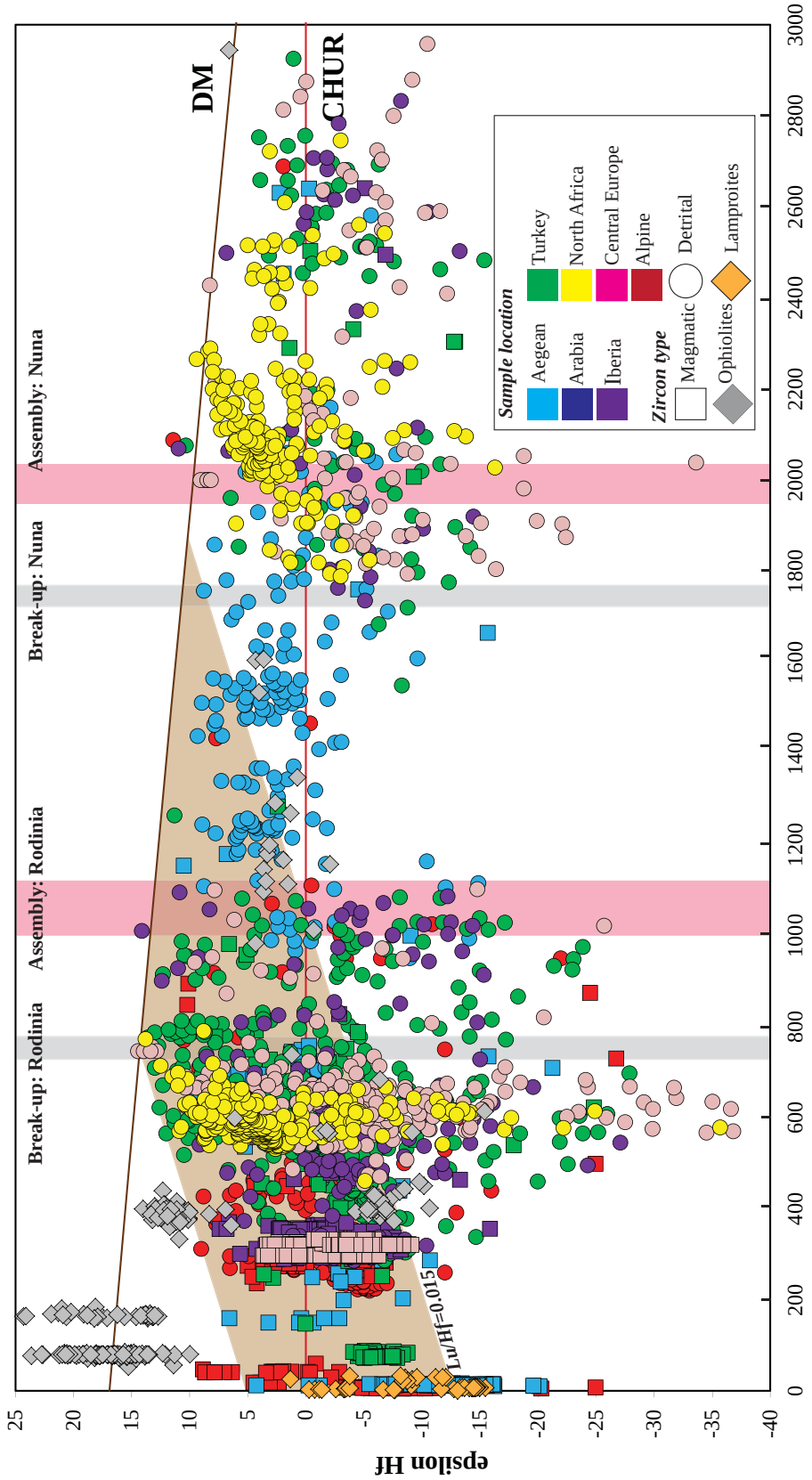

Figure 3
Hafnium array (εHf) and U-Pb spectra of detrital, magmatic, ophiolitic and lamproitic zircon grains from Phanerozoic Europe from 0-3500 Ma. For TDM constraints, the most evolved point within the array is used during the U-shaped excursion (600-550 Ma) for the older TDM limit, and the least evolved portion as the younger limit. These limits were projected to the depleted mantle using Lu/Hf ratio of average crust (0.015, Griffin et al., 2004), CHUR= chondritic uniform reservoir. Also shown are the intervals associated with the break-up and assembly of Nuna (Evans and Mitchell, 2011) and Rodinia (Li et al., 2008).

Europe, Africa, Arabia and Turkey (Figure 2, data tables in supplementary data). The new data are from five clastic Carboniferous-Permian rocks from the Cantabrian Zone in Iberia (Pastor-Galán et al., 2013). We use the mounts from Pastor-Galan et al., (2013) for the Lu-Hf isotopic analyses in the method following Henderson et al (2016) (A full description of the methods is included in the supplementary data.

Evolved Early Neoproterozoic-aged zircons (εHf< -5) reflect sediment dispersal from Pan-African terranes across Gondwana (Zlatkin et al., 2013). These Pan-African derived zircon grains are excluded from the major dataset (Fig. 1a) to highlight the initiation of arc magmatism on the northern margin of cratonic Gondwana, as constrained by geological evidence (Murphy et al., 2006). Without these and outlier data-points, the hafnium isotope array defined by zircons that crystallized between 900 Ma and the present day, is a surprisingly simple inverted "U-shaped" array that records only three major excursions of significance (Fig. 1b). The first excursion is a strongly developed spike to negative εHf values (0<εHf<-35) between 700-600 Ma, and the second is a return to more juvenile values (εHf >-10) between ~600-450 Ma. Thereafter to ~30 Ma, the εHf isotopic array is typical of crustal reworking (Lu/Hf=0.15) with upper and lower bounds (Fig. 1a) intersecting TDM (depleted mantle model age) at ~750 Ma and ~1.8 Ga respectively. An excursion towards negative εHf values in the mid Cenozoic (~30 Ma) marks the end of the "U-shaped" reworking array, and is consistent with the introduction of ancient crustal material into the Alpine orogenic system

The negative εHf excursion between ~700-600 Ma can be explained by either reworking of West African crust, or mixing of Eburnian and/or Late Archean crust with juvenile material, (see also Linnemann et al., 2014), which is attributed to continental arc magmatism (Linnemann et al., 2014) following accretion of composite Avalonia to the Gondwanan margin (Chapter 5).

The period between 600-450 Ma is characterised by a marked shift toward a more juvenile isotopic character (εHf +5 to -10). Such shifts reflect the transition from continental to oceanic arc magmatism, and typically associated with a retreating orogenic system, where arcs and ribbons migrated outboard (Kemp et al., 2009).

Between ~450 Ma and ~30 Ma, the zircon εHf record across Europe follows a typical crustal evolution path (Lu/Hf=0.015) indicating repeated reworking of this crust during tectonic events in this interval. With TDM ages ranging from ~1.8 to 0.75 Ga, the majority of the zircons indicate that the reworked crust was a mix of ~1.8 Ga Paleoproterozoic (probably younger than Eburnian), and juvenile peri-Gondwanan crust (0.75-0.55 Ga). Evolved εHf signatures in some Paleozoic ophiolites indicate that peri-Gondwanan sub-continental mantle lithospheric mantle (SCLM), possibly of Mesoproterozoic age (Martínez et al., 2011), was also reworked. However, most other ophiolites have high positive εHf values (Fig. 1a) indicating an asthenospheric source, and limited mixing with contemporaneous crust.

A trend to negative εHf values (-15 to -25) began in the Oligocene, and includes granitic rocks from Greece (Bolhar et al., 2012) and lamproitic rocks (Fig. 2) from Spain and Italy (Prelević et al., 2010), suggesting that ancient cratonic Gondwanan continental and mantle lithosphere became involved in subduction-related magmatism associated with back-arc basin retreat (Rosenbaum et al., 2002). Lamproites from Macedonia and Serbia have more positive εHf values, but also show evidence of mixing between ancient Gondwanan SCLM and asthenosphere (Prelević et al., 2010).

5. REVISED GEODYNAMIC MODEL OF EUROPE

The Hf isotopic data require that the Neoproterozoic active margin of northern Gondwana migrated outboard from ~600-450 Ma, resulting in a vast, extended peri-Gondwanan terrane that became the substrate to Variscan Europe. The negative εHf spike (Fig. 1a) at ~700-600 Ma is consistent with the development of a continental arc at ~650-640 Ma (Murphy et al., 2006) along the northern Gondwanan margin following accretion of Avalonia (Chapter 5). The subsequent major Hf isotopic shift toward more juvenile compositions between 600-450 Ma (Fig. 1a) is consistent with geological evidence for opening and closing of back-arc basins, including the 'Cadomian back-arc basin', which closed by ~540 Ma (Linnemann et al., 2014).

Ongoing arc magmatism throughout the Cambrian is sporadically recorded in the allochthonous complexes of Iberia, which progressively became more mafic and juvenile (Arenas et al., 2014), consistent with outboard arc migration. Late Cambrian high temperature metamorphism, Early Ordovician extension, and the emplacement of the widespread S-type Ollo de Sapo magmatism throughout Iberia (Díez, Fernández et al., 2012) provides critical evidence for alternating episodes of extension and contraction similar to the periodic emplacement of widespread S-type granites in the Tasmanides of eastern Australia, which herald new retreat phases (Collins & Richards, 2008).

460-450 Ma old bimodal volcanic rocks of Portugal may represent the external shelf of the peri-Gondwanan margin (Dias da Silva et al., 2014) and the opening of an oceanic tract. This oceanic tract is preserved in the allochthonous mafic units in Variscan Europe (Fig. 2), and the Early Ordovician Armorican Quartzite in Iberia and Brittany may represent remnants of the passive margin on either side of this tract (Ballèvre et al., 2014). The tract can be interpreted as a back-arc, consistent with the pervasive SSZ signature of most Paleozoic ophiolites (Table 1). In this model, the Cambrian to Carboniferous passive margin in northern Africa (Guiraud et al., 2005) and in the Cantabrian zone of Iberia (Pastor-Galán et al., 2013) are the inboard side of the back-arc rift (Ballèvre et al., 2014).

By the early Silurian, eastern Avalonia had docked with Baltica (Cocks and Torsvik, 2005), apparently triggering subduction beneath Variscan Europe and initiating closure of the Rheic Ocean (Murphy et al., 2006). Similarly, Avalonia docking in the northern Appalachians triggered subduction of Rheic oceanic crust beneath Laurentia (Chapter 3, van Staal et al. 2009; Torsvik and Rehnström 2003). Deep seismic and petrological evidence suggests S-dipping subduction beneath the Bohemian massif of central Europe from ~420 Ma (e.g Schulmann et al., 2014). Rare direct evidence for the arc and southward subduction is the 400-390 Ma Plounévez-Lochrist orthogneiss complex of NW France (Ballèvre et al., 2014). By contrast, Devonian SSZ ophiolites in Iberia reflect N-dipping subduction and subsequent accretion of the Paleozoic massifs to the inboard passive margin of peri-Gondwana (e.g., Arenas et al., 2014; Ballèvre et al., 2014). Similarly, N-directed subduction under Laurentia occurred farther along the orogen in the Appalachians.

The Late Paleozoic Variscan Orogeny was associated with widespread, voluminous syn-and post-collisional magmatism in Europe, but remarkably, did not significantly change the character of Hf isotopic array (Fig. 1a). Indeed, the abundant 400-250 Ma zircons cluster occurs within, and defines, the entire Phanerozoic reworking array. Thus, despite Pangean amalgamation, only the peri-Gondwanan terranes were reworked, consistent with relamination in the back-arc region (Hacker et al., 2011), producing a diffuse cryptic suture zone (Schulmann et al., 2014). The Hf isotopic data suggest that the Variscan Orogeny was closure of back-arc basins and/or limited oceanic tracts, which

juxtaposed Gondwana and Laurussia.

Early-Middle Triassic magmatic activity related to the opening of Neo-Tethys is recorded locally along the African margin (Guiraud et al., 2005), when the "Cimmerian ribbon" separated from northern Africa (Stampfli et al., 2013). The Jurassic magmatic gap (Fig. 1) is the expected hiatus as Neo-Tethys widened westward and the Central Atlantic Ocean opened (Guiraud et al., 2005). Numerous Jurassic ophiolite complexes developed in SE Europe (Table 1, Robertson et al., 2012) during ongoing dominantly N-directed subduction (Stampfli et al., 2013, Fig. 2), and have SSZ signatures consistent with a dominantly back-arc origin. The presence of peri-Gondwanan basement throughout Greece and northern Turkey, albeit dissected by Triassic-Jurassic back-arc rifts, implies that these terranes were part of the peri-Gondwanan ribbon (Zlatkin et al., 2013). N-directed subduction of the "Cimmerian" ribbon began in the Cretaceous and resulted, among other effects, in the Neogene lamproitic rocks of the Mediterranean region (Prelević et al., 2010). Lamproites are first-generation melts derived from volatile-rich mantle lithosphere, and their εHf values (Fig. 1a) indicate that ancient Gondwanan lithospheric mantle was underthrust and melted for the first time since the Neoproterozoic.

6. COMPARISONS WITH THE APPALACHIAN OROGEN

The ~600-300 Ma isotopic record of the Canadian Appalachians has remarkable similarities to the European array (Fig. x), with both orogens recording a transition towards increasingly radiogenic hafnium (εHf) values between ~600-450 Ma. The Hf isotopic arrays indicate that the "peri-Gondwanan" arc terranes of Variscan Europe and eastern Canada were part of a vast, retreating continental arc that was removed from the Gondwanan margin during subduction roll back in the Ediacaran (~600 Ma). The scale is similar to that of present-day Zealandia in the SW Pacific, which is a >4000 km long ribbon of highly extended continental crust, <10% of which is emergent (e.g., Grobys et al., 2008). Nonetheless, the lateral extension of the peri-Gondwanan terranes as part of a singular continental ribbon is not a new concept (Nance and Murphy et al., 1996; Stampfli et al., 2002; Keppie and Keppie 2014) and the hafnium isotopic record strongly supports this hypothesis.

The hafnium isotopic arrays of the Appalachian and Variscan orogens both indicate that crustal recycling processes occurred between ~450-300 Ma, in an upper-plate setting. Post-Variscan Europe has hosted predominantly N-dipping subduction regimes (see Stampfli et al., 2013) during the slow convergence of the African plate, which has led to the protracted opening-closing of ephemeral basins during intervals of extension and compression that have continued until the present day (Rosembaum et al., 2002; Jolivet and Brun 2010). The Appalachian margin also experienced protracted intervals of compression and extension, but only until Pangean amalgamation. They are interpreted as tectonic switching episodes between advancing and retreating subduction during closure of the Rheic Ocean (see Chapter 5). Such episodes are difficult to decipher in the Variscan orogenic record, due to subsequent Alpine reworking, but although the suggested "relamination" events in central Europe during the Devonian (e.g., Schulmann et al., 2014) could be the deep crustal expression of this process, it does not show the degree of homogenisation as indicated by the northern Appalachian array, as discussed below.

Magmatism associated with the Paleozoic assembly of Pangea in Variscan Europe (~450-300 Ma) records crustal recycling of the basement (~1.8-0.75 Ga) along a typical evolutionary array (Fig. 1, Lu/Hf= 0.015), anchored by the intersection with DM of the upper bound of the array at 750

Ma. Mafic complexes, termed ophiolites in the European literature, indicate that mantle input was occurring throughout, and continued up to the present-day. Nonetheless, zircons with primitive (high εHf) signatures are extremely rare, and non-existent in the detrital dataset, showing the dominance of crustal reworking, but apparently without crustal homogenisation. By contrast, although the northern Appalachians εHf array falls within the Paleozoic European array, it differs because it 'telescopes' around CHUR by ~300 Ma (see Fig. 15, Chapter 5). Thus, Paleozoic magmatism in the northern Appalachians is recorded by homogenisation of the late Neoproterozoic basement (TDM = 1.0-2.0 Ga). Accordingly, the Hf isotopic arrays of both regions can be broadly considered as 'reworking' arrays (i.e. Smits et al. 2014). In both orogenic systems, mantle-derived magmas did not mix significantly with the crustally derived melts that dominate the Hf record.

Interestingly, the beginning of both arrays are anchored at ~750 Ma, which is when the opening of proto-Iapetus is proposed (Chapter 5). It is melting of this juvenile proto-Iapetian arc crust that controls the Phanerozoic reworking arrays of both orogens, and it confirms the importance of proto-Iapetian opening in the evolution of the Iapetian Wilson cycle, and more broadly, in the establishment of the Gondwanan and Pangean supercontinental cycles.

Crustal reworking versus crustal homogenisation arrays suggests that the same section of crust was not involved in the subsequent reworking events, or that the conditions of melting were different, such as water fluxed melting versus dehydration melting. Water fluxing probably is confined to magmatic arcs and proximal back-arcs, producing relatively low-temperature S- and I-type granitic magmas (e.g. Frost et al., 2001, Collins and Richards 2008), whereas dehydration melting is generally confined to distal back-arcs and continental rifts, producing relatively hot A-type magmas (Collins et al., 2016). This difference might help explain the differences between the Variscan and northern Appalachian εHf arrays, particularly given the occurrence of Silurian-Early Devonian A-type magmatism in the latter. However, a detailed explanation of such petrological processes is beyond the scope of this thesis.

7. GLOBAL TECTONIC CYCLES

The inverted "U-shaped" European Hf isotopic reworking array (Fig. 1b) contrasts with the two fundamentally distinct Hf arrays evident from Phanerozoic orogenic systems recognised elsewhere on Earth (Collins et al., 2011) and requires a fundamental change in tectonic conditions (e.g. Smits et al., 2014); which is suggested to be a switch from an active continental arc on the northern Gondwanan margin, to outboard subduction retreat and the removal of an extended continental ribbon between ~650-400 Ma. The European array requires that the Paleozoic terranes now occupying Variscan Europe formed a large retreating orogen between ~600-450 Ma, which was then reworked throughout the remainder of the Phanerozoic by repeated back-arc opening and closing. Reworking was probably associated with small oceanic tract development, slow-moving plate convergence, hence limited mantle input in the back-arc regions, as is presently observed in the Aegean (e.g. Rosenbaum et al., 2002; Jolivet and Brun, 2010). In this predominantly extensional, back-arc dominated tectonic environment, magma mixing between crustal and mantle-derived components is more limited than in large hydrous arc systems that usually have extended crystallisation-hybridisation histories leading to magma mixing (Annen et al., 2006). Therefore, zircons from the Variscan and Appalachian orogens are almost exclusively derived from the reworked peri-Gondwanan crustal source. Only upon the introduction of Gondwanan crust during the Cenozoic Alpine Orogeny does mixing of an ancient cratonic source

become apparent (Prelević et al., 2010). This reworking style of Hf isotopic array is also evident in Mesoproterozoic Australia (Smits et al., 2014), showing that the broader geodynamic implications can be extended into Precambrian orogenic systems.

The Wilson cycle concept was formulated around Atlantic ocean-style opening and closing of oceans (Wilson, 1966). However, few zircon grains in either Europe or the Americas record any stage of that opening over the last 200 Ma. Once Atlantic closing begins, a burst of arc magmatism like the record of Neoproterozoic peri-Gondwanan arcs (Fig. 1a) should commence and may continue until continental collision, because ocean closure requires subduction and the second-order process of arc magmatism.

The European Hf isotopic record reflects a protracted ocean closure phase as the Gondwanan/Africa continent followed a slow, indirect path northward. Thus, the European Hf array is an inverted U-shape indicating ocean closure over a 600 Ma period, far greater than the length of the inferred Wilson cycle associated with Pangean amalgamation. Therefore, it is suggested the European Hf isotopic array records the final closure phase of a longer (600 Ma) supercontinent cycle, though the future magmatic record (the next 50 Myr) requires semi-continuous production of highly evolved zircons for that process to be adequately documented.

Surprisingly, the completion of the type-Wilson cycle in the northern Appalachians is marked simply by termination of magmatism as the εHf array converged on CHUR at ~300 Ma. Like Europe, collision of Gondwana with Laurentia to form Pangea is not reflected in the εHf array. What is recorded is "half" an inverted U-array, simply reflecting the reworking the composite Avalonia, like the Variscan orogeny reworked the peri-Gondwanan terranes of Armorica and Iberia. One must ask, therefore, whether the so-called Pangean supercontinental cycle is only part of a larger, longer-term supercontinental cycle?

For Europe, the εHf data indicates supercontinental cycle initiation is represented by the oldest εHf model age of the reworked peri-Gondwanan arc crust. The reworking array is bracketed between the upper Hf crustal evolutionary line with an εHf TDM age of 750 Ma (Fig. 1b), which may reflect the initial breakup of Rodinia, but more specifically relates to proto-Iapetus opening and formation of juvenile crust during subduction retreat as an oceanic arc developed on composite Avalonia (Chapter 5). The lower crustal evolution line has a εHf TDM age of ~1.8 Ga, which is slightly younger than the dominant 2.0 Ga (Eburnian) age of the West African Craton (WAC) (Fig. 3). This might also reflect opening of a major ocean during backarc spreading and oceanic arc development following Nuna amalgamation in the Paleoproterozoic.

The billion-year duration of the peri-Rodinian ocean inferred from Hf isotopic arrays largely coincides with the supercontinent cycle between Nuna (~1.8 Ga) and Rodinia (~750 Ma) breakup (Fig. 3), and is consistent with the inferred billion-year passive margin character of the WAC in many Proterozoic reconstructions (Zhang et al., 2012). The data presented here suggest that Hf isotopic arrays can be used to distinguish billion-year supercontinent cycles for individual cratons from second-order Wilson cycles, which more likely reflect the development of small oceans and the transfer of ribbons from one continent to another during supercontinental assembly. In this way, Hf isotopic arrays provide an excellent opportunity to reassess Precambrian supercontinent reconstructions at a cratonic scale, but less likely to recognise individual Wilson cycles unless they involve reworking of cratonic crust at the beginning and end of each cycle.

REFERENCES

Alinz, M., Floyd, P., and Goncuoglu, M., 1996, Supra-subduction zone ophiolites of Central Anatolia: geochemical evidence from the Sarikaraman ophiolite, Aksaray, Turkey: Mineralogical Magazine, v. 60, no. 402, p. 697-710.

Annen, C., Blundy, J., Sparks, R., 2006. The genesis of intermediate and silicic magmas in deep crustal hot zones. Journal of Petrology 47, 505-539.

Arenas, R., Díez Fernández, R., Sánchez Martínez, S., Gerdes, A., Fernández-Suárez, J., Albert, R., 2014. Two-stage collision: Exploring the birth of Pangea in the Variscan terranes. Gondwana Research 25, 756-763.

Arenas, R., Martínez, S. S., Gerdes, A., Albert, R., Fernández, R. D., and Andonaegui, P., 2013, Re-interpreting the Devonian ophiolites involved in the Variscan suture: U–Pb and Lu–Hf zircon data of the Moeche Ophiolite (Cabo Ortegal Complex, NW Iberia): International Journal of Earth Sciences, p. 1-18.

Azor, A., Rubatto, D., Simancas, J. F., González Lodeiro, F., Martínez Poyatos, D., Martín Parra, L. M., and Matas, J., 2008, Rheic Ocean ophiolitic remnants in southern Iberia questioned by SHRIMP U-Pb zircon ages on the Beja-Acebuches amphibolites: Tectonics, v. 27, no. 5, p. TC5006.

Bağcı, U., and Parlak, O., 2009, Petrology of the Tekirova (Antalya) ophiolite (Southern Turkey): evidence for diverse magma generations and their tectonic implications during Neotethyan-subduction: International Journal of Earth Sciences, v. 98, no. 2, p. 387-405.

Ballèvre, M., Bosse, V., Ducassou, C., Pitra, P., 2009. Palaeozoic history of the Armorican Massif: models for the tectonic evolution of the suture zones. Comptes Rendus Geoscience 341, 174-201.
Ballèvre, M., Catalán, J.R.M., López-Carmona, A., Pitra, P., Abati, J., Fernández, R.D., Ducassou, C., Arenas, R., Bosse, V., Castiñeiras, P., 2014. Correlation of the nappe stack in the Ibero-Armorican arc across the Bay of Biscay: a joint French–Spanish project. Geological Society, London, Special Publications 405, SP405. 413.
Bazylev, B. A., Popević, A., Karamata, S., Kononkova, N. N., Simakin, S. G., Olujić, J., Vujnović, L., and Memović, E., 2009, Mantle peridotites from the Dinaridic ophiolite belt and the Vardar zone western belt, central Balkan: A petrological comparison: Lithos, v. 108, no. 1–4, p. 37-71.

Bolhar, R., Ring, U., Kemp, A.S., Whitehouse, M., Weaver, S., Woodhead, J., Uysal, I.T., Turnbull, R., 2012. An integrated zircon geochronological and geochemical investigation into the Miocene plutonic evolution of the Cyclades, Aegean Sea, Greece: part 2—geochemistry. Contrib Mineral Petrol 164, 915-933.
Cocks, L.R.M., Torsvik, T.H., 2005. Baltica from the late Precambrian to mid-Palaeozoic times: The gain and loss of a terrane's identity. Earth-Science Reviews 72, 39-66.
Collins, W.J., Belousova, E.A., Kemp, A.I.S., Murphy, J.B., 2011. Two contrasting Phanerozoic orogenic systems revealed by hafnium isotope data. Nature Geoscience 4, 333-337.
Collins, W.J., Huang, H.Q., Jiang, X., 2016. Water-fluxed crustal melting produces Cordilleran batholiths, Geology, 44.
Collins, W., Richards, S., 2008. Geodynamic significance of S-type granites in circum-Pacific orogens. Geology 36, 559-562.

Costa, S., and Caby, R., 2001, Evolution of the Ligurian Tethys in the Western Alps: Sm/Nd and U/Pb geochronology and rare-earth element geochemistry of the Montgenèvre ophiolite (France): Chemical Geology, v. 175, no. 3–4, p. 449-466.

Dhuime, B., Hawkesworth, C., Cawood, P., 2011. When continents formed. Science 331, 154-155.

Dias da Silva, Í., Diez Fernandez, R., Gonzalez Clavijo, E., Diez Montes, A., 2014. Absolute age constraints on the Upper Parautochthon sedimentary sequence of the Morais allochthonous complex (Iberian Variscan belt, NE Portugal) based

on new magmatic zircon U-Pb data, In: Pankhurst, R.J., Castineiras, P., Sanchez Martinez, S. (Eds.), Gondwana 15: North meets South, Madrid, Spain.

Díez Fernández, R., Castiñeiras, P., Gómez Barreiro, J., 2012. Age constraints on Lower Paleozoic convection system: Magmatic events in the NW Iberian Gondwana margin. Gondwana Research 21, 1066-1079.

Dilek, Y., Furnes, H., and Shallo, M., 2008, Geochemistry of the Jurassic Mirdita Ophiolite (Albania) and the MORB to SSZ evolution of a marginal basin oceanic crust: Lithos, v. 100, no. 1–4, p. 174-209.

Dilek, Y., and Thy, P., 2009, Island arc tholeiite to boninitic melt evolution of the Cretaceous Kizildag (Turkey) ophiolite: Model for multi-stage early arc–forearc magmatism in Tethyan subduction factories: Lithos, v. 113, no. 1–2, p. 68-87.

Elmas, A., and Yiğitbaş, E., 2001, Ophiolite emplacement by strike-slip tectonics between the Pontide Zone and the Sakarya Zone in northwestern Anatolia, Turkey: International Journal of Earth Sciences, v. 90, no. 2, p. 257-269.

Evans, D.A.D., Mitchell, R.N., 2011. Assembly and breakup of the core of Paleoproterozoic-Mesoproterozoic supercontinent Nuna. Geology 39, 443-446.

Ewart, A., Collerson, K., Regelous, M., Wendt, J., Niu, Y., 1998. Geochemical evolution within the Tonga–Kermadec–Lau arc–back-arc systems: the role of varying mantle wedge composition in space and time. Journal of Petrology 39, 331-368.

Eyuboglu, Y., Bektas, O., and Pul, D., 2007, Mid-Cretaceous olistostromal ophiolitic melange developed in the back-arc basin of the eastern Pontide magmatic arc, northeast Turkey: International Geology Review, v. 49, no. 12, p. 1103-1126.

Frost, B.R., Barnes, C.G., Collins, W.J., Arculus, R.J., Ellis, D.J., Frost, C.D., 2001. A Geochemical Classification for Granitic Rocks. Journal of Petrology 42, 2033-2048.

Göncüoglu, M. C., Sayit, K., and Tekin, U. K., 2010, Oceanization of the northern Neotethys: geochemical evidence from ophiolitic melange basalts within the Izmir–Ankara suture belt, NW Turkey: Lithos, v. 116, no. 1, p. 175-187.

Griffin, W.L., Belousova, E.A., Shee, S.R., Pearson, N.J., O'Reilly, S.Y., 2004. Archean crustal evolution in the northern Yilgarn Craton: U–Pb and Hf-isotope evidence from detrital zircons. Precambrian Research 131, 231-282.

Grobys, J.W., Gohl, K., Eales, G., 2008. Quantitative tectonic reconstructions of Zealandia based on crustal thickness estimates GEOCHEMISTRY, GEOPHYSICS, GEOSYSTEMS 9.

Guiraud, R., Bosworth, W., Thierry, J., Delplanque, A., 2005. Phanerozoic geological evolution of Northern and Central Africa: An overview. Journal of African Earth Sciences 43, 83-143.

Hacker, B.R., Kelemen, P.B., Behn, M.D., 2011. Differentiation of the continental crust by relamination. Earth and Planetary Science Letters 307, 501-516.

Henderson, B., Collins, W.J., Murphy, B.J., Gutiérrez-Alonso, G., Hand, M., 2016. Gondwanan basement terranes of the Variscan-Appalachian orogen: Baltican, Saharan and West African hafnium isotopic fingerprints in Avalonia, Iberia and the Armorican Terranes. Tectonophysics.

Jolivet, L., Brun, J.-P., 2010. Cenozoic geodynamic evolution of the Aegean. Int J Earth Sci (Geol Rundsch) 99, 109-138.

Jones, G., and Robertson, A. H. F., 1991, Tectono-stratigraphy and evolution of the Mesozoic Pindos ophiolite and related units, northwestern Greece: Journal of the Geological Society, v. 148, no. 2, p. 267-288.

KARAOĞLAN, F., Parlak, O., Kloetzli, U., Thoeni, M., and Koller, F., 2013, U–Pb and Sm–

Nd geochronology of the Kızıldağ (Hatay, Turkey) ophiolite: implications for the timing and duration of suprasubduction zone type oceanic crust formation in the southern Neotethys: Geological Magazine, v. 150, no. 02, p. 283-299.

Kemp, A., Hawkesworth, C., Collins, W., Gray, C., Blevin, P., 2009. Isotopic evidence for rapid continental growth in an extensional accretionary orogen: The Tasmanides, eastern Australia. Earth and Planetary Science Letters 284, 455-466.

Kirby, G., 1984, The petrology and geochemistry of dykes of the Lizard Ophiolite Complex, Cornwall: Journal of the Geological Society, v. 141, no. 1, p. 53-59.

Kryza, R., Crowley, Q. G., Larionov, A., Pin, C., Oberc-Dziedzic, T., and Mochnacka, K., 2011, Chemical abrasion applied to SHRIMP zircon geochronology: An example from the Variscan Karkonosze Granite (Sudetes, SW Poland): Gondwana Research, no. 0.

Lanphere, M. A., Coleman, R. G., Karamata, S., and Pamić, J., 1975, Age of amphibolites associated with Alpine peridotites in the Dinaride ophiolite zone, Yugoslavia: Earth and Planetary Science Letters, v. 26, no. 3, p. 271-276.

Li, Z.X., Bogdanova, S.V., Collins, A.S., Davidson, A., De Waele, B., Ernst, R.E., Fitzsimons, I.C.W., Fuck, R.A., Gladkochub, D.P., Jacobs, J., Karlstrom, K.E., Lu, S., Natapov, L.M., Pease, V., Pisarevsky, S.A.,

Thrane, K., Vernikovsky, V., 2008. Assembly, configuration, and break-up history of Rodinia: A synthesis. Precambrian Research 160, 179-210.

Li, X. H., Faure, M., Lin, W., and Manatschal, G., 2013, New isotopic constraints on age and magma genesis of an embryonic oceanic crust: The Chenaillet Ophiolite in the Western Alps: Lithos, v. 160-161, no. 1, p. 283-291.

Linnemann, U., Gerdes, A., Hofmann, M., Marko, L., 2014. The Cadomian Orogen: Neoproterozoic to Early Cambrian crustal growth and orogenic zoning along the periphery of the West African Craton—Constraints from U–Pb zircon ages and Hf isotopes (Schwarzburg Antiform, Germany). Precambrian Research.

Martínez, S. S., Arenas, R., García, F. D., Catalán, J. R. M., Gómez-Barreiro, J., and Pearce, J. A., 2007, Careón ophiolite, NW Spain: suprasubduction zone setting for the youngest Rheic Ocean floor: Geology, v. 35, no. 1, p. 53-56.

Martínez, S. S., Gerdes, A., Arenas, R., and Abati, J., 2012, The Bazar Ophiolite of NW Iberia: a relic of the Iapetus–Tornquist Ocean in the Variscan suture: Terra Nova, v. 24, no. 4, p. 283-294.

Martínez, S.S., Arenas, R., Gerdes, A., Castiñeiras, P., Potrel, A., Fernández-Suárez, J., 2011. Isotope geochemistry and revised geochronology of the Purrido Ophiolite (Cabo Ortegal Complex, NW Iberian Massif): Devonian magmatism with mixed sources and involved Mesoproterozoic basement. Journal of the Geological Society 168, 733-750.

Murphy, J.B., Gutierrez-Alonso, G., Nance, R.D., Fernandez-Suarez, J., Keppie, J.D., Quesada, C., Strachan, R.A., Dostal, J., 2006. Origin of the Rheic Ocean: Rifting along a Neoproterozoic suture? Geology 34, 325-328.

Nicolae, I., Soroiu, M., and Bonhomme, G., 1992, Ages K-Ar de quelques ophiolites des Monts Apuseni du Sud et leur signification géologique (Roumanie): Géologie Alpine, v. 68, p. 77-88.

Ozvoldova, L., and Faupl, P., 1993, Radiolarien aus kieseligen Schichtgliedern des Juras der Grestener und Ybbsitzer Klippenzone (Ostalpen, Niederösterreich: Jahrb. Geol. Bundesanstalt. Wien, v. 136, p. 479-494.

Pamić, J., and Jurković, I., 1997, Alpine Magmatic-Metallogenic Formations of the Northwestern and Central Dinarides: Rudarsko-geološko-naftni zbornik, v. 9, no. 1, p. 1-9.

PARLAK, O., and ROBERTSON, A., 2004,

The ophiolite-related Mersin Melange, southern Turkey: its role in the tectonic–sedimentary setting of Tethys in the Eastern Mediterranean region: Geological Magazine, v. 141, no. 03, p. 257-286.

Pastor-Galán, D., Gutiérrez-Alonso, G., Murphy, J.B., Fernández-Suárez, J., Hofmann, M., Linnemann, U., 2013. Provenance analysis of the Paleozoic sequences of the northern Gondwana margin in NW Iberia: passive margin to Variscan collision and orocline development. Gondwana Research 23, 1089-1103.

Pearce, J.A., Lippard, S.J., Roberts, S., 1984. Characteristics and tectonic significance of supra-subduction zone ophiolites. Geological Society, London, Special Publications 16, 77-94.

Prelević, D., Stracke, A., Foley, S.F., Romer, R.L., Conticelli, S., 2010. Hf isotope compositions of Mediterranean lamproites: Mixing of melts from asthenosphere and crustally contaminated mantle lithosphere. Lithos 119, 297-312.

Rampone, E., Hofmann, A. W., and Raczek, I., 1998, Isotopic contrasts within the Internal Liguride ophiolite (N. Italy): the lack of a genetic mantle–crust link: Earth and Planetary Science Letters, v. 163, no. 1, p. 175-189.
Rautenschlein, M., Jenner, G. A., Hertogen,

J., Hofmann, A. W., Kerrich, R., Schmincke, H. U., and White, W. M., 1985, Isotopic and trace element composition of volcanic glasses from the Akaki Canyon, Cyprus: implications for the origin of the Troodos ophiolite: Earth and Planetary Science Letters, v. 75, no. 4, p. 369-383.

Ribeiro, A., Munhá, J., Fonseca, P., Araújo, A., Pedro, J., Mateus, A., Tassinari, C., Machado, G., and Jesus, A., 2010, Variscan ophiolite belts in the Ossa-Morena Zone (Southwest Iberia): geological characterization and geodynamic significance: Gondwana Research, v. 17, no. 2, p. 408-421.

Robardet, M., 2003. The Armorica 'microplate': fact or fiction? Critical review of the concept and contradictory palaeobiogeographical data. Palaeogeography, Palaeoclimatology, Palaeoecology 195, 125-148.

Roberts, S., Andrews, J., Bull, J., and Sanderson, D., 1993, Slow-spreading ridge-axis tectonics: evidence from the Lizard complex, UK: Earth and Planetary Science Letters, v. 116, no. 1, p. 101-112.

Robertson, A.H., 2002. Overview of the genesis and emplacement of Mesozoic ophiolites in the Eastern Mediterranean Tethyan region. Lithos 65, 1-67.

Robertson, A., and Shallo, M., 2000, Mesozoic–Tertiary tectonic evolution of Albania in its regional Eastern Mediterranean context: Tectonophysics, v. 316, no. 3–4, p. 197-254.

Robertson, A., and Waldron, J., Geochemistry and tectonic setting of late Triassic and Late Jurassic–Early Cretaceous basaltic extrusives from the Antalya Complex, SW Turkey, in Proceedings International Earth Sciences Congress on Aegean Region, Proceedings, 1990, Volume 2, p. 279-299.

Robertson, A.H., Parlak, O., Ustaömer, T., 2012. Overview of the Palaeozoic–Neogene evolution of Neotethys in the Eastern Mediterranean region (southern Turkey, Cyprus, Syria). Petroleum Geoscience 18, 381-404.
Robinson, P. T., Melson, W. G., O'Hearn, T., and Schmincke, H.-U., 1983, Volcanic glass compositions of the Troodos ophiolite, Cyprus: Geology, v. 11, no. 7, p. 400-404.

Rosenbaum, G., Lister, G.S., Duboz, C., 2002. Reconstruction of the tectonic evolution of the western Mediterranean since the Oligocene. Journal of the Virtual Explorer 8, 107-130.
Roddick, J., Cameron, W., and Smith, A., 1979, Permo–Triassic and Jurassic 40Ar–39Ar ages from Greek ophiolites and associated rocks.

Schulmann, K., Catalán, J.R.M., Lardeaux, J.M., Janoušek, V., Oggiano, G., 2014. The Variscan orogeny: extent, timescale and the formation of the European crust. Geological Society, London,

Special Publications 405, SP405. 415.

Slovenec, D., and Lugović, B., 2012, Evidence of the spreading culmination in the Eastern Tethyan Repno oceanic domain, assessed by the petrology and geochemistry of N-MORB extrusive rocks from the Mt. Medvednica ophiolite mélange (NW Croatia): Geologia Croatica, v. 65, no. 3, p. 345-466.

Smits, R.G., Collins, W.J., Hand, M., Dutch, R., Payne, J., 2014. A Proterozoic Wilson cycle identified by Hf isotopes in central Australia: Implications for the assembly of Proterozoic Australia and Rodinia. Geology.

Spray, J., and Roddick, J., 1980, Petrology and 40Ar/39Ar geochronology of some Hellenic sub-ophiolite metamorphic rocks: Contributions to Mineralogy and Petrology, v. 72, no. 1, p. 43-55.

Stampfli, G., Hochard, C., Vérard, C., Wilhem, C., vonRaumer, J., 2013. The formation of Pangea. Tectonophysics.

Thuizat, R., Whitechurch, H., Montigny, R., and Juteau, T., 1981, KAr dating of some infra-ophiolitic metamorphic soles from the eastern Mediterranean: New evidence for oceanic thrustings before obduction: Earth and Planetary Science Letters, v. 52, no. 2, p. 302-310.

Torsvik, T.H., Rehnström, E.F., 2003. The Tornquist Sea and Baltica–Avalonia docking. Tectonophysics 362, 67-82.

Ustaomer, T., and Robertson, A., 1997, AAPG Memoir 68: Regional and Petroleum Geology of the Black Sea and Surrounding Region. Chapter 14: Tectonic-Sedimentary Evolution of the North Tethyan Margin in the Central Pontides of Northern Turkey.

Uysal, İ., Ersoy, E. Y., Karslı, O., Dilek, Y., Sadıklar, M. B., Ottley, C. J., Tiepolo, M., and Meisel, T., 2012, Coexistence of abyssal and ultra-depleted SSZ type mantle peridotites in a Neo-Tethyan Ophiolite in SW Turkey: Constraints from mineral composition, whole-rock geochemistry (major–trace–REE–PGE), and Re–Os isotope systematics: Lithos, v. 132–133, no. 0, p. 50-69.

van Staal, C.R., Whalen, J.B., Valverde-Vaquero, P., Zagorevski, A., Rogers, N., 2009. Pre-Carboniferous, episodic accretion-related, orogenesis along the Laurentian margin of the northern Appalachians. Geological Society, London, Special Publications 327, 271-316.

Wilson, J.T., 1966. Did the Atlantic close and then re-open? Nature.

Worsley, T.R., Nance, D., Moody, J.B., 1984. Global tectonics and eustasy for the past 2 billion years. Marine Geology 58, 373-400.

Zhang, S., Li, Z.-X., Evans, D.A.D., Wu, H., Li, H., Dong, J., 2012. Pre-Rodinia supercontinent Nuna shaping up: A global synthesis with new paleomagnetic results from North China. Earth and Planetary Science Letters 353–354, 145-155.

Zlatkin, O., Avigad, D., Gerdes, A., 2013. Evolution and provenance of Neoproterozoic basement and Lower Paleozoic siliciclastic cover of the Menderes Massif (western Taurides): Coupled U–Pb–Hf zircon isotope geochemistry. Gondwana Research 23, 682-700.

Supporting information

Supplementary Table 1. Hafnium data from Iberia samples (new data)

Reference	Sample no.	Analysis number	U-Pb Age	Ehf value	Type	Region	Northing	Eastings
Henderson 2014	PG2	a12	1039.06506	-4.517640349	Detrital	Iberia	4788058.88 m N	358861.78 m E
Henderson 2014	PG2	a15	2045.057243	0.317955391	Detrital	Iberia	4788058.88 m N	358861.78 m E
Henderson 2014	PG2	a19	1770.838855	-2.879473202	Detrital	Iberia	4788058.88 m N	358861.78 m E
Henderson 2014	PG2	a23	2147.959788	-1.061460519	Detrital	Iberia	4788058.88 m N	358861.78 m E
Henderson 2014	PG2	a30	1048.895004	-3.021795068	Detrital	Iberia	4788058.88 m N	358861.78 m E
Henderson 2014	PG2	a34	1008.036965	-12.18622742	Detrital	Iberia	4788058.88 m N	358861.78 m E
Henderson 2014	PG2	a39	1026.21827	-14.31074857	Detrital	Iberia	4788058.88 m N	358861.78 m E
Henderson 2014	PG2	a46	1794.942294	-5.704870749	Detrital	Iberia	4788058.88 m N	358861.78 m E
Henderson 2014	PG2	a60	1949.56685	-4.860113496	Detrital	Iberia	4788058.88 m N	358861.78 m E
Henderson 2014	PG2	a7	1884.875371	-8.728613131	Detrital	Iberia	4788058.88 m N	358861.78 m E
Henderson 2014	PG2	a9	1076.608475	-6.624083916	Detrital	Iberia	4788058.88 m N	358861.78 m E
Henderson 2014	PG2	b10	1851.510947	-5.55117302	Detrital	Iberia	4788058.88 m N	358861.78 m E
Henderson 2014	PG2	b33	2718.799869	-2.205922613	Detrital	Iberia	4788058.88 m N	358861.78 m E
Henderson 2014	PG2	b36	2254.194629	-8.073851775	Detrital	Iberia	4788058.88 m N	358861.78 m E
Henderson 2014	PG2	b4	2119.706089	1.058045876	Detrital	Iberia	4788058.88 m N	358861.78 m E
Henderson 2014	PG2	b42	1029.142435	-10.10814581	Detrital	Iberia	4788058.88 m N	358861.78 m E
Henderson 2014	PG2	b45	2077.766407	10.79873709	Detrital	Iberia	4788058.88 m N	358861.78 m E
Henderson 2014	PG2	b55	1055.573498	-4.68640784	Detrital	Iberia	4788058.88 m N	358861.78 m E
Henderson 2014	PG2	b57	2123.850313	-9.824039291	Detrital	Iberia	4788058.88 m N	358861.78 m E
Henderson 2014	PG2	~~a03~~	600.25	-14.56142992	Detrital	Iberia	4788058.88 m N	358861.78 m E
Henderson 2014	PG2	a06	2093.461442	-3.436997223	Detrital	Iberia	4788058.88 m N	358861.78 m E
Henderson 2014	PG2	a11	2844.157023	-8.302566732	Detrital	Iberia	4788058.88 m N	358861.78 m E
Henderson 2014	PG2	a16	1743.033311	-5.199846857	Detrital	Iberia	4788058.88 m N	358861.78 m E
Henderson 2014	PG2	a17	301.4377342	-4.922022313	Detrital	Iberia	4788058.88 m N	358861.78 m E
Henderson 2014	PG2	a29	659.5472068	6.468232652	Detrital	Iberia	4788058.88 m N	358861.78 m E
Henderson 2014	PG2	a33	627.6020211	-1.381871041	Detrital	Iberia	4788058.88 m N	358861.78 m E
Henderson 2014	PG2	a35	294.0369559	-5.732856958	Detrital	Iberia	4788058.88 m N	358861.78 m E
Henderson 2014	PG2	a40	296.8056563	0.931841454	Detrital	Iberia	4788058.88 m N	358861.78 m E
Henderson 2014	PG2	a42	288.0510047	-4.248720958	Detrital	Iberia	4788058.88 m N	358861.78 m E
Henderson 2014	PG2	a47	684.9303128	7.643607806	Detrital	Iberia	4788058.88 m N	358861.78 m E
Henderson 2014	PG2	a50	293.6987703	-2.526975867	Detrital	Iberia	4788058.88 m N	358861.78 m E
Henderson 2014	PG2	a52	295.8078738	-3.86453452	Detrital	Iberia	4788058.88 m N	358861.78 m E
Henderson 2014	PG2	a53	744.2767943	-1.926111587	Detrital	Iberia	4788058.88 m N	358861.78 m E
Henderson 2014	PG2	b03	296.4976721	-5.068133449	Detrital	Iberia	4788058.88 m N	358861.78 m E
Henderson 2014	PG2	b11	2019.946543	-4.315403481	Detrital	Iberia	4788058.88 m N	358861.78 m E
Henderson 2014	PG2	b12	331.9106678	-4.325448624	Detrital	Iberia	4788058.88 m N	358861.78 m E
Henderson 2014	PG2	b17	2794.267409	-2.921780623	Detrital	Iberia	4788058.88 m N	358861.78 m E
Henderson 2014	PG2	b19	2572.744208	0.091995714	Detrital	Iberia	4788058.88 m N	358861.78 m E
Henderson 2014	PG2	b23	682.6178652	0.84990561	Detrital	Iberia	4788058.88 m N	358861.78 m E
Henderson 2014	PG2	b24	658.9590842	-8.800173888	Detrital	Iberia	4788058.88 m N	358861.78 m E
Henderson 2014	PG2	b35	2599.316325	-10.65637732	Detrital	Iberia	4788058.88 m N	358861.78 m E
Henderson 2014	PG2	b38	578.3062132	-12.36498394	Detrital	Iberia	4788058.88 m N	358861.78 m E
Henderson 2014	PG2	b41	630.9100333	5.905927328	Detrital	Iberia	4788058.88 m N	358861.78 m E
Henderson 2014	PG2	b43	295.39	-3.953167684	Detrital	Iberia	4788058.88 m N	358861.78 m E
Henderson 2014	PG2	b44	497.1992681	-1.454279545	Detrital	Iberia	4788058.88 m N	358861.78 m E
Henderson 2014	PG2	b51	511.775083	-0.70111061	Detrital	Iberia	4788058.88 m N	358861.78 m E
Henderson 2014	PG2	b52	654.0851513	-6.912019729	Detrital	Iberia	4788058.88 m N	358861.78 m E
Henderson 2014	PG2	b53	297.8538992	-5.822475419	Detrital	Iberia	4788058.88 m N	358861.78 m E
Henderson 2014	PG2	b54	2599.194942	-0.146098676	Detrital	Iberia	4788058.88 m N	358861.78 m E
Henderson 2014	PG2	b58	644.6299594	-5.130097504	Detrital	Iberia	4788058.88 m N	358861.78 m E
Henderson 2014	PG6	a16	644	-9.526	Detrital	Iberia	4796198.36 m N	279875.51 m E
Henderson 2014	PG6	a21	644.6309522	-6.773	Detrital	Iberia	4796198.36 m N	279875.51 m E
Henderson 2014	PG6	a22	2508.86165	6.550	Detrital	Iberia	4796198.36 m N	279875.51 m E
Henderson 2014	PG6	a3	644	6.959	Detrital	Iberia	4796198.36 m N	279875.51 m E
Henderson 2014	PG6	a30	635.9769665	-11.404	Detrital	Iberia	4796198.36 m N	279875.51 m E
Henderson 2014	PG6	a33	612.3732485	-5.810	Detrital	Iberia	4796198.36 m N	279875.51 m E
Henderson 2014	PG6	a34	978.542273	-2.679	Detrital	Iberia	4796198.36 m N	279875.51 m E
Henderson 2014	PG6	a36	996.8093947	-5.063	Detrital	Iberia	4796198.36 m N	279875.51 m E
Henderson 2014	PG6	a41	670.6497608	-19.453	Detrital	Iberia	4796198.36 m N	279875.51 m E
Henderson 2014	PG6	a45	1811.191816	-2.188	Detrital	Iberia	4796198.36 m N	279875.51 m E
Henderson 2014	PG6	a48	1901.518895	-10.263	Detrital	Iberia	4796198.36 m N	279875.51 m E
Henderson 2014	PG6	a5	623	-3.068	Detrital	Iberia	4796198.36 m N	279875.51 m E
Henderson 2014	PG6	a50	941.4028647	1.136	Detrital	Iberia	4796198.36 m N	279875.51 m E
Henderson 2014	PG6	a51	731.5251191	-14.887	Detrital	Iberia	4796198.36 m N	279875.51 m E
Henderson 2014	PG6	a53	738	8.729	Detrital	Iberia	4796198.36 m N	279875.51 m E
Henderson 2014	PG6	a54	813.5029621	-14.663	Detrital	Iberia	4796198.36 m N	279875.51 m E
Henderson 2014	PG6	a56	1091.026273	-12.171	Detrital	Iberia	4796198.36 m N	279875.51 m E
Henderson 2014	PG6	a59	1005.760778	-7.430	Detrital	Iberia	4796198.36 m N	279875.51 m E
Henderson 2014	PG6	a6	1015	14.259	Detrital	Iberia	4796198.36 m N	279875.51 m E
Henderson 2014	PG6	a7	1063.708223	-0.142	Detrital	Iberia	4796198.36 m N	279875.51 m E
Henderson 2014	PG6	a9	829	2.517096549	Detrital	Iberia	4796198.36 m N	279875.51 m E
Henderson 2014	pg6	PG6_A4	489.5515997	-6.130	Detrital	Iberia	4796198.36 m N	279875.51 m E
Henderson 2014	pg6	PG6_A10	518.4228979	-8.576	Detrital	Iberia	4796198.36 m N	279875.51 m E
Henderson 2014	pg6	PG6_A14	451.1354226	-3.415	Detrital	Iberia	4796198.36 m N	279875.51 m E
Henderson 2014	pg6	PG6_A19	970	-13.594	Detrital	Iberia	4796198.36 m N	279875.51 m E
Henderson 2014	pg6	PG6_A23	488.2242951	-6.683	Detrital	Iberia	4796198.36 m N	279875.51 m E

Henderson 2014	pg6	PG6_A24	343.2796266	-1.433	Detrital	Iberia	4796198.36 m N	279875.51 m E
Henderson 2014	pg6	PG6_A26	506.6929568	-2.751	Detrital	Iberia	4796198.36 m N	279875.51 m E
Henderson 2014	pg6	PG6_A27	339.856723	-6.389	Detrital	Iberia	4796198.36 m N	279875.51 m E
Henderson 2014	pg6	PG6_A39	486.558021	-2.387	Detrital	Iberia	4796198.36 m N	279875.51 m E
Henderson 2014	pg6	PG6_A42	321.743015	-10.500	Detrital	Iberia	4796198.36 m N	279875.51 m E
Henderson 2014	PG3	a01	1928	-14.55746919	Detrital	Iberia	4802182.68 m N	280485.99 m E
Henderson 2014	PG3	a05	549	-2.843392242	Detrital	Iberia	4802182.68 m N	280485.99 m E
Henderson 2014	PG3	a07	2693	-1.943925588	Detrital	Iberia	4802182.68 m N	280485.99 m E
Henderson 2014	PG3	a08	494	4.858959818	Detrital	Iberia	4802182.68 m N	280485.99 m E
Henderson 2014	PG3	a27	597	-1.067034115	Detrital	Iberia	4802182.68 m N	280485.99 m E
Henderson 2014	PG3	a28	948	-10.72449959	Detrital	Iberia	4802182.68 m N	280485.99 m E
Henderson 2014	PG3	a29	836	-2.913478208	Detrital	Iberia	4802182.68 m N	280485.99 m E
Henderson 2014	PG3	a34	541	-6.910983256	Detrital	Iberia	4802182.68 m N	280485.99 m E
Henderson 2014	PG3	a35	441	-7.591519692	Detrital	Iberia	4802182.68 m N	280485.99 m E
Henderson 2014	PG3	a37	298	-5.537205359	Detrital	Iberia	4802182.68 m N	280485.99 m E
Henderson 2014	PG3	a42	410	-1.513954926	Detrital	Iberia	4802182.68 m N	280485.99 m E
Henderson 2014	PG3	a47	513	-2.381128483	Detrital	Iberia	4802182.68 m N	280485.99 m E
Henderson 2014	PG3	a50	2146	-1.209841028	Detrital	Iberia	4802182.68 m N	280485.99 m E
Henderson 2014	PG3	a51	544	9.084970309	Detrital	Iberia	4802182.68 m N	280485.99 m E
Henderson 2014	PG3	a52	699	7.637496021	Detrital	Iberia	4802182.68 m N	280485.99 m E
Henderson 2014	PG3	a54	342	0.43218754	Detrital	Iberia	4802182.68 m N	280485.99 m E
Henderson 2014	PG3	a56	2521	-5.252849556	Detrital	Iberia	4802182.68 m N	280485.99 m E
Henderson 2014	PG3	a57	918	-15.45587881	Detrital	Iberia	4802182.68 m N	280485.99 m E
Henderson 2014	PG3	b02	502	-1.392008179	Detrital	Iberia	4802182.68 m N	280485.99 m E
Henderson 2014	PG3	b05	677	-0.657050719	Detrital	Iberia	4802182.68 m N	280485.99 m E
Henderson 2014	PG3	b06	387	-2.385009596	Detrital	Iberia	4802182.68 m N	280485.99 m E
Henderson 2014	PG3	b08	1034	-12.62296763	Detrital	Iberia	4802182.68 m N	280485.99 m E
Henderson 2014	PG3	b11	500	-2.730752579	Detrital	Iberia	4802182.68 m N	280485.99 m E
Henderson 2014	PG3	b21	482	6.712712014	Detrital	Iberia	4802182.68 m N	280485.99 m E
Henderson 2014	PG3	b22	738	5.793880532	Detrital	Iberia	4802182.68 m N	280485.99 m E
Henderson 2014	PG3	b26	600	0.334654523	Detrital	Iberia	4802182.68 m N	280485.99 m E
Henderson 2014	PG3	b32	1947	20.4377234	Detrital	Iberia	4802182.68 m N	280485.99 m E
Henderson 2014	PG3	b40	583	-0.1019719	Detrital	Iberia	4802182.68 m N	280485.99 m E
Henderson 2014	PG3	b43	557	-8.978202672	Detrital	Iberia	4802182.68 m N	280485.99 m E
Henderson 2014	PG3	b46	964	-9.304226459	Detrital	Iberia	4802182.68 m N	280485.99 m E
Henderson 2014	PG3	b49	440	-2.96454087	Detrital	Iberia	4802182.68 m N	280485.99 m E
Henderson 2014	PG3	b53	702	4.318732403	Detrital	Iberia	4802182.68 m N	280485.99 m E
Henderson 2014	PG3	b57	498	-24.44563068	Detrital	Iberia	4802182.68 m N	280485.99 m E

Henderson 2014	PG3	b58	581	0.262534949	Detrital	Iberia	4802182.68 m N	280485.99 m E
Henderson 2014	PG3	b59	1815	-3.203155601	Detrital	Iberia	4802182.68 m N	280485.99 m E
Henderson 2014	PG3	c02	2073	6.62195313	Detrital	Iberia	4802182.68 m N	280485.99 m E
Henderson 2014	PG3	c06	858	-2.544800084	Detrital	Iberia	4802182.68 m N	280485.99 m E
Henderson 2014	PG3	c09	607	6.361372874	Detrital	Iberia	4802182.68 m N	280485.99 m E
Henderson 2014	PG3	c11	475	-4.760212288	Detrital	Iberia	4802182.68 m N	280485.99 m E
Henderson 2014	PG3	c13	855	-8.248014605	Detrital	Iberia	4802182.68 m N	280485.99 m E
Henderson 2014	PG3	c16	674	-11.66797448	Detrital	Iberia	4802182.68 m N	280485.99 m E
Henderson 2014	PG3	c18	586	-10.20082929	Detrital	Iberia	4802182.68 m N	280485.99 m E
Henderson 2014	PG3	c27	636	-16.23892203	Detrital	Iberia	4802182.68 m N	280485.99 m E
Henderson 2014	PG3	c36	336	-2.787788849	Detrital	Iberia	4802182.68 m N	280485.99 m E
Henderson 2014	PG3	c44	615	-10.55015009	Detrital	Iberia	4802182.68 m N	280485.99 m E
Henderson 2014	PG3	c49	502	-5.448437544	Detrital	Iberia	4802182.68 m N	280485.99 m E
Henderson 2014	PG3	c51	602	-0.268233684	Detrital	Iberia	4802182.68 m N	280485.99 m E
Henderson 2014	PG3	c57	560	-2.506861105	Detrital	Iberia	4802182.68 m N	280485.99 m E
Henderson 2014	PG3	c59	550	-1.775152769	Detrital	Iberia	4802182.68 m N	280485.99 m E
Henderson 2014	pg5	PG5_A10	602	-10.51715294	Detrital	Iberia	4787226.91 m N	290206.27 m E
Henderson 2014	pg5	PG5_A15	326	-5.432580067	Detrital	Iberia	4787226.91 m N	290206.27 m E
Henderson 2014	pg5	PG5_A45	584	3.259271859	Detrital	Iberia	4787226.91 m N	290206.27 m E
Henderson 2014	pg5	PG5_B10	957	9.215117729	Detrital	Iberia	4787226.91 m N	290206.27 m E
Henderson 2014	pg5	PG5_B59	2718	-0.767901376	Detrital	Iberia	4787226.91 m N	290206.27 m E
Henderson 2014	pg5	pg5_a03	554	-3.496229399	Detrital	Iberia	4787226.91 m N	290206.27 m E
Henderson 2014	pg5	PG5_A12	613	7.282751737	Detrital	Iberia	4787226.91 m N	290206.27 m E
Henderson 2014	pg5	PG5_A14	572	-4.98567114	Detrital	Iberia	4787226.91 m N	290206.27 m E
Henderson 2014	pg5	PG5_A16	552	-3.573036907	Detrital	Iberia	4787226.91 m N	290206.27 m E
Henderson 2014	pg5	PG5_A19	335	-8.635765507	Detrital	Iberia	4787226.91 m N	290206.27 m E
Henderson 2014	pg5	PG5_a20	2638	-1.646305905	Detrital	Iberia	4787226.91 m N	290206.27 m E
Henderson 2014	pg5	PG5_A26	500	-4.143246168	Detrital	Iberia	4787226.91 m N	290206.27 m E
Henderson 2014	pg5	PG5_A30	1062	8.225059319	Detrital	Iberia	4787226.91 m N	290206.27 m E
Henderson 2014	pg5	PG5_A31	811	3.512063489	Detrital	Iberia	4787226.91 m N	290206.27 m E
Henderson 2014	pg5	PG5_A34	829	0.051426311	Detrital	Iberia	4787226.91 m N	290206.27 m E
Henderson 2014	pg5	PG5_A41	2636	-4.157040784	Detrital	Iberia	4787226.91 m N	290206.27 m E
Henderson 2014	PG5	pg5_A46	1064	-3.900087842	Detrital	Iberia	4787226.91 m N	290206.27 m E
Henderson 2014	pg5	PG5_A54	512	0.003605385	Detrital	Iberia	4787226.91 m N	290206.27 m E
Henderson 2014	pg5	PG5_A58	709	0.588602667	Detrital	Iberia	4787226.91 m N	290206.27 m E
Henderson 2014	pg5	PG5_A60	376	5.225926482	Detrital	Iberia	4787226.91 m N	290206.27 m E
Henderson 2014	pg5	PG5_b05	558	-5.089927383	Detrital	Iberia	4787226.91 m N	290206.27 m E
Henderson 2014	pg5	PG5_B08	905	12.35086885	Detrital	Iberia	4787226.91 m N	290206.27 m E
Henderson 2014	pg5	PG5_B13	346	-1.163957558	Detrital	Iberia	4787226.91 m N	290206.27 m E
Henderson 2014	pg5	PG5_B17	483	-11.25520412	Detrital	Iberia	4787226.91 m N	290206.27 m E
Henderson 2014	pg5	PG5_b18	814	5.505020762	Detrital	Iberia	4787226.91 m N	290206.27 m E
Henderson 2014	pg5	PG5_b20	335	-4.513407651	Detrital	Iberia	4787226.91 m N	290206.27 m E
Henderson 2014	PG5	pg5_b23	2513	-13.38142098	Detrital	Iberia	4787226.91 m N	290206.27 m E
Henderson 2014	PG5	pg5_b24	478	4.1209484	Detrital	Iberia	4787226.91 m N	290206.27 m E
Henderson 2014	pg5	PG5_b32	629	-6.268753373	Detrital	Iberia	4787226.91 m N	290206.27 m E
Henderson 2014	PG5	pg5_b33	340	-6.907315304	Detrital	Iberia	4787226.91 m N	290206.27 m E
Henderson 2014	PG5	pg5_b36	560	4.580370565	Detrital	Iberia	4787226.91 m N	290206.27 m E
Henderson 2014	pg5	PG5_B44	933	10.95206874	Detrital	Iberia	4787226.91 m N	290206.27 m E
Henderson 2014	PG5	pg5_b47	343	1.023071835	Detrital	Iberia	4787226.91 m N	290206.27 m E
Henderson 2014	PG5	pg5_b49	1100	10.82056109	Detrital	Iberia	4787226.91 m N	290206.27 m E
Henderson 2014	pg5	PG5_B50	2626	-2.614459024	Detrital	Iberia	4787226.91 m N	290206.27 m E
Henderson 2014	pg5	PG5_B52	2381	-4.472549965	Detrital	Iberia	4787226.91 m N	290206.27 m E
Henderson 2014	PG5	pg5_b56	585	-16.04720844	Detrital	Iberia	4787226.91 m N	290206.27 m E
Henderson 2014	PG5	pg5_b57	623	-2.451626142	Detrital	Iberia	4787226.91 m N	290206.27 m E
Henderson 2014	pg7	PG7_A03	476	-5.758260697	Detrital	Iberia	4800177.71 m N	709552.62 m E
Henderson 2014	pg7	PG7_A06	541	-10.30795128	Detrital	Iberia	4800177.71 m N	709552.62 m E
Henderson 2014	pg7	PG7_A08	481	-12.11089029	Detrital	Iberia	4800177.71 m N	709552.62 m E
Henderson 2014	pg7	PG7_A12	487	-4.674257581	Detrital	Iberia	4800177.71 m N	709552.62 m E
Henderson 2014	pg7	PG7_A19	509	-2.882727351	Detrital	Iberia	4800177.71 m N	709552.62 m E
Henderson 2014	pg7	PG7_A20	501	-11.86116665	Detrital	Iberia	4800177.71 m N	709552.62 m E
Henderson 2014	pg7	PG7_A45	487	-1.858984345	Detrital	Iberia	4800177.71 m N	709552.62 m E
Henderson 2014	pg7	PG7_A52	547	-14.29050232	Detrital	Iberia	4800177.71 m N	709552.62 m E
Henderson 2014	pg7	PG7_A53	507	-2.085926503	Detrital	Iberia	4800177.71 m N	709552.62 m E
Henderson 2014	pg7	PG7_B9	549	-27.2599467	Detrital	Iberia	4800177.71 m N	709552.62 m E
Henderson 2014	pg7	PG7_B13	478	-5.212977657	Detrital	Iberia	4800177.71 m N	709552.62 m E
Henderson 2014	pg7	PG7_B30	488	-0.634467094	Detrital	Iberia	4800177.71 m N	709552.62 m E
Henderson 2014	pg7	PG7_B34	430	4.689741559	Detrital	Iberia	4800177.71 m N	709552.62 m E
Henderson 2014	pg7	PG7_B46	490	-3.215450074	Detrital	Iberia	4800177.71 m N	709552.62 m E

References for the data from Figure 1, corresponding to locations shown in Figure 2

1. Beltrán-Triviño, A., et al. (2013). "Tracing Alpine sediment sources through laser ablation U–Pb dating and Hf-isotopes of detrital zircons." Sedimentology 60(1): 197-224.
2. Schärer, U., et al. (2012). "Major geological cycles substantiated by U–Pb ages and εHfi of detrital zircon grains from the Lower Rhine Basin." Chemical Geology 294–295(0): 63-74.
3. Schaltegger, U. and P. Brack (2007). "Crustal-scale magmatic systems during intracontinental strike-slip tectonics: U, Pb and Hf isotopic constraints from Permian magmatic rocks of the Southern Alps." International Journal of Earth Sciences 96(6): 1131-1151.
4. Stille, P. and R. Steiger (1991). "Hf isotope systematics in granitoids from the central and southern Alps." Contributions to Mineralogy and Petrology 107(3): 273-278.
5. Morag, N., et al. (2012). "1000–580Ma crustal evolution in the northern Arabian-Nubian Shield revealed by U–Pb–Hf of detrital zircons from late Neoproterozoic sediments (Elat area, Israel)." Precambrian Research 208: 197-212.
6. Fodor, L., et al. (2008). "Miocene emplacement and rapid cooling of the Pohorje pluton at the Alpine-Pannonian-Dinaridic junction, Slovenia." Swiss Journal of Geosciences 101(1): 255-271.
7. Prelević, D., et al. (2010). "Hf isotope compositions of Mediterranean lamproites: Mixing of melts from asthenosphere and crustally contaminated mantle lithosphere." Lithos 119(3–4): 297-312
8. Fu, B., et al. (2012). "O-Hf isotope constraints on the origin of zircon in high-pressure mélange blocks and associated matrix rocks from Tinos and Syros, Greece." European Journal of Mineralogy 24(2): 277-287.
9. Bolhar, R., et al. (2012). "An integrated zircon geochronological and geochemical investigation into the Miocene plutonic evolution of the Cyclades, Aegean Sea, Greece: part 2—geochemistry." Contributions to Mineralogy and Petrology 164(6): 915-933.
10. Avigad, D., et al. (2012). "Coupled U–Pb–Hf of detrital zircons of Cambrian sandstones from Morocco and Sardinia: Implications for provenance and Precambrian crustal evolution of North Africa." Gondwana Research 21(2–3): 690-703.
11. Villaseca, C., et al. (2012). "Recycled metaigneous crustal sources for S- and I-type Variscan granitoids from the Spanish Central System batholith: Constraints from Hf isotope zircon composition." Lithos 153(0): 84-93.
12. Pastor-Galán, D., et al. (2012). "Provenance analysis of the Paleozoic sequences of the northern Gondwana margin in NW Iberia: passive margin to Variscan collision and orocline development." Gondwana Research.
13. Rosa, D., et al. (2009). "U–Pb geochronology and Hf isotope ratios of magmatic zircons from the Iberian Pyrite Belt." Mineralogy and Petrology 95(1-2): 47-69.
14. Arenas, R., et al. (2013). "Re-interpreting the Devonian ophiolites involved in the Variscan suture: U–Pb and Lu–Hf zircon data of the Moeche Ophiolite (Cabo Ortegal Complex, NW Iberia)." International Journal of Earth Sciences: 1-18.
15. Martínez, S. S., et al. (2011). "Isotope geochemistry and revised geochronology of the Purrido Ophiolite (Cabo Ortegal Complex, NW Iberian Massif): Devonian magmatism with mixed sources and involved Mesoproterozoic basement." Journal of the Geological Society 168(3): 733-750.
16. Köksal, S., et al. (2012). "Crustal homogenization revealed by U–Pb zircon ages and Hf isotope evidence from the Late Cretaceous granitoids of the Agaçören intrusive suite (Central Anatolia/Turkey)." Contributions to Mineralogy and Petrology 163(4): 725-743.
17. Devechi, Z. (2013)." Detrital zircon ages and provenance of the Triassic (?) carpholite-bearing metaconglomerates in the southern Menderes massif", The graduate school of natural and applied sciences, Middle East Technical University, Master of Science Thesis
18. Zlatkin, O., et al. (2013). "Evolution and provenance of Neoproterozoic basement and Lower Paleozoic siliciclastic cover of the Menderes Massif (western Taurides): Coupled U–Pb–Hf zircon isotope geochemistry." Gondwana Research 23(2): 682-700.
19. Li, X. H., et al. (2013). "New isotopic constraints on age and magma genesis of an embryonic oceanic crust: The Chenaillet Ophiolite in the Western Alps." Lithos 160-161(1): 283-291.
20. Teixeira, R., et al. (2011). "Combined U–Pb geochronology and Lu–Hf isotope systematics by LAM–ICPMS of zircons from granites and metasedimentary rocks of Carrazeda de Ansiães and Sabugal areas, Portugal, to constrain granite sources." Lithos 125(1): 321-334.
21. Gagnevin, D., et al. (2011). "In-situ zircon U–Pb, oxygen and hafnium isotopic evidence for magma mixing and mantle metasomatism in the Tuscan Magmatic Province, Italy." Earth and Planetary Science Letters 305(1–2): 45-56.
22. Siebel, W. and F. Chen (2010). "Zircon Hf isotope perspective on the origin of granitic rocks from eastern Bavaria, SW Bohemian Massif." International Journal of Earth Sciences 99(5): 993-1005.
23. Schaltegger, U., et al. (2009). "Zircon and titanite recording 1.5 million years of magma accretion, crystallization and initial cooling in a composite pluton (southern Adamello batholith, northern Italy)." Earth and Planetary Science Letters 286(1): 208-218.
24. Abati, J., et al. (2012). "Insights on the crustal evolution of the West African Craton from Hf isotopes in detrital zircons from the Anti-Atlas belt." Precambrian Research 212: 263-274
25. Linnemann, U., et al. "The Cadomian Orogen: Neoproterozoic to Early Cambrian crustal growth and orogenic zoning along the periphery of the West African Craton—Constraints from U–Pb zircon ages and Hf isotopes (Schwarzburg Antiform, Germany)." Precambrian Research(0).
26. Bahlburg, H., et al. (2010). "Plate tectonic significance of Middle Cambrian and Ordovician siliciclastic rocks of the Bavarian Facies, Armorican Terrane Assemblage, Germany—U–Pb and Hf isotope evidence from detrital zircons." Gondwana Research 17(2): 223-235.
27. Zlatkin, O., Avigad, D. & Gerdes, A. Peri-Amazonian provenance of the Proto-Pelagonian basement (Greece), from zircon U–Pb geochronology and Lu–Hf isotopic geochemistry. Lithos 184, 379-392 (2014).
28. Samson, S.D., D'Lemos, R.S., Blichert-Toft, J., Vervoort, J., 2003. U–Pb geochronology and Hf–Nd isotope compositions of the oldest Neoproterozoic crust within the Cadomian orogen: new evidence for a unique juvenile terrane. Earth and Planetary Science Letters 208, 165-180.
29. Naydenov, K., Peytcheva, I., von Quadt, A., Sarov, S., Kolcheva, K., Dimov, D., 2013. The Maritsa strike-slip shear zone between Kostenets and Krichim towns, South Bulgaria — Structural, petrographic and isotope geochronology study. Tectonophysics 595–596, 69-89.
30. Morag, N., Avigad, D., Gerdes, A., Belousova, E., Harlavan, Y., 2011. Crustal evolution and recycling in the northern Arabian-Nubian Shield: New perspectives from zircon Lu-Hf and U-Pb systematics. Precambrian Research 186, 101-116.

Supplementary methodology for Chapter 6

The zircon mounts prepared for U–Pb LA-ICPMS analysis were also used for Lu–Hf isotopic studies undertaken with Laser Ablation Multi-Collector Inductively Coupled Plasma Mass Spectrometry (LA-MC-ICPMS) at the Waite campus, University of Adelaide, South Australia. Only grains with U–Pb LA-ICPMS analysis greater than 95% concordance were analysed for Lu–Hf isotope composition. Analysis spots were placed as close as possible to concordant U–Pb LA-ICPMS spots, and within the same CL zone. Zircons were ablated with a New Wave UP-193 Excimer laser (193 nm) using a spot size of 50 μm, frequency of 5 Hz, 4 ns pulse length and an intensity of ~ 10 J/cm2. Zircons were ablated in a helium atmosphere, which was then mixed with argon upstream of the ablation cell. Measurements were made using a Thermo-Scientific Neptune Multi Collector ICP-MS equipped with Faraday detectors and 1011 Ω amplifiers. Analyses used a dynamic measurement routine with: ten 0.524 s integrations on 171Yb, 173Yb, 175Lu, 176Hf (+ Lu + Yb),177Hf, 178Hf, 179Hf and 180Hf; one 0.524 s integration on 160Gd, 163Dy, 164Dy, 165Ho, 166Er, 167Er, 168Er, 170Yb and 171Yb, and one 0.524 s integration of Hf oxides with masses ranging from 187 to 196 amu. An idle time of 1.5 s was included between each mass change to allow for magnet settling and to negate any potential effects of signal decay. This measurement cycle is repeated 15 times to provide a total maximum measurement time of 3.75 min including an off-peak baseline measurement. The measurement routine is optimised to allow for the monitoring of oxide formation rates and REE content of zircon, and to provide the option to correct for REE-oxide interferences if required in high REE zircon. Hf oxide formation rates for all analytical sessions in this study were in the range 0.1–0.07%.

Hf mass bias was corrected using an exponential fractionation law with a stable 179Hf/177Hf ratio of 0.7325. Yb and Lu isobaric interferences on 176Hf were corrected for following the methods of Woodhead et al. (2004). 176Yb interference on 176Hf was corrected for by direct measurement of Yb fractionation using measured 171Yb/173Yb with the Yb isotopic values of Segal et al. (2003). The applicability of these values were verified by analysing JMC 475 Hf solutions doped with varying levels of Yb with interferences up to176Yb/177Hf = ~ 0.5. Lu isobaric interference on 176Hf was corrected using a 176Lu/175Lu ratio of 0.02655 (Vervoort et al., 2004) assuming the same mass bias behaviour as Yb.

Confirmation of accuracy of the technique was monitored using a combination of the Plesovice and Mudtank zircon standards. The average 176Hf/177Hf value for Mudtank for the analytical sessions was 0.282498 ± 0.0000020 (2SD, n = 19), which is comparable to the published value of 0.282504 ± 0.000026 (2SD) by Woodhead and Hergt (2005). εHf(T), TDMc and TDMc crustal were calculated using 176Lu decay constant after Scherer et al. (2001). TDMc crustal was calculated using the methods of Griffin et al. (2002) with an average crustal composition of176Lu/177Hf = 0.015.

Chapter 7

Conclusions and implications for further work

This thesis attempts to develop an understanding of how hafnium isotopic arrays record the opening and closure of oceanic basins (Wilson cycle tectonics) during continental break-up and assembly. The northern Appalachian orogen formed the focus of the study, with hafnium isotopic data also collected from the temporal Variscan orogen of Europe. In the preceding chapters the geochronological, hafnium isotopic and metamorphic history of the "peri-Gondwanan" terranes of Atlantic Canada and Europe were investigated in order to address the principle aims of the thesis. The following discussion summarises the key outcomes and presents a concise summary of the geodynamic evolution of the Appalachian-Variscan orogen during the Neoproterozoic-late Paleozoic. The fundamental learnings from investigating the large-scale use of the hafnium isotopic method are also briefly addressed.

1. Obtain a comprehensive hafnium isotopic record of Wilson cycle tectonics using the northern Appalachian orogen (the type area, Wilson, 1966) as a natural laboratory.

Chapter 2, 3, 5 and 6 present a comprehensive new zircon U-Pb and Hf isotopic data set of magmatic and detrital zircons from Cryogenian to Permian rocks in Ganderia, Avalonia, Meguma and Iberia. In addition, existing hafnium isotopic data was collated from Laurentia, Baltica, Amazonia, West Africa, Arabia and the central African terranes. The data demonstrate the power that U-Pb-Hf zircon datasets have with respect to provenance and paleogeography of dispersed terranes. A major conclusion from the comprehensive data sets is the similarities between the hafnium isotopic arrays of Avalonia, Ganderia and Meguma, so they are subsequently grouped as "composite Avalonia". The arrays indicate an early Neoproterozoic provenance for Avalonia from Baltica, and a late Neoproterozoic-early Cambrian affinity with northern Gondwana (Amazonia). The Hf arrays from Baltica and Amazonia are such that it is implausible to definitively separate them from one another. Most importantly, Hf data from mid-late Neoproterozoic arc-related zircons in all three terranes indicate a basement of similar composition that yields "Grenvillian-type" model ages between ~1.0-2.1 Ga. The autochthonous zones of NW Iberia are clearly traced back to the Saharan metacraton of north Africa, whereas the Upper Allochthon of Iberia is closer in isotopic character to Avalonia or Meguma. The data have implications for the paleogeography of the Upper Allochthon and suggests that the Upper Allochthon in NW Iberia may have been displaced from composite Avalonia during the assembly of Pangea. The Hf arrays indicate that the Paleozoic assembly of the Appalachian and Variscan orogens did not involve multiple Wilson cycles, recording only the closure of the Iapetus and Rheic Oceans.

2. To test the test the sensitivity of the hafnium isotopic arrays in documenting complex accretionary processes during continental ribbon transfer from one continental margin to another.

Chapter 3 presents hafnium isotopic data from Ganderia and the peri-Laurentian margin (Dashwoods terrane) in order to investigate the sensitivity of the Hf isotopic method against the complex accretionary processes and arc-magmatism associated with the closure of the Iapetus Ocean beneath the Laurentian (Notre Dame arc) and Ganderian margins (Penobscot-Popelogan-Victoria arcs). The data demonstrates that Hf isotopic arrays are capable of identifying plate tectonic changes on temporal scales of ~20-50 million years, which include: the onset of continental-arc magmatism on both margins, subduction roll-back and arc-retreat in Ganderia and the final

closure of Iapetus along both margins during the mid-Ordovician. Hafnium isotopes confirm the presence of an Archean basement beneath most outboard regions of peri-Laurentia in the Dashwoods terrane.

3. To test the metamorphic record against the hafnium isotopic record during continental ribbon transfer.

Chapter 4 addresses the timing and nature of metamorphism in the Gander Zone during continental ribbon transfer across the Iapetus Ocean. This chapter emphasises the power of multi-faceted geochronological, isotopic and mineral equilibria modelling with respect to unravelling polyphase orogenic systems. Ganderia records low pressure, high temperature metamorphism (3-4 kbar, 600°C) at 460 ± 7 Ma that coincides with the evolution of the Tetagouche-Exploits back-arc basin during the translation of the composite ribbon across Iapetus. The earlier event is overprinted by second event at 409 ± 6 Ma that involved initial higher pressures (5-6 kbar, ~600-650°C), and subsequent lower pressures (3-4 kbar, ~600-650°C). The later metamorphic event is attributed to the transition to an advancing subduction system in the northern Appalachians associated with the onset of the Acadian orogeny. The emplacement of the Hare Bay gneiss and associated A-type granites immediately follow the brief compressional interval, consistent with the return to an extensional environment. Ganderia forms a focal point for deformation and magmatism during the Paleozoic evolution of the Appalachians due to its thermally weakened and thinned lithosphere that is sandwiched between thick, cratonic Laurentia and the comparatively less deformed Avalonian terrane.

4. *To propose a geodynamic framework for the Neoproterozoic to late Paleozoic evolution of the Appalachian orogen (and to a lesser extent, the Variscan orogen) that accommodates both the hafnium isotopic and geological records..*

Chapter 5 and 6 synthesises the geochronological, isotopic and metamorphic data presented in this thesis in order to propose geodynamic models that attempt to encompass the geological record with the hafnium isotopic arrays for the Appalachian and Variscan orogens. There are a number of key conclusions to be taken from these chapters. First, the composite Avalonian terranes (Ganderia, Avalonia and Meguma) in the northern Appalachians are not built on ~1.0 Ga juvenile oceanic crust in the peri-Rodinian Mirovoi Ocean as had been previously suggested; instead, Hf model ages indicate a continental origin for the basement (TDM =~1.0-2.0 Ga). Continental-arc magmatism is interpreted to have commenced as early as 800 Ma on Mesoproterozoic-Paleoproterozoic crust. The model presented suggests that northeastern Laurentia, Baltica and possibly Amazonia began to rift apart during propagation of the Asgard sea spreading centre into the Grenville suture zone. The proto composite Avalonian terranes were rifted from the active margin and transferred to the northern Gondwana margin by ~650 Ma during subduction rollback associated with the Valhalla Orogen. Thus composite Avalonian terranes did not begin as 'peri-Gondwanan', but are interpreted to have an earlier Laurentian/Baltican origin. However, they did occupy a late Neoproterozoic-early Cambrian position along the Gondwanan margin as had been previously considered.

The Hf arrays from the composite Avalonian terrane of the northern Appalachians and Variscan Europe (The Iberian, Armorican, and Bohemian Massifs, Massif Central and the Pontides) all record subduction roll-back and retreat from the northern Gondwanan margin between ~600-450 Ma. The contiguity of the hafnium isotopic record indicates that the terranes may have formed a vast, extended continental ribbon that spanned the length northern Gondwanan margin, similar to Zealandia in the present-day southwest Pacific. The ribbon arrived diachronously along the Laurentian margin between ~450-

430 Ma, closing Iapetus and triggering outboard subduction into the trailing Rheic Ocean. The Hf isotopic arrays in both regions evolve towards a reworking array, whereby late Neoproterozoic juvenile arc rocks and the Mesoproterozoic-Paleoproterozoic basement was continuously recycled throughout the Paleozoic. The Silurian-Permian geologic record in Variscan Europe and Atlantic Canada is dominated by extensional tectonics punctuated by intervals of compression. The preferred interpretation is that the composite Avalonia on the Laurentian margin occupied an upper plate location during northward dipping subduction and closure of the Rheic Ocean. Magmatism was predominantly generated during the opening and closing of ephemeral back-arc basins, during which only crustal recycling is recorded in the Hf array rather than mixing with mantle derived magmas. In Europe, the reworking process continued throughout the Mesozoic as the African plate slowly moved northward, subducting beneath Eurasia. Gondwanan crust was recycled for the first time in the Cenozoic as the Neo-Tethyan ribbon finally arrived to the Mediterranean trench system.

The completion of the type-Wilson cycle in the northern Appalachians is marked only by termination of magmatism as the εHf array converged on CHUR at ~300 Ma. Similarly in Europe the collision of Gondwana with Laurentia to form Pangea is not reflected in the εHf array, and also reflects reworking of composite Avalonian-type crust. Therefore, the assembly of Pangea could form only part of a larger, longer-term supercontinental cycle.

Implications for the hafnium isotopic method and future work

The present study has highlighted the effectiveness of hafnium isotope arrays for assessing the tectonic evolution of a prescribed area from cratonic to plate tectonic scale. The method is strongest when used in conjunction with sound geological fieldwork and geochemical analysis (e.g. precise geochronology, calculated mineral phase equilibria) to allow the arrays can be tied into geological constraints. Ideally, detrital Hf arrays should be combined with a study of associated igneous rocks in the relevant orogens, to tie the array unequivocally to a particular orogen, and to gain further insights into the nature of the zircon-forming magmatism.

In addition, the thesis has identified areas for future research regarding hafnium isotopic arrays and Appalachian-Variscan geology, including the following:

- Unravelling the evolution of ancient orogenic regions is often complex due to the poly-cyclic nature of magmatism and deformation, commonly resulting in intricate evolutionary models that involve the inception of multiple oceanic basins. The inferred tectonic complexity of the northern Appalachians is a good example. Using hafnium isotopic arrays to recognise the nature and duration of "Wilson cycles", such as Atlantic- vs backarc type, may aid in reducing the complexities of models in these orogenic systems.

- The "arrowhead" reworking array found in the northern Appalachian orogen and Variscan belt during the Silurian- Permian was unexpected given the established accretionary nature of orogenesis during this interval. It is crucial to constrain what specific geological processes led to the reworking arrays, or if it is a manifestation of the size of the sample set. Given the high number of analyses from the Variscan belt, it is unlikely that the data is not statistically sound but further data would also be of benefit in the Appalachian orogen to confirm the veracity of the arrowhead array

- The study has implied that the reworking array is linked to tectonic switching in the northern Appalachians and similar processes in the Variscan orogen. A good assessment of the validity of the hypothesis could be achieved by investigating in great detail the whole rock geochemistry of plutonic and volcanic rocks, the timing of extension

and compression, and obtaining additional hafnium isotopic arrays from igneous rocks across both orogenic systems. The recognition of extension-compression cycles, combined with Hf arrays, provides an opportunity to understand the complex and distribution of magmatism in orogens – every magmatic belt does not need to be another arc-subduction system!

- The Upper Allochthon in NW Iberia and the Meguma terrane were not previously considered to be genetically related; however the arrays presented here are quite similar. The connection was not able to be tested within the confines of the thesis but further comparison and analysis of the geology of the two terranes may assist in unravelling the enigmatic Paleozoic evolution of the Upper Allochthon. A detailed study of the petrology and geochemistry of the turbidites from both terranes should strengthen the links between these two sedimentary sequences.